

## V. FOCUSED FUNDAMENTAL RESEARCH

Cathode Development

Anode Development

Electrolyte Development

Cell Analysis, Modeling, and  
Fabrication

Energy Frontier Research Centers

Integrated Lab-Industry  
Research Program



## V. Focused Fundamental Research

### V.A Introduction

The focused fundamental research program, also called the Batteries for Advanced Transportation Technologies (BATT) Program, is supported by the DOE's Vehicle Technologies Program (DOE-VTP) to research and analyze new materials for high-performance, next generation, rechargeable batteries for use in HEVs, PHEVs, and EVs. The effort in FY 2012 continued the increased emphasis on high-energy materials for PHEV and EV applications and expanded efforts into technologies for enabling the use of Li metal anodes.

#### Background and Program Context

The BATT Program addresses the fundamental problems of chemical and mechanical instabilities that have slowed the development of automotive batteries with acceptable cost, performance, life, and safety. The aim is to develop and test new materials and to use traditional and novel diagnostics and modeling methods to better understand cell and material performance and lifetime limitations before initiating battery scale-up and development. Emphasis is placed on the synthesis of components into cells with determination of failure modes, while continuing with materials synthesis and evaluation, advanced diagnostics, and improved model development. Battery chemistries are monitored continuously with timely substitution of more promising components. This is done with advice from within the BATT Program and from outside experts, including consultation with automotive companies and DOE. Also factored into the BATT Program direction is the monitoring of world-wide battery R&D activities. The Program not only supports research that leads to improvements to existing materials, but also into high-risk "leap-frog" technologies that might have a tremendous impact in the marketplace. An overview of the activities and focus of the Program is shown in Figure V - 1.

#### Solving applied problems using a fundamental approach

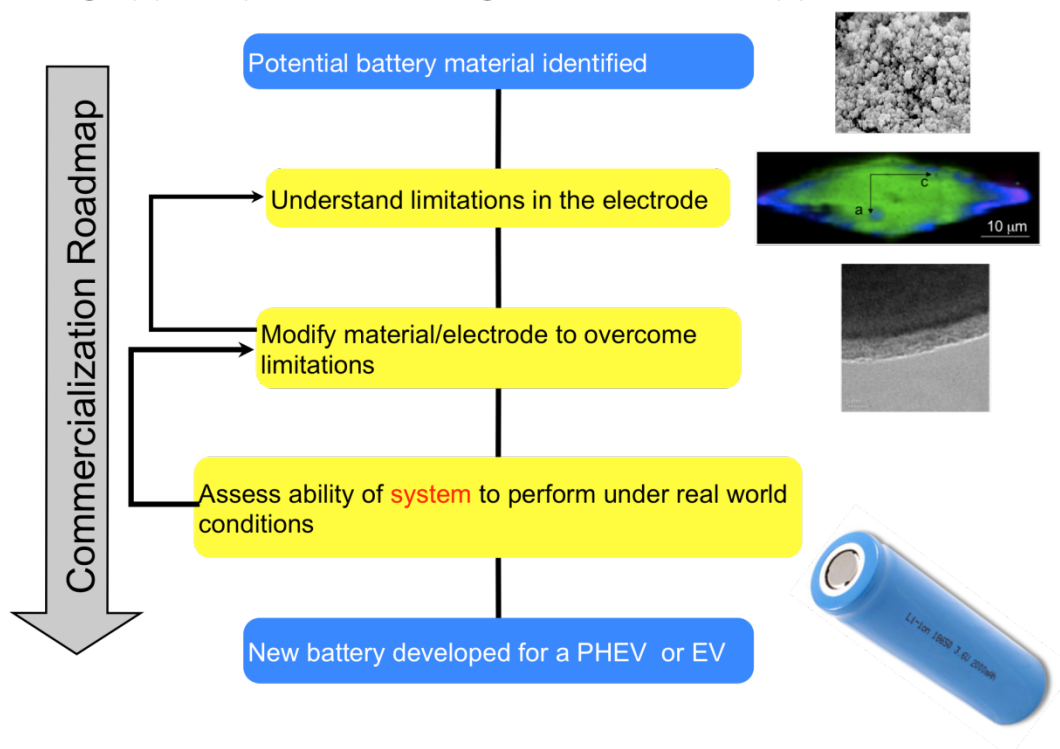


Figure V - 1: BATT Overview

The work is administered by the Lawrence Berkeley National Laboratory (LBNL), with principal researchers from LBNL, five additional national laboratories, fourteen universities, and two commercial companies. The program is organized into the following areas:

- New Cathode Systems, Performance and Limitations
- New Anode Materials
- Novel Electrolytes and their Characterization,
- Li-ion Modeling, Diagnostics, and Cell Analysis

The BATT Program has an enviable team of principal investigators, many of them world renowned, who push the battery field forward in each of these areas. The interaction among the four main focus areas is shown in Figure V - 2.

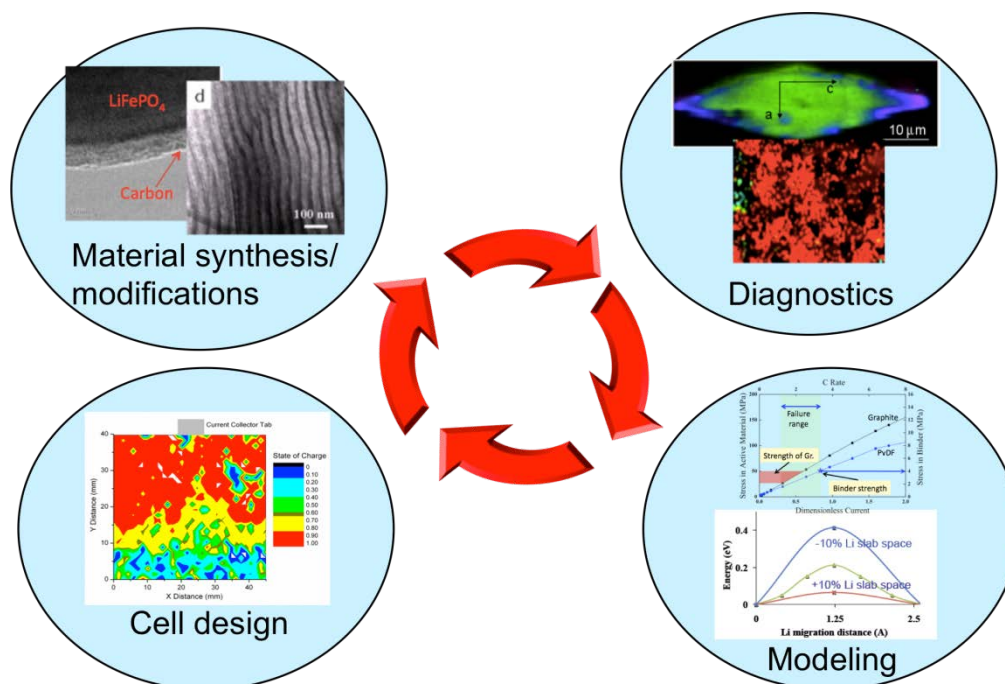


Figure V - 2: BATT Focus Areas

This section summarizes the research activities of this Program in FY 2012. The website for the BATT Program is found at <http://batt.lbl.gov>. Brief descriptions of each research area are as follows.

The **New Cathode Materials** task aims to find improved cathode materials that offer significant improvements in volumetric and specific energy and/or power over current state of the art materials, like  $\text{LiCoO}_2$ . Current projects include work on the high voltage, high-energy layered/layered or Li rich cathode materials, investigating Li bearing mixed polyanion glasses, investigating polyanions that may cycle more than one Li ion per transition metal ion (e.g., silicates), and developing *in situ* reactors designed to investigate solvothermal synthesis reactions in real-time using synchrotron.

The **New Anode Materials** task involves a significant focus on silicon, which offers ten times the capacity of currently used graphite anodes. Researchers are investigating several forms of Si, including nanowires, nanoparticles, clathrate structures, and others. They are also investigating methods for stabilizing Si and Sn composite negative electrodes, including the use of Cu foam current collectors, atomic layer deposition to stabilize alloy electrodes, and a number of Si/carbon nanocomposite materials.

The **Novel Electrolyte Materials** task includes research efforts focused on expanding the temperature range of cells, additives to stabilize the negative and positive interfaces, development of new overcharge shuttles to further stabilize Li-ion cells, new ionic liquids to enable higher voltage windows, and first principles modeling to understand and eventually to construct a more stable SEI.

The **Modeling, Diagnostics, and Cell Analysis** tasks involve the use of advanced diagnostics techniques, such as FTIR, X-ray absorption fine structure (XAFS), X-ray diffraction (XRD), nuclear magnetic resonance (NMR) and other techniques to investigate interfacial and other properties in Li-ion batteries. Several modeling approaches are used to understand cell and fundamental material properties, including *ab-initio* calculations, macroscopic cell calculations, and finite element simulations. Finally, standard cell making and testing techniques are developed and applied to provide a common evaluation process for new materials.

The Program is also studying issues critical to the realization of *Beyond Li-ion Technologies*. Two of the most promising (Lithium/Sulfur and Lithium/Air) require the use of a lithium metal anode. The main focus is to devise new methods to understand and stabilize lithium metal anodes (against mossy Li formation and dendrites) to bring about leaps in energy density without compromising durability and safety. LBNL, ANL and ORNL have partnered to design a series of projects that utilize recent advances in ceramic electrolyte materials, polymer science, and materials characterization to stabilize lithium metal anodes. Inorganic solid state lithium-ion conductors have been proposed as protective electrolyte layers in a lithium metal cell that contains a second, liquid electrolyte in contact with the cathode. The team is also studying various Li metal protective films and dopants that lead to a stable Li/electrolyte interface and permit long-term and stable cycling.

The BATT Program regularly solicits new proposals in each of the above-listed areas. BATT Program management regularly accepts unsolicited proposals on any advanced energy storage technology that can significantly advance the state-of-the-art and is appropriate for the R&D focus of the BATT Program. Unsolicited proposals are reviewed separately but by using a process similar to that for the solicited proposals.

## V.B. Cathode Development

### V.B.1 First Principles Calculations and NMR Spectroscopy of Electrode

#### Materials (MIT/U. Cambridge)

Gerbrand Ceder  
Massachusetts Institute of Technology  
Department of Materials Science and Engineering  
77 Massachusetts Ave, Rm 13-5056  
Cambridge MA 02139  
Phone: (617) 253 1581; Fax: (617) 258 6534  
E-mail: [gceder@mit.edu](mailto:gceder@mit.edu)

Clare P. Grey  
Cambridge University  
Department of Chemistry  
Lensfield Rd,  
Cambridge, CB2 1EW, UK  
Phone: +44 1223 336509; Fax: +44 1223 336362  
E-mail: [cpg27@cam.ac.uk](mailto:cpg27@cam.ac.uk)

Start Date: May 1, 2006  
Projected End Date: December 31, 2012

#### Objectives

- Determine the effect of structure on stability and rate capability of cathodes and anodes.
- Explore relationships between electro-chemistry and particle size and shape.
- Develop new materials.

#### Technical Barriers

- Low rate capabilities, high cost, poor stability of electrode materials, low energy density.

#### Technical Targets

- Specific power 300 W/kg, 10 year life, <20% capacity fade. Low cost.

#### Accomplishments

- NMR used (with Cabana) to investigate local structures in spinel.
- $^{27}\text{Al}$  and  $^{19}\text{F}$  NMR used to identify the composition of the coatings formed on layered lithium nickel manganate from aluminium fluoride solutions.
- *In situ* and *ex situ* micro-focused X-ray fluorescence mXRD, mXANES and mXRD were used to follow

Cu extrusion reactions. *In situ* NMR methods applied to paramagnetic spinels.

- Several novel intercalation cathodes proposed by high-throughput computing and tested.

✧ ✧ ✧ ✧ ✧

#### Introduction

Achieving DOE goals in this field requires both an understanding of how current materials function – with a view to improving rate, capacity and long term cycling performance – and the discovery of new materials and new mechanisms by which these materials function. This joint theoretical and experimental program attacks these issues by developing new *ex situ* and *in situ* tools to investigate battery materials, and then applies these to understand relationships between structure and function. One aim is to use these findings to optimize material function and/or develop new materials.

#### Approach

Use solid state NMR and diffraction/TEM to characterize local and long-range structure as a function of particle size, sample preparation method, state of charge and number of charge cycles (cathodes). Use electrochemistry to correlate particle size with rate performance. Continue to develop the use of *in situ* NMR methods to identify structural changes and reactivity in oxides and intermetallics and to examine Li dendrite formation. Use first principles calculations (density functional theory) to identify redox-active metals, relative stability of different structures, the effect of structure and particle size on cell voltages and rate capability. Use high-throughput computing to identify promising cathode materials for BATT applications. Anticipate possible instabilities in materials at high states of charge by using calculations. Use calculations and NMR to identify low activation energy pathways for cation migration and to investigate electronic conductivity. Extend approaches to Na systems.

#### Results

**High voltage spinels.** In collaboration with BATT members J. Cabana (LBNL) and M.S. Whittingham (Binghamton),  $^6\text{Li}$  and  $^7\text{Li}$  MAS NMR spectroscopy has been used to characterize a series of  $\text{LiNi}_{0.5}\text{Mn}_{1.5}\text{O}_4$

samples synthesized by J. Cabana. The results clearly show that NMR spectroscopy is extremely sensitive to the degree of ordering. Samples prepared at low temperatures (500 °C) show broad  ${}^6\text{Li}$  NMR resonances presumably due to kinetic limitations associated with the formation of an ordered phase (Figure V - 3). The signals sharpen and fewer resonances are observed as the calcination temperature approaches the order-disorder temperature (approx. 700 °C). The spectra just before this temperature can be modeled by assuming a model based on the Ni:Mn ordered structure with space group P4332, but allowing for some disorder between the two transition metal sites of this structure. The results are consistent with the diffraction results (neutron diffraction studies performed by Dr. M. Casas-Cabanas.)

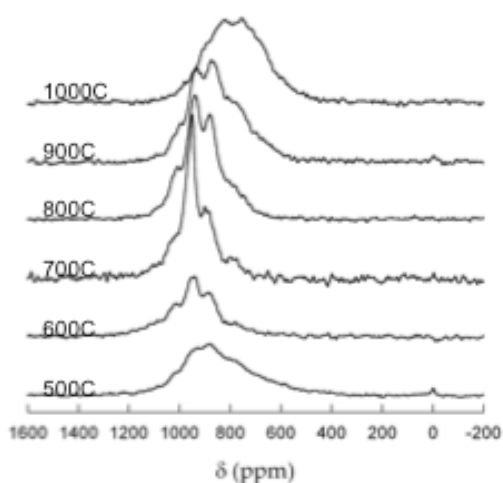


**Figure V - 3:**  ${}^6\text{Li}$  MAS NMR spectra of "LiNi<sub>0.5</sub>Mn<sub>1.5</sub>O<sub>4</sub>" samples as a function of calcination temperature.

The spectra become broader and contain multiple peaks above 700 °C as the disorder increases. A shift to lower frequencies is observed, which is consistent with increased  $\text{Mn}^{3+}$  in the sample and also the formation of a rock salt phase (seen by X-ray diffraction and electron microscopy). The NMR spectroscopy of these and a wider series of samples are being correlated with the electrochemical properties to understand the role that local structure plays in controlling performance.

**NMR Studies of Coatings.** A study of layered  $\text{Li}[\text{Li}_{1/9}\text{Ni}_{1/3}\text{Mn}_{5/9}]\text{O}_2$  positive electrodes nominally coated with aluminum fluoride has been completed. Coatings were prepared by using aluminum fluoride aqueous solutions with 0.25 – 10.0 mol%  $\text{AlF}_3$  and compared with samples treated under similar conditions but with aqueous HCl solutions. Samples were investigated following heat treatment at 120 and 400°C by X-ray diffraction, TEM and both  ${}^6\text{Li}$  &  ${}^{27}\text{Al}$  magic angle spinning (MAS) NMR spectroscopy. The TEM/EDS and  ${}^{27}\text{Al}$  NMR data provide support for an aluminum-rich amorphous coating that, following drying at 120 °C, comprises six-coordinate, partially hydrated aluminum environments containing no

more than one or two fluoride ion in the Al local coordination sphere (Figure V - 4). Heat treatment at 400 °C results in a phase that resembles partially fluorinated or  $\text{Al}_2\text{O}_3$ , at least locally. An Al:F elemental ratio of 2:1 is obtained in stark contrast to the ratio used in the original solution (1:3). The acidic coating procedures also result in significant structural rearrangements of the bulk, the acidic solutions leaching  $\text{Li}^+$  from the structure. Some evidence for the protonated phase is seen following drying at 120 °C. Heat treatment results in the development of local environments that more closely resemble those seen in  $\text{Li}_2\text{MnO}_3$ , which since no  $\text{Ni}^{2+}$  ions are lost during the acidic treatment, may result in some rock-salt like Ni-rich local structures.

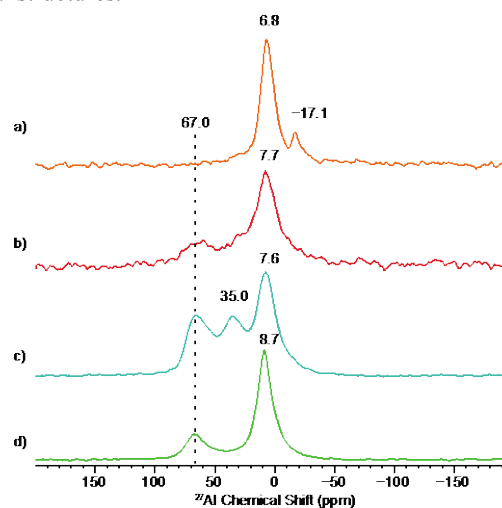


**Figure V - 4:**  ${}^{27}\text{Al}$  NMR of (a) 1% Al/F-coated  $\text{Li}[\text{Li}_{1/9}\text{Ni}_{1/3}\text{Mn}_{5/9}]\text{O}_2$  after heating at 120°C and (b) 400°C (in N<sub>2</sub>), (c) 5% reference  $\text{AlF}_3$ -coated  $\text{Li}[\text{Li}_{1/9}\text{Ni}_{1/3}\text{Mn}_{5/9}]\text{O}_2$  after heating at 400°C in N<sub>2</sub>, and (d) 5% Al/F-coated  $\text{Li}[\text{Li}_{1/9}\text{Ni}_{1/3}\text{Mn}_{5/9}]\text{O}_2$  after heating at 400°C in N<sub>2</sub>.

The results highlight the need to distinguish between the effect of the coating itself and the structural (bulk) effects induced by the coating method on the resulting electrochemical performance.

**Silicon Anode Materials.** A detailed  ${}^{29}\text{Si}$  NMR study of  ${}^{29}\text{Si}$ -enriched Si nanoparticles has now been complete. The results show three distinct types of Si on cycling.

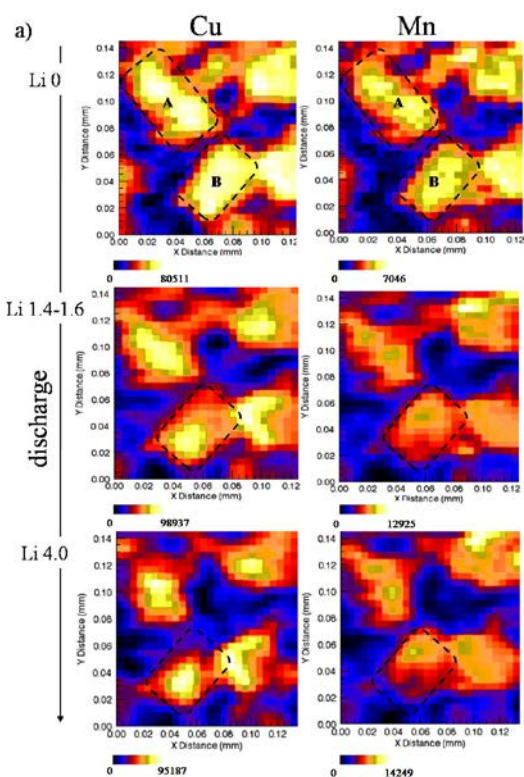


**Figure V - 5:** *In situ* X-ray fluorescence imaging maps at the Cu+ energy (8981 eV) for Cu K $\alpha$  and Mn K $\alpha$  of an *in situ* Sr<sub>2</sub>MnO<sub>2</sub>Cu<sub>3.5</sub>Li<sub>x</sub>S<sub>3</sub> cell at different stages of discharge, (from up to down): Li0, Li1.4-1.6 and Li4.0 (fully discharged) maps. The Li contents, denoted by x in Li<sub>x</sub>, indicate the amount of Li inserted in the Sr<sub>2</sub>MnO<sub>2</sub>Cu<sub>3.5</sub>-xLi<sub>x</sub>S<sub>3</sub> structure. The maps were collected at a same region on the electrode film of an area (120/130  $\mu$ m x 140  $\mu$ m) at 5  $\mu$ m/step with dwell time of 2s/pixel. 1

**In vs. Ex Situ Experiments.** *Ex situ* and *in situ* micro-focused synchrotron X-ray fluorescence imaging coupled with selective micro-focused X-ray absorption near edge spectroscopy ( $\mu$ XANES) and micro-focused X-ray diffraction methods were investigated as methods to image the elemental components within the battery electrode ( $\mu$ XRF) and to follow the metal oxidation states and phase distributions ( $\mu$ XANES and  $\mu$ XRD, respectively). The techniques were applied to investigate Sr<sub>2</sub>MnO<sub>2</sub>Cu<sub>3.5</sub>S<sub>3</sub>, a cathode material that operates by a combined insertion/displacement mechanism. After 2 moles of Li intercalation, Cu metal extrusion is observed by  $\mu$ XRD, which also reveals the formation of the Sr<sub>2</sub>MnO<sub>2</sub>Cu<sub>3.5</sub>-xLi<sub>x</sub>S<sub>3</sub> phase. *Ex situ*  $\mu$ XRF images of the electrode after 4 mol of Li intercalation show a segregation between the Cu metal particles while *in situ*  $\mu$ XRF imaging experiments reveal that the Cu and Mn elemental distribution maps are highly correlated with the particle orientation giving different results when the particle is oriented perpendicular or parallel to the incident beam (Figure V - 5). *In situ* electrochemical synchrotron XRF imaging has the advantage over *ex situ* mode of resolving the mechanism of single particles vs. time. *In situ*  $\mu$ XRF imaging data suggest that the microstructure of the

Sr<sub>2</sub>MnO<sub>2</sub>Cu<sub>3.5</sub>-xLi<sub>x</sub>S<sub>3</sub> electrode, on a micron-scale level, is not affected during the reaction process.

In a second method development, *in situ* <sup>7</sup>Li and <sup>6</sup>Li nuclear magnetic resonance (NMR) studies of working batteries have been performed to investigate paramagnetic cathode materials. Initial studies have focused on Li<sub>1.08</sub>Mn<sub>1.92</sub>O<sub>4</sub> and it has been shown that this method can be used to detect changes of lithium transport within the electrode, *in situ*. *Ex situ* lithium studies have been performed to determine the limits of Li substitution in this material. *In situ* studies have clearly shown changes in lithium mobility as a function of state of charge.

**Computational Study of Phosphates.** The Li<sub>x</sub>FeP<sub>2</sub>O<sub>7</sub> and Li<sub>x</sub>MnP<sub>2</sub>O<sub>7</sub> pyrophosphates have been considered as possible two-electron cathode materials. In collaboration with Professor Whittingham, these materials have been evaluated. The pair distribution function (PDF) profile, obtained from the X-ray total scattering data of the cycled samples, has been analyzed. It has been found that both oxidation of Mn<sup>2+</sup> to Mn<sup>3+</sup> and Fe<sup>2+</sup> to Fe<sup>3+</sup> is feasible, but oxidation to the 4+ state occurs at very high voltage for both Mn and Fe. These predictions indicate that cycling of one Li from Li<sub>2</sub>FeP<sub>2</sub>O<sub>7</sub> and Li<sub>2</sub>MnP<sub>2</sub>O<sub>7</sub> will be possible, but the second Li cannot be removed with any current electrolytes.

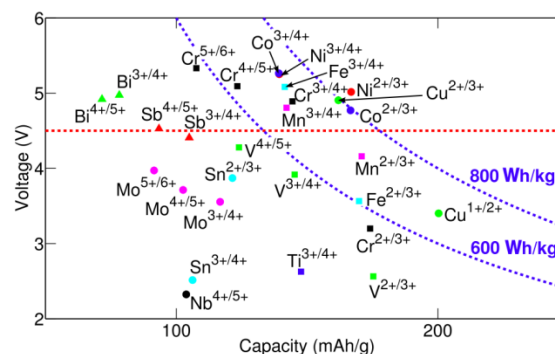


**Figure V - 6:** Average computed voltage for redox couples in phosphates

This is consistent with experimental work performed by the Whittingham group. These findings are consistent with the general trends that have been observed in phosphates. Using calculations on several thousand real and hypothetical phosphate compounds it has been possible to datamine the average potential for every possible redox couple. The result is shown in Figure V - 6. The results indicate that while in general, the Mn<sup>2+</sup>/Mn<sup>3+</sup> and Fe<sup>2+</sup>/Fe<sup>3+</sup> couple are in a reasonable voltage range, the Fe<sup>3+</sup>/Fe<sup>4+</sup> couple is very high in voltage. The Mn<sup>3+</sup>/Mn<sup>4+</sup> is marginally accessible in some phosphates, but clearly not in the pyrophosphate. The dependence of redox voltage on structure was also investigated in more detail (not shown).

**New Materials Predicted.** Lithium and sodium transition metal carbonophosphates have been suggested by previously reported high-throughput computing and screening to be promising intercalation compounds. Computational thermodynamic stability analysis indicates

that many of the sodium carbonophosphates are stable while all lithium compounds are not stable or meta-stable.  $\text{Na}_3\text{FePO}_4\text{CO}_3$  and  $\text{Na}_3\text{MnPO}_4\text{CO}_3$  were successfully synthesized by a hydrothermal method and then their lithium versions were obtained through Li-Na ion exchange. Stoichiometric  $\text{Li}_3\text{FePO}_4\text{CO}_3$  was obtained through fully complete ion exchange. However, for  $\text{Na}_3\text{MnPO}_4\text{CO}_3$ , only a part of Na can be replaced by Li and yield  $\text{Li}_{2.67}\text{Na}_{0.63}\text{Mn}_{0.96}\text{PO}_4\text{CO}_3$ . In collaboration with Yimei Zhu at Brookhaven National Laboratory, the crystal structure of  $\text{Li}_3\text{FePO}_4\text{CO}_3$  was solved by combining single particle electron diffraction and synchrotron powder diffraction. *In situ* battery cycling XRD experiments for both compounds were also performed at NSLS. Both *ex situ* and *in situ* XRD results indicate that Li ion intercalation/deintercalation in both Fe and Mn carbonophosphates are topotactic, with a solid solution pathway.

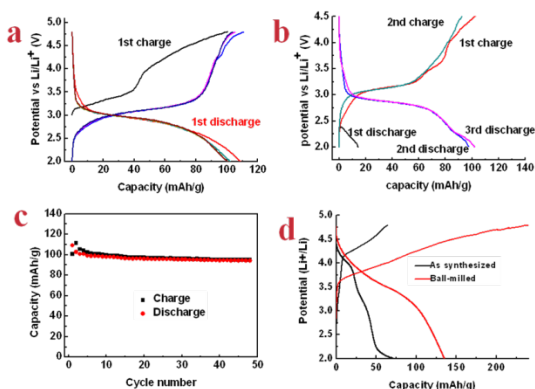


**Figure V - 7:** The voltage profile of  $\text{Li}_3\text{FePO}_4\text{CO}_3$  at C/5 at room temperature. (b) The voltage profile of non-ball-milled  $\text{Li}_3\text{FePO}_4\text{CO}_3$  at 60 °C and C/10. (c) The capacity retention of condition (a). (d) The voltage profile of  $\text{Li}_{2.67}\text{Na}_{0.63}\text{Mn}_{0.96}\text{PO}_4\text{CO}_3$ , both ball-milled and non-ball-milled samples, cycled at C/100 rate.

Both Fe and Mn carbonophosphates show good electrochemical performances.  $\text{Li}_3\text{FePO}_4\text{CO}_3$  shows a capacity of ~110 mAh/g at C/5 rate after ball-milling with carbon black and same capacity at 60°C without ball-milling. This capacity is approx. 100% of the 1-e theoretical capacity (115 mAh/g). The main plateau around 3 V agrees well with computationally predicted intercalation voltage (2.99 V) for  $\text{Fe}^{2+}/\text{Fe}^{3+}$  redox.  $\text{Li}_{2.67}\text{Na}_{0.63}\text{Mn}_{0.96}\text{PO}_4\text{CO}_3$  shows a capacity of ~135 mAh/g after ball-milling with carbon, corresponding to 1.2 Li intercalation per formula. This result indicates that not only  $\text{Mn}^{2+}/\text{Mn}^{3+}$  redox, but  $\text{Mn}^{3+}/\text{Mn}^{4+}$  redox couple is partially active, which is rare in polyanion cathode materials.

## Conclusions and Future Directions

In conclusion, a variety of *in situ* and *ex situ* structural probes has been pushed in order to characterize anode and cathode materials. Detailed NMR and impedance studies are in progress to track the change in coatings with cycling, while *in situ* NMR methods are being used to investigate cation dynamics during cycling.

The potential of novel phosphates as new electrode materials has been computationally evaluated, including some completely novel carbonophosphate compounds identified by high-throughput computing, and have outlined where future opportunities may be in phosphates.

## FY 2012 Publications/Presentations

1. R. Robert, D. Zeng, A. Lanzirotti, P. Adamson, S.J. Clarke, and C.P. Grey, *Chem. Mat.*, **24**, 684-2691, (2012).
2. J. Cabana, M. Casas-Cabanas, F.O. Omenya, N.A. Chernova, D. Zeng, M.S. Whittingham, C.P. Grey, "Composition-Structure Relationships in the Li-Ion Battery Electrode Material  $\text{LiNi}_{0.5}\text{Mn}_{1.5}\text{O}_4$ ," *Chem. Mat.*, **24**, 2952-2964, (2012).
3. K. Rossina, M. Jiang, D. Zeng, E. Salager, A. Best, C.P. Grey, "Structure of aluminum fluoride coated  $\text{Li}[\text{Li}_{1/9}\text{Ni}_{1/3}\text{Mn}_{5/9}]\text{O}_2$  cathodes for secondary lithium-ion batteries," *J. Mater. Chem.*, **22**, 20602-20610 (2012).
4. H. Chen, G. Hautier, A. Jain, C. Moore, B. Kang, R. Doe, L.J. Wu, Y.M. Zhu, Y.Z. Tang, G. Ceder, "Carbonophosphates: A New Family of Cathode Materials for Li-Ion Batteries Identified Computationally," *Chemistry of Materials*, **24**, 11, 2009-16 (2012).
5. G. Hautier, A. Jain, H. Chen, C. Moore, S.P. Ong, G. Ceder, "Novel Mixed Polyanions Lithium-Ion Battery Cathode Materials Predicted by High-Throughput *Ab Initio* Computations," *J. of Mat. Chem.*, **21**, 17147-17153 (2011).
6. S.P. Ong, V.L. Chevrier, G. Hautier, A. Jain, C.J. Moore, S. Kim, X. Ma., G. Ceder, "Voltage, Stability and Diffusion Barrier Differences Between Sodium-Ion and Lithium-Ion Intercalation Materials," *Energy & Environmental Science*, **4** (9), 3680-3688 (2011).

---

## V.B.2 Cell Analysis, High-energy Density Cathodes and Anodes (LBNL)

Thomas Richardson  
Lawrence Berkeley National Laboratory  
Department of Energy Storage and Distributed Resources  
1 Cyclotron Road  
Berkeley, CA 94720  
Phone: (510) 486-8619; Fax: (510) 486-8609  
E-mail: [tjrichardson@lbl.gov](mailto:tjrichardson@lbl.gov)

Start Date: October 1, 2004  
Projected End Date: September 30, 2012

### Objectives

- Investigate the relationships between structure, morphology and performance of cathode and anode materials.
- Explore kinetic barriers and utilize the knowledge gained to design and develop cells with improved energy density, rate performance and stability.

### Technical Barriers

- Low energy density
- Poor cycle life

### Technical Targets

- Available energy (Goal: 11.6 kWh)
- Cycle life (Goal: 5,000cycles/58 MWh)

### Accomplishments

- Determined the charge distribution in cathodes harvested from high power commercial cells using x-ray diffraction.
- Explored new methods to assess charge distribution using ultrafast laser-induced breakdown spectroscopy (LIBS) and infrared spectroscopy.
- Developed new optical microscopy methods for diagnosis of battery chemistries involving insoluble reactants and/or products.



### Introduction

The influence of electrode composition and structure on performance, especially at high charge-discharge rates is of considerable importance for both high power and high energy batteries. Improved utilization of active material and reduction of electrochemical stress by maximizing the uniformity of current distribution can increase capacity and extend cell life. It is therefore desirable to characterize the

internal structure of electrodes and correlate performance with the observed features. Methods have been developed for visualizing charge distribution in cathodes using spatially resolved x-ray diffraction (XRD). Focused ion beam (FIB) tomography has also been used to create 3D images of electrodes by sequential removal of thin vertical slices of the electrode followed by scanning electron microscopy (SEM) imaging of the revealed surfaces. Software reconstruction reveals the sizes, shapes and spatial distribution of voids and cracks as well as those of the active material, conductive additives and binder.

Our success in developing these *ex situ* methods enables a wide array of new experiments and the ability to evaluate the influence of charge homogeneity on cell performance and to monitor developing changes in structure and behavior. Some spectroscopic methods have now been added for mapping of the local state of charge SOC in harvested electrodes. These may eventually be applied to *in situ* cells.

### Approach

XRD, optical and electron microscopies, vibrational spectroscopies, and electroanalytical techniques are used to characterize known and modified electrode materials and to establish correlations between performance and factors such as composition, morphology, and surface chemistries. The results are used to provide guidelines for materials synthesis and electrode fabrication processes. Cells with lithium iron phosphate (LFP) cathodes were studied because redistribution of charge following charging or discharging does not occur in these electrodes.

### Results

**Charge Mapping.** Previously, XRD mapping of charge distribution was achieved using synchrotron radiation with a spot size of a few  $\mu\text{m}$ . In-plane mapping of a rapidly charged pouch cell cathode (Figure V - 8) shows a high SOC near the current collector tab. Electrolyte polarization resulted in a lower SOC near the center of the electrode. Isolated regions that were not charged were attributed to delamination or gas bubbles in the separator.

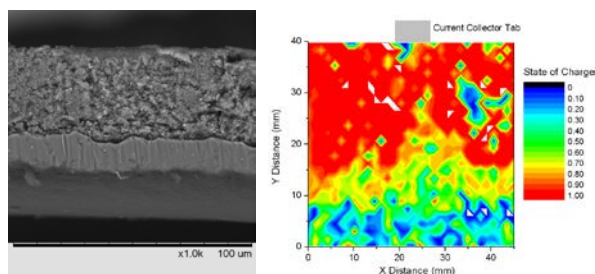


Figure V - 8: Charge mapping by XRD.

Due to lack of available synchrotron beam time, mapping of a cathode harvested from a commercial high-power 18650 cell rated for 30C continuous and 60C pulse discharging was carried out using a laboratory XRD instrument. The analyzed area (spot size) was 2 mm x 5 mm. A portion of the cathode was sectioned by Ar-ion milling (Figure V - 9), revealing a highly uniform particle size (ca. 50 nm) and a uniform bimodal pore structure (50 nm and 1 μm in size).

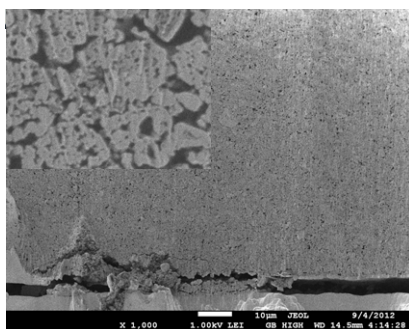


Figure V - 9: Top: A123 Nanophosphate cathode cross section (inset 30,000X).

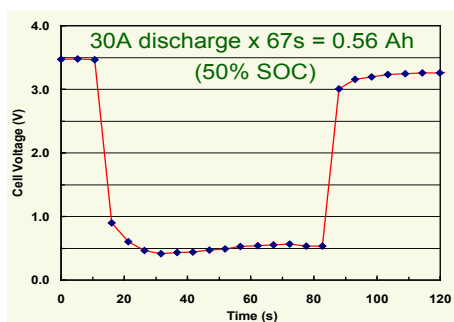


Figure V - 10: Cell voltage during fast discharge.

The cell was cycled once at C/25 to verify the 1.1 Ah capacity, then discharged at a current of 30 A (27C). The cell voltage (Figure V - 10) dropped quickly to less than 0.5 V, then slowly increased as the cell temperature rose. It recovered rapidly when the discharge ended.

After cell disassembly, the cathode was mapped using both XRD and infrared spectroscopy (FTIR). Non-destructive analysis of the cathode surface by attenuated total reflectance FTIR showed that the entire surface was fully discharged. Bulk samples scraped off the

current collector were dispersed in IR-transparent KBr powder and pressed into pellets for transmission measurements. SOC was determined by fitting these spectra to a linear combination of the end members, LFP and FP (Figure V - 11).

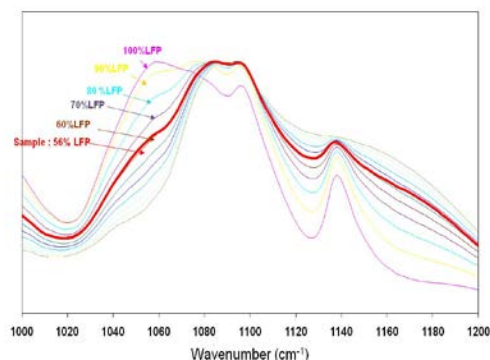


Figure V - 11: FTIR spectra of electrode samples and reference mixtures.

SOCs determined by XRD and FTIR at different distances from the single tab are compared in Figure V - 12. The overall SOC was much lower than expected, indicating that the cell may have been shorted during disassembly. The extent of discharge was significantly greater in the cathode area near the center of the jelly roll, perhaps due to higher compression or better electrolyte wetting. The substantial heat generated during discharge may also have resulted in a higher temperature in the interior of the cell.

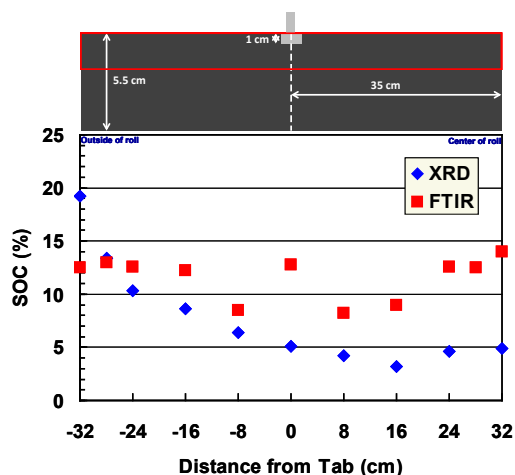


Figure V - 12: Measured SOC vs. distance from the tab.

**Laser Ablation SOC Depth Profiling.** In collaboration with Dr. Vasileia Zormpa of LBNL, ultrafast laser-induced breakdown spectroscopy (LIBS) was used to measure charge distribution in LFP electrodes. This technique offers elemental analysis with high spatial resolution (Figure V - 13), and is ideal for depth profiling because it does not require sample preparation such as mounting and slicing to expose the cross section.

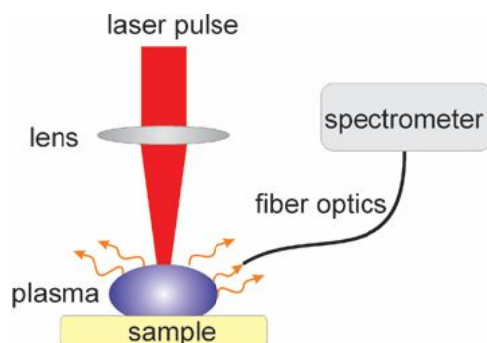


Figure V - 13: LIBS technique.

A coin cell cathode charged at 18C to 40 % SOC that had been previously mapped by synchrotron XRD was subjected to LIBS depth profiling by obtaining plasma emission spectra during repeated laser pulses (450 fs at 343 nm) directed at a single 100  $\mu\text{m}$  spot on the face of the electrode. The lithium-to-iron profiles (1 – SOC) measured by LIBS (Figure V - 14) were reproduced at three different locations.

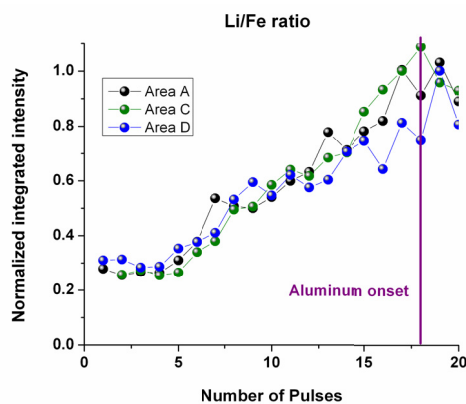


Figure V - 14: Li/Fe ratio vs. laser pulse number.

The depth accessed by each pulse was determined from the number of pulses before the aluminum signal from the current collector became apparent. The LIBS data compares well with the gradient obtained by XRD (Figure V - 15) except that the latter technique failed to access the top portion of the electrode, possibly due to loss of composite material during sectioning and polishing. When the data were offset to correct for this, the agreement was excellent.

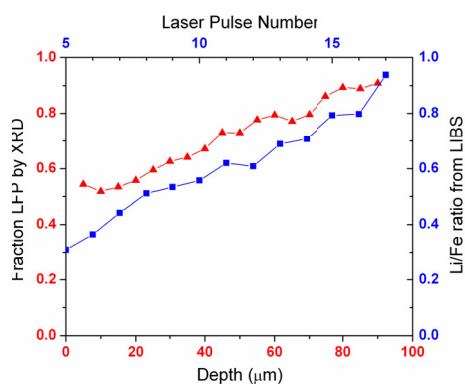


Figure V - 15: Comparison of XRD and LIBS results.

The LIBS technique is versatile and fast, requires little sample preparation, can map in-plane as well as cross section SOCs, and delivers the SOC from the Li/Fe ratio without further data processing. It was developed, however, for dense, homogeneous samples. Determination of the optimum laser parameters for analysis of composites containing a ceramic component along with a light weight polymer binder, carbon black, and considerable porosity is challenging, and it is necessary to rely on known standard samples for calibration.

**In situ Optical Microscopy.** Insoluble redox active materials in lithium-sulfur and lithium-air batteries can become isolated from the electrodes. In order to participate in cycling, they must be solubilized through intermediate species formed at the electrode surface. To identify these agents and their origin, cells were developed in which the gap between the electrode and an insoluble solid reactant is visible. An example is the dissolution of LiOH by a species generated at high potential. In a transparent cell (Figure V - 16), anodic polarization of an adjacent non-contacting electrode in PC on a LiOH•H<sub>2</sub>O crystal cluster produces an agent that breaks it up by dissolving the matrix surrounding the component crystals.

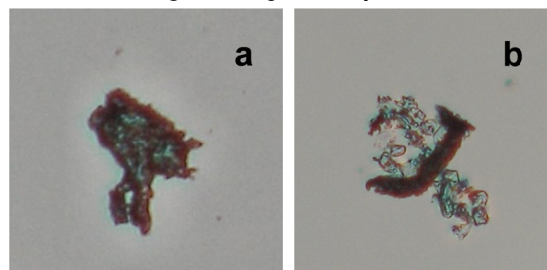


Figure V - 16: LiOH•H<sub>2</sub>O cluster in PC, a) before, b) after polarization at 5.0 V.

The addition of a color indicator sensitive to pH showed that an acidic species was responsible for the change.

## Conclusions and Future Directions

Determination of the current and charge distributions in laminated cells is essential to the improvement and

validation of models used to design batteries and optimize their performance. This has been achieved only in a small number of cases, using thermal imaging, magnetic imaging, element-specific beamline techniques, and by the methods described here. There is a great deal of potential for further exploration in this area.

This project has ended.

### FY 2012 Publications/Presentations

1. X. Liu, J. Liu, R. Qiao, Y. Yu, H. Li, L. Suo, Y.-S. Hu, Y.-D. Chuang, G. Shu, F. Chou, T.-C. Weng, D. Nordlund, D. Sokaras, Y. J. Wang, H. Lin, B. Barbiellini, A. Bansil, X. Song, Z. Liu, S. Yan, G. Liu, S. Qiao, T. J. Richardson, D. Prendergast, Z. Hussain, F. M. F. de Groot, and W. Yang, "Phase Transformation and Lithiation Effect on Electronic Structure of  $\text{Li}_x\text{FePO}_4$ : An In-Depth Study by Soft X-ray and Simulations," *Journal of the American Chemical Society*, **134**, 13708–13715 (2012).
2. R. Buonsanti, T. E. Pick, N. Krins, T. J. Richardson, B. A. Helms, D. J. Milliron, "Assembly Of Ligand-Stripped Nanocrystals Into Precisely Controlled Mesoporous Architectures," *Nano Letters*, **12**, 3872-3877 (2012).
3. T. J. Richardson, "Charge Distribution in Batteries: from Particles to Electrodes," *Gordon Research Conference on Batteries*, March 2012, Ventura, CA.
4. T. J. Richardson, "Determination and Evaluation of Charge Distribution in Lithium Battery Electrodes," *63<sup>rd</sup> Annual Meeting of the International Society for Electrochemistry*, August 2012, Prague, Czech Republic.

## V.B.3 Olivines and Substituted Layered Materials (LBNL)

Marca Doeff  
Lawrence Berkeley National Laboratory  
Environmental Energy Technologies Division  
1 Cyclotron Road  
Berkeley, CA 94720  
Phone: (510) 486-5821 Fax: (510) 486-4881  
E-mail: [mmdoeff@lbl.gov](mailto:mmdoeff@lbl.gov)

Start Date: Oct 1, 2011  
Projected End Date: September 30, 2015

- Showed that Ti-substituted NMCs consistently give up to 15% higher discharge capacities over baseline materials when substitution is limited to 4% or less and voltage range is extended to 4.7V vs Li/Li<sup>+</sup>.
- Showed that Ti-substituted NMCs cycle better than baseline materials when the upper voltage range is extended to 4.7V vs Li/Li<sup>+</sup>.
- Used synchrotron techniques to probe structural details of Li insertion processes in Ti-substituted NMCs.

### Objectives

- To develop high energy, high performance cathode materials including substituted Ni-Mn-Cos, composites of LiNi<sub>0.5</sub>Mn<sub>1.5</sub>O<sub>4</sub> and coated powders, using spray pyrolysis and other synthesis techniques.

### Technical Barriers

The cost of vehicle batteries is too high and the energy density needs to be improved. Cost on a \$/kWh basis will be lowered if higher energy density can be obtained without adversely affecting cycle life. However, the performance of high-energy high voltage electrode materials like LiNi<sub>0.5</sub>Mn<sub>1.5</sub>O<sub>4</sub> needs to be improved by reducing its reactivity with the electrolyte. Alternatively, higher utilization of NMC cathode materials could lead to higher energy density, provided cycling issues can be successfully addressed.

### Technical Targets

- Use simple one-step synthesis procedures like spray pyrolysis to prepare cathode materials with uniform spherical particle morphologies.
- Prepare materials with protective layers on particle surfaces or composite materials consisting of a lower voltage material on surfaces of a higher voltage material, using spray pyrolysis and infiltration techniques.
- Explore feasibility of increasing utilization of NMCs by partial Ti-substitution of Co and using higher voltage cutoffs during cycling.
- Understand origins of Ti-substitution effects in substituted NMCs.

### Accomplishments

- Demonstrated feasibility of preparing composite LiNi<sub>0.5</sub>Mn<sub>1.5</sub>O<sub>4</sub>/LiFePO<sub>4</sub> particles by combining spray pyrolysis with infiltration.

◇ ◇ ◇ ◇ ◇

### Introduction

Achieving DOE cost and energy goals for vehicular batteries based on Li-ion technologies requires improvement to existing cathode materials. Higher energy density can be achieved either by replacing conventional cathodes with high voltage materials such as LiNi<sub>0.5</sub>Mn<sub>1.5</sub>O<sub>4</sub>, or by increasing the utilization of NMC (LiNi<sub>x</sub>Mn<sub>x</sub>Co<sub>1-2x</sub>O<sub>2</sub>) cathodes. At present, either approach compromises the cycle life of the device, because of increased reactivity of the electrolytic solutions and/or the instability of the electrodes at high states-of-charge (in the case of the NMCs). Composites of LiNi<sub>0.5</sub>Mn<sub>1.5</sub>O<sub>4</sub> coated with a protective ion-conducting phase that can be delithiated at a potential below the voltage stability limit of the electrolyte could result in improved cycling stability while maintaining the high energy density of the high voltage phase. At present, we are exploring the feasibility of making LiFePO<sub>4</sub>/LiNi<sub>0.5</sub>Mn<sub>1.5</sub>O<sub>4</sub> composites prepared by spray pyrolysis followed by an infiltration process. A second aspect of the work is focused on Ti-substituted NMCs, which, for some formulations, show higher utilization and better cycling retention than the unsubstituted versions, when charged repeatedly to 4.7V vs. Li/Li<sup>+</sup>. Some work this year is directed towards understanding this effect and determining if this approach will be fruitful for designing higher energy density cells based on modified NMCs.

### Approach

Materials are synthesized by a variety of techniques, including co-precipitation, solid-state methods, combustion, and spray pyrolysis. For the latter, a precursor solution is sprayed through an ultrasonic nozzle into a heated furnace tube. Particle characteristics such as size, size distribution, morphology, porosity, etc. can be controlled by varying experimental conditions including nozzle frequency, type and concentration of precursors in solution, the use of additives, temperature, and post-

production thermal treatments. In some cases, hollow particles are produced. Solutions of  $\text{LiFePO}_4$  precursors can then be infiltrated into the hollow particles, and leave a coating on the surface. A variety of physical techniques are used to characterize materials including x-ray powder diffraction (XRD), scanning electron microscopy (SEM), and elemental analysis. Composite electrodes are tested in half-cell configurations. Pouch cells with lithium anodes and composite cathodes are assembled and cycled in the relevant SSRL beamline for *in situ* XAS and x-ray diffraction experiments. The Advanced Photon Source (APS) at Argonne National Lab is also used for structural characterization of powders and electrodes *ex situ*.

## Results

**$\text{LiNi}_{0.5}\text{Mn}_{1.5}\text{O}_4$ .** Figure V - 17 shows a scanning electron micrograph of a composite  $\text{LiFePO}_4@ \text{LiNi}_{0.5}\text{Mn}_{1.5}\text{O}_4$  particle. First, hollow spheres of  $\text{LiNi}_{0.5}\text{Mn}_{1.5}\text{O}_4$  were prepared using spray pyrolysis. These were then infiltrated with  $\text{LiFePO}_4$  precursors, dried and calcined to crystallize the  $\text{LiFePO}_4$ . Energy dispersive x-ray spectroscopy (EDS) (Figure V - 18) shows that Fe and P are located in the core of the particle and on the surface, while Ni and Mn are restricted to the shell in between.

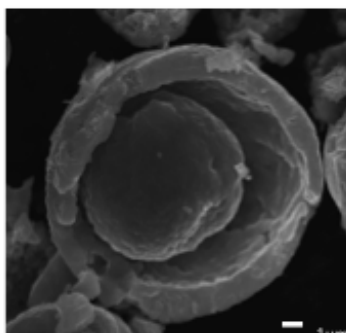


**Figure V - 17:** Scanning electron micrograph of a broken composite  $\text{LiFePO}_4@ \text{LiNi}_{0.5}\text{Mn}_{1.5}\text{O}_4$  particle prepared by spray pyrolysis and infiltration.

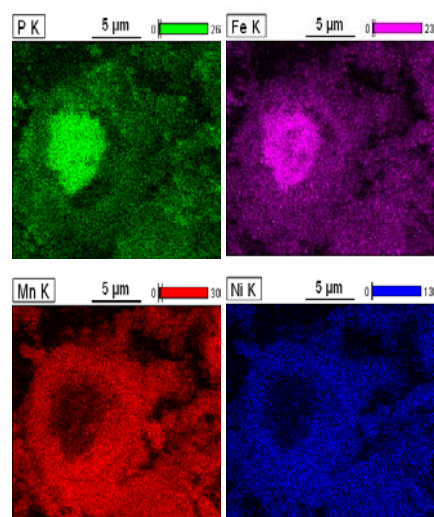


**Figure V - 18:** EDS mapping of a core-shell particle similar to the one pictured in Figure V - 17, showing distribution of P, Fe, Mn, and Ni.

At present, challenges with this approach include difficulty filling hollow particles completely and reactivity between the  $\text{LiFePO}_4$  precursors and the  $\text{LiNi}_{0.5}\text{Mn}_{1.5}\text{O}_4$ , particularly when they are in close contact. Images of cross-sectioned particles prepared by Ar ion-milling (Figure V - 19) show that most particles are only partially filled using the current infiltration process.

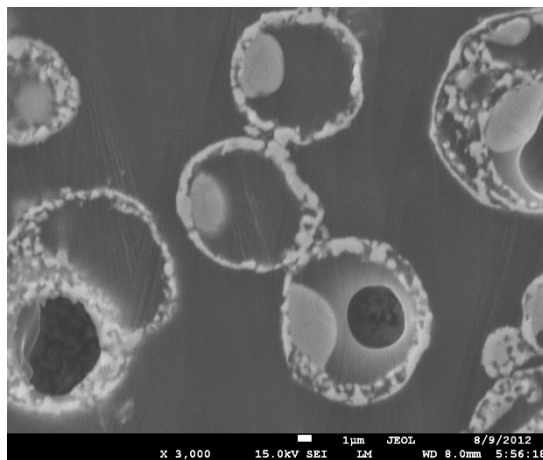


**Figure V - 19:** Scanning electron images of cross-sectioned particles showing that many core-shell particles contain large void spaces.

It may be necessary to use  $\text{LiMnPO}_4$  rather than  $\text{LiFePO}_4$  to fill and coat the hollow particles because of the chemical compatibility issues. Alternatively, lower temperature processing may be required. Further work on the composite systems will be directed towards exploring these and other options during FY2013.

**Ti-substituted NMCs.** Previously, it was shown that partial substitution of Co with Ti in NMCs has beneficial effects on discharge capacities and cycling retention for some formulations, particularly when the charge voltage cutoff is extended to 4.7V vs.  $\text{Li/Li}^+$ . During FY 2012, a comprehensive survey of Ti-substituted NMCs was carried

out to determine solid solution composition ranges, understand the mechanism of substitution, and find out what compositions gave the best results. X-ray powder diffraction experiments on two series of materials,  $\text{Li}[\text{Ni}_{1/3}\text{Mn}_{1/3}\text{Co}_{1/3-x}\text{Ti}_x]\text{O}_2$  (NMC-333) and  $\text{Li}[\text{Ni}_{0.4}\text{Mn}_{0.4}\text{Co}_{0.2-x}\text{Ti}_x]\text{O}_2$  (NMC-442), made either by combustion synthesis or by co-precipitation indicated that the maximum Ti content is less than about  $x=0.04$ . Only materials with Ti contents lower than  $x=0.04$  showed improved discharge and cycling characteristics. For some materials with low Ti contents, initial discharge capacities as high as 225 mAh/g were observed after charge to 4.7V in lithium half-cells (Figure V - 20).

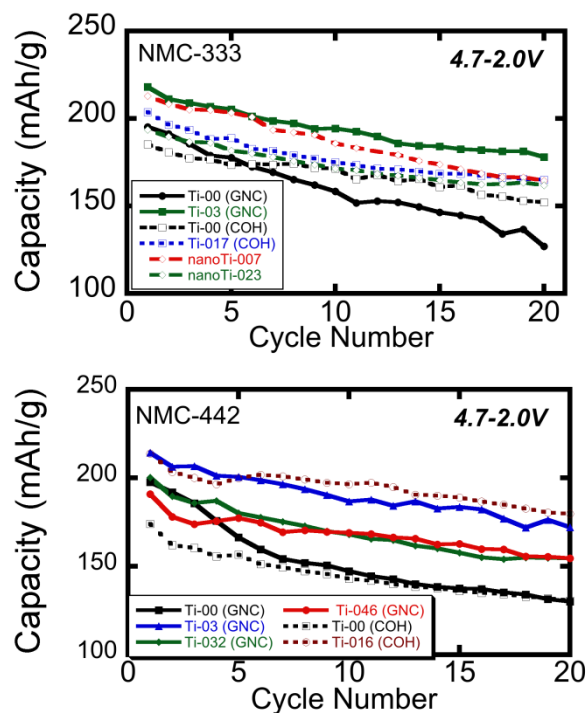


**Figure V - 20:** Discharge capacity as a function of cycle number for baseline and Ti-substituted NMC-333 (top) and NMC-442 (bottom) compounds in lithium half-cells, cycled between 4.7 and 2.0V. Legend indicates the amount of Ti-substitution ( $x$  in  $\text{Li}[\text{Ni}_{1/3}\text{Mn}_{1/3}\text{Co}_{1/3-x}\text{Ti}_x]\text{O}_2$  or  $\text{Li}[\text{Ni}_{0.4}\text{Mn}_{0.4}\text{Co}_{0.2-x}\text{Ti}_x]\text{O}_2$ ) and the synthesis method (GNC=glycine-nitrate combustion, nanoTi=combustion synthesis using a nano  $\text{TiO}_2$  precursor, and COH=co-precipitation).

Interestingly, capacity fading appears to be lower for the Ti-substituted materials compared to the baseline (unsubstituted) materials, in spite of the higher initial discharge capacities. Materials made by co-precipitation appear to cycle better under these conditions than those made by combustion, possibly due to lower surface areas, which may minimize losses due to irreversible oxidation of electrolyte by the NMCs at high states-of-charge. While some fading is still evident over twenty cycles even for the best Ti-substituted material, further improvements can be reasonably expected by utilizing high voltage electrolytes such as those made by Daikin and employing protective coatings.

Figure V - 21 shows changes in the lattice parameters as a function of state-of-charge, obtained by *ex situ* synchrotron x-ray diffraction experiments on electrodes harvested from partially or fully charged lithium half cells.

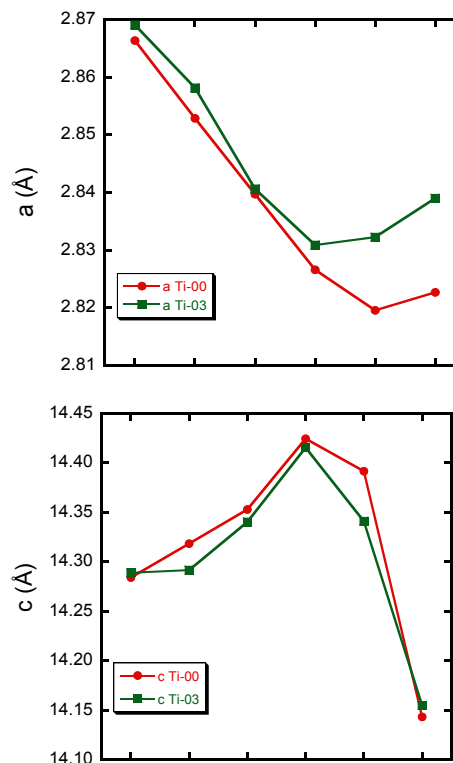


**Figure V - 21:** Lattice parameters (top and middle) and unit cell volume changes as a function of state-of-charge for the baseline NMC-333 (unsubstituted, labeled Ti-00) and an NMC-333 containing 3% Ti (labeled, Ti-03).

There is a smaller change in the  $a$  lattice parameter for the Ti-substituted material than for the baseline NMC-333, resulting in a lower overall volume change during delithiation. While the effect is small, this may be an additional factor in the improved cycling stability seen for the Ti-substituted materials compared to the baseline NMCs.

Unlike layered-layered composites consisting of an NMC component and  $\text{Li}_2\text{MnO}_3$ , no formation reaction occurs during the first charge. This has a number of important implications. The first cycle irreversible capacity exhibited in cells containing the Ti-substituted NMCs is much lower than that found for the composites because no irreversible removal of oxygen and lithium needs to occur. The first cycle inefficiencies tend to be lower than that of conventional NMCs as well. The improved efficiency may explain the higher discharge capacities seen in the Ti-substituted NMCs, although this needs to be explored further. Second, the Ti-substituted NMCs are expected to exhibit much better structural and voltage profile stability than the layered-layered composites upon cycling, because the additional capacity does not arise from activation of the  $\text{Mn}^{3+}/\text{Mn}^{4+}$  redox couple. It has long been known that

layered R3\_m structures containing Mn<sup>3+</sup> transform into spinel structures during electrochemical cycling. Finally, unlike the layered-layered composites, the rate capabilities of the Ti-substituted NMCs are not sacrificed (our studies indicate that they are the same as those found for the baseline NMC materials). Based on these observations, it is reasonable to expect that the reversible capacity of NMCs could be increased from the current 160 mAh/g to about 220 mAh/g by low level Ti-substitution.

### Conclusions and Future Directions

The main challenge in the preparation of the composites LiFePO<sub>4</sub>@LiNi<sub>0.5</sub>Mn<sub>1.5</sub>O<sub>4</sub> particles at present appears to be the reactivity of the LiFePO<sub>4</sub> precursors with the spinel phase, which is prepared by spray pyrolysis. It is difficult to fill the hollow shells completely and prevent deleterious reactions from occurring during calcination. For that reason, the use of other olivines such as LiMnPO<sub>4</sub> to use as the protective layer and core phase will be explored, and low temperature options for preparing the composites with LiFePO<sub>4</sub> will be considered as well. The next steps for the Ti-substituted NMCs include full-cell cycling (with V. Battaglia, LBNL), thermal characterization (with G. Chen, LBNL) and further experimentation to determine the origin of the enhanced performance. The latter include synchrotron surface techniques such as XPS to determine whether changes in composition of the particle surfaces lead to the higher discharge capacities (with P. Ross, Z. Liu and J. Cabana, LBNL).

### FY 2012 Publications/Presentations

1. Thomas E. Conry, Apurva Mehta, Jordi Cabana, and Marca M. Doeff, "XAFS Investigations of LiNi<sub>0.45</sub>Mn<sub>0.45</sub>Co<sub>0.1-y</sub>Al<sub>y</sub>O<sub>2</sub> Positive Electrode Materials," *J. Electrochem. Soc.* **159**, A1562 (2012).
2. Kinson C. Kam, Apurva Mehta, John T. Heron, and Marca M. Doeff, "Electrochemical and Physical Properties of Ti-substituted Layered Nickel Manganese Cobalt Oxide (NMC) Cathode Materials," *J. Electrochem. Soc.* **159**, A1383 (2012).
3. Thomas E. Conry, Apurva Mehta, Jordi Cabana, and Marca M. Doeff, "Structural Underpinnings of the Enhanced Cycling Stability upon Al-Substitution in LiNi<sub>0.45</sub>Mn<sub>0.45</sub>Co<sub>0.1-y</sub>Al<sub>y</sub>O<sub>2</sub> Positive Electrode Materials for Li-Ion Batteries," *Chem. Mater.*, **24**, 3307 (2012).
4. Kinson C. Kam, Apurva Mehta, John C. Heron and Marca M. Doeff, "Improved Layered Oxide Cathodes for Lithium-ion Batteries," *Beyond Lithium Ion V-Symposium on Scalable Energy Storage*, Berkeley, CA June 5-7, 2012.
5. Alpesh Shukla, Thomas Conry, Marca Doeff, and Thomas Richardson, "Transmission Electron Microscopy Studies on Lithium Battery Materials III:

Effect of Aluminum Substitution in Layered Oxides" *TMS 2012, Linking Science and Technology for Global Solutions*, Orlando, FL, March 11-15, 2012.

6. Marca M. Doeff, Kinson C. Kam, Thomas Conry, Jun Liu, and Thomas J. Richardson, "Spray Pyrolysis Synthesis of Hierarchically Structured Olivine Particles for Battery Applications," *7th International Symposium on Inorganic Phosphate Materials*, Argonne National Laboratory, November 8-11, 2011.
7. Kinson C. Kam, Anthony Chern, and Marca M. Doeff, "Ultrasonic Spray Pyrolysis of Hierarchically Structured Cathode Materials," *Abstract # 604, 220<sup>th</sup> Meeting of the Electrochemical Society*, Boston MA, October 2011.
8. Thomas E. Conry, Apurva Mehta, and Marca M. Doeff, "Characterization of the Effects of Al-Substitution in Layered Oxide Cathode Materials for Lithium-Ion Batteries," *Abstract # 1271, 220<sup>th</sup> Meeting of the Electrochemical Society*, Boston MA, October 2011.
9. Marca M. Doeff (Invited), "Spray Pyrolysis: Environmentally Friendly Synthesis of High Performance Electrode Materials," *Pacific Power Symposium 2012*, Waikoloa, HI, January 2012.

---

## V.B.4 Cell Analysis-Interfacial Processes: SEI Formation and Stability on Cycling (HQ)

Karim Zaghbi  
Hydro-Quebec IREQ  
1800 Lionel Boulet  
Varenes, QC, Canada J3X 1S1  
Phone: (450) 652 8019; Fax: (450) 652 8424  
E-mail: [Zaghbi.Karim@ireq.ca](mailto:Zaghbi.Karim@ireq.ca)

Start Date: January 1, 2006  
Projected End Date: December 31, 2012

- Developed *ex situ* and *in situ* SEM tools for understanding the SEI layer and the failure mode in Si-based anodes.
- Fabricated 20 m of laminated film coated with two different sources of LMNO (NEI and Toda) and delivered to LBNL.
- Prepared LMNO that was surface-coated with  $\text{LiMnPO}_4$  using  $\text{LiMnPO}_4$  and LMNO powders from PNNL and delivered to PNNL.

### Objectives

- Synthesize and evaluate high-voltage cathode (spinel Mn-Ni) with improved electrochemical stability.
- Reduce the oxidation of the cathode composition, electrolyte, and separator. Find the appropriate alternative anode material composition that meets the requirement for low cost and high energy.
- Continue the development of binders for the cathode and alternative anode to understand and improve the properties of the solid-electrolyte interphase (SEI) layer.

### Technical Barriers

- Low energy and poor cycle/calendar life.

### Technical Targets

- Identify a suitable technique to stabilize the interface reaction of the high-voltage oxide (Mn-Ni based, e.g.,  $\text{LiMn}_{1.5}\text{Ni}_{0.5}\text{O}_4$ ) cathode by surface coating with a more stable material such as an olivine. The emphasis is to improve electrochemical performance at high voltage.
- Investigate the effect of the type of binder, electrolyte composition, and separator on performance at high voltage.
- Develop high-capacity anodes based on Si compositions.

### Accomplishments

- Succeeded in stabilizing the high-voltage spinel  $\text{LiMn}_{1.5}\text{Ni}_{0.5}\text{O}_4$  by a doping process.
- Optimized a silicon-based composition as high-capacity anode material.

◇ ◇ ◇ ◇ ◇

### Introduction

BATT is looking for the next-generation systems for high energy batteries. Thus, the Hydro-Quebec project was directly affected with these changes, which were made to better integrate with the other DOE programs. The BATT program recommended working with; (i) spinel high-voltage cathode based on Mn-Ni, (ii) Si-based alloy anode and (iii) studies on SEI layers on alloy anode and cathode.

Following the strategy to develop high-energy batteries, high-voltage cathodes based on Mn-Ni spinel will be studied. In the first part of the project, HQ plans to protect the surface of the cathode by a thin layer of olivine  $\text{LiFePO}_4$ . By this process, we expect to reduce the oxidation of the electrolyte and enhance the safety of the high-voltage cathode. Dry or wet processes will be explored to modify the surface of the cathode.

The HQ strategy for the anode material is based on mixing particles of carbon-coated SiOx with graphite powder to reduce the volume expansion and increase the first-cycle coulombic efficiency. To increase the capacity of the anode, we evaluated nano-Si particles mixed with graphite as one configuration, and ternary compounds containing nano-Si-SiOx-graphite as a second configuration. Varying the Si-nano:graphite:SiOx compositions were investigated to determine the minimum content of graphite required in the anode. Due to the major effect of the binder on the performance of the anode, various types of binders were investigated.

To further improve our comprehension on the SEI layer with the Si-based anodes and Mn-Ni cathodes, two analysis methods were adopted: *Ex situ* SEM on cycled electrodes with liquid electrolytes and *in situ* SEM during anode cycling where a dry polymer was used as the binder in the anode to avoid electrolyte evaporation.

## Approach

Our approach is to develop an effective method to stabilize the interface reaction of the high-voltage oxide (Mn-Ni composition like  $\text{LiMn}_{1.5}\text{Ni}_{0.5}\text{O}_4$ ) by surface coating with a more stable material like olivine or by doping with  $\text{M}^{3+}$  metals. The emphasis is to improve electrochemical performance at high voltage. For the high-capacity anode, Si-based anode compositions will be optimized in terms of particle size (micro vs. nano), graphite and SiOx content. This study on the anode will be supported by SEM post-mortem analysis to better understand the failure mode and improve performance.

## Results

**Anode.** In order to develop anode alloys operating at 1200 mAh/g and higher, Si-based materials were considered, and optimizing the anode composition is necessary. The challenges are to reduce the volume expansion and to increase the first-cycle coulombic efficiency. From our recent work with alloy materials, C-SiOx and its mixture with graphite, we obtained a maximum capacity of ~900 mAh/g with the composition (1:1) graphite:C-SiOx. Our studies of the effect of the binder on the Si composite electrode included the polymer binders, PVDF, SBR, Polyimide, and EPDM.

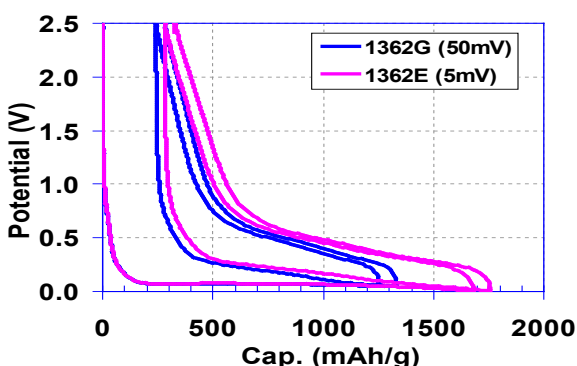


Figure V - 22: Li/C-SiOx that is fully discharged at 5mV and 50mV cut-off voltages in EC-DEC-1M LiPF<sub>6</sub>.

Currently, investigations have been extended using a new binder “Alginate origin”. With this binder, a water solvent is used to achieve lower cost. The anode was evaluated in Li-cells with EC-DEC-1M LiPF<sub>6</sub> and the discharge voltage was between 5 mV and 50 mV. The results of the first cycles are shown in Figure V - 22.

Reversible capacities of 1427 and 1048 mAh/g were obtained, respectively, for 5 mV and 50 mV cut-off voltages. In the first-cycle, the coulombic efficiency (CE1) was higher with cell discharged at 50 mV (83.2%) compared to 80.6% for discharge at 50mV. The CE in the second cycle was comparable at 96.5%. By using this new binder, the CE1 was improved, which was higher than

80% that was obtained with polyimide heated at a minimum temperature of 150°C.

The effort on C-SiOx was completed by addressing the effect of SiOx-graphite ratio in the electrode by using alginate-based binder. The effects of graphite content in the electrode compositions SiOx:graphite (50:50, 40:60, 30:70 and 20:80) were studied. The cycling evaluation was performed in Li-cells with EC-DEC-1M LiPF<sub>6</sub> at C/6. A constant voltage (CV) was applied on the discharge step, based on the previous result, where dendrites were formed with cells with CV at 5 mV, then the cut-off voltages was fixed at 50 mV. The reversible capacities (mAh/g) were 700, 482, 452 and 420, respectively. However, with a 50 mV cut-off voltage some capacity was sacrificed, which increased with the graphite content in the electrode because the capacity associated with the last graphite intercalation stage is still not used. The cycling life in Figure V - 23 shows quite good stability for some compositions. When the SiO:graphite ratio is higher, the capacity is higher but the cycling life is shorter.

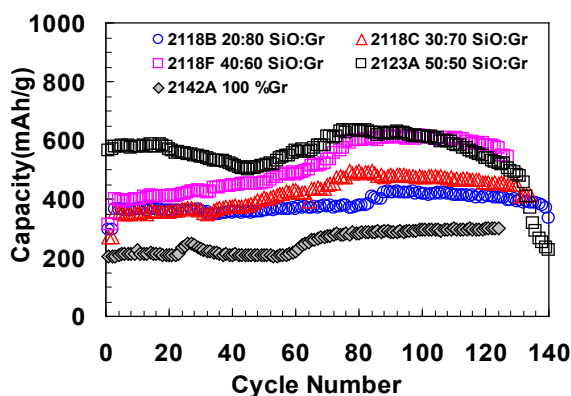


Figure V - 23: Li/EC-DEC-1M LiPF<sub>6</sub>/C-SiOx:Gr cells cycled at C/6 at 50 mV cut-off voltages with floating.

This data indicates that a capacity higher than that of graphite can be obtained by avoiding lithium dendrite formation. However, more effort on the anode composition should be devoted to optimize the electrode porosity and performance.

**Post mortem.** Some work on post-mortem analysis has also been conducted by using SEM. SiOx-Graphite in composite electrodes was analyzed after discharge to 5 mV in EC-DEC-1MLiPF<sub>6</sub>. From the *in situ* study, it was found that the bigger particles (ca. 13 μm) start to crack at around 0.1V, but the smaller particles (< 2μm) maintain their shape intact. It was observed in electrode plan view that many fractures were present in the larger particles (8-12 μm); however some internal cracks are also visible in the smaller particles (2-4 μm) (Figure V - 24.)

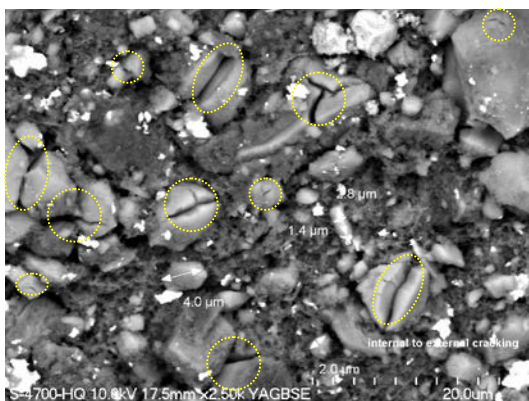


Figure V - 24: SEM photo for SiOx:Gr anode after discharged to 5 mV.

It was also observed that the cracks start from the bulk of the particle, then exploded to the surface, as indicated in Figure V - 24. These observations provide a better understanding of the cycling mechanism and the failure mode associated with its capacity fade.

**Cathode.** The influence of a vinyl carbonate (VC) additive in cells was investigated with various anode compositions and high-voltage-spinel cathode material ( $\text{LiMn}_{1.5}\text{Ni}_{0.5}\text{O}_4$ ). Lithium metal and graphite was compared in Li-ion cells with and without VC additive in EC-DEC-1M LiPF<sub>6</sub>. The first formation cycles at C/24 in Figure V - 25 clearly shows the effect of VC on the charging plateau. A side reaction from VC can occur during oxidation at 4.8-4.9 V. The reversible capacity with VC-containing cells was 83 mA/hg compared to 140 mA/g when VC was absent. The first/second coulombic efficiencies are 32%/46% and 75%/91%, respectively, with cells with and without VC. Furthermore, by removing lithium metal, the instability in the high-voltage plateau was eliminated, which could be associated with some oxidized species that affect the lithium surface. Further analysis will be performed to understand the effect of VC degradation on the LMNO cathode material.

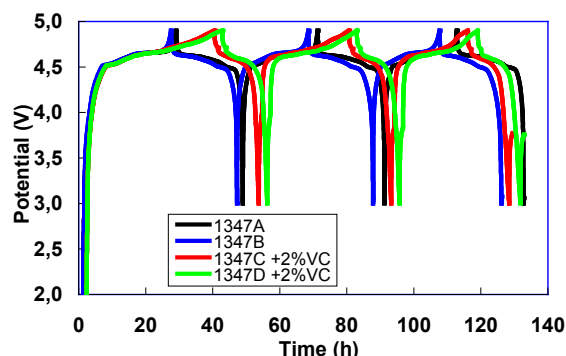


Figure V - 25: First few cycles of  $\text{LiMn}_{1.5}\text{Ni}_{0.5}\text{O}_4$ /Graphite in EC-DEC-LiPF<sub>6</sub> with VC and without VC.

Another technique adopted to stabilize  $\text{LiMn}_{1.5}\text{Ni}_{0.5}\text{O}_4$  was to utilize dopants. It was found that a post annealing step at lower temperature was beneficial to modify the

oxygen deficiency, while still maintaining the disordered structure. Cr<sup>3+</sup> was selected due to its electrochemical activity at ~ 4.8 V. A small amount of Cr<sup>3+</sup> was used to substitute Ni<sup>2+</sup> and Mn<sup>4+</sup> to keep the oxidation state unchanged ( $2\text{Cr}^{3+} = \text{Ni}^{2+} + \text{Mn}^{4+}$ ) and to improve cycling. It was observed that with Cr substitution, the impurity phase ( $\text{Li}_x\text{Ni}_{1-x}\text{O}$ ) was eliminated after re-annealing, and cycling was improved. Co and Fe doping did not show any improvement in either rate performance or cyclability. However, Cr-doped LMNO showed very good stability.

$\text{LiMn}_{1.45}\text{Cr}_{0.1}\text{Ni}_{0.45}\text{O}_4$ , obtained by co-precipitation at HQ, shows outstanding cyclability at 1C rate. The initial discharge capacity was about 120 mA/hg; after 385 cycles at 1C rate, with only 7% of capacity fade (Figure V - 26). The high-rate capability measurements of the LMCrNO show good performance with higher capacity and more stability at each rate compared to undoped LMNO. The cathode can deliver 88% and 68% of the capacity at 2C and 5C rates, respectively. After 230 cycles, less than 5% of the capacity loss was observed at 0.2C rate following the high-rate measurements (Figure V - 27, next page).

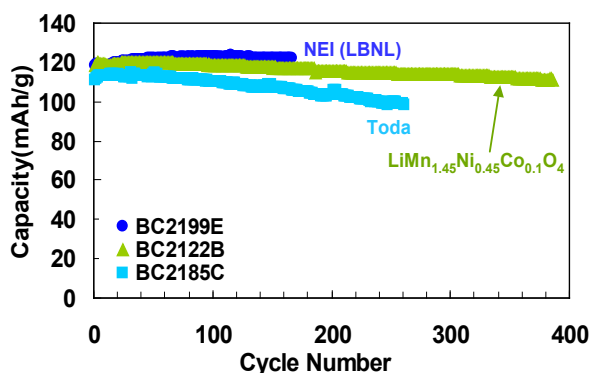


Figure V - 26: Cycling of HQ- $\text{LiMn}_{1.45}\text{Cr}_{0.1}\text{Ni}_{0.45}\text{O}_4$  compared to commercial materials vs. Li in EC-DEC-LiPF<sub>6</sub>.]

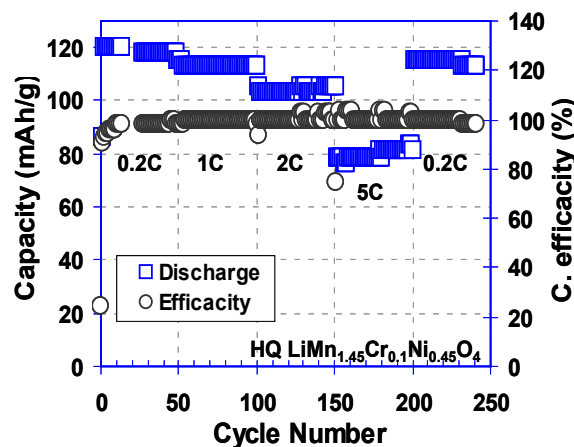


Figure V - 27: Cycling and rate capability of  $\text{LiMn}_{1.45}\text{Cr}_{0.1}\text{Ni}_{0.45}\text{O}_4$ /Li in EC-DEC-LiPF<sub>6</sub>.

## Conclusions and Future Directions

The LMNO spinel material was successfully stabilized by HQ utilizing a doping method. Cr<sup>3+</sup> was selected due to its electrochemical activity at ~ 4.8V. A small amount of Cr was used to substitute Ni<sup>2+</sup> and Mn<sup>4+</sup> to keep the oxidation state unchanged ( $2\text{Cr}^{3+} = \text{Ni}^{2+} + \text{Mn}^{4+}$ ) to improve cycling. We found that with Cr substitution, the impurity phase (Li<sub>x</sub>Ni<sub>1-x</sub>O) was eliminated after re-annealing. The cycle life and high-rate performance were improved compared to the undoped material; only 7% of capacity fade after 385 cycles at 1C.

The high-capacity fade of the Si-based anode material is a major challenge, and volume expansion has limited its progress. By using *in situ* and *ex situ* techniques, a better understanding of the cycling mechanism of the anode and the failure mode associated with its capacity fade was developed. Our studies revealed that the larger anode particles (ca. 13 μm) start to crack at around 0.1 V. In electrode plan view, it was found that some internal cracks are also visible in the smaller particles (2-4 μm), and that the cracks start from the bulk of the particle then exploded to the external surface.

The architecture of the Si-base should be revised by modifying the particle size and electrode composition with emphasis on the porosity and conductivity. For the spinel LMNCrO, a more scalable production method like a solid-state process should be explored and compared to a sample obtained by a co-precipitation method. In this manner, larger batches can be produced for other PIs in the BATT program to evaluate.

## FY 2012 Publications/Presentations

1. K. Zaghib, 2012 DOE Annual Peer Review Meeting Presentation, Washington, 2012.
2. A. Guerfi, P. Hovington, P. Charest, M. Lagacé, J. Trottier, M. Dontigny, A. Vijn and K. Zaghib, “Nanostructured Carbon Coated Si and SiO<sub>x</sub> Anodes for High Energy Lithium-ion Batteries,” *Abstract 1238, 220th ECS Meeting*, Boston, MA, October 9-14, 2011.
3. D. Liu, J. Trottier, P. Charest, J. Fréchet, A. Guerfi, A. Mauger, C.M. Julien and K. Zaghib, “Effect of nano LiFePO<sub>4</sub> coating on LiMn<sub>1.5</sub>Ni<sub>0.5</sub>O<sub>4</sub> 5 V cathode for lithium ion batteries,” *Journal of Power Sources*, **204-15**, 127-132 (2012).

---

## V.B.5 The Role of Surface Chemistry on the Cycling and Rate Capability of Lithium Positive Electrode Materials (MIT)

Yang Shao-Horn  
Massachusetts Institute of Technology  
Department of Mechanical Engineering, 3-344  
77 Massachusetts Ave  
Cambridge, MA 02139  
Phone: (617) 253-2259; Fax: (617) 258-7018  
E-mail: [shaohorn@mit.edu](mailto:shaohorn@mit.edu)

Subcontractor:  
A.N. Mansour, NSWCCD, West Bethesda, MD

Start Date: April 1, 2006  
Projected End Date: December 31, 2012

### Objectives

- Develop a fundamental understanding of processes associated with the interfacial instability between active materials and electrolyte.
- Design low cost positive electrodes with stable electrode-electrolyte interface with improved cycling performance and rate capability over wider operating temperatures.
- Develop a fundamental understanding of the role of catalyst on performance parameters of Li-O<sub>2</sub> cells.

### Technical Barriers

This project addresses the following technical barriers in relation to positive electrode materials for lithium-ion batteries:

- (A) High Cost
- (B) Poor cycle life
- (C) Poor calendar life
- (D) Abuse tolerance

### Technical Targets

- PHEV: Specific energy 56-96 Wh/kg; Specific power 316-750 W/kg; 15-year life (40 °C); 3,000-5,000 cycles.
- EV: Specific energy 200 Wh/kg; 1,000 cycles.

### Accomplishments

- Cycled LiNi<sub>0.5</sub>Mn<sub>1.5</sub>O<sub>4</sub> electrodes were characterized using conventional and synchrotron XPS with increasing depth as a function of cycling. Decomposition products consisting of Li<sub>x</sub>PF<sub>y</sub>O<sub>z</sub>,

OP(OR)<sub>3</sub>, and Li<sub>2</sub>CO<sub>3</sub> were found to increase with cycle number, suggesting that side reactions between the LiNi<sub>0.5</sub>Mn<sub>1.5</sub>O<sub>4</sub> electrode the electrolyte may lead to the formation of resistive films and contribute to capacity loss upon cycling.

- Created a solid-state lithium cell and applied *in situ* APXPS technique to achieve direction visualization of reversible oxygen reduction and evolution on an oxide surface and provide insights into the ORR and OER mechanisms.
- Prepared porous carbon electrodes packed with chemically synthesized Li<sub>2</sub>O<sub>2</sub> and variously catalyzed by Au, Pt, or Ru. These packed electrodes were then charged potentiostatically to oxidize the Li<sub>2</sub>O<sub>2</sub>. Pt and Ru were found to significantly reduce the potential required to oxidize the Li<sub>2</sub>O<sub>2</sub>.

◇ ◇ ◇ ◇ ◇

### Introduction

Achieving fundamental understanding of the role of coatings and synthesis conditions on the surface chemistry and structural integrity of positive electrode materials is necessary to design stable surfaces and structures for Li-ion batteries. The design of chemically and structurally-stable surfaces of Li storage materials is key to the development of low cost, high-energy, high-power, long-life, and thermally-stable Li rechargeable batteries.

### Approach

- Probe the surface chemistry of positive electrode materials before and after cycling using surface-sensitive electron microscopy, angle resolved X-ray photoelectron spectroscopy and electron-yield X-ray adsorption spectroscopy.
- Probe surface chemistry and reactions *in situ* using ambient pressure X-ray photoelectron spectroscopy
- Study the bulk structure of positive electrode materials before and after cycling using synchrotron X-ray diffraction and transmission X-ray absorption spectroscopy.
- Correlate surface chemistry and bulk structure information with electrochemical performance characteristics such as capacity retention and rate capability to determine the origin of surface instability.

## Results

**XPS Study of Cycled  $\text{LiNi}_{0.5}\text{Mn}_{1.5}\text{O}_4$  Electrodes.** In this study, synchrotron and conventional XPS was used to examine the surface chemistry of composite electrodes containing  $\text{LiNi}_{0.5}\text{Mn}_{1.5}\text{O}_4$  (LNMO) material, as a means of elucidating the mechanism responsible for electrochemical behavior upon cycling. Synchrotron XPS spectra were collected on beamline X24A of the National Synchrotron Light Source utilizing monochromatic X-rays with energies of 2493.6 and 3498.4 eV. In addition, XPS spectra was measured using a Physical Electronics model 5400 X-ray photoelectron spectrometer at room temperature using a non-monochromatic  $\text{Mg K}_\alpha$  (1253.6 eV) X-ray source operating at 400 W (15 kV and 27 mA).

By analyzing spectra obtained at different excitation energies, insights into chemical composition at different penetration depths into the electrodes are obtained. Penetration depths are approximately 11.7 and 15.9 nm for synchrotron XPS excitation energies of 2493.6 and 3498.4 eV respectively, and 4.1 nm for the  $\text{Mg K}_\alpha$  X-ray source. As shown in Figure V - 28, the O 1s region of the pristine LNMO is increasingly dominated by lattice oxygen in LNMO relative to  $\text{Li}_2\text{CO}_3$  as X-ray excitation energy is increased. After 5 and 10 cycles, this component disappeared at 1253.6 eV, which is the most surface-sensitive of the three excitation energies, while remaining at the two higher energies. This shows that the pristine electrode material becomes covered by decomposition products with increasing cycle number. After 5 and 10 cycles,  $\text{Li}_x\text{PF}_y\text{O}_z$  and  $\text{OP}(\text{OR})_3$  species, which are related to electrolyte decomposition, cover the surface of the electrode. The concentration of  $\text{Li}_2\text{CO}_3$  also increases relative to the pristine material, showing that side reactions between the LNMO electrode material and  $\text{LiPF}_6$  in the electrolyte may lead to the formation of resistive films on the surface of the electrode that may significantly contribute to capacity loss upon cycling.

***In Situ* Electrochemical XPS Spectroscopy of  $\text{Li-O}_2$  Cells during Discharge and Charge.** To probe the  $\text{Li-O}_2$  discharge and charge reaction mechanisms without interferences from the liquid electrolytes and possible contaminants associated with *ex situ* characterizations (e.g.,  $\text{CO}_2$  and  $\text{H}_2\text{O}$ ), *in situ* electrochemical, ambient-pressure XPS (APXPS) was applied to gain insights into the reaction products of oxygen reduction and evolution in presence of lithium ions at room temperature (Lu, Crumlin and Shao-Horn *et al.*, *Sci. Rep.* 2012).

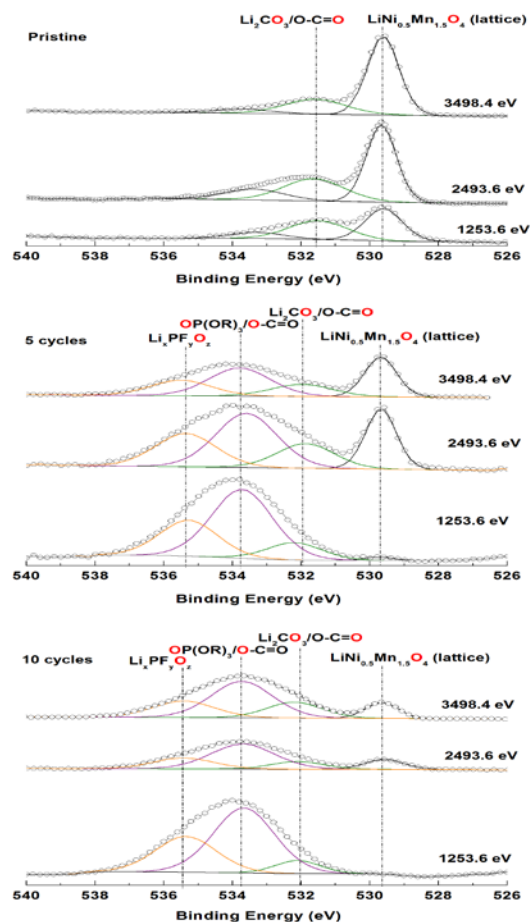


**Figure V - 28:** XPS of the O 1s region of (a) pristine LNMO, (b) LNMO after 5 cycles, and (c) LNMO after 10 cycles. Increasing incident energy corresponds to increasing penetration depth

This work was conducted in the environmental XPS chambers at Advanced Light Source at LBNL via ongoing collaborations with Dr. Zhi Liu. As aprotic electrolytes used in conventional  $\text{Li-O}_2$  electrolytes are volatile, they are not suitable for use in XPS, where the entire cell must be stable under ultra-high vacuum. Collaborations with Gabriel Veith and Nancy Dudney at ORNL created all solid-state  $\text{Li-O}_2$  cells. The cell consisted of lithiated lithium titanate  $\text{Li}_7\text{Ti}_5\text{O}_{12}$  (LTO) as the negative electrode, lithium phosphorus oxynitride ( $\text{LiPON}$ ) electrolyte, and  $\text{Li}_x\text{V}_2\text{O}_5$  electrode providing both ionic ( $\text{Li}^+$ ) and electronic conductivity facilitating lithium intercalation and  $\text{LiO}_x$  formation when exposed to an oxygen environment. It can be shown that such cells can reveal reversible lithium intercalation into  $\text{Li}_x\text{V}_2\text{O}_5$  in UHV (Figure V - 29a,b) and reversible oxygen reduction forming  $\text{Li}_2\text{O}_2$  and subsequent oxidation evolving  $\text{O}_2$  at 500 mtorr of oxygen pressure *in situ* as a function of cell potential, as shown in Figure V - 29. Interestingly, the oxidation of  $\text{Li}_2\text{O}_2$  began at much lower overpotentials ( $\sim 240$  mV) than the charge overpotentials of conventional  $\text{Li-O}_2$  cells with aprotic electrolytes ( $\sim 1000$  mV). This suggests that the OER

kinetics of decomposing thin (i.e., sub-nm layer) of  $\text{Li}_2\text{O}_2$  that formed under solid-state configuration is fast and does not require large overpotentials. This study has, for the first time, revealed reversible oxygen reduction and evolution on an oxide surface using a solid-state lithium cell using *in situ* APXPS. Through the direct visualization of the formation and disappearance of Li-O<sub>2</sub> reaction products, this study connects the electrical potential to oxygen redox chemistry in presence of lithium ions at room temperature, and leads to numerous opportunities for exploiting *in situ* APXPS to gain mechanistic insights into air-based electrochemical reactions for efficient energy storage.

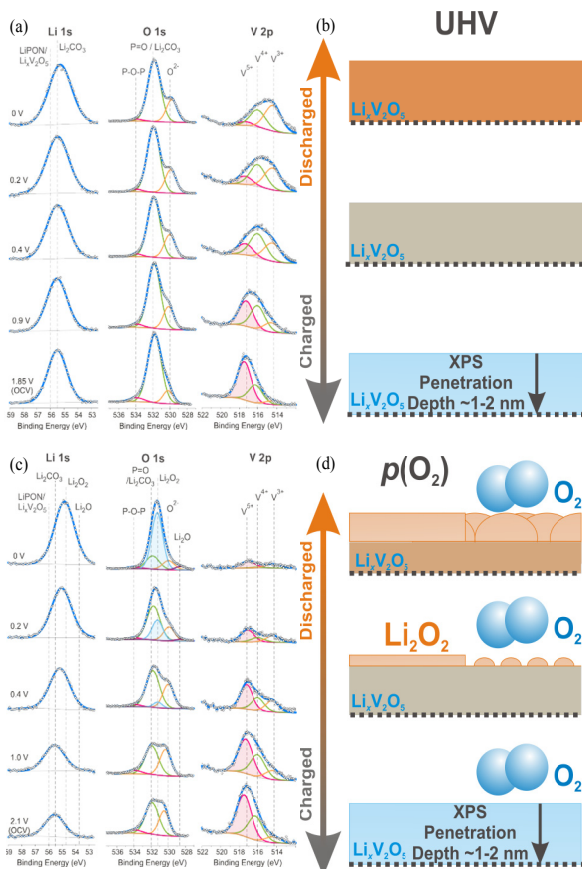


**Figure V - 29:** (a) *In situ* XPS data of Li 1s, O 1s, V 2p collected during discharge in UHV, (b) schematic representation of the solid-state cell cycling in UHV: lithium intercalation/deintercalation into the vanadium oxide, (c) *in situ* APXPS data of Li 1s, O 1s and V 2p collected during discharge in  $p(\text{O}_2) = 500$  mtorr, (d) schematic representation of the solid-state cell cycling in  $p(\text{O}_2) = 500$  mtorr: formation/oxidation of lithium peroxide on the vanadium oxide.

**OER Catalysis of  $\text{Li}_2\text{O}_2$ -Filled Electrodes.** The high over-potential required to charge Li-O<sub>2</sub> cells remains an important impediment to the development of Li-air batteries. Vulcan XC72 carbon-based electrodes (VC), in which commercially available  $\text{Li}_2\text{O}_2$  particles were introduced into the electrode during manufacture, have been developed. In this study, the electrochemical oxidative activity of Li-Li<sub>2</sub>O<sub>2</sub> cells with unmodified VC

and VC decorated with Au, Pt, and Ru nanoparticles is compared (Harding and Shao-Horn *et al*, Phys. Chem. Chem. Phys., 2012). VC was found to become active in catalyzing the oxidation of  $\text{Li}_2\text{O}_2$  at 4.0 V<sub>Li</sub> and higher. The net oxidation current obtained from VC+Li<sub>2</sub>O<sub>2</sub> was found to significantly increase with increasing applied potentials, as shown in Figure V - 30. A maximum current of 20 mA/g<sub>carbon</sub> was reached at 4.0 V<sub>Li</sub> while 1000 mA/g<sub>carbon</sub> was obtained at 4.4 V<sub>Li</sub>. Au/C was found to be no more active in catalyzing the oxidation of  $\text{Li}_2\text{O}_2$  than VC.

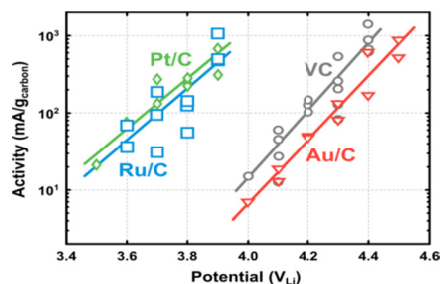


**Figure V - 30:** Oxidative activity of Pt/C+, Ru/C+, Au/C+, and VC+Li<sub>2</sub>O<sub>2</sub> cells. Pt/C+ and Ru/C+Li<sub>2</sub>O<sub>2</sub> are more than two orders of magnitude more active than VC+ and Au/C+Li<sub>2</sub>O<sub>2</sub>.

Pt/C and Ru/C was observed to be active several hundred millivolts below that of VC. At 3.9 V<sub>Li</sub>, the net oxidative current density of Ru/C and Pt/C approached 1000 mA/g<sub>carbon</sub>, in contrast with VC, where no net oxidative current was observed below 4.0 V<sub>Li</sub>. Ru/C remained reasonably active to 3.6 V<sub>Li</sub>, below which the majority of  $\text{Li}_2\text{O}_2$  could not be oxidized, while Pt/C exhibited very slow charging even at 3.5 V<sub>Li</sub>. XRD and SEM analyses indicate reduced  $\text{Li}_2\text{O}_2$  content in partially-charged electrodes, and do not indicate the presence of  $\text{Li}_2\text{O}_2$  after complete charging, which confirms that the measured oxidation currents are associated with oxidation of  $\text{Li}_2\text{O}_2$ . The mechanism of this activity enhancement remains unknown. Solid-state Li-air cells are being developed to be studied *in situ* in collaboration with Zhi Liu at the ALS in LBNL in order to resolve the chemical state of discharge product over the course of this reaction.

## Conclusions and Future Directions

XPS, XRD, APXPS and a number of electrochemical measurements have been used to probe the reactions that occur between electrode and electrolyte in lithium batteries. X-rays of different energies were used to probe the surface composition to different depths of  $\text{LiNi}_{0.5}\text{Mn}_{1.5}\text{O}_4$  before and after cycling. It was found that electrolyte decomposition products build up on the surface of LNMO during cycling, and may contribute to the loss of capacity observed in such cells. It was also observed that the formation of electrolyte decomposition products on the surface of Li-O<sub>2</sub> discharge product after a single cycle in an ether based electrolyte. Utilizing a solid-state lithium cell and *in situ* APXPS capability, direction visualization

of reversible oxygen reduction and evolution on an oxide surface was achieved and insights into the ORR and OER mechanisms were provided. Additionally, the kinetics and catalysis of the oxidation of  $\text{Li}_2\text{O}_2$  and  $\text{Li-O}_2$  discharge product were investigated and insights into the reaction mechanisms of the  $\text{Li-O}_2$  recharge were provided.

Future directions include 1) Understanding the relationship between surface film formation in cycled  $\text{LiNi}_{0.5}\text{Mn}_{1.5}\text{O}_4$  electrodes and surface chemistry/composition, nonstoichiometric defects and crystal structure, and 2) investigating the effect of secondary phases (such as rock salt-based impurities) on cycling performance. 3) Catalysis of  $\text{Li}_2\text{O}_2$  oxidation will be explored with non-precious metal containing metal oxides. 4) The use of polymer electrolytes will be studied for rechargeable  $\text{Li-O}_2$  cells, in particular investigating the behavior and discharge composition of air cathodes incorporating polymer gels as the lithium conducting matrix. 5) Conventional XPS and XRD will continue to be used to characterize the surface and bulk composition of lithium battery cathodes. Additionally, synchrotron XPS, XRD, and XAS will be used to probe the surface chemistry of  $\text{LiNi}_{0.5}\text{Mn}_{1.5}\text{O}_4$  and  $\text{Li-O}_2$  cathodes.

Hard X-rays at the National Synchrotron Light Source of Brookhaven National Laboratory will continue to be applied to increase the depth of the region analyzed by XPS and ARXS.

### FY 2012 Publications/Presentations

- N. Yabuuchi, Y.C. Lu, A.N. Mansour, S. Chen and Y. Shao-Horn, "The Influence of Heat-Treatment Temperature on the Cation Distribution of  $\text{LiNi}_{0.5}\text{Mn}_{0.5}\text{O}_2$  and its Rate Capability in Lithium Rechargeable Batteries," *Journal of The Electrochemical Society*, **158**, (2) A192-A200 (2011).
- Y.C. Lu, H.A. Gasteiger, and Y. Shao-Horn, "Method Development to Evaluate the Oxygen Reduction Activity of High-Surface-Area Catalysts for Li-Air Batteries," *Electrochem. Solid-State Lett.*, **14**(5) A70–A74 (2011).
- Y.C. Lu, D.G. Kwabi, K.P.C. Yao, J.R. Harding, J. Zhou, L. Zuin and Y. Shao-Horn, "The Discharge Rate Capability of Rechargeable  $\text{Li-O}_2$  Batteries," *Energy Environ. Sci.*, **4**(8) 2999-3007 (2011).
- R.R. Mitchell, B. Gallant, C. Thompson and Y. Shao-Horn, "All-Carbon-Nanofiber Electrodes for High-Energy Rechargeable  $\text{Li-O}_2$  Batteries," *Energy Environ. Sci.*, **4**(8) 2952-2958 (2011).
- Y.C. Lu, H.A. Gasteiger, and Y. Shao-Horn, "Catalytic Activity Trends of Oxygen Reduction Reaction for Nonaqueous Li-Air Batteries," *Journal of the American Chemical Society*, **133** (47) 19048-19051 (2011).
- J.R. Harding, Y.C. Lu, Y. Tsukada, and Y. Shao-Horn, "Evidence of catalyzed oxidation of  $\text{Li}_2\text{O}_2$  for rechargeable Li-air battery applications," *Phys. Chem. Chem. Phys.*, **14** 10540-10546 (2012).
- B.M. Gallant, R.R. Mitchell, D.G. Kwabi, J. Zhou, L. Zuin, C.V. Thompson, and Y. Shao-Horn, "Chemical and Morphological Changes of  $\text{Li-O}_2$  Battery Electrodes Upon Cycling," *J. Phys. Chem. C*, **116** (37) 20800-20805 (2012).
- Y.C. Lu, E.J. Crumlin, G.M. Veith, J.R. Harding, E. Muroto, L. Baggetto, N.J. Dudney, Z. Liu, and Y. Shao-Horn, "In Situ Ambient Pressure X-ray Photoelectron Spectroscopy Studies of Lithium-Oxygen Redox Reactions," *Sci. Rep.*, **2**, Article number 715 (2012).
- J.R. Harding, Y.C. Lu, Y. Tsukada, and Y. Shao-Horn, "The Influence of Catalysts on Electro-Oxidation Activity of Lithium Peroxide for Lithium-Air Batteries," *2011 MRS Fall Meeting*, Nov 30, 2011, Boston, MA, USA.
- R.R. Mitchell, B.M. Gallant, Y. Shao-Horn, and C.V. Thompson, "Morphological Evolution of  $\text{Li}_2\text{O}_2$  Discharge Product in Aligned Carbon Nanofiber Electrodes for Li-Air Batteries," *2011 MRS Fall Meeting*, Nov 30, 2011, Boston, MA, USA.
- Y.C. Lu, J.R. Harding, D.K. Kwabi, B.M. Gallant, K.P.C. Yao, and Y. Shao-Horn, "Challenges and Opportunities in Rechargeable Li-Air Batteries," *International Battery Association Pacific Power Source Symposium*, Jan 10, 2012, Kona, HI, USA.
- Y.C. Lu, J.R. Harding, E.J. Crumlin, D.K. Kwabi, K.P.C. Yao, and Y. Shao-Horn, " $\text{O}_2$ -Electrocatalysis for Rechargeable Li-Air Batteries: Challenges and Opportunities," *Gordon Research Conference*, Mar 8, 2012, Ventura, CA, USA.
- B.M. Gallant, R.R. Mitchell, C.V. Thompson, and Y. Shao-Horn, "Cycling Stability and Charging Behavior of Carbon Nanotube Electrodes for  $\text{Li-O}_2$  Batteries," *222nd ECS meeting*, Honolulu, HI, Oct 8, 2012.
- R.R. Mitchell, B.M. Gallant, Y. Shao-Horn, and C.V. Thompson, "Structure of  $\text{Li}_2\text{O}_2$  Discharge Products on Free-Standing Aligned Carbon Nanotube Electrodes for Li-Air Batteries," *222nd ECS meeting*, Honolulu, HI, Oct 8, 2012.

## V.B.6 Diagnostics – Battery Materials: Structure and Characterization

(Yang, Nam, BNL)

PI: Xiao-Qing Yang  
Brookhaven National Laboratory  
Chemistry Department  
Upton, NY 11973-5000  
Phone: (631) 344-3663; Fax: (631) 344-5815  
E-mail: [xyang@bnl.gov](mailto:xyang@bnl.gov)

PI: Kyung-Wan Nam  
Brookhaven National Laboratory  
Chemistry Department  
Upton, NY 11973-5000  
Phone: (631) 344-3202; Fax: (631) 344-5815  
E-mail: [knam@bnl.gov](mailto:knam@bnl.gov)

Start Date: October 1, 2008

End Date: September 30, 2012

### Objectives

- To determine the contributions of electrode materials changes, interfacial phenomena, and electrolyte decomposition to the cell capacity and power decline.
- To develop and apply synchrotron based *in situ* X-ray techniques such as x-ray diffraction (XRD) and x-ray absorption (XAS) to study materials in an environment that is close to the real operating conditions.
- To study the potentially low cost and high energy density cathode materials such as olivine structured  $\text{LiMn}_{0.4}\text{Fe}_{0.6}\text{PO}_4$  and spinel structured  $\text{LiNi}_x\text{Mn}_{2-x}\text{O}_4$
- To study the mechanism of solid-electrolyte interphase (SEI) formation and functionalities on anode and cathode surfaces.
- To develop new diagnostic tools for battery studies.

### Technical Barriers

- Li-ion batteries with long calendar and cycle life
- Li-ion batteries with superior abuse tolerance
- To reduce the production cost of a PHEV batteries

### Technical Targets

- To develop new *in situ* diagnostic techniques with surface and bulk sensitivity for studying the thermal stability of various cathode materials.
- To determine the contributions of electrode materials changes, interfacial phenomena, and electrolyte decomposition to the cell capacity and power decline.

- To develop and apply synchrotron based *in situ* x-ray techniques to study materials in an environment that is close to the real operating conditions.
- To study the potentially low cost materials such as layer structured composite  $\text{Li}_2\text{MnO}_3\text{-LiMO}_2$  and spinel structured  $\text{LiNi}_x\text{Mn}_{2-x}\text{O}_4$ .
- To develop new diagnostic tools for battery studies.

### Accomplishments

- Developed new “quick XAS” technique to do *in situ* studies on cathode materials for Li-ion batteries during both chemical and electrochemical delithiation.
- In collaboration with Institute of Physics, Chinese Academy of Sciences completed the *in situ* XRD studies of  $\text{LiMn}_{0.4}\text{Fe}_{0.6}\text{PO}_4$  cathode material with different particle size and morphology during electrochemical delithiation.
- In collaboration with Institute of Physics, Chinese Academy of Sciences completed the studies of electrochemical decompositions of  $\text{Li}_2\text{CO}_3$  above 4.1 V in both thin film and powder electrodes.
- Completed *in situ* XAS studies of high voltage cathode material  $\text{LiMn}_{2-x}\text{Ni}_x\text{O}_4$  with spinel structure (both ordered P4332 and disordered Fd-3m structures) during electrochemical cycling.

### Introduction

Achieving DOE goals of high energy and power density batteries for HEV, PHEV, and EV requires fundamental understanding of how current materials function – including how to improve rate capability, energy density, capacity retention and long-term cycling performance, safety characteristics, as well as the guidance on discovery of new materials and new mechanisms. This project attacks these issues by developing new diagnostic tools to investigate battery materials both *in situ* and *ex situ*, and then applies these techniques to obtain the fundamental understandings about the relationships between the structure and performance of materials for new material development.

### Approach

1. *In situ* XAS and XRD studies of new electrode materials such as  $\text{LiMn}_{0.4}\text{Fe}_{0.6}\text{PO}_4$  during electrochemical cycling to carry out the diagnostic studies to improve the energy density and cycle life of Li-ion batteries.

2. *In situ* XAS studies of  $\text{Li}_2\text{CO}_3$  during electrochemical decomposition and the potential application of this process.
3. *In situ* XRD and XAS studies of high voltage cathode material  $\text{LiMn}_{2-x}\text{Ni}_x\text{O}_4$  with spinel structure (both ordered  $P4_332$  and disordered  $Fd-3m$  structures) during electrochemical cycling.
4. *In situ* and *ex situ* transmission electron microscopy (TEM) coupled with selected area electron diffraction (SAED) to study the structural changes of electrode materials with high location specification and spatial resolution.

## Results

In FY2012, a quick X-ray absorption spectroscopy (XAS) technique was introduced to investigate fast chemical and electrochemical delithiation of cathode materials for Lithium-ion batteries. In standard XAS, it takes more than 15 minutes to collect one spectrum. Quick XAS replaces the stepwise scanning mode by a continuous mode of the monochromator. The scanning time of one spectrum can be as short as one minute, even less than one second. This quick XAS technique provides a method to study the structural changes of battery materials cycling at ultra-high C-rates (e.g., 100C). XAS technique has been applied to study the structural changes and reaction kinetics of Li-rich layered  $\text{Li}_{1.2}\text{Ni}_{0.15}\text{Co}_{0.1}\text{Mn}_{0.55}\text{O}_2$  material during fast constant voltage charge. Some of the results are shown in Figure V - 31.

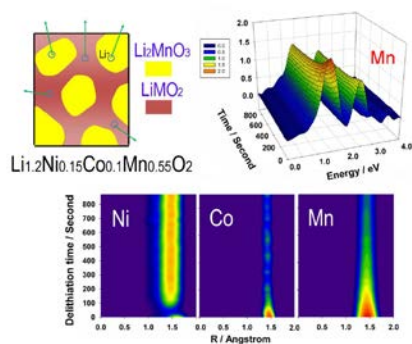


**Figure V - 31:** Quick XAS spectra at Ni, Co, and Mn K-edges of the Li-rich layered  $\text{Li}_{1.2}\text{Ni}_{0.15}\text{Co}_{0.1}\text{Mn}_{0.55}\text{O}_2$  cathode material during constant voltage charge at 5V.

In collaboration with Institute of Physics, Chinese Academy of Sciences, two types of NiO- $\text{Li}_2\text{CO}_3$  nanocomposite electrodes have been prepared for the electrochemical decomposition studies. The thin film electrode with a thickness of 225 nm and grain size around 5-8 nm was prepared by a pulsed laser deposition method. The powder sample was prepared by a solution evaporation and calcination method with primary particle size in the range of 20-50 nm. Using *ex situ* TEM, Raman and FTIR spectroscopy and synchrotron based *in situ* XRD, the electrochemical decomposition of  $\text{Li}_2\text{CO}_3$  phase in both types of the NiO- $\text{Li}_2\text{CO}_3$  nanocomposite electrodes

after charging up to about 4.1 V vs  $\text{Li}^+/\text{Li}$  at room temperature is clearly confirmed, but not in the electrode containing  $\text{Li}_2\text{CO}_3$  only. The NiO phase does not change significantly after charging process and may act as catalyst for the  $\text{Li}_2\text{CO}_3$  decomposition. Therefore, the potential of using NiO- $\text{Li}_2\text{CO}_3$  nanocomposite material as additional lithium source in cathode additive in lithium ion batteries has been demonstrated, which could compensate the initial irreversible capacity loss at the anode side. As shown in the *in situ* XRD patterns in Figure V - 32, during charge, the intensities of characteristic peaks for  $\text{Li}_2\text{CO}_3$  are decreased gradually. This confirms that the  $\text{Li}_2\text{CO}_3$  phase is electrochemically decomposed and the NiO/Ni phase in the nanocomposite acts as catalysts for the decomposition reaction.

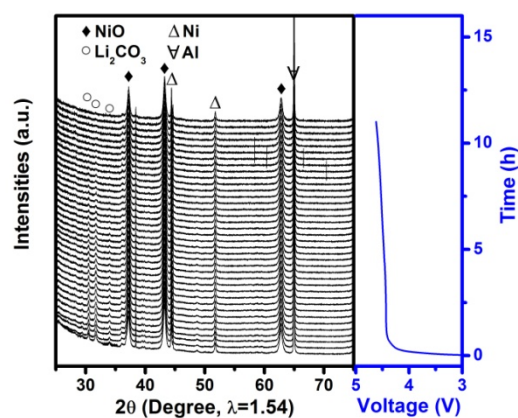


**Figure V - 32:** *In situ* XRD patterns of the NiO- $\text{Li}_2\text{CO}_3$  composite powder electrode during electrochemical decomposition.

The studies of structural changes of  $\text{LiNi}_{0.5}\text{Mn}_{1.5}\text{O}_4$  cathode materials have been completed. There are two types of structures, ordered  $P4_332$  and disordered  $Fd-3m$ , for  $\text{LiNi}_{0.5}\text{Mn}_{1.5}\text{O}_4$ . It is widely accepted that the disordered  $Fd-3m$  structure, which is closely related to the content of  $\text{Mn}^{3+}$  in the material, is the main contributor for good capacity retention and high rate capability. However, too high  $\text{Mn}^{3+}$  will severely reduce the capacity and cause poor capacity retention. Finding the optimum content of  $\text{Mn}^{3+}$  and synthesis conditions (annealing temperature, time and atmosphere, as well as cooling rate) are quite important. The local structure changes of the disordered  $\text{LiNi}_{0.5}\text{Mn}_{1.5}\text{O}_4$  ( $Fd-3m$ ) during charge-discharge were studied using *in situ* X-ray absorption spectroscopy (XAS) to monitor the changes of  $\text{Mn}^{3+}$  to  $\text{Mn}^{4+}$  and  $\text{Ni}^{2+}$  to  $\text{Ni}^{4+}$ . XAS results during first charge are shown in Figure V - 33. As shown in the Mn and Ni K-edges XANES spectra (Figure V - 33(b) and Figure V - 33 (c)), most of high voltage capacity at  $\sim 4.6$  V is originated from the redox reaction between  $\text{Ni}^{2+}$  and  $\text{Ni}^{4+}$  while the manganese does not contribute much on the high voltage capacity during charge. However, at early state of charge, where the low voltage plateau is appeared at  $\sim 4.1$  V, slight

increase in the Mn-O peak amplitude in the EXAFS spectra (Figure V - 33(d)) was observed suggesting that small amount of Mn<sup>3+</sup> ions oxidized to Mn<sup>4+</sup> ions which are not Jahn-Teller active. In the following high voltage capacity region above 4.6 V, the Ni K-edge EXAFS spectra in Figure V - 33(e) show typical peak feature changes for the first Ni-O bond confirming the major capacity contribution of the Ni<sup>2+/4+</sup> redox reaction. *In situ* XAS spectra of the disordered LiNi<sub>0.5</sub>Mn<sub>1.5</sub>O<sub>4</sub> during discharge showed very reversible local structure changes back to the pristine one via the redox reaction of Ni<sup>4+</sup> to Ni<sup>2+</sup> at high voltage followed by the small amount of redox reaction of Mn<sup>4+</sup> to Mn<sup>3+</sup>.

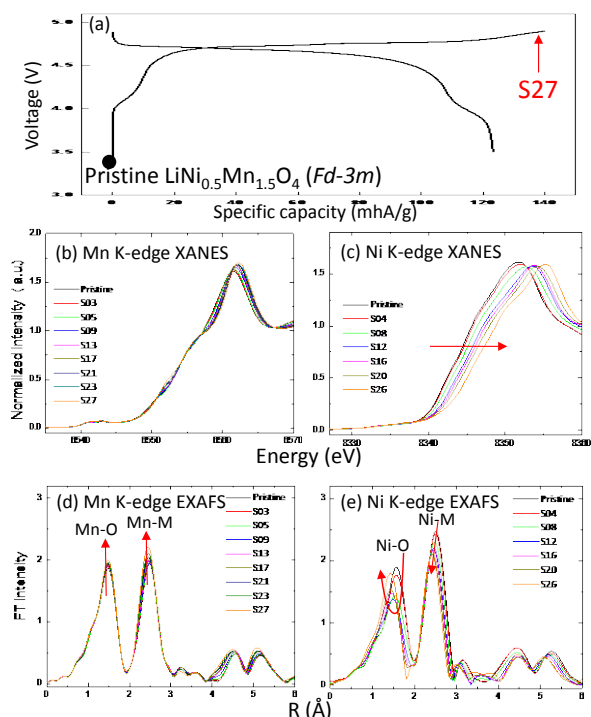


**Figure V - 33:** (a) charge-discharge profile of the disordered LiNi<sub>0.5</sub>Mn<sub>1.5</sub>O<sub>4</sub> cathode material during *in situ* XAS, and corresponding *in situ* XAS spectra at Mn K-edge (b) and (d) and Ni K-edge (c) and (e) during the 1<sup>st</sup> charge.

In comparison, the *in situ* x-ray absorption spectroscopy (XAS) at Ni and Mn K-edges were performed on the ordered *P4<sub>32</sub>* sample to study the local electronic and structure changes during 1<sup>st</sup> charge and discharge as shown in Figure V - 34. The first discharge curve in Figure V - 34(a) showed no detectable 4.0 V plateau, which is well agreed with the previous result for the ordered spinel LiMn<sub>1.5</sub>Ni<sub>0.5</sub>O<sub>4</sub>. As shown in Figure V - 34(b) and Figure V - 34(c), unlike the Ni K-edge XANES spectra, which show clear entire edge shift to lower energy, the Mn spectra do not show rigid edge shift, suggesting that most of high voltage capacity around 4.6 V is associated with the redox reaction from Ni<sup>4+</sup> to Ni<sup>2+</sup> while the manganese did not contribute much to the capacity during 1<sup>st</sup> discharge. One interesting feature observed in the Mn K-edge XANES spectra is the disappearance of two shoulder peaks located at the edge

rising region (marked by asterisk) in Figure V - 34(b) during discharge. The appearance of these shoulder peaks is due to the ligand to metal charge transfer (LMCT) which suggests that oxygen donates some electrons to metal 3d orbitals in a covalent bond manner. Appearance of strong two shoulder peaks at highly charged states (spectrum A) may suggest some contribution to the charge compensation reaction at high voltages from oxygen atoms bonded with Mn atoms. Disappearance of these two peaks during discharge reveals decreased oxygen contribution to the charge compensation reaction as the voltage decreased.

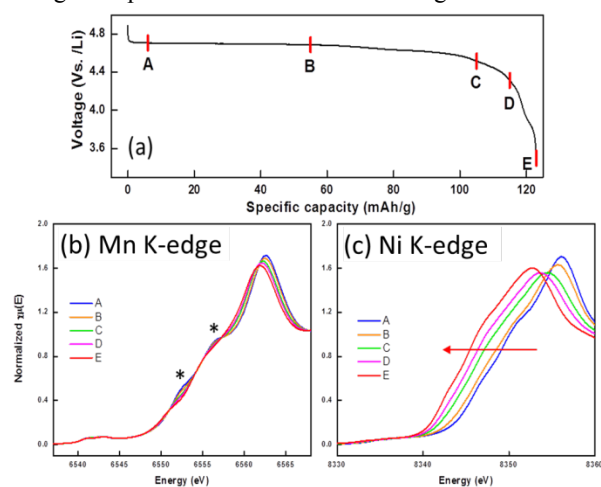


**Figure V - 34:** (a) 1<sup>st</sup> discharge profile of the ordered LiNi<sub>0.5</sub>Mn<sub>1.5</sub>O<sub>4</sub> cathode during *in situ* XAS, and corresponding *in situ* (b) Mn and (c) Ni K-edges XANES spectra.

## Conclusions and Future Directions

In FY2012, progress has been made by this project in diagnostic studies and collaborations with US industries and international research institutions.

The new quick XAS technique introduced for structural evolution studies during high rate delithiation both chemically and electrochemically is quite usable to obtain fundamental understandings of the structural changes at high rate cycling.

The studies on irreversible electrochemical decomposition of Li<sub>2</sub>CO<sub>3</sub> explored the possibility of using this compound as additional Li source to compensate the Li loss caused by SEI formation during formation cycling.

The *in situ* XAS studies of both ordered and disordered high voltage spinel LiMn<sub>1.5</sub>Ni<sub>0.5</sub>O<sub>4</sub> during charge-discharge cyclings provides important information about the charge compensation mechanism contributed by Mn, Ni, and O ions of these two types of materials at different states of charge, giving valuable information for the further development of these materials.

In the future, more *in situ* XRD and XAS will be carried out during heating to study the thermal stability of the high voltage spinel LiMn<sub>1.5</sub>Ni<sub>0.5</sub>O<sub>4</sub> materials, as well as for the Si-based high energy density anode materials. The

quick XAS technique will be applied to more BATT base-line electrode materials.

### FY 2012 Publications/Presentations

1. 2012 DOE Annual Peer Review Meeting Presentation, May 14-18 2012, Washington DC.
2. Xiao-Liang Wang, Wei-Qiang Han, Haiyan Chen, Jianming Bai, Trevor A. Tyson, Xi-Qian Yu, Xiao-Jian Wang, and Xiao-Qing Yang, "Amorphous Hierarchical Porous GeO<sub>x</sub> as High-Capacity Anodes for Li Ion Batteries with Very Long Cycling Life," *Journal of the American Chemical Society*, Vol. **133**. (2011), 20692-20695, DOI: 10.1021/ja208880f.
3. Ruigang Zhang, Xiqian Yu, Kyung-Wan Nam, Chen Ling, Timothy S Arthur, Wei Song, Angela Knapp, Steven N. Ehrlich, Xiao-Qing Yang, and Masaki Matsui, " $\alpha$ -MnO<sub>2</sub> as a Cathode Material for Rechargeable Mg Batteries," *Electrochem. Commun.* **23**, 110-113 (2012).
4. Min-Kyu Song, Shuang Cheng, Haiyan Chen, Wentao Qin, Kyung-Wan Nam, Shucheng Xu, Xiao-Qing Yang, Angelo Bongiorno, Jangsoo Lee, Jianming Bai, Trevor A. Tyson, Jaephil Cho, and Meilin Liu "Anomalous Pseudocapacitive Behavior of a Nanostructured, Mixed-Valent Manganese Oxide Film for Electrical Energy Storage," *Nano Lett.*, **12**(7), 3483-3490 (2012).
5. Rui Wang, Xiqian Yu, Jianming Bai, Hong Li, Xuejie Huang, Liqian Chen, Xiaoqing Yang, "Electrochemical decomposition of Li<sub>2</sub>CO<sub>3</sub> in NiO–Li<sub>2</sub>CO<sub>3</sub> nanocomposite thin film and powder electrodes", *Journal of Power Sources*, **218**, 113-118 (2012)
6. Xiangbo Meng, Xiao-Qing Yang, and Xueliang Sun, "Emerging Applications of Atomic Layer Deposition for Lithium-Ion Battery Studies," *Advanced Materials*, Volume **24**, Issue 27, July 17, 2012, Pages: 3589–3615, DOI: 10.1002/adma.201200397.
7. Eun-Sung Lee, Kyung-Wan Nam, Enyuan Hu and Arumugam Manthiram, "Influence of the Evolution of Two Tetragonal Phases on the Capacity Fade of LiMn<sub>1.5</sub>Ni<sub>0.5</sub>O<sub>4-δ</sub> for the High Energy Application," *Chemistry of Materials*, Vol. **24** (18), pp 3610 – 3620 (2012).
8. Xiaojian Wang, Xiao-Qing Yang, Bin Zhang, Yongning Zhou, Kyung-Wan Nam, Hai-Yan Chen, Jianming Bai, Hong Li, Xuejie Huang, Xiqian Yu, and Enyuan Hu, "Investigation of Phase Transition behavior in LiFePO<sub>4</sub> and Mesoporous LiFe<sub>1-x</sub>Mn<sub>x</sub>PO<sub>4</sub> during Charge-discharge Cycling Using Synchrotron Based X-ray Diffraction and Absorption Techniques," presented at International Conference on Advanced Electromaterials (ICAE2011), November 7-12, Jeju, Korea, Invited Keynote Speaker.
9. Xiqian Yu, Qi Wang, Kyung-Wan Nam, Yongning Zhou, Xiao-Qing Yang, Hong Li, Xuejie Huang, Wei Wang, Daiwon Choi, Jie Xiao, "Investigation on fast chemical and electrochemical delithiation of cathode materials for Lithium-ion batteries by using quick EXAFS technique," *2012 MRS Spring Meeting*, April 9-13, San Francisco, USA.
10. Kyung-Wan Nam, Xiqian Yu, Xiao-Qing Yang, Xiaojian Wang, Yongning Zhou, Enyuan Hu, Seong-Min Bak, Hung-Sui Lee, Lijun Wu, Yimei Zhu, Kyung-Yoon Chung, Hong Li, Xuejie Huang, Liqian Chen, and Kwang Bum. Kim, "Structural Changes of Cathode Materials for Lithium-ion Batteries during Heating Studied by the Combined *in situ* XRD, X-ray Absorption and TEM," *16th International Meeting of Lithium Batteries (IMLB-16)*, June 18 to 22, 2012, Jeju, Korea, Invited.
11. Xiqian Yu, Xiao-Qing Yang, Kyung-Wan Nam, Enyuan Hu, Yongning Zhou, Seong-Min Bak, Hung-Sui Lee, Daniel Abraham, Huiming Wu, and Khalil Amine, Hong Li, Xuejie Huang, and Liqian Chen, "Crystal and Local structure changes of Li<sub>1.2</sub>Ni<sub>0.15</sub>Co<sub>0.1</sub>Mn<sub>0.55</sub>O<sub>2</sub> cathode materials during multiple cycling," *5th International Conference on Advanced Batteries for Automobile Application*, September 17-20, 2012, Istanbul, Turkey, Invited.

## V.B.7 Development of High Energy Cathode (PNNL)

Ji-Guang Zhang  
Pacific Northwest National Laboratory  
902 Battelle Blvd., Mail Stop K2-44  
Richland, WA 99352  
Phone: (509) 372-6515; Fax: (509) 375-2186  
E-mail: [jiguang.zhang@pnnl.gov](mailto:jiguang.zhang@pnnl.gov)

Jie Xiao  
Pacific Northwest National Laboratory  
902 Battelle Blvd., Mail Stop K2-44  
Richland, WA 99352  
Phone: (509) 375-4598; Fax: (509) 375-2186  
E-mail: [jie.xiao@pnnl.gov](mailto:jie.xiao@pnnl.gov)

Start Date: October 1, 2011  
Projected End Date: September 30, 2015

### Objectives

- Develop high-energy cathode materials with improved safety.
- Develop low-cost synthesis routes for environmentally benign cathode materials with long cycle life.

### Technical Barriers

This project addresses the following technical barriers:

- High cost of materials and synthesis methods.
- Limited energy density and cyclability.
- Safety.

### Technical Targets

- Develop cost-effective methods to prepare high-energy cathode materials.
- Evaluate “inert” cell components at high voltages. Identify the key parameters that determine the electrochemical performance of the cathode material as well as the whole battery device.
- Develop electrolytes and/or additives for high-voltage spinel and layered composite cathode materials.

### Accomplishments

- Developed facile synthesis approaches for high-voltage spinel  $\text{LiNi}_{0.5}\text{Mn}_{1.5}\text{O}_4$  and Li-rich layered composite cathode materials.
- Identified the influences of disordered phase, element doping, residual  $\text{Mn}^{3+}$ , and oxygen deficiency on the structural and electrochemical performances of high-voltage spinel.

- Systematically evaluated the “inactive” cell components at high voltages; identified the baseline components and parameters for effective and reliable lab testing of advanced lithium ion batteries.
- Investigated  $x\text{Li}_2\text{MnO}_3 \cdot (1-x)\text{LiMO}_2$  ( $M = \text{Ni}, \text{Co}, \text{Mn}$ ) layered cathode material and decoupled  $\text{Li}_2\text{MnO}_3$  phase from the composite to understand the electrochemical reactions from bulk to the interfaces.
- Novel electrolyte additives have been developed to suppress capacity fade in these cathodes.

◇ ◇ ◇ ◇ ◇

### Introduction

High-energy-density cathode material is the key for the development of advanced lithium-ion batteries that can be employed for transportation electrification. Batteries operating in high-voltage conditions, however, involve complicated parasitic reactions in addition to the desired electrochemical processes.

During FY 2012, high-voltage spinel material itself was systematically investigated, as well as other key components used in high-voltage cells. The comprehensive understanding obtained from the study of high-voltage spinel ( $\text{LiNi}_{0.5}\text{Mn}_{1.5}\text{O}_4$ ) has been further applied to a high-capacity Li-rich, Mn-based cathode,  $x\text{Li}_2\text{MnO}_3 \cdot (1-x)\text{LiMO}_2$  ( $M = \text{Ni}, \text{Co}, \text{and Mn}$ ), to improve the performance of these high-energy cathode materials. In addition, novel electrolyte additives are also investigated, which will be finally incorporated in the whole system to improve the Columbic efficiency and long-term cycling stability of these high-energy composite cathodes.

### Approach

- Synthesize cathode materials through a rheological phase method to achieve homogeneous mixing of the starting materials from the molecular level.
- Use advanced characterization tools, including *in situ* XRD, TEM, and NMR, coupled with theoretical simulation to understand the failure mechanism in the electrochemical cells.
- Apply the systematic understanding to guide the material design and electrolyte development.

### Results

**1. Optimization of high-voltage spinel  $\text{LiNi}_{0.5}\text{Mn}_{1.5}\text{O}_4$ .** Synthesis conditions including calcination temperature, post-synthesis heating, cooling rate and elemental substitution were systematically investigated to prepare high-performance  $\text{LiNi}_{0.5}\text{Mn}_{1.5}\text{O}_4$ . The content of

the disordered phase (which can be tuned through oxygen deficiency and/or element substitution) was found to be one of the most critical parameters that determined the performance of  $\text{LiNi}_{0.5}\text{Mn}_{1.5}\text{O}_4$ . The cooling rate of spinel after high-temperature calcination, often ignored during synthesis, in fact significantly changes the amount of oxygen deficiency, which then modulates the residual  $\text{Mn}^{3+}$  and amount of disordered phase. Spinel cooled at different rates showed regular octahedral shape except the quenched one (Figure V - 35). At a cooling rate of  $3^\circ\text{C}/\text{min}$  or higher, only a typical spinel diffraction pattern (Fd-3m symmetry, disordered) was observed in [100] and [110] zones. When the cooling rate was lowered to  $1^\circ\text{C}/\text{min}$ ,  $\text{LiNi}_{0.5}\text{Mn}_{1.5}\text{O}_4$  exhibited superlattice diffraction, forbidden by the Fd-3m space group. The occurrence of the superlattice patterns was caused by the  $\text{Ni}^{2+}/\text{Mn}^{4+}$  ordering, which cannot be directly observed with XRD. Further lowering the cooling rate to  $0.5^\circ\text{C}/\text{min}$  led to the observation of more extra reflections, associated with the increase of ordered phase content. This observation was consistent with our earlier finding (reported in FY2011) on the effect of post-synthesis heating and Cr-doping, both of which also modified the relative contents between disordered and ordered phases.

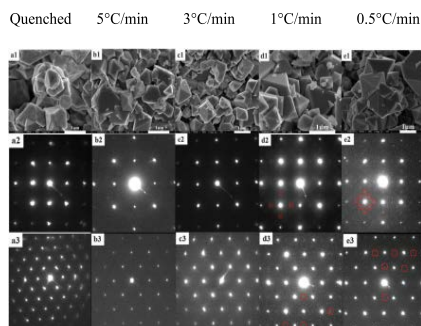


**Figure V - 35:** SEM images (a1 to e1) and electron diffraction patterns in the [100] (a2 to e2) and [110] (a3 to e3) zones of  $\text{LiNi}_{0.5}\text{Mn}_{1.5}\text{O}_4$  prepared with different cooling rates. (a) Quenched; (b)  $5^\circ\text{C}/\text{min}$ ; (c)  $3^\circ\text{C}/\text{min}$ ; (d)  $1^\circ\text{C}/\text{min}$ ; (e)  $0.5^\circ\text{C}/\text{min}$ .

The effects of the disordered phase on the properties of  $\text{LiNi}_{0.5}\text{Mn}_{1.5}\text{O}_4$  were investigated by *in situ* XRD measurements (see Figure V - 36). Three distinct phases (phase I:  $\text{LiNi}_{0.5}\text{Mn}_{1.5}\text{O}_4$ ; phase II:  $\text{Li}_{0.5}\text{Ni}_{0.5}\text{Mn}_{1.5}\text{O}_4$ ; phase III:  $\text{Ni}_{0.5}\text{Mn}_{1.5}\text{O}_4$ ) were identified in Figure V - 36a, for  $\text{LiNi}_{0.5}\text{Mn}_{1.5}\text{O}_4$  cooled slowly at  $0.5^\circ\text{C}/\text{min}$ , which contained the largest amount of ordered phase. When charged to ca. 30% state of charge (SOC), phase II appeared and became dominant with the diminishing of pristine phase I at ca. 70% SOC. The phase III started to emerge at ca. 80% SOC through another biphasic transition. For the  $5^\circ\text{C}/\text{min}$  cooled spinel (Figure V - 36c-d), however, a quite different phase evolution is observed in Figure V - 36b. From the pristine state to  $\sim 75\%$  SOC, a solid solution domain dominated. Cubic phase III growth through a two-phase transition was only observed near the end of charge. In general, the faster the cooling rate, the

more disordered phase in the lattice, and the wider the solid solution range during charge. The conversion of the first two-phase transition into a solid solution reaction definitely benefitted  $\text{Li}^+$  transport because of the reduced number of phase boundaries that  $\text{Li}^+$  ions had to overcome.

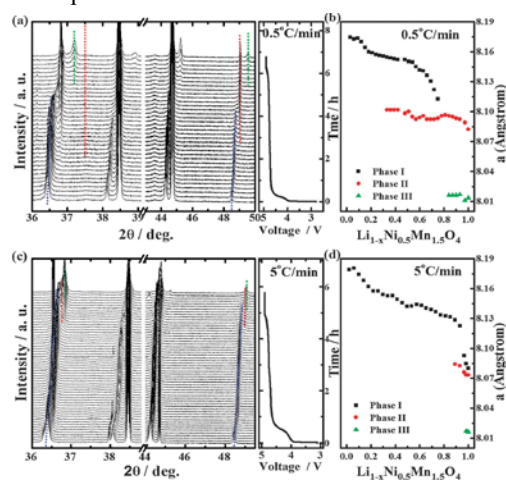


**Figure V - 36:** *In situ* XRD patterns of spinels at different SOCs and corresponding lattice parameter changes during  $\text{Li}^+$  extraction process for  $\text{LiNi}_{0.5}\text{Mn}_{1.5}\text{O}_4$  prepared with cooling rates of (a, b)  $0.5^\circ\text{C}/\text{min}$  and (c, d)  $5^\circ\text{C}/\text{min}$ .

The electrochemical behaviors of the spinels cooled at different rates were compared in Figure V - 37.

The charge-discharge curves of quenched spinel in Figure V - 37a exhibited an abnormally long plateau at  $\sim 4.0$  V, indicating the existence of a large amount of  $\text{Mn}^{3+}$  generated by the oxygen deficiency due to charge neutrality. When the long-term cycling stability and rate capability were compared in Figure V - 37b-d, rapidly cooled  $\text{LiNi}_{0.5}\text{Mn}_{1.5}\text{O}_4$  (3 or  $5^\circ\text{C}/\text{min}$ ) always demonstrated electrochemical properties superior to slowly cooled samples. For example, after 300 cycles,  $5^\circ\text{C}/\text{min}$  cooled spinel still maintains 112 mAh/g at 1C (Figure V - 37c), corresponding to a capacity fading of only 5.2% (0.017% per cycle). Even at 10C rate, the discharge capacity still approached 100 mAh/g for  $5^\circ\text{C}/\text{min}$  cooled spinel (Figure V - 37d). The improved performance can be attributed to the increased content of disordered phase in the rapidly cooled samples, which greatly promoted  $\text{Li}^+$  diffusion during repeated cycling.

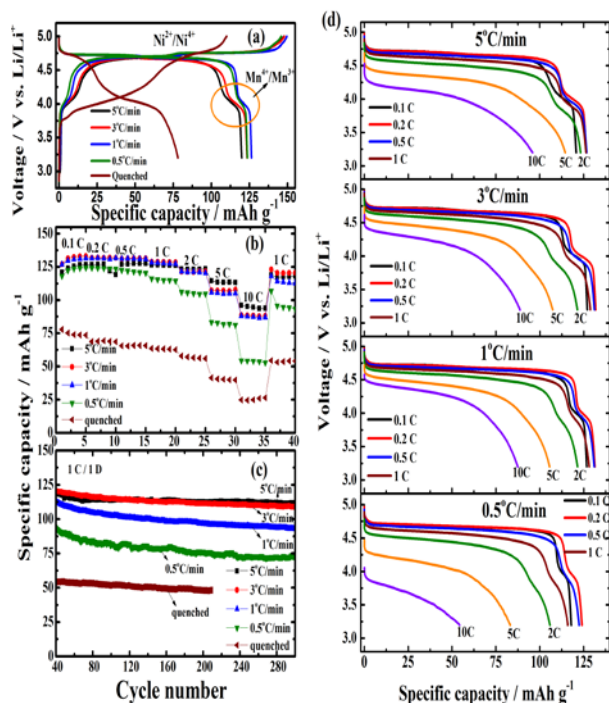


**Figure V - 37:** (a) Initial charge-discharge profiles at 0.1 C for  $\text{LiNi}_{0.5}\text{Mn}_{1.5}\text{O}_4$  prepared with different cooling rates. (b) Discharge capacity vs. cycle number at various C rates; (c) cycling performance; (d) rate capabilities for different  $\text{LiNi}_{0.5}\text{Mn}_{1.5}\text{O}_4$  at various C rates (1C = 140 mA/g).

**2. Investigation on the high-voltage stability of “inert” cell components.** Both high-voltage spinel and Li-rich Mn-based layered composite work at voltages beyond the stability limit of conventional electrolyte (>4.4 V). In high-voltage conditions, all the “inactive” cell components, such as cell cans, separator, and even carbon additives used in the electrode (which are normally stable in conventional Li-ion batteries) need to be reinvestigated.

For lab tests using button cells, aluminum (Al)-clad SS-316 positive cans had a much better resistance to oxidation than traditional stainless steel (SS-316) cathode pans at high voltages. It was also found that a polyethylene (PE)-based separator, such as Celgard K1640, is very stable at high voltage while a polypropylene (PP)-based separator (Celgard 2500) is not stable. Using a PE separator, or applying PVDF coating on Celgard 2500 to reduce direct contact between PP and  $\text{LiPF}_6$  can effectively improve the cell performance at high voltage.

Carbon additives in the cathode also may induce side reactions at high voltages. High-surface-area carbons, such as Ketjenblack (KB) or graphene not only accelerated electrolyte decomposition, the oxidation of functional groups on KB or graphene at high voltages further lowered the Coulombic efficiency of the cathode. Therefore, careful selection of carbon additives for high-voltage operation was required.

### 3. Investigation on the capacity fading mechanism in $x\text{Li}_2\text{MnO}_3 \cdot (1-x)\text{LiMO}_2$ (M = Ni, Co, Mn) layered

**composite.** In FY12, the work on Li-rich Mn-based layered composite was also initiated with an emphasis on the fundamental understanding of the failure mechanism. The  $\text{Li}_2\text{MnO}_3$  component has been decoupled from the layered composite and investigated separately. Figure V - 38a compares the XRD patterns of  $\text{Li}_2\text{MnO}_3$  calcined at different temperatures.  $\text{Li}_2\text{MnO}_3$  heated at  $700^\circ\text{C}$  delivered the highest reversible capacity of 175 mAh/g along with relatively stable cycling for the first 35 cycles. Large gaps were observed between charge and discharge in the first few cycles (Figure V - 38b). The low Coulombic efficiency in the beginning was closely related to the release of oxygen, which was also the challenge in the layered composite.

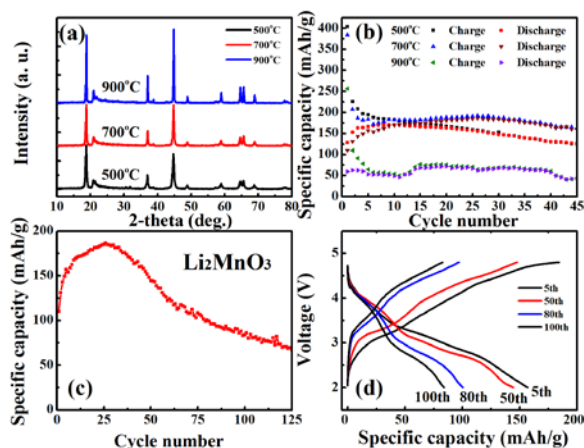


**Figure V - 38:** a) XRD patterns and b) cycling of  $\text{Li}_2\text{MnO}_3$  prepared at different temperatures; c) long-term cycling stability and d) voltage profiles of  $700^\circ\text{C}$ -prepared  $\text{Li}_2\text{MnO}_3$  at different cycles. The cells were cycled between 2.0 and 4.8 V at C/20 rate. (1C = 250 mA/g).

Figure V - 38c showed that the discharge capacity of  $\text{Li}_2\text{MnO}_3$  prepared at  $700^\circ\text{C}$  increased gradually during the first 40 cycles but decayed eventually after that. It was found that the duration of this activation process was related to the non-uniform extraction of  $\text{Li}^+$  during charge, depending on the cut-off charge voltage as well as the current density used in the test. The discharge voltage of  $\text{Li}_2\text{MnO}_3$  exhibited continuous drop during cycling (Figure V - 38d), exactly what is observed for the Li-rich layered composite. More characterizations are underway to understand and address these issues.

Finally, novel electrolyte additives have been developed to suppress the capacity fade in  $\text{Li}_{1.2}\text{Ni}_{0.2}\text{Mn}_{0.6}\text{O}_2$ . Initial results have verified the effectiveness of these additives. More investigations will be done to further improve the Coulombic efficiency and long-term cycling stability of the high-energy composite cathodes.

## Conclusions and Future Directions

The relationship of synthesis, structure and performance in high-voltage spinel cathodes has been systematically studied. It was found that the content of disordered phase in the spinel lattice significantly influence the materials properties. The content of the disordered phase relative to ordered phases can be modulated by controlling cooling rate, post-synthesis heating or element substitution. In addition, the disordered phase fundamentally changes the reaction pathways of spinel by converting the first biphasic transition into a solid-solution-like reaction. The end result was significantly improved cycling stability and rate capability in  $\text{LiNi}_{0.5}\text{Mn}_{1.5}\text{O}_4$  composed of more Ni/Mn disordered phase. Other cell components, which were assumed to be “inert” before, were also re-evaluated at high voltages. Stable cell pans and separators along with appropriate carbon additives have been identified to provide reliability and consistency in the investigation of high-voltage cathodes and the Li-rich layered composite. Preliminary results on the properties of  $x\text{Li}_2\text{MnO}_3 \cdot (1-x)\text{LiMO}_2$  ( $M = \text{Ni, Co, Mn}$ ) indicate that the instability of the  $\text{Li}_2\text{MnO}_3$  phase is probably the main initiator of the capacity decay and voltage fade phenomena, providing a baseline to understand the individual components in the layered composite.

Future work will focus on the investigation of bulk and surface reactions during repeated charge-discharge processes of the layered composite  $x\text{Li}_2\text{MnO}_3 \cdot (1-x)\text{LiMO}_2$  ( $M = \text{Mn, Ni, Co}$ ;  $0 \leq x \leq 1$ ). The key factors related to the oxygen release in these cathodes will be investigated. Sample preparation and post-synthesis conditions will be tuned to improve their cyclability. Novel electrolyte additives will be further investigated to suppress the capacity and voltage fade and improve the Coulombic efficiency of the high-energy cathode materials.

## FY 2012 Publications/Presentations

- J Xiao, X Chen, PV Sushko, ML Sushko, L Kovarik, J Feng, Z Deng, J Zheng, GL Graff, Z Nie, D Choi, J Liu, J-G. Zhang and MS Whittingham, “High Performance  $\text{LiNi}_{0.5}\text{Mn}_{1.5}\text{O}_4$  Spinel Controlled by  $\text{Mn}^{3+}$  Concentration and Site Disorder,” *Advanced Materials*, **24**, 2109-2116 (2012).
- J Zheng, J Xiao, X Yu, L Kovarik, M Gu, F Omenya, X Chen, X-Q Yang, J Liu, GL Graff, MS Whittingham and J-G Zhang, “Enhanced  $\text{Li}^+$  ion transport in  $\text{LiNi}_{0.5}\text{Mn}_{1.5}\text{O}_4$  through control of site disorder,” *Physical Chemistry Chemical Physics*, **14**, 13515-13521 (2012).
- X Chen, W Xu, J Xiao, MH Engelhard, F Ding, D Mei, D Hu, J Zhang, J-G Zhang, “Effects of cell positive cans and separators on the performance of high-voltage Li-ion batteries,” *Journal of Power Sources*, **213**, 160-168 (2012).
- W Xu, X Chen, F Ding, J Xiao, D Wang, A Pan, J Zheng, XS Li, AB Padmaperuma and J-G Zhang, “Reinvestigation on the state-of-the-art nonaqueous carbonate electrolytes for 5 V Li-ion battery applications,” *Journal of Power Sources*, **213**, 304-316 (2012).
- W Xu, AL Read, PK Koech, D Hu, C Wang, J Xiao, AB Padmaperuma, GL Graff, J Liu and J-G Zhang, “Factors Affecting the Battery Performance of Anthraquinone-based Organic Cathode Materials,” *Journal of Materials Chemistry*, **22**, 4032-4039 (2012).
- J Zheng, J Xiao, W Xu, X Li and J Zhang, “The Effects of Carbon Additive on Electrochemical Performance of High Voltage Spinel  $\text{LiNi}_{0.5}\text{Mn}_{1.5}\text{O}_4$ ,” *222<sup>nd</sup> ECS Meeting*, Honolulu, HI, October, 2012.
- J Xiao, J Zheng, X Chen, W Xu and J-G Zhang, “High Voltage Li-ion Batteries,” *7<sup>th</sup> Beijing International Forum on Li-ion Battery Technology & Industrial Development*, Beijing, China, September, 2012.
- J Xiao, J Liu, GL Graff and J-G Zhang, “Advanced Cathode Materials for Lithium Ion Batteries,” *10<sup>th</sup> China International Battery Fair*, Shenzhen, China, June, 2012.
- W Xu, X Chen, J Xiao, F Ding, D Wang, A Pan, and J-G Zhang, “Re-investigation of Non-aqueous Carbonate Electrolytes for High Voltage Lithium-ion Batteries,” *220<sup>th</sup> ECS Meeting*, Boston, MA, October, 2011.
- D Choi, J Xiao, W Xu, YJ Choi, JS Hardy, MS Bhuvanewari, V Murugesan, J Liu, W Wang, Z Yang, GL Graff and J-G Zhang, “Electrochemical Performance and Thermal Stability of  $\text{LiMnPO}_4$  Based Cathodes,” *220<sup>th</sup> ECS Meeting*, Boston, MA, October, 2011.
- X Chen, W Xu, J Xiao, F Ding, MH Engelhard, J Zheng, and J-G Zhang. “Effects of Non-Active Materials on the Performance of High Voltage  $\text{LiNi}_{0.5}\text{Mn}_{1.5}\text{O}_4$  Cathodes,” *221<sup>st</sup> ECS Meeting*, Seattle, WA, May, 2012.
- W Xu, X Chen, J Xiao, MH Engelhard, D Mei, F Ding and J-G Zhang, “Re-investigation of Non-active Materials for High Voltage Lithium Ion Batteries,” *International Meeting on Lithium Batteries (IMLB)*, Jeju Island, South Korea, June, 2012.

## V.B.8 Crystal Studies on High-energy Density Cathodes (LBNL)

Guoying Chen

Lawrence Berkeley National Laboratory  
Environmental Energy Technologies Division  
Berkeley, CA 94720

Phone: (510) 486-5843; Fax: (510) 486-5467

E-mail: [gchen@lbl.gov](mailto:gchen@lbl.gov)

Start Date: October 1, 2009

Projected End Date: September 30, 2012

### Objectives

- Investigate phase transition mechanisms, identify kinetic barriers, and evaluate stability of high-energy cathode materials.
- Establish direct correlations between structure, composition, size, morphology, performance, and thermal and cycling stabilities.
- Provide material's design guidelines and develop optimized high-energy cathodes.

### Technical Barriers

- Low energy density, low power density, poor cycle life and poor safety.

### Technical Targets

- PHEV40: 96 Wh/kg, 750 W/kg, 5,000 cycles.
- EV: 200 Wh/kg, 1,000 cycles.

### Accomplishments

- Determined transition-metal ordering and Mn<sup>3+</sup> content in Ni/Mn spinels by FTIR, NMR, and electrochemistry. Established the correlation between the three techniques.
- Identified the role of Mn<sup>3+</sup> content in Ni/Mn spinel structure, thermal behavior, redox properties, and rate capability.
- Investigates phase transition mechanisms in Ni/Mn spinels. Revealed the impact of phase boundary movement on kinetic behaviors.
- Demonstrated the dominating effect of spinel particle morphology on chemical diffusivity and kinetic properties.
- Demonstrated the effects of particle size and morphology on the kinetic properties of the Li-excess layered composite cathodes.

◇ ◇ ◇ ◇ ◇

### Introduction

To meet the DOE targets for Li-ion batteries for vehicular applications, it is necessary to employ electrode materials that offer high-energy density and high stability. The aim of the project is to improve the commercial viability of two oxide cathodes that are presently most promising to meet these targets: spinel LiNi<sub>x</sub>Mn<sub>2-x</sub>O<sub>4</sub> and layered Li<sub>1+x</sub>M<sub>1-x</sub>O<sub>2</sub> (M=Mn, Ni and Co).

Spinel LiMn<sub>1.5</sub>Ni<sub>0.5</sub>O<sub>4</sub> has a theoretical capacity of 147 mAh/g (700 Wh/kg) and fast three-dimensional lithium-ion diffusion paths within the cubic lattice. It has been reported that physical properties, such as crystal structures (ordered vs. disordered), size, morphology and Mn<sup>3+</sup> content, separately and collectively impact rate capability and stability of the material, but the individual contribution as well the synergy between them are unclear. Studies based on LiNi<sub>x</sub>Mn<sub>2-x</sub>O<sub>4</sub> single crystals with well-defined physical characteristics allow us to systematically investigate kinetic and thermodynamic behaviors, correlate material's specific property to the performance and stability, and ultimately achieve electrode optimization for minimized side reactions and improved transport properties.

Layered oxides are capable of delivering high capacity well over 200 mAh/g. The cathodes, however, exhibit large irreversible capacity loss when charged through the activation plateau in the first cycle and suffer low rate capability and poor cycle life thereafter. An in-depth understanding of material's intrinsic properties and processes is crucial to enabling its rational design and optimization for improved cathode performance.

### Approach

Prepare well-formed crystals with various structure, composition, size and morphology using wet chemistry synthesis routes, such as solvothermal and molten salt reactions. Characterize their physical properties and investigate their solid state chemistry using advanced spectroscopic, spectromicroscopic, scanning calorimetry and electron microscopic techniques. Optimize synthesis and processing conditions, improve performance and safety of the cathode materials based on the structural and mechanistic understandings.

### Results

**Spinel LiNi<sub>x</sub>Mn<sub>2-x</sub>O<sub>4</sub>.** With a goal to systematically investigate the effect of Mn<sup>3+</sup> content on rate performance and stability, the team has previously synthesized a series of LiNi<sub>x</sub>Mn<sub>2-x</sub>O<sub>4</sub> single crystals with 0.3 ≤ x ≤ 0.5 and 0 ≤ Mn<sup>3+</sup> content ≤ 23.5%. A qualitative measure of transition-metal ordering in the structure was established

by FTIR, which showed that while samples with higher Ni and low Mn<sup>3+</sup> contents were mostly ordered, an abrupt loss of ordering occurred at Ni content of 0.35. In collaboration with Prof. Grey's group, the changes in ordering scheme within the series were corroborated by <sup>6</sup>Li MAS NMR. Increasing the Ni content quickly reduced the line width and intensity of the peaks at low frequencies, with the spectrum at  $x=0.5$  showing a single peak at 1040 ppm, suggesting a near-perfect ordered structure in the sample.

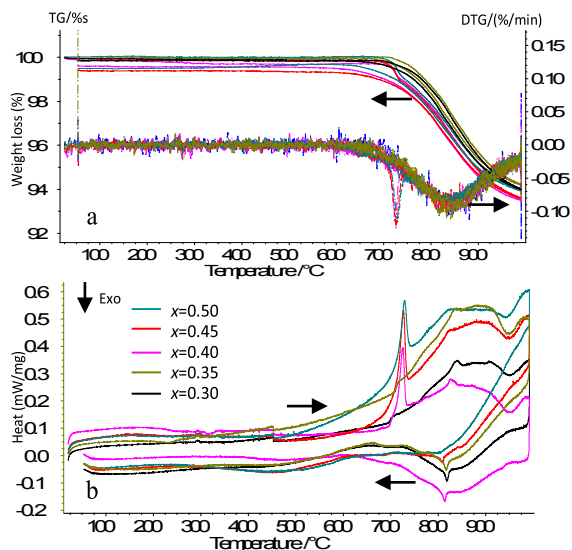


Figure V - 39: a) TGA and b) DSC profiles of the  $\text{LiNi}_x\text{Mn}_{2-x}\text{O}_4$  crystals.

The effect of Mn<sup>3+</sup> content on structural ordering was further investigated by thermal analysis. In a simultaneous thermogravimetric analysis (TGA) and differential scanning calorimetry (DSC) instrument, the  $\text{LiNi}_x\text{Mn}_{2-x}\text{O}_4$  crystals were heated and then cooled in air at a rate of 3 °C/min. As shown Figure V - 39a, the total weight loss on heating to 1000 °C ranged from 5.8 to 6.5%, depending on the Mn<sup>3+</sup> content in the samples. The broad reversible peaks which developed at 700 °C and centered at 830 °C on the differential TGA traces were attributed to the loss of oxygen. For the ordered samples with Ni content above 0.35, an additional peak corresponding to structural disordering was also observed at 720 °C, suggesting that disordering is promoted by the initial reduction of Mn<sup>4+</sup> to Mn<sup>3+</sup> and oxygen loss. In the DSC traces (Figure V - 39b), the sharp endothermic peaks at 720 °C imply that disordering is a first-order transition. The reversible peaks at 810 °C are likely due to the extrusion and incorporation of the rock salt phase,  $\text{Li}_x\text{Ni}_{1-x}\text{O}$ , during heating and cooling. The loss of oxygen between 700 to 950 °C was further indicated by the broad peaks on the DSC profiles.

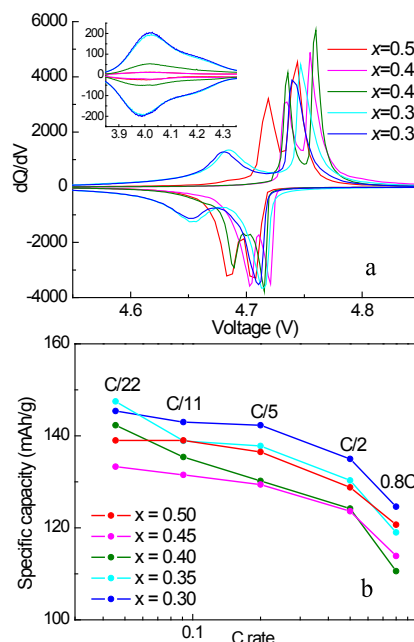
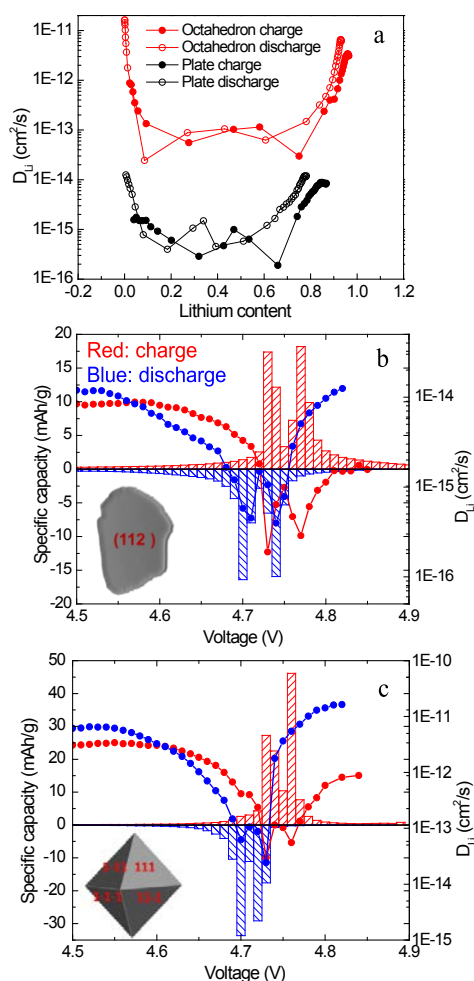


Figure V - 40: a) Integrated capacity and voltage profiles obtained at C/22 and b) rate capability comparison of  $\text{LiNi}_x\text{Mn}_{2-x}\text{O}_4$  crystals.

The effect of Mn<sup>3+</sup> content on structure, redox properties, and rate capabilities of the spinels was then evaluated by varying-rate cycling of  $\text{LiNi}_x\text{Mn}_{2-x}\text{O}_4$  half-cells between 3.0 and 5.0 V. In the integrated capacity and voltage profiles (Figure V - 40a), the peak separations between the Ni<sup>2+</sup>/Ni<sup>3+</sup> and Ni<sup>3+</sup>/Ni<sup>4+</sup> redox couples at 4.7 V were 20, 21, and 27 mV for  $x=0.5$ , 0.45, and 0.4, respectively. The separation increased to 60 and 63 mV for  $x=0.35$  and 0.3, suggesting a rapid decrease in transition metal ordering below a critical Ni content. The results are consistent with our FTIR and <sup>6</sup>Li MAS NMR observations and demonstrated the excellent correlation between the three techniques. At  $x=0.3$  and 0.35, the two peaks at 4.7 V were largely asymmetric, and significant lower-voltage peak broadening was observed. This suggests the existence of a solid-solution region during low SOC Li intercalation and de-intercalation in the disordered spinels. While the structurally more ordered spinels transform through two 2-phase transitions, indicated by the two sets of sharp redox peaks at 4.7 V, the disordered only go through one 2-phase transition. These differences dramatically affect transport properties, as evidenced by the rate capability study (Figure V - 40b). The disordered spinels consistently delivered higher capacities than the more ordered ones, and the best performance was obtained from  $x=0.30$  with the highest Mn<sup>3+</sup> content. Among the three ordered spinels, the sample with  $x=0.5$  and the lowest Mn<sup>3+</sup> content showed the best performance at nearly all rates tested, suggesting Mn<sup>3+</sup> may play a different role in the ordered spinels. By eliminating the influences of crystal size and morphology in this single-crystal study, the interdependence and the significance of Mn<sup>3+</sup> content, structural ordering, and phase transformation mechanism are clearly shown.



**Figure V - 41:** a) Chemical diffusivity comparison between the plate and octahedral shaped  $\text{LiMn}_{1.5}\text{Ni}_{0.5}\text{O}_4$  crystals, and incremental capacities and chemical diffusion coefficients in b) Plates and c) Octahedrons.

The impact of particle morphology on transport properties was evaluated by the comparative studies on similar-sized  $\text{LiMn}_{1.5}\text{Ni}_{0.5}\text{O}_4$  single crystals that have octahedron shape and (111) surface facets and plate shape and (112) surface facets. Potentiostatic Intermittent Titration Technique (PITT) measurements were performed on the composite electrodes composed of 80 wt% crystals, 10 wt% PVDF binder, 5 wt% graphite, and 5 wt% acetylene carbon. The experiments were performed between 3.5 and 4.9 V at a step size of 10 mV. The potential was stepped to next level when the current drops to 10  $\mu\text{A}$ , equivalent to  $C/150$ . The lithium chemical diffusion coefficient,  $D$ , was then calculated from the slope of the linear region in the  $\ln(I)$  vs.  $t$  plot, as defined in Equation (1):

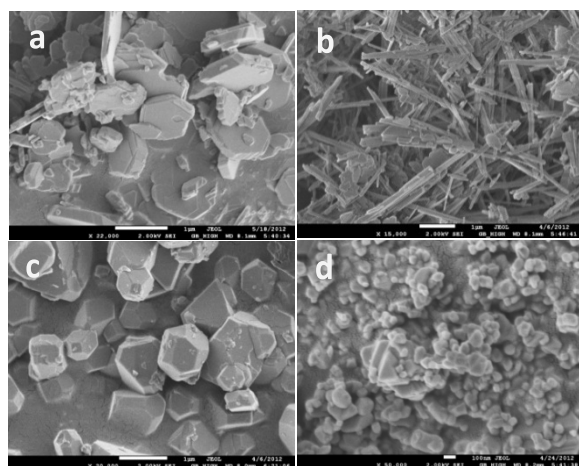
$$D = - \frac{d \ln(I)}{dt} \frac{4L^2}{\pi^2} \quad (1)$$

Figure V - 41a compares the chemical diffusion coefficients during charge and discharge. Lithium diffusion exhibited concentration dependent behavior in

both crystal samples, which ranged from  $1.9 \times 10^{-16}$  to  $1.2 \times 10^{-14} \text{ cm}^2/\text{s}$  in the plates and  $2.4 \times 10^{-14}$  to  $1.6 \times 10^{-11} \text{ cm}^2/\text{s}$  in the octahedrons. At any given Li content, diffusion in the octahedrons with (111) facets is at least two orders of magnitude higher than that in the plates with (112) facets.

The incremental capacities and chemical diffusion coefficient obtained during the charge and discharge of the plate-shaped crystals are superimposed in Figure V - 41b. Two diffusion minima were observed at 4.73 and 4.77 V on charge and 4.74 and 4.71 V on discharge, respectively, which correlated well with the capacity maxima. Similar behavior was also observed on the octahedral-shaped crystals (Figure V - 41c), where two minima were seen at 4.73 and 4.76 V on charge and 4.73 and 4.70 V on discharge). The appearance of a diffusion minimum at the occurrence of the first-order phase transition in  $\text{LiMn}_{1.5}\text{Ni}_{0.5}\text{O}_4$  implies that Li transport in the spinel is likely limited by the movement of phase boundaries, in addition to the limitation imposed by the electronic or ionic conductivities of the material. The octahedrons were found to have a substantially smaller solid solution region and more extended phase boundary movement, on top of a more ordered structure and a lower  $\text{Mn}^{3+}$  content in the structure. The superior transport properties, therefore, were attributed to the better particle morphology in the octahedrons. The study demonstrates the importance of spinel particle-morphology design for maximum Li transport.

**Layered Oxides.** Phase-pure  $\text{Li}_{1.2}\text{Mn}_{0.13}\text{Mn}_{0.54}\text{Co}_{0.13}\text{O}_2$  (alternatively  $0.5\text{Li}_2\text{MnO}_3 \cdot 0.5\text{LiMn}_{0.33}\text{Ni}_{0.33}\text{Co}_{0.33}\text{O}_2$ ) crystals with four different morphologies were synthesized by the molten-salt method. Synthesis temperature, time, precursors, and flux were found to largely control the size and shape of the crystals. For example, in the temperature range of 750-900°C, micron-sized hexagonal-shaped crystal plates were obtained when nitrate precursors and CsCl flux (m.p.= 645°C) were used (Figure V - 42a). Replacing CsCl flux with KCl (m.p.= 770°C) led to the formation of needle-shaped crystals in 2  $\mu\text{m}$  length and 100 nm diameter (Figure V - 42b). Regardless of the flux, cuboctahedral-shaped crystals were obtained when oxide precursors were used, with micron-sized crystals (Figure V - 42c) synthesized in CsCl and much smaller crystals of 100-200 nm (Figure V - 42d) made in NaCl flux (m.p.= 801°C).



**Figure V - 42:** a) SEM images of  $\text{Li}_{1.2}\text{Ni}_{0.13}\text{Mn}_{0.54}\text{Co}_{0.13}\text{O}_2$  single crystals synthesized from nitrate precursors in a) CsCl flux and b) KCl flux and oxide precursors in c) CsCl flux and d) NaCl flux.

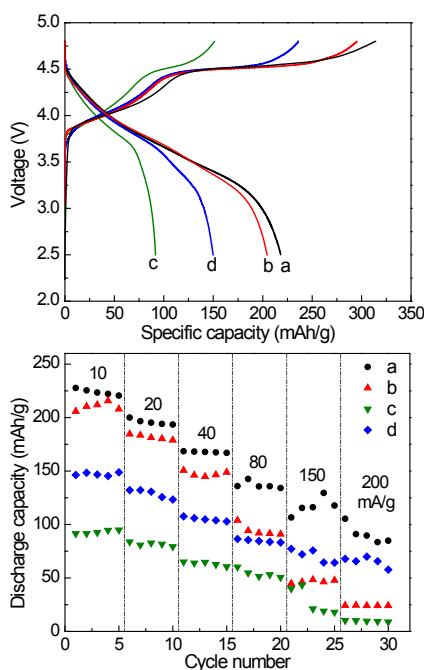


**Figure V - 43:** Top: First-cycle charge and discharge voltage profiles and Bottom: rate capability comparison of the  $\text{Li}_{1.2}\text{Ni}_{0.13}\text{Mn}_{0.54}\text{Co}_{0.13}\text{O}_2$  crystals.

Electrochemical performance of the crystal samples were evaluated by half-cell cycling of the composite electrodes made from the oxide crystals. Figure V - 43 (top) compares the first-cycle voltage profiles of the  $\text{Li}_{1.2}\text{Mn}_{0.13}\text{Mn}_{0.54}\text{Co}_{0.13}\text{O}_2$  cells when charged and discharged at a current density of 10 mA/g. All cells showed an activation plateau around 4.5 V, but higher polarization and much shorter plateau length were observed in the cell with the micron-sized cuboctahedrons. While both plate- and needle-shaped crystals delivered large capacities close to the theoretical value, the cuboctahedron samples had lower capacities that are directly proportional to the level of first-charge activation in these crystals. The effects of particle size and

morphology were further demonstrated on rate capability comparison, as shown in Figure V - 43 (bottom). The plates consistently delivered the highest capacity at all rates, while the large cuboctahedrons yielded the lowest capacities among the tested samples.

## Conclusions and Future Directions

The role of  $\text{Mn}^{3+}$  content in structure, phase transition mechanism and the rate performance of the Ni/Mn spinels were identified, and the impact of phase boundary movement on kinetic properties revealed. The dominant effects of particle size and morphology and the importance of morphology design in achieving the optimal rate performance in both spinel  $\text{LiNi}_x\text{Mn}_{2-x}\text{O}_4$  and layered  $\text{Li}_{1+x}\text{M}_{1-x}\text{O}_2$  cathodes were clearly demonstrated in our studies.

This project was completed as of September 2012. Future directions on the related research will focus on the examination of crystal-plane specific surface chemistries of the oxide cathodes and the stability of the interfacial layer between the cathode and the electrolyte.

## FY 2012 Publications/Presentations

1. B. Hai, A. K. Shukla, H. Duncan, and G. Chen, "Effect of Particle Surface Facets on the Kinetic Properties of  $\text{LiMn}_{1.5}\text{Ni}_{0.5}\text{O}_4$  Cathode Material," *J. Mater. Chem. A*, DOI:10.1039/C2TA00212D (2012).
2. G. Chen, B. Hai, A. K. Shukla, and H. Duncan, "Impact of Initial Li Content on Kinetics and Stabilities of Layered  $\text{Li}_{1+x}(\text{Ni}_{0.33}\text{Mn}_{0.33}\text{Co}_{0.33})_{1-x}\text{O}_2$ ," *Journal of the Electrochemical Society*, **159**, A1543 (2012).
3. G. Chen, A. Shukla, X. Song, and T. J. Richardson, "Improved Kinetics and Stabilities in Mg-Substituted  $\text{LiMnPO}_4$ ," *Journal of Materials Chemistry*, **21**, 10126 (2011).
4. "Structure and Performance of Layered  $\text{Li}_{1+x}\text{M}_{1-x}\text{O}_2$  Crystals," *ECS 220<sup>th</sup> Meeting*, Boston, MA, October 11, 2011.
5. "Impact of  $\text{LiMn}_{1.5}\text{Ni}_{0.5}\text{O}_4$  Crystal Surface Facets," *Gordon Research Conferences*, Ventura, CA, March 5, 2012.

## V.B.9 Developing Materials for Lithium-Sulfur Batteries (ORNL)

Chengdu Liang  
Oak Ridge National Laboratory  
Center for Nanophase Materials Sciences  
Building 8610 MS 6493  
Oak Ridge, TN37831-6493  
Phone: (865) 456-9185; Fax: (865) 574-1753  
E-mail: [liangcn@ornl.gov](mailto:liangcn@ornl.gov)

Collaborators:  
Nancy J. Dudney and Jane Howe

Start Date: June 2010  
Projected End Date: September 2014

### Objectives

- Expand the scientific understanding of lithium-sulfur chemistry to guide material development for practical Li-S batteries to meet the energy density and cost goals for PHEV and EV applications.
- Improve the reversibility of sulfur cathodes through optimization of the electrolyte composition.
- Establish a chemical and mechanical mechanism to enable long-term safe cycling of metallic lithium anodes.

### Technical Barriers

Using elemental sulfur and elemental lithium as cathode and anode, respectively, the lithium-sulfur (Li-S) battery represents the simplest battery chemistry for rechargeable batteries. In spite of the high theoretical energy density of 2,600 Wh/kg, Li-S batteries suffer from poor cyclability. There are three key limitations for cycling Li-S batteries that must be overcome to make practical Li-S batteries: (1) Sulfur is an electronic insulator. Its poor electronic conductivity leads to low utilization of active material in the electrode. (2) The charge and discharge products of sulfur are poor ionic conductors. In order to make the sulfur cathode rechargeable, a liquid electrolyte that has a high solubility of polysulfides is required to overcome the poor ionic conductivities of solid sulfur species. As a result of the dissolution of polysulfides in the liquid electrolyte, the diffusion of polysulfides from the cathode to the anode during the battery cycling leads to intrinsically short cycle-life. (3) The dendritic growth of lithium metal in liquid electrolytes and the ever-growing solid electrolyte interphase on the anode surface shorten the cycle-life of Li-S batteries and also cause safety concerns. New materials and novel design of batteries are crucial to enable Li-S battery chemistry in PHEV and EV applications.

### Technical Targets

- Optimize the structure of the sulfur cathode for the improvement of cycling performance.
- Invent new electrolyte compositions that are compatible with Li-S battery components.
- Achieve long cyclability of lithium metal anode in Li-S batteries.

### Accomplishments

- Discovered  $P_2S_5$  as new electrolyte additive for Li-S batteries with a liquid electrolyte.
- Achieved lithium metal anode protection through passivation.
- Developed novel nanostructured solid electrolytes as the enabler of metallic lithium anode.
- Designed and realized an all-solid battery configuration for Li-S batteries.
- Discovered a series of S-rich compounds as the cathode material for all-solid Li-S batteries.



### Introduction

The DOE Vehicle Technologies Program is tackling the challenges of electrified vehicle transportation to reduce U.S. petroleum consumption. Energy storage is a critical component in any electrified drivetrain. The cost and energy density targets that must be met to enable large scale deployment of electric vehicles will require the development of new battery materials. Compared to state-of-the-art lithium-ion batteries, Li-S batteries have obvious advantages of low cost and high energy density. The sheer abundance of elemental sulfur from both natural deposits of volcanos and waste from the petroleum industry offers opportunities to develop Li-S batteries at extremely low cost. Technologically, Li-S battery chemistry provides a theoretical energy density 2 to 5 times higher than any of the known Li-ion battery chemistries based on transition metal compounds. In spite of recent advances in Li-S batteries, the current Li-S batteries are still suffering from short cycle-life and poor efficiency. This project aims at innovating Li-S battery technology by discovering advanced materials that enable long-cycle life and high-efficiency Li-S batteries.

A conventional Li-S battery uses metallic lithium as the anode (also known as the negative electrode), sulfur-carbon composites as the cathode (the positive electrode), and an organic liquid electrolyte. With striking contrast to conventional lithium-ion batteries, the liquid electrolytes in

Li-S batteries are required to have a good solubility for lithium polysulfides, which are intermediate products of the cathode discharge process. The liquid electrolyte in a Li-S battery not only delivers lithium ions but also enables the electrochemical cycling of elemental sulfur which is an insulator of both electrons and ions. While the dissolution of polysulfides enables the electrochemical cycling of Li-S batteries, such a dissolution process is essentially the main cause of the short cycle-life and low energy efficiency of Li-S batteries. The dissolved active cathode materials lead to the diffusion-driven migration of sulfur inside the electrochemical cell. The migration of sulfur from the cathode to the anode results in permanent loss of capacity. Apart from the challenges of the sulfur cathode, the electrochemical cycling of the metallic lithium anode is a long-standing problem for lithium batteries with liquid electrolytes: the dendritic growth of lithium metal causes safety concerns and the continuous growth of solid electrolyte interphase (SEI) on the anode consumes Li and therefore results in capacity decay. The migration of sulfur species in Li-S cells add to the complication of cycling the metallic lithium anode: the chemical reaction between the lithium anode and polysulfides forms  $\text{Li}_2\text{S}$  on the surface of lithium and impedes the electrochemical reaction of lithium anode. Hence, the short cycle-life and low energy efficiency of a conventional Li-S battery are a combination of problems from both the sulfur cathode and metallic lithium anode. Innovative design of battery structures and new materials that enable new designs are of paramount importance for improving Li-S battery technology.

## Approach

The polysulfide shuttle phenomenon is the main cause of the short cycle-life of Li-S batteries with liquid electrolytes that dissolve lithium polysulfide. Since the dissolution of polysulfide is inevitable, the most viable approach to stop the polysulfide shuttle is to cut-off the shuttle path from the anode side. To this end, electrolyte additives have been developed to passivate the surface of lithium metal. The passivation layer functions as a physical barrier to prevent the direct contact of lithium with the dissolved lithium polysulfide, and thus blocks the polysulfide shuttle. Ideally the passivation layer should be a lithium-ion conductor that allows the transport of lithium ions during battery operations. The dissolved polysulfide will be the active material of the cathode. In this sense, the organic solvent is considered part of the electrode. The actual active material of the sulfur cathode is a solution of polysulfides that has been termed *catholyte*. The passivation layer is the actual electrolyte. In this design, the ionic conductivity of the sulfur cathode is provided by the solvated lithium ions in the catholyte. In addition to the polysulfide shuttle problem, the precipitation of  $\text{Li}_2\text{S}$  is another cause of capacity decay of Li-S batteries. In an ideal case, the additives will promote the dissolution of  $\text{Li}_2\text{S}$  in liquid electrolytes to alleviate the capacity decay.

In general, the use of electrolyte additives take advantage of dissolved lithium polysulfides while preventing the negative effect of the polysulfide shuttle. This part of the research focuses on the improvement of cyclability of the sulfur cathode under conventional cell design with a liquid electrolyte.

As elaborated in the introduction, the challenges of cycling Li-S batteries rise from both the metallic lithium anode and the sulfur cathode. Consideration of all the challenges introduced by soluble polysulfides led us to a key question: Is it possible to design a cell that enables the safe cycling of metallic lithium and sulfur without the dissolution of lithium polysulfide? It is known that metallic lithium can be cycled safely over 10,000 cycles in a thin film battery that uses a solid electrolyte. Using a solid electrolyte also benefits the sulfur cathode since there is no dissolution and shuttling of polysulfide in solid electrolytes. Thus, the polysulfide shuttle is completely eliminated in the all-solid Li-S batteries. This line of reasoning brought us to a second critical question: Can the Li-S battery be cycled well in an all-solid configuration? A second focus of this research is to identify the technical hurdles of all-solid Li-S batteries and develop new materials to overcome these hurdles. The key challenge of all-solid Li-S batteries is to meet the following conditions: (1) good electrolytes that have high ionic conductivity and excellent electrochemical stability with both the anode and cathode; (2) a cell design that can handle the mechanical stress of large volume changes and prevent the penetration of lithium dendrites; and (3) a sulfur cathode with high electronic and ionic conductivities. New solid electrolytes and sulfur compounds have been developed to meet these conditions.

## Results

**Electrolyte additives for conventional Li-S batteries with a liquid electrolyte.** Phosphorous pentasulfide ( $\text{P}_2\text{S}_5$ ) was discovered to be a novel electrolyte additive that can prolong the cycle-life of high-energy Li-S batteries. The function of the additive is two-fold: (1)  $\text{P}_2\text{S}_5$  promotes the dissolution of  $\text{Li}_2\text{S}$  and alleviates the loss of capacity caused by the precipitation of  $\text{Li}_2\text{S}$ ; and (2)  $\text{P}_2\text{S}_5$  passivates the surface of lithium metal and therefore eliminates the polysulfide shuttle phenomenon. Figure V - 44A shows that a Li-S test cell with the additive has a high reversible capacity of 900-1350  $\text{mAh g}^{-1}$  and a high coulombic efficiency of  $\geq 90\%$  for at least 40 stable cycles at 0.1 C.

The deployment of Li-S batteries is hampered by their poor cyclability due to the so-called polysulfide shuttle phenomenon: The migration of soluble sulfur species in the liquid electrolyte causes undesirable self-discharge, precipitation of lithium sulfide, corrosion of the lithium anode, and a low coulombic efficiency. We found that  $\text{P}_2\text{S}_5$  is able to form complexes with lithium sulfide and lithium polysulfide. These complexes prevent the precipitation of

lithium sulfide and passivate the surface of the lithium metal anode to reduce the polysulfide shuttle phenomenon. Shown in Figure V - 44B are two photos showing  $\text{Li}_2\text{S}$  in liquid electrolyte without (left) and with (right)  $\text{P}_2\text{S}_5$ . The turbid suspension of  $\text{Li}_2\text{S}$  in tetraglyme became a clear yellow solution when equimolar  $\text{P}_2\text{S}_5$  was added to the suspension. The high solubility of  $\text{Li}_2\text{S}$  in the organic electrolyte prevented the capacity decay that was caused by the precipitation of  $\text{Li}_2\text{S}$ .

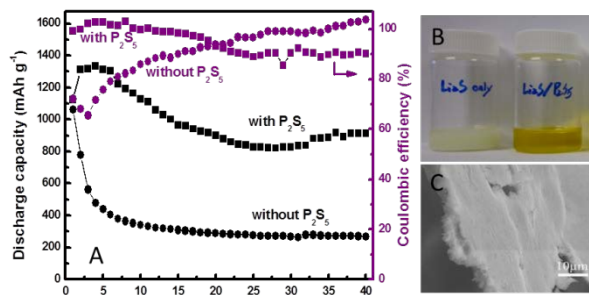


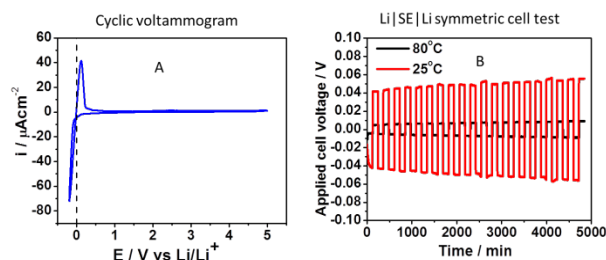
**Figure V - 44:** (A) Cycling performance of Li-S batteries with and without  $\text{P}_2\text{S}_5$ ; (B) Photos showing the promoted solubility of  $\text{Li}_2\text{S}$  in liquid electrolyte by  $\text{P}_2\text{S}_5$ ; (C) A micrograph of the passivation layer on lithium anode surface.

A passivation layer was formed on the surface of the lithium anode with  $\text{P}_2\text{S}_5$  in the electrolyte. Figure V - 44C is a micrograph of the passivation layer. The chemical composition of the passivation layer was checked by Energy-Dispersive X-ray (EDX) spectroscopy. Signals of phosphorous (P) and sulfur (S) dominate the EDX spectrum. X-ray diffraction (XRD) patterns of the cycled anode confirmed that the passivation layer contains  $\text{Li}_2\text{S}$ ,  $\text{Li}_3\text{P}$ ,  $\text{Li}_4\text{P}_2\text{S}_6$ , and  $\text{Li}_3\text{PS}_4$ . The primary component is  $\text{Li}_3\text{PS}_4$ , which is an excellent solid electrolyte. These results inspired the design of all-solid Li-S using  $\text{Li}_3\text{PS}_4$  as the solid electrolyte.

**Development of all-solid Li-S batteries.** In the research of  $\text{P}_2\text{S}_5$  as an additive for Li-S batteries with liquid electrolytes, we found that  $\text{Li}_3\text{PS}_4$  is the primary component of the passivation layer on the lithium anode. This discovery triggered the idea of using  $\text{Li}_3\text{PS}_4$  as the solid electrolyte for all-solid Li-S batteries. A collaborating project (funded by Office of Science, Basic Energy Science), developed nanoporous  $\beta\text{-Li}_3\text{PS}_4$  that has an ionic conductivity 1000 times higher than that of the bulk  $\text{Li}_3\text{PS}_4$ . This fundamental discovery enables the practical use of  $\beta\text{-Li}_3\text{PS}_4$  as the solid electrolyte for Li-S batteries. The chemical and electrochemical compatibility of the nanoporous  $\beta\text{-Li}_3\text{PS}_4$  was investigated by cyclic voltammetry (CV). Shown in Figure V - 45A is the CV of lithium with nanoporous  $\beta\text{-Li}_3\text{PS}_4$  as the solid electrolyte and a gold counter electrode. The CV shows an excellent compatibility of Li metal with  $\beta\text{-Li}_3\text{PS}_4$  and a broad electrochemical window of 5V that is suitable for Li-S batteries. A cold pressing procedure was developed to assemble the all-solid batteries. One of the key requirements of an all-solid battery is that the solid electrolyte should be able to tolerate the mechanical stress

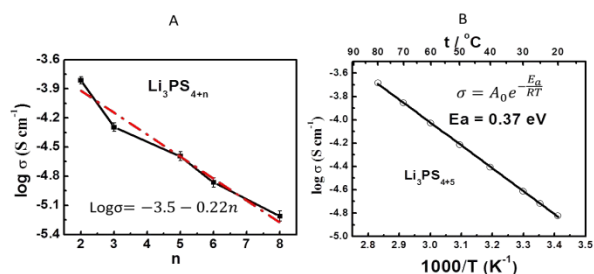
induced by volume changes and lithium dendrite formation during the battery cycling. A symmetric cell of  $\text{Li}|\text{solid electrolyte}|\text{Li}$  was employed to test the mechanical durability of the all-solid cell. The cell has been stably cycled over 1000 cycles with symmetric plating and stripping of lithium metal at a thickness of 1 micron. This test confirmed that the all-solid cell is highly durable.

Figure V - 45B shows representative stable cycles of the cell at 25 and 80°C. The ionic conductivity of the solid electrolyte is improved at the elevated temperature. Cell resistance has been significantly reduced at 80°C.



**Figure V - 45:** (A) A cyclic voltammogram of Li on nanoporous  $\beta\text{-Li}_3\text{PS}_4$  with a gold counter electrode. (B) Durability test of the solid electrolyte pellet in a symmetric cell configuration with both electrodes of metallic lithium. The thickness of solid electrolyte pellet is 500  $\mu\text{m}$ .

**Novel sulfur compounds for the cathode.** Sulfur and its discharge products are neither electronic conductors nor ionic conductors. In an all-solid cell, adding carbon to the cathode imparts its electronic conductivity. However, the ionic conductivity cannot be improved just by mixing sulfur with a solid electrolyte. As has been intensively studied in Li-ion batteries, the ionic conductivity of the cathode material is a limiting parameter for its cyclability. The same holds true in all-solid Li-S batteries. A conventional sulfur/carbon composite cannot be charged and discharged in an all-solid Li-S battery. A series of Li-ion conducting sulfur compounds with a general formula of  $\text{Li}_3\text{PS}_{4+n}$  ( $1 < n < 8$ ) were thus synthesized as cathode materials for all-solid Li-S batteries. The ionic conductivity of these compounds was measured by electrochemical impedance spectroscopy (EIS). Shown in Figure V - 46A is the ionic conductivity of these compounds as a function of sulfur atoms. In general, the ionic conductivity of these compounds decreases monotonically with the increase of sulfur atoms. Up to 60 wt. % of sulfur can be incorporated into these compounds with good ionic conductivity. The ionic conductivity of these new sulfur compounds are comparable to those of the cathode materials used in Li-ion batteries. Figure V - 46B shows the Arrhenius plot of  $\text{Li}_3\text{PS}_{4+n}$ . This sulfur compound has an ionic conductivity of  $3.0 \times 10^{-5} \text{ S cm}^{-1}$  at 25°C, which is 5 orders of magnitude higher than that of  $\text{Li}_2\text{S}$ , the discharge product of the sulfur cathode with an ionic conductivity of  $2.0 \times 10^{-10} \text{ S cm}^{-1}$  at room temperature. The activation energy of  $\text{Li}_3\text{PS}_{4+n}$  ( $n=5$ ) is 0.37 eV. The material has an ionic conductivity above  $10^{-4} \text{ S cm}^{-1}$  at 80°C.



**Figure V - 46:** (A) Ionic conductivity of sulfur-rich compounds as a function of sulfur numbers. (B) Arrhenius plot of  $\text{Li}_3\text{PS}_{4+5}$ .

The compound  $\text{Li}_3\text{PS}_{4+5}$  was selected for further electrochemical studies. Good cyclability was demonstrated at room temperature and an excellent cyclability was found at 60°C. A high specific capacity over 1200 mAh/g (550 mAh/g based on the mass of the cathode compound) was achieved after 300 cycles. This material has a good rate performance at 60°C. A capacity over 1200 mAh/g can be achieved at 0.1C. At a high cycling rate of 2C the cell retained a capacity of 700 mAh/g. (See Figure V - 47.)

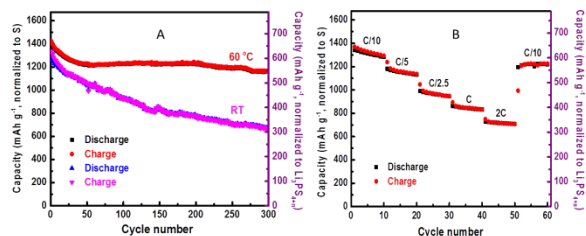


**Figure V - 47:** (A) Cycling performance of  $\text{Li}_3\text{PS}_{4+5}$  at room temperature and 60°C. (B) Rate performance at 60°C.

**Mechanistic studies of new cathode materials:** To understand the charge/discharge mechanism of these sulfur-rich compounds, Raman spectra (Figure V - 48) were taken on the pristine material and at the end of charge/discharge cycles. The peaks centered at 155 cm<sup>-1</sup>, 218/476 cm<sup>-1</sup>, and 180 cm<sup>-1</sup> of the pristine  $\text{Li}_3\text{PS}_{4+5}$  are attributed to the S-S bond. After the first discharge cycle, the characteristic peaks of the S-S bond at 155, 218/476, and 180 cm<sup>-1</sup> had vanished. New strong peaks at 375 and 418 cm<sup>-1</sup> and a weak peak at 283 cm<sup>-1</sup> appeared as evidence of the formation of  $\text{Li}_2\text{S}$  and  $\text{Li}_3\text{PS}_4$ . The discharge process breaks the S-S bond in  $\text{Li}_3\text{PS}_{4+5}$  and yields  $\text{Li}_2\text{S}$  and  $\text{Li}_3\text{PS}_4$ . When the cathode was charged again, S-S bond features reappeared with the disappearance of  $\text{Li}_2\text{S}$  and  $\text{Li}_3\text{PS}_4$  at the end of the charge cycle. The Raman spectra of the pristine material and the charged cathode are very much the same. These Raman spectra confirmed that the electrochemical insertion and removal of lithium ion in the cathode is a reversible reaction of  $\text{Li}_3\text{PS}_{4+5}$  to a mixture of  $\text{Li}_2\text{S}$  and  $\text{Li}_3\text{PS}_4$ .

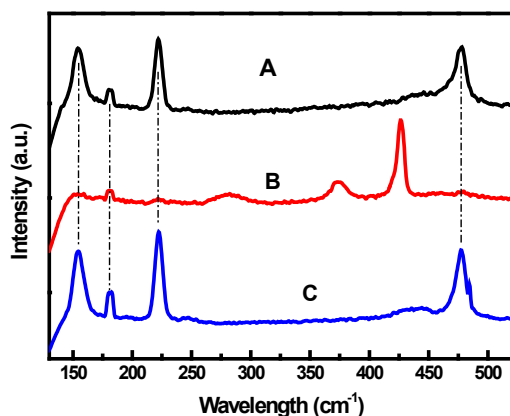


**Figure V - 48:** Raman spectra of  $\text{Li}_3\text{PS}_{4+5}$  (A) before cycling (black), (B) after discharge (red), and (C) after charge (blue). The signs of  $\diamond$ ,  $\nabla$ , and  $\star$  indicate the peaks of the S-S bond in  $\text{Li}_3\text{PS}_{4+5}$ , the P-S bond in  $\text{Li}_3\text{PS}_4$ , and  $\text{Li}_2\text{S}$ , respectively.

## Conclusions and Future Directions

Conventional Li-S batteries use organic liquid electrolytes that are required to have a high solubility of lithium polysulfide to enable the electrochemical cycling of the sulfur cathode. The dissolved sulfur species migrate inside the electrochemical cell and result in short cycle-life and low energy efficiency of Li-S batteries. Therefore, the poor performance of Li-S batteries is an intrinsic problem associated with the use of liquid electrolytes. Electrolyte additives such as  $\text{P}_2\text{S}_5$  mitigate the polysulfide shuttle problem and prolong the cycle-life of Li-S batteries to a certain extent. However, the short cycle-life cannot be completely solved if an effective protection of the lithium anode is missing. Apart from the cyclability problem of the sulfur cathode, the safe cycling of the metallic lithium anode in a liquid electrolyte is also a long-standing problem. Therefore, it is extremely challenging to make practical Li-S batteries using liquid electrolytes.

Replacing the liquid electrolyte with a solid electrolyte opens a new realm for the research of Li-S batteries. Particularly, the newly discovered thiophosphate-based solid electrolyte has an ionic conductivity higher than the current commercially used liquid electrolytes. There are tremendous opportunities to drive the Li-S battery technology to reality through innovative design of all-solid Li-S batteries. The use of the solid electrolyte eliminates the polysulfide shuttle and thus prevents the migration of sulfur. Meanwhile, the solid electrolyte enables the safe cycling of metallic lithium anode, which is a formidable challenge for batteries using liquid electrolytes. Critical problems of implementing all-solid Li-S batteries have been identified as the lack of appropriate solid electrolytes and cathode materials. The novel solid electrolyte lithium thiophosphate is an enabler of all-solid Li-S batteries. New series of sulfur-rich compounds have been discovered as sulfur cathode materials that have an unprecedented high ionic

conductivity among known electrochemically active sulfur compounds.

All-solid Li-S battery technology is in its infancy. Discovery of new materials with desirable electrochemical and mechanical properties will be the focus of future research. The immediate next step will be the optimization of cell components to achieve the best possible performance of all-solid Li-S batteries. In particular, there is much room for improvement in energy density by reducing the thickness of the solid electrolyte without affect the mechanical properties. Discovery of solid electrolytes with high ionic conductivity at room temperature will be a long journey that will benefit a large variety of energy storage technologies. All-solid batteries enable the safe operation of metallic lithium anodes. All-solid Li-S batteries have inherently high energy and safe design; they hold great promise for future development of electric vehicles.

Basic Energy Science project funded by the Materials Sciences and Engineering Division, Office of Science, US DOE.

### FY 2012 Publications/Presentations/Patent Applications

1. Z. Lin, Z. Liu, W. Fu, N. Dudney, and C. Liang, "Phosphorous Pentasulfide as a Novel Additive for High-Performance Lithium-Sulfur Batteries," *Advanced Functional Materials*, 2012. <http://dx.doi.org/10.1002/adfm.201200696>
2. "Carbon/Sulfur Nanocomposites and Additives for High-Energy Lithium Sulfur Batteries," 2012 DOE Annual Peer Review Meeting Presentation, May 2012.
3. "All-solid Li-S Batteries," 6th US-China Electric Vehicle and Battery Technology Workshop University of Massachusetts Boston, June 24, 2012.
4. "Nanostructured  $\beta$ -Li<sub>3</sub>PS<sub>4</sub> for All-Solid Lithium-Sulfur Batteries," 222<sup>nd</sup> ECS Meeting, Honolulu, HI, Oct. 7-11, 2012.
5. "Nanocrystalline Solid Electrolyte:  $\beta$ -Li<sub>3</sub>PS<sub>4</sub>," 222<sup>nd</sup> ECS Meeting, Honolulu, HI, Oct. 7-11, 2012.
6. "Lithium Sulfide Compositions for Battery Electrolyte and Electrode Coatings," C. Liang, Z. Liu, W. Fu, Z. Lin, N. Dudney, J. Howe, A. Rondinone; U.S. Patent Application N0. 13/463451; filed on May/3, 2012.

### Acknowledgment

This research at Oak Ridge National Laboratory, managed by UT Battelle, LLC, for the U.S. Department of Energy under contract DE-AC05-00OR22725, was sponsored by the Vehicle Technologies Program for the Office of Energy Efficiency and Renewable Energy. Parts of this research were performed at DOE user facilities including the Center for Nanophase Materials Sciences, the High Temperature Materials Laboratory, and the Shared Research Equipment (SHaRE) user facility. The solid electrolyte development was a collaboration with a

## V.B.10 Studies on High Energy Density Lithium-ion Electrodes (ORNL)

Jagjit Nanda (PI)  
Oak Ridge National Laboratory  
Materials Science and Technology Division  
Oak Ridge, TN 37934  
Phone: (865) 241-8361; Fax: (865) 574-4066  
E-mail: [nandaj@ornl.gov](mailto:nandaj@ornl.gov)

Collaborators:  
ORNL: Surendra Martha  
Ford Motor Co.: Andy Drews, Dawn Bernardi  
Toda America Ltd.

Start Date: October 2010  
Projected End Date: Continuing

density lithium-ion cathodes is a high priority area. Recent development of high voltage Mn-Ni spinel cathodes,  $\text{LiMn}_{1.5}\text{Ni}_{0.5}\text{O}_4$ , and Li-rich composite NMC cathodes are important steps in this direction. However, significant technical challenges still need to be addressed at the materials as well as the electrode level. These include: (i) structural and phase stability under continuous high voltage cycling ( $>4.5$  V); (ii) Mn dissolution leading to capacity fade; (iii) electronic and ionic transport limitations intrinsic to the electrode material; and (iv) higher 1<sup>st</sup> cycle irreversible capacity loss (ICL) due to interfacial issues and passive film formation. We report systematic studies on Lithium-rich NMC composite cathodes having nominal composition  $\text{Li}_{1.2}\text{Mn}_{0.525}\text{Ni}_{0.175}\text{Co}_{0.1}\text{O}_2$  and address the various technical barriers mentioned above.

### Objectives

- Investigate mechanisms behind capacity fade and voltage depression associated with high voltage Lithium-ion cathodes.
- Improve C-rate performance and cycle life of high voltage cathodes.
- Perform *ex situ* and *in situ* micro structural characterization to electrodes at various SOC and subjected to stress cycles; correlate structural changes to capacity fade and cycle life.

### Technical Barriers

Limited capacity utilization, transport and diffusion limited phenomenon at the electrode interface and bulk, C-rate performance limitation, transition metal dissolution, structural degradation.

### Accomplishments

- Improved interfacial stability and capacity utilization of Lithium rich NMC composite cathodes by coating a nanometer thick solid electrolyte, Lithium Phosphorus Oxynitride (LiPON).
- Improved the C-rate performance of Li-rich NMC by a factor of 3-5 (compared to uncoated electrode).
- Investigated the local structure of high voltage Li-rich NMC composition to study the structural phase transition associated with continuous high voltage cycling.



### Introduction

Current R&D efforts in lithium-ion batteries are directed towards increasing energy density with reduced cost and improved cycle-life and safety performance. Among other important factors, developing high energy

### Approach

We obtained high voltage Li-rich NMC cathode materials from a pilot scale facility of Toda-Kogyo Corporation (Japan) and fabricated them into electrodes using the slurry coating method. The electrodes were assembled into half cells (Li-metal as counter electrode) or full cells using modified graphite powders obtained from Conoco-Philips (now Philips 66). We performed life cycle studies in both coin cell as well as small pouch cell format to study capacity fade at room temperature as well as at 60 °C. The cells were cycled between 4.9-2.5 V using  $\text{LiPF}_6$  salt in an EC:DMC mixture. Apart from standard charge-discharge cycling, we also carried out impedance spectroscopy (EIS), cyclic voltammetry (CV) and various structural and surface spectroscopy techniques to characterize the electrodes to correlate between materials degradation and observed electrochemical performance. Materials modification such as nanoscale surface coating and electronic filler additives were also undertaken to improve the electrochemical performance. We summarize the main results below.

### Results

**Improving interfacial stability and capacity retention of high voltage Li-rich NMC composite cathodes using a nanometer scale surface coating of solid electrolyte. Lithium Phosphorous Oxynitride (LiPON).** High voltage Li-rich NMC compositions need to be cycled above 4.6 V for providing higher capacity ( $> 250$  mAh/g). This provides several challenges since most of the Li-ion electrolytes such as  $\text{LiPF}_6$  and carbonate solvents are unstable beyond 4.3 V. The electrolyte mixture decomposes on the surface of the cathode, producing thick insulating passivation films that significantly affect the capacity retention under continuous

high voltage cycling. LiPON was coated using rf-magnetron sputtering and the coating thickness was controlled by the deposition time. The microstructure of the Li-rich NMC particles remains unchanged after LiPON coating as shown in Figure V - 49. The Li-rich NMC composite comprises aggregated secondary particles having spherical morphology (Figure V - 49A) typically between 7-12  $\mu\text{m}$ .

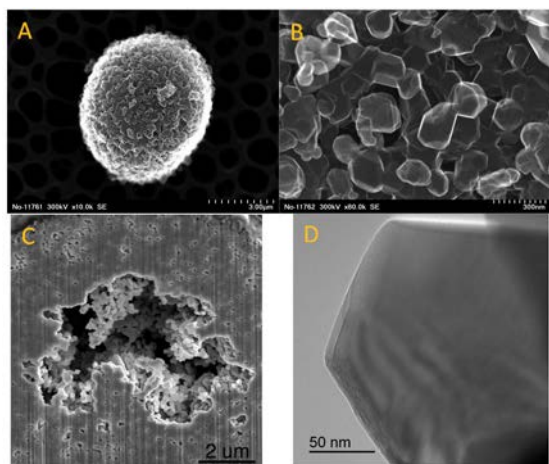
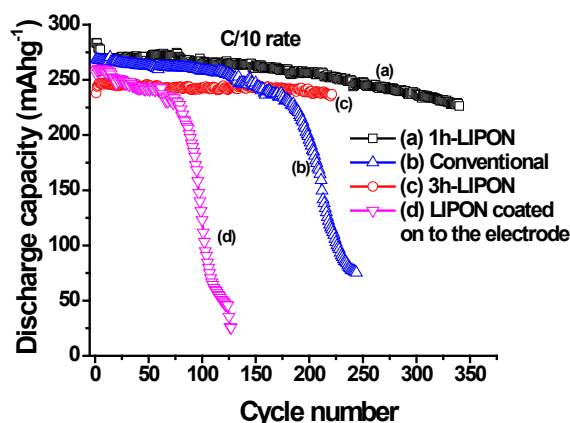


**Figure V - 49:** (a) A secondary Li-rich NMC composite cathode particle of spherical morphology (b) Faceted structures of primary Li-rich NMC particles having sizes in the range of 80-100 nm (c) Focused ion beam section of a secondary particle showing hollow interior core (d) A single Li-rich high voltage NMC primary particle with faceted surface.

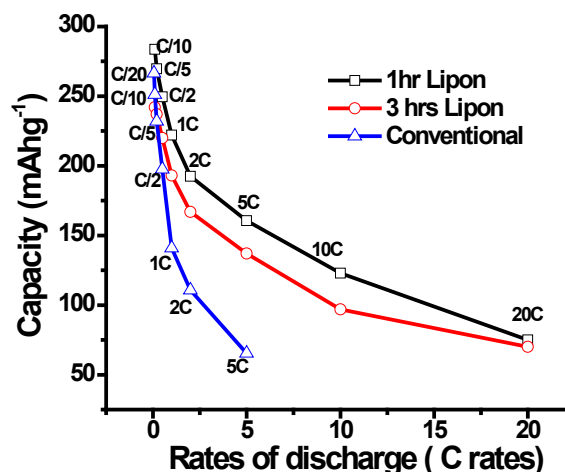
The secondary spherical aggregates comprise faceted primary particles in the range of 100 nm (Figure V - 49B). In order to explore the internal porosity of the spherical cathode particles, we performed focused ion beam (FIB) sectioning of an individual particle. The presence of internal pores and a hollow core enables liquid electrolyte to access internal primary particle surfaces for maximum capacity utilization. LiPON was coated around the particles for 1 hour and 3 hour durations. Typically, a 1 hour coating duration yielded a thickness of a few nanometers (nm) and a 3 hr coating resulted in an average LiPON thickness  $> 10$  nm. As a control, we also coated a thick LiPON layer ( $> 50$  nm) on the Li-rich NMC composite electrode surface to study the effect on the cycle life. X-ray Photoelectron spectroscopy (XPS) and electron microscopy results confirmed the presence of LiPON on the Lithium-rich NMC surface.

Figure V - 50a shows the capacity versus number of cycles for conventional (or pristine) and LiPON coated Li-rich NMC composite cathodes having nominal composition  $\text{Li}_{1.2}\text{Mn}_{0.525}\text{Ni}_{0.175}\text{Co}_{0.1}\text{O}_2$ . The electrode loading (thickness) and cycling conditions are kept similar for the coated and conventional electrodes for comparing the cycle-life performance. The results show a thin layer (1-2 nm) of LiPON coating has much improved capacity retention compared to thicker (3 hour) or conventional electrodes. The thicker coatings (Figure V - 50c and d) tend to be electrically insulating, blocking electron

transport on the surface and limiting capacity utilization. Detailed results are reported in [5].



**Figure V - 50:** Capacity vs. Cycle number for (a) 1h-LiPON coated Li-rich NMC, (b) uncoated Li-rich NMC, (c) 3h LiPON coated Li-rich NMC, and (d) LiPON coated on to the electrode surface.



**Figure V - 51:** Comparison of rate performance between conventional and LiPON coated high voltage Li-rich NMC composite cathode.

The presence of an optimally thick layer of LiPON at the interface also improves the C-rate performance of Li-rich NMC composite cathodes. Figure V - 51 shows the comparison of the rate performance between conventional and LiPON coated electrodes. The discharge capacity values are normalized to 2V for each of the current rates.

**Investigation on local structure changes during high voltage cycling of Li-rich NMC composite cathodes.** Under continuous high voltage cycling ( $>4.6\text{V}$ ), Li-rich NMC composite cathodes undergo a gradual loss in the discharge voltage plateau, resulting in a decrease in energy storage capacity. After hundreds of cycles the discharge profile gradually converges to a 3 V profile similar to spinels as shown in Figure V - 51. This

transition implies a gradual structural transformation from a layered-layered hexagonal structure to a spinel phase.

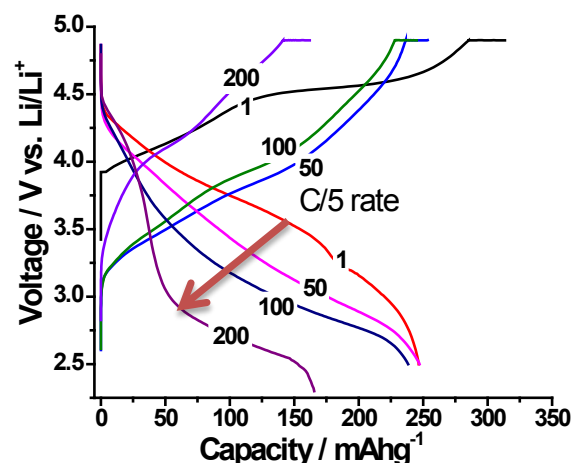


**Figure V - 52:** Voltage fade observed in Li-rich NMC composite cathodes as result of continuous high V cycling. The cells were cycled at room temperature between 4.9-2.5 volts using LiPF<sub>6</sub> in EC: DMC mixture.

We performed detailed high resolution transmission electron microscopy (HRTEM) and Electron Energy Loss Spectroscopy (EELS) at the atomic scale to characterize pristine (Figure V - 53) and cycled Li-rich NMC cathodes (Figure V - 54) to monitor local changes in transition metal (TM) coordination around Li atoms during cycling.

The majority of pristine Li-rich NMC composite particles have a R3m hexagonal phase as shown in the electron diffraction pattern (Figure V - 53(C)). However, there are local regions (marked by a red box in Figure V - 53(A)) showing Li<sub>2</sub>MnO<sub>3</sub> domains which have different local symmetry with respect to TM metal ordering (Figure V - 53(B)&(D)) corresponding to a monoclinic phase. After 200 high voltage cycles (as shown in Figure V - 51), we see a significant change in local structure. The majority of the sample does not exhibit the R3m phase, but rather a local structure representative of spinel (Figure V - 52(B)-(D)). Further, EELS spectrum of the cycled sample showed a Ni and Mn rich surface. Detailed studies are continuing to understand the diffusion of TM metal cations in Li-rich compositions.

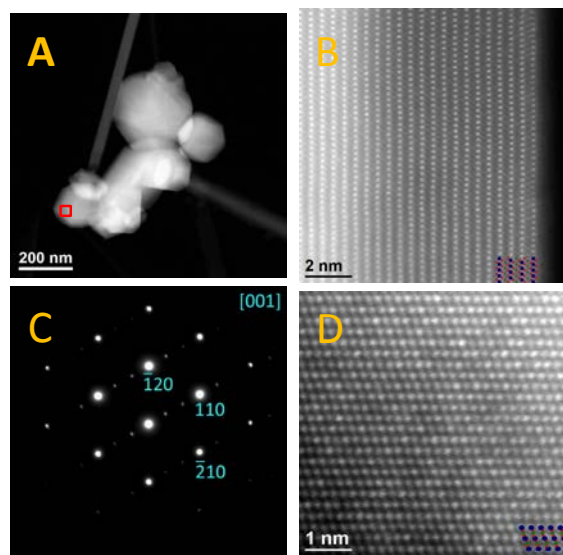


**Figure V - 53:** HRTEM images of pristine Li-rich NMC composite cathodes showing the majority of particles belonging to a hexagonal R3m structure.

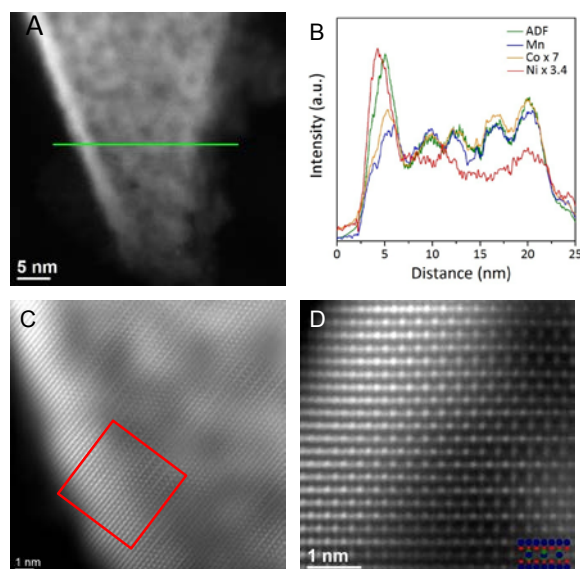


**Figure V - 54:** HRTEM and EELS study of cycled Li-rich NMC composite cathodes

## Conclusions and Future Directions

We have made significant improvements in the rate performance and interfacial stability of high voltage Li-rich composite cathodes. A coating of a solid electrolyte layer (LiPON) can significantly improve the charge transfer at the interface. Improved interfacial stability leads to better capacity retention at higher C-rates. EIS studies (not discussed here) also corroborate with our electrochemical performance results. The next phase of work involves stabilization of the Li-rich NMC phase against structural transitions and thereby suppressing the voltage fade phenomenon. Efforts will be directed towards

isovalent cation doping strategies that will stabilize the structure and/or prevent TM metal dissolution.

## FY 2012 Publications/Presentations

### Journal Publications

1. S. K. Martha, J. Nanda, Gabriel M. Veith, N. J. Dudney, Electrochemical and Interfacial Studies of High-Voltage Lithium-Rich Composition:  $\text{Li}_{1.2}\text{Mn}_{0.525}\text{Ni}_{0.175}\text{Co}_{0.102}$ , *J. Power Sources*, 199, 220, (2012).
2. S. K. Martha, Jagjit Nanda, G. M. Veith and N. J. Dudney, Surface studies on high voltage lithium-rich composition  $\text{Li}_{1.2}\text{Mn}_{0.525}\text{Ni}_{0.175}\text{Co}_{0.102}$ , *J. Power Sources*, 216, 179 (2012).
3. S. K. Martha, N. J. Dudney, J. Kiggans and Jagjit Nanda, Electrochemical Stability of Carbon Fibers Compared to Aluminum as Cathode Current Collectors for Lithium-Ion Batteries, *J. Electrochem. Soc.* 159, (10), A1-A7 (2012).
4. G. Veith, Jagjit Nanda, L. H. Delmau, N. J. Dudney Influence of Lithium Salts on the Discharge Chemistry of Li-Air Cells *J. Phys. Chem. Lett.* 3, 1242 (2012).
5. S. K. Martha, J. Nanda, Y. Kim, R.R. Unocic, S. Pannala and N. J. Dudney Solid Electrolyte Coated High Voltage Layered-Layered Lithium-rich Composite Cathodes:  $\text{Li}_{1.2}\text{Mn}_{0.525}\text{Ni}_{0.175}\text{Co}_{0.102}$ , Manuscript to be submitted to *Energy & Environ. Sci* (2012).

### Conference/ Meeting

1. 2012 DOE Annual Peer Review Meeting Presentation, May 2012 Washington DC.
2. Electrochemistry driven structural transitions in high voltage Lithium rich cathodes, DOE-EPSCOR Annual Meeting, Brown University, June 1st 2012 (invited).
3. Metal free binder free silicon carbon fiber composite anode architecture, J. Nanda, S. K. Martha, S. Pannala, N. J. Dudney, Electronic Materials and Applications 2012, American Ceramic Society, January 17-19th 2012 Orlando Florida.
4. Hierarchical Models for Batteries: Overview with Some Case Studies, S. Pannala, S. Allu, S. K. Martha,
5. J. Nanda et al., Advanced Automotive Battery Conference (AABC), Feb, 2012 Orlando, FL USA
6. A micro-macroscopic volume-averaged model for batteries, S. Pannala, P. Mukherjee, J. Nanda et al. Electronic Materials and Applications 2012, American Ceramic Society, January 17-19th 2012 Orlando Florida.
7. Improved Electrochemical Performance of High Energy Layered-Layered Mixed Oxide Lithium Rich Composition, S. K. Martha, J. Nanda, Nancy J.

Dudney, G. Veith, C. Narula, S. Pannala ECS Fall Meeting 2011 Oct 9th-14th Boston USA.

8. Silicon-Carbon Fiber Composite Li-Ion Electrode without Passive Components, S. K. Martha, J. Nanda, W. Porter and N. J. Dudney, ECS Fall Meeting, 2011 October 9-14th Boston, USA

## V.B.11 High -capacity Composite Cathode Materials: New Synthesis Routes and Structures (ANL)

Michael Thackeray  
Argonne National Laboratory  
9700 South Cass Avenue  
Argonne, IL 60439  
Phone: (630) 252-9184; Fax: (630) 252-4176  
E-mail: [thackeray@anl.gov](mailto:thackeray@anl.gov)

Collaborators:  
ANL: J. R. Croy, D. Kim, R. Benedek, V. G. Pol,  
S. V. Pol, C. S. Johnson, J. T. Vaughey,  
K. G. Gallagher, M. Balasubramanian (APS)  
LBNL: V. Battaglia

Start Date: October 1, 2011  
Projected End Date: September 30, 2015

### Objectives

- Design high capacity, high-power and low cost cathodes for PHEVs and EVs.
- Improve the design, composition and performance of Mn-based cathodes.
- Explore novel processing routes to prepare advanced electrodes with effective architectural designs.
- Use atomic-scale modeling as a guide to identify, design and understand the structural features and electrochemical properties of advanced cathode materials.

### Technical Barriers

- Low energy density
- Poor low temperature operation
- Abuse tolerance limitations

### Technical Targets (USABC - End of life)

- 142 Wh/kg, 317 W/kg (PHEV 40 mile requirement)
- Cycle life: 5,000 cycles
- Calendar life: 15 years

### Accomplishments

- Identified promising electrode compositions and syntheses to achieve high capacity electrodes with stable surfaces and high rate capabilities.

- Identified changes to  $\text{Li}_2\text{MnO}_3$ -like environments as a possible trigger for continued voltage fade on high voltage cycling.
- Evaluated the effect of coatings on voltage fade.

◇ ◇ ◇ ◇ ◇

### Introduction

$\text{Li}_2\text{MnO}_3$ -stabilized composite electrode structures, such as ‘layered-layered’  $x\text{Li}_2\text{MnO}_3 \bullet (1-x)\text{LiMO}_2$  ( $M=\text{Mn}, \text{Ni}, \text{Co}$ ), ‘layered-spinel’  $x\text{Li}_2\text{MnO}_3 \bullet (1-x)\text{LiM}_2\text{O}_4$  and even more complex ‘layered-layered-spinel’  $y\{x\text{Li}_2\text{MnO}_3 \bullet (1-x)\text{LiMO}_2\} \bullet (1-y)\text{LiM}_2\text{O}_4$  systems are receiving international attention because they can provide rechargeable capacities between 200 and 250 mAh/g between 4.6 and 2.0 V vs. lithium. They offer, today, perhaps the best opportunity to make a significant improvement to the energy output and to improve the abuse tolerance of state-of-the-art, commercial lithium-ion cell products in order to meet or exceed the 40-mile electric range targets of PHEVs. These manganese-rich composite cathode structures have to be electrochemically activated above 4.4 V in order to access the high capacity. Unfortunately, this process compromises the rate capability of these electrodes, which also suffer from voltage decay on cycling, thereby compromising the energy and power output of the cells and preventing their implementation in practical systems. This project directly addresses these limitations and challenges. A novel processing route using  $\text{Li}_2\text{MnO}_3$  as a precursor to synthesize composite electrode structures is advocated: it is based on promising results obtained over the past few months. The technique is simple, versatile and seemingly low cost; it offers the possibility of opening the door to wide exploitation and, in particular, of synthesizing and tailoring composite electrode structures, including new systems, thereby enhancing the electrochemical properties of lithium-ion cells to meet the performance targets of PHEVs.

### Approach

- Exploit the concept, and optimize the performance, of structurally-integrated, high-capacity electrodes, particularly ‘layered-layered’  $x\text{Li}_2\text{MnO}_3 \bullet (1-x)\text{LiMO}_2$  ( $M=\text{Mn}, \text{Ni}, \text{Co}$ ) and ‘layered-layered-spinel’  $y\{x\text{Li}_2\text{MnO}_3 \bullet (1-x)\text{LiMO}_2\} \bullet (1-y)\text{LiM}_2\text{O}_4$  electrodes.

- Explore new processing routes to prepare composite electrodes that provide acceptable capacity, power and life.
- Design effective surface structures to protect the underlying metal oxide particles from the electrolyte and to improve their rate capability when charged at high potentials.
- Use first principles modeling to aid the design of bulk and surface cathode structures and to understand electrochemical phenomena.

## Results

### Development of New Synthesis Method.

$x\text{Li}_2\text{MnO}_3 \cdot (1-x)\text{MO}_2$  ( $M = \text{Ni}, \text{Co}, \text{Mn}$ ) composite structures offer the possibility of significantly improving current state of the art lithium ion battery technology. Capable of attaining  $\sim 250$  mAh/g, these  $\text{Li}_2\text{MnO}_3$ -stabilized composites may be formed with a variety of integrated architectures such as ‘layered-layered’  $x\text{Li}_2\text{MnO}_3 \cdot (1-x)\text{LiMO}_2$  ( $M = \text{Mn}, \text{Ni}, \text{Co}$ ), ‘layered-spinel’  $x\text{Li}_2\text{MnO}_3 \cdot (1-x)\text{LiM}_2\text{O}_4$  and more complex ‘layered-layered-spinel’  $y\{x\text{Li}_2\text{MnO}_3 \cdot (1-x)\text{LiMO}_2\} \cdot (1-y)\text{LiM}_2\text{O}_4$ . Despite the advantages of such high capacities, these composites suffer from a continuous decrease in energy output brought about by a decaying voltage profile on high voltage cycling. This phenomenon, known as voltage fade, is believed to be a consequence of transition metal (TM) migration from TM to lithium layers and may also be exacerbated by the first-cycle activation process, e.g., oxygen loss and surface damage. This work is based on a newly developed approach whereby  $\text{Li}_2\text{MnO}_3$  is used as a layered, lithium-manganese-oxide ‘template’ in an ion-exchange process to form unique composite structures, the electrochemistry of which depends on the particular synthesis conditions. Figure V - 55a shows electrochemical cycling data of electrodes made from  $\text{Li}_2\text{MnO}_3$  precursors, ion-exchanged with nickel in a solution of nitric acid and nickel nitrate to target a  $0.5\text{Li}_2\text{MnO}_3 \cdot 0.5\text{LiNi}_{0.5}\text{Mn}_{0.5}\text{O}_2$  composition followed by annealing at  $450^\circ\text{C}$ .

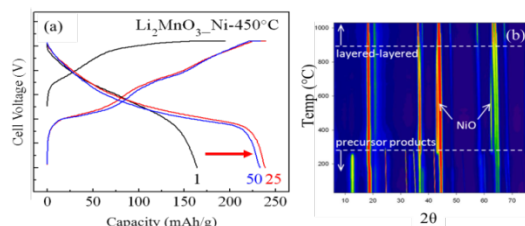


**Figure V - 55:** (a) Cycling of  $0.5\text{Li}_2\text{MnO}_3 \cdot 0.5\text{LiNi}_{0.5}\text{Mn}_{0.5}\text{O}_2$  synthesized with a  $\text{Li}_2\text{MnO}_3$  template and annealed at  $450^\circ\text{C}$ ; (b) *In situ* XRD of a  $\text{Li}_2\text{MnO}_3$ -based composite showing the incorporation of a NiO component on heating.

Clear differences in electrochemical performance were observed for samples annealed at  $450^\circ\text{C}$  vs. high temperature annealing. Figure V - 55b shows *in situ* X-ray diffraction data of the annealing processes undertaken after

the ion-exchange step. From these data it can be seen that low temperature samples contain a NiO component. These data reveal the discovery of a new class of ‘layered-rocksalt’ composite structures. The versatility of this technique to form a variety of composite structures is being explored to advance the understanding of structure-property relationships related to voltage fade.

Figure V - 56a shows rate data of a  $0.5\text{Li}_2\text{MnO}_3 \cdot 0.5\text{LiNi}_{0.5}\text{Mn}_{0.5}\text{O}_2$  electrode made from an ion-exchanged  $\text{Li}_2\text{MnO}_3$  precursor template and annealed at  $950^\circ\text{C}$ .

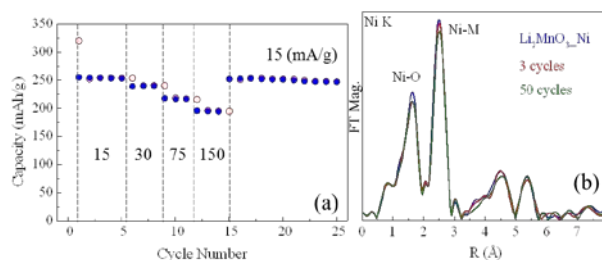


**Figure V - 56:** (a) Rate data of a  $\text{Li}_2\text{MnO}_3$ -based  $0.5\text{Li}_2\text{MnO}_3 \cdot 0.5\text{LiNi}_{0.5}\text{Mn}_{0.5}\text{O}_2$  cathode; (b) Ni K-edge EXAFS of fresh and cycled cathodes revealing the stability of the local nickel environment.

The data shows that the electrode provides 250 mAh/g at  $\sim 1\text{C}/15$ , and close to 200 mAh/g at  $\sim 1\text{C}$ . In order to understand the structure of these electrodes with cycling, X-ray absorption data were obtained. Manganese K-edge data (not shown) revealed that the local environment of Mn is that of  $\text{Li}_2\text{MnO}_3$  and that it undergoes significant changes during the initial cycles, particularly after first-cycle activation. In contrast, the Ni-K EXAFS data in Figure V - 56b reveals an unexpectedly stable Ni environment even after 50 high voltage cycles (4.6 – 2.0 V). Thus, the  $\text{Li}_2\text{MnO}_3$  template may allow the formation of a unique ordering of Mn and Ni conducive to the structural stability of local domains. Furthermore, it seems likely that the voltage fade is directly related to the activation process of the  $\text{Li}_2\text{MnO}_3$  component and is set in motion by structural and chemical changes which occur during that process and, in turn, affect the interior of Li- and Mn-rich  $\text{Li}_2\text{MnO}_3$ -like domains on extended cycling. Future work will focus on how  $\text{Li}_2\text{MnO}_3$  templates can be used to influence domain size, composition, and ordering to further stabilize  $\text{Li}_2\text{MnO}_3$ -based composite structures.

**Stabilization of Electrode-Particle Surfaces.** The attractive capacities achieved by composite electrode structures are only attainable if the first-cycle activation process is accompanied by oxygen loss from electrode-particle surfaces. This process induces surface damage and the rearrangement and migration of the transition metal ions, leading ultimately to poor rate performance and contributions to voltage fade. A unique sonochemical coating method was therefore explored in an attempt to combat the effects of voltage fade and first-cycle processes that affect high rate performance.

Figure V - 57a shows a 2.6 wt% nano-coating of ZrO<sub>2</sub> deposited on the surface of a standard 0.5Li<sub>2</sub>MnO<sub>3</sub>•0.5LiNi<sub>0.44</sub>Co<sub>0.25</sub>Mn<sub>0.31</sub>O<sub>2</sub> (LMR-NMC) cathode material. The coating was deposited by sonochemical decomposition of a Zr(NO<sub>3</sub>)<sub>3</sub> precursor in a solvent-bath of water and ethanol containing the LMR-NMC particles, followed by annealing at 450°C.

Cycling tests were performed at room temperature (Figure V - 57b), and 55°C (Figure V - 57c). Although coated and uncoated materials showed similar performance at low current rates, the coated materials showed marked improvements at higher rates. Despite this significant improvement in rate performance, indicating enhanced surface stability, a continuing decay of the voltage profile with cycling was still observed.

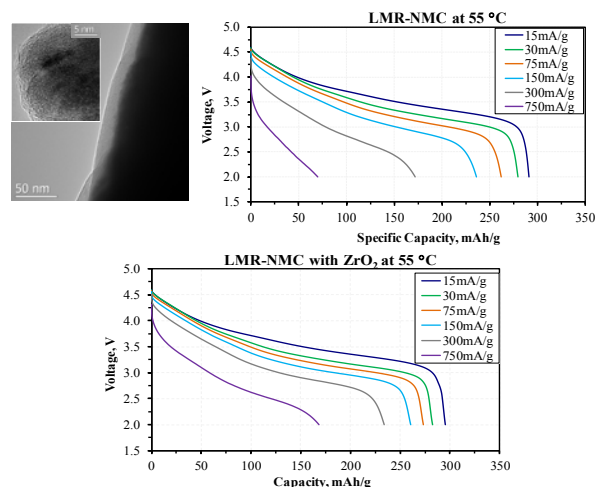


**Figure V - 57:** (a) HRTEM images of ZrO<sub>2</sub>-coated LMR-NMC. Rate data of Li cells with (b) uncoated and (c) coated electrodes.

A sonochemical coating has proven to be both a simple and versatile technique for coating lithium metal oxide cathode materials. Figure V - 58a shows rate data for a 0.5Li<sub>2</sub>MnO<sub>3</sub>•0.5LiMn<sub>0.5</sub>Ni<sub>0.5</sub>O<sub>2</sub> cathode synthesized using the above-mentioned Li<sub>2</sub>MnO<sub>3</sub> template technique and coated sonochemically with Al<sub>2</sub>O<sub>3</sub>. The electrode provides 250 mAh/g at low rates with no difference in early cycle performance compared to uncoated electrodes, i.e., no special formation cycles were required. Furthermore, first-cycle efficiencies of Al<sub>2</sub>O<sub>3</sub>-coated samples were improved to 85% (79% for uncoated samples). At a 150 mA/g rate (~1C), the electrode delivers ~210 mAh/g, ~20 mAh/g more than uncoated materials at the same rate. However, clear evidence of voltage fade with cycling is still observed. Nevertheless, the structure quickly reaches a fairly stable cycling profile consistent with the EXAFS data in Figure V - 56b and, despite major structural changes during the early cycles, the data in Figure V - 58b shows that the Al<sub>2</sub>O<sub>3</sub>-coated electrode maintains ~230 mAh/g above 3 V over the first 12 cycles.

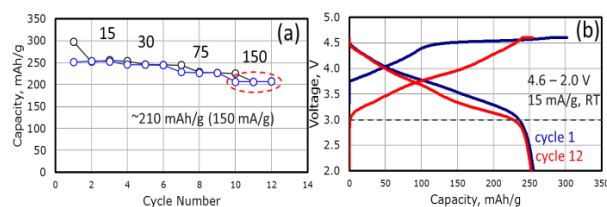


**Figure V - 58:** (a) Rate data of Al<sub>2</sub>O<sub>3</sub>-coated 0.5Li<sub>2</sub>MnO<sub>3</sub>•0.5LiMn<sub>0.5</sub>Ni<sub>0.5</sub>O<sub>2</sub>; (b) Voltage profiles of the sample in (a) showing ~230 mAh/g above ~3.0 V after 12 cycles to 4.6 V.

**Theory: Dissolution of LiMn<sub>2</sub>O<sub>4</sub>.** Dissolution of lithium manganate spinel electrodes in hydrofluoric acid is a significant source of degradation in lithium-ion batteries based on that cathode material. To elucidate the mechanism by which the acid promotes dissolution of LiMn<sub>2</sub>O<sub>4</sub>, constrained first principles MD was performed for simulation cells that comprised a spinel slab embedded in aqueous hydrofluoric acid. Initial work has focused on the effect of F ions on the energy required to detach Mn ions from a (110) surface, for which the low coordination number (3) makes surface Mn ions particularly vulnerable to dissolution. Whereas in neutral water, an energy greater than 1 eV is required to break the first bond of the dissolving Mn with the substrate, F ions strongly adsorb to Mn ions at a Mn-terminated (110) surface, which lowers the barrier substantially. The reduction to the divalent state of Mn as a member of a MnF complex occurs much closer to the surface than in the case of Mn<sup>3+</sup> ion in neutral water. Simulation of the dissolution of Mn ions with what may be the more typical coordination number CN=4 are in progress.

## Conclusions and Future Directions

- Li<sub>2</sub>MnO<sub>3</sub>-based synthesis has been verified as a versatile approach to fabricate structurally-integrated, high-capacity electrodes notably, ‘layered-layered’ xLi<sub>2</sub>MnO<sub>3</sub>•(1-x)LiMO<sub>2</sub> (M=Mn, Ni, Co) and ‘layered-layered-spinel’ y{xLi<sub>2</sub>MnO<sub>3</sub>•(1-x)LiMO<sub>2</sub>}•(1-y)LiM<sub>2</sub>O<sub>4</sub>.
- X-ray absorption data reveal that Li<sub>2</sub>MnO<sub>3</sub>-based, Ni-Mn systems show a unique stability of the local Ni environment. In addition, the continued decay of the voltage profile with cycling is a likely consequence of the changes which occur to the local Mn environments of Li<sub>2</sub>MnO<sub>3</sub>-like domains; initiated by the first-cycle activation process.
- A sonochemical coating method has proven to be easy and versatile, allowing for stable, uniform coatings on the surface of cathode particles. These coatings improve the rate capability and first-cycle efficiencies of composite electrode structures.
- Despite the electrochemical advantages associated with uniform coatings, protecting particle surfaces alone does not successfully mitigate voltage fade;

rather inherent bulk phenomena are responsible for the observed voltage fade in these electrodes.

- MD simulations have revealed that F<sup>-</sup> ions associated with undercoordinated, Mn surface atoms in LiMn<sub>2</sub>O<sub>4</sub> lower the barrier to Mn dissolution.
- Continue to explore the complex relationship between integrated composite structures when synthesized from a Li<sub>2</sub>MnO<sub>3</sub> precursor (e.g., ‘layered-layered’ structures) and their electrochemical properties.
- Explore other layered lithium-metal-oxide systems as precursors to control domain size and stability of unique composite cathode structures, in particular, the size and stabilization of Li<sub>2</sub>MnO<sub>3</sub>-like domains.
- Evaluate sonochemical coatings against wet-chemical and atomic layer deposition methods to identify optimum materials for protecting composite particle surfaces.
- Continue the use of theory to understand surface degradation in manganese-based cathode materials.

### FY 2012 Publications/Patents/Presentations

1. Jason R. Croy, M. Balasubramanian, Donghan Kim, S.-H. Kang, and M. M. Thackeray, “Designing High-Capacity, Lithium-Ion Cathodes Using X-ray Absorption Spectroscopy,” *Chem. Mater.* **23**, 5415 (2011).
2. D. Shin, C. Wolverton, Jason R. Croy, M. Balasubramanian, S.-H. Kang, C. M. Lopez Rivera, and M. M. Thackeray, “First-Principles Calculations, Electrochemical and X-ray Absorption Studies of Li-Ni-PO<sub>4</sub> Surface-Treated xLi<sub>2</sub>MnO<sub>3</sub> · (1-x)LiMO<sub>2</sub> (M = Mn, Ni, Co) Electrodes for Li-Ion Batteries,” *JES* **159**, A121 (2012).
3. Jason R. Croy, M. Balasubramanian, Donghan Kim, K. Gallagher, S.-H. Kang, M. M. Thackeray, “Countering the Voltage Decay in High Capacity xLi<sub>2</sub>MnO<sub>3</sub>·(1-x)LiMO<sub>2</sub> Electrodes (M=Mn, Ni, Co) for Li-Ion Batteries,” *JES* **159**, A781 (2012).
4. M. M. Thackeray, “Manganese Oxides for Lithium Batteries,” *J.B. Goodenough Symposium*, Austin, TX, October 2011.
5. J. R. Croy, M. Balasubramanian, D. Kim, S.-H. Kang and M. M. Thackeray, “Structural and Electrochemical Effects of LiNiPO<sub>4</sub> as a Surface Treatment for xLi<sub>2</sub>MnO<sub>3</sub>·(1-x)LiCoO<sub>2</sub> Electrodes,” *ISIPM 7*, Argonne, IL, November 2011.
6. J. R. Croy, D. Kim, S.-H. Kang, M. Balasubramanian, M.M. Thackeray, “Decoding the Structure of Composite, High-Capacity, Li-Ion Cathodes Using X-ray Absorption Spectroscopy,” *Argonne National Laboratory Postdoctoral Seminar*, Argonne, IL, March 2012.
7. M. M. Thackeray, J. R. Croy S.-H. Kang, D. Kim, K. G. Gallagher, “Recent Advances in High Capacity ‘Composite’ Electrode Structures for Li-ion Batteries,” *MRS Symposium*, San Francisco, CA, April 2012.
8. J. R. Croy, D. Kim, S.-H. Kang, M. Balasubramanian, M.M. Thackeray, “Decoding the Structure of Composite, High-Capacity, Li-Ion Cathodes Using X-ray Absorption Spectroscopy,” *221st Meeting of The Electrochem. Soc.*, Seattle, WA, May 2012.
9. M. M. Thackeray, J. R. Croy, S. Pol, R. Benedek, D. Kim, K. Ryan, M. Balasubramanian, Y. Ren, “Design and Evaluation of High-Capacity Cathodes,” *2012 Annual Merit Review*, Washington, D.C., May 2012.
10. M. M. Thackeray, J. R. Croy, D. Kim, G. Sandi-Tapia, K. G. Gallagher and M. Balasubramanian, “High Capacity Li- and Mn-rich Metal Oxide Electrodes: Challenges and Opportunities,” *IMLB 16*, Jeju, Korea, June 2012.
11. M. M. Thackeray, J. R. Croy, S. Pol, M. Balasubramanian, D. Kim and S.-H. Kang, “Structure, Surfaces & Electrochemistry of High-Capacity Cathodes for Li-Ion Batteries,” *IMLB 16*, Jeju Korea, June 2012.
12. J. R. Croy, M. Balasubramanian, D. Kim, S.-H. Kang, and M. M. Thackeray, Challenges of Composite, High-Capacity, “Li-Ion Cathodes, Advanced Photon Source User Science Seminar,” Argonne, IL, July 2012.

## V.B.12 *In Situ* Solvothermal Synthesis of Novel High Capacity Cathodes

(BNL)

Jason Graetz  
Brookhaven National Laboratory (BNL)  
Sustainable Energy Technologies Department  
Upton, NY, 11973  
Phone: (631) 344-3242; Fax: (631) 344-7905  
E-mail: [graetz@bnl.gov](mailto:graetz@bnl.gov)

Start Date: October 1, 2011  
Projected End Date: September 30, 2015

### Objectives

- Develop low-cost cathode materials that offer high energy density (>660 Wh/kg) and electrochemical properties (cycle life, power density, safety) consistent with USABC goals.

### Technical Barriers

Present day Li-ion batteries are incapable of meeting the 40-mile all-electric-range within the weight and volume constraints established for PHEVs by DOE and the USABC. Higher energy density cathodes are needed for Li-ion batteries to be widely commercialized for PHEV applications.

The development of new, safer lithium batteries requires new tools to better understand the physical and chemical processes that occur during cycling and the ability to predict and ultimately control the key electrochemical properties such as capacity (power and energy density), durability (calendar and cycle life), abuse tolerance (safety characteristics) and cost.

### Technical Targets

- Higher energy density cathodes.
- Lower cost.

### Accomplishments

- A new *in situ* capillary reactor (second generation) was developed to study hydrothermal synthesis at higher reaction pressures and temperatures.
- Two different procedures were identified for the synthesis of high-capacity copper vanadium oxides ( $\text{Cu}_{0.95}\text{V}_2\text{O}_5$ ) cathodes.
- Hydrothermal synthesis reactions of  $\text{LiFe}_x\text{Mn}_{1-x}\text{PO}_4$  and  $\text{Cu}_x\text{V}_2\text{O}_5$  were characterized using *in situ* reactor.

- Preliminary morphological and structural characterization of as-synthesized and (de)lithiated  $\text{Cu}_{0.95}\text{V}_2\text{O}_5$ .

◇ ◇ ◇ ◇ ◇

### Introduction

The synthesis of new lithium cathodes has proven to be slow and difficult since the preparation of new compounds or materials with unique properties often relies on trial and error. There are a variety of synthesis parameters (precursor concentration, temperature, pressure, cation choice and reaction time) each of which have a strong influence on the material properties (morphology, particle size, crystal structure) and electrochemical performance (e.g., capacity, rate capability, durability). Most solution-based reactions are carried out in a sealed autoclave and therefore the reactor is a black box – it is known what goes in and what comes out, but little about intermediate phases and the overall reaction pathway. The ability to probe synthesis reactions in real time would reveal which intermediate phases form and when, and provide a better understanding of how temperature, pressure, time and the initial concentrations affect the reaction pathways. This would allow us to optimize the reaction – increasing yield, decreasing waste (thereby lowering cost) and ultimately “dialing in” the desired phase and material properties.

### Approach

In this effort, specialized *in situ* reactors designed to investigate solvothermal synthesis reactions in real-time using synchrotron techniques were developed and utilized. *In situ* x-ray diffraction (XRD) and x-ray absorption/emission spectroscopy (XAS/XES) was used to investigate crystal growth and changes in chemical bonds while leaving the reaction undisturbed. This approach provides a real-time measurement of how reaction conditions affect nucleation and crystallization, bonding, particle size, morphology and defect concentration. In addition, *in situ* measurements reveal the formation crystalline intermediate and short-lived phases formed during the reaction without the need for quenching. These new tools and insights are being used to prepare novel high energy density lithium cathode materials.

### Results

**Development and testing of *in situ* reactor.** A new *in situ* capillary reactor was developed that is capable of

accommodating higher reaction pressures and temperatures and is suitable for a wide range of hydrothermal reactions. Last year an earlier version of this reactor was used to demonstrate a “proof of concept”, but it was only suitable for low temperature and pressure reactions, which limited its utility. The second-generation reactor (shown in Figure V - 59a) is considerably more flexible and makes use of a larger diameter quartz capillary. In addition to higher pressures and temperatures, this new design can accommodate both soluble and insoluble precursors, and is therefore suitable for a variety of reactions. Since a number of synthesis reactions of interest involve the release of gas, the reactor must be properly sealed after loading and high temperature sealants were identified for this purpose. In order to maintain a homogeneous reaction mixture, a small motor was used to rotate the capillary during the reaction. The heating gun was replaced with a coil wire to provide more uniform heating of the sample.

The *in situ* reactor was used to study the hydrothermal synthesis of  $\text{LiFe}_x\text{Mn}_{1-x}\text{PO}_4$  ( $0 \leq x \leq 1$ ) cathodes. Figure V - 59b shows the time-resolved XRD patterns acquired between 25°-250°C during the formation of  $\text{LiFe}_{0.4}\text{Mn}_{0.6}\text{PO}_4$ , which was found to follow a similar reaction path as that of  $\text{LiFePO}_4$  but much different than that of the pure Mn system, in which no phase transformation was observed. Interestingly, an unidentified phase (Li-Fe-Mn-O) was formed at ~100°C, which gradually transformed to  $\text{LiFe}_{0.4}\text{Mn}_{0.6}\text{PO}_4$  at 180°C.

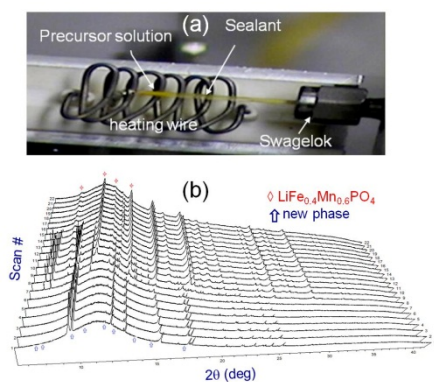


**Figure V - 59:** (a) Capillary reactor for investigating hydrothermal synthesis reactions by *in situ* x-ray diffraction. (b) Time-resolved XRD patterns acquired during the hydrothermal synthesis of  $\text{LiFe}_{0.4}\text{Mn}_{0.6}\text{PO}_4$  (25 - 240°C).

**Synthesis of  $\text{Cu}_{0.95}\text{V}_2\text{O}_5$  cathode.** FY 2012 efforts were focused primarily on developing methods for synthesis of high-quality  $\text{Cu}_{0.95}\text{V}_2\text{O}_5$  (CVO). A conventional hydrothermal synthesis was performed in deionized water at 200°C for 10 hrs:



where the reducing agent (RA) was acetophenone. Figure V - 60(a) shows the typical scanning electron microscopy (SEM) image of the as-synthesized CVO. The

individual particles have a rod-like morphology with dimensions of 1-2  $\mu\text{m}$  in the long direction and ~ 100 nm in the short direction. The crystal structure of the as-synthesized material was characterized using synchrotron x-ray diffraction (Figure V - 60b). The lattice parameters were determined from a profile fit to data giving  $a = 11.765 \text{ \AA}$ ,  $b = 3.694 \text{ \AA}$ ,  $c = 8.971 \text{ \AA}$ ,  $\alpha = \gamma = 90^\circ$ ,  $\beta = 111.57^\circ$ . The  $a$  parameter, which is the spacing parallel to the  $[\text{V}_2\text{O}_5]_n$  double layer, is slightly lower than the reported value, which suggests that the  $\text{VO}_6$  octahedron in the double layer stacking may be slightly distorted in this sample indicating further optimization of the synthesis procedure may be necessary. A small amount of impurities,  $\text{Cu}_3(\text{OH})_2\text{V}_2\text{O}_7 \cdot 2\text{H}_2\text{O}$  and  $\text{CuO}$ , were observed in the as-synthesized sample, primarily stuck to the wall of the reactor.  $\text{Cu}_3(\text{OH})_2\text{V}_2\text{O}_7 \cdot 2\text{H}_2\text{O}$  is expected to decompose to form  $\text{Cu}_{0.95}\text{V}_2\text{O}_5$  and, in the presence of a reducing agent,  $\text{CuO}$  should quickly decompose. The existence of these intermediate phases on the walls of the reactors suggests that there may be incomplete mixing of the slurry during the reaction.

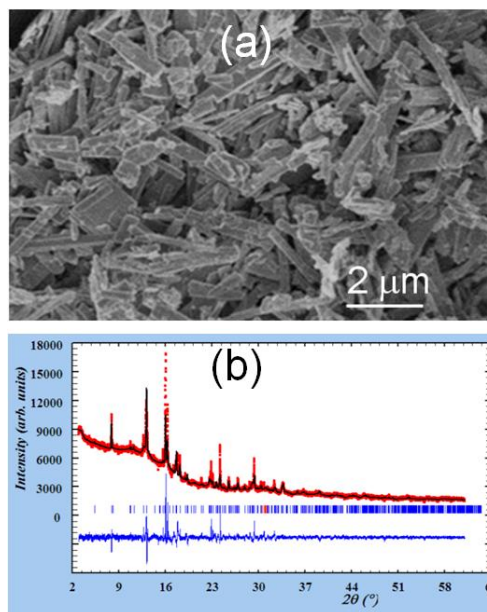
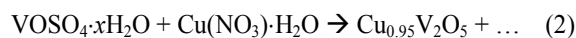


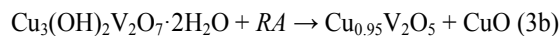
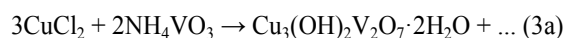
**Figure V - 60:** (a) SEM image of as-synthesized CVO nanorods prepared at 200°C for 10 h, (b) corresponding synchrotron XRD and profile fit from  $\text{Cu}_{0.95}\text{V}_2\text{O}_5$ .

Attempts were made to control particle morphology by using different precursors and organic additives such as cetyltrimethylammonium bromide (CTAB), dodecyltrimethyl-ammonium bromide (DTAB), D-sucrose, and L-ascorbic acid. A slight morphology change was observed with some additives, which also resulted in the formation of impurity phases and seemed to degrade the electrochemical performance.

A number of variations on the hydrothermal synthesis were explored, including the following hydrothermal reaction:



However, this reaction was unsuccessful and no  $\text{Cu}_{0.95}\text{V}_2\text{O}_5$  was formed. Another attempt utilized different precursors that react quickly to form an intermediate phase, followed by  $\text{Cu}_{0.95}\text{V}_2\text{O}_5$ :



In reaction 3b RA was acetophenone and the CuO was removed by a wash in HCl. Interestingly, reaction 3 leads to the formation of nanoparticles (100-300 nm) at 180°C for 48 hours, as shown in Figure V - 61a, rather than nanorods (obtained by reaction 1). XRD characterization of the product from reaction 3 is consistent with a high-purity phase of  $\text{Cu}_{0.95}\text{V}_2\text{O}_5$ , with rather poor crystallinity. Subsequent investigations of reaction 3 revealed that the crystallinity of the product seemed to increase with the concentration of the reducing agent (acetophenone). When the reaction temperature was increased to 200°C for 48 hours the product consisted of a mixture of different phases. In order to understand the chemical reaction process, *ex situ* XRD studies were performed on the products as a function of reaction time, as shown in Figure V - 61(b). A summary of the phase evolution is given in Table V - 1.

**Table V - 1:** Products obtained from reaction 3 as a function of time as determined by *ex situ* XRD (Figure V - 61).

| Reaction temperature and Time | Product  |
|-------------------------------|--|
| S 56 @200°C 1h                | $\text{Cu}_3(\text{OH})_2\text{V}_2\text{O}_7 \cdot 2\text{H}_2\text{O}$       |
| S 58 @200°C 3h                | $\text{Cu}_3(\text{OH})_2\text{V}_2\text{O}_7 \cdot 2\text{H}_2\text{O}$       |
| S 60 @200°C 6h                | $\text{Cu}_3(\text{OH})_2\text{V}_2\text{O}_7 \cdot 2\text{H}_2\text{O}$       |
| S 50 @200°C 10h               | $\text{Cu}_3(\text{OH})_2\text{V}_2\text{O}_7 \cdot 2\text{H}_2\text{O}$       |
| S 31 @200°C 20h               | $\text{Cu}_{0.95}\text{V}_2\text{O}_5$ (pure phase)                            |
| S 40 @200°C 24h               | $\text{Cu}_{0.95}\text{V}_2\text{O}_5$ (pure phase)                            |
| S 42 @200°C 48h               | Mixed phases ( $\text{Cu}_{0.95}\text{V}_2\text{O}_5$ with others more phases) |

The evolution of the XRD patterns indicate the formation of an intermediate phase,  $\text{Cu}_3(\text{OH})_2\text{V}_2\text{O}_7 \cdot 2\text{H}_2\text{O}$  in the early stage of the reaction. This phase is gradually consumed during the reaction and the final product is formed after ~20 hours. The crystallinity of the  $\text{Cu}_{0.95}\text{V}_2\text{O}_5$  seems to decrease after 24 hours, indicating that the product is not stable under these conditions. After an additional 24 hours (48 hours total) XRD results indicate that the  $\text{Cu}_{0.95}\text{V}_2\text{O}_5$  has partially transformed into a mixture of other phases.

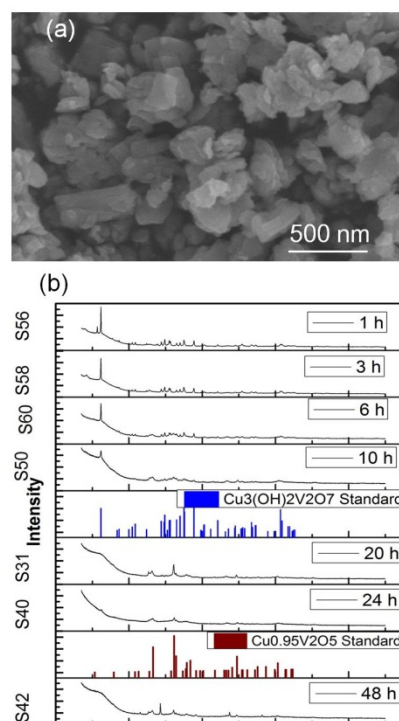


**Figure V - 61:** (a) SEM image of the as-synthesized CVO prepared via reaction 3 (180°C, 48 hours), (b) XRD patterns acquired during the synthesis of CVO (200°C).

**Preliminary *in situ* synthesis of  $\text{Cu}_x\text{V}_2\text{O}_5$ :** By using the newly-developed *in situ* reactor (Figure V - 59a), the phase transformations during the conventional hydrothermal synthesis of  $\text{Cu}_x\text{V}_2\text{O}_5$  series (using reaction 1) were investigated.

Figure V - 62 shows the XRD patterns from one of the tests. At the onset of the reaction the primary peaks are associated with the crystalline  $\text{V}_2\text{O}_5$  phase. As the temperature was increased to 180°C, the  $\text{V}_2\text{O}_5$  phase dissolved quickly and was followed by the growth of the  $\text{Cu}_x\text{V}_2\text{O}_5$  phase, indicating a dissolution-recrystallization reaction process. The  $\text{Cu}_x\text{V}_2\text{O}_5$  phase grew steadily with time until the reaction was stopped after approximately 17 hours. The final product consisted of a Cu deficient phase of  $\text{Cu}_{0.36}\text{V}_2\text{O}_5$ , which is isostructural with  $\text{V}_2\text{O}_5$ . Scanning transmission electron microscopy (STEM) and energy dispersive x-ray spectroscopy (EDS) analysis of the product revealed a rod-shaped morphology and a homogeneous distribution of Cu (not shown here). There was no evidence of an intermediate phase in this reaction, but intermediate phases were observed with different precursors and under different reaction conditions.

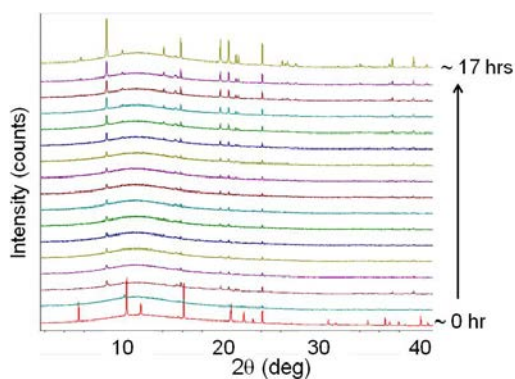


**Figure V - 62:** Resolved X-ray diffraction patterns from hydrothermal synthesis of CVO showing a direct transformation from the precursor ( $V_2O_5$ ) to CVO (no intermediate phase).

**Lithium reaction mechanisms.** Figure V - 63a shows the charge-discharge profiles and the specific capacities during the first cycle. The first discharge capacity was  $\sim 240 \text{ mAh g}^{-1}$ , which corresponds to a transfer of 2.17 Li, which is less than the previously reported value of  $292 \text{ mAh g}^{-1}$  (2.64 Li). The discharge profile is divided into three regions: (i) steep slope above 2.6 V ( $\sim 0.17 \text{ Li}$ ), (ii) gentle slope near 2.5 V ( $\sim 1.4 \text{ Li}$ ), and (iii) gentle slope below 2.2 V ( $\sim 0.6 \text{ Li}$ ). It is speculated that region (i) is due to Li intercalation into the CVO matrix, region (ii) is due to Cu extrusion, and region (iii) is due to further Li intercalation into the Li-V-O.

Electrochemical measurements (Figure V - 63b) showed the gradual decay of the capacity with cycling, which may be due to the structural degradation and irreversible Cu extrusion with cycling, according to preliminary STEM-EDS studies (Figure V - 63c).

## Conclusions and Future Directions

A second generation *in situ* capillary reactor was developed and used to track the hydrothermal synthesis of  $\text{LiFe}_{0.4}\text{Mn}_{0.6}\text{PO}_4$  and  $\text{Cu}_{0.95}\text{V}_2\text{O}_5$ . High purity  $\text{Cu}_{0.95}\text{V}_2\text{O}_5$  was synthesized using different methods, which exhibited a specific capacity of  $\sim 240 \text{ mAh g}^{-1}$  (2.17 Li) at the initial discharge. The capacity decreased gradually on subsequent cycling due to the irreversible segregation of metallic Cu and structural degradation during cycling. Improved performance may be achieved by tailoring particle morphology through reaction conditions (precursors, reducing agent, temperature, and time, etc.)

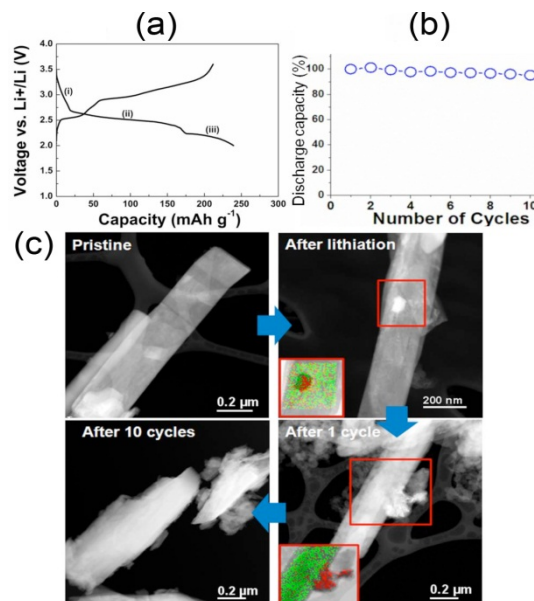


**Figure V - 63:** (a) Charge-discharge profiles for the first cycle, (b) cyclicability and (c) STEM-EDS images of the pristine, lithiated and cycled electrodes showing the extruded Cu identified by EDS mapping (red).

Investigations of the Cu-V-O cathodes will continue in 2013 and a number of different Cu-V-O compounds will be synthesized by the end of the year. The optimal procedure for the synthesis of  $\text{Cu}_{0.95}\text{V}_2\text{O}_5$  will be determined by evaluating a variety of precursors (Cu and V precursors and reducing agents) and reaction conditions (temperature and time). Electrochemical studies (*in situ* and *ex situ*) along with material characterization (e.g., particle size and morphology) will be determined to identify mechanism(s) of capacity fade. By the end of 2013 it is expected that feasibility studies of using hydrothermal and/or ion exchange reactions to prepare polyanion cathodes will be initiated.

It is our hope that new collaborations with other BATT members on synthesizing new materials and optimizing synthesis reactions will be initiated by sharing the resources and tools developed under this effort.

## FY 2012 Publications/Presentations

1. J. Hong, J.M. Bai, H.Y. Chen, F. Wang, J. Graetz, "Synthesis of  $\text{LiFe}_x\text{Mn}_{1-x}\text{PO}_4$  ( $0 \leq x \leq 1$ ) cathodes via solvothermal reaction and phase transformation mechanisms by *in situ* XRD," (*paper in preparation*)
2. F. Wang, Q. Wang, N.A. Chernova, M.S. Whittingham, J. Graetz, "*In situ* Studies of Cathodes for Li-ion Batteries by Simultaneous Quick X-Ray Absorption/Diffraction Spectroscopy (QXAS/XRD)," *MRS Fall Meeting*, Nov. 26-30, 2012. Boston. (*Oral*)

---

## V.B.13 Lithium-bearing Mixed Polyanion (LBMP) Glasses as Cathode Materials (ORNL)

Jim Kiggans (Oak Ridge National Laboratory) and Andrew Kercher (IMTECH)

Jim Kiggans  
Oak Ridge National Laboratory  
P.O. Box 2008; MS 6087  
Oak Ridge, TN 37831-6087  
Phone: (865) 574-8863; Fax: (865) 576-8424  
E-mail: [kiggansojr@ornl.gov](mailto:kiggansojr@ornl.gov)

Start Date: October 1, 2011  
Projected End Date: September 30, 2015

- Characterization of first baseline glass confirming amorphous structure and desired target elemental composition.
- Characterization of phosphate glass precursors and precursor mixtures by simultaneous differential thermal analysis and thermogravimetric analysis.



### Introduction

Polyanion framework materials, such as  $\text{LiFePO}_4$ , are promising cathode materials for lithium ion batteries for electric vehicle applications because they can have excellent safety and cycling performance due to their rigid covalently bonded structure. However, many crystalline polyanion framework materials with theoretically excellent properties, such as  $\text{LiCoPO}_4$ ,  $\text{LiFeBO}_3$ , and  $\text{Li}_2\text{MnSiO}_4$ , have not performed well as cathodes due to low electrical conductivity and/or crystal structure changes during cycling. Oak Ridge National Laboratory has proposed that mixed polyanion glasses can be excellent high capacity cathodes that can overcome the limitations of similar crystalline polyanion framework materials.

Mixed polyanion glasses have three key advantages over similar crystalline polyanion framework materials. First, with the proper choice of polyanion content, mixed polyanion glasses can have higher electrical conductivities than similar crystalline polyanion framework materials. For example, substitutions of molybdenum oxide, tellurium oxide, and vanadium oxide for phosphate in iron phosphate glasses have demonstrated increases in room temperature electrical conductivity by orders of magnitude. Second, the disordered covalently bonded structure of mixed polyanion glasses limits the ability of the structure to rearrange, which holds the promise to prevent undesirable microstructural arrangement during cycling. Third, the polyanion content of glasses can be tailored to produce a cathode with a maximized redox potential for a given electrolyte system. Changing the polyanion content of a polyanion cathode material has been shown to change the redox potential due to the inductive effect of the polyanion (Isono, et al., J. Power Sources, 2010, 195: 593-598). Depending on the amount and electronegativity of the polyanion substituted in the glass, the voltage of a glass cathode could be increased or decreased to the desired optimal voltage.

Most crystalline polyanion framework materials are phosphates, borates, or silicates. Phosphates, borates and silicates are renowned glass formers using conventional glass processing methods. Therefore, producing these

### Objectives

- Model and synthesize mixed polyanion glasses for use as active cathode materials in lithium ion batteries.
- Demonstrate enhanced material properties and electrochemical performance of glass cathode materials by varying the mixed polyanion content.
- Produce mixed polyanion glass cathode materials that undergo multivalent transitions in the transition metal cations during electrochemical cycling.
- Through laboratory-scale battery testing, demonstrate novel glasses with excellent overall cathode performance that are viable replacements for current cathode materials in electric vehicle applications.

### Technical Barriers

- Low energy density
- Poor high power performance
- Inadequate cycle life

### Technical Targets

- Produce a mixed polyanion glass cathode with significantly greater capacity at high discharge rates than crystalline  $\text{LiFePO}_4$ .
- Develop a mixed polyanion glass material with at least a 25% greater specific energy than  $\text{LiFePO}_4$ .
- Demonstrate multivalent glass cathodes with specific capacities exceeding 220 mAh/g.

### Accomplishments

- Production of first baseline glass cathode composition.

novel glass cathode materials will not likely require exotic processing methods, but could be produced by low-cost conventional glass processing methods.

## Approach

The research program on mixed polyanion glass cathodes is structured with five activities:

- structure and property modeling
- glass processing
- glass structure and property characterization
- cathode production
- electrochemical testing

The structure and property modeling will provide guidance on the most promising glass cathode materials to pursue based on glass forming ability and projected electrochemical properties. Classical heat/quench glass processing will be the primary processing method, but sol gel and rapid heating methods will be explored if required for certain glass compositions. Structural characterization will determine amorphous structure, transition metal valence, composition, and uniformity. Key property measurements are the thermal properties (such as glass transition and crystallization temperatures) and electrical conductivity. Cathode production will utilize submicron active cathode powder, PVDF binder, carbon black, and a metal foil current collector. Coin cells containing the glass cathode materials will be used to evaluate electrochemical performance under varied discharge rate and cycling.

## Results

**Precursor Characterization.** Iron phosphate glasses were chosen as baseline glass cathode materials, because their cathode performance can be readily compared to crystalline iron phosphate cathode materials. The precursors for iron phosphate glasses and related mixed polyanion glasses were chosen to be: ammonium dihydrogen phosphate (ADP), iron (III) oxide, lithium carbonate, and vanadium (V) oxide. Simultaneous differential thermal analysis & thermogravimetric analysis (DTA - TGA) has been used to understand the glass precursor reactions.

Understanding volatile loss and decomposition of precursors is necessary in order to control the composition of glasses produced by heat/quench processing. DTA - TGA analysis of phosphorous (V) oxide (from ADP) and vanadium (V) oxide showed that  $P_2O_5$  and  $V_2O_5$  are both volatile well below heat/quench processing temperatures for iron phosphate glass (volatile loss onsets of 575°C and 680°C, respectively). However, DTA - TGA analysis of an equimolar precursor mixture of  $P_2O_5$  and  $V_2O_5$  showed only slight volatile loss up to 1,100°C, which is well above the required heat/quench processing temperatures for iron phosphate/vanadate glasses. DTA - TGA analysis of an

equimolar mixture of iron (III) oxide and phosphorous (V) oxide (from ADP) showed only slight volatile loss from 605°C to 1200°C, but phosphate volatilization occurred between 500°C and 605°C prior to reaction with the iron oxide. Knowing this information, this phosphate volatilization can be minimized and compensated for during glass batching and processing.

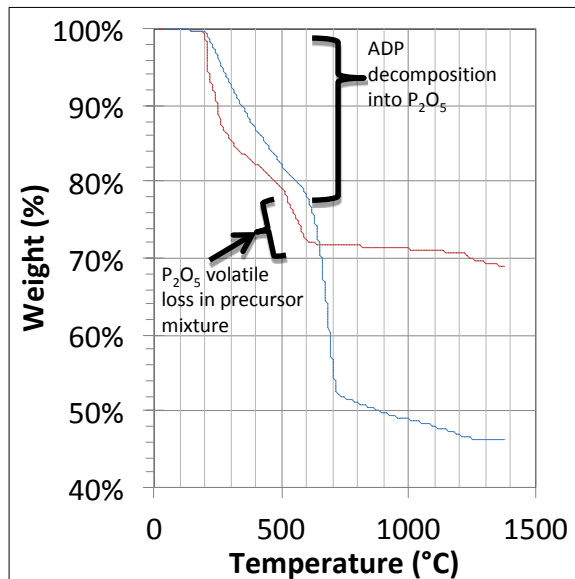


**Figure V - 64:** DTA - TGA analysis has provided insights into precursor behavior to aid glass processing development. DTA - TGA analysis of a mixture of iron (III) oxide and ammonium dihydrogen phosphate (red) showed volatile  $P_2O_5$  loss between 500°C and 605°C. (Blue curve is a sum of DTA - TGA analyses for iron (III) oxide and ammonium dihydrogen phosphate to show the expected weight loss assuming no reaction between the precursors.)

**Baseline Glass Cathode Materials.** The first baseline glass cathode composition,  $Fe_4(P_2O_7)_3$ , has been produced. The glass batch was heated in an alumina crucible to 1400°C and quenched on a graphite mold. An x-ray diffraction pattern of the  $Fe_4(P_2O_7)_3$  material was consistent with an amorphous glass structure. Elemental analysis of the glass by inductively coupled plasma atomic emission spectroscopy (ICP-AES) showed that the iron / phosphorous ratio was near the exact target ratio (0.82 measured; 0.83 target) and that a small percentage (0.85 wt.%) of aluminum was present, presumably from the alumina crucible. X-ray photoelectron spectroscopy of the material found a mixture of iron valences ( $\sim 2/3 Fe^{3+} / \sim 1/3 Fe^{2+}$ ). Glass processing parameters, such as melt temperature and dwell time, are being adjusted to obtain an improved baseline glass with a minimized  $Fe^{2+}$  content.



**Figure V - 65:** The first baseline glass cathode composition ( $\text{Fe}_4(\text{P}_2\text{O}_7)_3$ ) has been made. This glass was produced by quenching the melt in a graphite mold.

A glass processing run with an  $\text{FePO}_4$  target composition has also been performed. The  $\text{FePO}_4$  melt was rapidly quenched on a copper plate. X-ray diffraction analysis revealed a small fraction of crystalline iron phosphate inside the material. The critical cooling rate of iron phosphate glasses decreases with phosphate content. A future glass processing run is planned with a slightly higher phosphate content, which is anticipated to successfully produce the second baseline glass.

**Phosphate Glass Modeling.** CALPHAD (CALculation of PHase Diagram) modeling has been employed to predict the phase stability and electrochemistry of baseline glass cathode materials. The thermodynamic model of the crystalline  $\text{Li}/\text{FePO}_4$  phase has been modeled with a sublattice model of  $(\text{Li}^+, \text{Vacancy})(\text{Fe}^{2+}, \text{Fe}^{3+})(\text{P}^{5+})(\text{O}^{2-})_4$  and will serve as the basis for glass modeling. The thermodynamic model parameters have been self-consistently evaluated with phase equilibrium data from the literature with respect to lower order binary oxides.

### Conclusions and Future Directions

The first baseline glass cathode composition,  $\text{Fe}_4(\text{P}_2\text{O}_7)_3$ , has been synthesized and characterized, as scheduled in FY2012. Two baseline iron phosphate glasses,  $\text{Fe}_4(\text{P}_2\text{O}_7)_3$  and  $\text{FePO}_4$  with additional phosphate, are on schedule to be synthesized, characterized, and electrochemically tested by end of December 2012. After the two baseline phosphate glasses are synthesized, mixed polyanion glasses will be produced by substituting vanadate or molybdate for phosphate. These mixed polyanion glasses should provide proof-of-principle of the potential benefit of mixed polyanion glasses as cathode materials.

Thermodynamic modeling of  $\text{LiFePO}_4$  baseline glass is on schedule to be completed by end of December 2012. The next modeling task will be vanadate-based glass materials. First-principles calculations based on density

functional theory will be utilized to supplement scarce experimental thermochemical data, if needed.

### FY 2012 Publications/Presentations

None.

---

## V.B.14 High-capacity, High-voltage Cathode Materials for Lithium-ion Batteries (U. Texas)

Arumugam Manthiram  
University of Texas at Austin  
Materials Science and Engineering Program  
200 E. Dean Keeton Street, Stop C2200  
Phone: (512) 471-1791; Fax: (512) 475-8482  
E-mail: [manth@austin.utexas.edu](mailto:manth@austin.utexas.edu)

Start Date: January 1, 2012  
Projected End Date: December 31, 2015

- Establishment of the origin of the improved electrochemical performances of Fe-doped  $\text{LiM}_{1-x}\text{Fe}_x\text{PO}_4$  (M = Mn and Fe) olivine cathodes.
- Understanding the role of cationic substitutions in the high-voltage spinel  $\text{LiMn}_{1.5}\text{Ni}_{0.5-x}\text{M}_x\text{O}_4$  (M = Cr, Fe, Co, Zn, Al, and Ga) and utilizing the understanding to develop high-performance spinel cathodes.
- Establishing the factors causing the variations in the electrochemical properties of undoped high-voltage spinel  $\text{LiMn}_{1.5}\text{Ni}_{0.5}\text{O}_4$ .

### Objectives

- Develop high-performance cathodes for lithium-ion batteries and a fundamental understanding of their structure-composition-performance relationships.
- Develop novel synthesis approaches for polyanion-containing cathodes such as phosphates and silicates that can offer high energy, while exhibiting good thermal stability and safety.
- Develop high-voltage spinel oxide cathodes that can offer a combination of high energy and power, long cycle life, good storage properties, and good safety.

### Technical Barriers

This project addresses the following technical barriers of the lithium-ion battery technology, especially focusing on the cathode materials:

- Battery cost
- Safety
- Cycle life
- Energy and power

### Technical Targets

- Realization of high capacity with the insertion/extraction of more than one lithium ion per transition metal ion in silicate cathodes.
- Realization of high capacity and/or high voltage with novel phosphate cathodes.
- Realization of long cycle life and high rate with high-voltage spinel cathodes.

### Accomplishments

- Synthesis of  $\text{Li}_2\text{FeSiO}_4$  cathodes with unique morphologies by novel microwave-assisted solvothermal and microwave-assisted hydrothermal methods.



### Introduction

Cost is one of the major challenges hampering the adoption of lithium-ion technology for vehicle applications. Achieving the DOE targets for vehicle applications requires development of low-cost cathode materials that can offer high energy, high power, and long life with good safety. Accordingly, this project focuses on developing polyanion cathodes that offer high energy while keeping the cost low and exhibiting good safety characteristics. With an aim to increase the energy, we are focused on silicate and phosphate cathodes that offer high capacity with the insertion/extraction of more than one lithium ion per transition metal ion or polyanion cathodes that operate at high voltages. On the other hand, the major issue in employing the high-voltage spinel is the aggressive reaction of the cathode surface with the electrolyte at the high operating voltage of 4.7 V and the consequent degradation of cycle life and rate capability. Overcoming the difficulties by cationic substitutions and morphology control through novel synthesis approaches is the focus of this project.

### Approach

Focus is on the design and development of cathode materials based on polyanions that have the possibility for reversibly inserting/extracting more than one  $\text{Li}^+$  ion per transition metal ion  $\text{M}^{n+}$  and/or operating above 4.3 V. Some example systems to be pursued are  $\text{Li}_2\text{MSiO}_4$  and  $\text{Li}_2\text{MP}_2\text{O}_7$  (M = Mn, Fe, Co, and Ni). However, there are technical challenges in achieving the theoretical energy densities of many of these cathode materials. Synthesis and processing conditions play a critical role in realizing the full capacities of these polyanion cathodes with more than one  $\text{Li}^+$  ion per  $\text{Mn}^{2+}$  ion. Novel solution-based synthesis approaches such as microwave-assisted solvothermal methods that can offer controlled nanomorphologies are

pursued to maximize the electrochemical performances. The synthesized nanostructured polyanion cathodes are characterized by a variety of techniques including *ex situ* and *in situ* X-ray diffraction, electron microscopy (SEM, TEM, and STEM), X-ray photoelectron spectroscopy (ToF SIMS), time of flight – secondary ion mass spectroscopy, and in-depth electrochemical measurements. In addition, the role of cation doping, segregation of certain doped cations to the surface, cation ordering, and morphology on the electrochemical properties of 4.7 V spinel cathodes are investigated. Based on the characterization data gathered, a fundamental understanding of structure-composition-property-performance relationships is developed.

## Results

**Li<sub>2</sub>MSiO<sub>4</sub> Silicate Cathodes.** With an aim to increase the capacity while keeping the safety advantages associated with polyanion cathodes, the Li<sub>2</sub>MSiO<sub>4</sub> cathodes with unique morphologies have been synthesized by novel synthesis approaches; the Li<sub>2</sub>MSiO<sub>4</sub> cathodes offer the potential to reversibly extract/insert two lithium ions per transition metal ion and thereby to increase the capacity by a factor of two compared to the LiMPO<sub>4</sub> phosphate analogs. Accordingly, Li<sub>2</sub>FeSiO<sub>4</sub> was prepared by microwave-assisted hydrothermal (MW-HT) and solvothermal (MW-ST) synthesis approaches at < 300 °C for a short reaction time of < 30 min, followed by heat treatment with sucrose at 650 °C in argon atmosphere. Figure V - 66 compares the morphologies of the samples obtained by the MW-HT and MW-ST methods. While the MW-HT method offers walnut-shaped particles with a large particle size (1.5 – 2 μm) as seen in Figure V - 66a, the MW-ST method offers much smaller particles (20 – 50 nm) that are fused together into larger clusters as seen in Figure V - 66b. Both the MW-HT (C/50 rate) and MW-ST (C/20 rate) samples show low discharge capacities even at much slower C rates (Figure V - 66c); the lower rate capability of the MW-HT sample is due to the larger particle size. In order to improve the capacity, the MW-ST sample was prepared by incorporating graphene into the reaction medium. The MW-ST sample with graphene shows ~ 70 mAh/g higher capacity than the pristine MW-ST sample (Figure V - 66c) due to the improvement in electronic conductivity. The synthesis approach is now extended to other Li<sub>2</sub>MSiO<sub>4</sub> (M = Mn, Co, and Ni) cathodes and the Li<sub>2</sub>Fe<sub>1-x</sub>M<sub>x</sub>SiO<sub>4</sub> solid solutions.

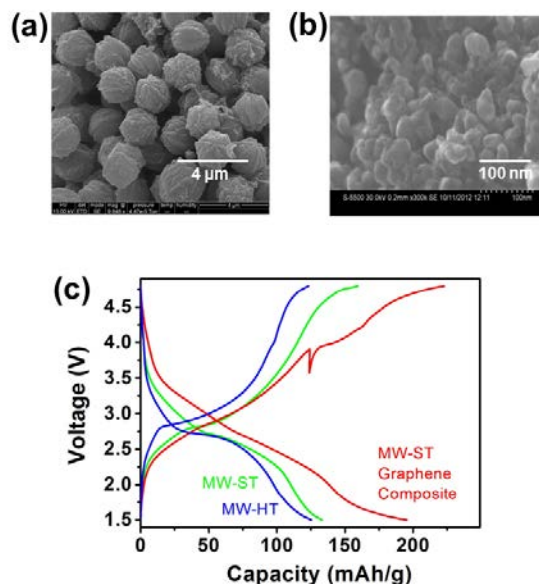


**Figure V - 66:** Morphologies of the (a) MW-HT and (b) MW-ST Li<sub>2</sub>FeSiO<sub>4</sub> samples, and (c) electrochemical performances of the MW-HT, MW-ST, and MW-ST-Graphene samples.

**LiM<sub>1-x</sub>Fe<sub>x</sub>PO<sub>4</sub> Phosphate Cathodes:** LiM<sub>1-x</sub>Fe<sub>x</sub>PO<sub>4</sub> (M = Mn and Co) solid solution cathodes were previously synthesized and it was found that the substitution of small amounts of Fe for Mn or Co greatly improves the electrochemical performance. Recognizing that the segregation of dopant ions like Fe<sup>3+</sup> in the high-voltage LiMn<sub>1.5</sub>Ni<sub>0.5-x</sub>M<sub>x</sub>O<sub>4</sub> (M = Cr, Fe, and Ga) spinel segregates to the surface and enhances the electrochemical performance, whether such segregations also occur in the LiM<sub>1-x</sub>Fe<sub>x</sub>PO<sub>4</sub> phosphate cathodes was investigated during this past year. Through time-of-flight – secondary ion mass spectrometry (ToF SIMS) and X-ray photoelectron spectroscopy (XPS), it was determined that segregation of Fe<sup>2+</sup> to the surface does not occur in LiM<sub>1-x</sub>Fe<sub>x</sub>PO<sub>4</sub> (M = Mn and Co). Figure V - 67 shows the surface-to-bulk ratio of iron in the Fe-substituted LiCo<sub>1-x</sub>Fe<sub>x</sub>PO<sub>4</sub> as a function of sputtering time. As can be seen, the iron concentration remains the same throughout the depth of the particle. It is concluded that segregation of Fe<sup>2+</sup> to the surface is not occurring, unlike in the case of the high-voltage spinel LiMn<sub>1.5</sub>Ni<sub>0.5-x</sub>M<sub>x</sub>O<sub>4</sub>. Therefore, the improvement in the electrochemical performances of LiM<sub>1-x</sub>Fe<sub>x</sub>PO<sub>4</sub> (M = Mn and Co) is not due to the segregation of Fe to the surface. The reason for the better performance on substituting Fe may be associated with the different affinities of transition metals to form carbides during carbon coating. For example, any iron carbide formed may enhance electronic conductivity and provide a better electrode-electrolyte interface. Future work will focus on determining whether or not iron carbide is forming during the carbon-coating process of LiM<sub>1-x</sub>Fe<sub>x</sub>PO<sub>4</sub>.

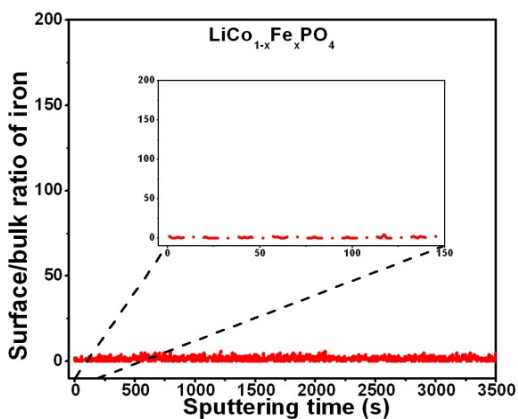


**Figure V - 67:** Surface-to-bulk ratio of iron in  $\text{LiCo}_{1-x}\text{Fe}_x\text{PO}_4$  as a function of sputtering time.

**High-voltage Spinel Cathodes.** Continuing the studies on understanding the factors that control the performances of the 4.7 V spinel  $\text{LiMn}_{1.5}\text{Ni}_{0.5}\text{O}_4$  cathode efforts have been focused on surface segregation, cation ordering, morphology, and  $\text{Mn}^{3+}$  content. A time-of-flight – secondary ion mass spectrometry (TOF-SIMS) study of  $\text{LiMn}_{1.5}\text{Ni}_{0.42}\text{M}_{0.08}\text{O}_4$  ( $M = \text{Al}, \text{Cr}, \text{Fe}, \text{Co}, \text{Zn},$  and  $\text{Ga}$ ) reveals that Al, Cr, Fe, and Ga segregate to the surface during the synthesis process, while both Co and Zn do not, resulting in a superior performance of the  $M = \text{Al}, \text{Cr}, \text{Fe},$  and  $\text{Ga}$  compositions compared to the  $M = \text{Co}$  and  $\text{Zn}$  compositions. Cation doping also eliminates the  $\text{Li}_x\text{Ni}_{1-x}\text{O}$  impurity phase. In addition, the effect of post-annealing at  $700^\circ\text{C}$  of the undoped  $\text{LiMn}_{1.5}\text{Ni}_{0.5}\text{O}_4$  and doped  $\text{LiMn}_{1.5}\text{Ni}_{0.42}\text{M}_{0.08}\text{O}_4$  ( $M = \text{Cr}, \text{Fe},$  and  $\text{Ga}$ ) samples already synthesized at  $900^\circ\text{C}$  has been investigated. While the undoped and Ga-doped samples transform into a more cation-ordered spinel with the  $P4_332$  space group on annealing at  $700^\circ\text{C}$ , as indicated by XRD and FTIR data, the Cr- and Fe-doped spinels sustain a high degree of cation disorder even after annealing at  $700^\circ\text{C}$  (Figure V - 68). Furthermore, the  $\text{Li}_x\text{Ni}_{1-x}\text{O}$  impurity phase in the undoped  $\text{LiMn}_{1.5}\text{Ni}_{0.5}\text{O}_4$  sample is eliminated after post-annealing at  $700^\circ\text{C}$ , indicating an increase in the solubility of Ni in the lattice accompanied by a decrease in the  $\text{Mn}^{3+}$  content.

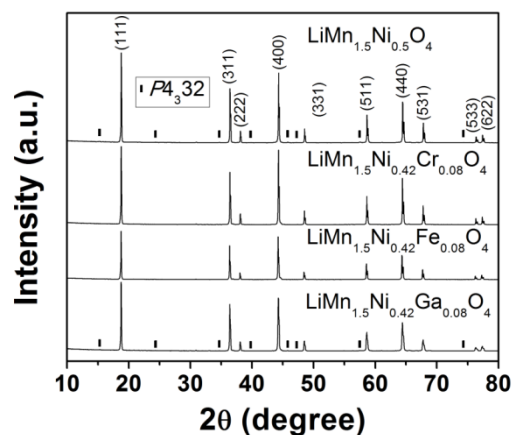


**Figure V - 68:** XRD patterns of the  $\text{LiMn}_{1.5}\text{Ni}_{0.5}\text{O}_4$  and  $\text{LiMn}_{1.5}\text{Ni}_{0.42}\text{M}_{0.08}\text{O}_4$  ( $M = \text{Cr}, \text{Fe},$  and  $\text{Ga}$ ) samples after post-annealing at  $700^\circ\text{C}$ . The rectangular points indicate the superstructure reflections for the ordered  $P4_332$  space group.

Previous focus was on how the cation ordering between  $\text{Mn}^{4+}$  and  $\text{Ni}^{2+}$  in the octahedral sites of the undoped and doped high-voltage  $\text{LiMn}_{1.5}\text{Ni}_{0.5}\text{O}_4$  spinels influences the cycle performances. A more detailed analysis of the electrochemical behavior has now been carried out using the  $dQ/dV$  plots ( $Q$  and  $V$  refer, respectively, to specific capacity and voltage) of a highly ordered undoped  $\text{LiMn}_{1.5}\text{Ni}_{0.5}\text{O}_4$  spinel and a highly disordered doped  $\text{LiMn}_{1.5}\text{Ni}_{0.42}\text{Fe}_{0.08}\text{O}_4$  spinel, as seen in Figure V - 69a and b. The wider voltage gap between the oxidation and reduction  $dQ/dV$  peaks at  $\sim 4.7$  V for the ordered spinel indicates higher polarization due to lower electronic and/or lithium-ion conductivity. Moreover, the voltage gap between the oxidation and reduction peaks of the ordered  $\text{LiMn}_{1.5}\text{Ni}_{0.5}\text{O}_4$  increases during 50 charge-discharge cycles, indicating a continuous increase in polarization, which is reflected in an increase in the charge-transfer resistance during cycling (Figure V - 69c). In contrast, the disordered  $\text{LiMn}_{1.5}\text{Ni}_{0.42}\text{Fe}_{0.08}\text{O}_4$  spinel exhibits lower polarization without much increase in polarization or charge-transfer resistance during cycling.

Additionally, the  $dQ/dV$  peaks in the 4.0 V region of the ordered undoped  $\text{LiMn}_{1.5}\text{Ni}_{0.5}\text{O}_4$  spinel exhibit an asymmetry in the intensity: the reduction peak area is larger than the oxidation peak area and the ratio of the reduction peak area to the oxidation peak area increases on cycling. It appears that a certain amount of  $\text{Mn}^{4+}$  ions in the ordered spinel is reduced to  $\text{Mn}^{3+}$  during discharge and then a fraction of the generated  $\text{Mn}^{3+}$  ions leaches out into the electrolyte during cycling, resulting in capacity fade. In contrast, the ratio of the reduction peak area to the oxidation peak area is almost constant during cycling for the disordered doped  $\text{LiMn}_{1.5}\text{Ni}_{0.42}\text{Fe}_{0.08}\text{O}_4$ , resulting in excellent capacity retention.

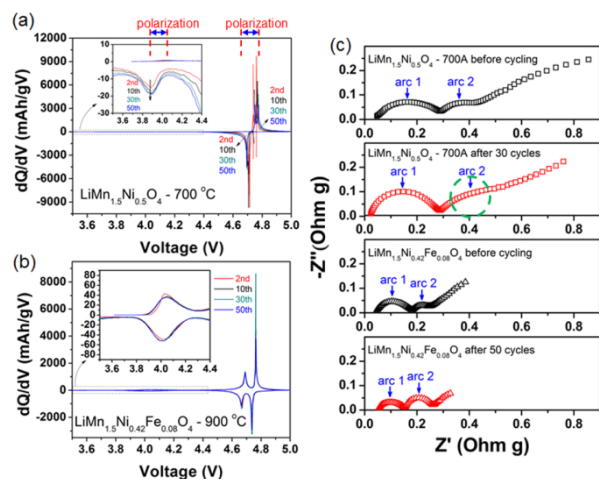


**Figure V - 69:** dQ/dV plots of the (a)  $\text{LiMn}_{1.5}\text{Ni}_{0.5}\text{O}_4$  spinel post-annealed at 700 °C, (b)  $\text{LiMn}_{1.5}\text{Ni}_{0.42}\text{Fe}_{0.08}\text{O}_4$  spinel synthesized at 900 °C, and (c) EIS spectra before and after cycling of both the spinels.

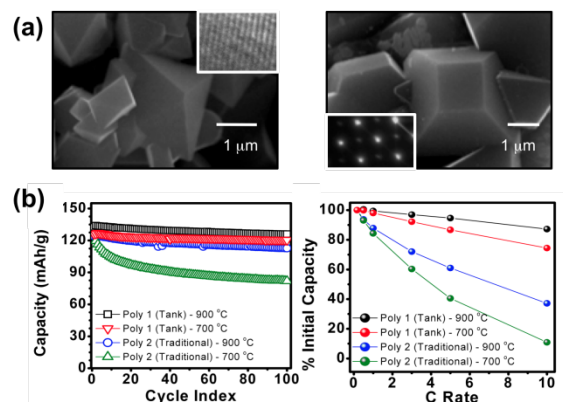


**Figure V - 70:** (a) Morphology and crystal planes of undoped  $\text{LiMn}_{1.5}\text{Ni}_{0.5}\text{O}_4$  spinel cathodes prepared by two different methods and (b) electrochemical performances of the samples fired at 900 °C and annealed at 700 °C.

Furthermore, with an aim to develop a better understanding of factors that lead to variations in the electrochemical performance of undoped  $\text{LiMn}_{1.5}\text{Ni}_{0.5}\text{O}_4$  spinel cathodes, focus has been placed on examining the orientation of the crystal planes facing the electrolyte and how these planes influence the cyclability and rate capability. By comparing two samples made by different wet-chemical routes but having identical undoped  $\text{LiMn}_{1.5}\text{Ni}_{0.5}\text{O}_4$  composition, we were able to determine that the Poly 1 sample (prepared with a tank reactor) with octahedral crystals in which the {111} family of planes are exposed to the electrolyte (Figure V - 70a) gives better rate capability and cyclability (Figure V - 70b) than the Poly 2 sample (prepared by traditional coprecipitation) with

truncated octahedral crystals in which the {100} family of planes are exposed to the electrolyte. The results illustrate that the surface planes and solid-electrolyte interface play a dominant role in controlling the performance of undoped  $\text{LiMn}_{1.5}\text{Ni}_{0.5}\text{O}_4$ .

## Conclusions and Future Directions

$\text{Li}_2\text{FeSiO}_4$  cathodes synthesized by a microwave-assisted solvothermal method, followed by the incorporation of graphene, exhibit high capacity. The improved performance of Fe-doped  $\text{LiM}_{1-x}\text{Fe}_x\text{PO}_4$  ( $M = \text{Mn}$  and  $\text{Co}$ ) appears to be due to the formation of iron carbide on the surface rather than due to surface segregation. The electrochemical performance of undoped high-voltage  $\text{LiMn}_{1.5}\text{Ni}_{0.5}\text{O}_4$  spinel cathodes is strongly influenced by the morphology and the surface planes in contact with the electrolyte. Cationic doping in  $\text{LiMn}_{1.5}\text{Ni}_{0.42}\text{M}_{0.08}\text{O}_4$  ( $M = \text{Cr}$ ,  $\text{Fe}$ , and  $\text{Ga}$ ) lowers the polarization losses and impedance growth during cycling due to a robust cathode-electrolyte interface offered by the decoration of the surface by the dopant cations. The doping also eliminates the  $\text{Li}_x\text{Ni}_{1-x}\text{O}$  impurity phase and promotes a disordering between  $\text{Mn}^{4+}$  and  $\text{Ni}^{2+}$  ions in the spinel lattice.

Future work is focused on the (i) synthesis and characterization of  $\text{Li}_2\text{MP}_2\text{O}_7$  ( $M = \text{Fe}$ ,  $\text{Mn}$ ,  $\text{Co}$ , and  $\text{Ni}$ ) as well as their solid solutions to realize high capacity with the insertion/extraction of more than one lithium per transition metal, (ii) assessment of surface segregation in  $\text{Li}_2\text{M}_{1-x}\text{Fe}_x\text{SiO}_4$  and  $\text{Li}_2\text{M}_{1-x}\text{Fe}_x\text{P}_2\text{O}_7$  ( $M = \text{Co}$ ,  $\text{Mn}$ , and  $\text{Ni}$ ), and (iii) assessing the role of morphology and surface planes on the electrochemical properties of doped  $\text{LiMn}_{1.5}\text{Ni}_{0.42}\text{M}_{0.08}\text{O}_4$  spinel cathodes.

## FY 2012 Publications/Presentations

1. A. Cao and A. Manthiram, "Shape-controlled Synthesis of High Tap Density Cathode Oxides for Lithium-Ion Batteries," *Physical Chemistry and Chemical Physics* **14**, 6724-6728 (2012).
2. Z. Moorhead-Rosenberg, D. W. Shin, K. R. Chemelewski, J. B. Goodenough, and A. Manthiram, "Quantitative Determination of  $\text{Mn}^{3+}$  Content in  $\text{LiMn}_{1.5}\text{Ni}_{0.5}\text{O}_4$  Spinel Cathodes by Magnetic Measurements," *Applied Physics Letters* **100**, 213909; doi: 10.1063/1.4722927 (2012).
3. D.W. Shin, C.A. Bridges, A. Huq, M.P. Paranthaman, and A. Manthiram, "Role of Cation Ordering and Surface-segregation in High-voltage Spinel  $\text{LiMn}_{1.5}\text{Ni}_{0.5-x}\text{M}_x\text{O}_4$  ( $M = \text{Cr}$ ,  $\text{Fe}$ , and  $\text{Ga}$ ) Cathodes for Lithium-Ion Batteries," *Chemistry of Materials* (in press).

# V.B.15 Novel and Optimized Phases for High-energy Density Batteries

(LBNL)

Jordi Cabana  
Lawrence Berkeley National Laboratory  
Environmental Energy Technologies Division  
1 Cyclotron Rd. MS62R0203  
Berkeley, CA 94720  
Phone: (510) 486-7097; Fax: (510) 495-8097  
E-mail: [jcabana@lbl.gov](mailto:jcabana@lbl.gov)

Start Date: October 1, 2008

Projected End Date: September 30, 2012

- The role of MgO as an electrode additive during high voltage cycling was evaluated.
- A lithium transition metal fluoride was synthesized and tested in Li metal half cells.

◇ ◇ ◇ ◇ ◇

## Introduction

Finding Li-ion battery electrode materials that can bring about increases in energy is a critical need if the social impact of their use in electric vehicles is to meet expectations. In order to fulfill this goal, the following strategies can be envisaged: i) raising the voltage of operation of the battery by using electrodes that react at very high and very low potentials, respectively, and/or ii) improving the storage capacity by switching to alternative electrode materials that can exchange a larger amount of electrons/Li<sup>+</sup> ions. Yet these changes cannot come with a penalty in terms of device safety and cycle life of the device, which implies that the mechanisms of their reaction with lithium need to be well understood in order to locate possible sources of failure.

Spinel-type LiNi<sub>0.5</sub>Mn<sub>1.5</sub>O<sub>4</sub> is a promising candidate for the positive electrode because lithium is extracted at very high potentials (around 4.7 V vs. Li<sup>+</sup>/Li<sup>0</sup>). While very high rate capability has been reported in several cases, it has not been fully ascertained what the role is of the crystal-chemistry of the compound, such as metal ordering and the existence of impurities of Mn<sup>3+</sup> in the spinel and segregated rock salt particles. During FY2011, the correlation between microstructure, crystal structure and composition was established, which enabled us, during FY2012, to establish further correlation with electrochemical properties.

The interface between an electrode and the electrolyte is critical to extended performance. The chemical and structural changes occurring at the surface of the LiNi<sub>0.5</sub>Mn<sub>1.5</sub>O<sub>4</sub> oxide particles during redox reaction will be followed using soft X-ray spectroscopy. Modifications based on the addition of basic oxides such as MgO in the form of coatings or simple additives will be introduced. Their effect on such side reactions will be assessed.

Current candidates for the cathode in Li-ion batteries only allow half to one electron per total transition metal to be extracted. In oxides, extensive Li de-intercalation induces irreversible destabilization of the O<sup>2-</sup> species toward O<sub>2</sub> evolution by polarizing metals at high formal oxidation states. Fluoride ions are less polarizable and, therefore, can provide chemical stability. It is proposed to

## Objectives

- Enable higher density Li-ion batteries through an increase in operation voltage and capacity of the cathode.
- Design electrode structures that maximize active material utilization and charge density.
- Understand the structure-composition-properties relationship for bulk and surface in electrodes.
- Discover and synthesize new phases showing potential as electrode materials.

## Technical Barriers

Low energy-density, poor cycle life, safety.

## Technical Targets

- PHEV: 96 Wh/kg, 5,000 cycles.
- EV: 200 Wh/kg; 1,000 cycles.

## Accomplishments

- Knowledge of the crystal/microstructure-composition correlation in LiNi<sub>0.5</sub>Mn<sub>1.5</sub>O<sub>4</sub> developed in FY2011 was used to synthesize a series of samples where morphology is decoupled from the crystal chemistry (Mn<sup>3+</sup> content, Ni-Mn ordering. Further decoupling of these two parameters was achieved through synthetic control.
- The correlation between crystal chemistry and properties in LiNi<sub>0.5</sub>Mn<sub>1.5</sub>O<sub>4</sub> was studied using the series of samples. Strong correlation with ordering was observed, whereas Mn<sup>3+</sup> contents were found to have a much more marginal role.
- Analysis of surface redox reactions in LiNi<sub>0.5</sub>Mn<sub>1.5</sub>O<sub>4</sub> during cycling was performed using soft X-ray absorption spectroscopy.

fluorinated systems for yet unreported phases that contain redox active metals, with the aim to discover new compounds that can have suitable properties.

## Approach

Employ and develop a variety of synthetic methods to produce materials with controlled purity, crystal structure and particle morphology. Use spectroscopic and diffraction techniques and controlled materials to get a complete picture of the different reactions involved in battery electrodes. Explore chemical spaces in search for new phases that may provide performance improvements. Establish the importance of the extended electrode structure on electrochemical performance.

## Results

All work on  $\text{LiNi}_{0.5}\text{Mn}_{1.5}\text{O}_4$  was done in coordination within the Spinel Focus Group. The work on new fluorinated phases is part of a new project started mid-FY2012.

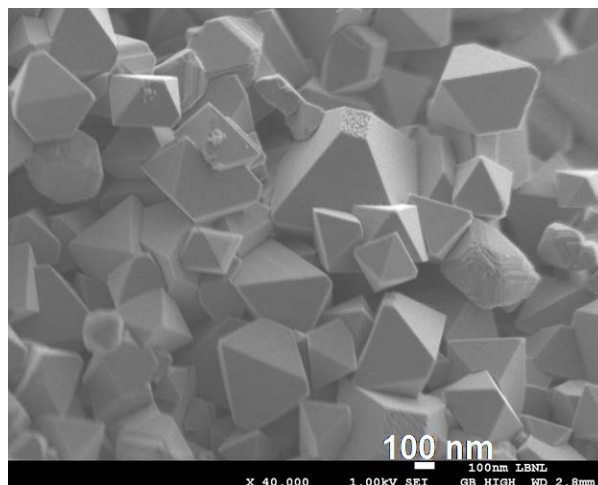


Figure V - 71: Representative SEM image of  $\text{LiNi}_{0.5}\text{Mn}_{1.5}\text{O}_4$  particles.

**Crystal-chemistry of  $\text{LiNi}_{0.5}\text{Mn}_{1.5}\text{O}_4$ .** During FY2012, a series of  $\text{LiNi}_{0.5}\text{Mn}_{1.5}\text{O}_4$  samples were synthesized using precursors annealed at  $900^\circ\text{C}$  for 1 h, followed by longer annealing at lower temperature. The first step induced grain growth (to  $\sim 1\mu\text{m}$ , Figure V - 71), whereas the second steps were performed at temperatures where coarsening largely does not occur. Changes in crystal chemistry were thus introduced. Differences were observed in the  $\text{Mn}^{3+}$  content, as determined from the capacity obtained at 4 V during charge. Good correlation with the magnetic moment of samples (measured by the Whittingham group, at SUNY Binghamton), which is also sensitive to transition metal oxidation states, was observed. As expected, differences were also observed in the degree of Ni/Mn disorder. Such differences were probed by  $^6\text{Li}$  MAS NMR (by the Grey group, at Cambridge University) and found to be in agreement with the separation between the two high voltage plateaus typically observed during Li

(de)intercalation. Higher  $\Delta V$  was found for the more disordered samples.

The rate capability, as well as the extended cycling behavior at various rates, of the series of samples was tested. Clear correlations between performance (defined as % capacity at the slowest rate and % capacity retention) and crystal-chemistry were observed (Figure V - 72). On one hand, a clear divide between disordered and ordered samples was found, with performance linearly correlating with  $\Delta V$ . In contrast, the  $\text{Mn}^{3+}$  contents were found to be less critical. While it varied notably in the case of the disordered samples, no correlation was found with electrochemical performance. In very ordered samples, small changes seemed to correlate with enhanced performance, suggesting that some  $\text{Mn}^{3+}$  is desirable in these samples. Whether this is due to an electronic effect (more electron carriers available) or simply to the fact that  $\text{Mn}^{3+}$  disrupts Ni-Mn ordering cannot be elucidated with

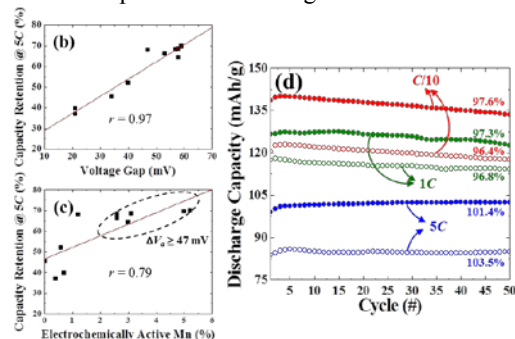


Figure V - 72: (Left) Electrochemical performance-crystal chemistry correlations in  $\text{LiNi}_{0.5}\text{Mn}_{1.5}\text{O}_4$  particles. (Right) Cycling of  $\text{LiNi}_{0.5}\text{Mn}_{1.5}\text{O}_4$  at different rates, within different voltage windows.

the available data. Future work, in collaboration with the Lucht group, at University of Rhode Island, will be directed at drawing similar correlations when cycling at high temperature.

Results hinted at the fact that, contrary to what is commonly believed in the field, the presence of  $\text{Mn}^{3+}$  does not critically determine rate capability. Further evidence was provided when cycling the same sample using two different discharge cutoff voltages: 3.5 and 4.4 V. The first enables the  $\text{Mn}^{3+}/\text{Mn}^{4+}$  redox activity, whereas the second one does not (Figure V - 72). Therefore, in the second case,  $\text{Mn}^{3+}$  was not regenerated during cycling. The results at different rates showed very similar capacity retention.

**Surface chemistry of  $\text{LiNi}_{0.5}\text{Mn}_{1.5}\text{O}_4$  during electrochemical operation.** The surface chemistry of pristine and cycled  $\text{LiNi}_{0.5}\text{Mn}_{1.5}\text{O}_4$  was characterized using soft X-ray absorption spectroscopy at the Ni and Mn  $L_{II, III}$  and O K edges (ALS, Berkeley). The sample was made at  $900^\circ\text{C}$  in air. Data from both total electron and fluorescence yield (TEY and TFY) detectors was collected. TEY probes 5-10 nm into the electrode, compared to ca. 100 nm in TFY mode. Therefore, comparisons between surface and bulk species can be

traced. Spectra were collected in the pristine state, at 40 and 100% state of charge (SOC), at 40% depth of discharge (DOD) and after 1 full cycle. While the spectra at the Mn edges (Figure V - 73a) show no shift or change in line shape, highlighting the role largely as formal spectator of these ions (changes occurring at 4 V are too small to be detected), the spectra at the Ni edges show notable changes (Figure V - 73b). For instance, the 2:1 doublet observed between 850 and 855 eV for the pristine sample turns into a broad 1:1 doublet at 100% SOC. This evolution is correlated with the oxidation of Ni in the compound. However, the doublet in the TEY spectrum at 100% SOC is shows a higher peak ratio than in TFY. It is concluded that the surface of the electrode is less oxidized than its bulk. Similar conclusions are reached from the O K edge spectra (Figure V - 73c). It can be seen that a shoulder at 524 eV appears on the pre-peak in TFY mode, which is associated to the change in the density of states at the O levels due to the oxidation of Ni. No such shoulder is observed in TEY mode. The fact that less electron depletion is found at the surface of the electrode is taken as indication that the electrode material directly participates on the decomposition of the electrolyte. The very highly acidic species that result from the oxidation of the oxide attack the electrolyte molecules in order to reduce to a less unstable state.

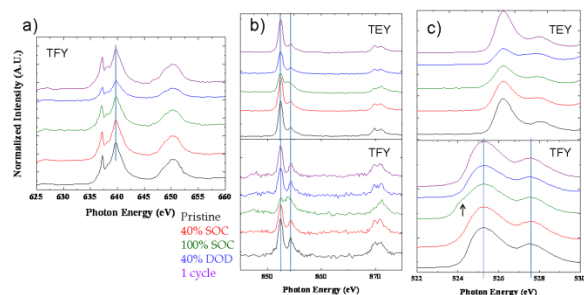


**Figure V - 73:** XAS for  $\text{LiNi}_{0.5}\text{Mn}_{1.5}\text{O}_4$  at different cycling states, as indicated, at the a) Mn, b) Ni L<sub>II,III</sub>, c) O K edges.

This work was extended to the study of modified materials. Fe L<sub>II,III</sub> edge XAS was performed on  $\text{LiFe}_{0.08}\text{Ni}_{0.42}\text{Mn}_{1.5}\text{O}_4$  (provided by the Manthiram group at UT-Texas) in its pristine state and after full lithium removal. The spectra showed noticeable differences in lineshape, indicative of a change in electronic structure of Fe and point at the electroactivity of this ion during electrochemical charging.

A baseline  $\text{LiNi}_{0.5}\text{Mn}_{1.5}\text{O}_4$  material was selected from the series of annealed samples, and coated post-synthesis using MgO. Two post-coating annealing procedures, at 500 and 800°C, were carried out on two different samples, respectively. Coating was found to be inhomogeneous after the 500°C treatment, but the sample following annealing at 800°C showed the same smooth surface of the baseline material. Porous composite electrodes, using PVDF and carbon as additives, were built with the three materials. MgO is a basic oxide that could harvest acidic

impurities in the electrolyte. Therefore, the importance of this mechanism of degradation with respect to protecting the electrode surface was evaluated by adding MgO as an additive to an electrode made with baseline material. Li metal half cells were cycled at 50°C. Both coated materials showed better capacity retention after 30 cycles than the baseline, whereas the performance of the electrode with MgO additive was worse. A significant difference in coulombic efficiency between baseline and the modified electrodes was also found, although the values were still to be too low for application. These data is in agreement with previous reports of a beneficial role of adding basic oxides to a high voltage electrode, whether in the form of coating or as an additive component, in preventing side reactions.

**Exploration of new fluorinated phases:** This task was initiated during FY2012. There has already been success in synthesizing the first fluoride phase,  $\text{Li}_2\text{NiF}_4$ , using conventional solid state methods. Attempts at electrochemically extracting lithium were made by ballmilling the material with as much as 30% carbon. No activity was found when tested in lithium half cells in any case. This observation is consistent with computational predictions that the potential of extraction is well above 5.0 V. Introducing oxygen is viewed as a strategy to introduce covalence in the compound that lowers the electrochemical potential as well as increase its electronic conductivity. The first reactions with oxygen in the reagent mixture have been initiated.

## Conclusions and Future Directions

The results obtained during FY12 have clearly revealed that  $\text{LiNi}_{0.5}\text{Mn}_{1.5}\text{O}_4$  can show very subtle variations in Ni/Mn ordering, as opposed to the black and white “ordered”/“disordered” picture that is commonly used. These subtle variations have more profound effects on electrochemical performance than composition and, hence,  $\text{Mn}^{3+}$  contents. The role of surface chemistry has also been clarified. XAS data suggests that the transition metals at the interface with the electrolyte are active toward its decomposition, especially when present in high oxidation, polarizing states. The result is surface reduction with respect to the bulk of the material. When oxide additives are present, either as barriers between electrode and electrolyte or as physically-mixed components, coulombic efficiencies at high temperature are higher, indicating that they alleviate some of the side reactions that cripple the performance of this material in the long term.

Work will continue under the Spinel Focus Group to ascertain the parameters that affect the bulk and surface properties of high voltage  $\text{LiNi}_{0.5}\text{Mn}_{1.5}\text{O}_4$ . The origin of the differences in performance with ordering will be linked to the mechanism of phase transformation. Leveraging the thorough understanding of the crystal-chemistry of this series of samples, the correlation between ordering and formation of solid solutions in  $\text{LiNi}_{0.5}\text{Mn}_{1.5}\text{O}_4$  upon cycling will be strengthened. For this purpose, X-ray diffraction

(XRD) will be performed during the electrochemical reaction. In parallel, understanding of how the different phases propagate within a single particle will be sought using recently developed protocols of transmission X-ray microscopy coupled with X-ray absorption spectroscopy.

Attention will be moved toward probing the chemistry and structure of the surface of  $\text{LiNi}_{0.5}\text{Mn}_{1.5}\text{O}_4$  during cycling. Well-characterized materials with controlled levels of coating and/or doping will be collected from fellow members of the Spinel Focus Group. Thin films of the material, with and without top “coating”, will also be prepared using physical vapor deposition methods. Changes on all these materials during cycling will be studied by combinations of X-ray and vibrational spectroscopy, in collaboration with ALS/SSRL researchers and the Kostecki group (LBNL).

Ramp-up of the materials discovery project will be completed early FY2013. During FY2013, protocols of fluorination reactions using PVDF as fluoride donor and moderate thermal treatments will be designed. These reactions will be performed on known oxides. In parallel, exploration of Li-M-O-F systems will be performed using direct synthesis. Several phase diagrams will be screened for stable phases. All new compounds will be characterized using diffraction and chemical analysis, and their performance as electrodes will be evaluated using lithium metal half cells.

### FY 2012 Publications/Presentations

1. T. E. Conry, A. Mehta, J. Cabana and M. M. Doeff, *J. Electrochem. Soc.*, **159**, A1562-A1571 (2012).
2. K. A. Aldi, J. Cabana, P. J. Sideris, J. Kim and C. P. Grey, *Amer. Miner.*, **97**, 883-889 (2012).
3. T. E. Conry, A. Mehta, J. Cabana and M. M. Doeff; *Chem. Mater.*, **24**, 3307 (2012).
4. J. Cabana, M. Casas-Cabanas, F. O. Omenya, N. A. Chernova, D. Zeng, M. S. Whittingham and C. P. Grey; *Chem. Mater.*, **24**, 2952 (2012).
5. C. Kim, N. S. Norberg, C. T. Alexander, R. Kostecki, J. Cabana; *Adv. Funct. Mater.* **2012**, In press, <http://dx.doi.org/10.1002/adfm.201201684>.
6. “Identification of critical parameters in electrochemical intercalation reactions,” *International Battery Association — Pacific Power Source Symposium (IBA-PPSS) 2012*. Waikoloa, HI (USA), January 9th-13th, 2012.
7. “Multiscale reactions in battery electrodes: importance and methods of characterization,” *Young Engineers + Scientists Symposium (YESS) 2012*. Berkeley, CA (USA), March 20th-22th, 2012.
8. “Multiscale reactions in battery electrodes: importance and methods of characterization,” *Symposium on “Challenges and Opportunities in Energy Storage Materials”*. Providence, RI (USA), June 1st, 2012.

---

## V.C Anode Development

### V.C.1 Nanoscale Composite Hetero-structures and Thermoplastic Resin

#### Binders (U. Pittsburgh)

Prashant N. Kumta  
University of Pittsburgh  
Department of Bioengineering, Chemical and Petroleum  
Engineering, Mechanical Engineering and Materials  
Science  
Pittsburgh, PA 15261  
Phone: (412) 648-0223; Fax: (412) 624-8069  
E-mail: [pkumta@pitt.edu](mailto:pkumta@pitt.edu)

Start Date: January 1, 2011  
Projected End Date: December 31, 2014

#### Objectives

- Identify new alternative nanostructured anodes to replace synthetic graphite providing higher gravimetric and volumetric energy densities.
- Similar or lower irreversible loss ( $\leq 15\%$ ) in comparison to synthetic graphite.
- Similar or better coulombic efficiency ( $>99.9\%$ ) in comparison to synthetic graphite.
- Similar or better cyclability and calendar life in comparison to synthetic graphite.
- Improve the coulombic efficiency, available energy density, rate capability and cycle life of high specific capacity Si based electrodes.
- Investigate nano-structured (*nc*-Si) and amorphous Si (*a*-Si) based composite or hybrid heterostructured anode.

#### Technical Barriers

The important technical barriers of alternative anodes for lithium ion batteries to be used in electrical vehicles or hybrid electrical vehicles are following:

- Low energy density
- Large first cycle irreversible loss ( $>25-30\%$ )
- Inadequate coulombic efficiencies
- Poor cycle life
- Poor rate capability
- Low charge/discharge rates

#### Technical Targets

- Synthesize nano-structured (*nc*-Si) and amorphous Si (*a*-Si) based composite or hybrid structured anodes using cost effective processing techniques.
- Achieve reversible capacity of  $\geq 1200$  mAh/g.
- Reduce first cycle irreversible loss to less than  $\sim 15\%$ .
- Improve coulombic efficiencies higher than  $99.5\%$ .
- Improve the rate capability.
- Characterize the nano-scale hetero-structures for structure and composition using electron microscopy techniques such as SEM, TEM and HREM.

#### Accomplishments

- Developed cost effective chemical and solid state approaches to nanostructured or amorphous Si based composites.
- Synthesized nanocrystalline Si and vertically aligned carbon nanotube (VACNT) hybrid nanostructures by combined simple, cost effective chemical vapor deposition (CVD) and pulsed laser deposition (PLD) method directly on Inconel 600 alloy.
- Binder free Si/VACNT heterostructured anode exhibited a specific capacity in excess of  $\sim 1500$  mAh/g and excellent rate capability.
- Identified interface control agents (ICA) to improve the interfacial strength of the Si and VACNT interface and as a result improved the cyclability.
- A novel binder system generated by layer by layer (LbL) assembly of chemically interactive polyelectrolyte layers consisting of silicon and super-P was developed.
- Synthesized amorphous Si films directly on Cu-foil by electrochemical reduction of silicon-salts which exhibit reversible capacity  $\sim 1300$  mAh/g with excellent stability, cyclability and rate capability.

◇ ◇ ◇ ◇ ◇

#### Introduction

Achieving the DOE-BATT technical targets will require improving the cycling stability, reduce the irreversible loss, improve the coulombic efficiency and rate capability of Si based anodes. Hence it is essential to

synthesize Si based nanocomposites using economical processes exhibiting excellent mechanical properties to endure the large cycling induced volumetric stresses of Li-Si alloys.

In 2011, a systematic investigation of the electrochemical properties of two step chemical vapor deposition (CVD) processes derived Si/VACNT based composite anodes was conducted and reported. The generated Si/VACNT structure exhibits very high specific capacities ( $\geq 2800 \text{mAh/g}$ ) with a very low 1<sup>st</sup> cycle irreversible loss of <15%. However, the Si/VACNT displayed continuous capacity fading especially in the case of Si film morphologies deposited directly on VACNT yielding a capacity of less than 1,500 mAh/g at the end of 25 cycles when cycled with a current density of  $\sim 100 \text{mA/g}$ . This capacity fade response of Si/VACNT is attributed to the weak interface between silicon and VACNTs causing delamination or clustering of the silicon film islands over long term cycling. Over the last year in 2012, Si/VACNT was synthesized by a combined chemical vapor deposition (CVD) and pulsed laser deposition (PLD) method in order to improve the mechanical property and as a result the cycling stability of Si structures. In addition, in order to further improve the mechanical properties of Si/VACNT, an interface control agent (ICA) was identified to improve the interfacial strength of the Si and VACNT interface, and as a result the composite based on Si/VACNT/ICA is expected to exhibit improved cycling stability during repeated lithium alloying and dealloying processes. Silicon nanotubes, because of their one dimensional structure and empty space allowing for silicon expansion during lithiation, have been identified as an excellent choice as high capacity lithium ion anodes. However, their large scale production has been a challenge limiting its use only as a potential anode in the next generation of lithium ion batteries. In 2012, a novel and simple high throughput technique to generate large quantities of silicon nanotubes (SiNT) using a template based approach was also developed.

In earlier reports (FY 2011), the synthesis of thin amorphous silicon films on copper foil by electrodeposition from  $\text{SiCl}_4$  based electrolyte was reported. These films showed a stable capacity of  $\sim 1300 \text{mAh/g}$  for over 100 cycles with very low capacity fade per cycle ( $<0.016\%$  per cycle for 100 cycles). In 2012, the rate capability of the deposited a-Si films have been studied at different current rates (different C rates) varying from C/4 to 4C. Also, morphological studies before and after cycling using scanning electron microscopy (SEM) and impedance spectroscopic studies during cycling were also performed to understand the excellent cyclability of the electrodeposited amorphous films.

## Approach

To achieve the aforementioned goals, several novel low cost approaches to develop: 1) binder free Si/VACNT

heterostructures using a combination of CVD and PLD, 2) nano-scale heterostructures of Si/VACNT/ICA by chemical vapor deposition (CVD), 3) high throughput synthesis of silicon nanotubes and 4) amorphous silicon films by electrodeposition have been explored.

The Si/VACNT heterostructures were directly grown on Inconel 600 alloy metallic substrates by a combined chemical vapor deposition and pulsed laser deposition (CVD-PLD) method. First, VACNTs were grown using the CVD approach reported earlier [1] and later silicon was deposited on these CNTs by PLD. A 30 min PLD deposition yielded approximately 15-20 nm thick silicon film which comprised of nanocrystalline and amorphous silicon. In the case of VACNT/Si/ICA based heterostructures, the VACNTs were grown on quartz substrate using ferrocene based floating catalyst approach and m-xylene as the carbon source. Subsequent to this, a thin layer ( $\sim 10 \text{nm}$  thick) of the ICA was electron beam deposited on the VACNTs at a growth rate of  $0.2 \text{\AA/s}$  following which silicon was deposited as a thick film by thermal cracking of silane ( $\text{SiH}_4$ ) gas in a CVD reactor.

Silicon nanotubes were generated by a simple two-step process. First, an inorganic nanowire template was synthesized by a simple and high throughput approach in a microwave reactor. The inorganic nanowire templates show a smooth rod like morphology, 5-10  $\mu\text{m}$  in length and diameters varying between 10-50 nm (Figure V - 74).

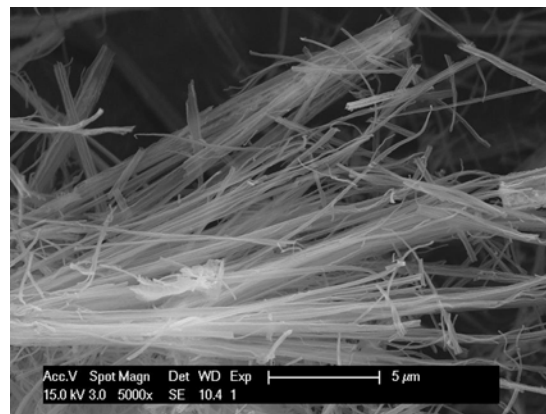


**Figure V - 74:** SEM image of inorganic oxide nanowires generated by hydrothermal synthesis techniques.

These nanowires were used as a template on which Si was deposited as a thin film by decomposing silane ( $\text{SiH}_4$ ) gas in a CVD reactor. Following silicon deposition, the silicon coated inorganic nanowires were dispersed in mineral acid to dissolve the nanowire template, thus generating silicon nanotubes (SiNTs). This method is a simple, convenient, and a facile technique to generate large quantities of silicon nanotubes in high yield involving simple and inexpensive processing techniques, and precursors.

A novel polyelectrolyte approach was used to develop a new binder system in which Si and super-P were dispersed in cationic and anionic polymers, respectively.

The solutions were coated as alternate layers akin to a layer by layer (LbL) approach on the current collector shown in Figure V - 75. The strong electrostatic interaction between the oppositely charged polymer layers provides powerful binding of the Si and Super-P during the cycling of the electrode.

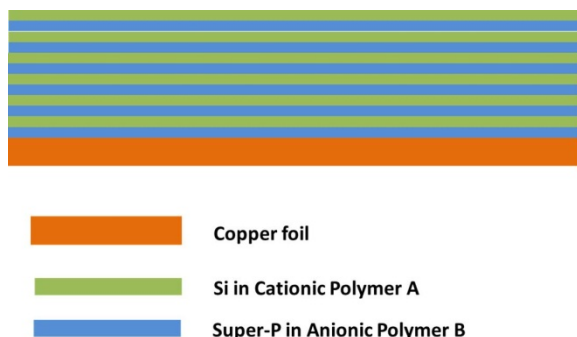


Figure V - 75: Schematic of the LbL assembly of polyelectrolyte layers consisting of Si and Super-P dispersions.

Amorphous Si (*a*-Si) films were deposited from non-aqueous electrolyte comprising 0.5M SiCl<sub>4</sub> and 0.1M of tetrabutylammonium chloride (TBACL) supporting electrolyte dissolved in propylene carbonate (PC). The *a*-Si films were obtained using galvanostatic deposition.

## Results

**1. Si/VACNT hybrid nanostructures synthesized CVD-PLD.** 15-20 nm Si film was deposited on the VACNTs grown on Inconel 600. These VACNT/Si heterostructures were used directly as anodes without binders and conductive agents. The heterostructures showed a low irreversible loss of <15% with a first discharge capacity ~2800 mAh/g (Figure V - 76) when cycled at ~100 mA/g in the 0.02-1.2V vs. Li<sup>+</sup>/Li voltage range. A stable reversible capacity >1600 mAh/g was obtained for 50 cycles with a capacity fade of 0.24% loss/cycle.

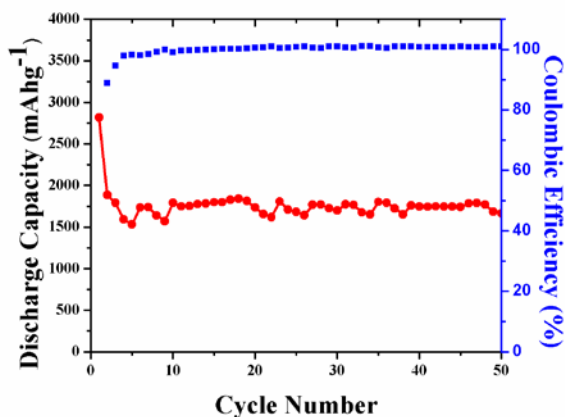


Figure V - 76: Cycling of Si/VACNTs by CVD/PLD approach.

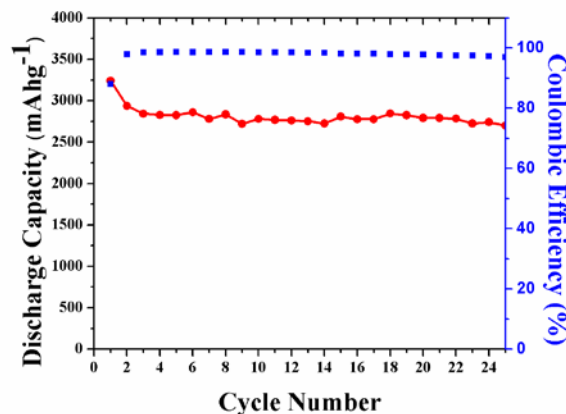


Figure V - 77: Charge-discharge plot of Si/ICA/VACNTs cycled at 300 mA/g between 0.02-1.2 V vs. Li<sup>+</sup>/Li.

**2. VACNT/ICA/Si heterostructures by eBeam/CVD.** Electrochemical cycling response (Figure V - 77) of the obtained VACNT/ICA/Si heterostructures, cycled at a discharge/charge rate of ~300 mA/g in the potential window between 0.02-1.2 V vs. Li<sup>+</sup>/Li, shows a first discharge capacity of ~3242 mAh/g with a very low first cycle irreversible loss of ~12%. At the end of 25 cycles, a reversible capacity ~2500 mAh/g capacity was obtained with a very low fade in capacity of ~0.3% loss per cycle and high coulombic efficiency (~99.8%). Si deposited as a thick film usually displays poor cyclability (fade rate >1.61%/cycle) compared to the silicon deposited as droplets. However, higher discharge capacity can be obtained in the case of films in contrast to droplets due to a greater weight ratio of Si to VACNT. The presence of the ICA layer between the VACNT and Si provides better support resulting in excellent cyclability of silicon as well as delivering reversible capacities ~2,500 mAh/g.

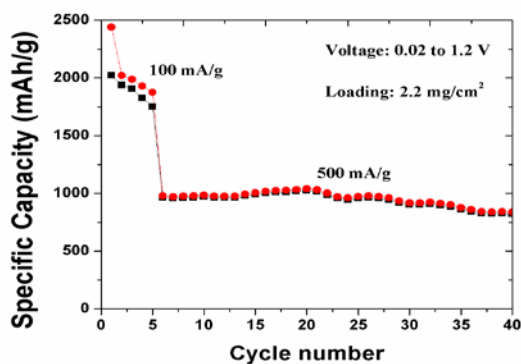


Figure V - 78: Variation of specific capacity vs. cycle number of SiNT cycled at different current densities.

**3. High throughput synthesis of Silicon nanotubes as high capacity anodes.** The obtained SiNTs were mixed with a binder and conductive additives to form a slurry which was coated on copper foils resulting in a mass loading of 2-3 mg/cm<sup>2</sup>. The obtained electrodes were

tested in a half cell configuration using Li foil as counter electrode within the voltage range of  $\sim 0.02\text{V}$  to  $1.2\text{V}$  vs.  $\text{Li}^+/\text{Li}$ . Figure V - 78 shows the electrochemical cycling behavior and stability of SiNTs cycled at current densities of  $\sim 100\text{ mA/g}$  and  $500\text{ mA/g}$ , respectively. The SiNTs exhibited a high first discharge capacity of  $\sim 2450\text{ mAh/g}$  and a low first cycle irreversible loss of 18%. These SiNTs when cycled at higher current densities of  $\sim 500\text{ mA/g}$  (C/2 rate) resulted in capacities of  $\sim 1000\text{ mAh/g}$  with very good cyclability and coulombic efficiency exceeding 99.5%. An initial fade rate less than 0.5%/cycle is obtained with a capacity retention of  $\sim 80\%$  at the end of 35 cycles.

#### 4. Synthesis of amorphous Si films directly on copper foil by electrochemical reduction of silicon salts.

In our 2011 Annual Report, it was reported that the amorphous silicon films deposited directly on copper showed a reversible capacity of  $\sim 1300\text{ mAh/g}$  for 100 cycles. In order to understand the cyclability of these films under high current rates, the *a*-Si films were discharged/charged at C/4, C/2, 1C, 2C and 4C rates, respectively (Figure V - 79). The capacity retained at the discharge/charge rate of 1C is  $\sim 1000\text{ mAh/g}$  which is  $\sim 77\%$  of capacity obtained at C/4 rate ( $\sim 1300\text{ mAh/g}$ ) thus indicating that electrodeposited *a*-Si is a promising anode for Li-ion systems involving medium charge/discharge rates ( $\sim 1\text{C}$ ) applications. However, a significant capacity loss is observed when cycled at higher rates (2C and 4C) resulting in a capacity of  $\sim 520\text{ mAh/g}$  for 4C rate. This is due to the poor electronic or ionic conductivity of *a*-Si rendering the charge transfer or lithium alloying to be kinetically hindered. However, no capacity fade was observed for a given C rate and the resulting capacity at 4C rate is still much higher than the capacity obtained using pure graphite as an anode indicating the promising nature of this approach.

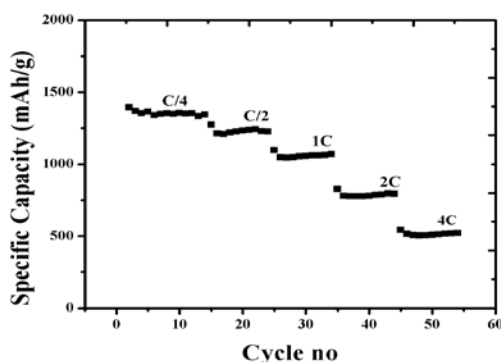


Figure V - 79: Specific capacity vs. cycle number of the *a*-Si film cycled at 0.25C, 0.5C, 1C, 2C and 4C.

**5. Novel binder system using Polyelectrolyte layers of Si and Super-P.** Following the polyelectrolyte layer approach, 10 alternating layers of Si dispersed in a cationic polymer and Super-P dispersed in an anionic polymer were coated onto the copper foil and annealed to generate a high strength ambipolar layered structure. These LBL layers

were mechanically strong and exhibited strong adhesion to the copper foil. Electrochemical characterization tests are currently ongoing, the results of which will be reported in subsequent quarterly and annual reports.

## Conclusions and Future Directions

Binder-free VACNT/Si heterostructures were developed using a combined CVD/PLD technique delivering stable reversible capacity  $> 1600\text{ mAh/g}$  for 50 cycles. This method can contribute to significant cost reduction in fabricating heterostructured anodes by eliminating inactive materials (Super-P and binder) and other processes (slurry making, tape casting, drying and rolling) which are typically used in battery manufacturing process. In order to improve the cyclability of the VACNT/Si (film) heterostructures, a thin interfacial layer (ICA) was grown between the CNT and Si film to improve the binding of the silicon film to the CNT. This interface control approach has resulted in heterostructures exhibiting capacities  $\sim 2500\text{ mAh/g}$  for (25 cycles) and a very low irreversible loss ( $\sim 12\%$ ). Also, a high throughput synthesis of silicon nanotubes (SiNTs) was developed for the first time wherein smooth inorganic nanowires synthesized in a microwave reactor were used as a template on which amorphous silicon was deposited by CVD. The template was eventually dissolved generating large quantities of SiNTs. These SiNTs exhibited reversible capacities  $\sim 1000\text{ mAh/g}$  at a current rate of  $500\text{ mA/g}$  (C/2) for 40 cycles with coulombic efficiencies exceeding 99.5%.

Future work will be dedicated to optimizing the interface control layer to further improve the mechanical stability for the VACNT/ICA/Si heterostructures. In order to lower the first cycle irreversible loss of the SiNTs, carbon coating of the Si/ICA/VACNTs will be attempted. Apart from developing the polyelectrolyte based binder system, new elastomeric and thermoplastic resin binders will be explored to improve the cyclability of nanostructured silicon. Also, efforts will be made to coat the electrodeposited *a*-Si film with a polymer or carbon layer to decrease the irreversible loss and improve the electron conduction to achieve better rate capability.

## FY 2012 Publications/Presentations

1. R. Epur, M. K. Datta & P. N. Kumta, *Electrochem. Acta*, **85**, 680-684 (2012).
2. R. Epur, M. Ramanathan, F. R. Beck, A. Manivannan and P. N. Kumta, *MSEB*, **177**, 14, 1157-1162 (2012).
3. W. Wang, R. Epur and P. N. Kumta, *Electrochem. Commu.* **13** 429-432 (2011).
4. M. K. Datta, J. Maranchi, S. J. Chung, R. Epur, K. Kadakia, P. Jampani and P. N. Kumta, *Electrochim. Acta*. **56** 4717-4723 (2011).
5. R. Epur, F. R. Beck, M. K. Datta, A. Manivannan & P. N. Kumta, *AIChE 2012 Conference – Pittsburgh, USA*

6. R. Epur, F. R. Beck, M. Ramanathan, M. K Datta, A. Manivannan & P. N Kumta, 2012, *ECS 221* Seattle Conference.

## V.C.2 Interfacial Processes - Diagnostics (LBNL)

Robert Kostecki  
Lawrence Berkeley National Laboratory  
Environmental Energy Technologies Division  
1 Cyclotron Road, MS 90-3062D  
Berkeley, CA 94720  
Phone: (510) 486-6002; Fax: (510) 486-5454  
E-mail: [r\\_kostecki@lbl.gov](mailto:r_kostecki@lbl.gov)

Start Date: October 1, 2008  
Projected End Date: September 30, 2012

### Objectives

- Establish direct correlations between BATT baseline electrodes' interfacial phenomena and surface chemistry, morphology, topology, and degradation mechanisms.
- Evaluate and improve the capacity and cycle life of intermetallic anodes and high voltage cathodes
  - Determine physico-chemical properties of the SEI i.e., chemical composition, reactions kinetics, morphology, ionic/electronic conductivity etc.
  - Investigate electrocatalytic behavior of intermetallic anodes in organic electrolytes
  - Provide remedies to interface instability e.g., new alloys and/or structures, electrolyte additives, codeposition of other metals etc.
  - Characterize degradation modes, improve SEI long-term stability in high-energy Li-ion systems.
  - Evaluate the effect of surface composition and architecture on electrochemical behavior of the electrode.

### Technical Barriers

This project addresses the following technical barriers related to the battery technology development effort of the DOE Office of Vehicle Technologies:

- Inadequate Li-ion battery energy (related to cost)
- Poor lithium battery calendar/cycle lifetime for PHEV and EV applications
- High electrode impedance that limits power density
- Need for new advanced battery materials and composite electrodes with acceptable specific energy, durability, costs, and safety characteristics.

### Technical Targets

- Cycle life: 5000 (deep) and 300,000 (shallow) cycles.
- (40 mile) · Available energy: 96 Wh/kg (40 mile).

- Calendar life: 15 years.

### Accomplishments

- Characterization of the interfacial phenomena occurring on  $\text{LiNi}_{0.5}\text{Mn}_{1.5}\text{O}_4$  was completed
  - Strong fluorescence signal that originates from the electrolyte decomposition products was detected at  $\text{Li}_x\text{Ni}_{0.5}\text{Mn}_{1.5}\text{O}_4$
  - Linear carbonates are responsible for the formation of a surface layer and soluble species at elevated potentials.
  - Electrolyte decomposition happens predominantly at  $\text{Ni}^{3+/4+}$  surface sites
- Study of interfacial properties of tin electrode, polycrystalline and single crystals was completed
- Preliminary near-field IR spectroscopy and imaging of SEI layer on Sn was carried out.
  - The chemical composition of the SEI could be correlated with the film surface morphology.

◇ ◇ ◇ ◇ ◇

### Introduction

A primary aim of this project is to develop and use advanced diagnostic techniques and experimental methodologies to characterize basic physico-chemical properties and function of Li-ion electrode active and passive components that are being developed for use in PHEV and EV applications. The focus of this task is to understand and correlate fundamental interfacial processes that occur in Li-ion batteries with the cell electrochemical performance. The diagnostic evaluation of composite and model electrodes are used to determine cell failure mechanisms, anticipate the system lifetime and develop new more-stable materials, composites and electrodes.

### Approach

The main focus of this project involves the development and application of new instrumental techniques and novel enabling experimental methodologies to investigate and understand the basic mechanism of operation of Li-ion batteries. Advanced analytic methods are being developed and used *in situ* to characterize materials and cell active and passive components. *In situ* enhanced spectroscopic, microscopic and diffraction techniques as well as standard post-test analyses are applied to investigate the morphology, topology, structure, and composition changes of electrode materials and electrode/electrolyte interfaces during cell cycling.

## Results

One objective of this project was to investigate surface phenomena occurring on high voltage cathode materials, e.g.,  $\text{LiNi}_{0.5}\text{Mn}_{1.5}\text{O}_4$ . *In situ* fluorescence spectroscopy (Figure V - 80) revealed the presence of a surface layer on the carbon- and binder-free model electrodes of LMNO. Exchanging  $\text{LiPF}_6$  with  $\text{LiClO}_4$  in the EC:DEC solution did not produce any difference in fluorescence intensity, indicating that it originates from the decomposition of organic carbonate solvents. Interestingly, no significant fluorescence signal was detected on a  $\text{LiMn}_2\text{O}_4$  electrode, which indicates, that the electro oxidation to the  $\text{Ni}^{3+/4+}$  is the main contributing factor, which facilitates the electrolyte decomposition.

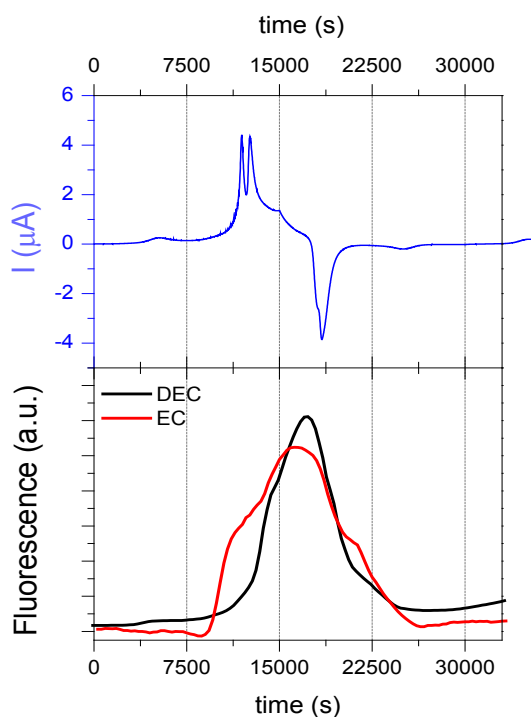


**Figure V - 80:** Current response (upper panel) and fluorescence intensity (lower panel) vs. time during a CV between 3.5 and 5.0 V at 0.1 mV/s for 1M  $\text{LiPF}_6$  EC (red curve) and 1M  $\text{LiPF}_6$  DEC (black curve).

The fluorescence spectroscopy studies indicate that (1)  $\text{LiPF}_6$  is not the source of the fluorescence in these systems, (2) origin of fluorescence is the decomposition of linear carbonates e.g., DEC, (3) nickel surface sites promote electrolyte decomposition at high potentials. However, similar interfacial studies on carbon black additives commonly used in composite electrodes also show strong fluorescence at elevated potentials (Figure V - 81).

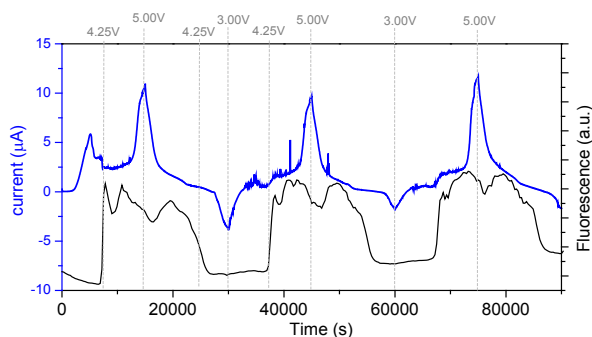


**Figure V - 81:** Current response (blue) and fluorescence intensity (black) vs. time during a CV of Super-P Li/PVdF (90/10) electrode between 3.5 and 5.0 V vs  $\text{Li/Li}^+$  at 0.1 mV/s, electrolyte EC:DEC 1:2 1M  $\text{LiPF}_6$ .

The fluorescence signal started to rise abruptly at 4.25 V and continued to increase up to 4.75 V, and then began to decrease at 4.75 V during the cathodic scan. Interestingly, the fluorescence signal decreased slightly around 5 V potential limit, and the intensity of residual fluorescence was higher at the end of the cycle. This pattern was repeated during the following cycles, indicating that electrolyte oxidation on CB additives also contributes to the interfacial side-reaction of the composite cathodes. These results point at a significant electrochemical activity of carbon blacks toward the electrolyte at such high potentials, which have to be mitigated in practical Li-ion cells.

Exploring near-field IR spectroscopy as a method for interfacial studies of Li-ion electrodes was the second objective. Near-field scanning optical microscopy enables the simultaneous topographical and sub-diffraction limited optical imaging of surfaces. Near-field spectroscopy using novel high-performance scanning optical microscopy probes (gold pyramid, bow tie or coaxial shaped antenna) overcomes the diffraction-limited resolution of regular confocal microscopy by showing spatial resolution down to 20 nm and provides near-field enhanced signature of surface compounds.

This research thrust toward milestones resulted in a pioneering *ex situ* near-field IR imaging of the SEI formed on polycrystalline tin electrode. The images were collected at three different wavelengths i.e., 9.6, 10.0 and 10.4  $\mu\text{m}$  for an Sn electrode that was cycled potentiostatically 5 times between 2.5 and 0.8 V.

The images shown in Figure V - 81 displayed strong variations in signal intensity and contrast as the function of the IR light energy. The image recorded at 10.4  $\mu\text{m}$  showed an inverted IR contrast, which is indicative of a complex composition and/or non-uniform distribution of the layer building components. Additional IR spectroscopic investigations of reference compounds such as  $\text{LiF}$ ,  $\text{Li}_2\text{CO}_3$ , lithium oxalate etc., will enable determination of the local chemical composition of the SEI with one simple mapping step.

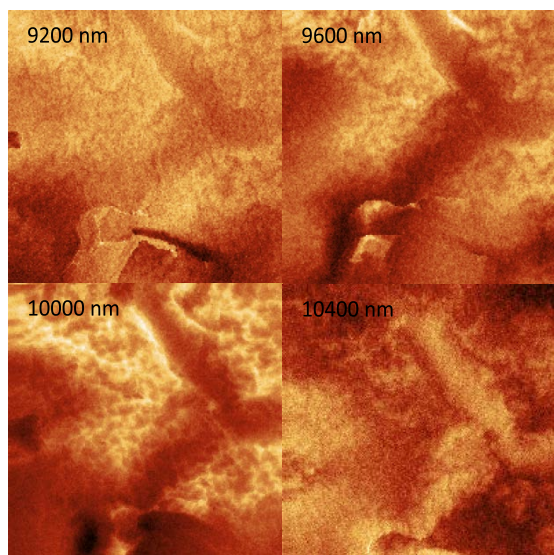


**Figure V - 82:** *Ex situ* near-field IR images at different wavelengths of the SEI layer on a polycrystalline Sn electrode after 5 cycles

## Conclusions

- *In situ* Raman and fluorescence spectroscopy unveiled the presence of a decomposition layer on carbon and binder free model  $\text{LiNi}_{0.5}\text{Mn}_{1.5}\text{O}_4$  electrodes.
- Fluorescence rise in this system can be correlated to the beginning of the  $\text{Ni}^{2+}$  oxidation and originates from the decomposition of organic carbonate solvents.
- Carbon black contributes side reaction on high-voltage cathodes, which may affect the overall chemistry of Li-ion cells.
- Near-field IR spectroscopy and imaging has been successfully introduced in the portfolio of powerful surface sensitive techniques to study electrochemical interfaces in Li-ion systems.

## Future Directions

- Design new and modify existing experimental setups to determine interfacial phenomena and characterize phase boundary reactions.
  - Development of *in situ* capabilities with near-field IR imaging.
- Investigate the effect of surface crystalline orientation and electrolyte additives on the interfacial activity of the baseline electrode materials.
- Conduct fundamental studies of the composition, function and operation of electrode surface layers in Li-ion systems at nanometer range i.e., scale that correspond to surface layer basic constituencies.
- Cooperate with the BATT Task Groups and industrial partners to investigate the effect of material structure, morphology on formation of the SEI layer on intermetallic anodes.

- Identify possible degradation mechanism and propose alternate routes to improve the performance of composite electrodes.

## FY 2012 Selected Publications/Presentations

1. Xiaobo Chen, Can Li, Michaël Grätzel, Robert Kostecki, Samuel S. Mao, “Nanomaterials for Renewable Energy Production and Storage,” *Chemical Reviews*, accepted.
2. Chunjoong Kim, Nick S. Norberg, Caleb T. Alexander, Robert Kostecki, Jordi Cabana, “Mechanism of phase propagation during lithiation in carbon-free  $\text{Li}_4\text{Ti}_5\text{O}_{12}$  battery electrode,” *Adv. Funct. Mater.*, accepted.
3. Nick S. Norberg, Robert Kostecki, “The Degradation Mechanism of a Composite  $\text{LiMnPO}_4$  Cathode,” *Journal of the Electrochemical Society*, in press.
4. Vassilia Zorba, Jaroslaw Syzdek, Xianglei Mao, Richard E. Russo and Robert Kostecki, “Ultrafast laser induced breakdown spectroscopy (LIBS) of electrode/electrolyte interfaces,” *Applied Physics Letters*, **100**, 234101 (2012).
5. Nick S. Norberg and Robert Kostecki, “Interfacial Phenomena at a Composite  $\text{LiMnPO}_4$  Cathode,” *Journal of the Electrochemical Society*, in press.
6. S.F. Lux, I.T. Lucas, E. Pollak, S. Passerini, M. Winter and R. Kostecki, “The mechanism of HF formation in  $\text{LiPF}_6$  based organic carbonate electrolytes,” *Electrochemistry Communications*, **14**, 47–50, 2012.
7. Nick Norberg, Robert Kostecki, “FTIR Spectroscopy of a  $\text{LiMnPO}_4$  Composite Cathode,” *Electrochimica Acta* **56** (2011) 9168–9171
8. Ivan T. Lucas, Jaroslaw Syzdek, and Robert Kostecki, “Interfacial Processes at Single-Crystal  $\beta$ -Sn Electrodes in Organic Carbonate Electrolytes,” *Electrochemistry Communications*, **11**, 1271-1275, 2011.

## V.C.3 Development of High Capacity Anodes (PNNL)

Ji-Guang Zhang  
Pacific Northwest National Laboratory  
902 Battelle Blvd., Mail Stop K2-44  
Richland, WA 99352  
Phone: (509) 372-6515; Fax: (509) 375-2186  
E-mail: [jiguang.zhang@pnnl.gov](mailto:jiguang.zhang@pnnl.gov)

Jun Liu (Co-PI)  
Pacific Northwest National Laboratory  
902 Battelle Blvd., Mail Stop K2-01  
Richland, WA 99352  
Phone: (509) 375-4443; Fax: (509) 351-6242  
E-mail: [jun.liu@pnnl.gov](mailto:jun.liu@pnnl.gov)

Start Date: October 1, 2010  
Projected End Date: September 30, 2014

### Objectives

- Develop Si-based anodes with high capacities, high cycle stabilities and high rate capabilities.
- Develop a low-cost synthesis route for Si-based anodes.

### Technical Barriers

- Low energy density, limited cycle life, and high cost.

### Technical Targets

- Identify the main failure mechanisms of the Si-based anode.
- Develop low-cost and scalable approaches to synthesize Si-based nanocomposite materials with improved performance (a capacity retention >700 mAh/g over 150 cycles).
- Select binders and electrolyte additive to improve the Coulombic efficiency of Si-based anodes to more than 99%.

### Accomplishments

- Developed high-capacity stable Si anodes using a low-cost and scalable synthetic method. Two-stage mechanical ball milling process has been developed to anchor Si on a rigid skeleton support and create continuous conductive paths. A stable capacity of ~800 mAh/g (based on the full electrode including the carbon additive and binder) over 150 cycles was obtained.
- Developed a hollow core-shell structured porous Si-C nanocomposite providing a capacity of ~650 mAh/g

(based on the full electrode including the carbon additive and binder) over 100 cycles.



### Introduction

Si-based materials have great potential to be used as high-capacity anodes for Li-ion batteries; however, their practical application has been hindered by several barriers, including large volume expansions and phase transformations during lithiation and delithiation, which lead to rapid capacity fading during charge/discharge cycles. The low conductivity and poor stability of these materials usually require the addition of conductive additives and/or coatings to enhance electron transport and electrical contact of the active materials. Good capacity retention could be obtained if a larger amount of carbon was added to the material, but this would lead to a decrease in the capacity of the full electrode. To increase the cycle life of the anode without sacrificing the capacity, novel structured anode composites, with capacities more than double that of the state-of-the-art graphitic anode, need to be developed.

### Approach

Two approaches have been developed for a highly stable, high-capacity anode based on silicon composite. First, a cost-effective and scalable approach is developed to prepare a core-shell structured Si/B<sub>4</sub>C composite with graphite coating with high efficiency, excellent rate performance and long-term stability. In this material, conductive B<sub>4</sub>C with high Mohs hardness serves not only as micro-/nano-millers in the ball-milling process to break down micron-sized Si but also as the conductive rigid skeleton to support the *in situ* formed sub-10 nm Si particles to alleviate the volume expansion during charge/discharge. The Si/B<sub>4</sub>C composite is coated with a few graphitic layers to further improve the conductivity and stability of the composite.

In another approach, hollow core-shell structured porous Si-C nanocomposites with void space up to tens of nanometers were synthesized to accommodate the large volume expansion during lithiation for high-performance Li-ion battery anodes. First, Si nanoparticles were oxidized under controlled conditions to form a layer of SiO<sub>2</sub> coating on the surface. CVD carbon deposition then was used to coat a layer of carbon on the core-shell structured Si@SiO<sub>2</sub>. After removal of the SiO<sub>2</sub> layer using HF etching, a void space was hence created between the Si core and the carbon shell, forming the hollow core-shell structured porous Si-C nanocomposite.

## Results

### 1. Si Anode with Conductive Rigid Skeleton

**Support.** High-capacity stable Si anodes with rigid skeleton support and continuous graphene coating have been developed. Figure V - 83 shows the schematic diagram of the synthesis process of Si/B<sub>4</sub>C/graphite (SBG) composite. Micron-sized Si and B<sub>4</sub>C were mixed in an appropriate ratio and milled using a high energy ball miller (HE Ball Milling) (Figure V - 83a) to form the Si/B<sub>4</sub>C composite. The *in situ* generated nano-sized Si particles were attached to the B<sub>4</sub>C particles, forming the Si-coated B<sub>4</sub>C core-shell structure. Graphite coating on the Si/B<sub>4</sub>C core-shell structure was achieved by a subsequent planetary ball milling (PBM) of Si/B<sub>4</sub>C and graphite, in which graphite was mechanically peeled, forming a graphite coating on the surface of Si/B<sub>4</sub>C. The effect of ball-milling-time, as well as the ratios among silicon, rigid skeleton, and conductive graphene coating were systematically investigated. All these parameters were found to affect the cycle stability of the anode (Figure V - 84.) The best composition (Si: rigid skeleton: graphene) was found to be 4: 3: 3 and a good ball milling condition is 8 hr high-energy ball milling (for Si/B<sub>4</sub>C) and 8 hr planetary ball milling (for graphite on Si/B<sub>4</sub>C).

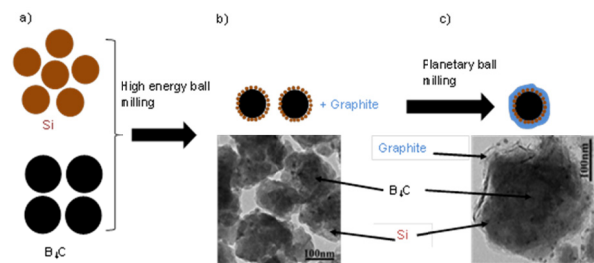


**Figure V - 83:** Schematic diagram of the synthesis process of conductive-rigid-skeleton-supported Si with TEM images for the intermediate product of Si/B<sub>4</sub>C and the final SBG product. a) Starting materials of micron-sized B<sub>4</sub>C and Si. b) Schematic diagram of the Si/B<sub>4</sub>C core-shell structure and TEM image. c) Schematic diagram of the SBG structure and TEM image.

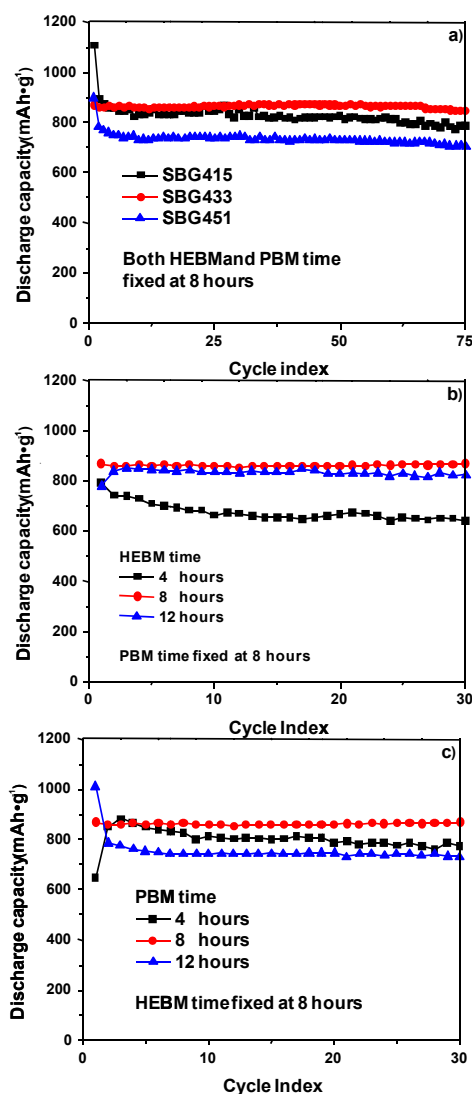


**Figure V - 84:** Effect of SBG composition and the synthesis condition on the cycling stability at a current density of 0.63 A/g based on the silicon weight. (a) Comparison of the long-term cycling stability for SBG composites with different compositions; (b) Cycling stability of SBG433 with different high-energy ball milling (HEBM) times; (c) Cycling stability of SBG433 with different PBM times.

For the optimized B<sub>4</sub>C-supported silicon anode, several binders and electrolyte additives were investigated to further improve the cyclability and Coulombic efficiency of the silicon-based anode. The samples using (CMC) binder and 10% FEC additive in the electrolyte (1 M LiPF<sub>6</sub> in ethylene carbonate and dimethyl carbonate (1:2 ratio in volume)) have demonstrated the best performance. a specific capacity of ~859 mAh/g (based on the whole electrode weight, including binder and conductive carbon) and a Coulombic efficiency of >99% have been obtained (Figure V - 85a). These Si-based anodes also exhibited very good rate performance. Figure V - 85b shows the cycling performance under different current densities

ranging from 0.5 to 2.5 A/g. The capacity is ~500 mAh/g at 2.5 A/g.

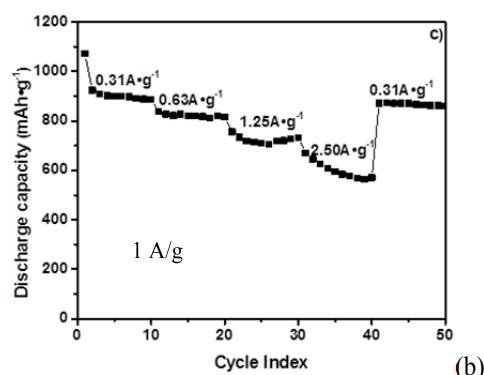
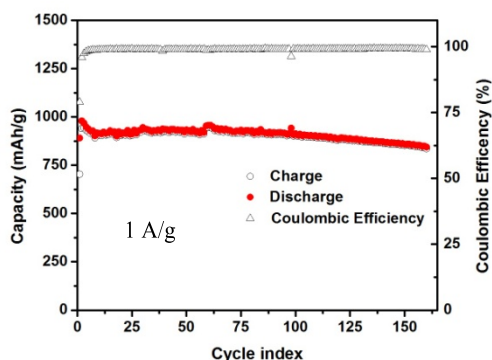


**Figure V - 85:** Electrochemical performance of SBG with optimized composition and ball-milling conditions. (a) Long-term cycling stability of SBG433 at a current density of 0.63 A/g. (b) Rate performance for SBG433 prepared by 8 h HEBM and 8 h PBM time.

**2. Hollow core-shell structured porous Si-C nanocomposite.** A hollow core-shell structured porous Si-C nanocomposite with rationally designed void space between the Si core and the carbon shell can accommodate a large volume change of Si (~300%) and at the same time retain good electrical contact between Si and carbon (Figure V - 86a). TEM analysis (Figure V - 86b) showed that a thin layer (~5 nm) of CVD-coated carbon stabilized the electrical contact among silicon particles and increased electrical conductivity of the silicon anode. The void space between Si and the CVD carbon can be controlled at up to tens of nanometers and can tolerate the volume change of silicon during charge and discharge.

The porous silicon anode designed can have more than 80% capacity retention after 100 cycles with the capacity ~ 650 mAh/g (based on full electrode weight) at a current density of 1 A/g (based on silicon) (Figure V - 87a). The composite also showed good rate performance. Figure V - 87b shows that the capacity at 100 mA/g current density is ~ 920 mAh/g and 530 mAh/g at 2 A/g. The capacity retention is > 630 mAh/g after testing for 113 cycles (3 formation cycles at 100 mA/g, 10 cycles each at current densities of 500 mA/g, 1 A/g, 2 A/g, 4 A/g and 8 A/g and then 60 cycles at 1 A/g), which demonstrates the

recovery of the composite material after subjecting it to different charge-discharge rates (Figure V - 87b).

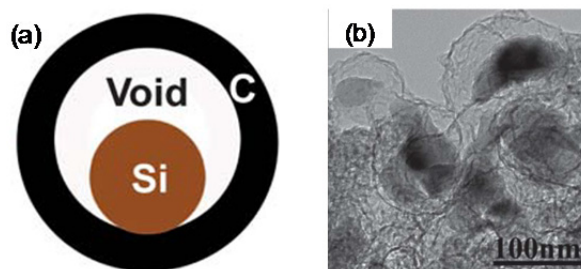


**Figure V - 86:** (a) Schematic structure and (b) TEM image of the hollow core-shell structured porous Si-C nanocomposite.

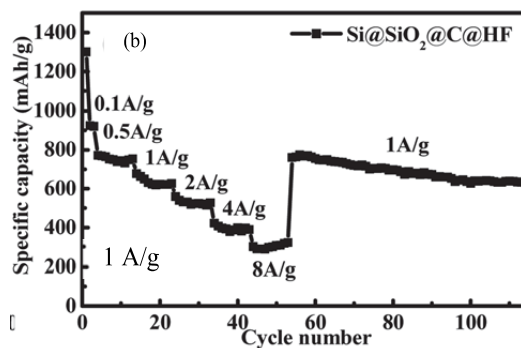
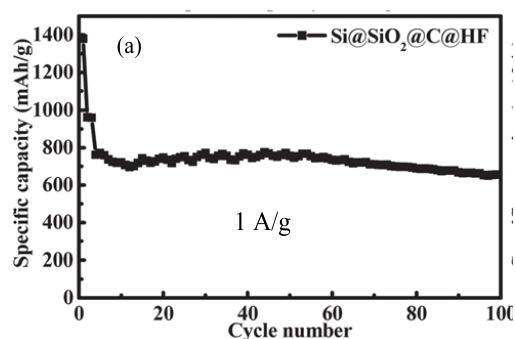


**Figure V - 87:** Electrochemical performance of the core-shell structured porous Si-C nanocomposite. (a) Long-term cycling stability of the composite. (b) Rate performance of the composite.

## Conclusions and Future Directions

Si anodes with rigid skeletons and the hollow core-shell structured porous Si-C nanocomposite showed significantly improved capacity and stability. The SBG composite anode shows excellent cyclability with a specific capacity of ~859 mAh/g (based on the weight of the entire electrode, including binder and conductive carbon) and ~94% capacity retention over 150 cycles at a 0.8C rate. This new structure has the potential to provide adequate storage capacity and stability for practical applications, and good prospects for large-scale manufacturing using commercially available materials and technologies. In a separate effort, a hollow core-shell structured porous Si composite designed and synthesized

using a low-cost and scalable approach demonstrated its promising practical application as stable, high-capacity anodes for Li-ion batteries. The pore-size effect of Si on the electrochemical performance was also elucidated and demonstrated that Si with large pore size has better cycling stability. The porous structured electrode material with hollow core-shell design is effective in accommodating the volume change during cycling and reveals a potential practical path for Si anodes.

Future work will focus on the following three aspects:

- Investigate new binders/electrolyte additives and their effects on the SEI layer using the B4C/Si/C composite as the baseline material.
- Optimize the hollow core-shell structured porous Si and the rigid skeleton-supported Si composite for high capacity and stable cycling.
- Develop new approaches to enable thick electrodes.

### FY 2012 Publications/Presentations

1. X Chen, X Li, F Ding, W Xu, J Xiao, Y Cao, P. Meduri, J Liu, GL Graff and J-G Zhang, "Conductive rigid skeleton supported silicon as high-performance Li-ion battery anodes," *Nano Lett.*, **12** (8): 4124-4130 (2012).
2. X Li, P Meduri, X Chen, W Qi, MH Engelhard, W Xu, F Ding, J Xiao, W Wang, C Wang, J-G Zhang and J Liu, "Hollow core-shell structured porous Si-C nanocomposites for Li-ion battery anodes," *J. Mater. Chem.*, **22**, 11014-11017, (2012)
3. F Ding, W Xu, D Choi, W Wang, X Li, M.H. Engelhard, X Chen, Z Yang and J-G Zhang, "Enhanced performance of graphite anode materials by AlF<sub>3</sub> coating for lithium-ion batteries," *J. Mater. Chem.*, **22**(25), 12745–2751 (2012).
4. J-G Zhang, "Nanostructured Materials for Energy Storage beyond Li-Ions," Presented (Invited Speaker) at *Materials Challenges in Alternative & Renewable Energy 2012* (MCRE12), Clearwater, FL on February 29, 2012.
5. X Chen, X Li, F Ding, W Xu, J Xiao, Y Cao, P. Meduri, J Liu, GL Graff and J.G. Zhang. "Silicon composites anode with rigid skeleton for lithium ion batteries," Presented at *MRS Spring Meeting*, San Francisco, CA on April 10, 2012.
6. W Xu, W Wang, F Ding, D Choi, X Chen, X. Li, CM Wang, MH Engelhard, Z Nie, Z Yang and J. Zhang, "Anode Materials with Non-carbon Coating for Stable and High Rate Lithium-ion Batteries," Presented at *221<sup>st</sup> ECS Meeting*, Seattle, WA on May 8, 2012.
7. J-G Zhang, "Nanostructured Materials for Energy Storage Systems beyond Li-ion," Presented at the *Rhode Island DOE EPSCoR Symposium on Challenges and Opportunities in Energy Storage Materials*, Brown Univ., Providence, RI on June 1, 2012.

## V.C.4 Advanced Binder for Electrode Materials (LBNL)

Gao Liu

Lawrence Berkeley National Laboratory  
Environmental Energy Technologies Division  
1 Cyclotron Rd., MS 70R108B  
Berkeley, CA 94720  
Phone: (510) 486-7207; Fax: (510) 486-7303  
E-mail: [Gliu@lbl.gov](mailto:Gliu@lbl.gov)

Start Date: October 1, 2008

Projected End Date: September 30, 2012

### Objectives

- Develop new conductive polymer binder materials to enable large volume change lithium storage materials to be used in lithium-ion electrode, focusing on Sn with Poly(9,9-dioctylfluorene-co-fluorenone-co-methylbenzoic ester (PFFOMB) conductive polymer optimization.
- Investigate conductive binder properties to Si electrode performance in various electrode compositions and configurations.
- Explore electrolyte and additives to increase coulomb efficiency (CE).

### Technical Barriers

This project addresses the following technical barriers from the Energy Storage section of the Vehicle Technologies Program Multi-year Research, Development and Demonstration Plan:

- Calendar and cycle life
- Energy density
- Cost

### Technical Targets

Relevant USABC goals

- EV
  - \$150/kWh.
  - 230 Wh/dm<sup>3</sup>.
  - 1000, 80% capacity, discharge cycles.
  - 10-year system life.
- PHEV 40-mile
  - \$220/kWh.
  - 193 Wh/dm<sup>3</sup>.
  - 2750, 75%-capacity, discharge cycles +80,000 HEV cycles.
  - 15-year system life.

### Accomplishments

- Successfully adapted the PFFOMB conductive polymer binder to Sn nanoparticles for lithium-ion negative electrode applications. Optimized the composition of the Sn/PFFOMB electrode composite. Demonstrated extended cycling of pure Sn nanoparticles with PFFOMB binder composite electrode at 500 mAh/g-Sn capacity.
- Developed secondary structures of Si/PFFOMB composite particles to fabricated higher area specific capacity electrode at 3.5mAh/cm<sup>2</sup>.
- Demonstrated the enhanced CE of the Si electrode in the electrolyte with vinyl ethylene carbonate (VC) and fluoroethylene carbonate (FEC) additives.



### Introduction

Achieving the DOE energy, cycle life and cost targets will require materials of higher capacity and improved coulombic efficiency or cells with higher voltage. High capacity Si or Sn alloy based anode material has the potential to fulfill the energy density requirements for EV/HEV applications. However, full capacity cycling of the alloy anode materials results in significant capacity fade due to a large volume change during Li insertion and removal. Decreasing the particle size to nanometer scale can be an effective means of accommodating the volume change. However, it is very challenging to make electric connections to all the alloy nanoparticles in the electrode by using similar size acetylene black conductive additive. The repeated volume change of the alloy nanoparticles during cycling can lead to repositioning of the particles in the electrode matrix and result in particle dislocation from the conductive matrix. This dislocation of particles causes the rapid fade of the electrode capacity during cycling. In order to address this issue, Si/conductive polymer composite electrodes were developed in this work. This new electrode can be fabricated with the current lithium-ion manufacturing processes. A new class of electric conductive binder materials was developed, which the Lowest Unoccupied Molecular Orbital (LUMO) energy is controlled to match the reduction potential of the alloy materials. The electrodes made with these binders have significantly improved cycling capability of Si or Sn type of alloy materials.

### Approach

Use functional polymer design and synthesis to develop new conductive polymers with proper electronic

properties, strong adhesion and improved flexibility to provide electric pathways in the electrode, and to accommodate large volume change of the Si or Sn alloy active material during lithium insertion and removal. The rational design of binder is assisted with advanced diagnostic techniques such as XAS at Advance Light Sources and with advanced molecular computation at National Energy Research Scientific Computing Center – both are DOE national user facilities.

## Results

### Conductive Polymer Binder with Tailored Electronic Properties for Si or Sn Alloy Materials. A

new class of conductive polymers was developed through a combination of material synthesis, X-ray spectroscopy, density functional theory, and battery cell testing (Figure V - 88). Contrasting other polymer binders, the tailored electronic structure of the new polymer enables lithium doping under the battery environment. The polymer thus maintains both electric conductivity and mechanical integrity during the battery operation.

The technical challenge stems from the reducing environment when the Si or Sn anode is lithiated. For example, the typically used p-type polyaniline (PAN) conductive polymer will not stay p-doped below potential 1 V (Li/Li+), therefore losing electronic conductivity when used in the Si anode, which is operated between the potential range of 0.01 V–1 V (Li/Li+). In order to solve the crucial problem of electric connectivity of the binder, polymer binders that could be cathodically (n-type) doped were developed for high electronic conductivity under the reducing environment for anodes. Our strategy for accomplishing the goal is to tailor the energy levels of the polymer conduction state, i.e., the lowest unoccupied molecular orbital (LUMO), so that the electrons could cathodically dope the polymer to achieve adequate electronic conductivity. Mechanically, it is also crucial that the polymer is intimately adhered to alloy particle surface. Both electrical and mechanical integrity of the electrodes will then be maintained throughout the battery operation.

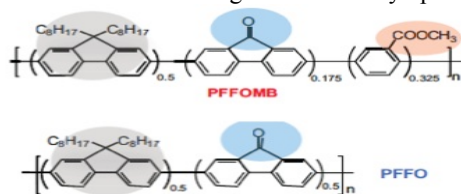


Figure V - 88: Molecular structure of conductive polymer binder.

The molecular structures of the developed polymers, PFFO and PFFOMB<sup>12</sup> are based on polyfluorene (PF)-type polymers (Figure V - 88) Two key function groups, carbonyl C=O and methylbenzoic ester -PhCOOCH<sub>3</sub>

<sup>12</sup> PFFO stands for Poly(9,9-dioctylfluorene-co-fluorenone); PFFOMB stands for Poly(9,9-dioctylfluorene-co-fluorenone-co-methylbenzoic ester).

(MB), were introduced for tailoring the LUMO electronic states and for improving the polymer adhesion respectively, as elaborated below.

In order to achieve a properly tailored electronic structure, synchrotron based soft x-ray absorption spectroscopy (XAS) was extensively applied on a series of polymers to monitor the unoccupied conduction states. XAS provides a simple but direct probe of the excitations of core level electrons to the unoccupied states, i.e., the lowest-energy XAS peaks directly correspond to the LUMO states. Figure V - 89 shows the XAS data collected on three selected PF type polymers and the traditionally used p-type PAN. It is evident that the carbonyl groups in PFFO and PFFOMB generate a new LUMO state at 284.7eV in XAS (blue arrow), much lower than that of the PF (black arrow) and PAN (purple arrow). The additional MB units in PFFOMB do not change the low energy position of this LUMO. Therefore, the carbonyl is the key function group that lowers the LUMO energy level.

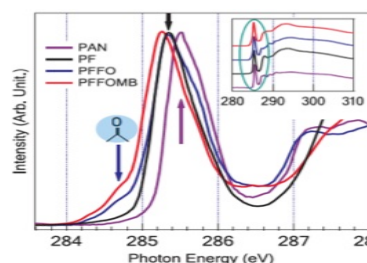


Figure V - 89: Carbon- 1s XAS spectra collected on a series of polymers.

Although the PFFOMB binder was initially designed for Si nanoparticles, Sn anode materials has the similar electronic properties requirements as for Si. The operational potential of Sn is between 0-1 V vs. lithium in the lithium-ion chemistry anode. The Sn oxide surface adheres strongly with the ester groups on the binders. PFFOMB binders with Sn nanoparticles were investigated during this period.

### Performance of Sn/Conductive Polymer Composite Electrode.

Since electronic conductive binders can provide molecular level electronic connection between the Sn particles and electric conducting medium at the interface, and provide inter-particle electronic connection, the usage of PFFOMB alone may be sufficient for the Sn electrode design. This will change the electrode to a two-composition system between Sn and PFFOMB. A limited optimization of the composition between Sn and PFFOMB was conducted. To optimize the composition of electrode, binder content was changed at 2 %, 5% and 10 % by weight (Figure V - 90). The testing results in Figure V - 90 show that electrode performance is sensitive to the binder content. With 5 % of polymer binder, the electrode can retain over 500 mAh/g of reversible capacity. On the contrary, the electrodes with 2 % of polymer binder fade dramatically. The electrode with 10% binder needs a few cycles of activation before it started to cycle normally. The PFFOMB functions both as binder to provide mechanical

stability of the electrode and provides electric conduction. The balance between the two functions is responsible for the optimum performance of this electrode composition.

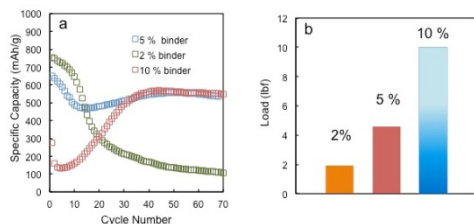


**Figure V - 90:** (a) Cycling performance of Sn electrode with different PFFOMB binder content. Cycling at 0.1 C rate in the range of 20 mV-1.5 V with electrolyte 1M LiPF<sub>6</sub> in EC/FEC 3/7. (b) Adhesion force of electrode laminates.

SEM surface images of the electrodes with different composition of PFFOMB/Sn were taken (Figure V - 91). Due to the high density (7.0 g/cm<sup>3</sup>) of the Sn particles, the 10% polymer by weight is equivalent to over 30% by volume ratio of polymer. The SEM images clearly show the 10% PFFOMB/Sn electrode sample has extensive coverage of polymer on the Sn particles. This extensive coverage leads to longer activation time needed to proper cycle the Sn particles. The 2% PFFOMB sample has low polymer content as binder, and low adhesion. This is the main reason the electrode fails fast during cycling. The 5% binder performs the best among three compositions. However, extended cycling of the electrode leads to particle reorganization in the binder, and possible Sn material aggregation. The reorganization and aggregation has created domain structures that are either binder rich or Sn rich in some areas. This may create a situation that the binder rich regions isolate the Sn rich domains from effective lithium-ion transport from the electrolyte.

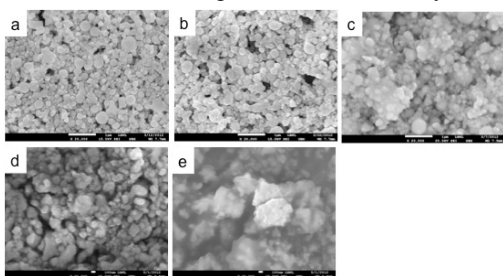


**Figure V - 91:** SEM images of the new PFFOMB/Sn electrode surface, PFFOMB content varies by weight in the pristine electrodes (a) 2%; (b) 5%; (c) 10%, and cycled electrode at 5% PFFOMB content electrode (d) after 1 cycle; (e) after 10 cycles.

The aggregation of Sn particles is detected by the TEM analysis of the electrode active material composite before and after cycling (Figure V - 92). The Sn particles are spherical particles before cycling, but become irregular shape after cycling. The cycled particles are also closer to each other than they are before cycling. The dynamic change of the composite electrode during cycling leads to capacity fade during cycling.

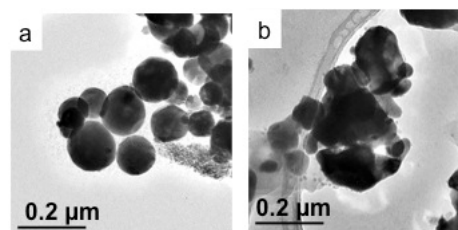


**Figure V - 92:** TEM image of the Sn particles in the electrode. (a) New electrode; (b) After 10 cycles.

**Developed secondary structures of Si/PFFOMB composite particles to fabricated higher area specific capacity electrode.** It is a challenge to fabricate Si particle based electrode at high area specific loading such as 3 mAh/cm<sup>2</sup> and above. The Si material volume expansion during the lithiation disrupts the integrity of the composite electrode. A 3-D secondary Si/PFFOMB composite particle approach was developed in order to stabilize the electrode level volume expansion (Figure V - 93). The composite particles have three components: Si nanoparticle, electrically conducting polymer, and has porosity build into it. During lithiation, the primary particles volume expanded into the conductive polymer and porosity, but secondary composite particles hold their shape and volume. The overall electrode structure was not interrupted during this process. This approach has shown promising cycling results for the electrode loading at 3.5 mAh/cm<sup>2</sup>.

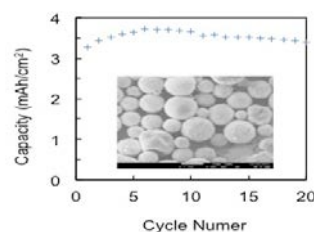


**Figure V - 93:** Si/PFFOMB conductive polymer electrode over 3.5 mAh/cm<sup>2</sup> area specific capacity. The in-set SEM image is the composite Si/PFFOMB particles (scale bar is 10 μm).

**Demonstrated the enhanced CE of the Si electrode in the electrolyte with additive.** The coulombic efficiency (CE) is another important parameter for Si based electrode. The CE is an indicator of the side reaction of the electrode materials. Due to the volume change, Si has a high surface reactivity. This causes a low CE and fast fading of cells made with Si anode. Electrolyte additive has routinely used to improve the cycling stability of graphite based lithium ion battery. Vinylencarbonate (VC) is an additive that well studied for graphite anode. Addition of VC can significantly improve the CE of the lithium ion battery. VC additive was used for Si/PFFPMB based electrode. It is demonstrated that increase the amount of VC in the electrolyte can significantly enhance the CE of the Si electrode, and stabilize the cycling capacity (Figure V - 94). At 10% of VC additive in the electrolyte, the CE reached 99.5% after 90 cycles.

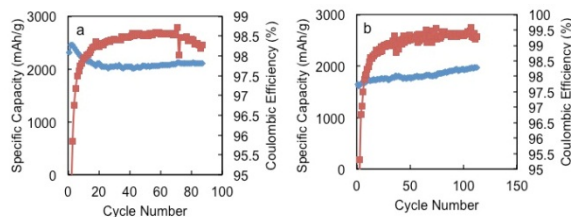


**Figure V - 94:** Cycling stability and coulombic efficiency of the Si/PFFOMB electrode at (a) 2% VC and (b) 10% VC in the electrolyte.

## Conclusions and Future Directions

The function of conductive polymer with alloy materials in the anode of the lithium-ion chemistry has been demonstrated in this period. A class of conductive polymer binder PFFOMB that is suitable for Si anode was developed in the past. Extended cycling tests have demonstrated the effectiveness to accommodate material volume change, provide electric conduction within the electrode, and the stability during cycling of the Si materials. The stable cycling performance of Sn/PFFOMB electrode was demonstrated. The performance characteristics of this Sn/PFFOMB electrode were studied. Composite Si/PFFOMB composite secondary particles were made. The electrode was fabricated with these secondary composite particles. Initial cycling at 3.5 mAh/cm<sup>2</sup> loading was demonstrated. Further development in the secondary particle structure is needed to improve the cycling stability. VC and FEC electrolyte additives have been demonstrated with improved performance in increasing CE. Further investigation in the additive area is warranted to improve the CE of alloy materials.

## FY 2012 Publications/Presentations

- Zheng, H.; Qu, Q.; Zhang, L.; Liu, G.; Battaglia, V. S., Hard carbon: a promising lithium-ion battery anode for high temperature applications with ionic electrolyte. *Rsc Advances* 2012, 2 (11), 4904-4912.
- Zheng, H.; Li, J.; Song, X.; Liu, G.; Battaglia, V. S., A comprehensive understanding of electrode thickness effects on the electrochemical performances of Li-ion battery cathodes. *Electrochim. Acta* 2012, 71, 258-265.
- Wu, S.-L.; Zhang, W.; Song, X.; Shukla, A. K.; Liu, G.; Battaglia, V.; Srinivasan, V., High Rate Capability of Li(Ni<sub>1/3</sub>Mn<sub>1/3</sub>Co<sub>1/3</sub>)O<sub>2</sub> Electrode for Li-Ion Batteries. *J. Electrochem. Soc.* 2012, 159 (4), A438-A444.
- Liu, X.; Liu, J.; Qiao, R.; Yu, Y.; Li, H.; Suo, L.; Hu, Y.-s.; Chuang, Y.-D.; Shu, G.; Chou, F.; Weng, T.-C.; Nordlund, D.; Sokaras, D.; Wang, Y. J.; Lin, H.; Barbiellini, B.; Bansil, A.; Song, X.; Liu, Z.; Yan, S.; Liu, G.; Qiao, S.; Richardson, T. J.; Prendergast, D.; Hussain, Z.; de Groot, F. M. F.; Yang, W., Phase Transformation and Lithiation Effect on Electronic Structure of Li<sub>x</sub>FePO<sub>4</sub>: An In-Depth Study by Soft X-

ray and Simulations. *J. AM. CHEM. SOC.* 2012, 134 (33), 13708-13715.

- Liu, G.; Zheng, H.; Song, X.; Battaglia, V. S., Particles and Polymer Binder Interaction: A Controlling Factor in Lithium-Ion Electrode Performance. *J. Electrochem. Soc.* 2012, 159 (3), A214-A221.
- Xun, S.; Song, X.; Wang, L.; Grass, M. E.; Liu, Z.; Battaglia, V. S.; Liu, G., The Effects of Native Oxide Surface Layer on the Electrochemical Performance of Si Nanoparticle-Based Electrodes. *J. Electrochem. Soc.* 2011, 158 (12), A1260-A1266.
- Xiao, J.; Wang, X.; Yang, X. Q.; Xun, S.; Liu, G.; Koech, P. K.; Liu, J.; Lemmon, J. P., Electrochemically Induced High Capacity Displacement Reaction of PEO/MoS<sub>2</sub>/Graphene Nanocomposites with Lithium. *Adv. Funct. Mater.* 2011, 21 (15), 2840-2846.
- Liu, G.; Xun, S.; Vukmirovic, N.; Song, X.; Olalde-Velasco, P.; Zheng, H.; Battaglia, V. S.; Wang, L.; Yang, W., Polymers with Tailored Electronic Structure for High Capacity Lithium Battery Electrodes. *Advanced Materials* 2011, 23 (40), 4679.
- Conductive polymer binder for lithium ion battery application - a scalable approach to assemble Si nanoparticles into electrode, DOE User Facility: The Molecular Foundry Annual Workshop, Berkeley, CA, October 2012.
- New Binder Approaches for Advanced Anode Electrode, 5th International Conference on Advanced Lithium Batteries for Automobile Applications, Istanbul, Turkey, September 2012.
- An ALS XAS characterization and DFT calculation guided materials discovery of conductive polymer binders for high capacity Si anode electrode, US-China Electric Vehicle and Battery Technology Workshop, Boston, MA, August 2012.
- An ALS XAS characterization and DFT calculation guided materials discovery of conductive polymer binders for high capacity Si anode electrode, ALS Seminar Series, Berkeley, CA, June 2012.
- Conductive Polymer Binders with Tailored Electronic Structure for Si Alloy Anode, MRS Spring Meeting, San Francisco, CA, 2012.

## V.C.5 Three Dimensional Anode Architecture and Materials (ANL)

Jack Vaughey  
Argonne National Laboratory  
9700 South Cass Avenue  
Argonne, IL 60439  
Phone: (630) 252-9184; Fax: (630) 252-4176  
E-mail: [vaughey@anl.gov](mailto:vaughey@anl.gov)

Collaborators:  
ANL: L. Trahey, Fulya Dogan, Fikile Brushett,  
Robert Winarski,  
Clemson: S.-J. Hwu, L. Duminda Sanjeeva

Start Date: October 1, 2010  
Projected End Date: September 30, 2014

### Objectives

- Design electrode architectures containing main group metal, metalloid or intermetallic components that can tolerate the volumetric expansion of the materials and provide an acceptable cycle life.
- Exploit electrochemical deposition reactions to improve the design and performance of silicon and tin-based electrodes.
- Develop methods to assess the internal changes within the electrode on cycling as a tool to improve performance.

### Technical Barriers

- Low energy
- Poor low temperature operation
- Abuse tolerance limitations

### Technical Targets

- 142 Wh/kg, 317 W/kg (PHEV 40 mile requirement)
- Cycle life: 5000 cycles
- Calendar life: 15 years

### Accomplishments

- Determined the role of interfacial compounds and processing in controlling the performance of silicon electrodes that use metallic copper binders.
- Devised methods to electrodeposit electrochemically active silicon in carbonate-based solvents into three-dimensional substrates. Determined which electrodeposition variables have a significant influence over morphology and cycle life.

- Utilized a cell designed last year for micro-CT tomography at APS to 'look inside' electrodeposited three dimensional electrode architectures based on silicon and tin.
- Interactions with the EFRC – Center for Electrical Energy Storage - Tailored Interfaces (Argonne-Northwestern University-University of Illinois (Urbana-Champaign) were continued around the micro CT tomography effort.



### Introduction

The search for an alternative anode material to replace graphite in lithium-ion batteries has been underway for many years. Several classes of materials have been investigated, notably: i) simple metal oxides, ii) main group elements, iii) and intermetallic compounds. Main group elements (e.g., Si, Sn) and intermetallic compounds (e.g.,  $\text{Cu}_6\text{Sn}_5$ ) are of particular interest because they offer significantly higher theoretical volumetric and gravimetric capacities when compared to graphite (372 mAh/g and 818 mAh/ml, respectively), and insert lithium several hundred millivolts above the potential of metallic lithium. However, the (near) close-packed structures of these materials have limited internal void volume and therefore expand considerably on reaction and insertion of lithium. Although this presently limits its utility, the high potential payoff associated has made silicon a focus for the BATT-Anode program.

A major objective of this research is to design microporous copper or carbon-based host architectures that can 1) simplify the lithium-ion battery electrode by combining requirements for a binder, and conductive additive and extending the current collector into the active phase, and 2) provide a sufficiently large void volume to accommodate the volumetric expansion that occurs during charging. This project is part of a combined synthetic - diagnostic effort to understand and adapt the excellent cycling performance seen for deposited silicon electrodes to laminated electrodes. When sputtered as thin films or vapor deposited to form nanowires (e.g., Cui, et al.), deposited electrodes show enhanced lifetimes and energy density due in part to the robustness of the connection between the current collector and active materials. The most common connection is formation of an intermetallic or alloy-based phase at the current collector (e.g.,  $\text{Ni}_3\text{Si}$ ,  $\text{Au}_3\text{Si}$ ) interface. By studying the interfacial region near the current collector, electrochemical cycling, and role of electrode porosity, new structure-property relationships can be examined and modified to improve the electrochemical performance of silicon-based electrodes.

## Approach

- Develop and utilize electrodeposition tools to control morphology and amount of active material being deposited into the porous electrode architectures.
- Characterize electrodes where copper metal acts as a binder and conductive additive for high capacity main group metals, e.g., silicon, to identify binding interactions for variety of compositions and processing conditions.
- Develop characterization methods that allow for a better understanding of the electrochemically active interfaces within the electrode architecture.

## Results

The initial focus was to develop a method to encase micron-sized Si particles within a Cu mesh formed *in situ*. In other words, control the interface by building the current collector around the active particles. The use of micron-size Si particles (10 to 20  $\mu\text{m}$ ) allowed for contact with the electrolyte and better metal-silicon binding. Last year the methods used to synthesize these electrodes were discussed and the electrodes were evaluated against conventional polymer-bound silicon-based laminates. A range of conditions that produced similar capacities, while offering significant power enhancements, were able to be identified. In this past year a diagnostic study using powder X-ray diffraction, impedance spectroscopy, and  $^{29}\text{Si}$  NMR spectroscopy was completed to examine in detail the relationship between cycling performance and interfacial compound formation (Figure V - 95). It was able to be shown that: (1) on annealing below 650 C, electrode samples (62-78% active Si) that showed no significant intermetallic formation had comparable performance to laminated electrodes, (2) higher copper ratios reduced the amount of detrimental surface  $\text{SiO}_x$  species in the electrodes, and (3) at higher temperatures, copper appears to diffuse over the surface faster than it moves into the bulk of the particle. Published studies on VLSI Si-nanowire electrodes indicate that the best performance is when the alloy formation is limited to the lower portion of the nanowire. In addition, silicon-based intermetallics are nearly all electrochemically inactive. Analysis of the interfacial region of the Cu-binder Si-based electrodes indicated phase relationships consistent with the known phases seen for Si-nanowire electrodes. Hot electrode structures, the best performing electrodes were ones that exhibited maximum copper annealing with minimal intermetallic formation as surface formation of  $\text{Cu}_x\text{Si}$  would shut down the underlying active material.

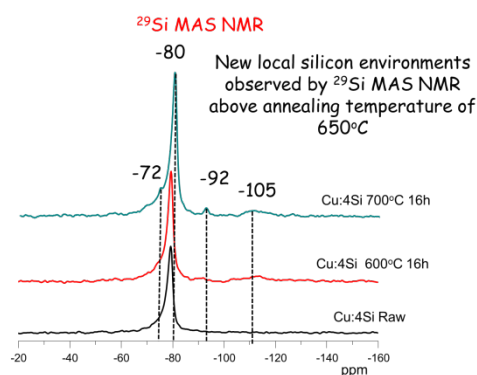


**Figure V - 95:** Evolution of new Si environments as a function of annealing temperature.

An alternative approach to building the current collector around the silicon is to use electrodeposition to control the morphology and amount of active material in the electrode. Using well defined porous copper substrates, the electrodeposition of silicon-thin films studied. This solution-based electrodeposition effort is in contrast to the vast majority of thin film studies that use chemical vapor deposition (CVD), thermal evaporation, or sputtering to make active crystalline materials. By using synthetic techniques based on electrodeposition, there is better control on the amount of silicon deposited, its morphology, and its dispersion within the substrate. A downside is the need to have extra non-Si species in the process (solvents, salts, counter-ions) that may incorporate into the film; however post processing can limit their detrimental properties.

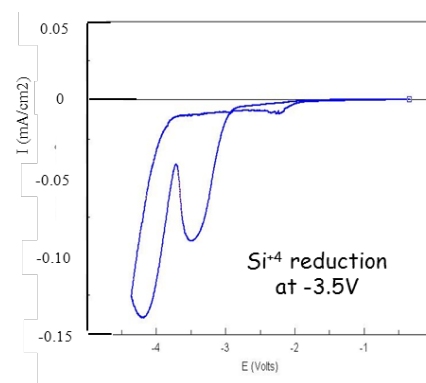


**Figure V - 96:** Reduction of Si (IV) is seen at -3.5 V (vs Pt) in a PC supporting electrolyte. The -4.2 V peak (vs Pt) is electrolyte decomposition.

To date, two methods have been used to make silicon films. One based on oxidation of anionic  $[\text{Si}_4]^{4-}$  clusters in the coordinating solvent glycol TEGDME, the other utilizing reduction of  $\text{SiCl}_4$  in PC. Because of its superior solubility, the reduction of  $\text{SiCl}_4$  has been focused on as the synthetic method. A typical deposition is shown in Figure V - 96.

The method used to electrodeposit silicon from solution (constant potential or constant current) has

been assessed on the morphology and thickness of film produced and its electrochemical performance. Figure V - 97 highlights the differences in morphology and appearance for two representative films.

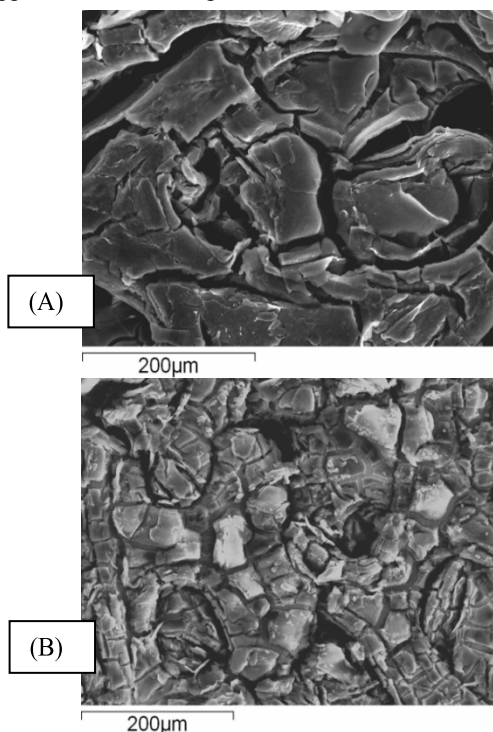


**Figure V - 97:** Post 1<sup>st</sup> cycle SEM of two films deposited over a 2-hr period and cycled vs Li in the range of 0.1-2 V in Gen2 electrolyte. Film (A) was made under constant potential (-3.3V), and Film (B) was done under constant current (-50 mA).

Using the method recently published by Kumta, et al., (*Mat Sci Eng B*, 2012) the amount of active material of Film (A) has been estimated to be 1.9 mg/cm<sup>2</sup> and 2.4 mg/cm<sup>2</sup> in Film (B). Based on preliminary data the rougher film produced under constant current conditions had superior capacity retention than the initially smoother constant potential film. In both cases the first cycle irreversible capacity was 60-70%, in agreement with literature values, as seen in Figure V - 98. This value is high versus dense Si films (~40-50%) but comparable to nanoparticles Si and laminates derived from SiO (~70%). The difference when compared to dense Si films and the observed similarities to Si nanoparticles, may arise from similar high surface areas (increased SEI formation) and from the inclusion of secondary phases within the electrode structure, e.g., Li<sub>2</sub>O, LiCl (from SiCl<sub>4</sub>), during formation. Other deposition variables are being assessed in an attempt to minimize the chloride content. Initial attempts at annealing at moderate temperatures (< 300 C) or placing it under vacuum to eliminate occluded solvents, was found to be detrimental to electrochemical performance.

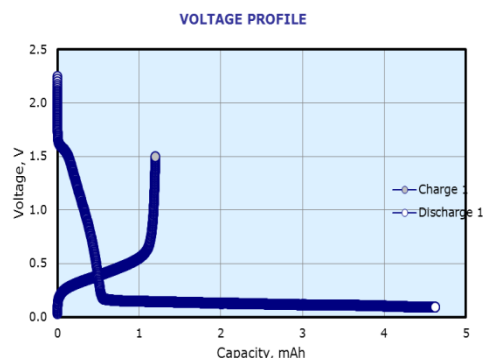


**Figure V - 98:** First cycle of silicon film (A) made via constant potential deposition.

**Tomography:** Improving the performance of silicon-based anodes requires knowledge of the three-dimensional structure as a function of synthesis parameters and cell operating conditions. High resolution, high speed synchrotron-based microtomography experiments have been used at the 2-BM-A beamline at Argonne's Advanced Photon Source to 'look inside' a cycling electrode. Microtomography enables non-destructive visualization of complex electrode architectures, including buried pore networks and sub-surface interfaces. Current *in situ* cell configuration is shown in Figure V - 99. The electrode pieces are located within a Torlon® tube and flattened stainless steel screws provides cell stacking pressure.

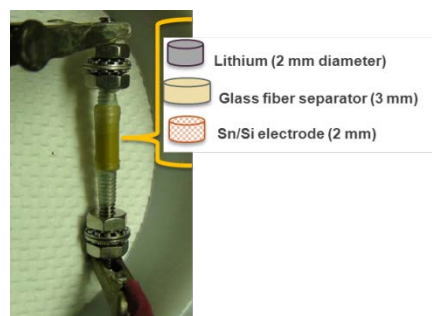


**Figure V - 99:** Optical image and schematic of *in situ* tomography cell

The electrodes initially analyzed were commercial copper foams roughly 100 μm thick with electro-less tin coatings. Electro-less tin plating was chosen for its conformal nature and because the tin provides a better X-ray contrast than the lighter silicon films. These carbon- and binder-free tin on copper anodes last ~30 cycles in coin cells before capacity fades. Initial results obtained show that 1 μm resolution can be achieved on the electrode. Figure V - 100 shows tomographic reconstructions of one electrode area, and highlights the type of surface features tracked and evaluated.

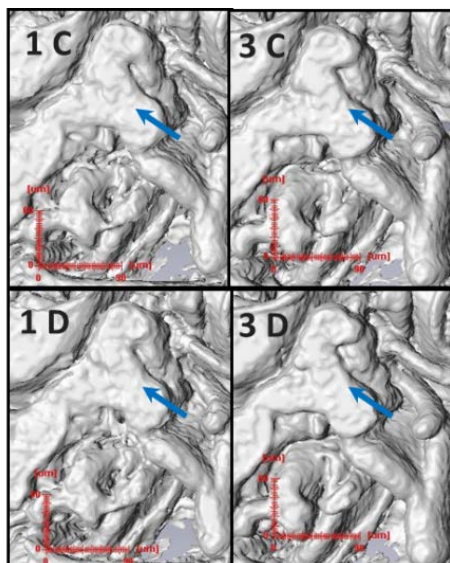


**Figure V - 100:** 3D reconstruction of Sn on Cu electrode during the 1<sup>st</sup> and 3<sup>rd</sup> discharge and charge cycles.

After proof-of-concept work with the tin system, 70% active silicon laminates were studied using 325 mesh commercial silicon. SEM analysis shows the particle size ranges from nanometers to 40 microns; all particles greater than 1 micron in diameter can be resolved. After several cycles the front surface of the electrode developed a higher level of porosity than the middle or rear of the electrode. This evolution in porosity may result from the more rapid lithiation of the amorphous silicon surface particles compared to the bulk, resulting in faster local volume expansion with all the resulting stresses built up being released as particle pulverization. This may even occur in cells cycled to a limited capacity (below theoretical capacity) as formation of  $\text{Li}_{15}\text{Si}_4$  (the crystalline end member of the cycling process) may form quickly. Methods to look at these laminates *in situ* while cycling and electrodeposited samples are underway.

### Conclusions and Future Directions

- The performance of electrodeposited silicon thin films is related to their deposition morphology. They have similar properties to laminates made using high surface area silicon nanoparticles or those derived from ‘SiO’.
- MAS-NMR studies of the Cu-Si electrodes have found that the best samples are created when copper self-diffusion maximized but surface-coating intermetallic formation minimized.
- Tomography experiments of two different types of silicon electrodes have identified differences in performance related to their cycling history. Notably the electrolyte side of the electrode shows greatly diminished particle sizes on cycling than the more protected inner parts of the electrode.

### FY 2012 Publications/Presentations

1. C. Joyce, L. Trahey, S. Bauer, F. Dogan, J. T. Vaughey “Copper Metal Binders: the Copper-Silicon System,” *J. Electrochem. Soc.*, **159**, A909 (2012).
2. Fulya Dogan, Christopher Joyce, John T. Vaughey “Formation of New Silicon Local Environments upon Annealing for Silicon Anodes: A  $^{29}\text{Si}$  Solid State NMR Study,” submitted, *J. Electrochem. Soc.*, 2012.
3. L. T. Trahey, T. Feckler, F. Brushett, M. Slater, C. S. Johnson, J. T. Vaughey, M. M. Thackeray “Electrodeposited Tin Electrodes for Electrochemical Energy Storage,” *Gordon Research Conference on Electrodeposition*, Biddeford, ME, July 2012.
4. L. Trahey, F. Brushett, X. Xiao, J. Vaughey “X-Ray Tomography on 3D Microporous Silicon-based Anodes,” submitted, *Chem. Mater.*, 2012.
5. L. Trahey, F. Brushett, B. Blaiszik, V. Rose, R. Winarski, X. Xiao, C. Johnson, J. Vaughey, and M. Thackeray “Synchrotron Tomography of Porous Lithium-Ion Battery Anodes,” *221st Meeting of the Electrochemical Society*, Seattle, WA, May, 2012.
6. Fulya Dogan, Lynn Trahey, Michael M. Thackeray, John T. Vaughey “Three-Dimensional Anode Architectures and Materials,” *219<sup>th</sup> Meeting of the Electrochemical Society*, Boston, MA, October, 2011.
7. Xianghui Xiao, Fikile Brushett, Susanna Neuhold, Lynn Trahey, John Vaughey “High-Energy X-Ray Tomography on 3D Microporous Composite Anode of Lithium-Ion Batteries,” *Materials Science and Technology 2011*, Columbus, OH, October 2011.
8. L. Trahey, F. Brushett, X. Xiao, J. Vaughey “X-Ray Tomography on 3D Microporous Tin-based Anodes,” BATT-Anode Workshop, Berkeley, CA, February 2012.
9. F. Dogan, A. Hubaud, K. Johnson, J. Vaughey “Synthesis and Interfacial Characterization of Silicon Electrodes,” BATT-Anode Workshop, Berkeley, CA, February, 2012.
10. J. Vaughey, L. Trahey, F. Dogan “Three Dimensional Battery Architectures,” DOE Hydrogen Program and Vehicle Technologies Program Annual Merit Review, Washington, DC, May, 2012.

## V.C.6 Metal-Based High Capacity Li-Ion Anodes (Binghamton U.)

M. Stanley Whittingham  
Binghamton University  
Department of Chemistry and Materials S&E  
Vestal Parkway East  
Binghamton, NY 13902-6000  
Phone: (607) 777-4623; Fax: (607) 777-4623  
E-mail: [stanwhit@binghamton.edu](mailto:stanwhit@binghamton.edu)

Start Date: January 1, 2011

Projected End Date: December 31, 2014

### Objectives

- Replace the presently used carbon anodes:
  - With safer materials that will be compatible with lower-cost layered oxide and phosphate cathodes and the associated electrolyte.
  - With materials having higher volumetric energy densities, twice that of carbon.

### Technical Barriers

This project addresses the following technical barriers facing the use of lithium-ion batteries in PHEV and all-electric vehicles:

- Materials and manufacturing cost of lithium-ion batteries.
- Safety of lithium-ion batteries.
- Volumetric capacity limitations of lithium-ion batteries.

### Technical Targets

- Synthesize nano-size tin materials by at least two different methods.
- Have the nano-size tin meet the gravimetric capacity of the Sn-Co-C electrode.
- Characterize these materials and determine their electrochemical behavior.
- Initiate studies on nano-silicon materials. Synthesize by at least one method.

### Accomplishments

- Synthesized nano-size tin compounds using two different techniques, mechanochemical reductive reaction and solvothermal reaction.
- Electrochemical behavior of the mechanochemical material is comparable or superior to that of the commercial Sn-Co-C material, both in gravimetric capacity and rate capability.

- Synthesized nano-size tin compounds solvothermally. Showed that capacity retention and cycling efficiency is improved by high energy ball milling the product with carbon. This showed that a protective layer of carbon is a critical component of a stable tin anode.
- Synthesized a nano-silicon material by a second method, using a SiAl alloy as starting material. It showed greater than 99% cycling efficiency after the first few cycles.
- Accomplished technology transfer through the placement of PhD professionals at many laboratories, including small and large Industry, National Laboratories and Academia.

◇ ◇ ◇ ◇ ◇

### Introduction

Achieving the DOE cost and energy/power density targets will require improved anode materials that have higher volumetric energy densities than carbon, and have lower cost production methods. At the same time the material must have higher lithium diffusion rates than carbon and preferably be at a slightly higher potential to improve the safety.

### Approach

Our anode approach is to synthesize, characterize and develop inexpensive materials that have higher volumetric energy densities than carbon. Emphasis will be placed on simple metal alloys/composites at the nano-size. Initially, emphasis will be placed on tin, building on what we learnt from our studies of the tin-cobalt anode, the only commercial anode besides carbon. All materials will be evaluated electrochemically in a variety of cell configurations, and for thermal, kinetic and structural stability to gain an understanding of their behavior. Ideally these will have a potential around 500 mV above that of pure lithium (to minimize risk of Li plating and thus enhance safety, whilst allowing for rapid charging).

### Results

**Nano-Tin Anode Materials.** Sn based alloy materials were prepared by several techniques. To date, this was accomplished optimally by mechanical milling using Ti as the reducing agent and soft iron grinding media. The reductive metal and grinding media significantly affect the material formed and the resulting electrochemical behavior. Titanium reduction provided materials with excellent capacity, 600 mAh/g close to the theoretical capacity, and excellent capacity retention on cycling. The use of soft iron grinding media resulted in the alloying of

most of the tin with iron giving  $\text{Sn}_2\text{Fe}$ . The capacity and rate capability of these iron containing materials is comparable to those of the Sn-Co-C compounds, and much better than bulk  $\text{Sn}_2\text{Fe}$ . The results are shown in Figure V - 101.

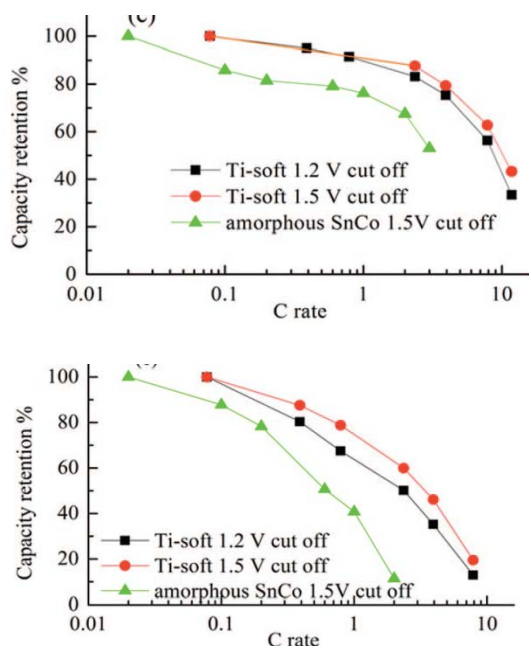


**Figure V - 101:** (top) Rate capability of lithium removal from the nano-tin anode, and (bottom) rate capability of lithium insertion into the nano-tin anode relative to the SONY SnCoC anode.

Nano-tin was synthesized by a second method, a solvothermal approach. In this approach,  $\text{FeCl}_3$  and  $\text{SnCl}_2$  were dissolved in ethanol and then transferred into a Teflon jar. Excess  $\text{NaBH}_4$  was poured into the solution before solvothermal treatment at  $200^\circ\text{C}$  for 24 hours. The XRD pattern in Figure V - 102 (top) shows that the resulting powder contains  $\text{FeSn}_2$  with a small amount of Sn metal. Ball-milling this compound with carbon removes the excess tin metal. The  $\text{Sn}_2\text{Fe}$  particle size is less than 100 nm. The electrochemical cycling of the Sn-Fe-C compound is also shown in Figure V - 102 (bottom) for two different voltage cycling regimes. The poor cycling efficiency was improved to over 99% by ball-milling with carbon; however this results in a drop in the capacity to between 400 and 500 mAh/g of total weight of SnFe material + carbon. High energy ball-milling was found to be more effective than planetary ball-milling. This behavior is being followed-up.

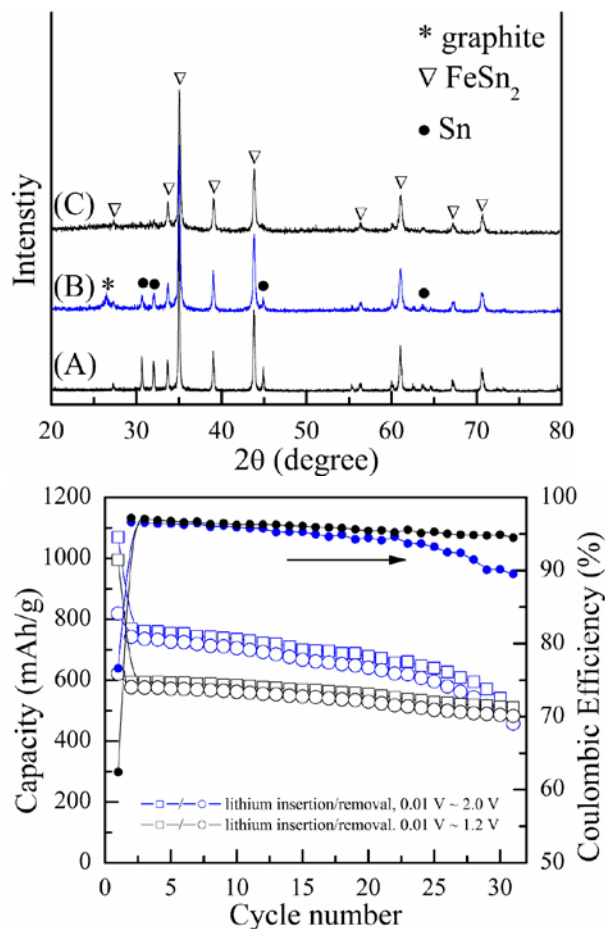


**Figure V - 102:** (top) XRD patterns of (A) Solvothermally formed Fe-Sn; (B) Planetary ball-milled (pBM) Sn-Fe-C composite; (C) High-energy ball-milled (HEBM) Sn-Fe-C composite. There is some Sn metal phase in the solvothermally formed material, but it is removed after high-energy milling with graphite. (bottom) Electrochemical cycling of this Sn-Fe alloy in two different voltage windows. The current was  $0.3\text{ mA/cm}^2$  in the 1<sup>st</sup> cycle and  $0.5\text{ mA/cm}^2$  thereafter.

**Nano-Silicon Anode Materials.** A nano-silicon material has been synthesized, and initial electrochemical measurements made on it. A low-cost Al-Si engine-block alloy was used as the starting material. We earlier reported on the electrochemical behavior of the alloy itself as a much improved aluminum-based anode. The powder was etched in aqueous HCl acid, resulting in the selective dissolution of the Al. The X-ray diffraction pattern showed only peaks from the silicon phase. The nanostructured porous Si sphere was retained after the etching as indicated in Figure V - 103 (top). Overnight etching with vigorous stirring caused these spheres to break. The average crystallite size of the Si in both the initial Al-Si powder and the etched sample is around 20 nm, as determined using the Scherrer Equation, showing no change in size during the aluminum removal. Their electrochemical behavior is shown in Figure V - 103 (bottom). On lithium insertion, 2.8 Ah/g of lithium were inserted per gram of silicon spheres and 2.1 Ah/g of this lithium was removed

in the first cycle. The capacity dropped to 1.5 Ah/g in the first 3 cycles, but then stabilized. After more than 60 cycles, the capacity was still 1.15 Ah/g. The coulombic efficiency of the broken Si, as indicated in Figure V - 103 was 76.5% in the first cycle and it went up to 99% after 10 cycles.

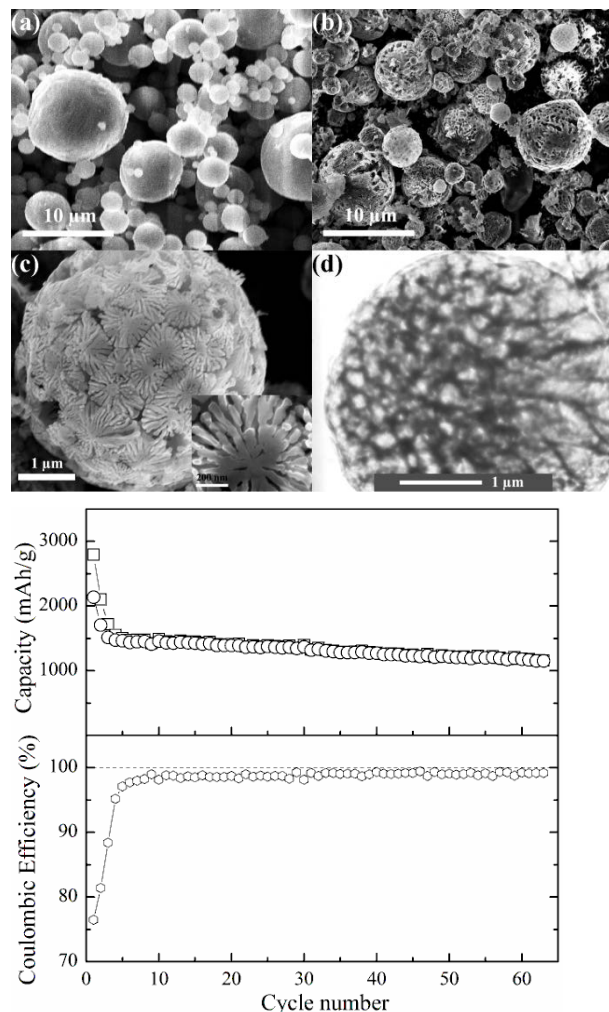


**Figure V - 103:** (top) SEM of (a) initial Al-Si, and of (b) and (c) porous Si spheres; (d) TEM of the Si spheres; (bottom) Electrochemical cycling of the porous Si spheres material at 0.5 mA/cm<sup>2</sup> between 0.01 V ~1.5 V. First cycle current density was 0.3 mA/cm<sup>2</sup>. The electrodes were made of Si, carbon black additive and binder in a weight ratio of 70:20:10. Capacities were calculated based on the weight of Si (2 ~ 3 mg/cm<sup>2</sup>).

## Conclusions and Future Directions

A clear result from this study of the cycling behavior of tin and silicon anode materials is that nano-sized materials work, and that bulk materials, with their high expansion on lithium reaction, do not, and are therefore unsuitable for batteries. This work also showed that SnFeC materials are just as good as the commercial SnCoC anode. The challenges and future directions are to solve the first cycle excess capacity, not only for tin but also for silicon, and to find low cost synthetic approaches. Our future work will therefore focus on the tin nanostructures, and determine the role of the carbon content and synthetic method on capacity and capacity retention. These nanoparticles will be protected from reaction with the electrolyte by a surface coating, for example carbon. If the above approaches are successful, we will substitute part of the tin to raise the redox potential and thus the safety.

As with tin, it appears that the silicon needs to be protected by a surface coating such as carbon. Some effort will continue on silicon materials using the learning from the tin studies. The goal is to attain at least double the volumetric capacity of carbon, whilst maintaining its high cycling efficiency.

## FY 2012 Publications/Presentations

1. M. Stanley Whittingham, "Metal-Based High Capacity Li-Ion Anodes," *DOE Annual Peer Review Meeting Presentation*, May 2012.
2. Ruigang Zhang, Shailesh Upreti and M. Stanley Whittingham, "Tin-Iron Based Nano-Materials as Anodes for Li-Ion Batteries," *J. Electrochem. Soc.*, **158** (12), A1498-A1504 (2011).
3. Wenchao Zhou, Ruigang Zhang, Shailesh Upreti, and M. S. Whittingham, "Sn-Fe Nano-Materials as Anodes for Li-Ion Batteries," *Materials Research Society*, San Francisco, April 9-13, 2012.
4. M. Stanley Whittingham, "Replacing the Carbon Anode in Li-Ion Batteries," *5<sup>th</sup> China – U.S. Workshop*, Hangzhou, China, April 14, 2012.
5. Wenchao Zhou, Shailesh Upreti and M. Stanley Whittingham, "Macroporous Si spheres as anode for lithium-ion batteries," *MRS Boston*, November 28-December 1, 2011.
6. M. Stanley Whittingham, "The Role of Nanomaterials: Are They the Answer to Reversibility, Lifetime and Rate?" *Infocast 10x Battery Meeting*, Santa Clara, CA, January 23, 2012.

## V.C.7 New Layered Nanolaminates for Use in Lithium Battery Anodes

(Drexel U.)

Yury Gogotsi  
Drexel University  
Materials Science and Engineering Department  
3141 Chestnut St, Philadelphia, PA 19104  
Phone: (215) 895-6446; Fax: (215) 895-1934  
E-mail: [gogotsi@drexel.edu](mailto:gogotsi@drexel.edu)

Michel W. Barsoum (Co-PI)  
Materials Science and Engineering Department  
Drexel University  
3141 Chestnut St, Philadelphia, PA 19104  
Phone: (215) 895-2338; Fax: (215) 895-6760  
E-mail: [barsoumw@drexel.edu](mailto:barsoumw@drexel.edu)

Start Date: January 1, 2011  
Projected End Date: December 2014

### Objectives

- To replace graphite in Li-ion battery (LIB) anode with new materials: layered ternary carbides and nitrides (MAX phases). The strategy may offer produce anodes with higher charge density than graphite, lesser expansion, longer cycle life and, potentially, a lower cost than Si nanoparticles.

### Technical Barriers

This project aims to address the following technical barriers facing the modern LIB technology:

- (A) short life-span of modern batteries,
- (B) low charge density, and
- (C) compromised safety.

### Technical Targets

- Perform the *ab initio* simulation of Li incorporation into MAX phase carbides.
- Screening electrochemical experiments on a variety of MAX phases to select the most promising ones for more detailed study.
- Studying the effect of particle size on the capacity of the three best MAX phase materials.
- Improvement of capacity by selective extraction of M or A atoms, to add space for the Li.
- Investigation of SEI formation on selected MAX phase carbides.

- Optimization of the material. Testing the rate capability of the anode.
- In situ* study of charge/discharge processes and better understanding of the mechanism of Li insertion.
- Comparison of powder vs. MAX phase solids with 10-20% porosity.

### Accomplishments

- Successful synthesis and electrochemical testing of several MXenes with different compositions ( $Ti_3C_2$ ,  $Ti_2C$ ,  $(Ti_{0.5}Nb_{0.5})_2C$ ,  $Ti_3(C_{0.5}N_{0.5})_2$ ,  $Ta_4C_3$ ) in LIBs.
- Completed a study on the effect of different carbon additives on the performance of MXenes in LIBs.
- Achieved gravimetric and volumetric capacities that are higher than graphite, especially at high cycling rates.
- Successful delamination of  $Ti_3C_2$ , producing additive-free  $Ti_3C_2$  anodes with a capacity of 410 mAh/g at a 1C cycling rate and 110 mAh/g at 36 C cycling rate for 200 cycles.



### Introduction

In FY 2011 a new 2-D material was successfully produced, viz.  $Ti_3C_2$ , by selectively etching Al from  $Ti_3AlC_2$  (a typical MAX phase), and found that  $Ti_3C_2$  had much better performance than  $Ti_3AlC_2$  as an anode material in LIB. The new 2-D material was labeled MXene to emphasize its similarity to graphene, and proposed that  $Ti_3C_2$  represents a family of materials, not just one phase. During FY 2012, it was proven that MXenes are, in fact, a family of 2-D transition metal carbides and carbonitrides, which have the potential for use as anodes in LIBs. Due to a better performance of MXenes over MAX phases, the research was focused on MXenes. Herein, some of the results obtained during FY 2012 are highlighted.

### Approach

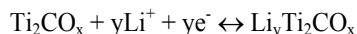
Since (at this time) the relationship between capacity and MAX phase chemistry is unknown, a rapid screening of as many MAX phases as possible shall be carried out to find out the most promising chemistry, by testing their performance in LIB. This process will be guided by *ab initio* calculations. Reducing particle size, selective etching of an A element from the MAX structure, and exfoliation of these layered structure also will be investigated to

increase the Li uptake of these structures and increase the charge density.

## Results

**Ti<sub>2</sub>C-Based Anodes.** HF treatment of Ti<sub>2</sub>AlC (10% HF for 10 h at RT) resulted in selective etching of Al and the exfoliation of the Ti<sub>2</sub>C layers.

Typical cyclic voltammetry curves, at a rate of 0.2 mV·s<sup>-1</sup>, for the exfoliated Ti<sub>2</sub>C are shown in Figure V - 104a. A broad, irreversible peak was observed around 0.6 V, during the first lithiation cycle (reduction); it was absent in subsequent cycles. This irreversible peak was preliminarily assigned to the formation of a solid electrolyte interphase (SEI) and/or to an irreversible reaction with the electrode material. In all subsequent cycles, broad reversible peaks were observed at 1.6 V and 2.0 V vs. Li<sup>+</sup>/Li during lithiation and de-lithiation, respectively. Because these peak potentials are similar to those reported for TiO<sub>2</sub> and lithiated titania, these peaks were tentatively assigned to the redox reaction:



The rationale for this assignment is that drying the MXene powders at 200 °C, prior to assembling the coin cells, rids it of water and leads to an oxygen terminated surface. Like in the case of the titanates, even if the potentials vs. Li are relatively high, it is an advantage from a safety standpoint.

Figure V - 104b shows the galvanostatic charge/discharge curves at a rate of C/10 (1 Li<sup>+</sup> per formulae exchanged in 10 h). The capacity loss in the first cycle can again be attributed to the formation of an SEI at potentials below 0.9 V vs. Li<sup>+</sup>/Li, as well as to the irreversible reduction of electrochemically active surface groups such as fluorine or possibly hydroxyls. At 160 mAh·g<sup>-1</sup>, the capacity of the treated powders is about 5 times higher than that of the as-received Ti<sub>2</sub>AlC (≈ 30 mAh·g<sup>-1</sup> at C/10) powders.

The specific capacities vs. cycle number at different cycling rates (C/25, C/6, 1C, 3C, and 10C) calculated from galvanostatic curves are shown in Figure V - 104c. The highest capacity was obtained at a rate of C/25. The specific capacity values stabilize after 5 cycles, for all scan rates. At a C/25 rate, the capacity is 225 mAh·g<sup>-1</sup>, which corresponds to  $y \approx 1$  in the above equation. At rates of 1 C and 3 C, the capacities, after 80 cycles, were, respectively, 110 mAh·g<sup>-1</sup> and 80 mAh·g<sup>-1</sup>. Even at rates of 10 C, a stable capacity of 70 mAh·g<sup>-1</sup> was obtained for more than 200 cycles.

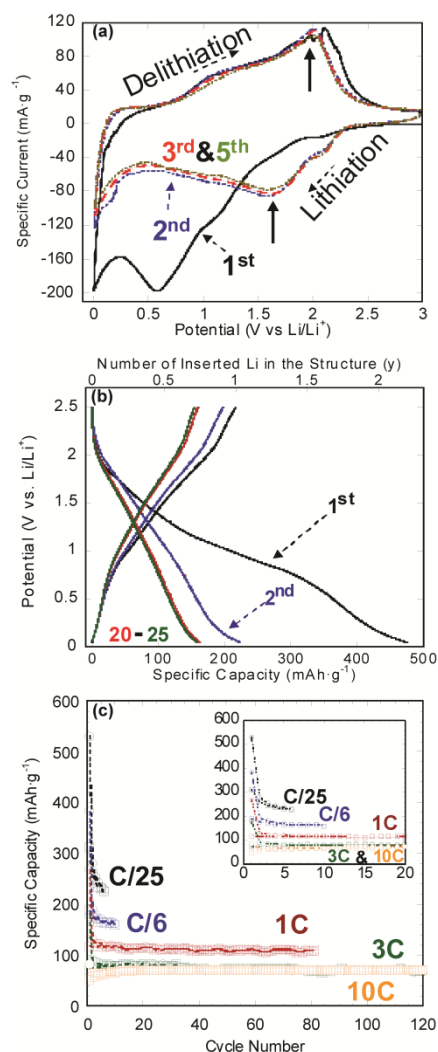


**Figure V - 104:** (a) Cyclic voltammetry curves of exfoliated Ti<sub>2</sub>C at a constant scan rate of 0.2 mV·s<sup>-1</sup>. The solid arrows refer to main peaks positions during lithiation and delithiation cycles. (b) The galvanostatic charge/discharge curves at a C/10 rate. (c) Specific lithiation (circles in the figure) and delithiation (squares in the figure) capacities (per mass of active material) vs. cycle number at different rates. The inset in Fig. 1c is a zoom of the first 20 cycles.

**Lithiation and Delithiation Mechanism.** Since Ti<sub>2</sub>C is a new material, its lithiation and delithiation mechanisms are not well understood. *In situ* XRD is one of the more powerful techniques to understand these mechanisms. The XRD diffraction patterns (not shown for the limited space) of Ti<sub>2</sub>C as a function of lithiation and de-lithiation are shown were obtained during a relaxation period of every 0.2 Li<sup>+</sup> ions per unit formulae of Ti<sub>2</sub>C. Before cycling, the diffractograms showed peaks associated with, mainly, Ti<sub>2</sub>C and Ti<sub>3</sub>C<sub>2</sub> and un-reacted Ti<sub>2</sub>AlC and Ti<sub>3</sub>AlC<sub>2</sub>. Note that despite the fact that the latter two were electrochemically inactive their presence was useful, since they acted as internal references for the other peak positions. No new peaks appeared during lithiation, but a progressive downshift of the 002 peaks was observed from  $2\theta = 11.4^\circ$  to  $9.4^\circ$ , corresponding to an

increase of the  $c$  lattice parameter from 15.46 Å to 18.72 Å. After delithiation, the  $c$  parameters decreased from 18.72 Å to 17.96 Å. In other words, after delithiation the  $c$  lattice parameter was  $\approx 16\%$  higher than its value before any cycling. This result can partially explain the large irreversibility observed during the 1<sup>st</sup> cycle as  $\text{Li}^+$  ions can be trapped between the *MXene* layers in addition to the formation of a SEI layer. No increase of the  $c$  parameter was observed at  $x$  values below 0.6, which is consistent with: i) an irreversible faradic reaction taking place at the surface of the particles, such as SEI layer formation, and possibly, ii) a fast  $\text{Li}^+$  ion intercalation in the bulk of the  $\text{Ti}_2\text{C}$  particles that does not involve any lattice volume expansion.

Based on the XRD results, it is reasonable to conclude that the charge storage in  $\text{Ti}_2\text{C}$  – and by extension all other MXenes – is due to  $\text{Li}^+$  ions intercalation between the  $\text{Ti}_2\text{C}$  layers and not due to a conversion reaction. This important conclusion supports the wisdom of changing research directions to focus on MXenes instead of MAX. More research is ongoing to further understand the lithiation and delithiation mechanisms for various MXenes.

**Other MXenes as Anodes in LIBs.** Two other MXenes were also tested as anode in LIBs:  $\text{Ti}_3\text{CN}$  and  $\text{Ta}_4\text{C}_3$ . The cyclic voltammetry (CV) curves for both  $\text{Ti}_3\text{CN}$  (Figure V - 105a) and  $\text{Ta}_4\text{C}_3$  (Figure V - 105b), again, show large first cycle irreversible lithiation peaks around 1 V. This can be explained by the presence of surface fluorine atoms from the HF treatment. Similar irreversible reactions were reported for transition metal fluorides due to the decomposition of the fluorides and the irreversible formation of  $\text{LiF}$  during the first cycle. After the first cycle, reversible capacity was obtained in both systems. So, controlling the surface chemistry of MXene and producing fluorine-free MXenes should help in minimizing the 1<sup>st</sup> cycle irreversibility.

The specific capacity vs. cycle number at different C rates was calculated from GV tests. At a C/8 rate, a stable capacity of more than 250  $\text{mAhg}^{-1}$  was obtained for  $\text{Ti}_3\text{CN}$ ; at 3C a stable capacity of 170  $\text{mAhg}^{-1}$  was obtained after 50 cycles.

For  $\text{Ta}_4\text{C}_3$  a stable capacity of 140  $\text{mAhg}^{-1}$  was obtained at C/3, while at 4C a stable capacity of 50  $\text{mAhg}^{-1}$  was obtained even after 50 cycles. Although the specific gravimetric capacities for  $\text{Ta}_4\text{C}_3$  are relatively low, volumetrically those capacities translate to  $\approx 1400 \text{ mAh.cm}^{-3}$  and  $500 \text{ mAh.cm}^{-3}$  at C/3 and 4C respectively, which are very high values, especially at such relatively high cycling rates.

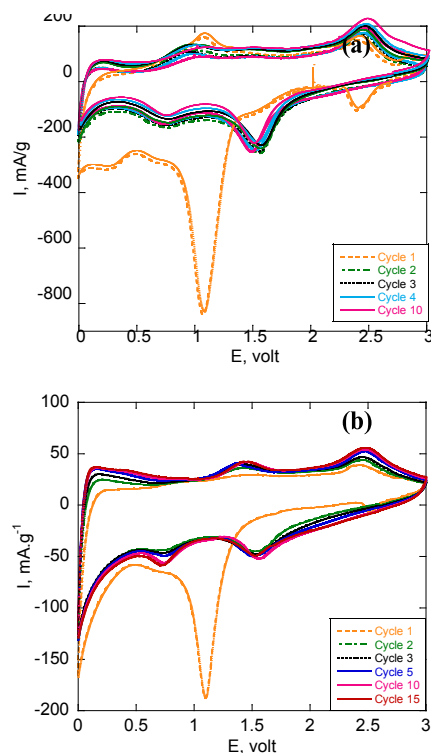


Figure V - 105: (a) Cyclic voltammetry curves for  $\text{Ti}_3\text{CN}$ , and (b)  $\text{Ta}_4\text{C}_3$ .

**Effect of Carbon Additives.** The effect of various carbon additives in different forms (carbon black, carbon onions, nanotubes, and carbide derived carbon) on the performance of MXene anodes was studied. Also, different binders were tested.  $\text{Ti}_3\text{C}_2$  was used as the active material and representative for all other MXenes.

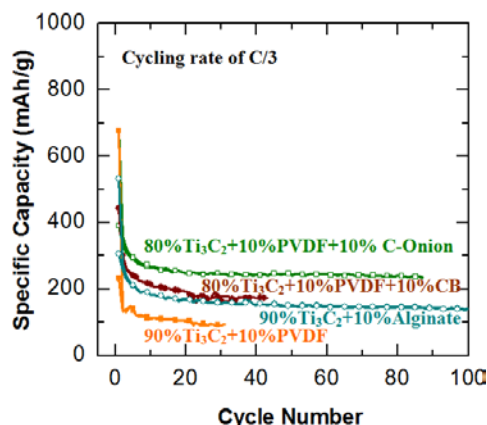
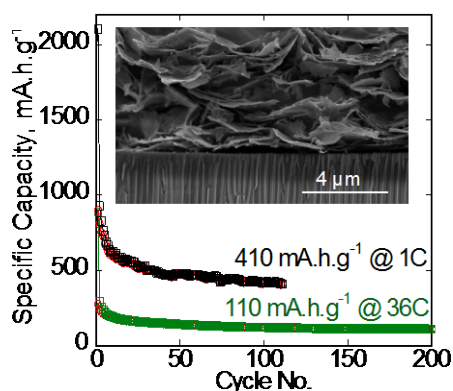


Figure V - 106: Specific capacities (per mass of active material) vs. cycle #, for  $\text{Ti}_3\text{C}_2$  with different binders and different carbon additives.

Figure V - 106 shows the effect of selected additives on the performance of  $\text{Ti}_3\text{C}_2$  anodes. Among the different binders, alginate (10 wt.%) yielded the best performance when no carbon additive was used. Adding 10 wt.% of C-onions to the conventional PVDF composition resulted in a stable capacity of  $\approx 240 \text{ mAh/g}$ . The capacity increase can be explained by an enhancement in conductivity. This was clear in emerging of new lithiation and delithiation peaks

in the CV (not shown) curves with the addition of alginate and/or C-onions. The highest capacity was obtained for a mixture of 80 wt.%  $\text{Ti}_3\text{C}_2$ , 10% PVDF and 10% C-onions (see Figure V - 106.)

**Additive-Free Delaminated  $\text{Ti}_3\text{C}_2$ .** Recently, full delamination of  $\text{Ti}_3\text{C}_2$  was successfully achieved. Additive-free anodes of  $\text{Ti}_3\text{C}_2$  (see inset in Figure V - 107) were made by filtering a dispersion of delaminated flakes in water. The new anodes showed a capacity of 410 mAh/g at a 1C cycling rate after 100 cycles, and a capacity of 110 mAh/g, at a cycling rate of 36 C for 200 cycles (Figure V - 107.) Such rates are significantly faster than what graphite can handle. It is important to note that the results shown in Figure V - 107 were obtained on *additive free* – no binders or other additive – anodes. This feature should prove useful commercially in simplifying LIB design and containing costs.



**Figure V - 107:** Specific capacities for delaminated  $\text{Ti}_3\text{C}_2$ . Inset shows SEM image of *additive-free*  $\text{Ti}_3\text{C}_2$  film used as anode.

## Conclusions and Future Directions

During FY 2012, all milestones were reached and in some cases surpassed. A number of MXenes (such as  $\text{Ti}_3\text{C}_2$ ,  $\text{Ti}_2\text{C}$ ,  $\text{Ti}_3(\text{C}_{0.5}\text{N}_{0.5})_2$ ,  $\text{Ta}_4\text{C}_3$ ) were produced by HF treatment of MAX phases at room temperature. It is now established that the MXenes represent a new family of 2-D materials with excellent potential as anode materials in LIB. Some of the MXenes were tested electrochemically as anode materials in LIBs. In all the cases, the MXenes showed an excellent ability for cycling at high rates with good gravimetric capacities and even better volumetric capacities. *In situ* XRD of  $\text{Ti}_3\text{C}_2$  anodes showed that the  $\text{Li}^+$  ion reversibility was due to its intercalation between the MXene layers and not due to a conversion reaction.

The effect of carbon additives on the performance of exfoliated but not delaminated  $\text{Ti}_3\text{C}_2$  in LIBs was studied. Carbon onions together with PVDF were found to be the best additives that boosted the capacity to 240 mAh/g at a rate of C/3. Totally *additive free* anodes made with delaminated  $\text{Ti}_3\text{C}_2$  showed outstanding performance at high rates (capacity of 410 mAh/g at 1C, and 110 mAh/g at 36C).

Future research will focus on the lightest MXene, viz.  $\text{Ti}_2\text{C}$ , and other compositions not tested to date. The focus will also shift to anodes made from *additive-free* delaminated films. The lithiation and delithiation mechanisms and the nature of the SEI will be further investigated, using various *in situ* techniques with the ultimate goal of optimizing the performance of MXenes in LIBs and minimizing the first cycle irreversibility.

## FY 2012 Publications/Presentations

1. Naguib, M. et. al., "Two-Dimensional Transition Metal Carbide," *ACS Nano* 2012, **6** (2), 1322-1331.
2. Naguib, M. et. al., "MXene: A Promising Transition Metal Carbide Anode Material for Lithium-ion Batteries," *Electrochem. Communications* 2012, **16** (1), 61-64.
3. Anasori, B. et. al. "The Cliff of the Two-Dimensional World," *Science*, 2012, 335, 527 - NSF/Science competition winner.
4. Come, J. et. al., "A Non-aqueous Asymmetric Cell with a  $\text{Ti}_2\text{C}$  Based Two-Dimensional Negative Electrode," *Journal of The Electrochemical Society* 2012, 159 (7) A1-A6.
5. Kurtoglu, M. et. al., "First Principles Study of Two-Dimensional Early Transition Metals Carbides," *MRS Communications* 2012, DOI: 10.1557/mrc.2012.25.
6. Lane, N. et. al., "First-Order Raman Scattering of the MAX phases  $\text{Ta}_4\text{AlC}_3$ ,  $\text{Nb}_4\text{AlC}_3$ ,  $\text{Ti}_4\text{AlN}_3$  and  $\text{Ta}_2\text{AlC}$ ," *J. Raman Spect.* 2012, **43** (7), 954-958.
7. Presser, V. et. al., "First-order Raman scattering of the MAX phases:  $\text{Ti}_2\text{AlN}$ ,  $\text{Ti}_2\text{AlC}_{0.5}\text{N}_{0.5}$ ,  $\text{Ti}_2\text{AlC}$ ,  $(\text{Ti}_{0.5}\text{V}_{0.5})_2\text{AlC}$ ,  $\text{V}_2\text{AlC}$ ,  $\text{Ti}_3\text{AlC}_2$ , and  $\text{Ti}_3\text{GeC}_2$ ," *J. Raman Spectroscopy* 2012, **43** (1), 168-172.
8. Lane, N.J. et. al., "Structure of a New bulk  $\text{Ti}_5\text{Al}_2\text{C}_3$  MAX Phase Produced by Topotactic Transformation of  $\text{Ti}_2\text{AlC}$ ," *J. Europ. Ceram. Soc.* 2012, **32** (12), 3485-3491.
9. Lane, N.J. et. al., Comment on " $\text{Ti}_5\text{Al}_2\text{C}_3$ : A New Ternary Carbide Belonging to MAX Phases in the Ti-Al-C System," *J. Amer. Ceramic Society* 2012, DOI: 10.1111/j.1551-2916.2012.05299.x.
10. 2012 DOE Annual Peer Review Meeting Presentation.
11. Several invited talks and oral presentations at MS&T, ACS, EMC, and ECS conferences

## V.C.8 Atomic Layer Deposition for Stabilization of Amorphous Silicon Anodes (NREL, U. Col)

Chunmei Ban (Anne C Dillon)  
National Renewable Energy Laboratory  
1617 Cole Blvd  
Golden, CO, 80401  
Phone: (303) 384-6504; Fax: (303) 384-6432  
E-mail: [Chunmei.ban@nrel.gov](mailto:Chunmei.ban@nrel.gov)

Steve M. George and Se-Hee Lee (Co-PIs)  
University of Colorado Boulder  
Department of Chemistry and Mechanical Engineering  
914 Broadway, Boulder, CO 80309  
Phone: (303) 492-7471 and (303) 492-7889  
E-mail: [steve.george@colorado.edu](mailto:steve.george@colorado.edu)  
[sehee.lee@colorado.edu](mailto:sehee.lee@colorado.edu)

Start Date: October 1, 2010  
Projected End Date: September 30, 2014

### Objectives

- Develop a novel conductive and elastic framework for Si anodes using Atomic Layer Deposition (ALD) & Molecular Layer Deposition (MLD).
- Demonstrate durable cycling performance of thick Si anodes by using new ALD/MLD coatings and electrode designs.
- Investigate effects of atomic surface modification on irreversible capacity loss & structural evolution during cycling.
- Explore the importance and mechanism of various coatings via the BATT Coating Group.
- Collaborate within the BATT program with the aim of developing high-rate plug-in hybrid electric (PHEV) compatible electrodes (both anodes and cathodes).

### Technical Barriers

Major barriers addressed include:

- (A) Cost: Inexpensive processing techniques are employed to fabricate conventional thick electrodes.
- (B) High Capacity: Silicon is predominantly being explored as a high capacity anode material. There is also a collaborative emphasis to enable high capacity cathode materials.
- (C) High Rate: Both ALD coatings and nanostructured materials are being developed such that high-rate capability is demonstrated for emerging materials.
- (D) Safety: The ALD coatings are targeted to improve

safety for a variety of electrode materials.

### Technical Targets

- Stabilize the high-capacity silicon anodes by employing the advanced surface coating techniques, ALD and MLD.
- Demonstrate the stable high-rate cycling performance of Si anodes
- Relevant to USABC goals: 200 Wh/kg (EV requirement); 96 Wh/kg, 316 W/kg, 3000 cycles (PHEV 40 mile requirement). Calendar life: 15 years. Improved abuse tolerance.

### Accomplishments

- Successfully developed the Si thick electrode ( $\geq 15 \mu\text{m}$ ) with a highly reversible capacity of at least 2,000 mAh g<sup>-1</sup> at C/20 (175mA/g).
- Demonstrated the high-rate capability (at C/3, ~1200mA/g) for Si-polyacrylonitrile (PAN) composite electrodes.
- Demonstrated mechanistic information about ALD coatings via *in situ* synchrotron X-ray diffraction (XRD), and *ex situ* X-ray photoelectron spectroscopy and time of flight secondary ion mass spectrometry (TOF-SIMS).
- Greatly improved cycling performance of full cells by applying Al<sub>2</sub>O<sub>3</sub> ALD coating on electrodes and separators.
- Density functional theory (DFT) simulations of lithiation in silica through partial reduction.

◇ ◇ ◇ ◇ ◇

### Introduction

Significant advances in both energy density and rate capability for Li-ion batteries will be necessary for implementation in next generation EVs. Due to the high theoretical capacity of Si, 3579 mAh g<sup>-1</sup> for Li<sub>15</sub>Si<sub>4</sub>, and its natural abundance, Silicon has attracted much attention as a promising Li-ion anode material. However, progress towards a commercially viable Si anode has been impeded by Si's rapid capacity fade caused by the large volumetric expansion. Such a massive volumetric change can result in cracking and pulverization of the Si particles, which then leads to the interruption of electronic transport pathways and the electrochemical isolation of pulverized particles. Using an ALD conformal nanoscale coating of Al<sub>2</sub>O<sub>3</sub> on

nano-MoO<sub>3</sub> has greatly improved the performance of these electrodes despite the volumetric expansion of nano-MoO<sub>3</sub> electrodes (> 100%). The nanoscale conformal coating of Al<sub>2</sub>O<sub>3</sub> is believed to stabilize the surface and enhance the mechanical integrity of MoO<sub>3</sub> electrodes. These past results suggest that new ALD and MLD coatings can be developed to accommodate the volumetric expansion of Si anodes, as well as ensure the electronic paths through the electrodes.

Both high rate and durable cycling of Si will be achieved by employing the ALD coating and new elastic (polymer-like) coatings with low elastic moduli that are similar to polysiloxanes. We collaborated with multiple outside organizations to investigate the effects of the ALD/MLD coatings and to demonstrate nano-structured materials. In the end, we are enabling the development of both high capacity anodes and cathodes within the BATT program that exhibit durable high rate capability.

## Approach

Chemical vapor deposition via silane decomposition on a hot filament was used to synthesis the amorphous silicon particles. Recently, a Nanocrystal RF Plasma Reactor has been utilized to synthesis silicon/alloy nanocrystals with uniform size and shape. Size may be tuned from <10 to ~100 nm by varying the plasma conditions that will allow the study of how Si nanocrystal size affects the electrochemical performance. Conventional electrodes containing active material, conductive additive and binder have been fabricated to evaluate the cycling properties.

ALD was employed to coat both Si particles and Si electrodes in order to enhance the surface stability and electrode integrity. Furthermore, MLD has been applied to develop a novel conductive and elastic framework in order to accommodate the volumetric changes in Si particles. Besides an Al-based precursor, other metal precursors are being used to enhance the conductivity in the MLD flexible coatings.

## Results

### Development of Si-cyclized PAN Composite

**Electrode.** Greatly improved cycling performance was achieved by using Si-cyclized polyacrylonitrile (PAN) hybrid material as a Li-ion anode. Optimal performance was achieved through the use of low-temperature heat-treated composite electrodes. The mechanical properties of the Si-cyclized PAN hybrid material were studied by nanoindentation. Figure V - 108 exhibits the hardness and reduced elastic modulus (Er) of the cyclized PAN at different synthesis temperatures. The Er of the cyclized-PAN, calculated by using nanoindentation, remains consistent below 500°C. It confirms that the low-temperature cyclized-PAN keeps the similar mechanical properties as the pristine polymer. However, an abrupt

increase in hardness was found at temperatures  $\geq 300^\circ\text{C}$ . This sudden increase in hardness is due to the cyclization of PAN at  $\sim 300^\circ\text{C}$ . The cyclization of PAN has been verified with the results from Raman spectroscopy.

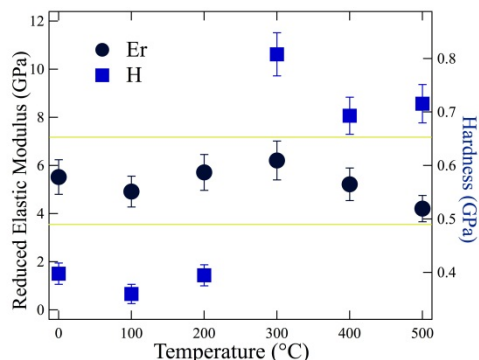


Figure V - 108: Hardness and Elastic Modulus of PAN with increasing annealing temperature.

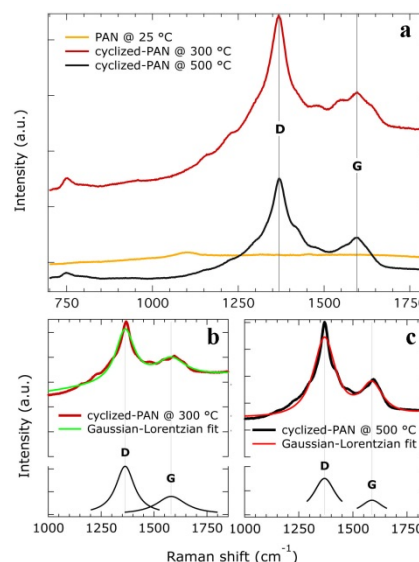
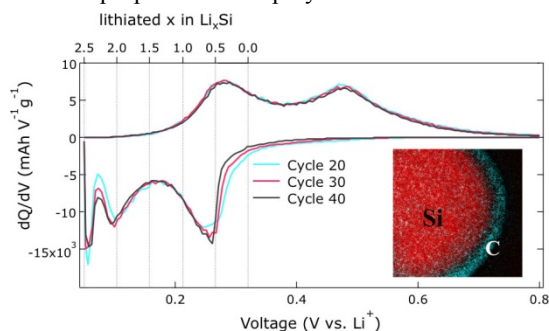


Figure V - 109: Raman spectrum of pristine PAN and cyclized PAN.

The formation of the sp<sup>2</sup> bonding in the Si-PAN hybrid material was confirmed with Raman spectroscopy. Figure V - 109 presents the Raman spectra for the pristine PAN, and Si-PAN cyclized at 300°C, and Si-PAN cyclized at 500°C. The two Raman shifts at 1600 cm<sup>-1</sup> and 1360 cm<sup>-1</sup> were obtained in both cyclized Si-PAN materials, which were attributed to the G band and D band from a graphite-like structure. However, these two peaks are absent in the Raman spectrum of the pristine PAN. The observation of both the D and G bands attests to the existence of graphite-like domains with varying degrees of crystallinity. The peaks in the cyclized PAN were fitted with a Gaussian-Lorentzian function, in order to compare the relative intensity of the G band (crystalline graphite-like structure) and D bands (disordered graphite-like structures). As indicated in Figure V - 109 b and c, a stronger relative G band for the sample treated at 500°C indicates a graphite-like structure with a higher degree of order than that for the sample treated at 300°C. The

evolution of a cyclized pyridine-ring structure occurs at a low temperature  $\sim 300^\circ\text{C}$ . These cyclized pyridine rings have  $\text{sp}^2$  bonding with delocalized  $\pi$  bonding which enables good electronic conductivity.

**Rate capability of Si-cyclized PAN Composite Electrode.** The development of the cyclic (ring) polymeric molecular structure at low temperatures enhances the electronic conductivity but also maintains the favorable mechanical properties of the polymer.



**Figure V - 110:** Differential capacity vs voltage curves represent the highly reversible cycling of Si-cyclized PAN electrodes, the inset shows EELS mapping image of the core-shell nanostructure.

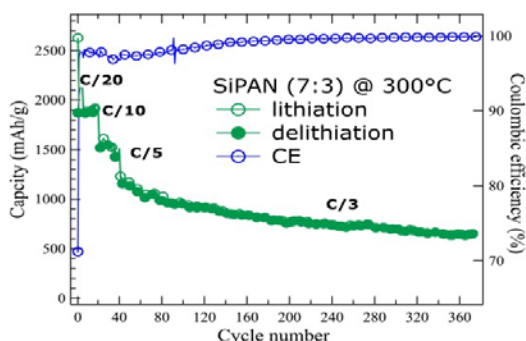


**Figure V - 111:** Sustainable cycling performance of Si-cyclized PAN electrodes at the higher cycling rates.

The Si-cyclized PAN nanostructure has demonstrated the stable cycling performance with minor degradation of the cycling capacity. Plotting of the differential capacity as a function of voltage confirms the structural stability after the first lithiation process, and shows highly reversible Li-alloying/dealloying over 50 cycles without degradation, as indicated in Figure V - 110. Electron Energy Loss Spectroscopy (EELS) overlay mapping image of the Si-C core-shell nanostructure, seen in the overlay of Figure V - 110, displays the cyclized-PAN shell covering the silicon core.

The rate-capability has been demonstrated in the half-cells with Li metal, as shown in Figure V - 111. The cells were cycled at C/20, followed by 20 cycles at C/10, then finally cycled at C/3. The Si-cyclized PAN has a reversible capacity of  $800 \text{ mAh g}^{-1}$  at a cycling rate of C/3 for more than 100 cycles, and retains a reversible capacity of  $600 \text{ mAh g}^{-1}$  after 300 cycles. Moreover, Coulombic efficiency of the Si/cyclized-PAN composite anodes approaches 100% after 150 cycles. The greatly improved cycling

performance at a rate of C/3 is believed to be due to the enhanced electronic and mechanical properties of the Si-cyclized PAN composite material.

#### Effect of $\text{Al}_2\text{O}_3$ ALD Coatings on SEI composition of Li-ion Electrodes.

The effect of  $\text{Al}_2\text{O}_3$  ALD coatings on solid electrolyte interphases (SEI) formation was also studied by using *ex situ* XPS and TOM-SIMS. The full cell composed of  $\text{LiCoO}_2$  (LCO) cathode and natural graphite anode (NG) was used as a platform. Figure V - 112 summarizes the XPS results from NG (a-e) and LCO (f-j) electrodes before and after cycling. The presence of  $\text{Al}_2\text{O}_3$  ALD layer has been observed on coated-NG (c-NG) XPS (Figure V - 112 d and e). Unexpected peaks at  $\sim 286.2 \text{ eV}$  for C 1s (Figure V - 112a) and  $\sim 686 \text{ eV}$  for F 1s (Figure V - 112b) on c-NG indicates a chemical interaction between  $\text{Al}_2\text{O}_3$  ALD species and the carbon in NG or PVDF - chemically changing the PVDF by ALD. The signals from the cycled c-NG also show the SEI signatures except for the  $\text{Li}_2\text{O}$ . Additionally, the cycled c-NG does not show the  $\text{Li}_2\text{CO}_3$  peak at  $\sim 290.3 \text{ eV}$  for C 1s while it is evident on bared NG (b-NG) (Figure V - 112a). A much higher intensity of the Li 1s peak was observed for the cycled b-NG than that for the cycled c-NG (Figure V - 112c). These above observations indicate that we have significantly mitigated side reactions by using  $\text{Al}_2\text{O}_3$  ALD coating. Overall, the analyses of XPS signals from NG suggest that the c-NG has a markedly different SEI from that of the b-NG in terms of the amount and also the composition. Furthermore, the  $\text{Al}_2\text{O}_3$  ALD coatings on the NG anodes result in a suppression of the side reactions on the bare LCO cathodes. A LiF peak at  $\sim 685 \text{ eV}$  for F 1s (Figure V - 112h) is very intense for the b-LCO cathode paired with a b-NG anode. The peak is negligible for b-LCO paired with c-NG. Secondly, the overall shape of O 1s spectra for b-LCO/b-NG is quite different from that for b-LCO/c-NG (Figure V - 112j), suggesting a b-LCO/c-NG pair leads to different SEI components from b-LCO/b-NG.

*Ex situ* TOF-SIMS has been performed to confirm the effect of  $\text{Al}_2\text{O}_3$  ALD on the thickness of SEI components. The depth profiling data of the ions on cycled NGs and LCOs by TOF-SIMS is shown in Figure V - 113a-f. For NG electrodes,  $\text{Al}^+$  signals and others ( $\text{Li}_2\text{O}^+$ ,  $\text{Li}_2\text{F}^+$ ,  $\text{CH}_3^+$ ) contributed to  $\text{Al}_2\text{O}_3$  ALD and inorganic ( $\text{Li}_2\text{O}^+$ ,  $\text{Li}_2\text{F}^+$ )/organic ( $\text{CH}_3^+$ ) components of the SEI, respectively. Two dramatic differences between b-NG and c-NG are: a) the thickness of  $\text{Li}_2\text{F}^+$  on b-NG ( $\sim 24 \text{ nm}$ ) is almost twice than that on c-NG; b)  $\text{CH}_3^+$  signals are very intense only for b-NG (arrow). *The TOF-SIMS results strongly reflect much thinner SEI layer with much less organics on c-NG than on b-NG.* In contrast, the signals for b-LCOs don't give any pronounced difference between b-LCO/b-NG and b-LCO/c-NG from the TOF-SIMS data (Figure V - 113e, f). This observation may indicate that the key to govern the degradation of b-LCO may not be related to the thickness of the SEI. From the combined analyses by *ex situ* XPS and TOF-SIMS, the following conclusions are possible: i)

The Al<sub>2</sub>O<sub>3</sub> ALD coating significantly mitigates the surface reaction on NG, forming thinner SEI with significantly reduced organic species. ii) Compared with b-LCO paired with b-NG, b-LCO paired with c-NG shows similar thickness of the SEI but a different composition. Thus, improved durability has been achieved in the full cell of b-LCO/c-NG.

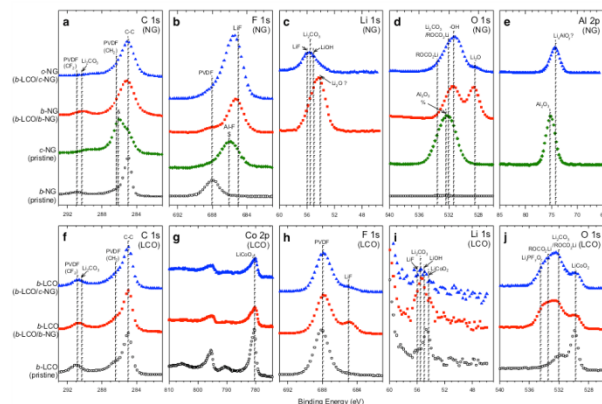


**Figure V - 112:** XPS spectra of NG and LCO electrodes before and after the charge-discharge cycles.

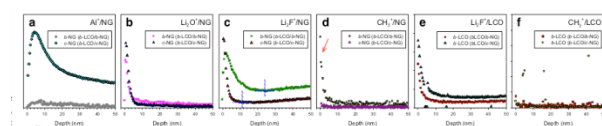


**Figure V - 113:** Time-of-flight secondary ion mass spectrometry (SIMS) analyses of cycled NG and LCO electrodes from b-LCO/b-NG and b-LCO/c-NG full cells.

## Conclusions and Future Directions

By cyclizing commercially available polyacrylonitrile (PAN), a pyridine-based conjugated polymer is obtained to accommodate Si's volumetric expansion during lithiation. Pyridine also has delocalized  $sp^2 \pi$  bonding for intrinsic electronic conductivity. Good ionic conductivity of cyclized-PAN coatings is assumed based upon good electrochemical performance at fast cycling rates. And for increased electrode energy density, cyclized-PAN coatings serve as both conductive additive and binder singly. Therefore, the cyclized-PAN acts both as a binder and conductive additive because of its good mechanical resiliency to accommodate silicon's (Si) large expansion as well as its good ionic and electronic conductivity. The Si-cyclized PAN electrodes exhibit a specific charge capacity of nearly  $1500 \text{ mAh g}^{-1}$  when cycling at C/10, and deliver the reversible capacity of  $800 \text{ mAh g}^{-1}$  at a cycling rate of C/3 for more than 100 cycles, and retains a reversible capacity of  $600 \text{ mAh g}^{-1}$  after 300 cycles. The enhanced electronic and mechanical properties of the Si-cyclized PAN composite material enable the durable cycling performance with greatly improved rate capability.

The effect of Al<sub>2</sub>O<sub>3</sub> ALD coatings on the structure and SEI composition have been demonstrated by using *in situ* synchrotron XRD and *ex situ* XPS and TOF-SIMS. Al<sub>2</sub>O<sub>3</sub>

ALD has mitigated the side reaction on the surface of electrodes and preserved the structure during severe cycling at higher voltage.

In the FY13, our research will focus on: 1) developing a hybrid metal-organic coating on Si anode; 2) optimizing the coating materials for ALD/MLD to reduce the irreversible capacity loss; and 3) demonstrating the effect of new coatings on the electrochemical performance and structural evolution of Si anodes.

## FY 2012 Publications/Presentations

1. Y. Jung, L. Peng, A. S. Cavanagh, C. Ban, S. Lee, S. J. Harris, G. Kim, A. Dillon, "Unexpected Improved Performance of ALD Coated LiCoO<sub>2</sub>/Graphite Li-ion Batteries", *Adv. Energy Mater.* DOI: 10.1002/aenm.201200370.
2. C. Ban, B. Kappes, Q Xu, C. Engrakul, C.V. Ciobanu, A. C. Dillon and Y Zhao, "Lithiation of silica through partial reduction" *Appl. Phys. Lett.* (2012) 100, 243905.
3. Jung, Y. S., Cavanagh, A. S., Gedvilas, L., Widjonarko, N. E., Scott, I. D., Lee, S.-H., Kim, G.-H., George, S. M. and Dillon, A. C." Improved Functionality of Lithium-Ion Batteries Enabled by Atomic Layer Deposition on the Porous Microstructure of Polymer Separators and Coating Electrodes" *Adv. Energy Mater*, 2: 1022–1027. 2012.
4. 2012 DOE Annual Peer Review Meeting Presentation
5. (Invited talk) Electrochemical and *In situ* Structural Study of Coated Li[NMC]O<sub>2</sub> Cathodes for Durable High-voltage Cycling, International Battery Association-Pacific Power Source Symposium, 2012, Hawaii.
6. (Invited talk) Improving Electrochemical Performance of Li-ion Electrodes via Advanced Surface Modification, 10X Advanced Battery R&D, 2012, Santa Clara, CA.

## V.C.9 Synthesis and Characterization of Si/SiO<sub>x</sub>-Graphene Nanocomposite Anodes and Polymer Binders (Penn State U)

Donghai Wang and Michael A. Hickner  
The Pennsylvania State University  
Department of Mechanical and Nuclear Engineering  
Department of Materials Science and Engineering  
328 Reber Building University Park, PA 16802  
Phone: (814) 863-1287; (814) 867-1847  
E-mail: [dwang@psu.edu](mailto:dwang@psu.edu); [mah49@psu.edu](mailto:mah49@psu.edu)

Start Date: January 1, 2011  
Projected End Date: December 31, 2014

### Objectives

- Design, synthesize and test novel polymer binders with varying mechanical properties and surface linker groups for Si anodes.
- Synthesize and characterization of Si/SiO<sub>x</sub>-graphene nanocomposites.
- Identify and evaluate the electrochemical performance of the Si/SiO<sub>x</sub>-graphene nanocomposites and the polymer binder.
- Improve management of volume change characteristics of Si-based anodes, impede the capacity fading with enhanced capacity reliability, decrease initial irreversible capacity loss, and improve the specific capacity and coulombic efficiency of Si/SiO<sub>x</sub>-based anodes.

### Technical Barriers

There are several technical barriers to developing Si/SiO<sub>x</sub>-based anodes for lithium-ion batteries including:

- Poor capacity cycling.
- Large initial irreversible capacity and corresponding low coulombic efficiency.
- Need to add a high percentage of conductive carbon to obtain good rate performance.

### Technical Targets

- Prepare Si nanoparticles with controlled particle size, and demonstrate Si-graphene nanocomposite anodes.
- Synthesize and evaluate novel polymer binders with controlled SiO<sub>x</sub> binding groups and Li-conducting blocks.
- Determine electrochemical properties of Si/SiO<sub>x</sub> nanoparticle, Si/SiO<sub>x</sub>-graphene nanocomposites and the polymer binders in lithium half cell.

- Achieve stable reversible capacity in excess of ~1,000 mAh/g.
- Obtain above 40% first cycle coulombic efficiency as well as 90% coulombic efficiency cycle to cycle.

### Accomplishments

- Successful synthesis of SiO<sub>x</sub> nanoparticle with high cycling ability (capacity retention >95% after 350 cycles) and high coulombic efficiency (>99%).
- The novel series of porous Si/C composites exhibit specific capacity in excess of ~1500mAh/g with good cycling stability and rate capability.
- New classes of binders were demonstrated with commercial Si nanoparticles that showed between 2500 and 3500 mAh/g (based on Si) over 45 cycles.
- Demonstrated key properties of binders including electrolyte swelling and functional group composition for high capacity and low capacity fade.

◇ ◇ ◇ ◇ ◇

### Introduction

An increase in energy and power densities of Li-ion cells depends in a decisive way on improvements in electrode materials performance. As the commercial anode, graphite has the theoretical capacity of 372 mAh/g, which is low relative to the requirement of high-energy application fields. Thus, the search for an alternative anode to replace graphite in Li-ion batteries has been underway for many years. So far, silicon has the highest theoretical capacity (Li<sub>4.4</sub>Si ≈ 4200 mAhg<sup>-1</sup>) of all known materials, and is abundant, inexpensive, and safer than graphite (it shows a slightly higher voltage plateau than that of graphite, and lithiated silicon is more stable in typical electrolytes than lithiated graphite). Unfortunately, the practical use of Si powders as anodes in Li-ion batteries is still hindered several problems. One of the problems is severe volume change during Li insertion/extraction, leading to loss of electric contact and poor cycling performance.

One approach to obtain a high-performance Si anode is to use silicon/carbon composites. Graphene is an excellent conductive carbon substrate to host active Si nanomaterials due to its high conductivity, large surface area, flexibility, and chemical stability. In this project, the aim is to develop novel Si/SiO<sub>x</sub>-graphene nanocomposite to improve cycling performance of Si anodes. On the other hand, many important battery characteristics, including

stability and irreversible capacity losses, are critically dependent on the polymer binder's properties. High capacity electrochemically active Si particles that exhibit significant volume changes during insertion and extraction of Li require improved binder characteristics to ensure electrode integrity during use.

Inspired by these features, this project sought to mitigate the electrochemical limitations of Si-based anodes during charge/discharge by designing novel Si/SiO<sub>x</sub>-graphene nanocomposite and polymer binders to tolerate volume change, improve electrode kinetics, and decrease initial irreversible capacity loss. The new electrodes made with these polymer-coated SiO<sub>x</sub>-graphene nanocomposites have significantly improved the cycling capability of Si-based anodes.

### Approach

The approach is to 1) to synthesize different Si-based nanocomposites and identify novel commercially available binders to tolerate volume change upon lithiation/delithiation so as to improve cycling performance; and 2) to develop novel polymer binder with controlled elastic properties, ion-conductive moieties, and SiO<sub>x</sub> surface binding functionality in order to stabilize and bridge SiO<sub>x</sub> particles to improve cycling performance of Si anodes from both commercial sources and novel Si-based nanomaterials.

### Results

**Si-based anode materials.** A new series of Si-hollow carbon (Si@HC) nanocomposites composed of commercial Si nanoparticles and hollow carbon spheres were developed to accommodate the volume changes during lithiation for high-performance Li-ion battery anodes. The TEM image of the Si@HC (Figure V - 114) clearly shows that the Si contained within the carbon spheres with void in between the Si and carbon. In such structures, Si contents can expand/shrink freely during discharge/charge processes in the void space. In order to optimize the void/Si volumetric ratio, three different Si@HC nanocomposites with void/Si volumetric ratios of 1.5:1, 3:1, and 6:1 were synthesized and investigated.

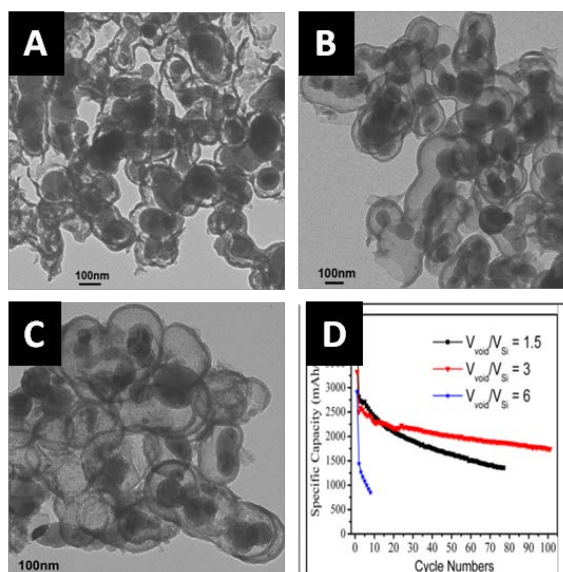


**Figure V - 114:** TEM images of the Si@HC nanocomposite (A) Void/Si = 1.5:1 (B) Void/Si = 3:1 (C) Void/Si = 6:1 and (D) Capacity comparison of three Void/Si ratios

Electrochemical tests were performed on the Si@HC nanocomposite anode materials between a lower cut-off voltage of 0.01 V and an upper cut-off voltage of 1.5 V (Figure V - 114D). The Si@HC material with ratio of Void/Si = 1.5:1 showed the highest first cycle discharge capacity of around 4050 mAh/g Si (equivalent C/10 rate). After 80 cycles, the sample with ratio of Void/Si = 3:1 shows the best capacity among three materials of ca. 2000mAh/g based on the Si content. As a comparison, the Si@HC with void/Si = 6:1 yielded the lowest first cycle discharge capacity of ca. 2900 mAh/g. After 10 cycles, it only showed discharge capacity of ca. 750 mAh/g. Therefore, the Si@HC material with void/Si = 3:1 is shown to provide both promising first cycle discharge capacity and good cycling stability.

In order to achieve long cycling ability, a novel SiO<sub>x</sub> nanocomposite was prepared by a wet synthesis method. The average particle size of the SiO<sub>x</sub> composite is about 10 nm, which was confirmed by TEM (Figure V - 115A, B). The structure of the nanocomposite can be described as a Si core surrounded by SiO<sub>x</sub> layer. The composite structure was further characterized by various of physical methods including XPS, EDS and FT-IR spectroscopy.

The first cycle discharge capacity of the SiO<sub>x</sub> material was 2190 mAh/g and stabilized at ca. 650 mAh/g for the cycles thereafter (Figure V - 115D). After the initial cycle, the electrode showed good capacity retention after 100 cycles (>90%) and 350 cycles (>85%). The coulombic efficiency after 30 cycles reached 99% and grew to >99.5%. The SiO<sub>x</sub> also showed excellent cycling stability at different current densities. Further studies are undergoing to improve cycling capacity and first cycle coulombic efficiency.

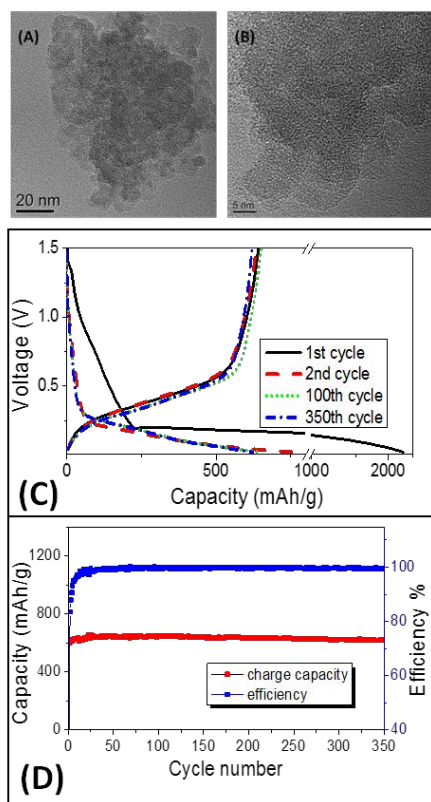


**Figure V - 115:** (A) (B) HRTEM images of the SiO<sub>x</sub> nanocomposite (C) Discharge-charge profiles obtained after 1st, 2nd, 100th and 350th cycles. (D) Discharge capacity and coulombic efficiency of 350 cycles between 0.01 and 1.5V.

Based on the synthesis developed for the SiO<sub>x</sub> composite, a series of porous Si materials was synthesized by a modified method. The corresponding Si/C porous materials (labeled as PSiC-1, 2 and 3) based on such Si materials were also prepared by carbon deposition. XRD spectra of the porous Si materials clearly showed phases of crystalline Si. These porous Si and Si/C materials were further characterized by a variety of methods such as SEM, TEM and EDS.

The first cycle discharges of all three Si/C materials were 2303 mAh/g, 1709 mAh/g and 2557 mAh/g (Figure V - 116A). The coulombic efficiencies of the first cycle (>60%) of all three materials were much improved compared to the previous SiO<sub>x</sub> material (~30%). After the initial cycles (3 cycles at a current density of 0.4 A/g), the electrodes showed capacity retention of >90% after 50 cycles at a current density of 1 A/g. The charge capacity after 100 cycles of PSiC-1 and PSiC-3 were still above 1000 mAh/g at a current density of 1 A/g. The PSiC-2 showed excellent rate performances of >400 mAh/g at high electron density (12.8 A/g) (Figure V - 116B). Further investigations on pore size effect are ongoing.

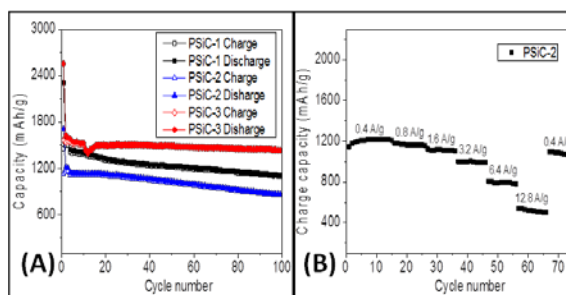


**Figure V - 116:** (A) Charge and discharge capacities of all three porous Si/C materials in 100 cycles between 0.01-1.5V. (B) Rate performances of the PSiC-2 materials.

### Synthesis and Evaluation of Polymer Binders.

Aromatic backbone polymers were synthesized with a variety of functional groups to determine the important properties for creating new binders for commercial Si nanoparticles. The goal of this work is to design new binders that enable good cycling of commercially available Si and to determine chemical motifs for advanced binder design. In previous work it was found that flexible backbone random and block copolymers did not perform well in battery cycling tests. Therefore, current work is focused on stiff backbone polymers.

The swelling of new binders in EC:DMC solvent has been measured (Figure V - 117). It was observed that binders that reached their equilibrium swelling quickly tend to cycle better in cell performance tests. Binders that swell slowly over 100s of hours tend to not cycle well. This swelling experiment gives a method to screen new binders for Si-based anodes.

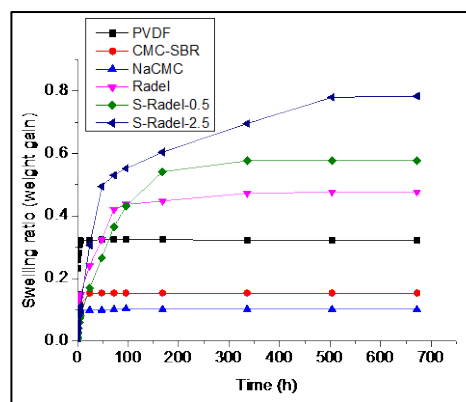


**Figure V - 117:** Swelling of various binders including PVDF and CMC-SBR in EC:DMC electrolyte. Binders that swell quickly and stabilize their electrolyte uptake tend to cycle better.

The sulfonated Radel (S-Radel) or sulfonated poly(sulfone) binders were shown to swell over long periods and did not show good cycling stability (Figure V - 118). Sulfonate groups were attached to the stiff Radel polymer backbones to improve their ionic conductivity. It is hypothesized that the slow swelling of these binders caused them not to hold the electrode structure together well and thus lead to lower cycling stability.

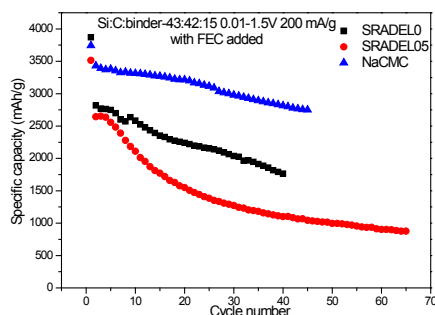


**Figure V - 118:** Cycling of Na-CMC and S-Radel binders with commercial Si-nanoparticles showing significant capacity fade and low performance in the case of S-Radel samples.

New binders containing ketone and sulfonate groups, SPEEK or sulfonated poly(ether etherketone), were synthesized, Figure V - 119. These binders are meant to have ketone groups that mimic NaCMC and also uptake some electrolyte with the sulfonate groups to promote ion conductivity in the binder. The cycling performance of cells with commercial Si powder anodes and added fluoroethylene carbonate (FEC) is shown in Figure V - 119. The SPEEK binder shows nearly equivalent cycling to the NaCMC when FEC is added to the electrolyte.

This promising result helps to clarify the needed functional groups in the polymer binder. A series of ketone/carboxylate/sulfonate-containing binders are now being designed for parametric tests of binder composition and cycling performance.

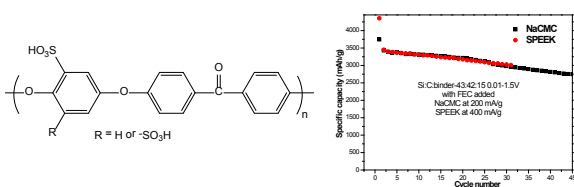


**Figure V - 119:** Chemical structure of sulfonated poly(ether etherketone) and its cycling performance with commercial Si nanoparticles compared to NaCMC.

## Conclusions and Future Directions

Three different Si-based composite (Si@HC, SiO<sub>x</sub> and porous Si/C) have been designed, synthesized and characterized. The electrochemical performance of all Si-based materials has been evaluated in coin-type cells. Results demonstrate that 1) the Si@HC composites exhibit ability to accommodate the volume changes during lithiation and also high capacities (> 2,000 mAh/g); 2) the SiO<sub>x</sub> nanocomposite shows an excellent long cycling ability (>85% after 350 cycles) and good coulombic efficiency (>99%), 3) the porous Si/C composites achieve good cycling ability and good high rate performance (>400mAh/g at 12.8A/g).

During the remainder of the project period, future work will focus on: 1) Optimizing composition and nanostructures of Si/SiO<sub>x</sub>-carbon nanocomposites (including Si/SiO<sub>x</sub> ratio, Si/C ratio, nanoparticle size, nanoporous structures) 2) Electrochemical characterization of the Si/SiO<sub>x</sub>-carbon nanocomposites;

For polymeric binders, how electrolyte swelling and the presence of carbonyl functional groups influence the cycling of commercially available Si-nanoparticle-based anodes has been investigated. It has been determined that slow swelling profiles over long times are not advantageous to binder performance as too much binder swelling cannot maintain the structure of the electrode. Polymers with only sulfonate groups seemed to swell too much to give good cycling stability. Stiff backboned polymers containing both sulfonate and ketone groups appear to show similar cycling performance to Na-CMC in current battery tests with commercially available Si-nanoparticles. With these new compositional insights in mind, a series of polymers with controllable ketone and ionic group functionalities will be pursued.

## FY 2012 Publications/Presentations

- Dai, F., Yi, R., Gordin, M. L., Chen, S. R., Wang, D. H., *RSC Advances* 2012. Accepted.
- Chen, S. R., Gordin, M. L., Yi, R., Howlett, G., Sohn, H. S. and Wang, D. H., *PCCP* 2012, **14** (37), 12741 – 12745.
- Vaughn, D. D., Hentz, O. D., Chen, S. R., Wang, D. H. and Schaak, R. E., *Chem. Comm.* 2012, **48**, 5608.
- Song, Z. P., Xu, T., Gordin, M. L., Jiang, Y. B., Bae, I. T., Xiao, Q.; Zhan, H., Liu, J., Wang, D. H., *Nano Lett.* 2012, **12** (5), 2205-11.
- Xu, Y., Yi, R., Yuan, B., Wu, X. F., Dunwell, M., Lin, Q. L., Fei, L., Deng, S. G., Andersen, P., Wang, D. H., Luo, H. M., *J Phys Chem Lett* 2012, **3** (3), 309-314.
- Wang, D. H., In Symposium of Frontiers of Energy and Fuel Research, Division of Energy and Fuel, *244th American Chemical Society (ACS) National Meeting*, Aug 2012, Philadelphia.
- Chen, S. R., Yi, R., Xu, T., Gordin, M. L., Howlett, G. Wang, D. H. *American Chemical Society (ACS) National Meeting*, Aug 2012, Philadelphia.
- Song, Z. P., Xu, T., Gordin, M. L., Wang, D. H., *ACS Spring Meeting*, Mar 2012, San Diego.
- Wang, D. H., *36th International Conference on Advanced Ceramics and Composites*, Jan 2012, Daytona Beach.
- Wang, D. H., Chen, Z. X., Gordin, M. L. Xu, T., *International Materials Research Congress*, Aug 2011, Cancun.

## V.C.10 Synthesis and Characterization of Silicon Clathrates for Anode Applications in Lithium-ion Batteries (SwRI)

Kwai S. Chan and Michael A. Miller  
Department of Materials Engineering  
Mechanical Engineering Division  
Southwest Research Institute  
6220 Culebra Road  
San Antonio, TX 78238  
Phone: (210) 522-2053; Fax: (210) 522-6965  
E-mail: [kchan@swri.org](mailto:kchan@swri.org); [mmiller@swri.org](mailto:mmiller@swri.org)

Start Date: January 1, 2011  
Projected End Date: December 31, 2014

### Objectives

- Develop scalable synthesis methods for producing empty and substituted silicon clathrates.
- Design, synthesize, and characterize silicon clathrate compounds for anode applications in Li-ion batteries.
- Fabricate and characterize prototype silicon clathrate anodes designed to exhibit small volume expansion during lithiation, high specific energy density, while avoiding capacity fading and improving battery life and abuse tolerance.

### Technical Barriers

This project addresses the following technical barriers of the lithium-ion battery technology, especially focusing on the silicon clathrate anode materials:

- Low-energy density
- Low-power density
- Short calendar and cycle lives

### Technical Targets

Develop silicon clathrate anodes to meet PHEV and EV goals by exceeding current benchmarks (Conoco Phillips CPG-8 Graphite/1 M LiPF<sub>6</sub>+EC:DEC (1:2)/ Toda High-energy layered (NMC) in the following metrics:

- Energy density
- Power density
- Calendar and cycle lives

### Accomplishments

- Selected a solution-based approach for synthesizing empty Type I silicon clathrates (Si<sub>46</sub>) and selected vacuum arc-melting for synthesizing alloyed Al-substituted silicon clathrates (Ba<sub>x</sub>Al<sub>y</sub>Si<sub>46-y</sub>).
- Predicted the Li<sup>+</sup> occupancy and lattice expansion potential of Type I metal-silicon clathrate alloys using classical and *ab initio* calculations.
- Identified possible reaction pathways for the formation of empty clathrates Si<sub>46</sub>, Li<sub>x</sub>Si<sub>46</sub>, Li<sub>15</sub>Si<sub>4</sub>, and Li<sub>x</sub>M<sub>y</sub>Si<sub>46-y</sub>.
- Synthesized hundreds of grams of metal-silicon Type I clathrate alloys with complementary determination of structural purity



### Introduction

To achieve the DOE's performance targets for PHEV and EV applications, low-cost advanced anode materials with high-energy density, high-power density, and longer calendar and cycle lives are needed. To address this need, the project focuses on the development of synthesis methods, characterization of electrochemical performance, and the design and fabrication of prototype silicon clathrate anodes for potential applications in Li-ion batteries for PHEV and EV.

Silicon clathrate, a polymorph of silicon, is an emerging anode material that is composed of sp<sup>3</sup> bonded silicon atoms arranged in cage-structures. The silicon clathrate, Si<sub>46</sub>, consists of crystalline Si with a regular arrangement of 20-atom and 24-atom cages fused together through five atom pentagonal rings (Type I clathrate). It has a simple cubic structure with a lattice parameter of 10.335 Å and 46 Si atoms per unit cell. The crystal structure (Space Group  $Pm\bar{3}n$ ) of the Si<sub>46</sub> clathrate is different from the common form of crystalline Si (c-Si), which is diamond cubic (Space Group  $Fd\bar{3}m$ ) with a lattice parameter of about 5.456 Å.

First-principles computations performed at Southwest Research Institute® (SwRI®) have revealed that significant amounts of Li ions can be inserted into and extracted from the cage structure of silicon clathrates without substantial volume changes or pulverization of the cage structure. Theoretical computations of the total volume, occupiable volume, and accessible volume within the Type I silicon clathrate structures indicate that the empty spaces within

the cage structure are accessible to Li and amenable to Li intercalation through electrochemical means, thus making silicon clathrate a potential anode material for Li-ion battery applications, while overcoming the usual problems of irreversible volume expansion encountered in *d*-Si-based anodes.

## Approach

SwRI is working with LBNL to develop silicon clathrate anodes for PHEV and EV applications. The approach is to synthesize guest-free Type I silicon clathrate (Si46) using a number of high-temperature processing methods, while concurrently exploring an investigational route for direct synthesis of guest-free clathrate and performing ab initio and classical molecular dynamics (MD) computations to identify lithiation pathways. Silicon clathrates will be utilized to fabricate prototype anodes. Electrochemical characterization will be performed to evaluate and improve, if necessary, anode performance including cyclic stability. The final year of the program will be directed at the design, assembly, and characterization of a complete (anode/cathode) small-scale, prototype battery suitable for concept demonstration.

## Results

### Batch Synthesis via Soft Oxidation of BaSi<sub>2</sub>.

A systematic approach toward synthesizing and isolating guest-free Type I silicon clathrate (Si46) was undertaken using a solution-based, batch process (Hoffman-type elimination and soft oxidation reaction) under relatively mild conditions (~300°C). Three different trial syntheses were carried out starting from a fine powder of BaSi<sub>2</sub> dispersed in a series of ionic liquids (ILs) in which the hexafluorophosphate (HFP), bis(trifluoromethylsulfonyl)imide (BTFMSI), and aluminum tetrachloride (ATC) anions were employed. In this series, partial structural transformation of BaSi<sub>2</sub> was observed in the powder XRD spectra only for the ATC system, but this reaction was accompanied by significant thermal degradation of the IL. To further improve the thermal stability of the reaction, a new IL consisting of the BTFMSI salt, which formed a liquid-phase eutectic near room temperature, was first synthesized and then incorporated into a fourth trial synthesis. The PXRD (Figure V - 120) and Raman characterization of the isolated product showed substantial transformation of the silicide to form Si46. Efforts are currently underway to improve the purity of the reaction product by removing unreacted silicide and secondary phase byproducts (i.e., Si<sub>4</sub>). Additionally, process methods were devised to enable the phase transformation of fuel-grade NaSi to the required Zintl phase (Na<sub>4.5</sub>Si<sub>9</sub>) under mild conditions. This more reactive precursor will be used in place of BaSi<sub>2</sub> in the solution synthesis of empty Si<sub>46</sub>.

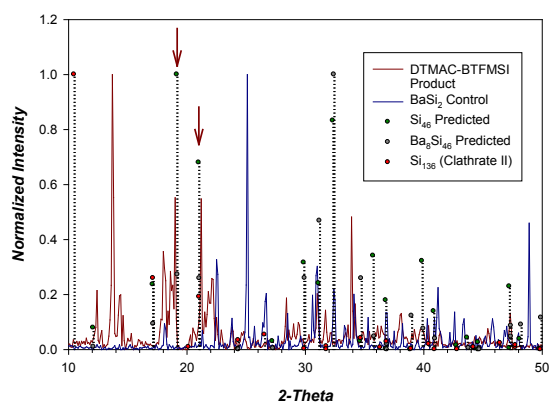


Figure V - 120: PXRD spectra of unpurified synthesis product compared with that of other compounds.

**Vacuum Arc-Melting Synthesis.** The framework-substituted Type I clathrate alloy, Ba<sub>8</sub>Al<sub>8</sub>Si<sub>38</sub>, was successfully synthesized in bulk (200 g) using a large-volume vacuum arc-melting technique. By making adjustments to the starting materials, process conditions and hardware, an improved degree of crystallographic purity was achieved as compared with previously-obtained (and evaluated) product (Figure V - 121). Earlier and on-going electrochemical measurements are showing that Li<sup>+</sup> can be intercalated reversibly in this clathrate slightly beyond the theoretical limit with negligible lattice expansion despite the presence of Ba guest atoms.

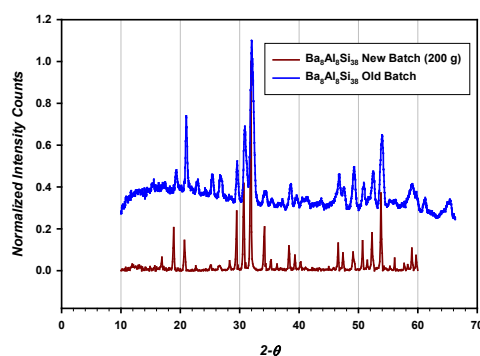
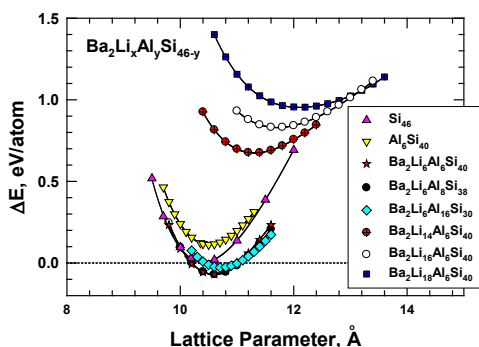


Figure V - 121: Powder XRD patterns for Type I clathrate alloys as formed from a revised (200 g) and old vacuum arc-melting process.

### Molecular Modeling of Silicon Clathrates.

Electrochemical (EC) cycling measurements made on the metal-substituted Type I silicon clathrate, Ba<sub>8</sub>Al<sub>6</sub>Si<sub>40</sub>, previously synthesized using a vacuum arc-melting technique, indicated that 300-350 Li atoms can be intercalated into the Ba-occupied clathrate lattices, equivalent to a specific capacity in excess of 4,000 mAh/g. EC experiments further indicated that Ba atoms cannot be extracted (deintercalated) from as-prepared Ba<sub>8</sub>Al<sub>6</sub>Si<sub>40</sub> even at large over potentials. In order to gain a fundamental understanding of the thermodynamic stability of these compositions when intercalated with lithium atoms, first-principles molecular dynamics computations based on the Carr-Parrinello theory (CPMD) were

performed over a range of lattice parameters for each composition. The results, shown in Figure V - 122, indicate that certain compositions already containing Ba as guest atoms are further stabilized by the presence of Li guest atoms, up to six, with little change in the lattice parameter. Large changes in both the thermodynamic stability and lattice parameters occur as the clathrate framework is occupied by a larger number (14-18) of Li atoms, suggesting that the large specific capacities measured experimentally ( $\gg 18$  Li atoms) would be far from the lattice equilibrium of  $\text{Ba}_8\text{Al}_6\text{Si}_{40}$  and would render the bulk anode material structurally metastable. The results of these computations will be compared with the cyclic capacity losses measured electrochemically.



**Figure V - 122:** Computed energies of formation for various Type I clathrate compositions.

The appropriate amounts of Ba and Al additions to attain a stable alloyed Si clathrate structure with limited volume expansion during Li insertion were identified through first-principles computations via the CPMD code. Two clathrate compositions,  $\text{Ba}_6\text{Li}_x\text{Al}_8\text{Si}_{38}$  and  $\text{Ba}_6\text{Li}_x\text{Al}_6\text{Si}_{30}$ , have been found to improve Li insertion without Ba removal over  $\text{Ba}_8\text{Li}_x\text{Al}_8\text{Si}_{38}$ . Both exhibit small increases in the lattice constant upon insertion of up to 24 Li atoms, as shown in Figure V - 123 (a). The corresponding energy change is negative, as shown in Figure V - 123 (b), indicating that lithiation is energetically feasible and relatively easier compared to delithiation.

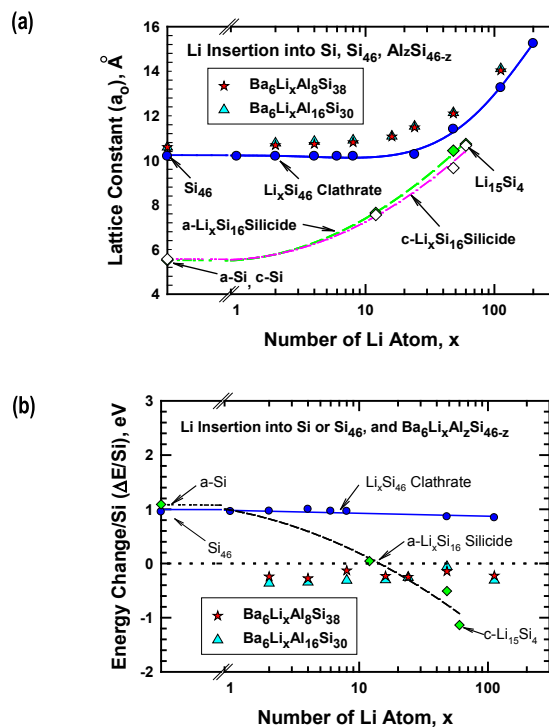


**Figure V - 123:** Comparisons of computed lattice constant and energy change as a function of Li insertion in  $\text{Ba}_6\text{Li}_x\text{Al}_8\text{Si}_{38}$ ,  $\text{Ba}_6\text{Li}_x\text{Al}_6\text{Si}_{30}$ ,  $\text{Li}_x\text{Si}_{46}$ , and  $\text{Li}_x\text{Si}_4$ : (a) lattice constant, and (b) energy change/Si atom.

The possible use of Na guest atoms to stabilize the empty  $\text{Si}_{46}$  structure was evaluated by computing the energy of formation of  $\text{Na}_x\text{Li}_y\text{Si}_{46}$  as a function of the lattice constant. These results, summarized in Figure V - 124, indicate that Na guest atoms stabilize the  $\text{Si}_{46}$  structure by producing a slightly negative energy of formation. Insertion up to 6 Li atoms into the  $\text{Na}_2\text{Si}_{46}$  structure reduces the energy of formation without a volume expansion. The energy of formation becomes positive and the unit cell expands by 8% when the number of Li inserted is increased to 22. The results suggest that Li insertion into Na-stabilized  $\text{Si}_{46}$  may be easier compared to Ba-stabilized  $\text{Si}_{46}$ .

**Figure V - 124:** Computed energy change of  $\text{Na}_x\text{Li}_y\text{Si}_{46}$  as a function of lattice constant.

#### Half-Cell Electrochemical Characterization.

Electrochemical measurements were performed to explore

the effects of binder and conductive additives on the net capacity, cycle loss, and SEI formation of the anode when combined with the intermetallic clathrate  $\text{Ba}_8\text{Al}_8\text{Si}_{38}$  previously synthesized by the vacuum arc-melting technique. Overall, the results suggest that the compounded anodes formed by mechanical compression into free-standing disks (1 cm diam.  $\times$  3  $\mu\text{m}$  thick) tend to be diffusionally constrained at rates  $\geq C/14$ , particularly on intercalation of  $\text{Li}^+$ , with a first-cycle net (irreversible) loss 24% of the theoretical capacity (259 mA-h/g, exemplary cycles shown in Figure V - 125). Additionally, potential and/or current fluctuations during anodic deintercalation of  $\text{Li}^+$  point to instabilities in SEI formation that persist beyond the second cycle.

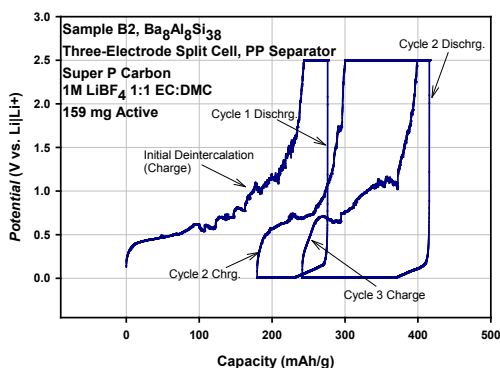


**Figure V - 125:** Half-cell voltage profiles for the first few delithiation-lithiation cycles of clathrate anode.

To overcome these gaps in half-cell performance, anodes were formed by casting slurries composed of  $\text{Ba}_8\text{Al}_8\text{Si}_{38}$ , carbon additive, and binder into thin layers. Furthermore, to address the instability of the SEI, the half-cells containing the thin-cast anodes were combined with a fluoroethylene carbonate (FEC)-based electrolyte. These changes resulted in marked improvements in the anode material's capacity: 1,500 mAh/g of active materials (Figure V - 126).

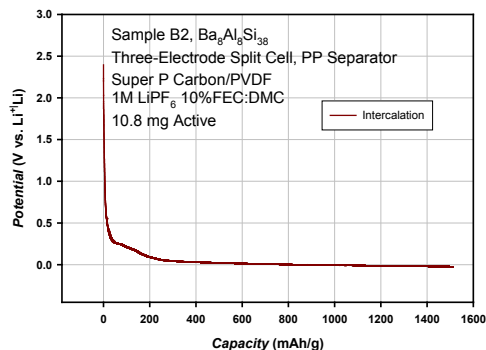


**Figure V - 126:** Electrochemical intercalation of  $\text{Li}^+$  into thin-film  $\text{Ba}_8\text{Al}_8\text{Si}_{38}$  anode composition using FEC-based electrolyte.

## Conclusions and Future Directions

1. While a solution-based approach to synthesizing empty Type I silicon clathrate ( $\text{Si}_{46}$ ) starting from  $\text{BaSi}_2$  and a novel IL eutectic has been shown to be efficacious, further improvements are needed to decrease the formation of secondary phases and increase product purity. Efforts are currently underway to prepare and employ the more reactive Zintl species  $\text{Na}_{4.5}\text{Si}_9$  and characterize the reaction yield.
2. Bulk synthesis (200 g) of the Type I clathrate alloy,  $\text{Ba}_8\text{Al}_8\text{Si}_{38}$ , via the vacuum arc-melting technique has been successfully demonstrated by employing process improvements in material form and hardware. A marked improvement in crystallographic purity and yield has been achieved, thus allowing the use of contemporary processes to form and evaluate nano-phase anode materials in the near future.
3. First-principles computational studies indicate that the stability of  $\text{Ba}_x\text{Al}_y\text{Si}_{46-y}$  Type I clathrates and the extent to which they can accommodate Li atoms (in the presence of Ba guests) without significant volume expansion is improved by restricting Ba guest atoms to six. Thus, bulk synthesis and electrochemical analysis of this improved composition will be undertaken during in the following year.
4. Theoretical predictions further suggest that Type I silicon clathrates accommodating Na guest atoms (in place of Ba) are thermodynamically stable even when intercalated with six Li atoms. Future work will be directed at the trial bulk synthesis of such compositions for experimental evaluation.
5. Marked improvements in SEI stability and cycle losses for silicon clathrate anodes have been realized by employing FEC-based electrolytes in combination with thin-film casting techniques. Further improvements in the reversible capacity are forthcoming by implementing process methods that yield nano-phase material of bulk-synthesized clathrate alloys.

## FY 2012 Publications/Presentations

1. 2012 DOE Annual Peer Review Meeting Presentation.
2. Miller, M.A. and Chan, K.S., "Development and Characterization of Energy Materials", *Plug-In 2012 Conference*, July 23, 2012.

---

## V.C.11 Wiring up Silicon Nanoparticles for High Performance Lithium Ion Battery Anodes (Stanford U)

Yi Cui  
Stanford University  
476 Lomita Mall, McCullough 343  
Stanford, CA 94305  
Phone: (650) 723-4613  
E-mail: [yicui@stanford.edu](mailto:yicui@stanford.edu)

Start Date: January 1, 2011  
Projected End Date: December 31, 2014

### Objectives

- Go beyond the charge capacity limitation of conventional carbon anodes by designing nano-architected silicon electrodes.
- Design, synthesize and characterize Si nanostructure-based anodes to overcome the volume change-induced materials challenges and to realize high performance.
- Understand the fundamental structure-property relationship on electrode materials with large structure and volume changes.
- Develop low-cost materials processing methods.

### Technical Barriers

The large structure and volume changes of Si during battery cycling cause multiple materials challenges: 1) mechanical breaking; 2) unstable solid electrolyte interface; 3) difficulties in maintaining good electrical connections. These fundamental challenges result in the following technical barriers to good battery performance:

- Large first cycle irreversible capacity loss.
- Poor cycle life.
- Inadequate Coulombic efficiencies.

### Technical Targets

- Develop fundamental materials guidelines through structure and property correlations and design nanostructured Si anodes with these features to address the three material challenges outlined above.
- Develop synthesis techniques to produce the designed nanostructured Si anodes.
- Develop and pursue techniques for structure-property correlation at the single nanostructure level.

### Accomplishments

- Developed a variety of synthesis strategies to make hollow Silicon core-carbon shell nanostructures with controlled porosity
- Developed nanostructures in which the directionality of volume expansion is controlled during lithiation.
- Used electrospinning (a cheap and scalable manufacturing method) to fabricate Si nanostructures.
- Used *in situ* transmission electron microscopy (TEM) methods to examine the nature of expansion in these hollow nanostructures.
- Used *in situ* TEM to observe the effect of conductive metal coatings on Si volume expansion during lithiation.
- Used *in situ* TEM to determine the controlling kinetic factors during the lithiation of crystalline silicon nanostructures.
- Developed conductive polymer coatings that improve Coulombic efficiency in Si nanowire electrodes.

◇ ◇ ◇ ◇ ◇

### Introduction

Next generation high capacity electrode materials are needed in order to generate high energy battery technology to meet the demands of the transportation sector. Silicon is an exciting and promising anode material for replacing carbon in Li-ion batteries due to: 1) a high gravimetric capacity of ~4,200 mAh/g, ten times higher than graphite (~370 mAh/g); 2) a high volume capacity of 9786 mAh/cm<sup>3</sup>; 3) its relatively low working potential (~0.5 V Vs Li/Li+), which makes it suitable as an anode; 4) the abundance and environmentally friendly nature of Si; and 5) the ability to leverage the fundamental and manufacturing knowledge that has been established in the Si semiconductor industry and solar industry. However, there exist several scientific and technical challenges for silicon anodes: 1) Mechanical fracture caused by large volume changes. The electrochemical alloying reaction of Li with Si involves volume expansion of up to 300% and significant contraction during lithium extraction. The stress induced by the large volume changes causes cracking and pulverization of silicon, which leads to loss of electrical contact and eventual capacity fading. 2) Unstable solid electrolyte interface (SEI). The repetitive volume expansion/contraction causes the continuous movement of the interface between Si and organic electrolyte, which

makes it challenging to form a stable SEI layer, resulting in low Coulombic efficiency and capacity loss during cycling. 3) It is challenging to maintain good electrical contact between Si materials and the current collector. Even though mechanical fracture does not take place in Si nanostructures below critical sizes, large volume changes can still cause the movement of Si nanostructures and their detachment from the conducting framework during long-term battery cycling. 4) Challenges associated with generating Si materials to address the above three challenges with low-cost and scalable processing.

The goal of this project is to study the fundamental principles related to alloy anodes, to design nanostructured Si anodes to solve the three fundamental challenges and to develop low-cost and scalable processing for these materials.

### Approach

This project takes a two-pronged approach to solving these problems. First, *ex situ* and *in situ* observation techniques are developed and used to uncover the fundamental nature of the Li-Si reaction and volume changes. Insight gained from this fundamental study is used as the framework for designing new nanostructured anodes that feature minimal structural damages and dimensionally stable surface/electrolyte interface regions. A focal point of the project is to also develop low-cost and scalable methods to synthesize these designed nanostructured Si anodes.

### Results

#### Double-walled Si nanotubes with an outer constraining layer for high Coulombic efficiency.

Electrodes that were made up of hollow Si nanofibers delivered promising electrochemical results. This structure is designed for SEI control: the surface region of the thin (~40nm) tube wall is oxidized, and this oxide layer acts as a constraint to promote inward expansion of the silicon material during lithiation. In this way, outward expansion of silicon and repeated SEI fracture and electrolyte exposure is avoided, and thus SEI formation is expected to be limited and less severe than in traditional geometries. This is demonstrated by the SEM images in Figure V - 127.

The top image (A) shows that a relatively extensive SEI film grows on tubes without an external oxide constraining layer after 200 cycles. Tubes with the oxide layer after 2,000 cycles are shown in the bottom image (B); the SEI that forms is much more compact and uniform. This leads to better Coulomb efficiency and lower overpotential in the cell. This geometry leads to remarkable cycling behavior; shows good capacity retention for 6,000 cycles at a rate of 5C.

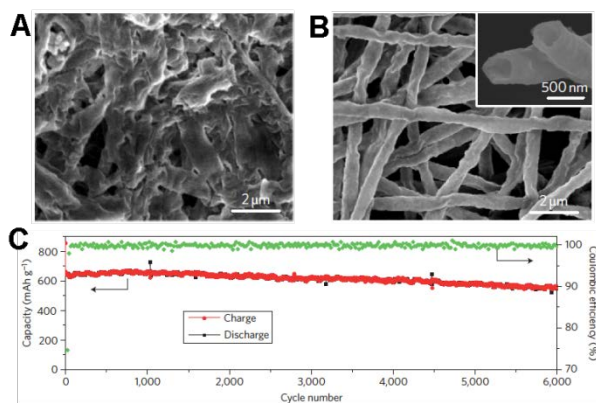


**Figure V - 127:** A, Image of SEI on Si nanotubes without oxide after 200 cycles. B, Similar image of SEI on nanotubes with an oxide constraining layer. C, Cycling capacity of Si nanotube battery anode showing superior performance.

**A yolk-shell design for Si anodes with good cycle life.** To create a low-cost high-performance anode material, a yolk-shell structure based on Si nanoparticles is fabricated primarily with solution-based methods. This yolk-shell structure consists of Si nanoparticles encapsulated within a thin (~30 nm) carbon shell with empty space between the Si particle and the shell. This empty space is rationally designed to accommodate the volume expansion that occurs during lithiation. An example TEM image of this structure is shown in Figure V - 128, where the Si particles (darker contrast) are seen to be surrounded by the outer carbon shell. This structure is fabricated via a sacrificial templating method: Si nanoparticles are first coated with ~100 nm of SiO<sub>2</sub> via TEOS decomposition in solution, and then carbon coating is applied. Finally, the SiO<sub>2</sub> layer is removed with HF etching, leaving the yolk-shell structure behind.

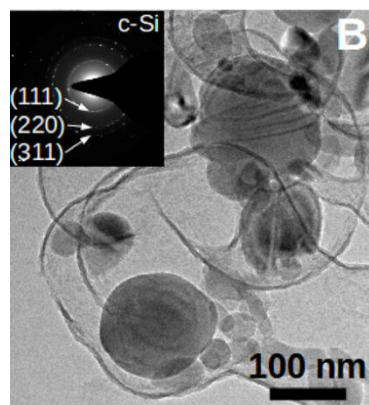


**Figure V - 128:** Yolk-shell structure

The idea behind this structure is that when it is used as the active material in a Li battery anode, the electrolyte will only contact the outer carbon surface, while the Si particles can expand and contract within the hollow pockets via lithium diffusion through the outer carbon layers. In this way, the surface in contact with the electrolyte (the carbon coating) undergoes only minor

mechanical deformation, which allows for a stable, compact SEI to grow on the outer carbon layer. *In situ* TEM was carried out to examine this material, and it was observed that the Si particles become fully lithiated via Li diffusion through the outer carbon layers.

The yolk shell material shows excellent electrochemical behavior when tested in half cells. Example data are shown in Figure V - 129. Here, a Si nanoparticle yolk-shell electrode was cycled 1000 times at 1C with little capacity decay. Although during the first ~100 cycles the average Coulombic efficiency is about 99%, from cycle 500 to 1,000 the average Coulombic efficiency increases to 99.84%.

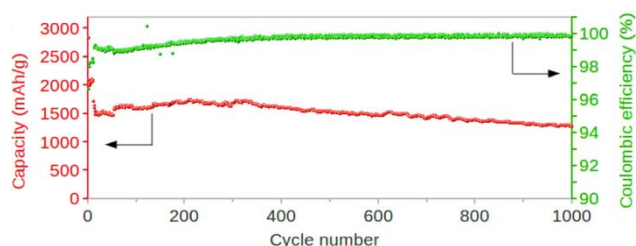


Figure V - 129: Capacity with cycling of yolk-shell anodes.

***In situ* TEM reveals the lithiation kinetics of individual crystalline Si nanoparticles.** To better design silicon-based anodes for Li-ion batteries, it is important to understand both the phase transformations and the details of the lithium-silicon reaction. Here, *in situ* TEM experiments are reported in which Si nanoparticles of different sizes were observed in real-time during lithiation. Example data of a group of nanoparticles being lithiated are shown in Figure V - 130. At 148 sec (c), the particles have been lithiated and are expanded compared to the pristine particles (a). To analyze the reaction kinetics, the diameter of the crystalline Si core and the total particle diameter were measured as a function of time for dozens of individual nanoparticles. Example data of this type are shown in Figure V - 131. It is evident from this data that the reaction front velocity slows significantly as the lithiation reaction progresses. This is rather surprising, since if the kinetics were only controlled by the short-range interactions at the reaction front (as has been previously suggested), the velocity of the reaction front should be constant.

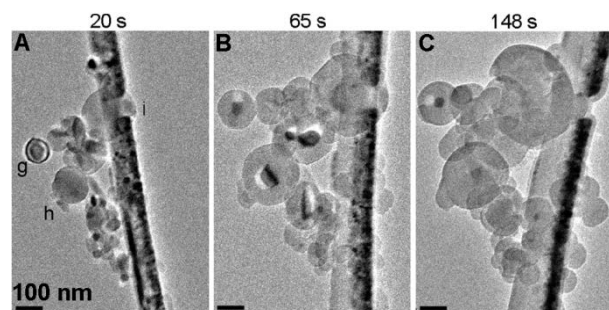


Figure V - 130: *In situ* TEM of Si nanoparticle lithiation.

Based on analysis of the reaction front trajectories and analytical models of the mechanical stress evolution during the lithiation of silicon, the reaction front slowing behavior is attributed to the effect of mechanical stress on the reaction. As a spherical particle is lithiated, significant hydrostatic pressures develop on either side of the reaction front, and the stress become more compressive with the degree of lithiation. This hydrostatic stress affects the driving force the reaction, and if the reaction rate is assumed to depend exponentially on the driving force, this would explain the slowing reaction front. Overall, these findings have implications for the rate behavior of actual Si-based anodes. In addition, this study shows that stress can significantly affect the reaction in addition to causing physical changes such as fracture.

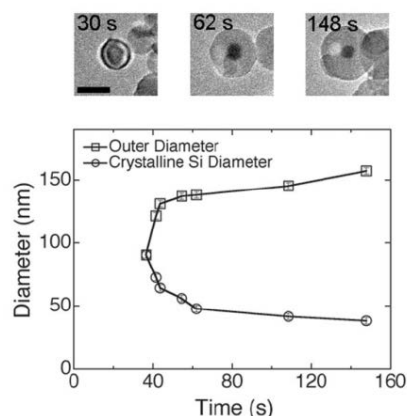
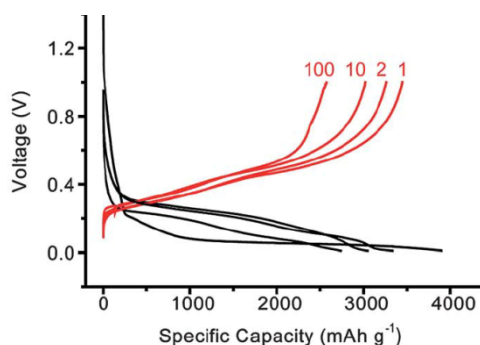


Figure V - 131: Diameter during lithiation of a single Si particle.

***In situ* TEM to determine the effect of metallic coatings on volume expansion.** Metallic coatings have been shown to improve the Coulombic efficiency of Si anodes, but their effect on volume expansion is less well understood. To understand their effect, *in situ* TEM experiments were performed to observe the lithiation of Cu-coated Si nanowires (NWs). NWs with Cu coated on one side were observed to expand primarily away from this coating. Conformal copper coatings fracture when the underlying Si alloys with Li. These results indicate the importance of creating coatings with the correct thickness and mechanical properties to withstand the volume expansion of Si without fracture, or alternatively to create hollow coated nanostructures.

**Conducting polymer coatings to improve the performance of Si NW anodes.** For silicon nanowires to be used as a successful high capacity lithium-ion battery anode material, improvements in cycling stability are required. Here it is shown that a conductive polymer surface coating on the Si NWs improves cycling stability. Conformal PEDOT polymer coatings were applied to NWs via a facile electropolymerization method, and the coatings were uniform and ~100 nm thick. Coating the NWs with PEDOT causes the capacity retention after 100 charge-discharge cycles to increase from 30% to 80% over bare NWs. The improvement in cycling stability is attributed to

the conductive coating maintaining the mechanical integrity of the cycled Si material, along with preserving electrical connections between NWs that would otherwise have become electrically isolated during volume changes.



**Figure V - 132:** Galvanostatic voltage profiles during cycling of PEDOT-coated SiNW anodes.

### Conclusions and Future Directions

Much progress has been made on these projects this year. A variety of *in situ* and *ex situ* microscopy techniques have been used to determine the effect of nanostructure size, shape, and crystallinity on volume expansion/contraction and structural changes. Based on these fundamental studies, tailored nanostructured anodes were designed and fabricated that showed high capacity, high Coulombic efficiency, and good cycle life. Hollow nanostructures were designed with the following engineering guidelines in mind: 1) volume expansion should be accommodated within the hollow nanostructure, 2) the surface of the structure should not expand or contract so that a stable SEI film can grow there, and 3) the nanostructures must be electronically connected to the electrode framework.

Future directions include: 1) further developing and exploring conducting polymer additives, coatings, and binder to improve the connectedness of the Si electrode framework during cycling. This includes the use of viscous polymers for a self-healing effect. In addition, the use of micron-scale Si particles will be explored in conjunction with polymer coatings. 2) The next focus will be on determining the effect of porosity and surface coatings on SEI thickness and properties. 3) Finally, *in situ* TEM and *ex situ* SEM will be used to compare single-crystalline, amorphous, and polycrystalline lithiation/delithiation and volume expansion/contraction, with emphasis on structural transformations. These results will be useful for designing future nanostructures.

### FY 2012 Publications/Presentations

1. S.W. Lee, M.T. McDowell, L.A. Berla, W.D. Nix, Y. Cui, "Fracture of crystalline silicon nanopillars during electrochemical lithium insertion," *PNAS*, March 2012, **109**, 11, 4080-4085.

2. M.T. McDowell, S.W. Lee, C.M. Wang, Y. Cui, "The effect of metallic coatings and crystallinity on volume expansion of silicon during electrochemical lithiation/delithiation," *Nano Energy*, May 2012, **1**, 3, 401-410.
3. H. Wu, G. Zheng, N. Liu, T.J. Carney, Y. Yang, Y. Cui, "Engineering empty space between silicon nanoparticles for lithium-ion battery anodes," *Nano Letters*, January 2012, **12**, 2 904-909.
4. N. Liu, H. Wu, M.T. McDowell, Y. Yao, C.M. Wang, Y. Cui, "A yolk-shell design for stabilized and scalable Li-ion battery alloy anode," *Nano Letters*, May 2012, **12**, 6, 3315-3321.
5. H. Wu, G. Chan, J.W. Choi, I. Ryu, Y. Yao, M.T. McDowell, S.W. Lee, A. Jackson, Y. Yang, L. Hu, Y. Cui, "Stable cycling of double-walled silicon nanotube battery anodes through solid-electrolyte interphase control," *Nature Nanotechnology*, March 2012, **7**, 310-315.
6. Y. Yao, N. Liu, M.T. McDowell, M. Pasta, Y. Cui, "Improving the cycling stability of silicon nanowire anodes with conducting polymer coatings," *Energy and Environmental Science*, April 2012, **7**, 5, 7927-7930.
7. M.T. McDowell, I. Ryu, S.W. Lee, C.M. Wang, W.D. Nix, Y. Cui, "Studying the kinetics of crystalline silicon nanoparticle lithiation with *in situ* transmission electron microscopy," *Advanced Materials*, September 2012, DOI: 10.1002/adma.20120274.

---

## V.D Electrolyte Development

### V.D.1 Polymer Electrolytes for Advanced Lithium Batteries (UC, Berkeley)

Nitash P. Balsara  
University of California  
Department of Chemical and Biomolecular Engineering  
201 C Gilman Hall  
Berkeley, CA 94720  
Phone: (510) 642-8973; Fax: (510) 643-4778  
E-mail: [nbalsara@berkeley.edu](mailto:nbalsara@berkeley.edu)

Start Date: October 1, 2009  
Projected End Date: September 30, 2013

#### Objectives

- Fundamental characterization of self-assembled block copolymer electrolytes for stabilizing lithium metal anodes.
- Development of self-assembled polymer separators.
- Development of electronically and ionically conducting polymer binders.

#### Technical Barriers

Current lithium-ion cells use polymers for two applications: they serve as a binder to hold the active materials in place and as a porous separator to hold the liquid electrolyte and keep the electrodes physically separated. The cost of the porous separators is large due to the delicate processing steps that are used in manufacturing. Defects in the separator can cause catastrophic failures. The binder is essentially an inactive component, while electron and ion transport are mediated by separate components - carbon and liquid electrolyte that floods the pores of a porous electrode, respectively. Cell energy and power performance deteriorate if the active materials loses contact with charge transporting components. Lithium metal electrodes are not used in rechargeable batteries due to dendrite growth.

#### Technical Targets

- Enable the use of a lithium metal electrode stabilized by a block copolymer electrolyte.
- Synthesize and characterize self-assembled porous battery separators.
- Synthesize and characterize electronically and ionically conductive polymer binders.

#### Accomplishments

- First quantification of the stability block copolymer electrolytes against Li metal anodes in full cells.
- The relationship between conductivity and morphology of self-assembled, porous block copolymer separators revealed by combination of ac impedance spectroscopy and resonant soft X-ray scattering.
- Successful characterization of electronic- and ionic-conductivity of a polymer binder.



#### Introduction

The objective of this work is to comprehensively examine the role that polymers can play in the development of advanced lithium batteries – specifically addressing issues of safety, cycle life, and cost. Replacing conventional liquid electrolytes with a solid block copolymer enables the use of a lithium metal anode, which improves the energy density of the battery. The block copolymer comprises a hard non-conducting block that suppresses the formation of lithium dendrites while a soft block enables rapid transport of lithium-ions. There has been the first demonstration of stability of block copolymer electrolytes in full cells with a lithium metal anode. In more recent work, the hard non-conducting block was replaced with an electronically conducting block to serve as a polymer binder. It is obvious that the conductivity of these materials is due to the transport of both ionic and electronic charge. A robust approach for independently determining electronic and ionic conductivity in these materials is demonstrated. Finally, a processing route for nanoporous separators has been developed which may be more cost-effective and environmentally friendly than those under current industrial use. The separators are made via templated block copolymer self-assembly. Thus far, however, the tools for characterizing when the templating worked and when it failed are lacking. It is shown here that resonant soft X-ray scattering (RSOXS) provides a route for characterizing templating.

#### Approach

Sequential polymerization is used to synthesize the block copolymers for all of the projects. Physical characterization includes determination of morphology by

soft X-ray and X-ray scattering and electron microscopy, and electrochemical characterizations are performed using either blocking or non-blocking electrodes.

## Results

**Material.** Three different kinds of block copolymers have been synthesized: poly(styrene)-*b*-poly(ethylene oxide) (SEO) copolymers for stabilizing the lithium metal electrode, polystyrene-*b*-polyethylene-*b*-polystyrene (PS-PE-PS) copolymers for self-assembled porous separators and poly(3-hexylthiophene)-*b*-polyethylene oxide (P3HT-PEO) copolymers for electronically and ionically conducting binders.

**Stability of Block Copolymer Electrolytes at Lithium Metal Anodes.** Lithium dendrite formation was studied in polymer electrolytes consisting of lithium bis(trifluoromethanesulfonimide) salt (LiTFSI) dissolved in polystyrene-*b*-poly(ethylene oxide) (SEO) block copolymers. Both Li-polymer-FePO<sub>4</sub> batteries and Li-polymer-Li symmetric cells were cycled at constant current until voltage responses characteristic of dendritic failure were observed. The amount of charge passed before this observation,  $C_D$ , was defined as the lifetime of the cell. Battery lifetimes were found to be significantly longer than symmetric cell lifetimes. Both battery and symmetric cell lifetimes increased with increasing electrolyte thickness, as predicted by the model of Monroe and Newman (Figure V - 133). Post-mortem analyses of the lithium surfaces were conducted after failure. The lithium electrodes from failed batteries were much smoother than those from failed symmetric cells. Dendritic structures with characteristic length scales in the 10-30  $\mu\text{m}$  range were seen in batteries. In contrast, the length scales of the dendritic structures seen in symmetric cells were in the 100-300  $\mu\text{m}$  range.

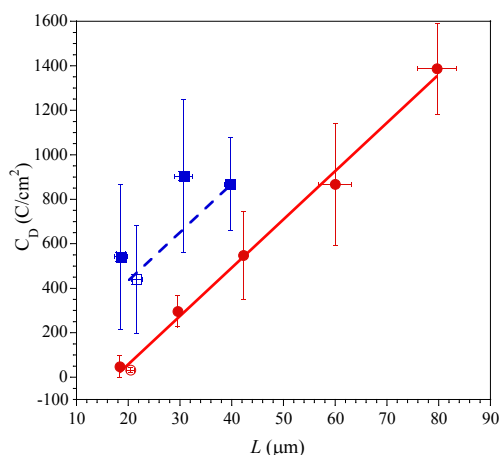


**Figure V - 133:** Battery (blue) and symmetric cell (red) lifetime,  $C_D$ , as a function of electrolyte thickness. Filled symbols: SEO diblock copolymers. Open symbols: SEOS tri-block copolymer. Lines are linear regressions. [details in ref. 1].

**Self-assembled Separators.** Nanoporous battery separators were made by blending a poly(styrene-block-ethylene-block-polystyrene) copolymer (SES) and polystyrene (PS) homopolymers, casting films of the blend, and selectively dissolving the homopolymer. The volume previously occupied by the homopolymer chains in the cast films are thus converted into pores. This approach enabled systematic variation of the pore structure at fixed void fraction by changing the normalized chain length of the sacrificial PS homopolymer. The efficacy of the resulting separators was determined by measurement of the ionic conductivity of separators soaked in a standard lithium battery electrolyte, 1M lithium hexafluorophosphate in ethylene carbonate/diethyl carbonate (1:1 v/v, Novolyte Technologies, Inc.). The effect of the chain length of the sacrificial homopolymer on separator morphology and ion transport was then determined using impedance measurements.

The main advantage of this approach relative to conventional separator manufacturing is that the pore structure is determined by equilibrium thermodynamics and thus strict control over processing conditions is not necessary.

The use of contrast-matched Resonant Soft X-ray Scattering (RSOXS) for studying the morphology of the separators is demonstrated. If the PS homopolymer chains are initially located within the PS microphase of the SES copolymer, then one obtains a porous film wherein the pores are lined with PS. This is referred to as the templated morphology. The membranes are thus composed of three phases: voids, PS, and PE. Conventional techniques such as Small Angle X-ray Scattering (SAXS) and Scanning Electron Microscopy (SEM) only distinguish between the polymer and the voids. It has been shown that microphase separation between PS and PE can be studied by using contrast-matched RSoXS in spite of the presence of voids. Under certain circumstances, mesoporous membranes that are not templated by the SES copolymer are obtained. It has been shown that RSOXS can be used to distinguish between templated and non-templated mesoporous films.

The properties of SES separators with a fixed void fraction of 0.43 as a function of  $\alpha$ , the molecular weight of the PS homopolymer normalized by that of the PS block in the SES copolymer, have been studied. The conductivity of SES separators peaked at  $\alpha$  values between 0.2 and 0.5 (Figure V - 134.) Thus, the templating is expected to have worked in this regime. RSOXS data (Table V - 2) shows that this is indeed the case, but that the templating failure in the low and high  $\alpha$  regimes is entirely different. The characteristic length scales determined by RSOXS ( $d_{280\text{eV}}$  and  $d_{284.4\text{eV}}$ ) reveal the nature of templating. When templating is effective the observed values of  $d_{280\text{eV}}$  and  $d_{284.4\text{eV}}$  are about 52 and 39 nm, respectively.  $d_{280\text{eV}}$  represents the average distance between adjacent pores while  $d_{284.4\text{eV}}$  At low  $\alpha$  ( $\alpha=0.13$ ) both  $d_{280\text{eV}}$  and  $d_{284.4\text{eV}}$  decrease dramatically to 44 and 34 nm, respectively. This

is a signature of a collapsed pore structure. At high  $\alpha$  ( $\alpha=1.65$ ) both  $d_{280\text{eV}}$  and  $d_{284.4\text{eV}}$  are about 39 nm respectively. This is a signature of macrophase separation of the block copolymer. Thus, while the conductivity data in Figure V - 134 suggests that the separators at  $\alpha=0.13$  and 1.65 are equally poor, RSOXS reveals that the reasons for this are entirely different. Note that traditional probes such as SEM and SAXS are unable to distinguish the  $\alpha=0.13$  and 1.65 cases (Table V - 2).

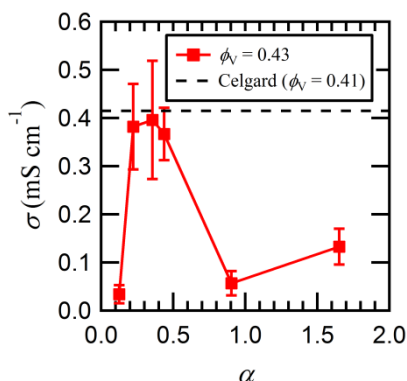


**Figure V - 134:** Ionic conductivity,  $\sigma$ , of SES separators soaked in 1M LiPF<sub>6</sub> in EC/DEC 1:1 v/v as a function of the normalized chain length of the sacrificial homopolymer,  $\alpha$ . The dashed line represents the conductivity of Celgard® 2400 soaked in the same electrolyte [details in ref. 2].

**Table V - 2:** Summary of length scales,  $d_i$ , as a function of the normalized chain length of the sacrificial homopolymer,  $\alpha$  [details in ref. 2].

| $\alpha$ | $d_{SEM}$<br>(nm) | $d_{SAXS}$<br>(nm) | $d_{280\text{eV}}$<br>(nm) | $d_{284.2\text{eV}}$<br>(nm) |
|----------|-------------------|--------------------|----------------------------|------------------------------|
| 0.13     | -                 | 44.9               | 44.1                       | 33.5                         |
| 0.22     | 65.1              | 53.5               | 51.5                       | 38.5                         |
| 0.36     | 53.4              | 57.9               | 51.2                       | 38.8                         |
| 0.44     | 56.3              | 64.1               | 53.6                       | 38.8                         |
| 0.90     | 62.9              | 69.4               | 61.4                       | 39.1                         |
| 1.65     | -                 | 45.6               | 39.3                       | 39.2                         |

**Characterization of Simultaneous Ionic and Electronic Current in a Novel Binder.** A detailed study of charge transport in mixtures of poly(3-hexylthiophene)-b-poly(ethylene oxide) (P3HT-PEO) block copolymers and lithium bis(trifluoromethanesulfonyl) imide salt (LiTFSI) has been completed. The P3HT-rich microphase conducts electronic charge while the PEO-rich microphase conducts ionic charge. The nearly symmetric P3HT-PEO copolymer used in this study self-assembles into a lamellar phase (Figure V - 135). In contrast, the morphologies of asymmetric copolymers with P3HT as the major component are dominated by nanofibrils. A combination of ac and dc impedance measurements was used to determine the electronic and ionic conductivity of the samples (Figure V - 136). The ionic conductivities of

P3HT-PEO/LiTFSI mixtures are lower than those of mixtures of PEO homopolymer and LiTFSI, in agreement with published data obtained from other block copolymer/salt mixtures. In contrast, the electronic conductivities of the asymmetric P3HT-PEO copolymers are significantly higher than those of the P3HT homopolymer. This is unexpected because of the presence of the non-electronically-conducting PEO microphase. This implies that the intrinsic electronic conductivity of P3HT the microphase in P3HT-PEO copolymers is significantly higher than that of P3HT homopolymers. To our knowledge, ref. 3 contains the first complete characterization of simultaneous ion and electron transport in a polymer.

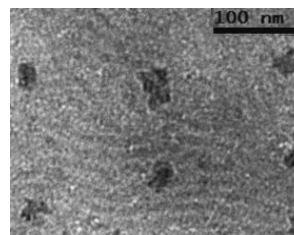


**Figure V - 135:** TEM of a symmetric P3HT-PEO copolymer showing a lamellar phase.

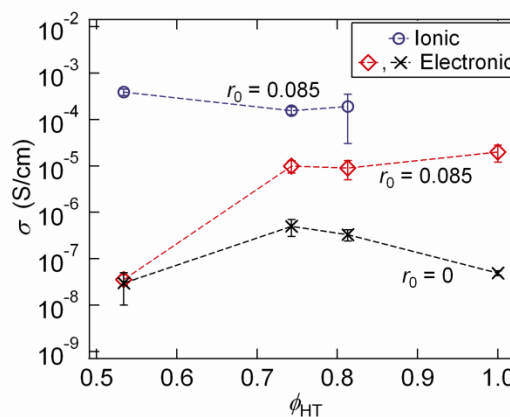


**Figure V - 136:** Electronic conductivity of P3HT homopolymer and P3HT-PEO block copolymers as a function of the P3HT volume fraction,  $\phi_{HT}$ , at 90 °C. Measurements were made with ( $r_0 = 0.085$ ) and without ( $r_0 = 0$ ) added salt;  $r_0$  is the molar ratio of LiTFSI to ethylene oxide monomers. All samples are ionic insulators without salt.

## Conclusions and Future Directions

Study of nanostructured block copolymer electrolytes demonstrating by quantifying the lifetime of full cells with lithium metal anodes has been completed. Polymer separators with self-assembled pores have been successfully synthesized, and new characterization tools for quantifying the relationship between ion transport and morphology have been discovered. The relationship between morphology and ionic- and electronic-conductivity in a novel P3HT-PEO block copolymer binder has also been quantified. Study of the structure-

function relationships of the first generation of self-assembled separator, and the effect of applied potential on charge transport in P3HT-PEO block copolymers, will be completed by 2013.

### FY 2012 Publications/Presentations

1. D.T. Hallinan, S.A. Mullin, G.M. Stone, N.P. Balsara, "Lithium Metal Stability in Batteries with Block Copolymer Electrolytes", *Journal of the Electrochemical Society*, under review, 2012 (revision requested by journal).
2. D.T. Wong, C. Wang, K.B. Beers, J.B. Kortright, N.P. Balsara, "Mesoporous Block Copolymer Morphology studied by Resonant Soft X-ray Scattering", *Macromolecules*, accepted, 2012.
3. S.N. Patel, A.E. Javier, G.M. Stone, S.A. Mullin, N.P. Balsara, "Simultaneous Conduction of Electronic Charge and Lithium Ions in Block Copolymers", *ACS Nano*, vol. 6, p. 1589-1660, 2012.
4. D.T. Wong, S.A. Mullin, V.S. Battaglia, N.P. Balsara, "Relationship Between Morphology and Conductivity of Block Copolymer-Based Battery Separators", *Journal of Membrane Science*, vol. 394-395, p. 175-183, 2012. (Paper was under review when last report was due.)
5. S.A. Mullin, G.M. Stone, A.A. Teran, D.T. Hallinan, A. Hexemer, N.P. Balsara, "Current-Induced Formation of Gradient Crystals in Block Copolymer Electrolytes", *Nano Letters*, vol. 12, p. 464-468, 2012.
6. G.M. Stone, S.A. Mullin, A.A. Teran, D.T. Hallinan, A.M. Minor, A. Hexemer, N.P. Balsara, "Resolution of the Modulus versus Adhesion Dilemma in Solid Polymer Electrolytes for Rechargeable Lithium Metal Batteries", *Journal of the Electrochemical Society*, vol. 159 (3), p. A222-A227, 2012.
7. S.N. Patel, A.E. Javier, K.M. Beers, J.A. Pople, R.A. Segalman, N.P. Balsara, "Morphology and Thermodynamic Properties of a Copolymer with an Electronically Conducting Block: Poly(3-ethylhexylthiophene-block-Poly(ethylene oxide))", *Nano Letters*, on the web, 2012.
8. Invited Lecture. "Block Copolymers for All-Solid Lithium Batteries", Physics Department of Physics and Astronomy, Simon Fraser University, British Columbia, Canada, October 26, 2012.
9. Invited Lecture, "Block Copolymers for All-Solid Lithium Batteries", Physics Department of Physics and Astronomy, University of Victoria, British Columbia, Canada, October 24, 2012.
10. Invited Lecture, "Nanostructured Polymers for Lithium Battery Electrodes and Electrolytes", Department of Chemical and Biomolecular Engineering, University of Delaware, Newark, Delaware, September 7, 2012.
11. Plenary Lecture, "Characterization of Block Copolymer Electrolytes", *International Symposium on Polymer Electrolytes*, Selfoss, Iceland, August 26, 2012.
12. Invited Lecture, "Simultaneous Electron and Ion Transport in Block Copolymers", *IUPAC World Polymer Congress*, Blacksburg, Virginia, June 26, 2012.
13. Keynote Lecture, "Nanostructured Block Copolymer Electrolytes for Lithium Batteries", *Nanotech Conference and Expo*, Santa Clara, California, June 19, 2012.
14. Invited Lecture, "Nanostructured Electrolytes for Lithium Batteries", Department of Physics, Boston University, May 4, 2012.

## V.D.2 Interfacial Behavior of Electrodes (LBNL)

John B. Kerr

Lawrence Berkeley National Laboratory,  
MS 62R0203, 1 Cyclotron Road,

Berkeley, CA 94720

Phone: (510) 486-6279; Fax: (510) 486-4995

E-mail: [jbkerr@lbl.gov](mailto:jbkerr@lbl.gov)

Start Date: October 1, 2009

Projected End Date: September 30, 2013

### Objectives

- Determine the role of electrolyte structure upon bulk transport and intrinsic electro-chemical kinetics and how it contributes to cell impedance (energy/ power density.)
- Determine chemical and electrochemical stability of electrolyte materials to allow elucidation of the structure of and the design of passivating layers (e.g., SEI.)

### Technical Barriers

This project addresses the following technical barriers

- Poor cycle and calendar life.
- Low power and energy densities.
- High manufacturing cost.
- Safety.

### Technical Targets

- Determine the contribution to the interfacial impedance of the salt structure in terms of reactivity versus intrinsic electrode kinetics.
- Determine the contribution to the interfacial impedance of the solvent or polymer structure in terms of reactivity versus intrinsic electrode kinetics.
- Determine the contribution to the interfacial impedance of the physical properties of the electrolyte – liquid vs. gel. vs. solid polymer electrolyte.
- Determine the effects of surface treatments of composite electrode particles on electrode morphology and resulting performance.
- Develop analytical methods for determination of side reaction products and chemical characterization of the SEI layer.

### Accomplishments

- Prepared and tested new single ion conductor materials based on fluoroalkylsulfonylimide anions which appear stable to 5 Volts or higher.
- Carbon conducting components of composite electrodes have been successfully surface modified by a number of routes to allow control of ionic concentration in composite electrodes.
- The surface modified carbon particles have been shown to display morphological properties that improve particle dispersion and uniformity in coated electrodes resulting in improved rate performance.



### Introduction

The choice of electrolyte used in lithium-ion batteries presents significant challenges. The material has to transport lithium ions from one electrode to the other with minimum resistance and facilitate the transfer of charge across the interfaces with a minimum of irreversible electrochemical and chemical reactions that reduce capacity and shorten lifetime. Since high energy electrodes are desirable, this represents a major challenge for the design of electrolytes. The presence of large resistances within the battery results in heat generation which imposes further stress upon the electrolyte and hence it is important not only for power and energy density but also for lifetime to minimize the impedances within the cell.

The impedances presented by the electrolyte are the bulk ohmic resistance (conductivity), concentration polarization (transport properties) and interfacial impedance (intrinsic electrochemical kinetics of charge transfer at the electrodes). Single-ion polyelectrolyte lithium conductors possess the solution for many of the problems with present electrolytes. They can be used with no liquid electrolyte thereby reducing the safety problem. They can be prepared and deployed in ways that avoid many of the reactivity issues both in the bulk of the electrolytes and at the interfaces. Because they possess a unity transference number, there is no concentration polarization through the composite electrodes. Thus, provided the conductivity is in excess of  $10^{-4}$  S/cm, the single ion conductors (SIC) can facilitate the use of thicker composite electrodes thereby leading to higher energy and power densities. In past years, this group has demonstrated that SIC materials, both dry and as gels, possess the bulk transport properties required. However, the interfacial behavior of these materials has exhibited disastrously high impedances rendering the SIC materials unusable. It is

imperative that the source of this impedance be elucidated and reduced to manageable values.

The FY2011 annual report for this project described the progress of preparation of SIC materials and a demonstration of the benefits of their benefits in removing concentration polarization in terms of power and energy density improvements. Examples of the materials are shown in Figure V - 137a. However, the interfacial impedances are just barely acceptable for practical operation and they need to be reduced further. Figure V - 137b shows our approach to this problem. The interfacial impedance is in large part due to the exchange current density at the electrode. This can be increased by increasing the concentration of lithium ions at the surface of the electrode and can be accomplished by using polymer binders in the composite electrode that have high ionic concentrations. However, such high ionic concentrations tend to degrade the bulk conductivity of the polymers. The alternative is to attach the ions to the surface of the carbon conducting elements in the composite electrodes as shown in Figure V - 137b. This report will describe progress in this activity.

## Approach

A physical organic chemistry approach is taken to electrolyte design, where the molecular structure is varied to provide insight into the processes that may affect the performance of the battery. These processes include transport properties, electrochemical kinetics, electrode side-reactions, thermal stability of the bulk material and interfacial behavior. The work involves use of model compounds as well as synthesis of new materials to test hypotheses which may explain battery behavior. Examples include:

- Different solvents and salts, including polymer
- Gels and solid polymer electrolytes.
- Electrode materials with different reaction potentials.
- Single-ion conductor polyelectrolytes (dry polymers and gels) as separators and binders in composite electrodes.
- Functionalized surfaces for electrode components.

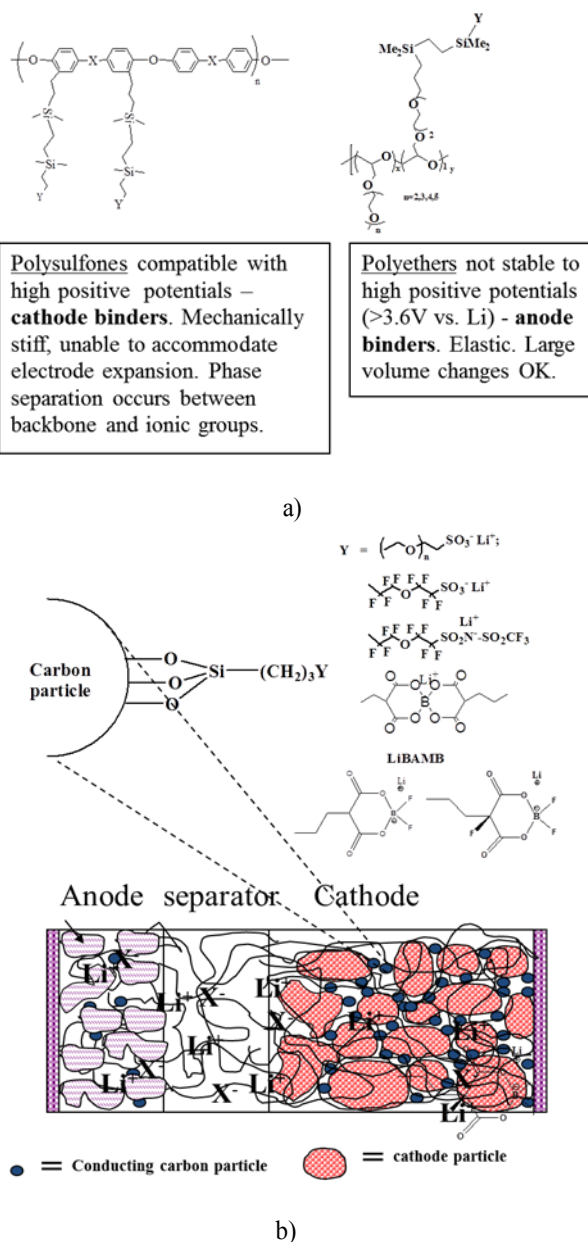


**Figure V - 137:** Methods of immobilizing electrolyte anions in lithium ion batteries. (a) Polyelectrolyte ionomers for use as separators and binders; (b) surface modified carbons for incorporation into composite electrodes to control lithium ion concentration.

To accomplish this work requires collaboration with other groups in BATT.

- Surface analysis groups to identify side reaction products and reactive intermediates by combination of spectroscopy and product distribution analysis.
- Sharing data and materials with other electrolyte developers.
- MD and electrochemical systems modeling groups to provide experimental data.
- Deliver promising materials to cell testing group

## Results

**Preparation of Carbon Surfaces.** Multiwalled carbon nanotubes (MWCNT) were modified with hydroxyl groups by a hydrothermal process using glucose as the precursor.

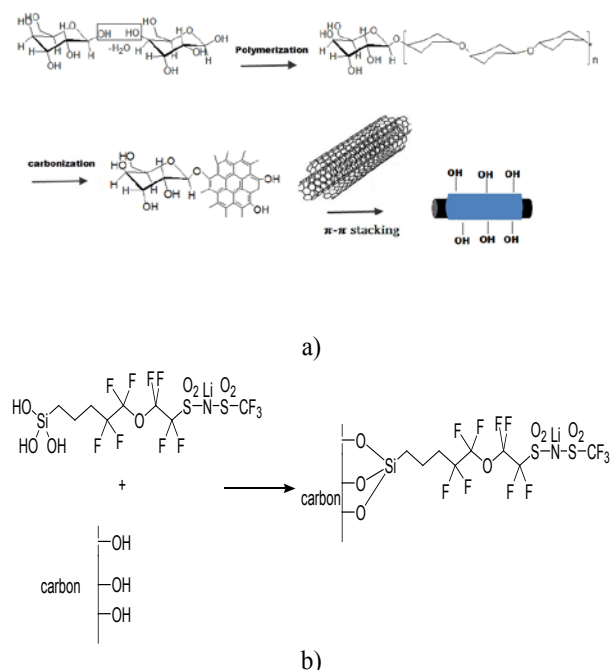


**Figure V - 138:** Preparation of functionalized Carbon surfaces. a) Preparation of carbon nanocables on MWCNT templates. b) functionalization of carbon surfaces with imides (Harmer et al, JCS Chem. Commun., 1997 1803)

Glucose is polymerized on the MWCNT and then carbonized to leave a high concentration of hydroxyl groups on the surface of the MWCNT that can then be functionalized with anions such as triflate or fluoroalkylsulfonate imides. The functionalized MWCNTs are then used as conducting additives for composite electrodes where the attached anions can influence the rates of the electrochemical reactions in the composite electrodes. The unfunctionalized MWCNTs show excellent performance themselves which appears to be due to the effect of the surface groups on the dispersion of the carbons in the electrode inks. The rate capability and impedance of lithium half cells with  $\text{LiFePO}_4$  cathodes is shown below which shows much better performance than the unmodified MWCNT electrodes and similar to those previously modified with sulfonated polystyrenes. This last observation indicates that the improvement in performance derives from better dispersion of the carbons in the electrodes. Examples of the improvement in the electrode morphology are shown in Figure V - 140 which shows Scanning Electron Microscopy images of composite electrodes prepared with functionalized and non-functionalized conducting elements.

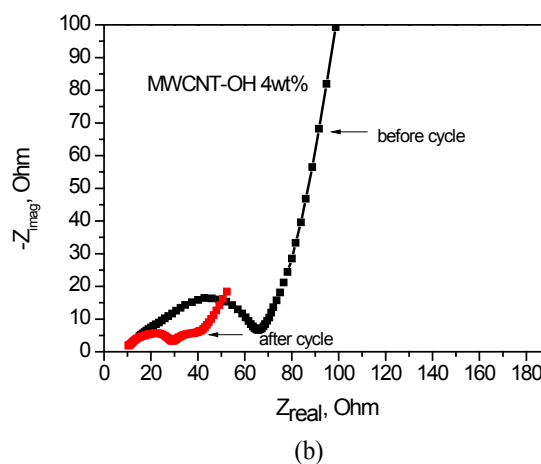
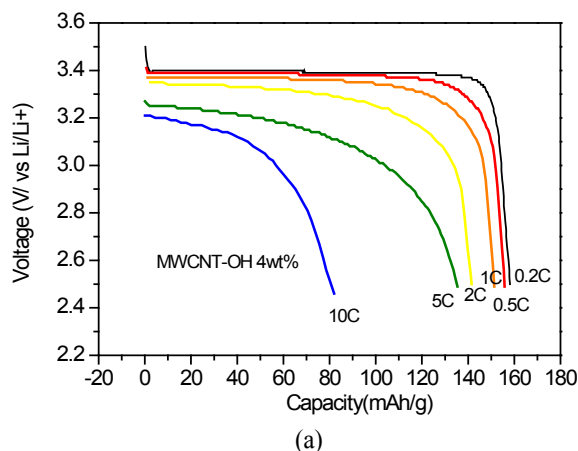


**Figure V - 139:** Discharge performance of Li- $\text{LiFePO}_4$  cells (EC, EMC- $\text{LiPF}_6$  electrolyte) at RT (a) and EIS Nyquist plot before and after cycling (b).

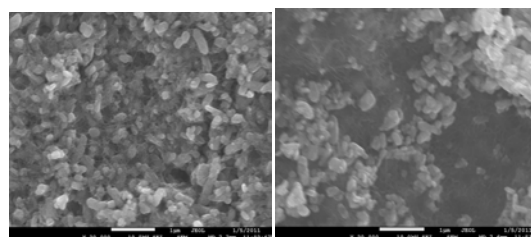


**Figure V - 140:** SEM images of  $\text{LiFePO}_4$  composite cathode. (a) PSSLi-MWCNT, (b) pristine MWCNT

The surface modified carbon elements have been used to prepare a variety of composite electrodes both anodes and cathodes. Their use with  $\text{SnO}_2$  electrodes appears to improve the cyclability

## Conclusions and Future Directions

### Conclusions

A variety of polyelectrolytes have been prepared with sufficient bulk conductivity for EV performance both as gels with solvents and as dry polymers. Testing of composite electrodes with SIC gel electrolytes has demonstrated the elimination of concentration polarization.

Capacities at high rates are doubled due to this and thicker electrodes are possible which will lead to increased energy and power densities.

Modification of the electrode surfaces alters the surface concentration of ions. It is apparent that improvement of performance is due to better distribution of conducting additives in the composite electrodes. Improvement in the intrinsic rates of the electrochemical reactions is necessary to achieve adequate room temperature performance – this will be achieved by control of ion concentrations in the electrodes.

#### Future Directions

- Continued Synthesis of polyelectrolyte materials
- TFSI and fluoroalkylsulfonate anions attached to both polyether and polysulfone backbones with a range of equivalent weights (concentrations of ions).
- Complete attachment of anions to conducting carbons using nanocable method.
- Test SIC polyelectrolytes combined with surface modified carbons to determine the limits of improvements in performance that can be expected.

#### Characterization of materials.

- Thermal, mechanical and chemical testing as dry materials and gelled with organic solvents (carbonates, GBL, ethers, sulfones.)
- Bulk conductivity, morphology measurements (SAXS/WAXS at LBNL ALS), dielectric relaxation measurements (Penn State U) and Neutron relaxation measurements (NIST.)

#### Composite Electrode Characterization.

- Cathodes. Focus on Low voltage materials (LiFePO<sub>4</sub> if available) for polyether materials. Reduce interfacial impedance enough to build completely dry (no solvents), solid-state cells.
- Cathodes. LiCoO<sub>x</sub> and LiMn<sub>2</sub>O<sub>4</sub> for polysulfone materials. Characterize composite electrodes thermally, mechanically and electrochemically. Particular emphasis on electrode kinetics and electrode thickness behavior - thicker electrodes.
- Anodes. Graphite: Characterize composite electrodes thermally, mechanically and electrochemically. Particular emphasis on electrode kinetics and electrode thickness behavior.
- Expanding anodes. Test Si and Sn based materials as they are available. Collaborate with other groups investigating these materials and determine whether elimination of concentration polarization helps to resolve cycling issues.
- Continue development of chemical analysis methods for characterization of SEI layers.

#### FY 2012 Publications/Presentations

1. John B. Kerr, Li Yang, Jianli Cheng and Peter Driscoll, "Electrolytes - R&D for Advanced Lithium Batteries. Interfacial and Bulk Properties," Poster Presentation #ES089, 2012 DOE Annual Peer Review Meeting, May 15, 2012.
2. John B. Kerr, Li Yang, Xiaoguang Sun, Adam Miller, Peter Driscoll and Ravindra Potrekar, "Single Ion Conductor Polyelectrolytes for Increased Capacity, Dendrite Inhibition and Safety," *Dow-Kokam Technology Exchange*, October 21, 2011.
3. Li Yang, Peter F. Driscoll, Matthieu Gervais, Ravindra Potrekar, Jianli Cheng, John Kerr, "Synthesis of Lithium Malonate Difluoro Borate (LiMDFB) and Lithium Bis(Trifluoromethanesulfonyl) Imide (LITFSI) based single ion conductor and its Electrochemical Performance."
4. Jianli Cheng, Li Yang, John B. Kerr, "Polymer modified MWCNT as conductive additive in LiFePO<sub>4</sub> cathode with high rate capability," *ECS Fall Meeting 2011*, Boston, MA.

---

## V.D.3 Molecular Dynamics Stimulation Studies of Electrolytes and Electrolyte/Electrode Interfaces (Univ. Utah, ARL)

Dmitry Bedrov and Feng Liu  
University of Utah  
Department of Materials Science & Engineering  
122 S. Central Campus Dr., Rm. 304  
Salt Lake City, Utah, 84112  
Phone: (801) 673-7452; Fax: (801) 581-4816  
E-mail: [d.bedrov@utah.edu](mailto:d.bedrov@utah.edu)

Oleg Borodin  
Army Research Laboratory  
Department of Electrochemistry Branch  
2800 Powder Mill Rd  
Adelphi, MD 20783  
Phone: (301) 394-0066  
E-mail: [oleg.a.borodin.civ@mail.mil](mailto:oleg.a.borodin.civ@mail.mil)

Start Date: January 1, 2009  
Projected End Date: December 31, 2012

### Objectives

- Use molecular simulations to gain understanding into the chemical composition of the electrode/electrolyte interface as a function of electrode potential.
- Use ab initio calculations to gain insight into electrolyte oxidation (cathode) and reduction (anode) mechanisms.
- Gain molecular level understanding of Li<sup>+</sup> cation transport mechanisms in electrolytes comprised of new salts and solvents and through SEI layers.
- Use modeling to understand the role of additives in the formation of SEI layer.
- Provide guidance for design of electrolytes with improved Li<sup>+</sup> transport, reduced interfacial resistance and/or improved electrochemical stability.

### Technical Barriers

- Poor low-temperature operations.
- Poor transport through SEI layers.
- High interfacial transport resistance.
- Oxidative stability of the electrolyte in contact with high voltage cathode materials.

### Technical Targets

- Develop a cell to meet the 10-mile PHEV goal.

- Develop an electrolyte or electrolyte additives that allow use of cathodes in the high-potential range (4V–5V vs. Li/Li<sup>+</sup>).
- Develop and utilize a high-potential, stable electrolyte system that can operate in the temperature range of -30°C to 55°C.

### Accomplishments

- Systematic understanding of the influence of local environment on oxidation potential and decomposition pathways for main electrolyte components.
- Improved understanding of the electrode/electrolyte interfacial structure and composition as a function of electrode potential and composition of electrolyte.
- Correlations between molecular level information obtained from MD simulations and experimental data on electrochemical stability at non-active electrodes.
- Detailed understanding of Li ion transport mechanisms in various electrolytes and model SEI layers.

◇ ◇ ◇ ◇ ◇

### Introduction

Design of electrolytes for secondary lithium batteries is a complicated task as an electrolyte has to satisfy a number of often conflicting requirements such as low bulk electrolyte and charge-transfer ionic resistance over a wide temperature range, low volatility and flammability, compatibility of the electrolyte with a separator and electrode materials. The latter requirement implies that electrolyte should be either electrochemically stable at the operating voltages of electrodes or, if decomposes, to form a stable passivation layer often called the solid electrolyte interphase (SEI) on the anode side and a passivation film on the cathode. The passivation layer stability, ionic conductivity and mechanical properties are critical for reversible ion intercalation into electrodes, preventing the capacity loss and achieving high Coulombic efficiency.

### Approach

The approach to simulation of bulk electrolytes, SEI components, and electrode/electrolyte interfaces is multifold. High-level quantum-chemistry calculations using both DFT and correlated methods are used to study the structure of electrode materials, their surfaces,

interactions between electrodes and electrolytes (including reactions), and the interaction between electrolyte components. Non-reactive molecular dynamics (MD) simulations are used to study structural, thermophysical and transport properties in bulk electrolytes, model SEI layers and electrode/electrolyte interfaces. The electroactive interface model is employed to study electrolyte structure and charge transfer processes at electrode/electrolyte interfaces where control of electrode potential is paramount. Finally, reactive atomistic MD simulations were utilized, using the ReaxFF force field to study important chemical and structural reorganization during SEI formation.

## Results

**Oxidative Stability of Solvents.** Previous studies of the oxidation-induced decomposition reactions of PC/PF<sub>6</sub><sup>-</sup> and PC/ClO<sub>4</sub><sup>-</sup> complexes have been extended to a number of additional solvent/anion pairs as shown in Table V - 3 below. Calculations were performed with PCM model for several solvents with dielectric constants 4.2, 20.5 and 78.4 and gas-phase  $\epsilon=1$ . The spontaneous proton abstraction from the solvent by anions was observed for a number of solvent/anion complexes and lowered oxidation stability of solvents by as much as 1 V. Such H- and F-spontaneous abstraction reactions were found for complexes where *both* solvent and anion had high intrinsic oxidative stability. In the case of TMS/BF<sub>4</sub><sup>-</sup> oxidized complex a small barrier (~0.1 eV) for the F-transfer from BF<sub>4</sub><sup>-</sup> to the open TMS ring was observed. However, in the solvent/anion complexes where one of the components had significantly lower oxidative stability than another no proton abstraction from the solvent was observed and anions with low oxidative stability such as difluoro(oxalate)borate (DFOB<sup>-</sup>) or dicyanotriazolate (DCTA<sup>-</sup>) oxidized. Similarly, in VC/BF<sub>4</sub><sup>-</sup> complex VC oxidized without any proton abstraction. Oxidation stability of EC/LiBF<sub>4</sub> was found 0.4-0.6 V higher than for EC/BF<sub>4</sub><sup>-</sup> indicating the increase of the electrolyte oxidation stability in the cases when all solvent is bound to Li<sup>+</sup> at the cathode interface.

**Table V - 3:** Oxidative stability of the solvent/anion complexes from M05-2X/cc-pvTz DFT calculations.

| complex                          | H or F transfer | $\epsilon=20.5$<br>(implicit solvent dielectric constant) |
|----------------------------------|-----------------|---|
| DMC/BF <sub>4</sub> <sup>-</sup> | Yes             | 6.21  |
| EC/BF <sub>4</sub> <sup>-</sup>  | Yes             | 6.28  |
| EC/LiBF <sub>4</sub> (v1)        | Yes             | 6.64  |
| EC/LiBF <sub>4</sub> (v2)        | Yes             | 6.82  |
| PC/BF <sub>4</sub> <sup>-</sup>  | Yes             | 6.25  |
| FEC/BF <sub>4</sub> <sup>-</sup> | Yes             | 6.62  |
| TMS/BF <sub>4</sub> <sup>-</sup> | Small barrier   | 6.49  |
| VC/BF <sub>4</sub> <sup>-</sup>  | No              | 5.46  |
| EC/ClO <sub>4</sub> <sup>-</sup> | YES             | 6.65  |
| EC/DFOB <sup>-</sup>             | No              | 6.10  |
| EC/DFOB <sup>-</sup>             | No              | 6.18  |
| EC/DCTA <sup>-</sup>             | No              | 5.83  |
| EC/ClO <sub>4</sub> <sup>-</sup> | YES             | 6.65  |

The oxidative stability, initial decomposition reactions, transport and structural properties were investigated for *N,N*-Dimethylmethanesulfonamide (DMMSA)/LiTFSI electrolyte in collaboration with (I. Halalay (GM), D. Aurbach, M. Levy (Israel)) and compared with those for carbonate-based electrolytes. The DMMSA-based electrolytes showed quite different oxidative decomposition behavior compared to carbonates with LiTFSI and LiFSI salts. DFT calculations performed at B3LYP/6-311++G(d) level on a single DMMSA, DMMSA dimer and DMMSA/anions showed that while oxidation stability of DMMSA is about 70kJ/mol (0.7V) lower than that for carbonate solvents (EC and PC) the barrier for the DMMSA decomposition is significantly higher (~200kJ/mol) than that for EC, EC<sub>2</sub>, PC and PC/ClO<sub>4</sub> and PC. Therefore, the oxidized DMMSA species will have a long life time before they decompose suggesting that DMMSA-based electrolytes operating above its oxidative stability limit will act as a redox shuttle.

**Electrolyte/Electrode Interface.** The double layer structure of tetramethylene sulfone (TMS)-based electrolytes (TMS)<sub>x</sub>:DMC<sub>y</sub>/LiPF<sub>6</sub> were investigated in order to obtain molecular insight into experimental observations indicating that addition of high oxidative stability TMS solvent noticeably increases oxidative stability of electrolyte. In MD simulation, a link between bulk and interfacial compositions as well as the composition of the interfacial lithium solvation shell was established and compared these properties with EC-based electrolytes. MD simulations revealed that despite relative similarity of TMS and EC molecular dipole moments, a significant difference in electrolyte double layer composition is observed for TMS- and EC-based

electrolytes. Analysis of solvent molecules composition in the interfacial layer as a function of electrode potential showed that on the anode the fraction of polar TMS increases as the magnitude of electrode potential increases. Similar effect was observed for EC-based electrolytes. At the cathode-electrolyte interface TMS oxygen atoms strongly adsorbed on the surface, while DMC carbonyl groups desorbed from the positive electrode with increasing potential. The DMC oxygen atoms in TMS:DMC/LiPF<sub>6</sub> do not approach the surface of the positive electrode as close as in EC:DMC/LiPF<sub>6</sub>, thus, DMC molecules in TMS:DMC/LiPF<sub>6</sub> are likely to experience a lower electrochemical potential and, hence, are less likely to be oxidized than in the EC:DMC/LiPF<sub>6</sub>. This trend is consistent with experimental observations reporting that electrolytes containing mixture of linear carbonates and TMS show high oxidative stability, similar to that observed in TMS-only electrolytes, which is higher than what is observed for electrolytes with carbonates mixture. Analysis of molecular level differences in interfacial structure obtained from MD simulations provides potential rationale for this trend.

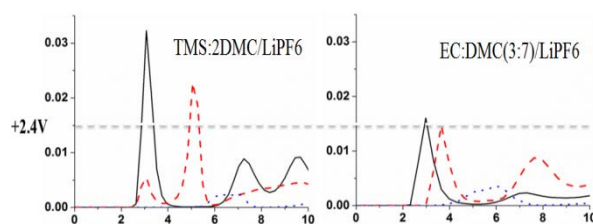


**Figure V - 141:** Density profiles of oxygen atoms in TMS or EC (solid black line) and DMC (red line) in TMS:DMC(1:2)/LiPF<sub>6</sub> (left panel) and in EC:DMC(3:7)/LiPF<sub>6</sub> (right panel) electrolytes at 2.4 V electrode potential. Zero on x-axis is the position of the electrode surface.

MD simulations also showed that on the negative electrode Li<sup>+</sup> accumulates faster (with respect to magnitude of the electrode potential) in TMS solvent and remains strongly bound with TMS oxygen atoms even below -2 V generating surprisingly large interfacial concentration of negatively charged TMS oxygen atoms in the interfacial layer. On the positive electrode there is a significantly smaller concentration of Li<sup>+</sup> in the outer part of the interfacial layer in TMS-based electrolytes than in EC-based electrolyte, due to the fact that both oxygen atoms of TMS molecule are adsorbed on the positively charged surface and therefore are unavailable to participate in Li<sup>+</sup> coordination and retain it near the surface. The LiPF<sub>6</sub> salt is completely dissociated on the negative electrode (Li<sup>+</sup> and PF<sub>6</sub><sup>-</sup> are well separated) but are mostly associated in cation-anion pairs at the positive electrode.

The mechanism for improvement of DMC oxidation stability by mixing it with TMS solvent obtained based on analysis of MD simulations was further complemented by DFT calculations exploring influence of BF<sub>4</sub><sup>-</sup> on TMS oxidation stability and decomposition reactions. Presence

of BF<sub>4</sub><sup>-</sup> next to TMS during oxidation significantly reduced the barrier for TMS ring opening reaction to 0.17 eV. This result should be contrasted with the barrier-less H-transfer reaction observed upon oxidation of EC<sub>2</sub>, EC<sub>4</sub> and EC/BF<sub>4</sub><sup>-</sup> clusters. The most probable reaction observed in DFT calculations of the oxidized TMS/BF<sub>4</sub><sup>-</sup> complex involved F-transfer from BF<sub>4</sub><sup>-</sup> anion to TMS highlighting the role of anion on the oxidation of electrolytes.

## Conclusions and Future Directions

Simulations have demonstrated that redox chemistry of electrolyte components strongly depends on their local environment. The latter can be a strong function of proximity to the electrode surface, electrode potential and electrolyte chemical composition. Hence, no single simulation methodology is currently capable of accurate prediction of electrolyte redox decomposition reactions at electrode surfaces, SEI formation, ionic transport in SEI, and initial stages of cathode dissolution indicating that multiple simulation methodologies have to be integrated to effectively tackle these issues. In the future, it is hoped that our multiscale, multifold modeling approach will be continued in order to address (i) molecular level understanding of reactivity at the LiNi<sub>0.5</sub>Mn<sub>1.5</sub>O<sub>4</sub> spinel cathode – electrolyte interface with a wide range of electrolytes, additives, and contaminants that will lead to mitigation of the cathode dissolution and electrolyte oxidation, (ii) molecular level details on the electrolyte reduction reactions and SEI formation on SiNW anodes, (iii) computational screening of additives beneficial to the SiNW SEI formation and cathode passivation composition and properties.

## FY 2012 Publications/Presentations

- Xing, L.; Borodin, O. "Oxidation induced decomposition of ethylene carbonate from DFT calculations – importance of explicitly treating surrounding solvent," *Phys. Chem. Chem. Phys.* **14** (37), 12838 – 12843 (2012).
- Xing, L.; Vatamanu, J.; Borodin, O.; Smith, G. D.; Bedrov, D. "Electrode/Electrolyte Interface in Sulfolane-Based Electrolytes for Li-Ion Batteries: A Molecular Dynamics Simulation Study," *J. Phys. Chem. C* 2012, ASAP.
- Seo, D. M.; Borodin, O.; Han, S.-D.; Ly, Q.; Boyle, P. D.; Henderson, W. A. "Electrolyte Solvation and Ionic Association (II): Acetonitrile-Lithium Salt Mixtures – Highly Dissociated Salts," *J. Electrochem. Soc.*, **159** (9), A1489-A1500 (2012).
- Seo, D. M.; Boyle, P. D.; Borodin, O.; Henderson, W. A. "Li<sup>+</sup> cation coordination by acetonitrile—Insights from crystallography," *RSC Adv.*, **2**, 8014-8019. <http://pubs.rsc.org/en/Content/ArticleLanding/2012/R/A/C2RA21290K> (2012).

5. Seo, D. M.; Borodin, O.; Han, S.-D.; Ly, Q.; Boyle, P. D.; Henderson, W. A. "Electrolyte Solvation and Ionic Association (I): Acetonitrile-Lithium Salt Mixtures - Intermediate and Highly Associated Salts," *J. Electrochem. Soc.* 2012, 159 (5), A553-A565.
6. Li, Z; Bedrov, D.; Smith, G.D.; "Li<sup>+</sup> Solvation and Transport Properties in Ionic Liquid/Lithium Salt Mixtures: A Molecular Dynamics Simulation Study," *J. Phys. Chem. B.*, 2012 ASAP.
7. Bedrov, D.; Smith, G.D.; van Duin A.D.T., "Reactions of singly-reduced ethylene carbonate in lithium battery electrolytes. A molecular dynamics study using the ReaxFF," *J. Phys. Chem. A.*, **116**, 2978-2985 (2012).
8. Borodin, O. "Insight into Electrolyte Stability and Transport from Simulations" *Gordon Research Conference – Batteries*, "Advanced Characterization, Theory and Mechanisms of Processes in Rechargeable Batteries Across Length Scales," Invited talk, March 4-9, 2012, Ventura, CA.
9. Borodin, O., T. R. Jow, L. Xing, "Insight into Electrolyte Stability, Decomposition and Transport Properties from DFT and MD Simulations," *PRiME 2012, 222nd Meeting of Electrochem. Soc.*, Invited talk, Honolulu, Hawaii, October 7-12, 2012.
10. Borodin, O., Vatamanu, J.; Xing, L.; Bedrov, D.; Smith, G. D. "Insight into Ionic Liquid and Liquid Electrolyte Behavior at Electroactive Interfaces," *The 63rd Annual Meeting of the International Society of Electrochemistry for Advanced Materials, Technologies and Instrumentation*, Invited talk, 19-24 August, 2012, Prague, Czech Republic.  
<http://event12.ise-online.org/>
11. Borodin, O., E. Fox, W. Henderson "Molecular insight into ionic liquid mixtures with solvents and lithium salts," *243rd American Chemical Society Meeting*, Invited talk, San Diego, March 25-29, 2012.
12. Borodin, O., Jow, T. R.; Xing, L. X. "Electrolyte Oxidative Stability and Decomposition Pathways from DFT Calculations," "Insight into Ionic Liquid and Liquid Electrolyte Behavior at Electroactive Interfaces," *The 63rd Annual Meeting of the International Society of Electrochemistry for Advanced Materials, Technologies and Instrumentation*, Contributed presentation, 19-24 August, 2012, Prague, Czech Republic.
13. Bedrov, D., Vatamanu, J.; Borodin O., "Electrolyte Structure Near Charged Electrode Surfaces: A Molecular Dynamics Simulation Study," *Electrochemical Society PRiME Meeting*, Contributed talk, Honolulu, 2012.
14. Bedrov, D.; Xing, L.; Hooper, J.; Halalay, I.; Aurbach, D.; Levi, M.D.; Shilina, Y.; Geiculescu, O.E.; Desmarteau, D.D.; "Joint Theoretical and Experimental Study of Novel Electrolytes Based on Eutectic Mixtures of DMMSA with LiFSI and LiTFSI Salts," *Electrochemical Society PRiME Meeting*, Contributed talk, Honolulu, 2012.
15. Smith, G. D.; Borodin, O. "Lithium Battery Electrolyte Stability and Performance from Molecular Modeling and Simulations," in *Encyclopedia of Sustainability Science and Technology*, Springer, ISBN 978-0-387-89469-0, September 15, 2012.

## V.D.4 Bifunctional Electrolytes for Lithium-ion Batteries (CWRU)

Daniel Scherson  
Case Western Reserve University  
Department of Chemistry  
10900 Euclid Avenue, Cleveland, OH 44106  
Phone: (216) 368-5186  
E-mail: [dxs16@case.edu](mailto:dxs16@case.edu)

John Protasiewicz  
Case Western Reserve University  
Department of Chemistry  
10900 Euclid Avenue, Cleveland, OH 44106  
Phone: (216) 368-5060  
E-mail: [jdp5@case.edu](mailto:jdp5@case.edu)

Start Date: April 1, 2009  
Projected End Date: March 31, 2013

### Objectives

- Design, synthesize, and characterize physical, electrochemical, and interfacial characteristics of functionalized Li-salt anions containing phosphorus moieties known to impart materials with flame retardant properties (Flame Retardant Ions or FRIONs) and additional functional redox active groups capable of providing overcharge protection.
- Develop and implement ATR-FTIR spectroscopic methods for monitoring *in situ* the nature of products generated at Li-ion battery anodes under highly controlled conditions

### Technical Barriers

This project addresses the abuse tolerance barriers from the BATT program.

### Technical Targets

- Demonstrate superior abuse characteristics compared to a baseline cell: Conoco Philips CPG-8 Graphite/1 M LiPF<sub>6</sub>+EC:DEC (1:2)/Toda High-energy layered (NMC)

### Accomplishments

- A new class of diphosphinato catecholate (DPC) FRIONs were prepared and characterized.
- Optimization of the synthesis of cyclic triol borate (CTB) type FRIONs has been performed and results show an improvement over previously reported FRIONs.



### Introduction

The main objectives of this project are to develop rational guidelines for the design and synthesis of new classes of Li-based salts endowed with flame retardant properties. In addition, such bifunctional electrolytes should be weakly coordinating and of low molecular weight, exhibit low toxicity, promote formation of low impedance solid electrolyte interfaces (SEI) and from an economic viewpoint be relatively inexpensive.

### Approach

Develop methods for the chemical functionalization of anions known to improve the performance of Li-ion batteries with covalently linked groups displaying flame retardant and/or overcharge protection attributes. Establish guidelines for the rational design and synthesis of optimized FRIONs and FROPs based on the analysis of results of testing in actual Li-ion batteries. Develop new *in situ* tactics for the application of attenuated total reflection Fourier transform infrared ATR-FTIR for the characterization of solution products generated at Li-ion battery anodes and solid electrolyte interfaces formed therein.

### Results

**Synthesis: a) Cyclic triol borate (CTB) salts.** optimized routes have been developed for the synthesis of CTBs allowing a series of such materials to be prepared. Previous methods involved long heating times, and the products required additional steps for purification leading to overall yields of ca. 50% for LiC<sub>Et</sub>B<sub>Ph</sub> with a 3 day total synthesis. In stark contrast, the new method, which lends itself to large scale synthesis, involves heating the reactants in a sand bath at 220°C for 20 min, followed by deprotonation with LiOtBu in diethyl ether, and can achieve in just one day, yields of ca. 90% without the need for any further purification beyond drying (See Figure V - 142, Scheme 1).

Based on thermogravimetric analysis (TGA) data, the onset for decomposition of the LiC<sub>Me</sub>B<sub>Ph</sub> and LiC<sub>Et</sub>B<sub>Ph</sub> salts was found to be at 200°C and 150 °C, respectively (see Figure V - 143), i.e., much higher than the normal range of operation of lithium ion batteries.

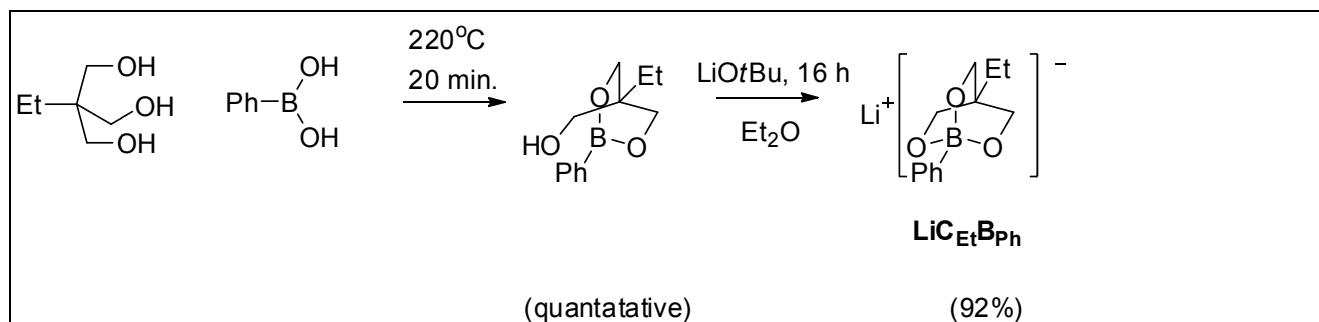
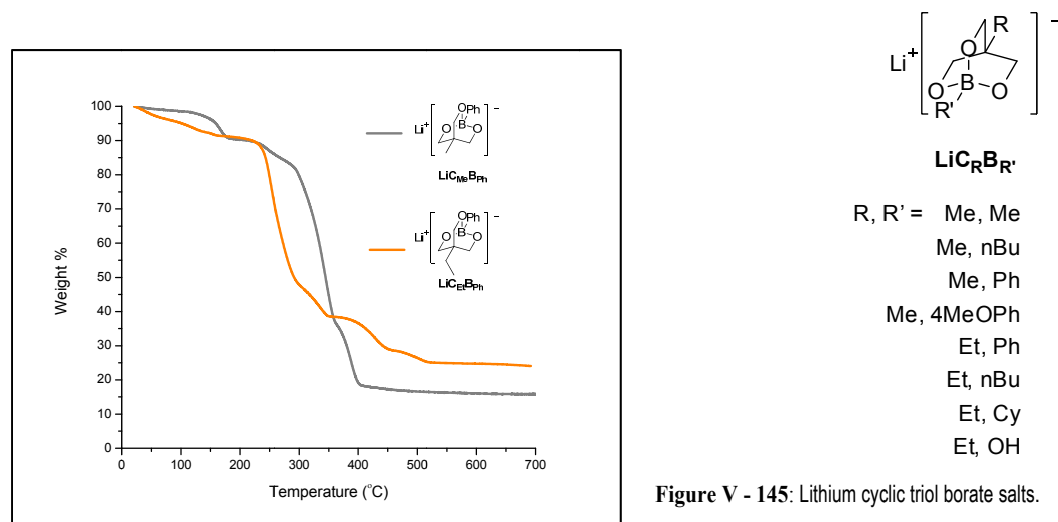
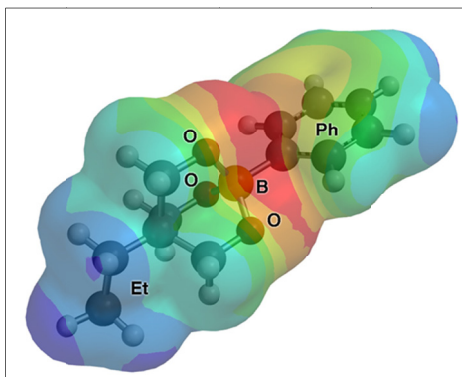
Figure V - 142: Scheme 1–Improved synthesis of  $\text{LiC}_{\text{Et}}\text{B}_{\text{Ph}}$ .

Figure V - 143: TGA of LiCTB Salts.

Figure V - 144: Electrostatic potential map of the  $\text{C}_{\text{Et}}\text{B}_{\text{Ph}}$  anion performed at BLY3P/6-31G\*.

Quantum mechanical calculations using DFT methods (B3LYP with a basis set of 6-31G\*) yielded an electrostatic potential map for the CTB anion, which, as shown in Figure V - 144, places the majority of the charge on the B atom, but is also distributed to an appreciable degree on the benzene ring attached to B.

Figure V - 145: Lithium cyclic triol borate salts.

**Synthesis: b) Diphosphinato Catecholates:** Over the past year, a new class of FRIONs was synthesized featuring the diphosphinato catecholate (DPC) ligand around a boron center. FRION 1 features four organophosphorus moieties per anion whereas FRION 2, a lower molecular weight molecule, features two units of organophosphorus. The synthetic route for the preparation of these salts is shown in Scheme 2 (see Figure V - 146). Salt 1 was prepared using two equivalents of a diphosphorylated catechol, boric acid and lithium t-butoxide,  $\text{LiOtBu}$ . For salt 2, one equivalent of oxalic acid replaced one equivalent of the diphosphorylated catechol. Both salts have displayed higher solubility in organic solvents than our other classes of FRIONs. This may be due in part to the manner in which the DPC ligands bind to the positively charged lithium and negatively charged boron, encapsulating the cation and anion inside the molecule, thus reducing the overall polarity of the molecule and making it much more soluble in organic solvents.

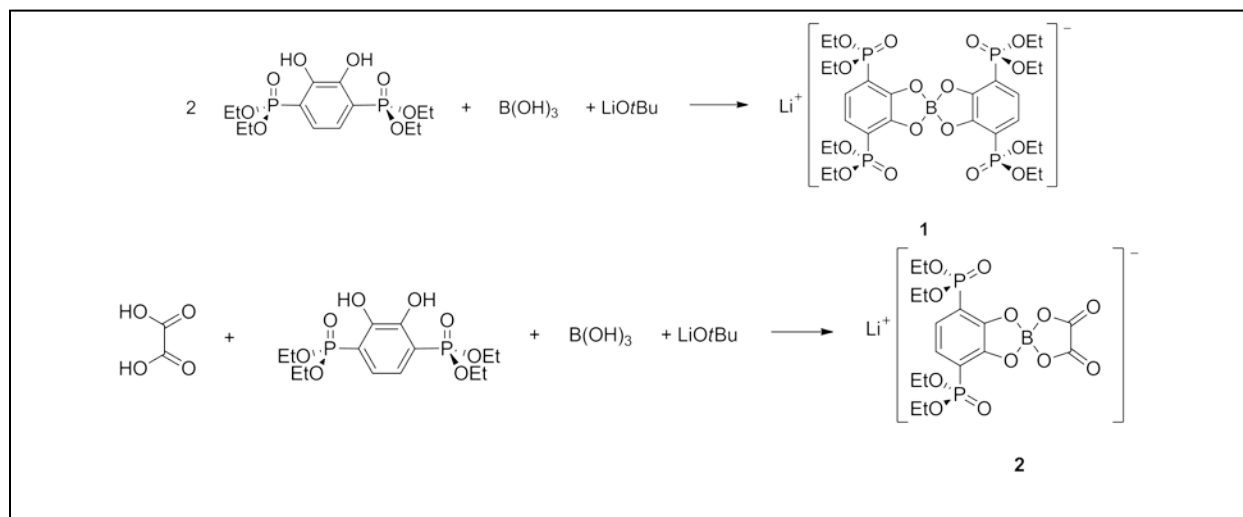


Figure V - 146: Scheme 2–Synthesis of FRION salts.

The structure of salt 2, determined using single crystal X-Ray diffraction methods (Figure V - 148), showed a DPC group and an oxalato group both bound to boron in a bidentate fashion. The lithium ion coordinates with the oxygen atom on the phosphoryl group and with an internal oxygen atom of the catechol. The negative charge on boron should be delocalized via resonance on the aromatic ring.

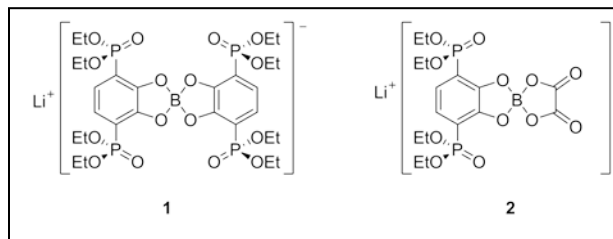


Figure V - 147: New DPC FRIONs

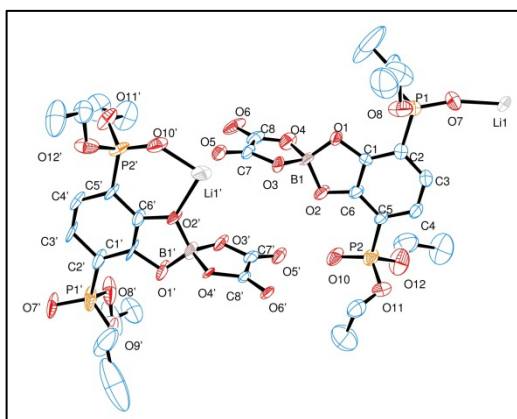


Figure V - 148: Single Crystal X-Ray Structure of 2 in Figure 4.

Char yields of the DPC salts determined by pyrolysis combustion flow calorimetry are listed in Table V - 4 yielded higher values for salt 2 compared to Salt 1.

Table V - 4: Char yields of DPC salts as determined by pyrolysis combustion flow calorimetry.

| Char Yields (%) |       |       |
|-----------------|-------|-------|
| Compound        | 1     | 2     |
| Trial 1         | 42.54 | 49.65 |
| Trial 2         | 42.34 | 49.55 |
| Trial 3         | 41.71 | 49.59 |

**Synthesis: c) New Salt Battery Performance.** The electrochemical performance of a new salt, i.e., CaseY, at the 1 and 2% level was examined at room temperature in 1 M LiPF<sub>6</sub> in EC/EMC (3:7 by volume) using a 650 mAh graphite anode and a 111 NMC Cathode at a C rate of 1 between 4.2 and 3.0 V. As shown in Figure V - 149, the results obtained for Salt 1 were slightly lower than those found for the base electrolyte.

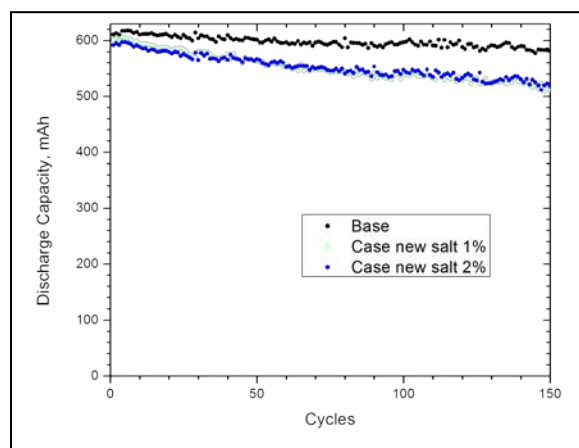


**Figure V - 149:** Comparison between the charge discharge curves for the base electrolyte before and after addition of Case Y salt at the 1 and 2% levels.

## Conclusions and Future Directions

The synthesis of previously reported CTB FRIONs was optimized allowing a series of new materials to be prepared. In addition, a new class of FRIONs based on diphosphinato catecholates was synthesized and found to display higher solubility than previous classes of FRIONs and also to feature an increased number of organic phosphorus units per unit of molecular weight. New salts denoted as CaseY were prepared and their performance as electrolyte additives tested in prismatic type Li-ion batteries.

Efforts will continue toward finding new strategies toward further optimization of salts in terms of electrochemical and flame retardant performance. In particular, the carbon atom at the bicyclic bridgehead of CTB salts will be replaced with an organophosphorus unit. Lastly, a new approach will be developed for acquiring *in situ* FTIR data in a configuration that will significantly decrease the contribution to the signal derived from the liquid electrolyte.

## FY 2012 Publications/Presentations

1. Rectenwald, M.; A. Shaffer; and J. Protasiewicz "Bifunctional Electrolytes for Lithium Ion Batteries," *ACS National Meeting*, Philadelphia, PA, August 22, 2012.
2. Rectenwald, M.; A. Shaffer; and J. Protasiewicz "Bifunctional Electrolytes for Lithium Ion Batteries," *Ohio Inorganic Weekend*, Detroit, MI, October 20, 2012.

## V.D.5 Advanced Electrolyte and Electrolyte Additives (ANL)

Khalil Amine  
Argonne National Laboratory  
Chemical Sciences and Engineering Division  
Argonne, IL 60439  
Phone: (630) 252-3838; Fax: (630) 252-4672  
E-mail: [amine@anl.gov](mailto:amine@anl.gov)

Start Date: October 1, 2009  
Projected End Date: September 30, 2013

### Objectives

- Use advanced quantum chemical model to predict functional additives that form stable Solid Electrolyte Interfaces (SEI) on electrodes and for overcharge protection.
- Use the model to predict how additives interact with the surface of anode and cathode to form good protective films.
- Synthesize suitable additives predicted by the modeling, characterize them and carry out extensive cycle and calendar life test.

### Technical Barriers

This project addresses the following technical barriers in lithium ion battery technology

- (a) Cycle/calendar life
- (b) abuse tolerance

### Technical Targets

- New additives that form stable film formation on anodes and cathodes
- Increased cycle life
- Improved safety

### Accomplishments

- Using an improved quantum chemical model for screening of reduction and oxidation potentials, additions have been made to a database of potential additives for SEI formation and overcharge protection. The database now has over 400 additive molecules.
- Many of the molecules have been further screened for decomposition pathways that are needed for SEI formation and some of these have been tested experimentally.
- The molecule 2,4,6-tris(2-propen-1-yloxy)-1,3,5-triazene has been investigated as an SEI additive for Li ion batteries. DFT calculations show that when this

molecule is reduced, an allyl radical detaches via an apparent charge-spin segregation mechanism. In experimental studies it has been shown to be a promising SEI additive.

- Density functional calculations have been carried out on a series of anhydride derivatives to gauge their suitability as SEI additives for Li-ion batteries. Decomposition pathways for the anhydride derivatives were investigated based on ring opening. The maleimide anion radicals do not form open structures but have large reduction potentials nonetheless. In contrast, the open anion radicals for all oxaxolidinedione, oxadiazolidinedione and thiazolidinedione species were more stable and are good candidates.
- Several substituted maleic and succinic anhydrides were investigated. experimentally and theoretically as possible additives. One of the anhydrides, 3-oxabicyclohexane-2,4-dione, did not form the traditional SEI indicating the formation of a new SEI at higher reduction potential than the Gen 2 carbonate electrolytes. The SEI may involve a polymerization of the reduced 3-oxabicyclohexane-2,4-dione anion radical with ethylene carbonate.

◇ ◇ ◇ ◇ ◇

### Introduction

The development of advanced electrolytes with functional additives that provide for stabilization of the interface of lithium ion batteries to prevent detrimental degradation is important for enhancing the cycle life and safety of lithium ion batteries. In addition, electrolyte additives can provide protection against overcharge at the cathode. This project involves the use of high level quantum chemical methods for accurate energy assessment to screen for electrolyte additives that can be added to the electrolyte and form a protective solid electrolyte interphase (SEI) during the initial charging to prevent the conventional passivation film from taking place first. These additives must form a thin and a uniform film that protects the electrode. Similar quantum chemical methods are being used to screen for new additives for redox shuttles to provide for overcharge protection in Li-ion batteries.

### Approach

A joint theoretical/experimental approach is being used for design and discovery of new electrolytic additives that react in a preferential manner to prevent detrimental decomposition of cell components. Quantum chemical screening, based on density functional theory and wave-

function based methods, is used to predict accurate oxidation and reduction potentials and decomposition pathways that form desirable coatings, and to find stable additives for overcharge protection. Synthesis of the new additives and testing of them is done to determine the cycle life of the batteries followed by characterization.

## Results

**Electrolyte additives for SEI.** Over 400 candidate additives have been screened for their reduction and oxidation potentials using a quantum chemical model and have been stored in a database. In addition, the candidates are further down selected on the basis of reaction pathways for decomposition. These calculations are being used to suggest additives for protective film formation on anodes and cathodes and some have been studied experimentally. Following, the results for some of the additives that have been investigated are presented.

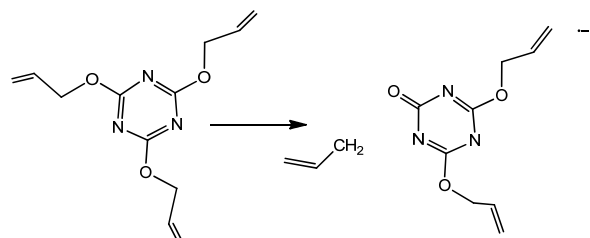


Figure V - 150: Decomposition of TPYT additive upon reduction

**2,4,6-Tris(2-propen-1-yloxy)-1,3,5-triazene.** A good solid electrolyte interphase (SEI) prevents further electrolysis of the electrolyte and increases battery cycle life. Density functional theory (DFT) has been used to investigate the molecule 2,4,6-Tris(2-propen-1-yloxy)-1,3,5-triazene (TPYT) as an SEI additive for Li ion batteries. The DFT calculations using B3LYP and a continuum model for the surrounding electrolyte show that when this molecule is reduced, an allyl radical detaches via an apparent charge-spin segregation mechanism as shown in Figure V - 150. DFT calculations show that upon reduction an allyl radical can separate with a small energy barrier. This allyl radical can initiate free radical polymerization by attacking C=C bonds of TPYT species in solution to form an effective SEI. The pores of this SEI layer are likely to be large enough to allow uninterrupted  $\text{Li}^+$  transport. Thus, calculations indicate that allyl groups are promising substituents for the design of SEI additives for lithium-ion batteries. In experimental studies (TPYT) has been shown to be a promising SEI additive.

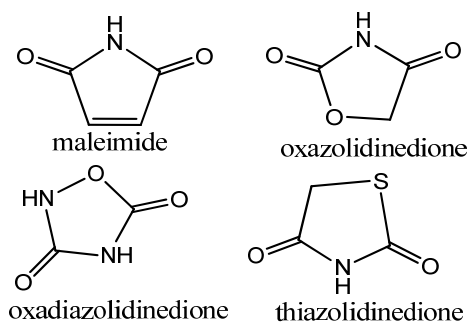


Figure V - 151: Structures of the of the anhydride derivatives investigated as SEI additives

**Anhydride derivatives.** Density functional calculations of anhydride derivatives, including thiazolidinedione, oxazolidinedione, oxadiazolidinedione and maleimide derivatives (shown in Figure V - 151), have been carried out to gauge their suitability as SEI additives for Li-ion batteries. The maleimide species are derivatives of maleic anhydrides, which are good additives, while thiazolidinedione, oxazolidinedione, oxadiazolidinedione are substituted derivatives of succinic anhydrides, which are also good additives. The anion radical of these species is stabilized by conjugation. Maleimide has a somewhat smaller reduction potential than maleic anhydride. Replacing the imide NH hydrogen or CH hydrogens in the maleimide ring can influence the reduction potential. The oxadiazolidinedione species (with an extra nitrogen in the ring) has a larger reduction potential than oxazolidinedione due to a larger electron affinity. An extra nitrogen in the ring of the sulfur containing species also increases the reduction potential. The sulfur containing species (e.g., thiazolidinedione) have smaller reduction potentials than the corresponding oxygen containing species (e.g., oxazolidinedione) and open spontaneously upon reduction. Substituting imino C=NH for carbonyl C=O lowers the reduction potentials. Two extra nitrogens in the ring also decreases the reduction potential. All have higher reduction potentials than succinic anhydride so they should be good SEI additive candidates. Decomposition pathways for the anhydride derivatives were investigated based on the initial ring opening step. The ring opening decomposition of reactions of thiazolidinedione, oxazolidinedione, oxadiazolidinedione and maleimide derivatives were studied using a density functional model. The maleimide anion radicals do not form open structures but have large reduction potentials nonetheless. In contrast, the open anion radicals for all oxazolidinedione, oxadiazolidinedione and thiazolidinedione species were more stable and are good candidates.

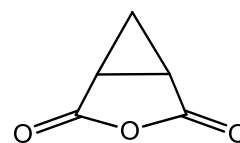
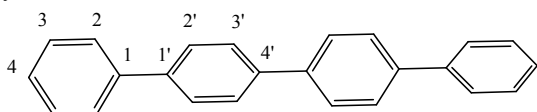


Figure V - 152: Structure of 3-oxabicyclohexane-2,4-dione

**3-oxabicyclohexane-2,4-dione.** Density functional calculations were used to investigate how 3-oxabicyclohexane-2,4-dione shown in Figure V - 152 can form a solid-electrolyte interphase (SE) before ethylene carbonate (EC) forms an SEI upon reduction. The calculations show that the ring form of 3-oxabicyclohexane-2,4-dione has a reduction potential of 0.66 V and an open form reduction potential of 1.04 V, compared to a calculated reduction potential of 1.43 V (Expt. 1.36 V) for the open form of EC. In order for a new SEI film to form before EC is reduced, the reduction potential of an additive must be significantly larger than that of EC. If the ring anion of 3-oxabicyclohexane-2,4-dione breaks various CC bonds followed by a hydrogen transfer, then the resulting species will have a much larger reduction potential. Several isomers were investigated. The results showed that citraconic anhydride anion gives the highest reduction potential relative to 3-oxabicyclohexane-2,4-dione (2.75 V). This suggests that a larger reduction potential of an additive can be achieved by using a high energy isomer (3-oxabicyclohexane-2,4-dione) that can rearrange to the anion radical of a lower energy isomer (citraconic anhydride). The resulting citraconic anhydride anion radical can then polymerize with either 3-oxabicyclohexane-2,4-dione or EC to form the new and potentially improved SEI compared to EC, consistent with experimental studies showing improved performance when a small amount is added to the electrolyte. The 3-oxabicyclohexane-2,4-dione species was investigated experimentally as a possible additive. A new peak is observed at 2.25 V upon addition of a small amount of 3-oxabicyclohexane-2,4-dione. However, the traditional SEI is not formed, indicating the formation of a new SEI at higher reduction potential than the Gen 2 carbonate electrolytes. This may involve a polymerization of the reduced 3-oxabicyclohexane-2,4-dione anion radical with ethylene carbonate.



**Figure V - 153:** Illustration of possible substituent sites on p-quaterphenyl.

**Redox Shuttle Screening.** Density functional investigation of potential redox shuttles has focused on p-quaterphenyls shown in Figure V - 153. Over 70 different possible substituted p-quaterphenyls were investigated. It was found that substituent effects are approximately additive and allow the oxidation potential to be tailored for a range of oxidation potentials for this class of potential redox shuttles. By variation of the functional groups in the positions shown in Figure V - 153 it is possible to tailor this class of molecules for redox shuttles.

## Conclusions and Future Directions

The development of electrolyte additives for SEI formation and overcharge protective is important for

improving the safety and lifetime of Li-ion batteries. Results during the past year have shown how advanced quantum chemical methods can be used to screen potential molecules as candidates for these additives for experimental exploration. The results of the calculations described here have been used to help find new additives described in this report and to understand the mechanism by which the protective film is formed. Based on experimental feedback, further candidates will continue to be screened. In future work density functional calculations will be used to help understand the properties of shuttle molecules for overcharge protection that are being studied experimentally and then using this information to help design new shuttle molecules.

## FY 2012 Publications/Presentations

1. 2012 DOE Annual Peer Review Meeting Presentation.
2. W. Weng; Z. Zhang, J. A Schlueter; P. C. Redfern; L. A. Curtiss; K. Amine, J. "Improved synthesis of a highly fluorinated boronic ester as dual functional additive for lithium-ion batteries," *Power Sources*, **196**, 2171-2178 (2011).
3. L. Zhang, Z. C. Zhang, P. C. Redfern, L. A. Curtiss, and K. Amine, "Molecular engineering towards safer lithium-ion batteries: a highly stable and compatible redox shuttle for overcharge protection," *Energy & Environmental Science* **5**, 8204-8207 (2012).
4. G. Ferguson, P. Redfern, L. Cheng, D. Bedrov, G. Smith and L. A. Curtiss, "A Theoretical Study of the Reaction of Reduced Ethylene Carbonates in Lithium-Ion Batteries", to be submitted.
5. G. Ferguson and L. A. Curtiss, "Atomistic Modeling of the Electrolyte Organic Solvents used in Lithium-ion Batteries," submitted.

## V.D.6 Inexpensive, Nonfluorinated (or Partially Fluorinated) Anions for Lithium Salts and Ionic Liquids for Lithium Battery Electrolytes (NCSU)

Wesley Henderson  
North Carolina State University  
Ionic Liquids & Electrolytes for Energy Technologies  
(ILEET) Laboratory Department of Chemical &  
Biomolecular Engineering  
911 Partners Way, Campus Box 7905  
Raleigh, NC 27695  
Phone: (919) 513-2917; Fax: (919) 515-3465  
E-mail: [whender@ncsu.edu](mailto:whender@ncsu.edu)

Collaborators: Michel Armand (co-PI)

Start Date: April 1, 2009

Projected End Date: March 31, 2013

- Determined the crystal structures of numerous solvates to identify how the anions coordinate the  $\text{Li}^+$  cations and to facilitate the spectroscopic analysis of electrolyte solution ionic association interactions.
- Identified that electrolytes with LiDFOB and LiBOB are much more dissociated than anticipated (with a correspondingly higher conductivity than  $\text{LiBF}_4$  solutions).
- Demonstrated that concentrated electrolytes with a variety of solvents and salts have remarkably different properties from more dilute mixtures.



### Objectives

- Develop new anions as replacements for  $\text{PF}_6^-$  or as additives for electrolytes.
- Establish characterization methods for electrolyte solvent-lithium salt and ionic liquid-lithium salt mixtures to aid in understanding structure-property relationships and optimization of cell performance.

### Technical Barriers

This project addresses the following technical barriers from the VT Research & Development plan regarding electrolytes:

- Improved cell performance, calendar life and abuse tolerance.
- Improved low-temperature performance.
- Reduced cost.

### Technical Targets

- Obtain electrolyte salt materials that can operate in the potential range (4-5 V vs.  $\text{Li}/\text{Li}^+$ ) enabling the use of high-voltage cathode materials.
- Develop electrolyte materials which enable cell operation in the temperature range -30 to 55°C or higher.
- Improve cycle life and safety.

### Accomplishments

- Synthesized several lithium salts for characterization.
- Determined the phase behavior of the salts with nitrile, carbonate and ester solvents.

### Introduction

Electrolyte materials are key components in terms of both the cost and performance (power, safety, lifetime) of a battery. The properties of salts (either lithium salts or ionic liquids) containing new anions are being explored to determine their utility for lithium battery applications.

### Approach

To explore new anions for alternative salts to  $\text{LiPF}_6$ , ionic liquids and electrolyte additives, two classes of nonfluorinated (or partially fluorinated) anions were synthesized and characterized: 1) chelated and non-chelated organoborate anions (related to bis(oxalate) borate or BOB<sup>-</sup>), and 2) Hückle-type anions in which the charge is stabilized on a 5-member azole ring and noncyclic cyanocarbanions. The physical properties of these new anions, incorporated in both lithium salts and ionic liquids, are being examined including the thermal phase behavior (phase diagrams); thermal, chemical and electrochemical stability; transport properties; interfacial properties; molecular interactions and cell performance. These salts will be compared with current salts of interest such as  $\text{LiBF}_4$ ,  $\text{LiPF}_6$  and LiBOB and ionic liquids based upon the bis(trifluoromethanesulfonyl)imide anion.

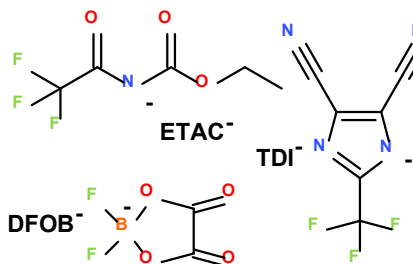
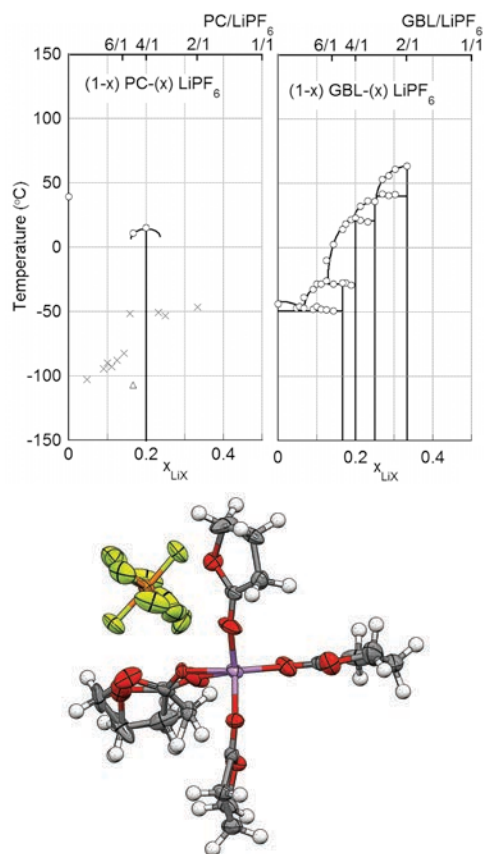


Figure V - 154: Anions synthesized as part of the present study.



**Figure V - 155:** Phase diagrams for  $(PC)_n\text{-LiPF}_6$  and  $(GBL)_n\text{-LiPF}_6$  mixtures and ion coordination in the crystal structure of the  $(GBL)_4\text{:LiPF}_6$  solvate (Li-purple, O-red, P-orange, F-green)—x and triangle symbols indicate a  $T_g$  for fully amorphous and partially crystalline mixtures, respectively.

## Results

**Anion Synthesis.** The synthesis of lithium ethyl-*N*-(2,2,2-trifluoroacetyl)carbamate (LiETAC), lithium difluoro(oxalato)borate (LiDFOB) and lithium 4,5-dicyano-2-(trifluoromethyl)imidazolidine (LiTDI) was scaled up to facilitate the full characterization of these salts (Figure V - 154). Modifications to the synthesis procedures have been made to improve the salt purity and yields.

### Characterization of Solvent-Lithium Salt

**Mixtures.** The study of the phase behavior and transport properties of (solvent) $_n\text{-LiPF}_6$  mixtures with EC, PC, GBL and GVL has been completed (e.g., Figure V - 155 shows partial phase diagrams for  $(PC)_n\text{-LiPF}_6$  and  $(GBL)_n\text{-LiPF}_6$  mixtures and a portion of the  $(GBL)_4\text{:LiPF}_6$  crystalline solvate). This information has been compared with the phase behavior and properties of  $\text{LiBF}_4$ , LiDFOB and lithium bis(oxalato)borate (LiBOB) mixtures. Interestingly, the average solvent coordination numbers (from Raman spectroscopy) suggest that the  $\text{Li}^+$  cations in the LiDFOB solutions are more solvated than those in  $\text{LiBF}_4$  solutions. Numerous solvate crystal structures have been determined for LiDFOB (i.e.,  $(G1)_2\text{:LiDFOB}$  with

monoglyme - Figure V - 156) to examine how this anion coordinates  $\text{Li}^+$  cations and to correlate this with the Raman bands for the DFOB $^-$  anion which reflect specific known forms of DFOB $^- \dots \text{Li}^+$  cation coordination.

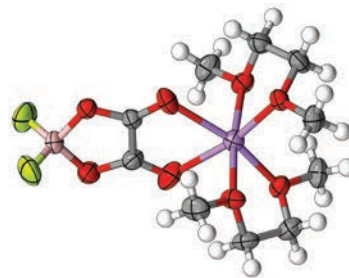


**Figure V - 156:** Ion coordination in the crystal structure of the  $(G1)_2\text{:LiDFOB}$  solvate (Li-purple, O-red, B-tan, F-green).

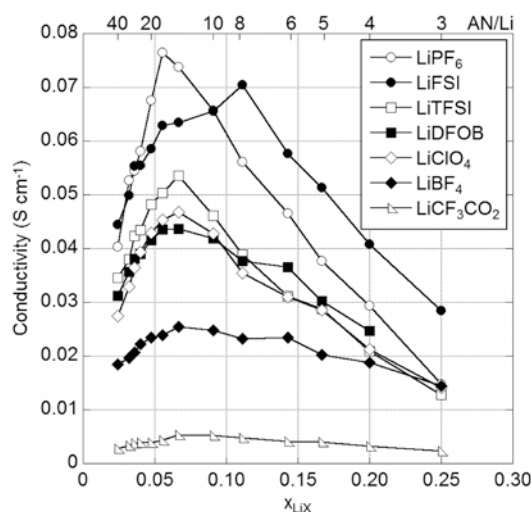


**Figure V - 157:** Isothermal ionic conductivity of  $(AN)_n\text{-LiX}$  solutions at  $60^\circ\text{C}$ .

Using the anion Raman bands to examine ionic association, the characterization of acetonitrile solutions,  $(AN)_n\text{-LiDFOB}$ , suggests that this salt is less associated than the corresponding  $\text{LiBF}_4$  solutions, in agreement with the solvent coordination numbers. Further, the conductivity (Figure V - 157) and viscosity data for the AN mixtures also supports this surprising conclusion.  $(\text{Solvent})_n\text{-LiDFOB}$  mixtures with the cyclic carbonates or esters are also consistently found to have a comparable or higher ionic conductivity than the analogous  $\text{LiBF}_4$  mixtures (Figure V - 158). It is also interesting to note that LiBOB solutions with PC, GBL and GVL (but not EC) are more conductive than the corresponding  $\text{LiBF}_4$  solutions (Figure V - 159).

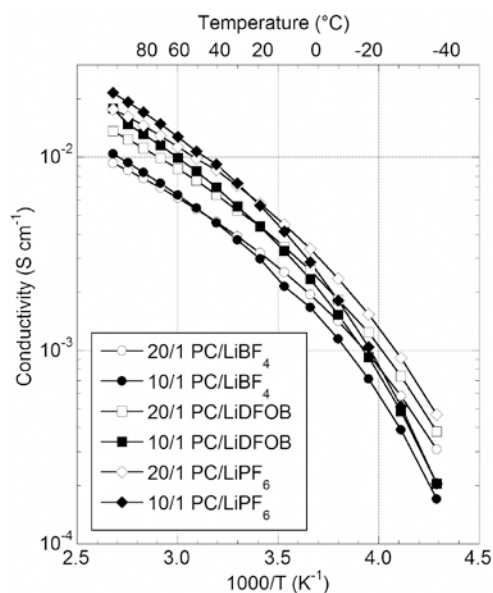


Figure V - 158: Ionic conductivity of (PC)<sub>n</sub>-LiX solutions.

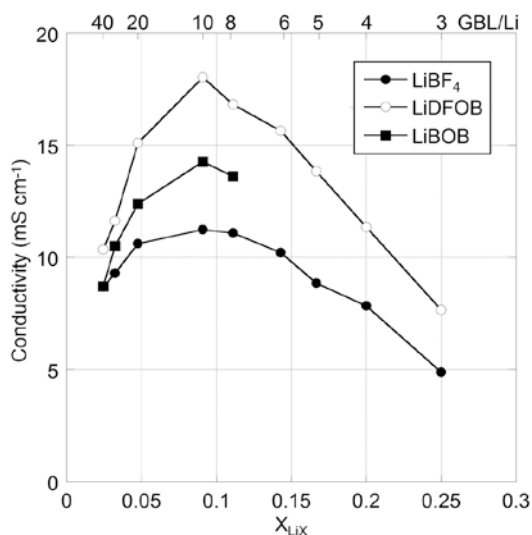


Figure V - 159: Isothermal ionic conductivity of (GBL)<sub>n</sub>-LiX solutions at 60°C.

A number of crystal structures for LiTDI solvates have also been determined—examples with diglyme (G2) and AN are shown in Figure V - 160 and Figure V - 161—to facilitate the assignment of TDI-anion Raman band positions to specific forms of TDI...Li<sup>+</sup> cation coordination. This enables the solution structure (i.e., ionic association) behavior of this salt to be fully characterized.

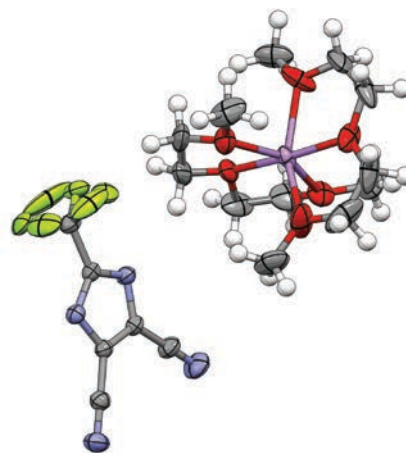


Figure V - 160: Ion coordination in the crystal structure of the (G2)<sub>2</sub>:LiTDI solvate (Li-purple, O-red, N-blue, F-green).

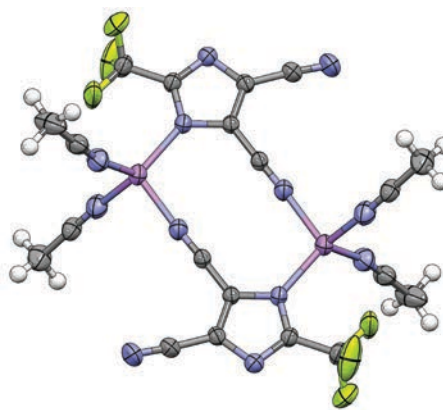


Figure V - 161: Ion coordination in the crystal structure of the (AN)<sub>2</sub>:LiTDI solvate (Li-purple, O-red, N-blue, F-green).

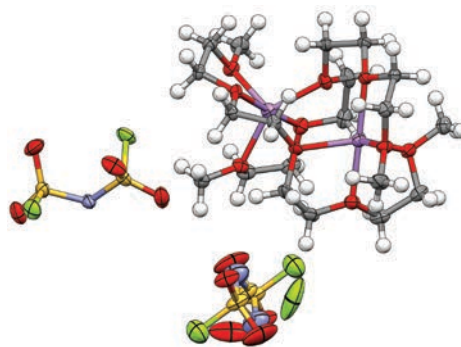
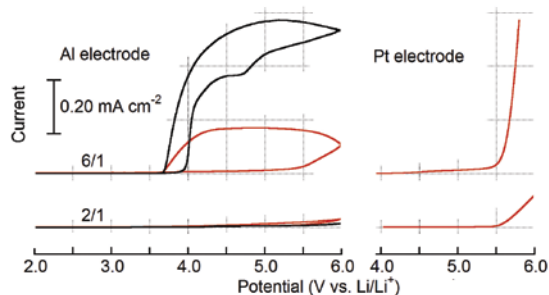


Figure V - 162: Ion coordination in the crystal structure of the (G4)<sub>1</sub>:LiFSI solvate (Li-purple, O-red, N-blue, S-yellow, F-green) (one of the FSI<sup>-</sup> anions is disordered).

The characterization of LiFSI electrolytes is also underway. Such solutions have an exceptional conductivity (i.e., Figure V - 157)—comparable to LiPF<sub>6</sub> solutions. The first known solvate with LiFSI has been determined with tetraglyme (i. e., (G4)<sub>1</sub>:LiFSI in Figure V - 162).



**Figure V - 163:** CVs of (EC)<sub>n</sub>-LiTFSI electrolytes with n = 6 or 2 (i.e., 6/1 or 2/1) on Al and Pt working electrodes.

**Concentrated Electrolytes.** From the information gleaned from the phase diagrams, concentrated electrolytes have also been selected for characterization. Such solvent-LiX mixtures contain little to no uncoordinated solvent. The properties of these mixtures differ markedly from those of more dilute mixtures. For example, the oxidative stability of (EC)<sub>n</sub>-LiTFSI mixtures is shown in Figure V - 163. The 2/1 mixtures not only has an improved stability (relative to the 6/1 electrolyte) on the Pt electrode, but also exhibits negligible Al corrosion (in sharp contrast to the 6/1 electrolyte). Such properties suggest that salt concentration may be one effective means of tailoring electrolyte properties.

### FY 2012 Publications/Presentations

1. Han, S.-D.; Allen J. L.; Jónsson, E.; Johansson, P.; McOwen, D. W.; Boyle, P. D.; Henderson, W. A. J., "Solvate Structures and Computational/Spectroscopic Characterization of Lithium Difluoro(oxalato)borate (LiDFOB) Electrolytes," *Phys. Chem. C*, 2012, in-press.
2. McOwen, D. W.; Delp, S. A.; Boyle, P. D.; Henderson, "W Dilithium 1,2,5-Thiadiazolidine-3,4-dione 1,1-dioxide dehydrate," *A. Acta Crystallogr.*, E68, m1228 (2012).
3. Allen, J. L.; Boyle, P. D.; Henderson, "Lithium Bis(2-methylactato)borate Monohydrate," *W. A. Acta Crystallogr.*, E68, m749 (2012).
4. Seo, D. M.; Afroz, T.; Han, S.-D.; Allen, J. L.; Boyle, P. D.; Henderson, "Delving into Solvation and Ionic Coordination Interactions in Lithium Salt Solvates," *W. A.* 2012, submitted.
5. "Delving into the Depths of Solution Structure. Developing Tools for Lithium Battery Electrolyte Characterization," *CIC-Energigune*, Vitoria, Spain, Mar 8, 2012.
6. Electrolyte Projects – Overview, *U.S. Drive Tech Team Workshop*, Berkeley, CA, Mar 28-29, 2012.
7. "Inexpensive, Nonfluorinated (or Partially Fluorinated) Anions for Lithium Salts and Ionic Liquids for Lithium Battery Electrolytes," DOE Annual Merit Review & Evaluation Meeting—Hydrogen Program and Vehicle

Technologies Program, Crystal City, VA, May 9-12, 2012.

8. "Inexpensive, Nonfluorinated (or Partially Fluorinated) Anions for Lithium Salts," DOE BATT Electrolytes Review, Berkeley, CA, Sep 18, 2012.
9. "Concentrated Electrolytes: Improving Oxidative Stability for Use in High-Voltage Li-Ion Batteries," *PRiME ECS Meeting*, Honolulu, HI, Oct 7-12, 2012.
10. "Delving into the Properties and Solution Structure of Nitrile-Lithium Difluoro(oxalato)borate (LiDFOB) Electrolytes for Li-ion Batteries," *PRiME ECS Meeting*, Honolulu, HI, Oct 7-12, 2012.
11. "Thermal Phase Behavior and Electrochemical/Physicochemical Properties of Carbonate and Ester Electrolytes with LiBF<sub>4</sub>, LiDFOB and LiBOB," *PRiME ECS Meeting*, Honolulu, HI, Oct 7-12, 2012.

## V.D.7 Development of Electrolytes for Lithium-ion Batteries (URI)

Brett L. Lucht  
University of Rhode Island  
Department of Chemistry  
51 Lower College Rd., Pastore  
Kingston, RI, 02881  
Phone: (401) 874-5071; Fax: (401) 874-5071  
E-mail: [blucht@chm.uri.edu](mailto:blucht@chm.uri.edu)

Start Date: April 1, 2009  
Projected End Date: March 31, 2013

### Objectives

- Develop novel electrolytes with superior performance to state of the art (LiPF<sub>6</sub> in carbonates).
- Develop understanding of the source of performance fade in LiNi<sub>1.5</sub>Mn<sub>0.5</sub>O<sub>4</sub> cathodes cycled to high voltage (4.9 V vs Li).
- Develop an electrolyte formulation that allows for superior performance of LiNi<sub>0.5</sub>Mn<sub>1.5</sub>O<sub>4</sub> cathodes.

### Technical Barriers

This project addresses the following technical barriers from the Batteries for Advanced Transportation Technologies Research Development Plan regarding electrolytes: improving the cell performance, cell life, and cost; improving the calendar life of lithium ion batteries; expanding the survival temperature range.

### Technical Targets

- Cell performance, life, cost: Calendar life: 40 °C, 15 years.
- Survival Temp Range: -46 to +66 °C.
- Unassisted Operating & Charging Temperature Range, -30 to + 52 °C.

### Accomplishments

- Developed an understanding of the role of electrolytes in capacity fade and poor cycling efficiency of LiNi<sub>0.5</sub>Mn<sub>1.5</sub>O<sub>4</sub> cathodes. (March 2012).
- Designed electrolyte formulations to improve efficiency (>99 %) and decrease capacity fade (50 % of SOA) for high voltage Ni-Mn spinel cathode materials in coin cells. (July 2012).
- Optimized a LiPF<sub>4</sub>(C<sub>2</sub>O<sub>4</sub>) electrolyte for graphite/LiNi<sub>x</sub>Co<sub>1-2x</sub>Mn<sub>x</sub>O<sub>2</sub> cells for high and low temperature performance (50 % of SOA capacity fade.) (September 2012).



### Introduction

While commercial lithium-ion batteries (LIBs) perform well for most home electronics applications, currently available LIB technology does not satisfy some of the performance goals for Plug-in Hybrid Electric Vehicles (PHEV). In particular, currently available LIB technology does not meet the 15 year calendar life requirement set by the United States Advanced Battery Consortium (USABC).

The most extensively used LIB electrolytes are composed of LiPF<sub>6</sub> dissolved in organic carbonates. However, LiPF<sub>6</sub> based electrolytes have poor thermal stability and performance when cycled to high voltage (> 4.5 V vs Li). Significant energy fading occurs after several years at room temperature and over only a few months the moderately elevated survival temperature of 66 °C required by the USABC. While there are several different factors that limit the thermal stability, calendar life and voltage window of LIBs, the reactions of the electrolyte with the surface of the electrode materials are frequently reported to be most important.

### Approach

Optimize properties of LiPF<sub>4</sub>C<sub>2</sub>O<sub>4</sub>/carbonate electrolytes in small Li-ion cells at low temperature (-30 °C) after accelerated aging. Investigate electrode surface films for cells cycled with LiPF<sub>4</sub>(C<sub>2</sub>O<sub>4</sub>) to determine source of performance differences. Investigate cathode film forming additives for high voltage (> 4.5 V) cathode materials. Investigate the surface of cathodes and anodes cycled with novel electrolytes, with or without additives, to develop a mechanistic understanding of interface formation and degradation.

### Results

**Role of electrolyte in LiNi<sub>0.5</sub>Mn<sub>1.5</sub>O<sub>4</sub> performance fade.** A detailed analysis of the role of electrolytes in capacity fade and poor cycling efficiency of LiNi<sub>0.5</sub>Mn<sub>1.5</sub>O<sub>4</sub> cathodes cycled to high voltage was conducted. The reaction of electrolyte with the surface of uncycled LiNi<sub>0.5</sub>Mn<sub>1.5</sub>O<sub>4</sub> particles upon storage of the particles in SOA electrolyte at elevated temperature to simulate accelerated aging was analyzed. After storage, the particles were analyzed via SEM (Figure V - 164), XPS, and IR to monitor changes to the solid materials and the liquid electrolytes were analyzed via ICP-MS to detect Mn or Ni. The SEM images clearly indicate that the electrolyte significantly damages the cathode particles. Analysis of

the surface of the cathode particles with XPS suggests a high concentration of electrolyte decomposition products on the cathode surface. Analysis of the electrolyte by ICP-MS indicates that 0.9 % of the Mn and 0.3 % of the Ni were dissolved into the electrolyte. Similar results were observed for storage at 55 °C for two weeks.

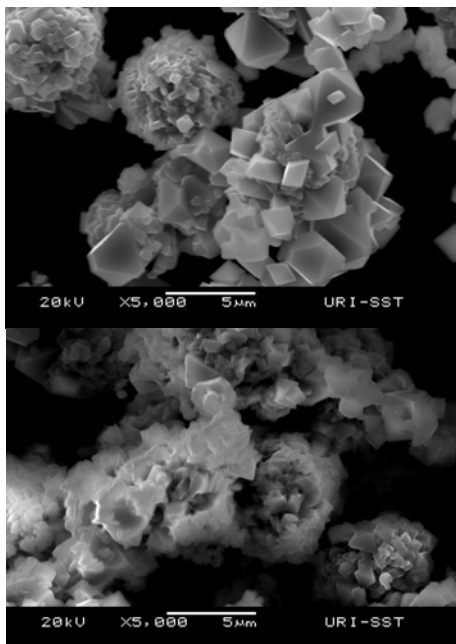


**Figure V - 164:**  $\text{LiNi}_{0.5}\text{Mn}_{1.5}\text{O}_4$  before storage in the SOA electrolyte (top) and after storage in SOA electrolyte for 2 weeks at 55 °C.

Investigations into the mechanism of performance fade in  $\text{LiNi}_{0.5}\text{Mn}_{1.5}\text{O}_4$  cathodes cycled to high voltage has led to an understanding of two primary sources of performance fade. First, decomposition of the  $\text{LiPF}_6$  salt leads to the generation of Lewis acidic species that corrode the cathode surface and dissolve transition metals (Mn and Ni). Second, the high oxidation potentials of the cathode result in the oxidation of carbonate solvents to generate polyethylene carbonate. Experiments suggest that Mn dissolution is the primary problem; Mn dissolution is worse at high voltage and that electrolyte oxidation is a secondary contributor. However, investigations of graphite/ $\text{LiNi}_{0.5}\text{Mn}_{1.5}\text{O}_4$  cells suggest that performance is worse in full cells than in  $\text{Li}/\text{LiNi}_{0.5}\text{Mn}_{1.5}\text{O}_4$  cells and that there may be cross reactions between the graphite anode and the  $\text{LiNi}_{0.5}\text{Mn}_{1.5}\text{O}_4$  cathode. Finally, mechanistic investigation has led to the development of several additives which improve the performance of  $\text{LiNi}_{0.5}\text{Mn}_{1.5}\text{O}_4$  cycled to high voltage (4.9 V vs Li).

**Development of electrolyte additives to improve performance of  $\text{LiNi}_{0.5}\text{Mn}_{1.5}\text{O}_4$ .** Electrolyte formulations to optimize the performance of  $\text{LiNi}_{0.5}\text{Mn}_{1.5}\text{O}_4$  cathodes cycled to 4.9 V (vs Li) are being designed. Two primary types of additives are being investigated. First, Lewis basic species which inhibit the thermal decomposition of  $\text{LiPF}_6$  are being investigated. Preliminary investigations suggest

that incorporation of Lewis basic additives, such as Diethyl Methyl Phosphonate (DMMP), inhibits Mn dissolution and improves cycling performance at high voltage. The second type of additive that is being investigated is cathode film forming additives such as LiBOB. Cathode film forming additives are preferentially oxidized on the cathode surface to generate a passivation layer which inhibits electrolyte oxidation. A novel cathode film forming additive (Additive 1) has been incorporated into  $\text{Li}/\text{LiNi}_{0.5}\text{Mn}_{1.5}\text{O}_4$  cells. The incorporation of the additive resulted in a significant reduction in the capacity loss during the first 55 cycles (Figure V - 165). The standard electrolyte lost 28 % of the capacity while the electrolyte with additive lost only 13 %, a 54 % reduction in capacity loss. In addition, the efficiencies were improved from 98.2 to 99.3 %. *Ex situ* surface analysis of the electrode after cycling suggests that incorporation of the novel additive reduced the thickness of the cathode surface film and reduced the detrimental reactions of the electrolyte with the cathode surface. Further investigation on the optimization of electrolyte additives is in progress.

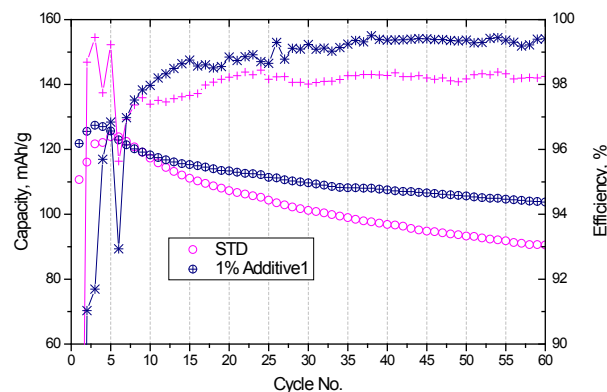


**Figure V - 165:** Cycling capacity and efficiency of  $\text{Li}/\text{LiNi}_{0.5}\text{Mn}_{1.5}\text{O}_4$  cells with and without DMMP.

**Optimization of  $\text{LiPF}_4\text{C}_2\text{O}_4$  (LiFOP) for low and high temperature performance.** Lithium-ion coin cells were constructed with 1.2 M  $\text{LiPF}_6$  in 3:7 EC/EMC, 1.2 M  $\text{LiPF}_6$  in 2:2:6 EC/EMC/MB (Methyl Butyrate) and 1.2 M LiFOP in 2:2:6 EC/EMC/MB with natural graphite/ $\text{LiNi}_{1/3}\text{Co}_{1/3}\text{Mn}_{1/3}\text{O}_2$  electrodes to probe low temperature performance. The first cycle efficiency of all cells was similar (~85 %). After initial formation cycles the cells with MB electrolytes have a similar cycling performance, which is slightly higher than the EC/EMC cells (Figure V - 166). When the cells were cooled to -10 °C for low temperature discharging, the discharge capacities of all three sets of coin cells decreased, but cells containing MB outperformed the EC/EMC cells. Then cells were stored at 55 °C for one week to simulate accelerated aging.

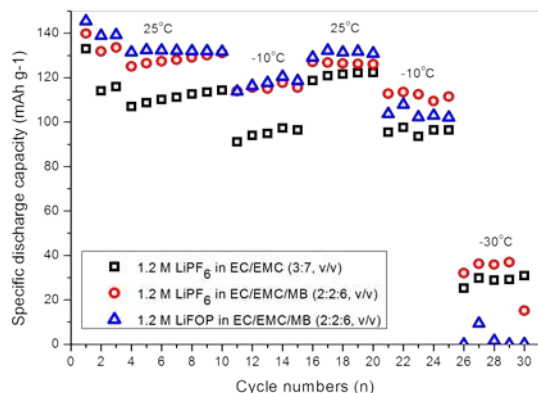


**Figure V - 166:** Cycling performance of different electrolytes with graphite/LiNi<sub>1/3</sub>Co<sub>1/3</sub>Mn<sub>1/3</sub>O<sub>2</sub>.

After aging, the RT cycling performance was comparable to the initial RT performance. Upon cycling at -10 °C after aging, all sets of cells had similar performance although the cell with LiPF<sub>6</sub> and MB had the highest discharge capacity. Upon dropping the temperature further (-30 °C), the differences in performance were greater. Cells containing LiPF<sub>6</sub> and MB provided the best performance, followed by LiPF<sub>6</sub> in carbonates, while LiFOP with MB gave the worst performance at -30 °C. Similar poor low temperature performance was observed for LiFOP electrolytes with PC after aging.

Electrochemical impedance spectroscopy suggests that both the film resistance and the charge-transfer resistance of the cells containing the LiFOP/MB electrolyte are much larger than the LiPF<sub>6</sub> electrolytes. The IR spectrum of the natural graphite anode after accelerated aging with LiFOP/MB electrolyte is quite different from that of the natural graphite anode after accelerated aging with LiPF<sub>6</sub> electrolytes (see Figure V - 167). The presence of lithium oxalate is supported by peaks at ~1640 cm<sup>-1</sup> and 1323 cm<sup>-1</sup>, and poly(ethylenecarbonate) is supported by a peak at 1760 cm<sup>-1</sup>. The IR results are consistent with the XPS data of anodes cycled with LiFOP/MB electrolyte and suggest that the surface film is thicker for cells cycled with LiFOP/MB electrolyte and have high concentrations of lithium oxalate. The increased impedance and poor cycling performance at -30 °C for cells with LiFOP/MB electrolyte is likely due to the thicker surface films on the anode.

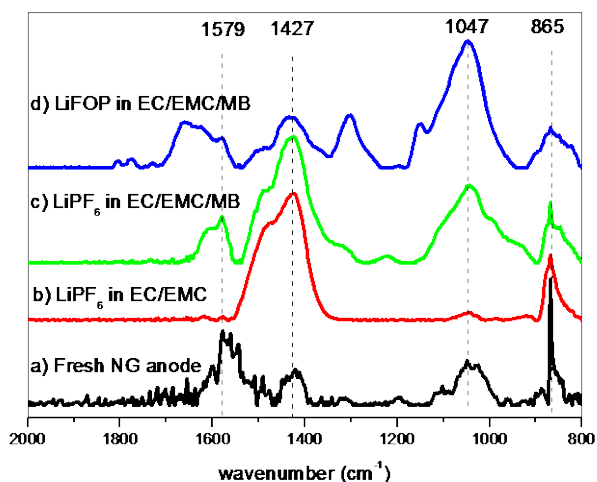


**Figure V - 167:** FT-IR spectra of natural graphite anode cycled with LiNi<sub>1/3</sub>Co<sub>1/3</sub>Mn<sub>1/3</sub>O<sub>2</sub> cathode, fresh and after accelerated aging.

## Conclusions and Future Directions

A detailed investigation of the electrolyte based failure mechanisms of LiNi<sub>0.5</sub>Mn<sub>1.5</sub>O<sub>4</sub> cycled to high voltage (4.9 V vs Li) has been conducted. The two main decomposition mechanisms are Mn dissolution and electrolyte oxidation. Our data suggests that the Mn dissolution is the primary problem while electrolyte oxidation is secondary. The development of a mechanistic understanding of performance fade has led to the development of electrolyte additives which improve the performance of LiNi<sub>0.5</sub>Mn<sub>1.5</sub>O<sub>4</sub> cathodes. The two primary types of additives are Lewis basic additives such as DMMP which inhibit Mn dissolution and cathode film forming additives such as LiBOB which inhibit electrolyte oxidation. Future investigations will focus on understanding the role of electrolyte in performance fade of graphite/ LiNi<sub>0.5</sub>Mn<sub>1.5</sub>O<sub>4</sub> cells cycled to high voltage (4.8-4.9 V vs Li) at moderately elevated temperature (55 °C). Electrolyte additives will also be developed and optimized to improve the performance of graphite/ LiNi<sub>0.5</sub>Mn<sub>1.5</sub>O<sub>4</sub> cells.

LiPF<sub>4</sub>C<sub>2</sub>O<sub>4</sub> electrolytes were further investigated with a focus on the optimization of low temperature performance. Incorporation of methyl butyrate (MB) improved the low temperature (-10 °C) performance of both LiPF<sub>6</sub> and LiPF<sub>4</sub>C<sub>2</sub>O<sub>4</sub> electrolytes. Unfortunately, the performance of LiPF<sub>4</sub>C<sub>2</sub>O<sub>4</sub>/MB electrolytes at low temperature (-30 °C) after accelerated aging (1 week storage at 55 °C) was inferior to LiPF<sub>6</sub> electrolytes. Future investigations will focus on the development of novel non-fluorinated salts for lithium ion battery electrolytes.

## FY 2012 Publications/Presentations

1. Swapnil Dalavi, Mengqing Xu, Brandon Knight and Brett L. Lucht, "Effect of added LiBOB on High Voltage

- (LiNi<sub>0.5</sub>Mn<sub>1.5</sub>O<sub>4</sub>) Spinel Cathodes,” *Electrochem. Solid State Lett.* **15**, A28-A31 (2012).
2. Liu Zhou and Brett L. Lucht, “Performance of Lithium Tetrafluorooxalatophosphate (LiFOP) Electrolyte with Propylene Carbonate,” *J. Power Sources*, **205**, 439-448 (2012).
  3. M. C. Smart, B. L. Lucht, S. Dalavi, F. C. Krause, and B. V. Ratnakumar, “The Effect of Additives upon the Performance of MCMB/ LiNi<sub>x</sub>Co<sub>1-x</sub>O<sub>2</sub> Li-Ion Cells Containing Methyl Butyrate-Based Wide Operating Temperature Range Electrolytes,” *J. Electrochem. Soc.* **159**, A739-A751 (2012).
  4. M. Xu, D. Lu, A. Garsuch, and B. L. Lucht, “Improved Performance of LiNi<sub>0.5</sub>Mn<sub>1.5</sub>O<sub>4</sub> Cathodes with Electrolytes Containing Dimethylmethylphosphonate (DMMP),” *J. Electrochem. Soc.* In Press.
  5. L. Zhou, M. Xu, B. L. Lucht, “Performance of lithium tetrafluorooxalatophosphate in methyl butyrate electrolyte,” *J. Power Sources*, submitted.
  6. Mengqing Xu, Liu Zhou, Dinesh Chalasani, Swapnil Dalavi, and Brett L. Lucht, “Investigation of the Solid Electrolyte Interphase on Graphite Electrodes with Lithium Tetrafluorooxalatophosphate [LiPF<sub>4</sub>C<sub>2</sub>O<sub>4</sub>] Electrolyte,” *Meeting of the Electrochemical Society*, Boston, MA, October 2011.
  7. Mengqing Xu, Swapnil Dalavi, Janak Kafle, and Brett L. Lucht, “Detrimental reactions of electrolyte with LiNi<sub>0.5</sub>Mn<sub>1.5</sub>O<sub>4</sub>,” *Meeting of the Electrochemical Society*, Boston, MA, October 2011.
  8. “New developments in high voltage electrodes, electrolytes and alternative red-ox chemistries,” *Electronic Materials and Applications Conference*, Orlando, FL, January 2012.
  9. “Development of Electrolytes for High Voltage Lithium Ion Batteries,” *Advanced Automotive Battery Conference*, Orlando, FL, February 2012.
  10. “Spinel Focus Group: Electrolytes,” *US Drive Partnership Tech Team Meeting*, Berkeley, CA, March 2012.
  11. “Development of Electrolytes for Lithium Ion Batteries,” *DOE Annual Merit Review*, Washington, DC, May 2012.

## V.D.8 Sulfones with Additives as Electrolyte (ASU)

C. Austen Angell  
Arizona State University  
Department of Chemistry and Biochemistry  
Tempe, AZ 85287-1604  
Phone: (480) 965-7217; Fax: (480) 965-2437  
E-mail: [Austenangell@gmail.com](mailto:Austenangell@gmail.com)

Start Date: May 1, 2010  
Projected End Date: April 30, 2014

### Objectives

- To complete study of sulfone electrolytes for high voltage cells.
- To demonstrate the possibility of alternative electrolytes that are less likely to have capacity-limiting side reactions.
- Complete the development of amorphous MOF nanoporous membranes as electrolyte supports.

### Technical Barriers

Technical barriers to sulfone electrolyte development lie in the unexpected inability of sulfone solutions to withstand high voltage cathodes, evidently due to inability to establish a suitable SEI between cathode material and the solution. Intrinsic oxidative stability, which seemed so high at manganate cathode, and platinum cathode, is not found a LNM spinel cathode. For success it seems SEI-forming additives need to be developed.

For alternative electrolytes, in which side reactions can't occur, electrolytes without oxidizable components are needed. The barriers to such developments lay in the difficulty of finding physical states that are not liquid that have high enough conductivity to replace the liquid electrolytes.

For amorphous and glassy MOF studies, there are technical barriers to be overcome in measuring accurately the available internal surface areas, and in the manipulation of films to achieve the state in which they have been first fully voided and then properly filled with liquids or solutions of technical interest.

### Technical Targets

- Finding suitable additives for sulfone solvent SEIs.
- Finding novel physical systems for electrolytes in which mobile species are the alkali cations, targeting inorganic ionic liquid systems.
- For glassy MOFs, finding suitable starting materials to permit formation of mixed metal linker center

linkers with similar kinetics of reaction with the same or different spacer units.

### Accomplishments

- In collaboration with Kang Xu at NRL, viscosities and glass temperatures of possible additives for sulfone electrolytes have been evaluated.
- Inexpensive, non-toxic, salts with mobile alkali cations have been identified. These were initially thought to be liquid in character, but prove to be a new class of inorganic crystal of the plastic (rotator phase) type. While initial formulations were only of moderate lithium-ion conductivity, later modifications have proven remarkably highly conducting, and indeed rival the best known molecular liquid ionic solutions in this property, while no doubt exceeding them in actual lithium ion mobility. While these very high-conducting formulations initially showed decay of conductivity with time, the method of mixtures has proved successful in generating stable conductivities at the highest values. Patent disclosures have been written, and provisional patent applications are being generated.
- For glassy MOFs, a range of amorphous structures, with pore sizes ranging from 7 to 25 Å have been formulated. Most of these can be converted to monolithic films using cresol solutions and methanol cleanup. Their physical properties are being evaluated.



### Introduction

**Electrolytes for high voltage cells.** The end of the second full year of support of this project comes with some very promising achievements. Although the project in which the success has been achieved was initiated in consequence of a perceived failure of the original aims of the proposal to develop high voltage sulfone solvent-based electrolytes, the consequences may prove to be very beneficial. This is because a quite new class of electrolytes has been developed in the past year and it is a development that could provide the answer to many of the problems that are currently afflicting the field of high voltage cathode systems.

To put this in context, the original objectives of the project are briefly revisited. In the search for electrolytes that might be able to avoid the side reactions that afflict the current generations of lithium batteries that incorporate very high voltage cathodes (such as the high rate capable LiMNO spinel cathode, electrolytes based on molecular solvents believed to be the most resistant to oxidation of

all, were being investigated. These were the sulfones, the known high oxidative stability of which was attributed to the character of the dipolar group of the molecule (the sulfone group). However after finding sulfones that behaved very well at the graphite anode, intractable problems with stability at the cathode were encountered. The cathode half cells could not be charged beyond the first stage, and evidence of gaseous products was found. This implied that the alkyl groups comprising the remainder of the molecules were being attacked, and implied that a favorable SEI (that must be invoked to explain the success of the intrinsically more oxidizable carbonate solvent based electrolytes) was not being formed. Success in improving cycle life of high voltage cathodes by incorporation of phosphite additives, by the NRL labs, had been reported from by Xu at NRL and it was implied that the only route to success for sulfones would be through research on additives. This was deemed contrary to research group strengths, and was discarded in favor of seeking a quite different solution based on removing all oxidizable elements and focusing on single ion conductors, such as those bringing limited success (at expense of high current) to glassy electrolyte technologies. These systems have yielded cyclic voltammograms with sharp lithium deposition and stripping, but zero oxidation currents up to 14 volts!

An approach aimed at generating inorganic ionic liquids of large (low Coulomb potential) anions was commenced. Sharp transitions observed to accompany onset of high conductivity were initially taken to indicate success. However it was later found that the apparent melting was actually a softening, and that the substances synthesized were of the plastic crystal variety.

**Nanoporous supports for Li cell electrolytes.** This branch of the project had just achieved an initial success at the time of the previous report, after months of frustration in which attempts to emulate the success of researchers in self-assembly of DNA derivatives, had been failing. The new ideas are discussed in following sections.

## Approach

**Electrolytes (i) sulfone electrolytes.** Sulfone electrolytes, now appearing to need SEI development, are being approached by collaboration with other laboratories expert in additives. Activities are limited to testing physical properties of promising additives provided by collaborating laboratories.

**(ii) New generation solid state alkali cation conducting electrolytes:** As an alternative to using liquid electrolytes with oxidizable carbon-containing groups, all-inorganic materials, in which alkali cations are the least strongly bound elements, have been sought. Alternative to alkali-metal conducting glasses, systems with low melting inorganic salts, or systems in which there is rapid ion rotation within a crystal lattice (rather than alkali cation migration alone), have been sought.

**Nanoporous electrolyte supports.** At the last annual report, a hydrogen-bonded self-assembly strategy has just been abandoned in favor of the direct synthesis of covalently bonded networks followed by a film-making strategy - an approach which had been immediately successful. This approach has been continued during the past year, and has led to a complete series of glasses related to the ideal strain-free assemblages of constraint theory, as described below.

## Results

**Electrolytes (i) sulfone electrolytes.** Some further tests of the cathode half cells, that had been found unsatisfactory in the previous annual report, were carried out in the Japanese laboratory of our returning post-doctoral fellow because of the superior cathode preparation facilities available there. The results did not improve. Therefore this line of study was discontinued in favor of the new approach to high voltage inorganic electrolytes for which favorable results are described below. Some physical characterizations (viscosities, glass temperatures, and fragilities) of potential SEI-forming additives for sulfone electrolytes (of the fluorinated phosphite variety from Kang Xu at NRL) have been made.

**New generation solid state alkali cation conducting electrolytes.** The first sign that a new line of electrolytes was in prospect came from a synthesis in which an improbable tetravalent lithium salt was found to provide unexpectedly high conductivity. This salt exhibited a sharp first order phase transition, at 80°C in DSC scans, followed by a long stable range extending to >200°C. It was thought at first that it was a liquid above 80°C but further tests showed this was not the case. The initial results from the first quarterly report, are shown in Figure V - 168.

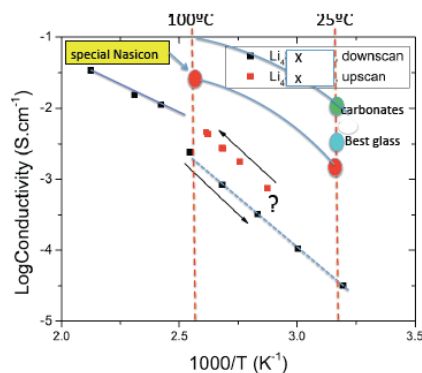


**Figure V - 168:** Initial results for the new lithium ion conducting electrolyte compared with some rival materials.

A subsequent preparation, in which a divalent anion of the same type was prepared in the expectation of much better performance, was disappointing in that the conductivity did not reach the levels needed for a competitive electrolyte. Considerable time was devoted to optimizing synthetic procedures and to characterization of the waxy material obtained. It was not until the trivalent

anion equivalent was prepared and found to be almost as conductive as the best available liquid electrolytes that it became clear that an exciting electrolyte development was at hand. The comparison of the Li4, Li3 and Li2 materials with other state-of-the-art lithium electrolytes is given in Figure V - 169. Of those shown, only the crystalline germanium thiophosphate and the present material are lithium ion conductors, and only the present material is nontoxic, non-brittle and cheap. It has not yet been tested in half cells or full cells.

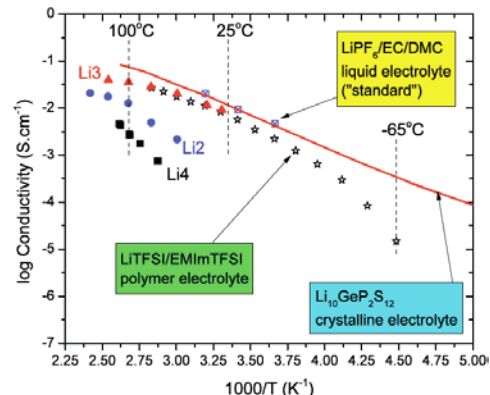


**Figure V - 169:** Comparison of Li4, Li2 and Li3 solid electrolytes preparations with other state of the art lithium cell electrolytes (carbonate liquid electrolyte, EMImidazolium TFSI ionic liquid gel electrolyte, and germaniumthiophosphate crystal electrolyte.)

The evidence that the material was a crystal came from Xray powder patterns, now reproduced for the trivalent material in Figure V - 170.

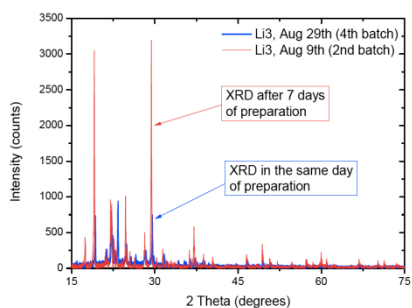


**Figure V - 170:** X-ray powder pattern of preparation Li3 immediately after preparation, and after 7 days.

There was a remaining problem with the high-conducting phase, evident in Figure V - 170 that has now been solved. Until very recently, the high level conductivity (seen in Figure V - 169.) decayed with passing time, losing an order of magnitude in conductivity over one week. This problem has now been solved by preparing mixtures of Li<sub>3</sub> and Li<sub>2</sub>. The difference in conductivity behavior over time between Li<sub>2</sub> and Li<sub>3</sub>-Li<sub>2</sub> mixtures is shown in Figure V - 171.

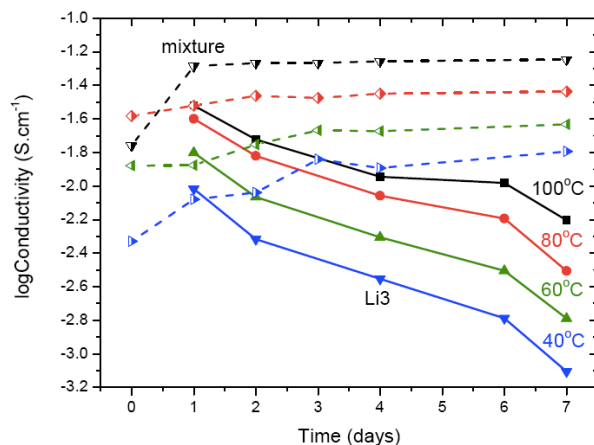


**Figure V - 171:** Time dependence of conductivity at different temperatures for Li3 alone (solid lines) and after mixing with Li2 (by ball milling) at mass fraction 1:1 (dashed lines, same colors and symbols)

The final stabilized conductivities are seen to be essentially the same as those of the Li<sub>10</sub>GeP<sub>2</sub>S<sub>12</sub> crystal, hence equal to that of the standard carbonate electrolyte, with the *major advantage* that the mobile species is the lithium ion itself. The cell used in establishing these results is not well suited for low temperature measurements but preliminary data suggest that the low temperature conductivity will behave favorably, like the Ge-based crystal of Figure V - 168, rather than like the standard electrolyte.

**Nanoporous electrolyte supports.** Direct synthesis of nanoporous structures held together by covalent bonds between metal centers and hydrocarbon struts of either rigid or flexible character has been revived from its early versions in this lab of some ten years ago to produce powders that contain nanoscale pores in their amorphous structures. The new development has been the finding of particular solvents that are capable of dissolving the powders and the regenerating the as monolithic films that retain the pore structure when the solvent has been completely removed, by vacuum drying and finally washing with low molecular weight alcohol. The porosity was characterized by obtaining the powder XRD pattern of the powder and film, and transforming to real space. A comparison is made in Figure V - 172 and Figure V - 174.

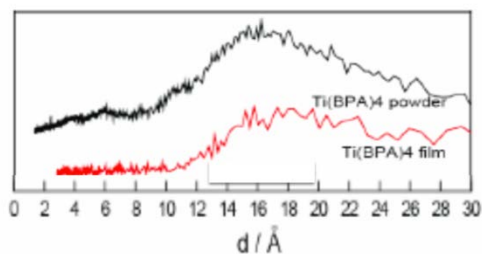


**Figure V - 172:** Comparison of powder and corresponding monolithic film nanopore distributions.

By mixing 3- and 4-coordinating metal centers with the right mole fraction of divalent struts, the composition of our nets can be related to the compositions of covalently

bonded glasses of the chalcogenide variety, for which constraint theory expectations have been worked out by Phillips and Thorpe. There is nothing in the constraint counting procedures that require the shapes of the low valent species to be spherical, so the conditions for stress-free glass formation deduced for the chalcogenides should apply equally to the present generation of covalent glasses. If the bond angles as well as the bond distances are considered constrained then ideal strain-free glasses should be formed when the average number of bonds per structural unit is 2.4. If only distances are constrained the bond density should 2.66. The phase diagram showing the relation of chalcogenide glasses to the present system for the compositions  $\text{AlTi(BPP)}_2$ , and  $\text{Al}_2(\text{BPP})_3$ . The corresponding XRD patterns and their real space representations are shown in Figure V - 174. The composition  $\text{Al}_2(\text{BPP})_3$  shows extraordinarily large pore sizes compared to the corresponding boron-based composition (not shown), presumably due to a distribution of Al between 3- and 4-coordination. This will be explored by solid state NMR studies in future work. At the moment, measurements of internal surface area are being made in collaboration with Don Seo of ASU.

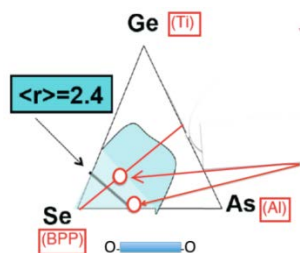


**Figure V - 173:** Composition relations between inorganic covalent glasses and present nanoporous glass compositions.

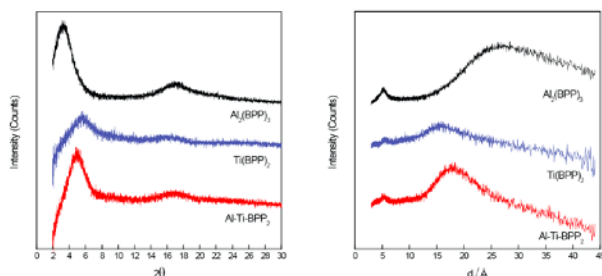


**Figure V - 174:** Powder X-ray pattern, showing the large low angle peak due to the pore-pore correlation function and its real space representation, showing the presence of a share distribution of pore sizes around an 18Å mean size for the mixed metal net, and very large average pore size for the  $\text{Al}_2(\text{BPP})_3$  net.

The mixed metal net has good solution properties and is being cast on to Celgard for support and use as separator in coin cells. The effect of different length spacers is under evaluation. Nets made with smaller spacers are dark red and are electronically conducting.

## Conclusions and Future Directions

While serious problems have been encountered in the search for sulfone-based electrolyte solvent systems for high cathode voltage lithium cells, some important progress has been made in developing alternative electrolytes of a novel class. These offer even higher lithium ion mobilities, and may prove very suitable for use with high voltage cathodes. The conductivities are already shown to be exceptional and stable. Important future work characterizing  $\text{Li}^+$  diffusivities, and their performance in half cells, and full cells, is an immediate evaluation challenge. In separate studies nanoporous films for separators have been successfully developed and characterized, and now need to be characterized as cell components with both separator and cathode electronic conducting elements, as research objectives.

Collaborations: Kang Xu (NRL): Don Seo (ASU): Vince Battaglia (LBL): Guoying Chen

## FY 2012 Publications/Presentations

1. 2012 DOE Annual Peer Review Meeting Presentation.
2. Seung-Yul Lee, Kazuhide Ueno, and C. Austen Angell, Lithium Salt Solutions in Mixed Sulfone and Sulfone-Carbonate Solvents: A Walden Plot Analysis *J. Phys. Chem.* (in press) dx.doi.org/10.1021/jp3067519.

## V.D.9 Lithium Batteries of Higher Capacities and Voltage (U. Texas)

John B. Goodenough  
University of Texas at Austin  
Department of Texas Materials Institute  
ETC 9. 184, University of Texas at Austin  
Austin, TX 78712  
Phone: (512) 471-1646; Fax: (512) 471-7681  
E-mail: [jgoodenough@mail.utexas.edu](mailto:jgoodenough@mail.utexas.edu)

Start Date: January 1, 2009  
Projected End Date: December 31, 2012

### Objectives

- To increase cell voltage (a) by enabling use of a lithium anode and (b) by allowing use of a liquid catholyte compatible with higher-voltage cathodes.
- To increase capacity by (a) the elimination of the irreversible loss of Li from the cathode on first charge and (b) the introduction of cathode strategies other than insertion-compound hosts.

### Technical Barriers

Identification and fabrication as a robust, thin membrane a ceramic  $\text{Li}^+$  electrolyte with a conductivity  $\sigma_{\text{Li}} > 10^{-4} \text{ S cm}^{-1}$  at room temperature that is stable in different liquid environments and on contact with lithium.

### Technical Targets

- To fabricate a thin and dense garnet membrane with  $\sigma_{\text{Li}} > 10^{-4} \text{ S cm}^{-1}$  that can be directly contacted with lithium.
- To fabricate a thin and robust garnet/polymer composite electrolyte with high  $\text{Li}^+$  conductivity.
- To test the stability of the garnet electrolyte in an aqueous solution with different pH.
- To construct a rechargeable Li-Br<sub>2</sub> battery with organic electrolyte.

### Accomplishments

- A garnet membrane less than 10 m thick has been deposited on a porous substrate by pulsed laser deposition. Both nonconductive (YSZ) and conductive (garnet) substrates have been evaluated.
- The stability of the garnet electrolyte has been tested in aqueous solution as well as in ambient storage.
- A polymer coating approach has been investigated to stabilize the garnet electrolyte in water.

- A rechargeable Li-Br<sub>2</sub> battery with organic electrolyte on both cathode and anode sides has been built and tested.
- A flexible garnet/polymer composite has been made, but the garnet content and polymer chain length need to be optimized.

◇ ◇ ◇ ◇ ◇

### Introduction

With present strategies, realization of a rechargeable battery of large enough energy and power density to power an electric car at a price that can compete with the internal combustion engine is problematic. This project is motivated by the possibility of alternative strategies that can use a lithium anode and sulfur, liquid (stationary or flow-through), or air electrode. The essential requirement is fabrication of a thin, dense  $\text{Li}^+$  solid-electrolyte separator that allows use of different liquid electrolytes, anolite and catholite, on the anode and cathode sides.

### Approach

A lithium anode is viable with a solid  $\text{Li}^+$ -electrolyte separator that blocks any lithium dendrites from reaching the cathode. Moreover, the  $\text{Li}^+$  of the passivating SEI layer on the lithium would come from the anode, not the cathode. However, this strategy requires identification of a solid  $\text{Li}^+$  electrolyte having a  $\sigma_{\text{Li}} > 10^{-4} \text{ S cm}^{-1}$  at room temperature that is stable on contact with lithium and can be fabricated into a thin, dense membrane that is mechanically robust. Moreover, this strategy would allow use of a liquid cathode (aqueous or organic) providing a higher capacity than can be achieved with a Li-insertion host. A garnet  $\text{Li}^+$  electrolyte with a  $\text{Li}^+$  conductivity  $\sigma_{\text{Li}} \approx 10^{-3} \text{ S cm}^{-1}$  has been developed, but fabrication into a thin, mechanically robust membrane remains a challenge. One approach is to fabricate a dense, thin film on top of a porous substrate to make a highly conductive electrolyte with proper mechanical strength and then to test it in a dual-electrolyte cell. A second approach is to prepare a polymer/oxide electrolyte composite to improve the mechanical strength of the oxide  $\text{Li}^+$  solid electrolyte while keeping its  $\text{Li}^+$  conductivity.

### Results

**A dense and thin garnet membrane has been prepared.** Figure V - 175 shows a scanning electron microscope (SEM) image of the garnet membrane deposited on the top of a porous substrate. The substrate is also made of the garnet electrolyte. The porous substrate, which can be clearly seen from the image of the cross

section, is made to allow the liquid electrolyte to reach the thin film. The pore size and porosity of the substrate is adjustable by controlling the ratio of garnet powder and the polymer additive during annealing. A larger pore size and higher porosity provides a higher active surface and lower resistance, but it also decreases the mechanical strength. Therefore, the structure of such an electrolyte needs further optimization.

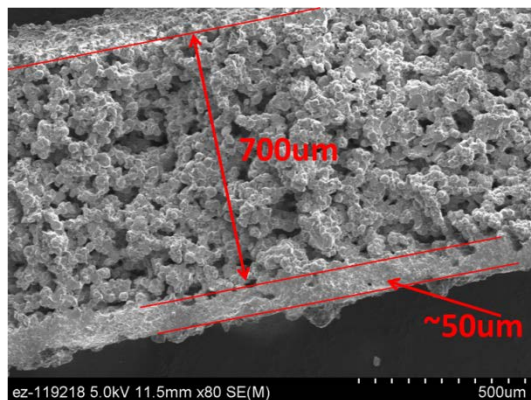


Figure V - 175: SEM image of the cross section of garnet membrane deposited on a porous substrate.

**Stabilization of garnet electrolyte in water.** A garnet electrolyte  $\text{Li}_{7-x}\text{La}_3\text{Zr}_{2-x}\text{Ta}_x\text{O}_{12}$  showing  $\sigma_{\text{Li}} \approx 10^{-3} \text{ S cm}^{-1}$  with  $x=0.4$  has been prepared. However, this electrolyte is not stable in water. Experiment shows that  $\text{H}^+/\text{Li}^+$  exchange occurs as soon as the garnet pellet is put into water, which leads to a pH increase from 7 to 11. The situation becomes worse when the electrolyte is put into a strong acidic solution (0.1 M HCl) where it decomposes slowly. Moreover, the electrolyte can also absorb water from air when stored in ambient condition. In order to make a dual-electrolyte with aqueous catholyte feasible, a polymer coating approach has been developed to stabilize the garnet electrolyte in water. After coating a thin layer of polydopamine with polyethylene oxide tails on the surface of the garnet electrolyte, no  $\text{H}^+/\text{Li}^+$  exchange reaction was observed when the oxide was put into water. The measured lithium-ion conductivity is  $5.5 \times 10^{-4} \text{ S cm}^{-1}$ , which is higher than the that of commercial LISICON electrolyte.

**A 4 V rechargeable Li-Br<sub>2</sub> battery.** Bromine has a theoretical capacity of 370 mAh/g and a redox potential of 4.13 V vs.  $\text{Li}^+/\text{Li}$  according to the reaction

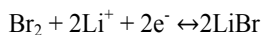


Figure V - 176 shows the discharge/charge curves of a dual-electrolyte Li-Br<sub>2</sub> battery with a garnet electrolyte separator. With bromine in the catholyte, the cell shows a flat discharge plateau at 3.9 V. A low current density of  $0.042 \text{ mA cm}^{-2}$  was needed because the substrate of the separator was not sufficiently porous. The working potential is as high as state-of-the-art cathode materials of a lithium-ion battery. Moreover, the Li-Br<sub>2</sub> battery does not have the big voltage gap between charge and discharge that exists in the Li-air battery with organic electrolytes.

The Li-Br<sub>2</sub> battery also shows a stable capacity retention; no capacity fade has been observed (Figure V - 177) since the potential is well-matched to the HOMO of the organic liquid-carbonate electrolyte.

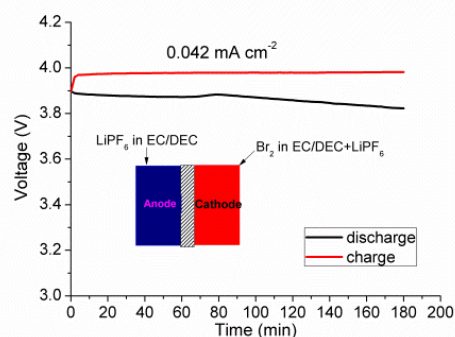


Figure V - 176: Voltage profiles of a Li-Br<sub>2</sub> cell.

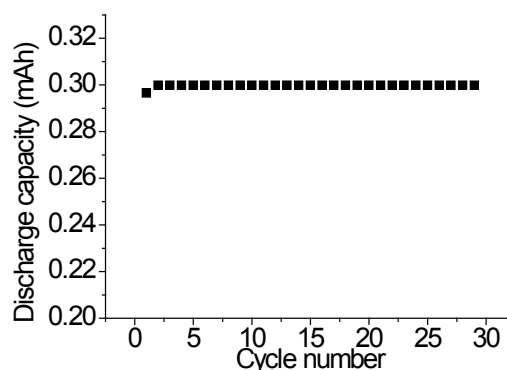


Figure V - 177: Capacity retention of a Li-Br<sub>2</sub> cell. The cell was charged and discharged for 1 h with a current of 0.3 mA. (30% of the theoretical capacity).

## Conclusions and Future Directions

Deposition of a dense and thin garnet electrolyte onto a porous substrate with acceptable mechanical strength is demonstrated to be feasible. It has allowed us to build a dual-electrolyte battery with a lithium metal anode that can be cycled, but the porous substrate needs to be optimized for realization of a high current density. Coating a polymer layer on top of such a solid electrolyte to make it stable in water is also planned so that a high-performance Li-air battery with aqueous catholyte will be feasible. A 4 V Li-Br<sub>2</sub> battery is promising for its high voltage and high theoretical capacity. Different catholytes in which LiBr has different solubility will be studied to optimize its performance.

## FY 2012 Publications/Presentations

- 2012 DOE Annual Peer Review Meeting, "Solid electrolytes for the next generation batteries."

2. J.B. Goodenough, "Evolution of Strategies for Modern Rechargeable Batteries," *Acc. Chem. Res.*, DOI: 10.1021/ar2002705.
3. H. Xie, K.S. Park, J. Song, J.B. Goodenough, "Reversible lithium insertion in the garnet framework of  $\text{Li}_3\text{Nd}_3\text{W}_2\text{O}_{12}$ ," *Electrochem. Comm.* **19**, 135 (2012).
4. H. Xie, Y.T. Li, J. T. Han, Y.Z. Dong, M.P. Paranthaman, L. Wang et al., " $\text{Li}_6\text{La}_3\text{SnMO}_{12}$  (M = Sb, Nb, Ta), a Family of Lithium Garnets with High Li-Ion Conductivity", *J. Electrochem. Soc.* **159**, A1148 (2012).
5. A. Gupta, R. Murugan, M. P. Paranthaman, Z. Bi, C.A. Bridges, M. Nakanishi et al. "Optimum lithium-ion conductivity in cubic  $\text{Li}_{7-x}\text{La}_3\text{Hf}_{2-x}\text{Ta}_x\text{O}_{12}$ ", *J. Power Sources*, **209**, 184 (2012).
6. Y.T. Li, J.T. Han, C.A. Wang, S.C. Vogel, H. Xie, M.W. Xu, J.B. Goodenough, "Ionic distribution and conductivity in lithium garnet  $\text{Li}_7\text{La}_3\text{Zr}_2\text{O}_{12}$ ," *J. Power Sources*, **209**, 278 (2012).

---

# V.E Cell Analysis, Modeling, and Fabrication

## V.E.1 Electrode Fabrication and Failure Analysis (LBNL)

Vincent Battaglia  
Lawrence Berkeley National Laboratory  
Environmental Energy Technologies  
1 Cyclotron Road  
Berkeley, CA 94720  
Phone: (510) 486-7172; Fax: (510) 486-4260  
E-mail: [vsbattaglia@lbl.gov](mailto:vsbattaglia@lbl.gov)

Start Date: October 1, 2008  
Projected End Date: September 30, 2012

### Objectives

- Benchmark baseline material performance.
- Provide electrodes, cells, and/or cycled cell components to BATT researchers.
- Identify key performance failure modes.

### Technical Barriers

The cost of batteries is too high to make EVs commonplace. The energy density of batteries is too low to allow for enough battery on board a vehicle to achieve comparable miles on a single charge as achieved by a gas combustion vehicle on a tank of fuel. The potential safety issues are too uncertain to allow for large size cells.

### Technical Targets

- Energy density (PHEV) 207 Wh/l.
- Energy density (EV) 300 Wh/l.
- Cost (PHEV) 207 \$/kWh (40 miles).
- Cost (EV) 150 \$/kWh (150 miles).

### Accomplishments

- Tested two common sources of electrolyte and identified the one that was more stable at 5 V.
- At short mixing times (less than 2/3 hour) the variability of mixing with a hand held homogenizer creates the bulk of the cell-to-cell variability.
- The addition of VC to the electrolyte results in less side reaction in a cell with NCM cathode.



### Introduction

Millions of Li-ion batteries are produced every day for the portable electronics industry; these same battery

chemistries are used in automobiles today. However, none of these batteries meet the targets established by DOE and the USABC: their life is too short making the need for replacement a certainty, the cost is too high to allow these vehicles to compete favorably with traditional vehicles, and the safety issues typically lead to lower energy density chemistries that in turn lead to even higher system costs.

The life limitations of commercially available technologies are poorly understood, yet, there is little time to spend on these issues as the push for the next generation of technologies is ever present. The Cell Analysis Group's responsibility is to establish the baseline performance of cutting edge technologies and develop methodologies for measuring performance limitations of any technology. The Group's method for making electrodes is fairly robust and is shared with other researchers through an online manual. All steps for cell making are continuously reviewed, with a focus on improved cell-to-cell repeatability. The present focus is on mixing time. Some preliminary tests on short-duration cycling were reported; longer-duration mixing tests are underway.

The BATT program has started focus groups in an attempt to bring a critical mass of research to a particularly difficult challenge.  $\text{LiNi}_{1/2}\text{Mn}_{3/2}\text{O}_4$  was selected by PIs in the BATT Program approximately 2 years ago. The Cell Analysis Group identifies baseline materials and evaluates their rate and cycling performance. This year much of the effort went toward understanding the cycling limitations of  $\text{LiNi}_{0.5}\text{Mn}_{1.5}\text{O}_4$  spinel when cycled against graphite.

It is anticipated that the next focused effort on a cathode material will be moving away from the  $\text{LiNi}_{1/2}\text{Mn}_{3/2}\text{O}_4$  spinel, due to its low capacity, and to a NiCoMn-based material. Some effort has gone toward finding a material which cycles well and to understand the effect of certain additives on its cyclability.

A second Focus Group is on Si-based electrodes. This group has taken some time to identify a single material to rally behind; however, a relationship with Umicore has accelerated and a baseline material identified through this collaboration. Materials were recently shipped to LBNL and three other BATT PIs outside of LBNL.

### Approach

The effort here requires a combination of repetitive tasks that need to be performed in a very reproducible way, and innovative, cutting-edge research. This work is therefore conducted by a combination of Research Associates and Post-docs. The Research Associates provide a means of making electrodes the same way every

time; a means for acquiring surface area, particle size, and SEMs of all materials that enter the lab; and a means for developing new techniques for measuring capacity fade, power fade, and cell data between 25 and 55 °C. The Post-docs bring with them a fresh set of problems to investigate, a fresh way of looking at problems, and new energy and skills to solving problems. The basic approach taken is the same as any other scientific team: identify an important problem of Li-ion batteries, develop a theory that may explain the foundation of the problem, and then find independent ways to test the theory. Efforts are performed through collaborations whenever possible to reduce duplication of effort and to tap previously developed expertise.

## Results

**Baseline Electrolyte.** Although it is named the High-Voltage Ni-spinel Focus Group, several materials in a cell had to be evaluated for their stability, not the least of which the electrolyte. In this case, two sources of a common electrolyte 1 M LiPF<sub>6</sub> in EC:DEC 1:2 were evaluated. It was previously shown that the majority of the intercalation capacity occurs at around 4.7 V *versus* a Li/Li<sup>+</sup> electrode. Thus, it is important that the electrolyte be stable to 4.8 V or higher. In Figure V - 178, cyclic voltammetry curves are given for two newly assembled cells with two different electrolytes. Electrolyte A shows a current that tracks back on itself as the voltage sweep is reversed at 5.0 V. This suggests that the reaction occurring is an oxidation in both directions of the voltage sweep and is indicative of a side reaction. Electrolyte B shows a current that also tracks back on itself for some of the reverse sweep of the potential, but not to the severity of Electrolyte A. Figure V - 179 shows the cyclic voltammetry of the cells after 4 cycles and at a slower sweep rate. Here one sees that Electrolyte A is showing an additional peak at 4.8 V. Additional currents are absent in the sweep of Electrolyte B by the 4<sup>th</sup> cycle. The combination of these two results indicates that Electrolyte B is more stable against oxidation than Electrolyte A. It is for this reason that Electrolyte A was selected as the baseline electrolyte. Samples of this electrolyte were subsequently delivered to all members of the Ni-spinel Focus Group directly from the manufacturer.

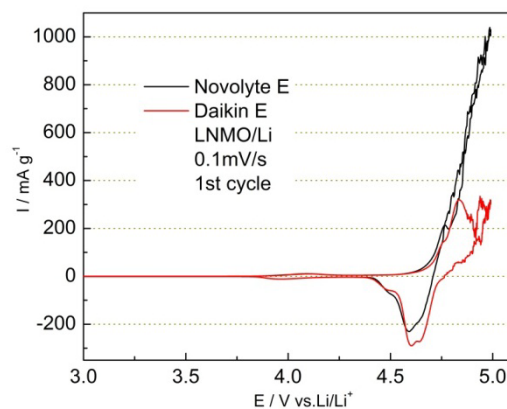


**Figure V - 178:** Cyclic voltammogram of a fresh cell at 0.1 mV/s of a Ni-spinel cathode in two different electrolytes.

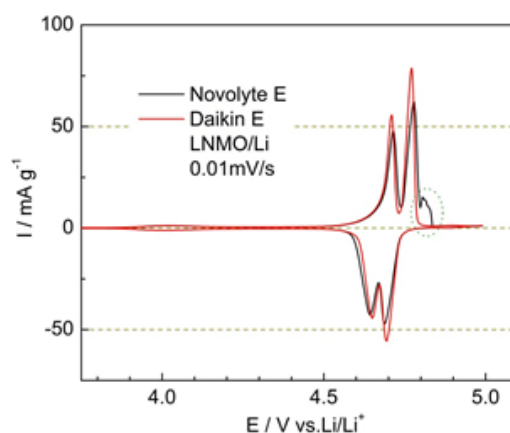


**Figure V - 179:** Cyclic voltammogram after 4 cycles at 0.01 mV/s of a Ni-spinel cathode in two different electrolytes.

Other materials evaluated this year for their stability included the cell hardware and carbon additive. From this analysis it was determined that the high Cr content positive cans of the coin cell hardware from NRC passivate after one cycle and that a new carbon additive from Timcal is superior to others tested at high voltage.

**Short Mixing Times.** A Li-ion electrode consists of active material, for energy, in the form of nano particles, for power; a polymer binder to hold the particles together; and conductive carbon powder of <100 nm size to enhance the transport of electrons. These materials are mixed together in a solvent to make slurry, which can easily and uniformly be spread onto metal substrates that act as current collectors when assembled in a cell. The mixer being used is a homogenizer. It is uniformly acknowledged that proper mixing is a critical step to the fabrication process. In the past, this group evaluated the order by which the materials were mixed and determined that it was better to mix the active material and conductive carbon together in solvent and then add the binder than to mix the carbon additive and binder together in solvent and then add the active material (mixing binder with active material and

then adding the conductive additive has yet to be tested.) Better was defined as the electrodes cycled for over a thousand cycles by adding the carbon to the active material first as opposed to only cycling 400 cycles when the carbon was first mixed with the binder.

In these experiments, the group is investigating the time of mixing. Typically, the final slurry composition is mixed for an hour. That is, the first two components are mixed for 8 minutes and then the binder is added and mixed for an additional hour. In this first set of experiments the second mixing step was varied from 16 minutes to 37 minutes, as shown in Figure V - 180. The electrodes were cycled at C/10 for the first few cycles than at C/2. C/10 cycles were performed every 50 cycles. There appears to be no monotonic correlation of performance with mixing time. The electrode mixed for 16 and 30 minutes showed the greatest drop-off in fractional capacity when the cycling switched from C/10 to C/2. After 50 cycles, the electrodes cycled for 16 and 30 minutes showed the C/10 capacity. The cell mixed for 30 minutes showed the least overall fade after 150 cycles and the cell mixed for 23 minutes showed the greatest amount of fade. Such results suggest that for short mixing times, the time of mixing may not matter as much as the technique used for mixing. In other words, the way in which the homogenizer is hand manipulated in the jar may be more important than the time it is in the jar.

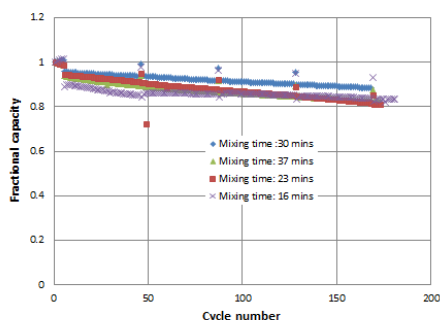


**Figure V - 180:** Cycling data for cathodes of NCM, carbon, and binder mixed for different durations.

**Effect of Additives.** The Ni-spinel Focus Group has made great strides towards correlating physical properties with performance and will start turning its attention to the interfacial reactions. It is clear that the Ni-spinel does not have the specific capacity necessary to advance Li-ion technology and may move to an NCM-based material. It is anticipated that the program can glean additional understanding of cathode materials by comparing and contrasting the side reactions at Ni-spinel with NCM. Therefore, the Cell Analysis Group has started evaluating the side reactions on  $\text{LiNi}_{1/3}\text{Co}_{1/3}\text{Mn}_{1/3}\text{O}_2$  material; in particular, the effects of the additive VC on the rate of the side reaction of the electrolyte with NCM. Provided in Figure V - 181 is the rate of side reaction as the voltage of

the material is stepped up by 100 mV intervals from 4.1 to 4.6 V vs.  $\text{Li}/\text{Li}^+$  for electrolyte with and without VC.

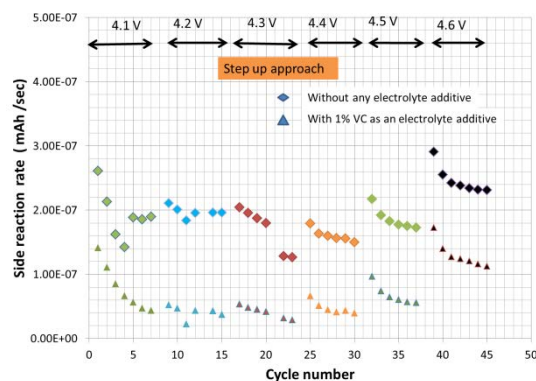


**Figure V - 181:** Rate of side reaction of an electrolyte of 1 M LiPF<sub>6</sub> in EC:DEC 1:2 with and without VC.

Careful inspection of Figure V - 181 indicates that the cells with and without VC show that the side reaction decreases through the first 5 cycles at 4.1 V, although the rate is much less for the cell with VC. The rate is fairly constant for the next 7 cycles at 4.2 V, and then steadily declines at 4.3 V. At 4.4 V, the side reaction jumps up and then falls to a steady rate. This is repeated for the next two voltage steps to 4.6 V. For the entire voltage range, the side reaction with VC is approximately 25 to 50% less than the electrolyte without VC. It is interesting to note that tests of Ni-spinel with VC (not shown) were dramatically different. The VC-containing electrolytes were extremely unstable resulting in poor coulombic efficiency and rapid capacity fade.

## Conclusions and Future Directions

Side reactions in Li-ion batteries may play an important role with regard to the life. It is important that the rate of these reactions at the very least is measured. Once measured, establishing whether correlations to energy and/or power fade is important. The process of measuring the rate of the side reactions for different components and of electrolytes that include additives has begun. It has been shown that the rate of capacity fade of a cell is less than the rate of the side reaction in the cell, and, thus, 100% of the current going toward the side reaction is not resulting in a loss of cycleable lithium. In other words, some fraction of the side reaction is reversible. In the future, the intent is to further understand the role of the side reaction toward capacity fade and to understand the effects additives have on the side reaction and capacity fade.

The fabrication of electrodes consists of many steps and many variables. The mixing step is considered crucial to cell performance and to cell-to-cell repeatability. This group has examined mixing order and short-time mixing. In the future, it intends to investigate longer mixing times as some have reported changes in the slurry physical

properties as a result of extended cycling, different methods of making coatings, and different slurry formulations all in an attempt to fabricate films more economically, with more repeatability, and more capability.

### FY 2012 Publications/Presentations

1. 2012 DOE Annual Peer Review Meeting Presentation.
2. Honghe Zheng, Li Tan, Gao Liu, Xiangyun Song, Vincent S. Battaglia, "Calendaring effects on the physical and electrochemical properties of  $\text{Li}[\text{Ni}_{1/3}\text{Mn}_{1/3}\text{Co}_{1/3}]\text{O}_2$  cathode," *Journal of Power Sources*, Volume **208**, 15 June 2012, Pages 52-57.
3. Honghe Zheng, Qingna Sun, Gao Liu, Xiangyun Song, Vincent S. Battaglia, "Correlation between dissolution behavior and electrochemical cycling performance for  $\text{LiNi}_{1/3}\text{Co}_{1/3}\text{Mn}_{1/3}\text{O}_2$ -based cells," *Journal of Power Sources*, Volume **207**, 1 June 2012, Pages 134-140.
4. Paul Ridgway, Honghe Zheng, A. F. Bello, Xiangyun Song, Shidi Xun, Jin Chong, and Vincent Battaglia, "Comparison of Cycling Performance of Lithium Ion Cell Anode Graphites," *J. Electrochem. Soc.* **159** A520 (2012).
5. G. Liu, H. Zheng, X. Song, and V. S. Battaglia, "Particles and Polymer Binder Interaction: A Controlling Factor in Lithium-Ion Electrode Performance," *J. Electrochem. Soc.* **159** A214 (2012).
6. E.V. Thomas, I. Bloom, J.P. Christophersen, V.S. Battaglia, "Rate-based degradation modeling of lithium-ion cells," *Journal of Power Sources*, Volume **206**, 15 May 2012, Pages 378-382.
7. Zheng Honghe; Yang Ruizhi; Liu Gao; Song, X.Y., and Battaglia, V.S., "Cooperation between Active Material, Polymeric Binder and Conductive Carbon Additive in Lithium Ion Battery Cathode," *Journal of Physical Chemistry C* Volume: **116** Issue: 7 Pages: 4875-4882.
8. Zheng Honghe; Chai Lili; Song Xiangyun; et al., "Electrochemical cycling behavior of  $\text{LiFePO}_4$  cathode charged with different upper voltage limits," *Electrochimica Acta*, Volume: **62** Pages: 256-262.
9. Jin Chong, Shidi Xun, Xiangyun Song, Paul Ridgway, Gao Liu, Vincent S. Battaglia, "Towards the understanding of coatings on rate performance of  $\text{LiFePO}_4$ ," *Journal of Power Sources*, Volume **200**, 15 February 2012, Pages 67-76.
10. Zheng Honghe; Qu Qunting; Zhang Li; Liu, G; and Battaglia, V. S., "Hard carbon: a promising lithium-ion battery anode for high temperature applications with ionic electrolyte," *RSC Advances*, Volume: **2** Issue: 11 Pages: 4904-4912.
11. Shao-Ling Wu, Wei Zhang, Xiangyun Song, Alpesh K. Shukla, Gao Liu, Vincent Battaglia, and Venkat Srinivasan, "High Rate Capability of  $\text{Li}(\text{Ni}_{1/3}\text{Mn}_{1/3}\text{Co}_{1/3})\text{O}_2$  Electrode for Li-Ion Batteries," *J. Electrochem. Soc.* **159** A438 (2012).
12. Same, Adam; Battaglia, Vincent; Tang Hong-Yue; et al., "In situ neutron radiography analysis of graphite/NCA lithium-ion battery during overcharge," *Journal of Applied Electrochemistry*, Volume: **42** Issue: 1 Pages: 1-9.
13. Jin Chong, Shidi Xun, Honghe Zheng, Xiangyun Song, Gao Liu, Paul Ridgway, Ji Qiang Wang, Vincent S. Battaglia, "A comparative study of polyacrylic acid and poly(vinylidene difluoride) binders for spherical natural graphite/ $\text{LiFePO}_4$  electrodes and cells," *Journal of Power Sources*, Volume **196**, Issue 18, Pages 7707-7714 (2011).
14. Jordi Cabana, Honghe Zheng, Alpesh K. Shukla, Chunjoong Kim, Vincent S. Battaglia, and Muharrem Kunduraci, "Comparison of the Performance of  $\text{LiNi}_{1/2}\text{Mn}_{3/2}\text{O}_4$  with Different Microstructures," *J. Electrochem. Soc.*, **158** (9) A997-A1004 (2011).

---

## V.E.2 Modeling - Thermo-electrochemistry, Capacity Degradation, and Mechanics with SEI Layer (U. Michigan)

Jonghyun Park  
University of Michigan  
Department of Mechanical Engineering  
2350 Hayward St.  
Ann Arbor, MI 48109  
Phone: (734) 998-0013; Fax: (734) 998-0028  
E-mail: [jhparkvt@umich.edu](mailto:jhparkvt@umich.edu)

Ann Marie Sastry (Co-PI)  
Sakti3  
1490 Eisenhower Place, Building 4  
Ann Arbor, MI 48108  
Phone: (734) 827-2583  
E-mail: [ams@sakti3.com](mailto:ams@sakti3.com)

Start Date: January 1, 2009  
Projected End Date: December 31, 2012

- Investigation of anisotropic features of graphite material in a single particle and its extension to cell-level scale via a micro-macro mechanical and electrochemical modeling.
- Development of a variational multi-scale model including microscopic structures of the active materials and validation of the developed model.
- Investigation of the additive effects on the interface between the active material and the electrolyte.



### Introduction

The SEI layer is a necessary and important phenomenon, enabling the reversible and safe operation of lithium ion batteries. As such, a great deal of research has been devoted to understanding and optimizing this complex system. To-date, however, a detailed study of the impact of the SEI on the active material has not been undertaken.

Graphite material exhibits a drastic capacity decrease, especially during the initial stage of the electrochemical reactions. This is related to the formation of the SEI layers, which causes an electrochemical impedance rise and, eventually, capacity fade. Graphite also experiences volume changes during intercalation/de-intercalation. The resultant local stresses may cause a disordering of the surface structure of the anode. In addition, the misfit between the graphite and the SEI layer can cause physical damage to the SEI layer, negating the passivation effect and forming a new SEI layer. Further, lithium transport in graphite is highly anisotropic. The resulting concentration gradient induces significant local stress and lattice deformation in the graphene layers in the vicinity of their edges.

To make matters worse, the phenomena above occur at the microscopic level, which requires multiscale and multiphysics solutions. In addition, microstructural details are necessary to design a better battery system. To address these non-linear coupled electrochemical phenomena at separated scales, a simulation tool based on the variational multiscale principal has been developed.

Practically, the use of electrolyte additives has been considered one of the most effective ways to improve the thermal stability of lithium-ion batteries. The additive is electrochemically decomposed on the graphite before the main organic solvents reductively decompose, thus providing a stable SEI layer both electrochemically and thermally. Fluoroethylene carbonate (FEC), vinylene

### Objectives

- Multiscale FE modeling considering phase transition and mismatch between the active material and the SEI layer.
- Simulation in Li-ion batteries including microscale features.
- Measurement of mechanical properties (i.e., Young's modulus and thickness) of the SEI layer.

### Technical Barriers

- Prediction of capacity and power degradation.
- Excessive additive materials compromises energy and power density; it also increases cost.

### Technical Targets

- Available energy for CD mode: 3.4 kWh (10 miles) and 11.6 kWh (40 miles).
- Cycle life: 5000 cycles (10 miles) and 300,000 cycles (40 miles).
- 10- s discharge power: 45 kW (10 miles) and 38 kW (40 miles).
- Calendar life: 15 years (40°C).

### Accomplishments

- Development of a stress and fracture analysis model including intercalation-/misfit-induced stress in/between graphite and the SEI layer

carbonate (VC), and vinyl ethylene carbonate (VEC) have been typically selected to enhance thermal stability of the SEI layer formed on the anode surface. However, the effects of additives on the interface between a cathode and an electrolyte have been relatively overlooked. In this work, an experimental study was done by incorporating electrochemical measurement and ICP-OES (Inductively Coupled Plasma-Optical Emission Spectrometry) to investigate the correlation between the additive-derived surface layer and manganese dissolution.

## Approach

**Intercalation- and misfit-induced stress in the graphite electrodes.** Stress and fracture analysis was conducted to evaluate the effect of the SEI layer on the stress level in the active materials and crack propagation in the SEI layer. The volume expansion due to intercalation and the misfit between the graphite and SEI layer was modeled. Next, channel formation due to cracks through the SEI layer was predicted as a function of SEI layer thickness and volume expansion ratio between the graphite and SEI layer.

Anisotropic features in a graphite electrode were also examined via an electrochemical-mechanical modeling in a particle with multiple grains at a galvanostatic condition. The orientation of each grain was controlled with a fixed number of grains in the particle, and the particle size was controlled by changing the number of grains in a fixed volume. Next, this model was extended into the cell-level model by developing a micro-macro multiscale modeling considering the grain boundaries in the active materials. In this model, representative particles with grain boundaries communicated with the cell-level homogenized domain to exchange current density and concentration at each region.

**Multiscale modeling with self-assembly.** In this work, variational multiscale enrichment was adopted. In this approach, the response fields are expressed in terms of microscale and macroscale counterparts. The battery cell was represented at the coarse-scale, and the electrode particle aggregates were represented at the fine-scale, respectively. At the fine-scale, geometrical complexities, multiphysics phenomena, and interactions between different species were considered, and each fine-scale domain was assigned to a macroscopic finite element for the coarse scale solution.

**Characterization of SEI layer.**  $\text{LiMn}_2\text{O}_4$  powders were used as the cathode active materials. A slurry was prepared by mixing 90 wt % of the powder, 5 wt % of carbon black, and 5 wt % of a polyvinylidene fluoride binder dissolved in anhydrous N-methyl-2-pyrrolidinone. The slurry was cast on an aluminum foil. The composite electrode was then dried in the vacuum oven at  $110^\circ\text{C}$  for 24 h. The reference electrolyte solution was 1.0 M lithium hexafluorophosphate ( $\text{LiPF}_6$ ) dissolved in a mixture of ethylene carbonate (EC) and dimethyl carbonate (DMC) with a volume ratio of 1:1. VEC-containing electrolyte and

FEC-containing electrolyte were prepared by adding 5 wt % of VEC and FEC into the reference electrolyte solution, respectively. Coin-type half cells ( $\text{LiMn}_2\text{O}_4$ /lithium) were assembled in an Ar-filled glove box. A cycling test was galvanostatically performed at a rate of 0.14 C for the first three cycles and 0.25 C for the subsequent cycles using charge-discharge equipment. The cells (no additive-containing cells, FEC containing cells) were cycled 50 times at room temperature, followed by 30 times at  $50^\circ\text{C}$ . ICP-OES was used to measure the amount of Mn dissolution.

## Results

**Intercalation- and misfit-induced stress in the graphite electrodes.** Figure V - 182a shows that the stress intensity factor increases as crack thickness increases. Also, cracks can propagate through the SEI thickness before being arrested at the interface. At this point, a connected channel can be created. Figure V - 182b shows the channeling criteria. The lines represent relative  $K_{IC}$  values to 2  $\text{MPa}\cdot\text{m}^{-1/2}$  (a) 1.15 (b) 1.12 (c) 1.10 (d) 1.05.

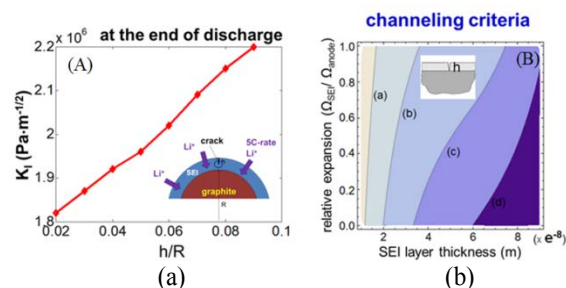


**Figure V - 182:** (a) stress intensity factor (b) channeling criteria

Figure V - 183a (next page) shows the misorientation distribution for 5 different cases and the Li concentration distribution for case 1 and case 5, with the single grain case as the reference. Each misorientation distribution for each case was averaged with 5 different random generations. As the mean misorientation angle was increased, the concentration distribution became more irregular, as seen in the figure. As a result, the relative maximum principal stress was increased as the misorientation angle increased, as shown in Figure V - 183b.

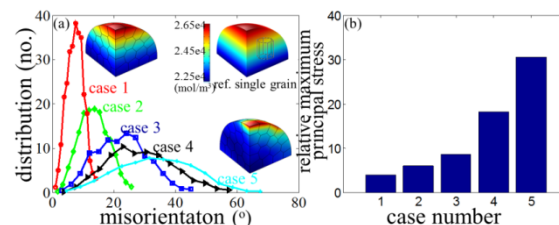


**Figure V - 183:** (a) misorientation distribution (b) relative max. principal stress

Figure V - 184a shows the normal probability of each case, and Figure V - 184b shows the maximum principal stress, with the dotted-blue line indicating the case of

random angle distribution and the solid-green line indicating the case of controlled angle distribution ( $<10^\circ$ ). The maximum stress increased as the angle was more irregular due either to random selection or increase of the grain number. This tendency coincided with the previous result: that maximum principal stress was increased as the misorientation angle increased.

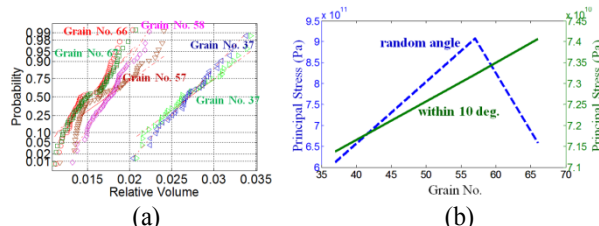


Figure V - 184: (a) probability, (b) relative max. principal stress

Figure V - 185 shows the voltage profile during 1C cell discharge. As shown in the figure, the case of the single-grain particle results in lower capacity compared to the case of multiple-grain particles. This is due usage limitations of the particle in local regions: Li-ions cannot intercalate effectively through the basal plane of the graphite.

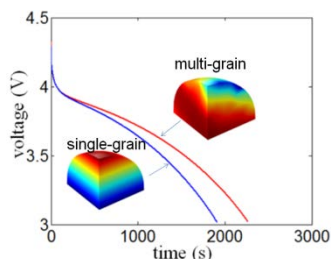


Figure V - 185: Voltage profiles from a single-grain particle (blue) and a multi-grain particle (red)

**Multiscale modeling with self-assembly and dissolution.** The variational multi-scale simulation (VMS) model for Li-ion batteries was validated by comparison with a direct numerical simulation (DNS) model. One particle-cluster in each electrode was modeled to reduce computational cost (Figure V - 186). The cell was discharged at a rate of 1C. As shown in Figure V - 187, cell potential (a) and the concentration profile in the particles and electrolyte (b) are almost identical.

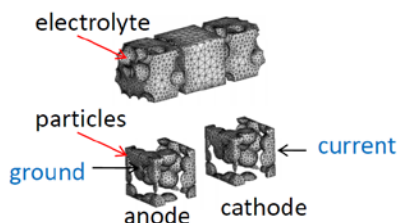


Figure V - 186: FE mesh for VMS and DNS

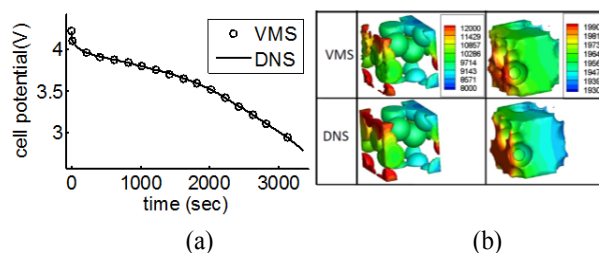


Figure V - 187: (a) Cell potential, (b) Li-ion concentration (mol/m<sup>3</sup>)

The developed VMS and the pseudo 2D model were compared based on the effective properties (Table V - 5) evaluated from a randomly generated microstructure. Even though the same material properties were used in both models, the discharge curves (Figure V - 188) from both approaches showed different patterns. This is because the VMS result included the aggregated network effect in the electrode.

Table V - 5: Effective material properties obtained from a 3D micro model.

| parameter                    | unit              | value                  |
|------------------------------|-------------------|------------------------|
| solid phase volume fraction  | -                 | 0.4104                 |
| specific surface area        | 1/m               | $1.26 \times 10^3$     |
| solid phase tortuosity       | -                 | 1.2803                 |
| electrolyte phase tortuosity | -                 | 1.2307                 |
| ionic diffusivity            | m <sup>2</sup> /s | $1.64 \times 10^{-11}$ |
| electronic conductivity      | S/m               | 0.9514                 |
| parameter                    | unit              | value                  |
| solid phase volume fraction  | -                 | 0.4104                 |
| specific surface area        | 1/m               | $1.26 \times 10^3$     |
| solid phase tortuosity       | -                 | 1.2803                 |
| electrolyte phase tortuosity | -                 | 1.2307                 |
| ionic diffusivity            | m <sup>2</sup> /s | $1.64 \times 10^{-11}$ |
| electronic conductivity      | S/m               | 0.9514                 |

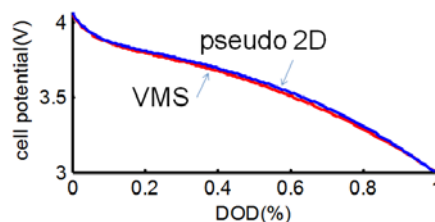
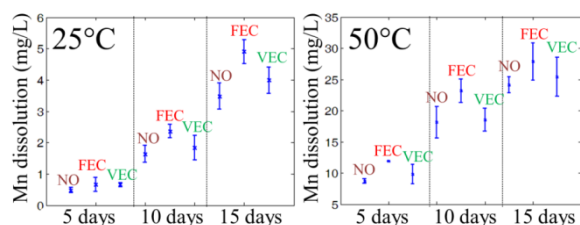


Figure V - 188: 1C discharge curves predicted by multi-scale and pseudo 2D model.

**Effects of additive on Mn dissolution.** Surface layers were formed in the electrolyte with different additives (5 wt % FEC and 5 wt % VEC) over five days. The amount of Mn dissolution was then observed as a function of time at different temperatures. As shown in Figure V - 189, Mn dissolution increased as both the temperature and the storage time increased. Also, the FEC-derived surface layer clearly resulted in relatively significant Mn dissolution compared to the normal (without additive) surface layer. However, the VEC-derived surface layer showed less effect on Mn dissolution compared to the normal surface layer.



**Figure V - 189:** Quantity of Mn dissolution as a function of storage time at (a) 25°C and (b) 50°C

To clarify the negative effect of FEC on cathode, half-cell (LMO/Li) cycling performance is compared with/without 5 wt % of FEC additive. FEC additive (5%) was added to the 1M LiPF<sub>6</sub> EC/DMC(1:1 v/v) solution. The cells were cycled 45 times at room temperature, then cycled 10 more times at 50°C. The additive FEC had little influence on capacity fade at room temperature (Figure V - 190a). At high temperatures, however, the added FEC clearly affected capacity fade (Figure V - 190b). Based on the previous ICP results, the additive FEC resulted in the acceleration of Mn dissolution. The combined results imply that the FEC additive is advantageous for generating a stable SEI layer on the anode at high temperatures. However, it can also result in aggravated Mn dissolution on the cathode at high temperatures. This may be related to the HF attack. FEC can lose HF molecules to form VC molecules, and the HF can increase Mn dissolution.

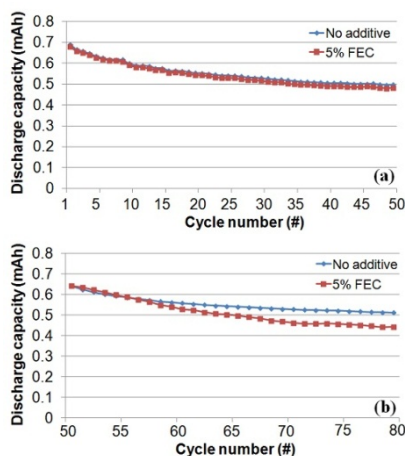


**Figure V - 190:** Discharge capacity retention at 25°C (a) and 50°C (b)

## Conclusions and Future Directions

Stress and fracture analysis considering anisotropic features of graphite material and misfit between the graphite material and SEI layer have revealed the effects of the grain orientation and grain size on the maximum stress level. Also, the extension of analysis to the cell-level scale has demonstrated the effects of the grain boundary on cell performance. This study can be further extended to examine the relationship between the anisotropic features of graphite materials and SEI layer formation.

The Li-ion battery cell performance with respect to microstructures has been explored using the macro-/micro-coupled variational multiscale simulation model. The developed multi-scale model (VMS) was well matched with the DNS model. Also, the VMS model has demonstrated that the microscopic particle network plays an important role in characterizing battery performance. The developed model will be utilized in studying of degradation at microscale.

The combined ICP-OES measurement and cycling test have revealed that while the FEC additive may be suggested as a good SEI layer stabilizer, it has a negative effect on the cathode side, resulting in acceleration of Mn dissolution. In order to clarify the effects of additives on both the anode and cathode interfaces, further electrochemical measurement, such as EIS, will be conducted with three-electrode cells.

## FY 2012 Publications/Presentations

1. M. Zhu, J. Park, and A.M. Sastry, "Fracture Analysis of the Cathode in Li-Ion Batteries: A Simulation Study", *Journal of the Electrochemical Society*, **159** (4), pp. A492-498 (2012).
2. S. Lee, J. Park, M. Zhu, A.M. Sastry, "Variational multi-scale enrichment for electrochemical-mechanical Li-ion battery cell," *221st ECS Meeting*, May, 2012, Seattle, WA.
3. J. Park, M. Zhu, Y.-K. Lee, S. Han, H. Shin, S. Lee, W. Lu, and A.M. Sastry, "Degradation modeling of Li-ion battery cells" *16th International Meeting on Lithium Batteries*, Jeju, South Korea (2012).
4. H. Shin, J. Park, W. Lu, and A.M. Sastry, "The effects of temperature on the formation/growth of the SEI layer near the anode surface" *16th International Meeting on Lithium Batteries*, Jeju, South Korea (2012).

## V.E.3 Mathematical Modeling of Next-generation Li-ion Chemistries (LBNL)

Venkat Srinivasan  
Lawrence Berkeley National Laboratory  
1 Cyclotron Rd. MS 70R0108B  
Berkeley, CA 94720  
Phone: (510) 495-2679; Fax: (510) 486-4260  
E-mail: [vsrinivasan@lbl.gov](mailto:vsrinivasan@lbl.gov)

Start Date: October 1, 2008  
Projected End Date: September 30, 2012

### Objectives

- Predict behavior of thick porous electrodes under PHEV operating conditions.
- Estimate transport properties of liquid electrodes.
- Understand and model the mechanical degradation in battery electrodes.

### Technical Barriers

- Low energy efficiency; low calendar/cycle life; high cost.

### Technical Targets

- Available energy: 56 Wh/kg (10 mile) and 96 Wh/kg (40 mile).
- 10-s discharge power: 750 W/kg (10 mile) and 316 W/kg (40 mile).

### Accomplishments

- Quantified the liquid phase limitations in porous cathodes and understood the effect of thickness and porosity.
- Measured the activity coefficient as a function of concentration in LiPF<sub>6</sub> in EC:DEC (1:1 by weight).
- Extended mechanical degradation models of particles to include the binder.



### Introduction

High energy density and long cycle life are critical for reducing cost of ownership of vehicles powered by Li-ion batteries. One possible way of achieving high energy densities is by using thick porous electrodes. However, operating the battery at high charge, discharge rates results in transport limitations in the electrolyte phase of such electrodes. In addition, mechanical degradation results in severe capacity fade which in turn reduces the cycle life of batteries. This problem is particularly pronounced in silicon anodes (which have an order of magnitude higher

theoretical capacity than existing carbon anodes) where large volume expansions occur due to Li lithiation and delithiation. The goal of this project is to develop continuum mathematical models and controlled experiments to: (a) better understand mass transport in porous electrodes; (b) investigate mechanical degradation mechanisms in Li ion batteries.

### Approach

**Porous-electrode-scale study.** Rate limitations from the porous electrode were studied by using the macro-homogeneous model developed by Newman and coworkers. The Li diffusion coefficient inside the NMC particles obtained from the particle-scale study was applied in the porous-electrode model. The electrolyte transport properties, i.e., diffusivity and conductivity for LiPF<sub>6</sub> in EC/DEC (1/1 by weight), were taken from the literature (Stewart and Newman, 2008) and corrected by the Bruggeman relation. Also, a series of experiments were performed on NMC electrodes of varying thickness with similar porosity and of varying porosity with similar thickness to understand the deviation of model predictions from the experimental data.

**Transport properties.** According to Onsager reciprocal relations, there are  $n(n-1)/2$  independent transport properties, where  $n$  is the number of species in the electrolyte. If the solvent mixture (EC and DEC) is treated as a single species, the number of transport properties become three: (a) conductivity; (b) salt diffusion coefficient; (c) transference number. In addition to these three properties, the salt activity coefficient (which is a thermodynamic property) also needs to be measured. The salt diffusion coefficient and the transference number determine the concentration gradients that form under polarization whereas the salt activity coefficient determines the concentration overpotential resulting from the gradient.

The functionality of the salt activity coefficient as a function of concentration was obtained using a concentration cell. The cell consisted of two separate chambers that were separated by a glass frit to prevent rapid mixing of the electrolyte. The concentration in one of the chambers was kept constant at 2M whereas in the other chamber it was varied in between 0.2M to 2M. The open circuit voltage was measured for each concentration and lithium metal was used as the electrode in the experiments.

A diffusion cell has been designed and work is in progress to measure the other transport properties of the electrolyte using the restricted diffusion and galvanostatic polarization methods.

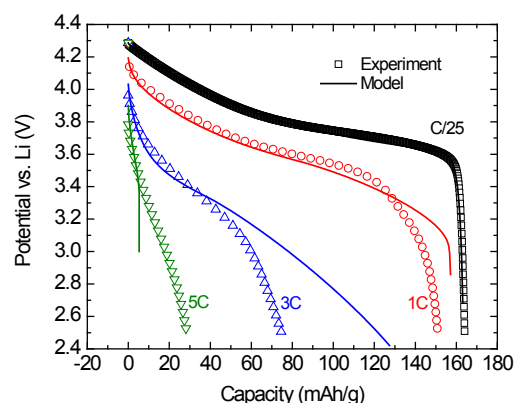
**Stress study.** Christensen and Newman (2006) describe a large-deformation model for a spherical

electrode particle undergoing lithiation and delithiation and incorporating pressure-driven diffusion. This model has been implemented as a finite-volume method and with an alternative coordinate transform, requiring extensive changes to the original equations but allowing for the relatively straightforward addition of a surrounding binder layer. Displacement and stress are guaranteed to be continuous at the particle-binder interface, and the material properties of the particle and binder, as well as binder thickness, are easily specified by users. This implementation has also included the effect of composition on the Young's modulus and Poisson's ratio in the lithiated silicon particle, as described by Shenoy, Johari and Qi (2010). Finally, this implementation interfaces with standard open-source data storage libraries to generate data files that are easily accessible by other researchers.

Insight gained through exploring this model suggested that a fundamentally new model be developed for materials such as lithiated silicon, in which the inserted material presumably experiences the same stress as the surrounding host material--the model of Christensen and Newman, on the other hand, may be more suitable for intercalation materials. The development of this new model has drawn from both finite deformation solid mechanics and classical thermodynamics.

## Results

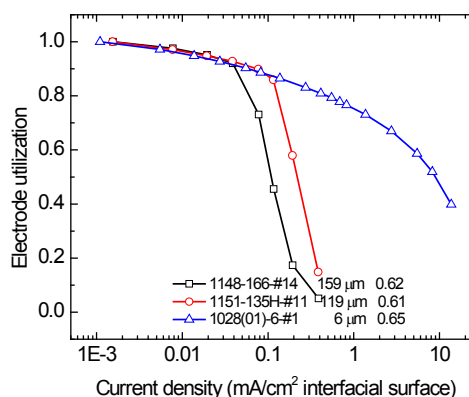
**Porous-electrode-scale study.** The model-experiment comparison of the electrode potential at different discharge rates is shown in Figure V - 191. The typical value of the Bruggeman coefficient used in the literature is 1.5. The simulation obtained using this value did not fit the experimental data. Decreasing the effective diffusion coefficient and conductivity by increasing the Bruggeman coefficient from 1.5 to 3.0 improves the model predictions but still cannot fit the experimental data at the rate of 3C. To understand experimentally the cell limitation, the transport resistance in the electrolyte was increased by increasing the electrode thickness.



**Figure V - 191:** Model-experiment comparisons at various discharge rates. The experimental data (dots) was obtained on a NMC electrode with a

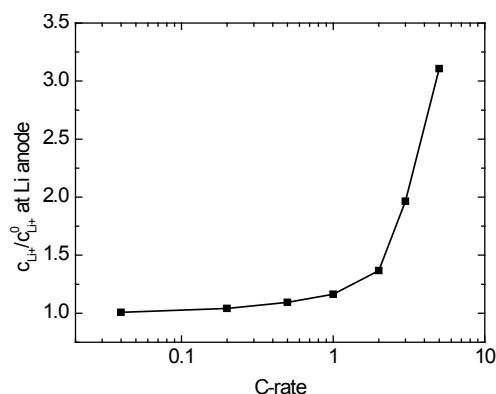
thickness 159  $\mu\text{m}$  and porosity of 0.62. The calculated potentials (lines) were obtained using the Bruggeman coefficient of 3.0.

Figure V - 192 shows the electrode utilization for three different thicknesses a function of current density based on the interfacial area of NMC particles. All the electrodes show a gradual decrease in electrode utilization when the applied current is small. This was previously shown to be caused by the decrease in the diffusion coefficient of Li in the solid cathode particles toward the end of discharge. As the current density was increased further, the thicker electrodes show a rapid capacity loss. This suggests that the electrode limitation has changed as thickness increases. However, as the total current also changes when the thickness is changed, it is not clear where this limitation occurs.



**Figure V - 192:** Experimental capacity of NMC electrode as a function of discharge current density based on the interfacial area of active material.

To further examine the cause of the electrode limitation, the concentration distribution in the solution phase was calculated using the porous-electrode model. Figure V - 193 shows the calculated  $\text{Li}^+$  concentration at the Li-metal counter/reference electrode at different rates. The simulation results indicate that the current densities on these electrodes could lead to a large concentration buildup on the Li anode, possible inducing the saturation of salt, and could be the cause of the utilization drop seen on the thick electrodes.



**Figure V - 193:** Calculated  $\text{Li}^+$  concentration at the Li-metal counter/reference electrode at different discharge rates. The initial  $\text{Li}^+$  concentration ( $c_{\text{Li}^+}^0$ ) is 1 M.

However, replotting Figure V - 192 as the electrode utilization against the current density based on the cross-sectional area of the porous electrode (Figure V - 194) shows an apparent deviation of the thick electrodes from the thin electrode at the same current density. This deviation suggests that the limitation occurs on the electrolyte phase within the porous electrode, rather than the Li-metal electrode. The model's inability to predict the experimental data is due to the lack of knowledge in the electrolyte transport properties. While the calculated salt concentration was over 3 M at a rate of 5C as seen in Figure V - 193, the concentration dependency of electrolyte transport properties reported in the literature is rarely beyond 2 M. For the salt used in the present study,  $\text{LiPF}_6$  in EC/DEC (1/1 by weight), the diffusion coefficient reported by Stewart and Newman (2008) showed a great error bar at the concentration of 1 M. Therefore, to improve the model predictions it is crucial to investigate the transport properties of the battery electrolyte.

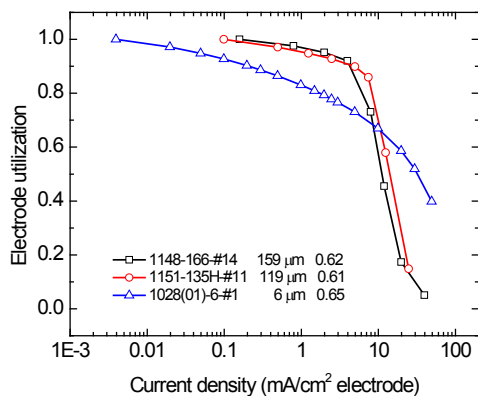


**Figure V - 194:** Experimental capacity of NMC electrode as a function of discharge current density based on the cross-sectional area of the porous electrode.

**Transport Properties.** Figure V - 195 shows the thermodynamic factor as a function of concentration for  $\text{LiPF}_6$  in EC:DEC (1:1 by weight). This curve was calculated from the open-circuit voltage data obtained from the concentration cell. A concentration dependent fit

for the thermodynamic factor was obtained from the Debye Huckel theory for concentrated solutions.

$$1 + \frac{d \ln f}{d \ln c} = 1 + c \left[ \frac{-1.0178}{2(1 + 0.9831\sqrt{c})} \left( \frac{1}{\sqrt{c}} - \frac{0.9831}{(1 + 0.9831\sqrt{c})} \right) - 2.54898\sqrt{c} + 0.58685 c + 2.05021 c^{\frac{3}{2}} - 0.50322 c^2 + 1.5842 \right]$$

In the above expression,  $c$  is in M. For comparison, Figure V - 195 also shows the thermodynamic factor for  $\text{LiPF}_6$  in EC:EMC (1:1 by weight) as measured by Stewart and Newman (2008) and  $\text{LiPF}_6$  in PC:EC:DMC as measured by Valoen and Reimers (2005).

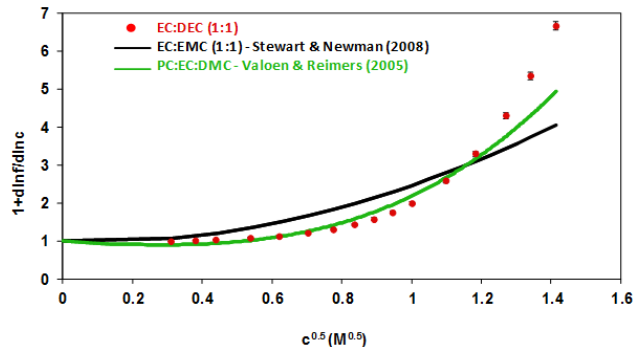


**Figure V - 195:** Thermodynamic factor ( $1 + d \ln f / d \ln c$ ) as a function of concentration for  $\text{LiPF}_6$  in EC:DEC (1:1), EC:EMC (1:1) and PC:EC:DMC.

At infinite dilution (where the thermodynamic factor is unity), the slope of open-circuit voltage vs. concentration curve obtained from the concentration cell data gave the transference number of  $\text{LiPF}_6$  in EC:DEC (1:1 by weight) to be 0.38. This number is very close to the transference number obtained for  $\text{LiPF}_6$  in EC:EMC (1:1 by weight), Stewart and Newman (2008) and  $\text{LiPF}_6$  in PC:EC:DMC, Valoen and Reimers (2005).

In future, the diffusion coefficient will be measured using restricted diffusion method. In this technique free standing  $\text{LiPF}_6$  in EC:DEC (1:1 by weight) will be placed between Li-Li electrodes. Constant current will be passed for certain time, which will build up a concentration gradient. The current will then be stopped and the cell potential would be monitored during this open-circuit relaxation period. Chapman and Newman (1980) have shown that at long relaxation times the slope of  $\ln V$  vs. time curve is a straight line, which is proportional to the salt diffusion coefficient at that particular electrolyte concentration. The procedure will be repeated for different electrolyte concentrations and at different polarization times to check for reproducibility. Using the method of

restricted diffusion the salt diffusion coefficient can be obtained independently i.e., without the use of any other transport property.

The transference number will be measured using galvanostatic polarization. In this technique free standing  $\text{LiPF}_6$  in EC:DEC (1:1 by weight) will be placed between Li-Li electrodes and constant current will be passed for certain time. The polarization time chosen would be such that the concentration fronts on each side of the Li electrodes do reach the center of the cell. In other words the system would be solved with a semi-infinite boundary condition. Current would then be stopped and the cell potential would be monitored during this open-circuit relaxation period. For a given electrolyte concentration, this procedure would be repeated several times to obtain a slope  $m$  of the straight line of  $\Delta\Phi$  vs.  $It^{1/2}$ , where  $\Delta\Phi$  is the open circuit voltage,  $I$  is the current density and  $t$  is the polarization time. An accurate extrapolation method of obtaining  $m$  as shown by Hafesi and Newman (2000) will be used. By the value of salt diffusion coefficient obtained from the restricted diffusion experiments, open circuit data obtained from the concentration cell experiments and the value of  $m$  obtained from the galvanostatic polarization technique, the transference number will be calculated.

**Stress study.** The finite-volume method simulation of the particle-binder system, based on Christensen and Newman's large-deformation particle model, yields accurate results that are consistent with an implementation of the original equations, even at much lower spatial resolutions than used by Christensen and Newman. However, radially-symmetric models cannot describe the full range of particle-binder interactions that are likely sources of mechanical damage, so this implementation must be coupled with additional modes of particle-binder interaction in order to provide a more comprehensive understanding of mechanical damage in porous electrodes.

Thermodynamic relations forming the foundation of the new large deformation model for lithiated silicon have been developed, and the relationship between potential and stress has been explored in a reanalysis of existing data (Sethuraman, et al., 2010). This relationship has been incorporated into the modified kinetic expression proposed by Monroe and Newman (2004)--their modified Butler-Volmer equation is stress-dependent, although its application involves an assumption of small material deformation. Additional equations consistent with the new thermodynamic framework will be developed to describe dynamic phenomena such as diffusion and inelastic deformation, with the goal of producing a comprehensive set of equations suitable for dynamic simulation.

## Conclusions and Future Directions

**Porous-electrode-scale study.** Experimental results obtained from the thin and thick NMC electrodes indicated that the electrode limitation occurs on the solution phase within the porous electrode, rather than the Li-metal anode. The comparison of the model to the experiment shows that the model's inability to predict the data is due to the lack of knowledge in the electrolyte transport properties. Therefore, future work will be focused on understanding the transport properties of the electrolyte and to improve the mathematical model.

**Stress study.** It is anticipated that the two present lines of inquiry will converge in the next year. With the eventual goal of describing mechanical damage at the porous electrode level, the spherical electrode particle model based on Christensen and Newman's work will provide estimates of local stresses for insertion materials. A similar implementation based on new dynamic equations would describe materials such as silicon. These radially-symmetric implementations will be complemented with simple models of particle-binder systems in different geometries and of mechanical interactions among particles within a porous electrode. In combination, these should allow one to estimate rates of mechanical damage accumulation in porous electrodes constructed from a wide range of materials.

## FY 2012 Publications/Presentations

1. S.-L. Wu, W. Zhang, X. Song, A. K. Shukla, G. Liu, V. Battaglia, and V. Srinivasan, "High Rate Capability of  $\text{Li}(\text{Ni}_{1/3}\text{Co}_{1/3}\text{Mn}_{1/3})\text{O}_2$  Electrode for Li-Ion Batteries," *J. Electrochem. Soc.*, 159(2012), A438-A444.

---

## V.E.4 Analysis and Simulation of Electrochemical Energy Systems (LBNL)

John Newman  
Lawrence Berkeley National Lab  
Environmental Energy Technologies  
1 Cyclotron Road MS: Hildebrand  
Berkeley, CA 94720  
Phone: (510) 642-4063; Fax: (510) 6424478  
E-mail: [newman@newman.cchem.berkeley.edu](mailto:newman@newman.cchem.berkeley.edu)

Start Date: October 1, 2008  
Projected End Date: September 30, 2012

### Objectives

- Develop experimental methods for measuring transport, thermodynamic, and kinetic properties.
- Model electrochemical systems to optimize performance, identify limiting factors, and mitigate failure mechanisms.

### Technical Barriers

This project addresses the following technical barriers from the USABC:

- (A) Capacity and power fade
- (B) Safety and overcharge protection
- (C) Low calendar/cycle life

### Technical Targets

This project contributes to the USABC Requirements of End of Life Energy Storage Systems for PHEVs and EVs:

- 300,000 shallow discharge cycles
- 15 year calendar life

### Accomplishments

- Obtained ferrocene kinetic measurements of SEI on HOPG.
- Compared through-film ferrocene kinetics for SEI formed in presence of VC and FEC.
- Developed model to explain current-time curves for film formation.

◇ ◇ ◇ ◇ ◇

### Introduction

In FY12 the main project was the experimental study of SEI formation reactions and the interaction of the SEI with redox shuttles. Our novel method of SEI characterization contributes to understanding of

passivation in nonaqueous electrolytes, which is, in turn critical to battery performance and lifetime. Additionally, studies were expanded from glassy carbon, a model surface, to highly-oriented pyrolytic graphite (HOPG), which more accurately resembles the carbon found in a lithium-ion battery. The ferrocene kinetic measurements on HOPG were obtained and compared the kinetics of the through-film for SEI formed in presence of VC and FEC. Additionally, a model was developed to explain current-time curves for film formation.

### Approach

- Utilize classical electrochemistry experiments to understand the fundamental growth kinetics of the SEI, as well as how it interacts with a redox shuttle.
- Measure shuttle reduction kinetics in the presence and absence of passivating films to determine the relative transport and kinetic inhibitions to reaction.
- Use a rotating-disk electrode (RDE) to measure the steady-state through-film reduction current, and electrochemical impedance spectroscopy (EIS) to measure the frequency response of the ferrocene reaction in the presence and absence of the SEI.

### Results

Previously, our ferrocene characterization method was used to find that the SEI products formed at lower potential are inherently more passivating than those formed at higher potential. Both the through-film limiting current ( $i_{lim,r}$ ) and effective rate constant ( $k_{eff}$ ) are smaller for the same amount of formation charge when formation potential decreases. Previous work has suggested that a decrease in the film porosity is responsible for the similar trend of transport and kinetics. In this year, the study was continued and a manuscript was submitted to the Journal of the Electrochemical Society. It is currently under review. A BATT Program seminar on the subject was also given on June 11 at Lawrence Berkeley Lab.

Figure V - 196 (below) shows the porosity of the SEI calculated using either the value of  $i_{lim,f}$  or  $k_{eff}$ . Only data at 0.45 V formation are shown. The two methods both yield reasonable values, but do not agree exactly. Although adjusting the assumed thickness can improve the agreement slightly, the difference between the calculated values increases at greater amounts of formation charge. The same trends apply for data at different formation potentials (not pictured). While this disagreement may seem to contradict the explanation of decreasing porosity, the disagreement could also point to the existence of a porosity gradient through the SEI. If the porosity is smaller at the compact/porous layer interface than it is at the porous layer/ electrolyte interface, the accessible area for charge-transfer reaction will be smaller than the area limiting transport through the SEI.

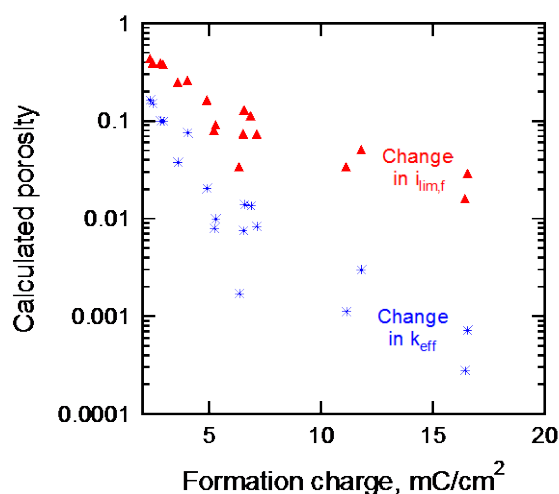


Figure V - 196: Calculated porosity of 0.45 V formation

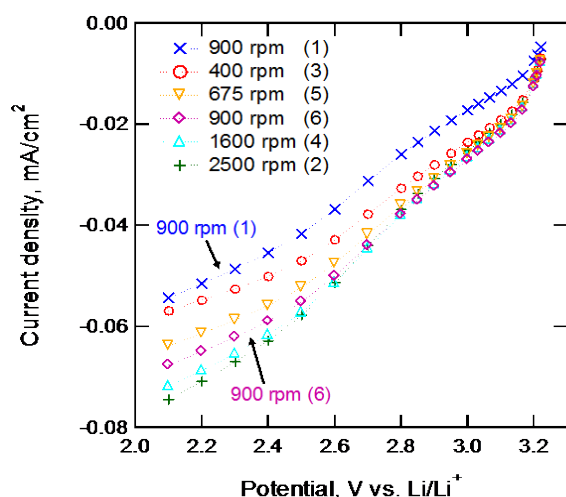
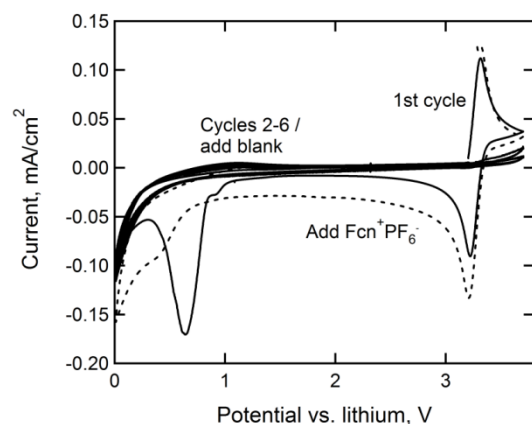


Figure V - 197: Instability of SEI formed at 0.1 V

Figure V - 197 shows another result that suggests that porosity is indeed the limiting phenomenon for through-film ferrocenium reduction. The data shown are for through-film reduction after 10 seconds of formation at 0.1

V. The order of measurement is shown in parentheses. Figure V - 197 shows that current increases with order of measurement (parentheses) and rotation speed; thus, the film is unstable. However, the open circuit potential does not change, and from fitting the curves (not pictured), both  $i_{lim,f}$  and  $i_0$  increase with time. Thus, either the thickness and the rate constant decrease simultaneously at open-circuit conditions, or the porosity increases, possibly because intermediates diffuse away and open up void space in the film.

It has been found that the SEI formed rapidly in  $\text{LiClO}_4$ -based electrolyte but slowly in  $\text{LiPF}_6$ -based electrolyte. Either differences in anion precipitation kinetics or SEI dissolution by HF, a product of  $\text{PF}_6$  decomposition, was proposed as an explanation. To understand whether the difference is caused by precipitation kinetics or HF attack, the SEI was formed in 1.0 M  $\text{LiClO}_4$  EC:DEC. 2 mM. Ferrocene was included in the electrolyte in order to monitor the electronic passivation as the SEI was formed. This experiment is shown in Figure V - 198 (next page.) Ferrocene oxidation was observed only on the first cycle, before the SEI was formed. On the first cycle to low potential, SEI reduction peaks occurred at approximately 0.9 and 0.65 V, after which they disappeared completely. After six cycles, one mL of the same electrolyte was added to the cell. The cell was gently agitated to mix the contents, and the sweep was repeated. No change was observed after adding the blank, demonstrating that introducing new electrolyte does not dissolve the SEI. Next, 1 mL of solution containing 8 mM ferrocenium hexafluorophosphate was added to the cell and the procedure repeated. The dashed line in Figure V - 196 shows that the ferrocene peak completely reappears, with the same reversible separation of peaks. Reappearance of an SEI formation peak can also be seen at 0.5 V, separate from the limiting current for ferrocenium reduction. The renewed activity for both ferrocene oxidation and electrolyte reduction demonstrates that adding hexafluorophosphate dissolves the SEI chemically, not electrochemically.



**Figure V - 198:** Adding ferrocenium hexafluorophosphate to an electrode passivated in  $\text{LiClO}_4$  causes the SEI to dissolve.

## Conclusions and Future Directions

Potentiostatic experiments show that electrochemical activity is higher on the edge than the basal plane of graphite, in agreement with literature results. At a constant potential of 0.6 V vs. lithium, current increases with increasing fractional edge plane density. Plotting formation charge vs. square root of time suggests transport-limited growth, regardless of the value of  $f_e$ . Glassy carbon exhibits similar behavior under the same conditions, although the measured value of  $f_e$  and the measured rate of film growth are not consistent with the correlation for that on HOPG. During potentiodynamic SEI formation experiments, the edge plane exhibits higher currents for both SEI formation reactions, which appear only on the first cycle, and for lithium de/intercalation currents, which reach a steady-state profile for oxidation and reduction. Future work will continue to use ferrocene to study the effect of different electrolytes on electrode passivation.

## FY 2012 Publications/Presentations

1. Maureen Tang and John Newman. *J. Electrochem. Soc.* **159** (12): A1922-A1927, 2012.
2. Maureen Tang, Sida Lu, and John Newman. *J. Electrochem. Soc.* **159** (11): A1775-A1785, (2012).
3. Maureen Tang, Kohei Miyazaki, Takeshi Abe, and John Newman. *J. Electrochem. Soc.* **159** (5): A634-A641, (2012).
4. Maureen Tang and John Newman. *J. Electrochem. Soc.* **159** (3): A281-A289, (2011)
5. *Gordon Conference for Batteries*, Mar., 4-9, 2012, Ventura CA (poster).
6. *220<sup>th</sup> ECS Meeting*, Oct., 9-14, 2011, Boston, MA. (presentation).

---

## V.E.5 Modeling - Predicting and Understanding New Li-ion Materials Using *Ab Initio* Atomistic Computational Methods (LBNL)

Kristin Persson (Chemist Research Scientist, LBNL)  
Lawrence Berkeley National Laboratory  
Advanced Energy Technology  
1 Cyclotron Rd, MS 62-0203  
Berkeley, CA 94720  
Phone: (510) 486-7218  
E-mail: [kapersson@lbl.gov](mailto:kapersson@lbl.gov)

Start Date: October 1, 2008

Projected End Date: September 30, 2012

### Objectives

- Predict new chemistries and crystal structures for improved electrodes as defined by the goals of USABC.
- Understand performance-limiting behavior in current electrode materials in order to target and design optimized materials.

### Technical Barriers

Investigating electrode materials with atomistic modeling require rigorous bench marking as well as insight into the materials chemistry and its effect on electrode performance. For example, the relevant surfaces of the electrodes are generally not well characterized in terms of chemistry and structure. Both the cathode materials as well as the graphitic anode have solid electrolyte interfaces (SEIs) that depend on the synthesis conditions as well as the electrolyte composition and the conditions under which the battery is operated. The calculations are systematically benchmarked and the assumptions under which the modeling is made are carefully monitored to make sure that the results are relevant and provide useful information and insights for electrode materials design.

### Technical Targets

- Investigate graphene and few-layer graphene for anode applications.
- Identify and elucidate the coupling – on an atomistic level - between cation ordering and performance in the high-voltage spinel.
- Find the surface structure of the manganese spinel cathode material to correlate morphology and highly reactive surfaces with performance degradation.
- Create a high-throughput computational Materials Genomic Design Center at LBNL.

### Accomplishments

- It was found that single-layer graphene does not exhibit any Li absorption on the [0001] surface (as previously proposed) – for any Li ordering - unless there are defects in the carbon structure.
- Similarly, few-layer graphene only exhibits intercalation (no surface absorption), and the Li capacity increases with the number of layers. This means that the capacity will always be inferior to that of graphite.
- Bi-layer graphene exhibits a slightly higher voltage profile due to increased ionicity in the bonding between the carbon and Li atoms.
- While the cation-disordered high-voltage Ni-Mn spinel material can transform via a Li/Va solid solution reaction for most of the Li composition range, the ordered material reacts through a very stable two-phase region. Our study shows that the more ‘uniformly’ disordered the cations are distributed in the high-voltage spinel, the better long-term cycling performance can be expected due to less strain associated with the Li intercalation process.
- The Materials Project ([www.materialsproject.org](http://www.materialsproject.org)), which was launched in Oct 2011, now has over 3,000 users and exhibits properties for more than 30,000 inorganic materials. A 5-year Materials Genome Center, recently awarded by DOE/BES will focus on data production, dissemination and materials design for functional electronic materials.



### Introduction

There is increasing evidence that many of the performance limiting processes present in electrode materials are highly complex reactions occurring on the atomic level. The Persson group at LBNL is studying these processes using first-principles density-functional theory modeling tools. By understanding the underlying reasons for the electrode materials working performance improvements can be suggested or design schemes directed at the root cause of the process.

During this project cycle, first studied was graphite. It was found that it exhibits excellent inherent diffusivity, which should make possible very high rate anodes with the right surface and electrode engineering. It was also found that the most stable surface in graphite – the 0001 facet –

does not absorb Li in its perfectly crystalline defect-free state. This presents a significant kinetic bottleneck for Li intercalation. As nano-engineering has been shown to drastically change materials properties, this year single and few-layer graphene was investigated for enhanced Li reactivity as compared to graphite.

Work on the Li manganese spinel surface structures, as a first step towards understanding the different surface reactivities as a function of the surface orientation, was concluded. This project generated the thermodynamic stable morphology of the  $\text{LiMn}_2\text{O}_4$  particle as well as lithium voltage profiles for the low-index surface facets.

A collaborative study within the BATT focus group on the high-voltage spinel was also concluded this year. A strong coupling between the Li arrangement and the underlying cation lattice which results in a different response (voltage profile as well as phase transformation mechanism) of the material when synthesized under different conditions was elucidated. Furthermore, the Li/Va arrangement as a function of temperature was investigated, as well as the Li kinetics as a function of cation order.

Finally, the Materials Project ([www.materialsproject.org](http://www.materialsproject.org)) was successfully launched. The Materials Project is a freely available materials design resource encompassing over 30,000 inorganic materials. The Center has already attracted over 3,000 users and continuously incorporates more data, analysis and design capabilities.

## Approach

The Persson group uses atomistic modeling to study the relevant thermodynamic and kinetic processes. The calculations are performed on the Lawrence Livermore cluster at LBNL and at NERSC. In the case of the high voltage spinel first-principles zero-temperature calculations and a coupled cluster expansion have been used to establish the relationship between the cation order and the electrochemical signature of the materials.

For the investigation on the carbonaceous anode materials and the high-voltage spinel systems, a combination of density-functional theory is being used to describe the low temperature characteristics of the material as well as statistical mechanics to calculate the phase diagram and the Li chemical diffusivity. For the Li-carbon systems phenomenological models have also been incorporated to capture the van der Waals interactions.

## Results

**The  $\text{Li}_x\text{Ni}_{0.5}\text{Mn}_{1.5}\text{O}_4$  Spinel.** As part of the high-voltage spinel focus effort in the BATT group the cation ordering influence on the performance as a function of Li content in the  $\text{Li}_x(\text{Ni}_{0.5}\text{Mn}_{1.5})\text{O}_4$  spinel was investigated. Monte Carlo simulations show that the ordered cation arrangement has a strong two-phase reaction which

persists to high temperatures (see Figure V - 199), while the more ‘cation-disordered’ material favors a solid solution reaction mechanism across most of the Li composition range. Since a solid solution reaction is generally associated with less strain in the material (as compared to a two-phase reaction) during cycling, the disordered material is considered superior in this aspect. Li diffusion as a function of cation ordering was also investigated and it was found that the high-voltage spinel has intrinsically very high rate capability, irrespective of cation ordering.

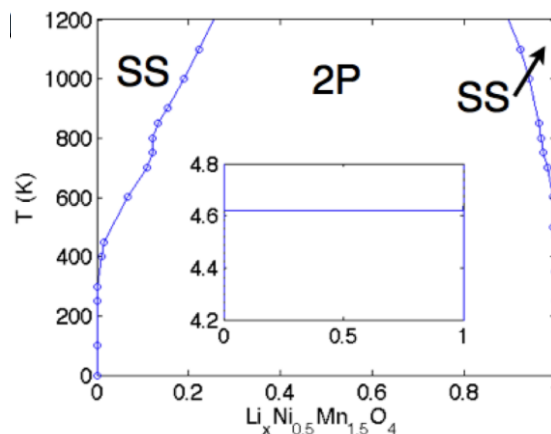


**Figure V - 199:** Li/Vacancy phase diagram for the ordered high-voltage spinel and voltage profile at RT (see inset).

**Carbonaceous Anode Materials.** Our study of Li absorption on graphite surfaces has been concluded. It was found, in agreement with experimental evidence, that the 0001 surface is the most thermodynamically stable surface. More surprisingly it was also found that Li does not absorb on the predominant 0001 surface, if that surface is defect-free.

Furthermore, the Li absorption and intercalation was studied as a function of increasing number of layers of graphene and Li content. It is predicted that there exists no Li arrangement, which stabilizes Li absorption on the surface of single layer graphene unless that surface includes defects. From this result follows that defect-poor single layer graphene exhibits significantly inferior capacity compared to bulk graphite. For few layer graphene, the same results hold but intercalation is possible. However, the intercalation process does not reach stage I until the layers increase in number and become bulk-like, which means that the capacity for the nano-phase will always be inferior to that of bulk graphite. Interestingly, bi-layer graphene has a different bonding character between the Li and the C, which results in a slightly higher voltage profile. These results were recently published in Nanoletters [2].

**The  $\text{LiMn}_2\text{O}_4$  Spinel Surface Morphology.** The  $\text{LiMn}_2\text{O}_4$  spinel system exhibits charge-ordering and magnetic ordering among the  $\text{Mn}^{3+}$  and  $\text{Mn}^{4+}$  as well as

Jahn-Teller distortion on the  $Mn^{3+}$  sites. Once a satisfactory bulk description was obtained, surface calculations were approached, using the ground state bulk magnetic and electronic state as a starting point. Many different terminations and reconstructions - exploring O, Mn, Li and combinations thereof - of the low-index surfaces and their electronic structure were calculated and evaluated for stability using both GGA and GGA+U. Using the most stable surface configurations, we were able to predict the thermodynamically stable morphology of  $LiMn_2O_4$ , (see Figure V - 200.) As can be seen from the figure, the favorable shape is a cuboctahedra with predominant [111] surface facets, in agreement with numerous reports for compounds with the spinel phase. Surface voltage profiles and the electronic structure of the surfaces were also obtained.

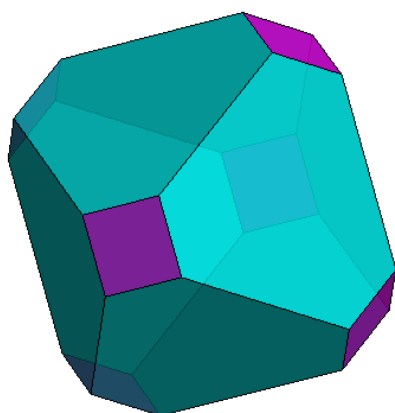


**Figure V - 200:** The calculated  $LiMn_2O_4$  particle equilibrium cubo-octahedral shape with majority (111) facets (aqua) and minority (100) facets (purple) from the calculated (GGA+U) surface energies.

**The Materials Project.** In October 2011, the first Materials Project web site and database ([www.materialsproject.org](http://www.materialsproject.org)) was successfully launched. Today, the web site has over 3,000 registered users and provides free searchable access to general materials properties covering >30,000 inorganic compounds and the number of compounds increases continuously. The site contains tools ('apps') designed to aid in materials design for specific application areas such as Li-ion battery technology. For example, the Li BATT App contains over 400 intercalation materials and over 14,000 conversion materials, which are available with computed voltage profiles, capacities, Li sites, oxygen evolution as a function of charge etc. The Materials Project was recently awarded one of the Materials Genome DOE/BES Centers and through this funding will expand into new areas of materials design and capabilities.

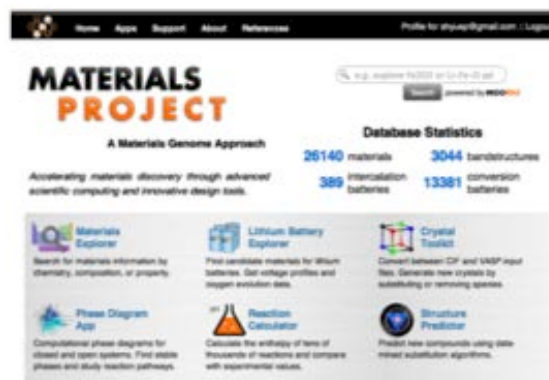


**Figure V - 201:** The Materials Project front page ([www.materialsproject.org](http://www.materialsproject.org)).

## Conclusions and Future Directions

For the high voltage spinel system, it has been demonstrated that the reaction with Li follows a two-phase behavior for the ordered spinel with increasing solid solution reactions as a function of cation disorder. Also, it was found that the intrinsic Li diffusivity enables very high rate (> 100C) but is rather insensitive to the cation ordering. Hence, the disordered high-voltage spinel is considered a better match for vehicle applications as it will exhibit better cyclability combined with excellent rate capability.

For single and few layer graphene, there is no Li absorption on the surface for any Li ordering. Few layer graphene intercalates Li at higher stages for potentials comparable to graphite but the capacity is always lower than for graphite.

The equilibrium morphology of the Li manganese spinel was derived, which yielded a cubo-octahedral shape, in agreement with most experimental results for the spinel system.

Finally, the Materials Project has over 3,000 registered users since its launch in Oct 2011 and comprises the calculated energy storage properties of more than 400 Li intercalation compounds, 14000 Li conversion compounds and general materials properties for more than 30,000 inorganic compounds.

This concludes the Persson 2008 BATT project.

## FY 2012 Publications/Presentations

1. 2012 DOE Annual Peer Review Meeting Presentation.
2. Eunseok Lee and Kristin A. Persson, "Li Absorption and Intercalation in Single Layer Graphene and Few Layer Graphene by First Principles," *Nanoletters*, DOI: 10.1021/nl3019164, (2012).
3. Kristin A. Persson, Bryn Walldwick, Predrag Lazic, and Gerbrand Ceder, "Prediction of Solid Aqueous Equilibria: An Effective Scheme to Combine First-Principles Solid Calculations with Experimental Aqueous States," *Physical Review B Phys. Rev. B* **85**, 235438 (2012).
4. Göran Grimvall, Blanka Magyari-Köpe, Vidvuds Ozolins, Kristin A. Persson, "Lattice Instabilities in Metallic Elements," *Reviews of Modern Physics*, Rev. Mod. Phys. **84**, 945–986 (2012).
5. Eunseok Lee and Kristin A. Persson, "Revealing the Coupled Cation Interactions behind the Electrochemical Profile of  $\text{Li}_x\text{Ni}_{0.5}\text{Mn}_{1.5}\text{O}_4$ ," *Energy Environ. Sci.* **5**, 6047-6051, (2012).
6. The Materials Project – *YESS Symposium*, Berkeley CA Jan. 2012 (Invited).
7. "The Materials Project – A Materials Genome Approach," *The Advanced Manufacturing Workshop*, Berkeley CA Dec. 2011 (Invited).
8. "The Materials Project – A Public Materials Design Platform," *Harnessing the Materials Genome*, Vail, September 2012 (Invited).
9. "Towards Rechargeable Magnesium Batteries," oral 10-min highlight presentation, *IMLB South Korea* 2012.
10. "Prediction of Solid - Aqueous Equilibria for Materials Design," *ModVal 9*, Switzerland April 2012.
11. "First-principles design of multivalent energy storage materials," *Molecular Foundry User Meeting*, Oct 2012 (Invited).

## V.E.6 New Electrode Designs for Ultra-high Energy Density (MIT)

Yet-Ming Chiang  
Massachusetts Institute of Technology  
Department of Materials Science and Engineering  
Room 13-4086  
77 Massachusetts Avenue  
Cambridge, MA 02139  
Phone: (617) 253-6471; Fax: (617) 253-6201  
E-mail: [ychiang@mit.edu](mailto:ychiang@mit.edu)

Subcontractor: Antoni P. Tomsia, LBNL

Start Date: May 1, 2010

Projected End Date: December 31, 2012

active material (positive and negative combined); automotive-grade cells have even lower utilization. The high intrinsic energy density of lithium-ion couples is therefore significantly diluted by inactive materials, limiting lithium-ion battery specific and volumetric energies. While a great deal of past and ongoing research is focused on the discovery of new active materials and cell chemistries as a route to increased energy, there has been proportionally less effort on new cell designs that can leapfrog existing technology by reducing inactive fraction. The objectives of this project are to develop a scalable, high density, binder-free electrode fabrication approach to enable rechargeable lithium batteries of increased active materials utilization.

### Objectives

- Develop a scalable high density binder-free low-tortuosity electrode design and fabrication process to enable increased cell-level energy density compared to conventional Li-ion technology for a range of electrode-active materials.
- Characterize transport properties in high voltage Ni-Mn spinel.

### Technical Barriers

- Low energy density and poor cycle life of EV battery systems.

### Technical Targets

- EV: 200 Wh/kg; 1000 cycles (80% DoD)

### Accomplishments

- Determined mesoscale porosity distributions theoretically and experimentally that minimize net tortuosity and maximize rate capability for electrodes of a given energy density.
- Applied directional freeze-casting method to  $\text{LiNi}_{0.5}\text{Mn}_{1.5}\text{O}_4$  and  $\text{Li}(\text{Ni},\text{Co},\text{Al})\text{O}_2$ .
- Conducted electronic and ionic transport measurements on sintered  $\text{LiNi}_{0.5}\text{Mn}_{1.5}\text{O}_4$  that shed light on rate-limiting chemical diffusion mechanisms.



### Introduction

The well-established laminated cell construction and manufacturing paradigm for current lithium-ion batteries has recognized limitations in the mass and volume utilization of active material that is possible. For example, state-of-art 2.9Ah 18650 cells have by volume only 50%

### Approach

Mesoscale porosity distributions that optimize rate capability were modeled for a fixed total porosity (i.e., electrode energy density). Theory and experimental results showed that periodically spaced aligned pore channels in a porous matrix are highly effective. In collaboration with Antoni P. Tomsia of LBNL, a fabrication approach was developed that produces binder-free sintered electrodes with aligned, low-tortuosity porosity. Directional freeze-casting of aqueous suspensions of electrode particles produces ice microstructures that upon lyophilization produce desired pore morphologies. The solid particles rejected from the ice growth front are subsequently sintered to produce high density consolidated electrodes. These electrodes were then structurally characterized and electrochemically tested in lithium half-cells.

The directional freeze-casting approach was been applied to  $\text{LiNi}_{0.5}\text{Mn}_{1.5}\text{O}_4$  and  $\text{Li}(\text{Ni},\text{Co},\text{Al})\text{O}_2$ . For the former material, sintered additive-free samples have also been used to measure the electronic and ionic conductivity as a function of lithium content (state of charge), allowing the chemical diffusion coefficient to be determined for comparison with values determined by electrochemical measurements such as PITT.

### Results

**Mesoscale Porosity Distributions to Optimize Power/Energy Tradeoff.** Porosity distributions that are amenable to economical powder based processing were considered. At one limit lies a dense electrode with appropriately spaced straight channels (of  $\tau=1$ ), while at the other limit is an electrode with homogeneous random porosity, e.g., as determined by particle packing. The fundamental question addressed is whether periodic pore channels of unit tortuosity, embedded in a porous matrix (Figure V - 202), can improve ion transport under conditions of fixed total porosity (i.e., fixed electrode

energy density, with aligned porosity being introduced at the expense of reduced matrix porosity.) In the model, the *effective electrode tortuosity* was determined for all possible arrangements of the channel array.

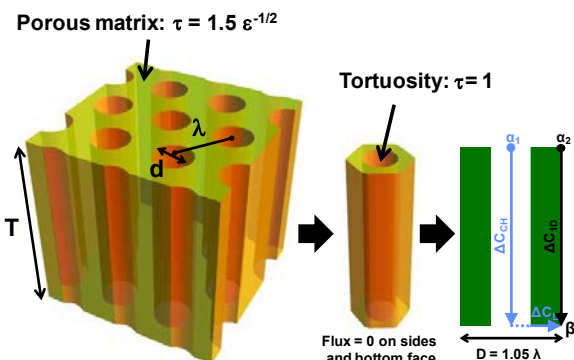


**Figure V - 202:** Model for porous electrode with aligned linear pores of unit tortuosity where available porosity may be distributed between the pore channels and porous matrix.

For a periodic array of cylindrical channels forming “unit cells” with a porous matrix surrounding each channel, when electrode thickness,  $T$ , and overall electrode porosity,  $P$ , are fixed, so are the charge capacity per unit area of current collector (areal capacity,  $\text{mAh}/\text{cm}^2$ ) and the energy density of the electrode ( $\text{Wh}/\text{L}$ ). The remaining parameters defining a design are  $\lambda$ , the channel spacing, and  $P_C$ , the pore fraction of the channels.  $P_C$  is bounded by zero for a homogenous electrode and  $P$  for a fully dense matrix with all porosity located within channels. The channel diameter and matrix porosity,  $\varepsilon$ , are also fixed upon selecting  $P$ ,  $\lambda$  and  $P_C$ . The channel is assigned unit tortuosity, while tortuosity in the porous matrix follows a modified Bruggeman relationship,  $\tau = \gamma \varepsilon^{-1/2}$ , in which the coefficient  $\gamma$  is assumed equal to 1.5, corresponding to sintered ceramics having porosity  $\varepsilon = 0.15 - 0.5$ .<sup>[20]</sup>

The porous electrode model of Doyle and Newman was modified to obtain the *steady state concentration drop across the electrode during discharge*,  $\Delta C$ . For the electrode in Figure V - 202, bounded by a separator above and a current collector below, there exists a fastest path across the electrode which may be along the channel alone, through the matrix alone, or some combination of the two. An effective tortuosity is found by calculating  $\Delta C$  and comparing to the value for an electrode of unit tortuosity. Details are given in a recently published paper (C.-J. Bae and C.K. Erdonmez, *et al.*, *Adv. Mater.*, in press).

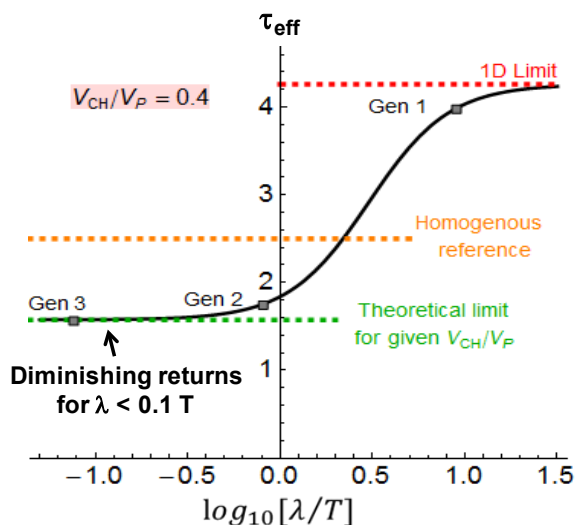


**Figure V - 203:** Results from model showing effective tortuosity as a function of the pore channel spacing relative to thickness, for an electrode of fixed total porosity (36%) and in which 40% of the available porosity resides in the channels.

The channel spacing relative to electrode thickness,  $(\lambda/T)$ , and the channel pore fraction,  $(P_C/P)$ , emerge as logical independent variables. An example of the results, Figure V - 203, shows the effective tortuosity,  $\tau_{\text{eff}}$ , against the ratio of channel spacing to electrode thickness,  $\log_{10}(\lambda/T)$ , for an electrode of fixed porosity  $P=0.36$  and in which the fraction of the porosity residing in the channels,  $P_C/P$ , is 0.4. The plot shows  $\tau_{\text{eff}}$  for the limiting cases of large and small channel spacings, compared to the value for the homogenous case (horizontal line). The upper limit (right side) corresponds to the instance where channels are too far apart to be effective and diffusion occurs mainly through the matrix. Here, the tortuosity is actually *higher* than the homogenous value because 40% of the available porosity is devoted to channels that are not effective transport paths. At the lower limit (left side), one has channels with very small spacings. Structures approximating this case can be fabricated by the directional freeze-casting process. In the example in Figure V - 203, transport through the channels predominates, but the tortuosity is not reduced all the way to unity since 60% of porosity is assumed to remain in the matrix. The asymptotic approach to a limiting tortuosity toward the left in Figure V - 203 is a key result: it shows that reducing  $\lambda/T$  below  $\sim 0.1$  provides diminishing returns. This is a reasonable objective for scalable processing. Thus, the analysis identifies the largest relative spacings,  $\lambda/T$ , that provide essentially all of the benefits of straight pore channels.

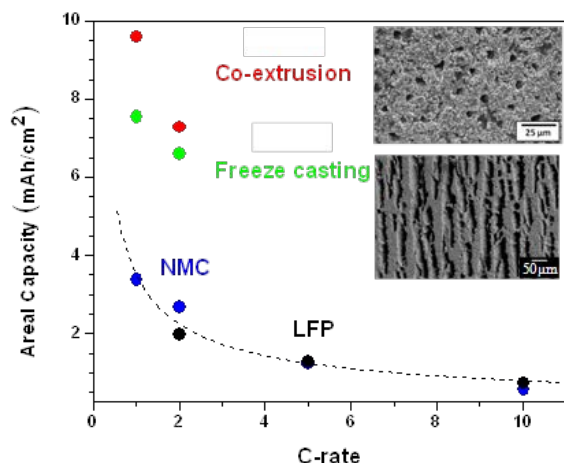


**Figure V - 204:** Maximum C-rate vs. areal capacity of sintered  $\text{LiCoO}_2$  electrodes with oriented mesoscale porosity prepared by two methods, compared to conventional calendared Li-ion electrodes.

The predictions of the model have been experimentally validated in the directionally freeze-cast and sintered electrodes developed in this project, as well as cathodes produced by an iterative co-extrusion and sintering approach (C.-J. Bae and C.K. Erdonmez, et al., *Adv. Mater.*, in press). Figure V - 204 compares results for the maximum C-rate that is possible vs. the areal capacity of the electrode ( $\text{mAh}/\text{cm}^2$ ). In the inset figure, the threading pore channels of the co-extruded electrode can be seen in a transverse section, and that of the freeze-cast sample in plain view. The curve labeled “conventional Li-ion electrode” represents results from a recent systematic study from LBNL (H. Zheng, J. Li, X. Song, G. Liu, V.S. Battaglia, *Electrochimica Acta* **2012**, *71*, 258). Zheng *et al.* found very similar power law relationships between areal capacity and maximum C-rate for cathodes prepared with NMC and LFP active materials. The common scaling of capacity with increasing electrode thickness (up to  $\sim 100 \mu\text{m}$ ) with all other experimental parameters held constant, was attributed to ion transport limitations in the electrolyte, as in the present case. Comparing at 2C rate, a practical upper limit for most portable device and PHEV/EV applications, Figure V - 204 shows that the engineered-porosity electrodes provide almost 3 times the areal capacity. In practical terms, this could allow proportionately fewer separator layers, current collectors layers, tabs, and packaging for the same energy, thereby improving cell-level energy density and reducing costs associated with the electrochemically inactive components.

**Transport Measurements in High Voltage Spinel  $\text{Li}_x\text{Ni}_{0.5}\text{Mn}_{1.5}\text{O}_4$  (LNMO).** The availability of additive-free sintered samples allowed the conductivity of the spinel phase alone to be reliably measured. The fact that the sintered samples are porous allowed them to be electrochemically titrated to a desired lithium content  $x$ . By measuring transport under small-signal conditions, the composition remains fixed under measurement conditions and effects of phase transformations were excluded. The

electronic and ionic conductivity were measured independently by using different electrode configurations (Figure V - 205). Compacted powder samples were fired to maximum temperatures of  $900^\circ\text{C}$  or  $1,000^\circ\text{C}$ , following which a 48h hold at  $650^\circ\text{C}$  in air atmosphere was applied in those cases where the ordered phase was desired. Electrochemical delithiation was conducted to obtain a range of  $x$  values. Ag paste electrodes were used as ion-blocking electrodes for the measurement of electronic conductivity (Ag/LMNO/Ag), while PEO-based solid polymer electrolyte was used as ion-conducting/electron-blocking electrodes (Li/PEO/LMNO/PEO/Li) for the measurement of ionic conductivity. The latter measurements were conducted at  $\sim 50^\circ\text{C}$  to ensure sufficient ionic conductivity in the electrodes.

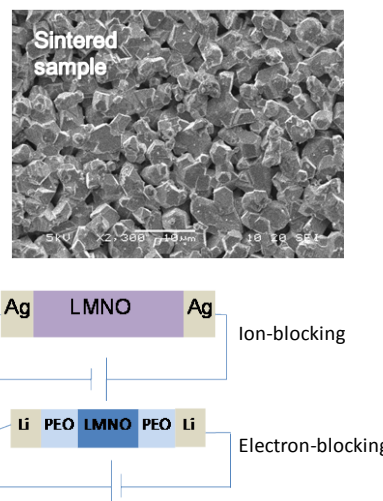


**Figure V - 205:** Sintered additive-free LMNO samples were measured using ion-blocking Ag electrodes in order to measure electronic conductivity, and electron-blocking/ion-conducting PEO+Li electrodes to measure ionic conductivity

Electronic conductivity results at  $30^\circ\text{C}$  are shown in Figure V - 206. The electronic conductivity of fully lithiated, disordered spinel is one and a half orders magnitude higher than that of fully lithiated ordered spinel. In the ordered samples, the electronic conductivity increased monotonically with increasing  $x$ . However, in disordered LMNO, the electronic conductivity is initially higher, but dropped, to about the same value as in the ordered LMNO at  $x \sim 0.04$ . Thereafter, the conductivity increases monotonically with increasing  $x$ . The initial drop in conductivity in disordered LMNO is attributed to the oxidation of residual  $\text{Mn}^{3+}$  to  $\text{Mn}^{4+}$ , after which further Li extraction activates the  $\text{Ni}^{2+}/\text{Ni}^{4+}$  couple. Except for this initial transient, the electronic conductivity is similar in disordered and ordered LMNO, exhibiting an increase by over an order of magnitude upon delithiation. With respect to temperature dependence, both ordered and disordered LMNO exhibit semiconducting behavior at all lithium concentrations, wherein the electronic conductivity increases with temperature. The activation energy is highest in lithiated LMNO at  $0.53\text{eV}$  and decreases to

0.30-0.37eV in delithiated samples. Overall, it is seen that the electronic conductivity of LMNO at room temperature lies in the range  $10^{-6}$  to  $10^{-4}$  S/cm.

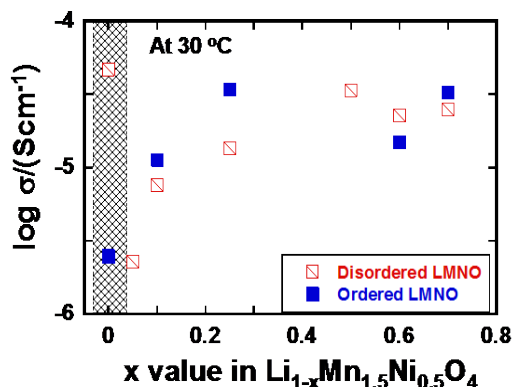


Figure V - 206: Electronic conductivity measurements of disordered and ordered LMNO at 30°C.

The ionic conductivity of fully-lithiated samples of both ordered and disordered spinel was measured using both the dc polarization and ac impedance spectroscopy methods. Independent measurement of the conductivity of the PEO + LiI electron-blocking electrodes (shown in Figure V - 203) was first conducted over the measurement temperature range for calibration purposes. Good agreement was obtained between the two measurement methods. In both disordered and ordered LMNO, the ionic conductivity is  $\sim 5 \times 10^{-8}$  S/cm at  $\sim 50^\circ\text{C}$ . The lithium diffusion coefficient at the same temperature is  $5 \times 10^{-8}$  to  $10^{-7}$  cm<sup>2</sup>/s. The chemical diffusion coefficient is expected to be of the same magnitude, given that the electronic conductivity is  $\sim 10^3$  higher than the ionic conductivity at the same temperature. The results clearly show that chemical diffusion is limited by ionic rather than electronic transport. Furthermore, at these values of chemical diffusivity, lithium transport should not be rate-limiting for spinel particles of up to  $\sim 10$   $\mu\text{m}$  diameter, assuming a 2.5C current rate. These are, to our knowledge, the first direct measurements of ionic conductivity in LMNO, and the first determination of chemical diffusivity in LMNO in the absence of electrochemical reaction. Preliminary results of partially delithiated ordered spinel ( $x = 0.1$ ) indicates that ionic conductivity decreases upon delithiation.

## Conclusions and Future Directions

It has been shown theoretically and experimentally that the introduction of mesoscale low-tortuosity porosity allows approximately 3-fold higher areal capacity at equivalent C-rates compared to conventionally processed Li-ion electrodes. Electrodes of such design may enable higher energy density rechargeable batteries for transportation. Using the same type of sintered electrodes, measurements of electronic and ionic conductivity in the high voltage spinel  $\text{Li}_x\text{Ni}_{0.5}\text{Mn}_{1.5}\text{O}_4$  in the absence of phase boundary effects were conducted. Results show that

electronic conductivity is not rate-limiting for chemical diffusion in either ordered or disordered LMNO. Thus, in the absence of phase boundary effects, chemical diffusion should be limited by ion diffusion. However, chemical diffusivities measured using PITT elsewhere in the BATT program are orders of magnitude lower than the values obtained here. These results together show that chemical diffusion in LMNO, and therefore its rate capability, is determined by strong coupling to phase transition kinetics. LMNO shares these characteristics with other compounds with kinetics limited by a first-order phase transition such as the olivines.

Future directions in this project are as follows:

- Modeling of mesoscale porosity effects will be extended to the specific microstructures resulting from the freeze-casting approach in which the pore morphology is defined by ice crystal shapes.
- The freeze-casting + sintering approach will be applied to electrode materials with electronic conductivities intermediate between highly conductive compounds such as  $\text{LiCoO}_2$  and highly insulating ones such as conventional  $\text{LiFePO}_4$  in order to determine the relative limitations of electronic and ionic transport on capacity utilization.
- Due to the large capacity per unit area, the pulse power performance of such electrodes may differ from conventional electrodes of much lighter active loading. This behaviour will be characterized, using PHEV and EV specific “drive cycles.”

## FY 2012 Publications/Presentations

1. C.-J. Bae, C.K. Erdonmez, J.W. Halloran and Y.-M. Chiang, “Design of Battery Electrodes with Dual-Scale Porosity to Minimize Tortuosity and Maximize Performance,” *Adv. Mater.*, in press.
2. Y.-M. Chiang, “Materials Research for Electrochemical Storage at Transportation and Grid Scales,” *Peter G. Winchell Distinguished Lecture Series*, Purdue School of Materials Engineering, Purdue Univ., West Lafayette, IN, Sept. 24, 2012.
3. Y.-M. Chiang, “Materials, Systems, and Manufacturing Challenges for Electrochemical Storage at Transportation and Grid Scales,” *R.E. Tressler Distinguished Lecture in Materials*, Pennsylvania State University, March 22, 2012.
4. Y.-M. Chiang, “New Device Architectures,” *Gordon Research Conference*, Ventura, CA, March 8, 2012.

---

## V.E.7 *In Situ* Electron Microscopy of Electrical Energy Storage Materials (ORNL)

Raymond R. Unocic  
Oak Ridge National Laboratory  
Materials Science and Technology Division  
One Bethel Valley Rd  
PO Box 2008 MS-6064  
Oak Ridge, TN 37831-6030  
Phone: (865) 574-0096; Fax: (865) 576-5413  
E-mail: [unocicrr@ornl.gov](mailto:unocicrr@ornl.gov)

Collaborators: Nancy J. Dudney, Gabriel M. Veith, Loic Baggetto, and Karren L. More (ORNL)

Start Date: January 2010  
Projected End Date: N/A

### Accomplishments

- Developed an *in situ* TEM liquid cell capable of performing electrochemical measurements of electrical energy storage materials.
- Demonstrated the ability to study SEI formation mechanisms on natural graphite anodes in organic electrolytes.
- Developed a method for directly depositing electrode material on MEMS based microchips.
- Demonstrated the capability of extracting chemical information within the *in situ* electrochemical liquid cell using electron energy loss spectroscopy.

◇ ◇ ◇ ◇ ◇

### Objectives

- Develop and perform quantitative *in situ* electron microscopy experiments on electrical energy storage materials using an electrochemical cell holder built specifically for *in situ* transmission electron microscopy (TEM) characterization.
- Perform controlled nanoscale electrochemistry experiments within the high vacuum environment of the TEM column.
- Image electrochemical processes at high spatial and temporal resolution.
- Investigate critical nm-scaled microstructural and micro-chemical changes as a function of battery test conditions, electrode materials, electrolyte, and electrolyte additives.

### Technical Barriers

- At present, there is a lack of high-resolution electrochemical characterization techniques, which allow for direct observations of dynamically evolving electrochemical reactions during charge/discharge cycling.

### Technical Targets

- Develop *in situ* characterization technique and methodology to investigate dynamically evolving electrochemical reaction mechanisms.

### Introduction

The accelerated development of materials for electrical energy storage systems will hinge critically upon our understanding of how interfaces (particularly electrode-electrolyte solid-liquid interfaces) control the electrochemical processes during charge and discharge. Insight into dynamically evolving electrochemical reaction mechanisms and kinetics remains limited due to the present lack of *in situ* high-resolution characterization methodologies. Electrochemical fluid cell microscopy is an emerging *in situ* method that allows for the direct, real-time imaging of electrochemical processes within a fluid environment. This technique is facilitated by the use of MEMS-based biasing microchip platforms that serve the purpose of sealing highly volatile electrolyte between two electron transparent SiN<sub>x</sub> membranes; these membranes also serve as a means to interface electrodes to an external potentiostat for controlled nanoscale electrochemistry experiments.

### Approach

In this program, we have developed an electrochemical liquid cell for *in situ* TEM studies of electrochemical reactions that take place in electrical energy storage material systems. The core challenge of preventing the evaporation of volatile organic liquid electrolytes is overcome by sealing the liquid electrolyte between thin electron transparent viewing membranes. The general concept for conducting *in situ* TEM characterization is as follows: MEMS based silicon microchip devices containing a central thin electron transparent silicon nitride (SiN<sub>x</sub>) viewing membrane are stacked upon one another and placed within the tip of a

precision machined TEM holder. Liquid electrolyte is delivered through the TEM holder with a microfluidic delivery system to wet the space between the SiN<sub>x</sub> membranes. Gold or platinum biasing contacts that are deposited onto the lower chip/window of the cell serve as a platform for attaching battery electrodes and for interfacing with an external potentiostat for electrochemical testing. A 500 nm thick spacer material patterned on the upper chip controls the thickness of the liquid electrolyte layer in the cell.

In order to elucidate both structural and chemical changes during such *in situ* electrochemical experiments, it is important to first improve upon the spatial resolution by utilizing energy-filtered transmission electron microscopy (EFTEM) to minimize chromatic aberration, then to determine the chemical changes via electron energy loss spectroscopy (EELS). This presents a formidable challenge since the overall thickness through which electrons are scattered through the multiple layers of the cell can be on the order of hundreds of nanometers to microns. Scattering has the deleterious effects of degrading image resolution and decreasing signal-to-noise for spectroscopy.

## Results

To demonstrate the feasibility of utilizing this technique to study the dynamics of SEI formation we studied the electrolyte decomposition mechanisms from 1M LiPF<sub>6</sub> EC:DEC electrolyte onto a natural graphite anode. Furthermore, we developed a lithium counter electrode that is connected to the cell in a manner similar to an electrolyte bridge so that we can better quantify the electrochemistry. Figure V - 207(a) shows a bright-field TEM image of the graphite anode sandwiched between the SiN<sub>x</sub> membranes. Figure V - 207(b-c) depict a time-lapse series of images of SEI formation from the edge of the graphite anode. Here we observe that the SEI is growing from the electrode-electrolyte interface, reminiscent of interface-controlled growth.

Extracting chemical information during *in situ* TEM characterization of electrochemical processes is also an important facet of this research program. Radio frequency (RF) magnetron sputtering was used to deposit thin films of LiMn<sub>2</sub>O<sub>4</sub> onto the surface of the SiN<sub>x</sub> membrane. The target materials for sputtering were prepared by high temperature solid-state reaction. Figure V - 208 shows a typical bright-field TEM image of the spinel cathode material deposited onto the surface of the SiN<sub>x</sub> membrane. The inset selected area electron diffraction (SAED) ring pattern confirms the nanocrystalline nature of the thin film electrode material.

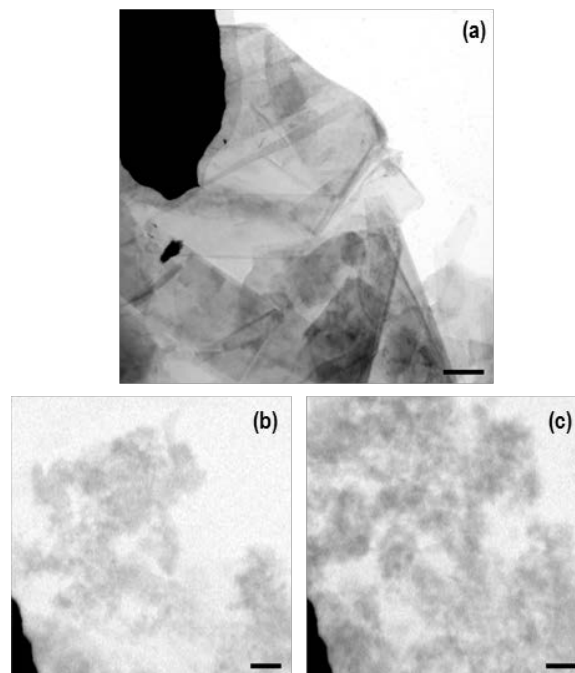


**Figure V - 207:** (a) Bright-field TEM image of the natural graphite anode materials within the electron transparent SiN<sub>x</sub> membrane region of the electrochemical cell (imaged without liquid electrolyte). (b-c), time-lapse images extracted from *in situ* TEM video showing SEI growth dynamics. Scale bar is 1 micron.

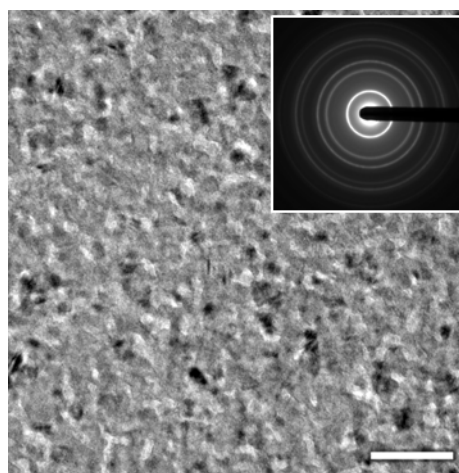


**Figure V - 208:** RF magnetron sputtered LiMn<sub>2</sub>O<sub>4</sub> thin films on SiN<sub>x</sub> membrane. Inset SAED reveals the spinel structure and the nanocrystalline nature of the thin film electrode material. Scale bar is 100 nm.

To demonstrate this feasibility of extracting chemical information through the components of the liquid cell, low-loss and core-loss EEL spectra were acquired with liquid present and without liquid in the cell. Note: for demonstration purpose dimethyl carbonate (DMC) was used as the liquid in the study. Figure V - 209 shows a Fourier-log deconvoluted spectrum showing the O-K and the Mn L<sub>2,3</sub> core-loss ionization edges (a) without DMC and (b) with DMC. It is clear that the signal-to-noise ratio decreases when liquid is present within the cell; however, there is still sufficient signal to allow for the extraction of

chemical information such as what elements are present. Furthermore, with this method, it is possible to extract information on the oxidation state of the transition metals through analysis of the  $L_3$  and  $L_2$  intensities from the Mn  $L_{2,3}$  edge through analysis of the so-called white-line intensity ratio method.

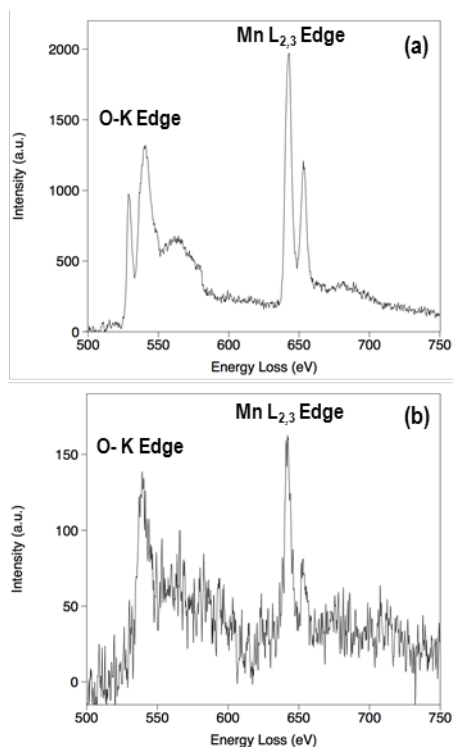


**Figure V - 209:** Fourier-log deconvoluted EEL spectra of  $\text{LiMn}_2\text{O}_4$  thin film electrodes deposited on MEMS based *in situ* microchip platform: (a) dry and (b) with DMC present within the cell.

## Conclusions and Future Direction

The *in situ* electrochemical liquid cell microscopy technique is a versatile characterization method that is useful for characterizing dynamically evolving electrochemical processes in a liquid environment. When coupled with analytical characterization methods such as EELS, it is also possible to characterize chemical changes during battery cycling. In future work, more emphasis will be placed on characterizing the role of additives and electrolyte solvent on SEI formation, degradation mechanisms in electrode materials during charge-discharge cycling, and correlating microstructural and microchemical changes with battery performance, lifetime, and capacity.

## FY 2012 Publications/Presentations

1. Unocic RR, Baggetto L, Unocic KA, Veith GM, Dudney NJ, More KL, "Coupling EELS/EFTEM Imaging with Environmental Fluid Cell Microscopy," *Microscopy and Microanalysis*, 18, Suppl 2, 1104-1105, (2012).
2. Unocic RR, Sun X-G, Adamczyk LA, Dudney NJ, More KL, Alsem DH, Salmon NJ, "Development of *In situ* Electrochemical Fluid Cells for Electrical Energy Storage Research," Batteries Gordon Conference, Ventura, CA, March 2012.
3. Unocic RR, Alsem DH, Salmon NJ, Chi M, Veith GM, Adamczyk LA, Dudney NJ, More KL, "The Versatility of *In situ* Environmental Fluid Cells for Materials Science Research," MS&T 2011, Columbus, OH, October 2011.

## FY 2012 Awards

Microanalysis Society Birks Award for Best Contributed Paper: Unocic RR, Adamczyk LA, Dudney NJ, Alsem DH, Salmon NJ, More KL, "*In situ TEM Characterization of Electrochemical Processes in Energy Storage Systems*," *Microscopy and Microanalysis*, Nashville, TN, August 2011.

Description: The Birks Award is presented annually to the best-contributed paper from the previous year's Microscopy and Microanalysis annual meeting (held August 7-11, 2011) and is judged from the quality of both the paper and the oral presentation. The winning award was judged best out of a total of 120 nominations. Award was presented at the 2012 Microscopy and Microanalysis meeting held July 29-Aug 2, in Phoenix, AZ.

## Acknowledgements

*In situ* Transmission Electron Microscopy was performed at the Shared Research Equipment (ShaRE) at ORNL which is sponsored by the DOE Office of Basic Energy Sciences Scientific User Facilities Division.

---

## V.F Energy Frontier Research Centers

### V.F.1 Energy Frontier Research Center at ANL

Michael Thackeray  
Argonne National Laboratory  
9700 South Cass Avenue  
Argonne, IL 60439  
Phone: (630) 252-9184; Fax: (630) 252-4176  
E-mail: [thackeray@anl.gov](mailto:thackeray@anl.gov)

Collaborators:  
ANL: J. R. Croy, M. Balasubramanian (APS)

Start Date: October 1, 2010  
Projected End Date: September 30, 2014

#### Accomplishments

- A detailed electrochemical/structural study of surface treated  $0.5\text{Li}_2\text{MnO}_3 \bullet 0.5\text{LiCoO}_2$  was accomplished.
- Structural features of composite electrode materials prepared from a  $\text{Li}_2\text{MnO}_3$  precursor were evaluated using X-ray absorption techniques.
- One paper published; one patent application; two presentations made at ECS and IMLB meetings.

◇ ◇ ◇ ◇ ◇

#### Introduction

Bulk and interfacial electrochemical processes are of fundamental scientific interest as well as of technological importance. The performance of energy storage and power supply systems is largely dependent on these processes, which can occur at an electrode-electrolyte interface or in the bulk of the electrode. In this project, the structural features, ionic transport phenomena and charge-transfer reactions at the electrode/electrolyte interface of lithium battery electrode materials, notably high potential metal oxide cathodes are studied. The electrode materials under investigation are selected specifically from those being investigated in the Batteries for Advanced Transportation Technologies (BATT) program and on their potential for making significant advances in electrochemical performance; the studies complement the research being conducted by the Energy Frontier Research Center, the *Center for Electrical Energy Storage – Tailored Interfaces* led by Argonne National Laboratory, with Northwestern University and the University of Illinois, Urbana-Champaign as partners.

Of particular importance to this project is Argonne's research in the BATT program on electrodes with integrated 'composite' structures, which has highlighted the possibility of designing new, high-potential and high capacity electrodes with  $\text{Li}_2\text{MnO}_3$  as a stabilizing component. It has been demonstrated, in particular, that it is possible to integrate  $\text{Li}_2\text{MnO}_3$  with layered  $\text{LiMO}_2$ - or spinel  $\text{LiM}_2\text{O}_4$  components (e.g.,  $\text{M}=\text{Mn, Ni, Co}$ ) at the atomic level, and that these composite materials can provide an exceptionally high capacity (240-250 mAh/g), which is significantly higher than that offered by conventional layered  $\text{LiCoO}_2$ , spinel  $\text{LiMn}_2\text{O}_4$  and olivine  $\text{LiFePO}_4$  electrodes. These lithium- and manganese-rich composite materials have complex structures that are surprisingly stable when delithiated at high potentials (~5

#### Objectives

- Conduct studies of electrode materials relevant to the BATT program to complement the research being conducted by the EFRC, *Center for Electrical Energy Storage – Tailored Interfaces* led by Argonne National Laboratory, with Northwestern University and the University of Illinois, Urbana-Champaign as partners.
- Specifically, use X-ray spectroscopy, including "in situ" experiments, at Argonne's Advanced Photon Source to probe and characterize the surface and bulk structures of high capacity  $x\text{Li}_2\text{MnO}_3 \bullet (1-x)\text{LiMO}_2$  ( $\text{M}=\text{Mn, Ni, Co}$ ) electrode materials in lithium cells.

#### Technical Barriers

- Low energy density.
- Poor low temperature operation.
- Abuse tolerance limitations.

#### Technical Targets (USABC - End of life)

- 142 Wh/kg, 317 W/kg (PHEV 40 mile requirement).
- Cycle life: 5,000 cycles.
- Calendar life: 15 years.

V). Despite this stability, it is still necessary to passivate the electrode surface to prevent electrode/electrolyte reactions from occurring, and to improve lithium-ion transport at the surface, thereby enhancing the power capability of the cell. In this respect, several coating techniques and passivating agents, such as metal oxides ( $\text{Al}_2\text{O}_3$ ,  $\text{ZrO}_2$ ), fluorides ( $\text{AlF}_3$ ) and phosphates ( $\text{AlPO}_4$ ) have been used to improve surface stability but little is known about surface structures, or the mechanisms by which lithium-ion transport occurs at the electrode surface. The knowledge gained from these studies will be used to improve the composition and structure of electrode surfaces and advancing the overall performance of the electrodes to meet DOE's 40-mile PHEV battery requirements.

## Approach

Analytical techniques for probing the structure-electrochemical property relationships of lithium battery electrode materials, notably at electrode surfaces, include neutron scattering, x-ray absorption, scattering and photoelectron spectroscopy, nuclear magnetic resonance, Raman spectroscopy, Fourier transform infrared spectroscopy, and electron microscopy. In this project, analytical efforts are focused predominantly on x-ray spectroscopic techniques, including “*in situ*” experiments, and high-resolution electron microscopy. Major facilities are available at Argonne to conduct these experiments, notably at the Advanced Photon Source (APS) and the Electron Microscopy Center (EMC).

Surface-protected ‘coated’ cathode materials being studied include those with integrated ‘composite’ structures in which the coating contains specific 3d/4d transition metals which are not present in the core structure. Coatings are applied by various techniques, for example, from solution by standard sol-gel methods, sonication or by atomic layer deposition (ALD). “*In situ*” synchrotron hard X-ray spectroscopic techniques including X-ray absorption spectroscopy (XAS), resonant and non-resonant X-ray emission spectroscopy (XES) and X-ray Raman scattering (XRS) can be used to monitor the interfacial reactions at the electrode-electrolyte interface. The important traits of these spectroscopic techniques, specifically the element specific nature and the sensitivity to dilute constituents, allow the monitoring of changes in the electronic and atomic structures of the surface and the bulk during charge and discharge. It is envisioned that the studies will provide key information at the molecular level on the structure of coatings, the mechanism of lithium-transport at the electrode-electrolyte interface and provide insights into degradation mechanisms. Another aspect is the effect of the coating on the bulk structure of the composite material itself, particularly on deintercalation at high voltages, for example 4.6 V, during the initial charge. The knowledge gained from both the bulk and interface using x-ray spectroscopic methods will feed into the

design of improved electrodes to meet the 40-mile PHEV goals. These spectroscopic investigations complement the X-ray based scattering approaches, which are currently an integral part of the efforts of Argonne's EFRC, the *Center for Electrical Energy Storage - Tailored Interfaces* (CEES).

## Results

In an initial study,  $0.5\text{Li}_2\text{MnO}_3 \cdot 0.5\text{LiCoO}_2$  ( $\text{Li}_{1.2}\text{Mn}_{0.4}\text{Co}_{0.4}\text{O}_2$ ) cathode materials were surface-treated in an acidic solution of  $\text{Li-Ni-PO}_4$  with the goal of forming a protective coating on the cathode particles at high states of charge to combat degradation [1]. It was subsequently shown that both capacity retention and rate performance were significantly improved relative to untreated samples, indicating that the surface treatment had desired effects. XRD and XAS analyses revealed that surface treatment resulted not only in the precipitation of a  $\text{Li}_3\text{PO}_4$ -like surface phase but also in modifications to the bulk of the cathode structure. Nickel ions, introduced via the acidic solution, were incorporated into the transition metal layers of the  $\text{Li}_2\text{MnO}_3$ -like regions within the structure. Electrochemical cycling showed that despite the enhanced capacity retention and rate performance, the voltage fade phenomenon still persisted in these cells.

XANES and EXAFS studies were conducted to explore the structural changes in cycled,  $\text{Li-Ni-PO}_4$  treated cathodes. Figure V - 210a and Figure V - 210b show Mn and Co K-edge XANES, respectively, of a fresh cathode (black) and a cathode that had been cycled 21 times at room temperature between 4.6 – 2.0 V. The data indicate that both the Mn and Co appear to be somewhat reduced with respect to their initial oxidation states of 4+ and 3+, respectively, consistent with the activation of the  $\text{Li}_2\text{MnO}_3$  component and the oxygen loss that accompanies lithium extraction. The Co K-edge EXAFS data in Figure V - 210c reveal a high degree of structural disorder in the cycled electrode (red) associated with  $\text{LiCoO}_2$  domains, as well as the possibility of tetrahedral  $\text{Co}^{2+}$ , as indicated by the arrow in accordance with the shifting Co edge. The data also show that some Co ions are mobile leading to disordered regions associated with local  $\text{LiCoO}_2$  environments; these bulk-average changes are similar to those observed by XAS in untreated materials. The implications of this study are two-fold: 1) effective surface modifications can lead to stable surfaces which enhance both capacity retention and rate capability; 2) stable surfaces do not lead to the suppression of voltage fade, which appears to be an inherent property of Mn-rich composite electrode structures.

To address voltage fade, a synthesis approach was developed in the BATT program that uses  $\text{Li}_2\text{MnO}_3$  as a layered ‘template’ to fabricate composite structures. In this method,  $\text{Li}_2\text{MnO}_3$  is treated in an acidic solution in the presence of any desired cation (e.g.,  $\text{Ni}^{2+}$ ) to be incorporated into the composite structure. This method

produces a variety of structure types, such as ‘layered-layered’, ‘layered-layered-spinel’, and ‘layered-layered-rocksalt’ configurations. For the structural studies in this project, a series of temperature-dependent XAS measurements was made on a material with nominal composition  $0.5\text{Li}_2\text{MnO}_3 \cdot 0.5\text{LiMn}_{0.5}\text{Ni}_{0.5}\text{O}_2$ .

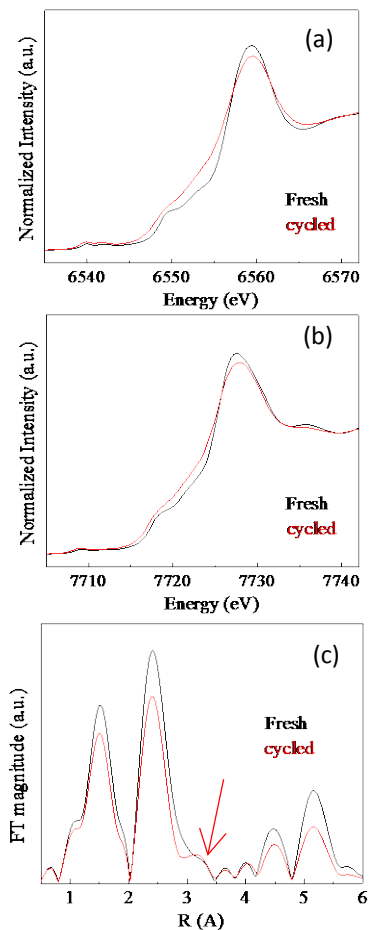


**Figure V - 210:** (a) Mn and (b) Co K-edge XANES of fresh (black) and cycled (red)  $0.5\text{Li}_2\text{MnO}_3 \cdot 0.5\text{LiCoO}_2$  treated with Li-Ni- $\text{PO}_4$ . (c) Magnitude of Fourier transformed Co K-edge data; the arrow indicates tetrahedral Co.

Figure V - 211a and Figure V - 211b show the Fourier transformed magnitude of Mn and Ni K-edge EXAFS data, respectively, at various annealing temperatures between 550 and 1050 °C. Of significance is the observation that the local manganese environment of the  $\text{Li}_2\text{MnO}_3$  template does not change significantly over the entire range of temperatures. Clear changes, however, do appear in the increasing amplitude of the second peak at  $\sim 2.5$  Å related to the first-shell, Mn-metal coordination. Figure V - 211b reveals several interesting features; 1) the first-shell Ni-metal correlations at  $\sim 2.5$  Å decrease with increasing temperature; 2) Ni-O-metal correlations at  $\sim 4$  Å decrease with temperature indicating less Ni in the transition metal layers with increasing temperature; and 3) the increasing amplitude of the ‘focusing’ peak above

$\sim 5$  Å with increasing temperature indicates increasing long range order between metal atoms within the transition metal layers.

Figure V - 211c shows the results of EXAFS analysis with respect to first-shell, metal-metal coordination numbers for manganese (red) and nickel (blue). The dashed lines at 3 and 6 represent the ideal metal-metal coordination numbers of  $\text{Li}_2\text{MnO}_3$  and  $\text{LiMO}_2$  (e.g., M =

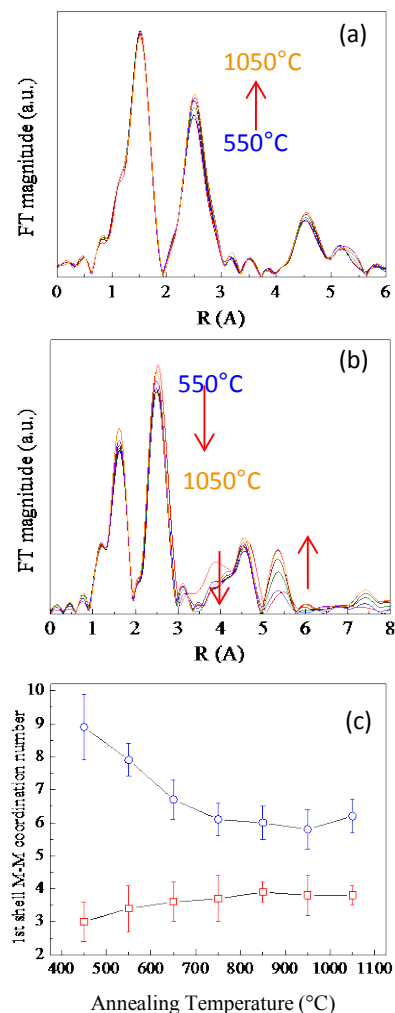


**Figure V - 211:** Magnitude of Fourier transformed Mn (a) and Ni (b) K-edge EXAFS data of composite  $0.5\text{Li}_2\text{MnO}_3 \cdot 0.5\text{LiMn}_{0.5}\text{Ni}_{0.5}\text{O}_2$  synthesized via an acid/nickel-treated  $\text{Li}_2\text{MnO}_3$  precursor followed by annealing at various temperatures. (c) EXAFS determined coordination numbers as a function of temperature. Arrows denote direction of change with T.

Co, Ni, Mn), respectively. As shown in Figure V - 211c, increasing the annealing temperature increases the coordination of manganese relative to its initial  $\text{Li}_2\text{MnO}_3$ -like state and decreases the coordination of nickel towards the ideal  $\text{LiMO}_2$  state. The large amplitude of Ni-O-metal correlations at  $\sim 4$  Å (Figure V - 211b) reveals integrated, NiO domains within the composite structure at lower synthesis temperatures. With increasing temperature, these domains ‘decompose’; nickel is incorporated into the Li sites of the transition metal layers of the  $\text{Li}_2\text{MnO}_3$  template

[1], as evident from the increasing coordination number of manganese. This effect decreases the coordination of nickel away from that of NiO (12) towards the value of 6 in ideal layered  $\text{LiMO}_2$  structures, thus enhancing longer-range, Ni-metal-metal interactions within the transition metal layers, consistent with the increasing peak amplitude at  $\sim 5.2 \text{ \AA}$  (Figure V - 211b).

Recent XAS studies have shown that the voltage fade phenomenon is closely linked to dramatic changes which take place on activation, and during early cycles, associated with local manganese environments. These studies showed that Mn-Ni correlations result in a much more stable manganese environment whereas Li- and Mn-rich,  $\text{Li}_2\text{MnO}_3$ -like domains suffer more drastic, irreversible changes. In order to maintain the electrochemical benefits of  $\text{Li}_2\text{MnO}_3$  domains, while minimizing overall structural changes, the above-mentioned synthesis method has been extended to other layered precursors in an attempt to control local compositions as well as domain sizes within composite structures.

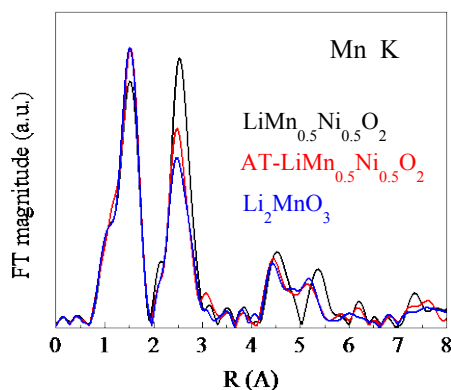


**Figure V - 212:** Magnitude of Fourier transformed Mn K-edge EXAFS data of layered  $\text{LiMn}_{0.5}\text{Ni}_{0.5}\text{O}_2$  (black), an acid/Li-treated (AT) analogue (red), and a  $\text{Li}_2\text{MnO}_3$  standard (blue).

Figure V - 212 shows Mn K-edge EXAFS data of a layered  $\text{LiMn}_{0.5}\text{Ni}_{0.5}\text{O}_2$  (black) precursor material together with the EXAFS data of a product derived from this precursor after treatment in an acidic solution containing 10% excess lithium (with respect to the initial lithium content) and thereafter annealed at  $950^\circ\text{C}$  (red). A  $\text{Li}_2\text{MnO}_3$  standard is shown for comparison (blue). The data show that the local environment of manganese shifts from an almost ideal  $\text{LiMO}_2$ -type arrangement to one in which manganese is found in a less coordinated,  $\text{Li}_2\text{MnO}_3$ -type environment. The data also reveal that this synthesis approach was successful in affecting lithium and manganese ordering by introducing  $\text{Li}_2\text{MnO}_3$ -like domains into the  $\text{LiMn}_{0.5}\text{Ni}_{0.5}\text{O}_2$  precursor. This approach is currently being explored further to investigate the influence that different layered precursors, compositions and synthesis parameters have on domain size, local ordering, and on bulk electrochemical properties, such as voltage fade and hysteresis.

## Conclusions and Future Directions

### Conclusions

X-ray absorption spectroscopy (XANES and EXAFS) has been extensively used to understand surface and bulk structural processes of high-capacity composite cathode materials. A surface-treated  $0.5\text{Li}_2\text{MnO}_3 \cdot 0.5\text{LiCoO}_2$  material, which has greatly enhanced electrochemical properties vs. untreated samples, was found to undergo similar bulk-average structural changes as untreated analogues. These processes likely include oxygen loss around manganese with subsequent manganese migration and reduction. These spectroscopic studies of surface and bulk structural effects are revealing important information that may help to address and combat voltage fade.

### Future Work

Future work will continue to focus on determining structure-electrochemical property relationships of high capacity composite electrode structures and to characterize both surface and bulk properties using primarily X-ray spectroscopic techniques; the ultimate goal is to achieve stable capacities and optimized electrochemical properties. Sonochemical techniques will be investigated, in particular, to apply surface coatings and/or to modify surface compositions to control surface stability. These studies on technologically important electrode materials complement the basic research being conducted by the Energy Frontier Research Center, the *Center for Electrical Energy Storage – Tailored Interfaces*.

## FY 2012 Publications/Patents/Presentations

### Publications

1. J. R. Croy, S.-H. Kang, M. Balasubramanian and M. Thackeray, *Designing High-Capacity, Lithium-Ion Cathodes Using X-ray Absorption Spectroscopy*, *Chem. Mater.*, **23**, 5415 (2011).

### Patents

1. M. Thackeray, S.-H. Kang, M. Balasubramanian and J. R. Croy, *Electrode Structures and Surfaces for Li Batteries*, US Patent Application (CIP) 20120263998 (18 October, 2012).

### Presentations

1. J. R. Croy, M. Balasubramanian, D. Kim, S. Kang, and M. Thackeray, *Recent Advances in Manganese Oxide Materials for Lithium Battery Applications*, 221<sup>st</sup> ECS Meeting, Seattle, WA, 6-10 May (2012).
2. M. M. Thackeray, J. R. Croy, D. Kim, G. Sandi-Tapia, K. G. Gallagher and M. Balasubramanian, *High Capacity Li- and Mn-rich Metal Oxide Electrodes: Challenges and Opportunities*, 16<sup>th</sup>

International Meeting on Lithium Batteries, Jeju,  
Korea, 17-22 June, 2012.

## V.G. Integrated Lab-Industry Research Program

### V.G.1 Integrated Lab-Industry Research Project (LBNL, ANL)

Jordi Cabana<sup>1</sup>, John T. Vaughey<sup>2</sup>  
Lawrence Berkeley National Laboratory  
<sup>1</sup>Environmental Energy Technologies Division  
1 Cyclotron Rd. MS62R0203  
Berkeley, CA 94720-8168  
E-mail: [jcabana@lbl.gov](mailto:jcabana@lbl.gov)

<sup>2</sup>Chemical Sciences and Engineering Division  
9700 S Cass Ave  
Argonne National Laboratory  
Lemont, IL 60439  
E-mail: [vaughey@anl.gov](mailto:vaughey@anl.gov)

#### Participants:

Guoying Chen, Tom Richardson, Robert Kostecki,  
Marca Doeff, Gao Liu, John Kerr, Vince Battaglia,  
Brian Ingram, John Zhang, D. Schroeder (NIU)

Start Date: October 1, 2010

Projected End Date: September 30, 2013

#### Objectives

- Design, synthesize and characterize structures based on solid lithium ion conductors, organic and/or inorganic, that enhance the cycle life of lithium metal based anodes in a lithium battery.
- Develop characterization tools that contribute to an understanding of how ionically conducting ceramic coatings and lithium metal interact in an electrochemical cell environment.
- Design, synthesize and characterize organic lithium ion conducting materials that enhance the cycle life of lithium metal based anodes.

#### Technical Barriers

This project addresses the following technical barriers from the Energy Storage section of the DOE Vehicle Technologies Program Multi-Year Research, Development and Demonstration Plan:

- (A) 40 mile range for PHEVs.
- (B) Abuse tolerance.
- (C) Cell life.

#### Technical Targets

- EV: 200 Wh/kg; 1,000 cycles.

#### Accomplishments

- Developed a procedure to synthesize the garnet phase  $\text{Li}_{7-3x}\text{Al}_x\text{La}_3\text{Zr}_2\text{O}_7$  (LLZ) at temperatures as low as 700 C. Evaluated the role of Al-substitution as a function of crystal class and temperature ( $700\text{ C} > x > 1150\text{ C}$ ).
- Carried out detailed MAS-NMR, ionic conductivity, and XRD studies to determine relationship between annealing temperature, phase formation, and cation ordering in LLZ. Identified the position the Al cation substitutes in the structure as being one of the Li-sites. This in contrast to the most widely used ceramic lithium-ion conductor,  $\text{Li}(\text{Ti},\text{Al})_2(\text{PO}_4)_3$ , where aluminum substitution occurs on the transition metal site.
- Synthesized phase-pure  $\text{Li}_7\text{La}_2\text{Zr}_3\text{O}_{12}$ , studied the conditions that lead to impurity formation and developed a protocol to produced dense (>92%) sintered membranes and thin films.
- Identified a series of nanoscale silane-based coatings for lithium metal that work by size exclusion rather than packing density.
- Prepared the first ceramic-polymer composites based on LATP,  $\text{TiO}_2$  and PEO-PS block copolymers.
- Completed the first set of studies of bottlenecks for ion conduction in systems based on dual phase electrolytes (ceramic, liquid).



#### Introduction

Achieving the DOE 40 mile range target for PHEVs will require significant advancements in energy storage technology. One of the most straightforward ways of achieving this goal is the use of a lithium metal anode. This monolithic anode is an enabling technology that can be paired with a number of elemental, organic, or charged cathodes to meet EEREs mid and long term energy storage goals. The main focus of this project is to devise new methods to understand and stabilize lithium metal anodes in a battery environment. Previous literature work has focused on the electrolyte reactivity and electrodeposition problems and the effects of these issues on long term cycling stability. ANL, in collaboration with LBNL, has designed a series of projects that utilize recent advances in ceramic electrolyte materials, polymer science, and materials characterization to stabilize lithium metal

anodes. With advantages for lithium metal that include a significant increase in anode capacity versus most alternatives, increased options for cathode materials, and a factor of four reduction in coating volume, new approaches to stabilizing this class of anodes is a benefit to researchers seeking next generation energy storage systems.

The work under this program leverages the unique expertise of the groups at ANL and LBNL to address the challenge of developing a lithium metal electrode for an electrochemical cell. The team comprises materials scientists, as well as inorganic, organic and physical chemists with expertise in the synthesis, characterization and electrochemical evaluation of battery materials. Thus, a variety of synthetic methodologies can be employed, from classical solid state to thin film growth, and an array of diagnostics tools leveraged to evaluate the interfaces in the system, as well as the surface of the electrode. With this aim, cells that are suitable for experiments with simultaneous cycling and probing have been designed. During FY2012, a new synergistic task has been phased-in, in which the effort on polymer and ceramic materials has been combined to develop novel ionically conducting composite membranes.

### Approach

The work under this program leverages the unique expertise of the groups at ANL and LBNL to address the challenge of developing a lithium metal electrode for an electrochemical cell. To evaluate the surface of the electrode, vibrational and scanning probe microscopies have been employed to study changes on lithium metal anode surface with different modifications. These include stabilizing the metal interfaces using organosilane coatings or by addition of polymeric single ion conductor electrolytes to reduce the overall cell impedance.

Solid state lithium-ion conductors based on transition metal based framework structures have great promise as a new generation of materials have been identified that conduct lithium cations at room temperature as very high rates. Two approaches have been taken toward applying these materials towards a practical cell – bulk ceramic processing and thin film (via sputtering) on porous substrates. LBNL has developed a thin film effort that has focused on synthesis by PLD and ALD on dense substrates.

### Results

**Ceramics.** Initial work on transition metal containing lithium ion conducting ceramics was focused on LATP. A scheduled go/no-go decision resulted in a no-go (mainly due to sintering stability) and studies of the lithium-ion conducting oxides (LiLa)TiO<sub>3</sub> (LLTO) and Li<sub>7</sub>La<sub>3</sub>Zr<sub>2</sub>O<sub>12</sub> (LLZ) were initiated. The choices were based on commercial interest and high lithium ion conductivity at room temperature.

Although high conductivity cubic LLZ has been investigated since its report in 2005 by Weppner, et al., issues relating to the role of Al(III) substitution, sintering stability, and stability to lithium metal have not been resolved. Initial efforts have focused on evaluating the role of Al(III) doping in LLZ. Literature reports have noted several theories, including its inclusion mainly at grain boundaries, that it substitutes for Zr in the fixed lattice, or that it substitutes for Li in the conducting channels. Samples were synthesized by either a sol-gel derived (700°C) or high temperature (1050°C) ceramic method. The lower temperature sol-gel samples show much smaller particle size and but poor sinterability due to excess lithia.

Highlights the effects of small amounts of Al(III) substitution on the tetragonal to cubic phase transition. The high temperature ceramic samples gave more crystalline samples but were more likely to have La<sub>2</sub>Zr<sub>2</sub>O<sub>7</sub> impurities due to surface lithia evaporation.

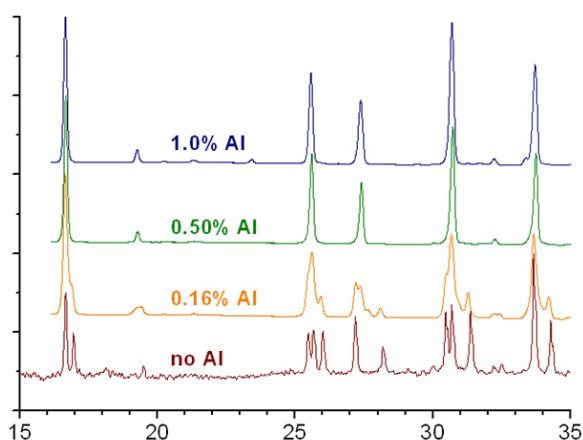


**Figure V - 213:** Synthesis of LLZ as a function of Al(III) content for a series of samples synthesized using a sol-gel method. The material undergoes a tetragonal to cubic transition around 0.5% Al (III).

Combining characterization data from the NMR, TGA, high resolution synchrotron powder XRD, and synthesis studies, it was shown that in the tetragonal samples the Al was widely distributed over three different crystallographic sites whereas at the cubic transition the Al coalesces into one specific tetrahedral Li cation site with a dramatic increase in lithium-ion conductivity.

Ionic conductivity measurements on samples sintered at 1000°C with varied Al content show the expected differences between the tetragonal and cubic forms of LLZ.

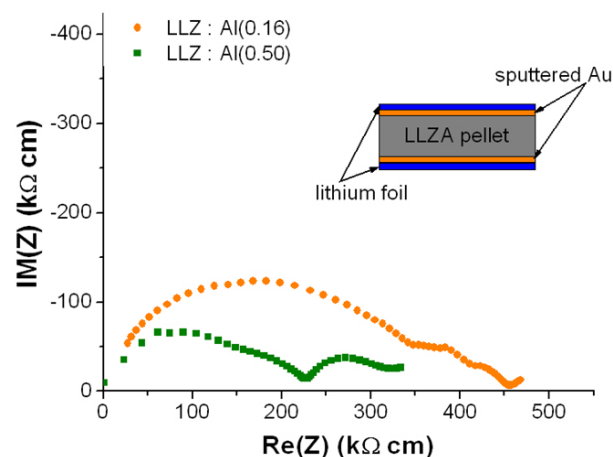


**Figure V - 214:** EIS ionic conductivity measurements on Al-substituted tetragonal LLZ (orange) and Al-substituted cubic LLZ (green) are shown. No significant conductivity differences were noted for samples that did not use Au (or Li<sub>x</sub>Au) protective coating.

Pellets sintered from either synthetic process showed densities (vs. theoretical density) ranging from 60 to 80%. The higher densities were achieved for samples that were annealed above 1100°C using sol-gel derived powders. Figure V - 215 is an SEM micrograph of an ~80% dense pellet.

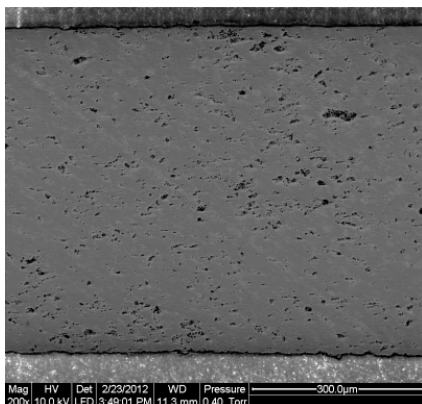


**Figure V - 215:** Cross-sectional SEM micrograph of a cubic-LLZ pellet.

Efforts to increase the density by lithium borate addition have had mixed results. The pellets appear denser in SEM studies but the conductivity is reduced as the Li-B-O phase appears to accumulate at grain boundaries in the amounts evaluated (1-3 wt %).

Cabana and Doeff at LBNL have devised a processing and sintering methodology for LLZ powder to get as high as 92% theoretical density in pellets. ANL is in the process of applying their methodology to their samples as previously only hot isostatically pressing (HIP) LLZ could achieve such high compaction.

Modeling of this type of solid electrolyte containing system from Kevin Gallagher has highlighted the opportunities available from making thin films of any of these high conductivity Li-ion conducting phases.

Figure V - 216 highlights the modeling results at three different energy density values. The values chosen reflect 1) PHEVs (red), 2) consumer electronics (blue), and 3) optimized Li-S cells (black).

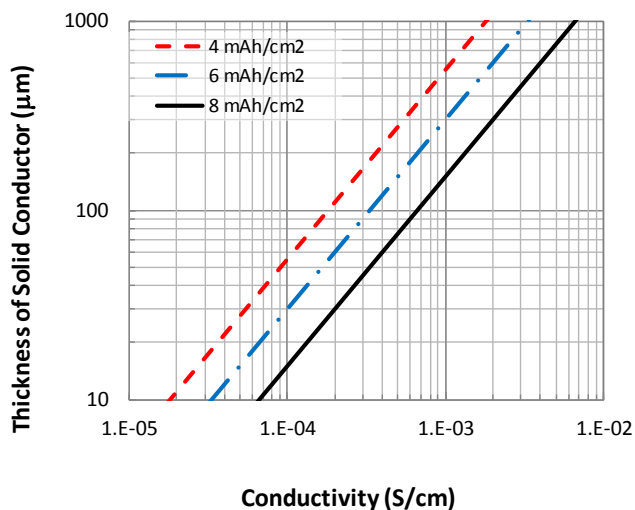


**Figure V - 216:** Modeling energy density requirements for a series of materials at various solid state conductivities and sintered plate thickness.

State-of-the-art materials and sintered plates typically are manufactured with thicknesses between 100-200 μm. This translates to end-user required conductivities of 10<sup>-3</sup> S/cm to 10<sup>-4</sup> S/cm. However synthesizing 50-100 nm thin films would allow materials with conductivities as low as 10<sup>-5</sup> S/cm to be viable for transportation applications.

To this, efforts were directed at the deposition of Li<sub>3.4</sub>Si<sub>0.4</sub>P<sub>0.6</sub>O<sub>4</sub> and Li<sub>7</sub>La<sub>3</sub>Zr<sub>2</sub>O<sub>12</sub> in thin film form using pulsed laser deposition (PLD) and rf sputtering. Figure V - 217 shows the scanning electron microscope (SEM) cross-section image of a thin Li-La-Zr-O film deposited by PLD at LBNL. X-ray diffraction (XRD) indicated that the film was amorphous. The thin film was dense, around 200 nm thick and generally had a smooth surface without large droplets that can generally form during laser deposition. Laser induced breakdown spectroscopy confirmed that the film contains only Li, La, Zr and O with relative molar ratios close to the stoichiometry of the Li<sub>7</sub>La<sub>3</sub>Zr<sub>2</sub>O<sub>12</sub> target. The dependence of the conductivity of the thin films with temperature was measured by AC impedance spectroscopy. The response was assigned to the ionic conductivity of the thin film. An Arrhenius relationship between conductivity and inverse of absolute temperature was found (Figure V - 214). The activation energy of the amorphous Li-La-Zr-O thin film was calculated to be 0.43eV, similar to reported bulk values for Li<sub>7</sub>La<sub>3</sub>Zr<sub>2</sub>O<sub>12</sub>. The ionic conductivity of the film at room temperature was extrapolated from the Arrhenius relation, and found to be 4.6×10<sup>-7</sup> S/cm. This value is comparable to that of Li<sub>7</sub>La<sub>3</sub>Zr<sub>2</sub>O<sub>12</sub> crystallizing in a tetragonal structure, which was the material used as target. Despite the low conductivity of the thin film, its' very low

thickness resulted in an area specific resistance (ASR), which measures the ohmic loss during ion transport, of  $43.5 \text{ Ohm}\cdot\text{cm}^2$  at room temperature.

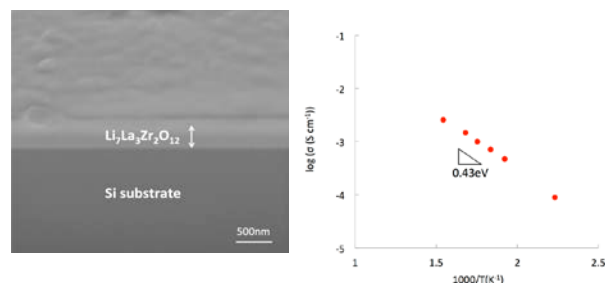


**Figure V - 217:** (Left) SEM cross-section image of 200nm thick Li-La-Zr-O films. (Right) Arrhenius plot of the thin films grown on MgO, measured by AC impedance spectroscopy.

ANL has initiated an effort to synthesize thin films of LLZ and LLTO using RF sputtering. On dense substrates several methods to make LLZ films have been evaluated. Initial work showed the need for a copper layer between the  $\text{Al}_2\text{O}_3$  or  $\text{SiO}_2$  substrate due to high lithia reactivity (formation of  $\text{LiAlO}_2$  or  $\text{Li}_4\text{SiO}_4$ ). An SEM micrograph of a typical film is shown in Figure V - 218. XRD characterization of these films shows either amorphous materials (similar to results from Doeff, et al.) or, at high temperatures, formation of poorly crystalline  $\text{La}_2\text{Zr}_2\text{O}_7$ .

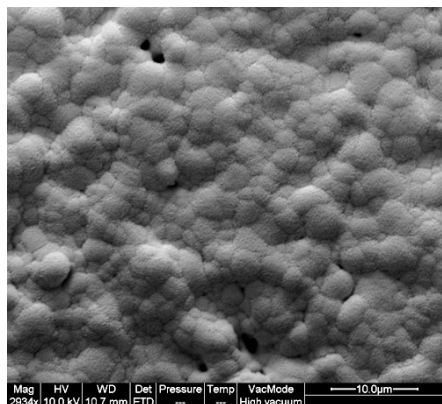


**Figure V - 218:** SEM micrograph of an LLZ sputtered film.

**Polymer-ceramic composites.** Researchers at Argonne National Laboratory (ANL) supplied LAMP nanoparticles synthesized using a solution method during FY11 to the team at LBNL for their assembly into composite structures with SEO block copolymers. The LBNL leveraged their recent developments in the assembly of inorganic nanoparticles of active Li-ion electrode materials and mixed ion-electron conducting polymers to produce purely ionically conducting composites. The resulting membranes showed a certain degree of inhomogeneity, but were found to be ionically conductive. Complete control of the assembly process was sought by preparing dispersible nanoscale inorganic particles with a stabilizing ligand. These particles could be

dispersed in a solution with polymer monomers that is easily cast into a relatively thin membrane (20  $\mu\text{m}$  or less). Using this strategy, complete control of the assembly process will be achieved so that the beneficial mechanical properties of both types of materials as well as the conductivity of the whole can be maximized. Proof of concept was obtained with  $\text{TiO}_2$  nanoparticles prepared in colloidal, fully dispersible form. An example of the morphology of the composite is provided in Figure V - 219. An extremely high degree of homogeneity was achieved. Cycling of these SEO- $\text{TiO}_2$  structures proved that dispersed ceramics significantly increase the stiffness of the structure, with a manageable decrease in ionic conductivity. As a result, Li/Li symmetric cells based on these composites could be cycled more extensively than ceramic-free counterparts before dendritic growth was observed.

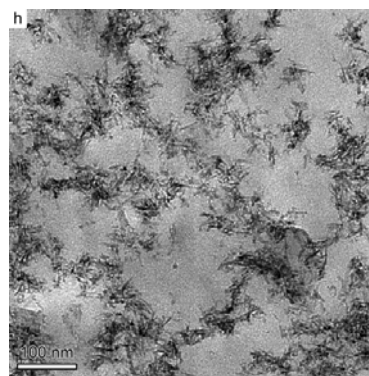


**Figure V - 219:** SEM of a  $\text{TiO}_2$ /SEO Composite

**Organic Coatings.** The organic coatings effort has focused on two research pathways. In a continuation of organosilane coatings effort, earlier findings that utilized a packing density argument to explain the significant cycle life enhancement observed by small R-group organosilane (e.g., trimethylsilane) based coatings has been extended. In this effort the effect of using larger more sterically hindered organosilanes, (e.g., triphenylsilane) on the cycle life of coated lithium surfaces was examined, and again a significant increase was noted. Since the amount of silane on the surface is much lower, modeling of the system indicated a correlation between volume the R-group occupies and the enhancement of cycle life, as seen in Figure V - 220. An effort to study the reactivity of these R-groups and its effect on cycle life has been initiated.

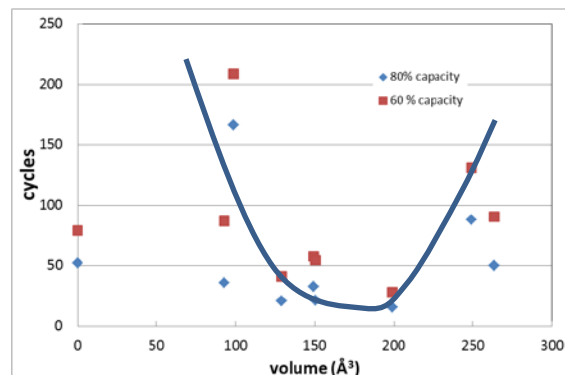


**Figure V - 220:** Cycle life (to 80% of initial capacity) for a series of organosilane coated lithium anodes versus volume of organosilane component.

Cycling data for the different silane treated lithium, along with a control sample are depicted in Figure V - 221. Out of all these surface modifications, TEOS demonstrated the lowest polarization resistance and curve hysteresis. Both, pristine lithium and Li-TMS anodes portray elevated hysteresis during galvanostatic plating and stripping. This resulted in a lowered stability and performance in regards of prolonged cycling. Moreover, the increased polarization resistance of the lithium anodes resulted in elevated overpotentials. The TMS surface layer appeared to be relatively unstable; cycling data was comparable to the unmodified lithium anode. The observed “noise” along the Li-TMS cycling data was indicative of dendrite growth and instable resonance behavior of the surface layer. During the stripping process, the TMS was easily removed from the lithium surface, resulting in a complete absence of the siloxane modified layer during the second galvanostatic plating/stripping. TEOS appeared to stabilize the lithium surface during cycling and seems to form a stable surface layer.

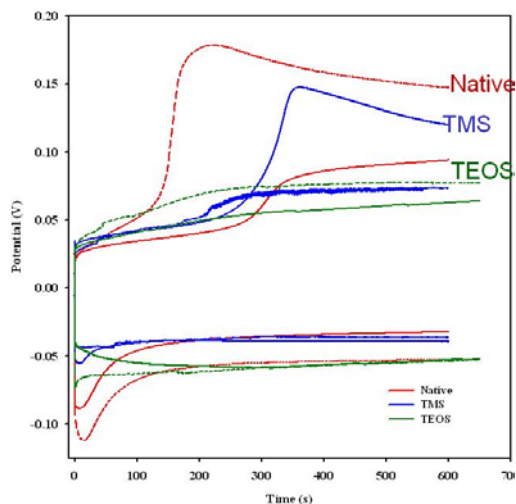


**Figure V - 221:** Cycling data on native lithium, chlorotrimethylsilane-coated lithium, and tetraethyl orthosilicate coated lithium anodes.

Studies of interfacial processes in hybrid solid/liquid lithium-ion cells reveal that electrolyte composition affects

the interfacial impedance. Mixed electrolytes help to elucidate the contribution of both, solvents and salts to interfacial impedance. Figure V - 222 shows 4 probe impedance data for 1M LiPF<sub>6</sub>/Tetra glyme (I), 1M LiClO<sub>4</sub> in PC (II) & EC: DEC (III). The reactance component of the systems (I & II) at low frequencies decreased with an increase in voltage. This indicated that the solid/liquid interface is dynamic. Under large potentials, this capacitive component (interfacial thickness) decreased. The resistance decrease was due to a possible buildup of lithium degradation products on the ceramic surface. Spectrum III indicated little effect under the polarization for the LiClO<sub>4</sub>-based electrolyte, contrary to what was observed in the LiPF<sub>6</sub>-based electrolytes. This observation suggested that the interfacial region is highly dependent on the solvent environment i.e., (how well Li is solvated).

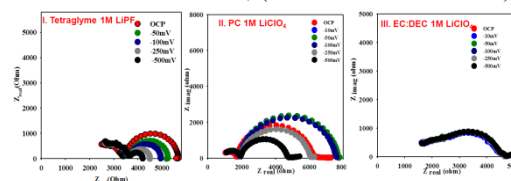


**Figure V - 222:** Four probe cole-cole plots for hybrid solid (LTP) and liquid 1M LiPF<sub>6</sub>/Tetra glyme (I), 1M LiClO<sub>4</sub> in PC (II) & EC: DEC (III) cells at 323K. All electrodes were lithium.

## Conclusions and Future Directions

- Li<sub>7</sub>La<sub>3</sub>Zr<sub>2</sub>O<sub>12</sub> (garnet, LLZ) has been studied as a bulk material and in thin film form. Initial studies on the role of Al(III) substitution have shown that the Al(III) substitutes for a Li-site and that this arrangement is different than the tetragonal form where it is more dispersed.
- Modeling studies have indicated many of the EERE-OVT goals for energy storage can be met if a stabilized lithium metal can be connected in some form to a dense thin film of a lithium-ion conducting phase. Strategies to achieve this have been discussed between ANL and LBNL and coordinated work has been initiated.
- A second surface protection mechanism has been identified for silane coated lithium surfaces. In addition to the surface packing density mechanism studied earlier, a second mechanism based on surface volume coverage has also been shown to be viable.
- An effort to embed conducting ceramic particles in polymers has been initiated. Synthesis optimization, chemical identity and phase fraction will be developed to ensure good synergy between mechanical stability and low resistivity.

## FY2012 Publications/Patents/Presentations

1. Rebecca Thompson, David J. Schroeder, Carmen M. Lopez, Susanna Neuhold, J. T. Vaughey

- “Stabilization of Lithium Metal Anodes using Silane-based Coatings,” *Electrochem. Comm.*, **13**, 1369 (2011).
2. C.M. Lopez, J. T. Vaughey, D. W. Dees “The Role of Interfacial Morphology on the Electrochemical Properties of Metallic Lithium Electrodes,” *J. Electrochem. Soc.*, **159**, A873 (2012).
  3. W. Lu, C. M. Lopez, N. Liu, J. T. Vaughey, A. N. Jansen, D. Dees “Overcharge Effect on Morphology and Structure of Carbon Electrodes for Lithium-ion Batteries,” *J. Electrochem. Soc.*, **159**, A566 (2012).
  4. B. Key, D. Schroeder, B. Ingram, J. Vaughey “Solution-based Synthesis and Characterization of Lithium-ion Conducting Phosphate Ceramics for Lithium-Metal Batteries,” *Chem. Mater.* **24**, 284 (2012).
  5. S. Neuhold, D. Schroeder, J. T. Vaughey “Effect of Surface Preparation and R-group Size on the Stabilization of Lithium Metal Anodes with Silanes,” *J. Power Sources*, **197**, 295, (2012).
  6. B. Ingram, D. Schroeder, J. Vaughey, B. Key “Ceramic Electrolytes: Synthesis and Characterization,” ANL-LBNL ILIRP Workshop, Berkeley, CA, October, 2011.
  7. S. Neuhold, J. Vaughey, D. Schroeder “Organic Coatings for Lithium Metal: Synthesis and Characterization,” ANL-LBNL ILIRP Workshop, Berkeley, CA, October, 2011.
  8. Baris Key, David J. Schroeder, Brian Ingram, John Vaughey “Synthesis and Characterization of Lithium-ion Conducting Ceramics for Lithium Metal Batteries,” *219<sup>th</sup> Meeting of the Electrochemical Society*, Boston, MA, October, 2011.
  9. Baris Key, David J. Schroeder, Brian Ingram, John Vaughey “Solution-Based Synthesis and Characterization of Lithium-ion Conducting Ceramics,” *7th International Symposium on Inorganic Phosphate Materials*, Argonne, IL, November, 2011.
  10. S. Neuhold, D. Schroeder, J.T. Vaughey “Silane-based Coatings for Lithium Metal Anodes,” *Gordon Conference on Battery Materials*, Ventura, CA, March 2012.
  11. C. M. Lopez, J. T. Vaughey, D. W. Dees “Morphologically Dynamic Electrodes: Metallic Lithium and the Effect of Morphology on its Electrochemical Response,” *Powering Our Future 2012*, Palacio Villasuso, Vitoria-Gasteiz, Spain, March 2012.
  12. J. Vaughey, D. Schroeder, B. Key, B. Ingram, A. Hubaud, S. Neuhold “Lithium Metal Anodes,” DOE Hydrogen Program and Vehicle Technologies Program Annual Merit Review, Washington, DC, May, 2012.
  13. B. J. Ingram, D. Schroeder, S. Neuhold, A. Hubaud, B. Key, J. Vaughey “New Protection Strategies for Lithium Metal,” *Beyond Lithium V*, Berkeley, CA, June, 2012.
  14. B. Key, F. Dogan, D. Schroeder, A. Hubaud, B. Ingram, J. Vaughey “Solution Based Synthesis and Characterization of Lithium-Ion Conducting Ceramics for Lithium Metal Batteries,” *54th Annual Rocky Mountain Conference on Magnetic Resonance*, Copper Mountain, CO, July 2012.
  15. L. Zhang, L. Cheng, J. Cabana, G. Chen, M. M. Doeff, and T. J. Richardson, “ $\text{Li}_4\text{SiO}_4\text{-Li}_3\text{PO}_4$  Solid Solutions as Ceramic Electrolytes in Li Metal Cells,” *220th meeting of the Electrochemical Society*, October 2011, Boston MA, Abstract # 1288.
  16. L. Cheng, L. Zhang, J. Cabana, G. Chen, M. M. Doeff and T. J. Richardson, “Effect of Lithium Borate Addition on the Physical and Electrochemical Properties of the Lithium Ion Conductor  $\text{Li}_{3.4}\text{Si}_{0.4}\text{P}_{0.6}\text{O}_4$ ” *36th International Conference and Exposition on Advanced Ceramics and Composites, ICACC 12*, Daytona Beach, FL, January 22-27th, 2012, Abstract # ICACC-S14-029-2012.
  17. J. Cabana, L. Zhang, L. Chen, J.-S. Park, T. J. Richardson, G. Chen, M. M. Doeff, “Protective layers for the lithium electrode based on ceramic phases,” *Beyond Lithium Ion V-Symposium on Scalable Energy Storage*. Berkeley, CA (USA), June 5th-7th, 2012.
  18. L. Zhang, L. Cheng, Guoying Chen, Marca M. Doeff, Thomas J. Richardson and Jordi Cabana, *Solid State Ionics*, **2012**, In press, <http://dx.doi.org/10.1016/j.ssi.2012.09.002>.

## V.G.2 Integrated Lab Research Project II (LBNL, ANL, FMC, Saft)

### DOE National Laboratories Participants

Gao Liu, Vince Battaglia and Venkat Srinivasan  
Lawrence Berkeley National Laboratory  
Environmental Energy Technologies Division  
1 Cyclotron Rd., MS 70R108B  
Berkeley, CA 94720  
Phone: (510) 486-7207; Fax: (510) 486-7303  
E-mail: [gliu@lbl.gov](mailto:gliu@lbl.gov); [vsbattaglia@lbl.gov](mailto:vsbattaglia@lbl.gov);  
[vsrinivasan@lbl.gov](mailto:vsrinivasan@lbl.gov)

Zhengcheng Zhang and Khalil Amine  
Argonne National Laboratory  
Chemical Sciences and Engineering Division  
9700 S. Cass Ave., Building 205  
Argonne, IL 60439-4837  
Phone: (630) 252-7868; Fax: (630) 972-4440  
E-mail: [zzhang@anl.gov](mailto:zzhang@anl.gov); [amine@anl.gov](mailto:amine@anl.gov)

### Industrial Participants

Marina Yakovleva  
FMC Corporation  
Lithium Division  
2801 Yorkmont Road, Suite 300  
Charlotte, NC 28208  
Phone: (704) 426-5391; Fax: (704) 426-5387  
E-mail: [marina.yakovleva@fmc.com](mailto:marina.yakovleva@fmc.com)

Bridget Deveney  
Saft America, Inc.  
Space and Defense Division - US  
107 Beaver Court,  
Cockeysville, MD 21030  
Phone (410) 568-6415; Fax (410) 771-0234  
E-mail: [bridget.deveney@saftbatteries.com](mailto:bridget.deveney@saftbatteries.com)

Start Date: October 1, 2010

Projected End Date: September 30, 2013

### Objectives

Applications of Stabilized Lithium Metal Powder (SLMP) in Lithium-ion Batteries to achieve lower cost and higher energy density. This project is designed to address two main issues in regard to the current lithium ion technology - the high cost associated with formation process, which accounts for over 20% of the production cost of lithium-ion battery; and first cycle loss of capacity (10-30%) depending on the chemistry. Lawrence Berkeley National Laboratory (LBNL) and Argonne National Laboratory (ANL) are teaming with FMC-Lithium and

Saft USA to work on problems that impede or prevent the Stabilized Lithium Metal Powder (SLMP®) from being used as a performance enhancing additive in the electrode in commercial rechargeable batteries. If successful, this will lead to commercialization of batteries with simplified formation process, lower irreversible capacity losses (leading to higher energy densities) and allow for a wider range of cathode materials to be utilized for transportation applications.

### Technical Barriers

This project addresses the following technical barriers from the Energy Storage section of the Vehicle Technologies Program Multi-year Research, Development and Demonstration Plan:

- Performance: High first cycle irreversible capacity, low coulombic efficiency, and poor cycle life.
- Life: Poor calendar life.
- Cost: High manufacture cost.
- Research in high-energy system.

### Technical Targets

- Relevant USABC goals (EV)
  - \$150/kWh
  - 230 Wh/dm<sup>3</sup>
  - 1000, 80% capacity, discharge cycles
  - 10-year system life
- Relevant USABC goals (PHEV, 40-mile)
  - \$220/kWh
  - 193 Wh/dm<sup>3</sup>
  - 2750, 75%-capacity, discharge cycles +80,000 HEV cycles
  - 15-year system life

### Accomplishments

- Investigated the SLMP stability towards various solvents and developed new binder and solvent combinations, which are stable toward SLMP in the slurry making process.
- Investigated the physical and chemical properties of the SLMP particles and developed new processes to activate the SLMP particles.
- Demonstrated the improved first cycle performance with the new SLMP in co0peration process and activation process.

◇ ◇ ◇ ◇ ◇

## Introduction

Lawrence Berkeley National Laboratory (LBNL) and Argonne National Laboratory (ANL) are teaming with lithium metal provider FMC-Lithium (Charlotte, NC) and lithium battery manufacturer Saft America to work on problems that impede or prevent the Stabilized Lithium Metal Powder (SLMP®), Figure V - 223a,b) from being used as a performance enhancing additive in the negative electrode in commercial rechargeable batteries. This effort will lead to commercialization of batteries with lower irreversible capacities (leading to higher energy densities) and allow for a wider range of cathode materials to be utilized for transportation applications. The joint effort between DOE National Laboratories and US materials and battery industries addresses technical issues preventing the utilization of SLMP, a carbonate-coated lithium metal powder, as an additive for negative electrode of rechargeable batteries for vehicles, encompassing hybrid, plug-in hybrid, and fully electric vehicles.

There is a growing trend of experimenting SLMP in the advanced lithium-ion chemistries and super capacitors by both small and large companies in the recent years. However, the efforts appear to be less coordinated, repetitive and lack of fundamental work to truly understand the SLMP material properties, and short of an objective evaluation of long-term cell performance. The integrated national lab and industry project is aimed to solve the fundamental issues associated with the  $\text{Li}_2\text{CO}_3$  surface coating on SLMP, and the application of this material in the lithium-ion battery. The material is used in applications to reduce irreversible capacity in conventional lithium-ion cells or as an independent source of lithium in batteries that do not use a lithiated cathode, and to facilitate formation process. The success of this material will have a broad impact to the lithium-ion industry.

Although numerous forms of lithium metal are available in the marketplace, including lithium foils, wires, and ingots, they all require special handling due to reactivity with air/moisture and low yield strength (0.5 MPa). An emerging alternative is SLMP, an air stable coated lithium metal powder material manufactured by FMC-Lithium. The product consists of a metallic sphere of lithium metal with an average particle diameter of 40-50  $\mu\text{m}$  with a coating consisting primarily of a 100 nm layer of  $\text{Li}_2\text{CO}_3$ . The lithium metal content is over 98% by weight. Initially developed as an easy-to-handle reducing agent for synthetic organic chemists, FMC-Lithium has also explored potential applications of SLMP as a lithium source in primary and secondary lithium-ion batteries. Initial work has demonstrated its utility as an additive in the battery manufacturing process. Three issues have been identified that limit its widespread acceptance with battery manufacturers. First issue is the chemical incompatibility between the SLMP and common battery manufacturing solvents, notably NMP, used to formulate electrode slurries. To increase acceptance, methodologies to enable

addition of SLMP during the anode slurry mixing and coating process should be developed. Second, SLMP can be used as an additive in the negative electrode to accelerate the formation of SEI on negative material surface, e.g., graphite. The long-term stability of the direct SEI formation by SLMP is unknown. Third is related to the activation of SLMP. As supplied, the coating on SLMP is very robust and activation to expose the active lithium metal is typically done using compression in the calendar process to physically break the coating. The effects of compression to the SLMP particles and electrode have not been well studied. With these identified limitations SLMP has achieved only limited marketplace penetration. The team focused on understanding the properties of SLMP and solving the problems, which impede the wide-industrial application of SLMP.

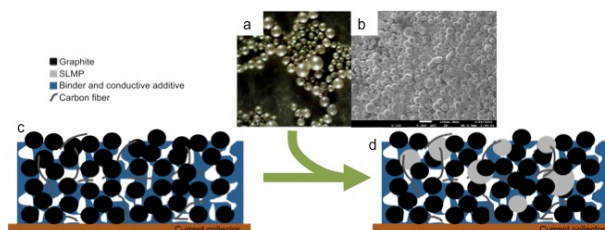


**Figure V - 223:** Develop an industrial compatible process to incorporate SLMP into the lithium-ion electrode. a. Optical image of SLMP; b. SEM image of SLMP; c. regular graphite electrode; d. graphite with SLMP electrode.

## Approach

To date several different methods have been investigated to introduce SLMP into lithium-ion cells, including spraying onto the surface of the negative electrode, addition into the slurry mixing process, and direct addition and pressure activation on a pre-formed laminate (Figure V - 223c,d). The specific amount of SLMP added to the negative electrode depends on application. Because SLMP is an active form of lithium that is easy to handle in a standard dry-room environment, our effort focused on three cell manufacturing applications that can lead to low cost manufacture and higher energy density of the lithium ion cell: Acceleration of the lithium-ion cell formation process, compensation for first cycle loss and prelithiation of anode materials and laminates.

For these applications, three issues have been identified that limit its widespread acceptance with battery manufacturers, and corresponding approaches to address these issues have been developed. The first issue is the chemical incompatibility between the SLMP and common battery manufacturing solvents, notably NMP, used to formulate electrode slurries. To increase acceptance, new binder and solvent compositions that are stable towards SLMP have been jointly developed. The second issue is related to the activation of SLMP. The carbonate coating on SLMP is very robust and activation to expose the active lithium metal is typically done using compression in the

calendar process to physically break the coating. The coating chemistry and the effect of compression to the SLMP particles have been investigated. New activation processes are being developed and tested. Third, SLMP can be used as an additive in the negative electrode to accelerate the formation of SEI on negative material surface, e.g., graphite. The long-term stability of the direct SEI formation by SLMP has been investigated.

## Results

The customized method for lithium-ion battery electrode fabrication employs a slurry coating/heating process using N-methyl pyrrolidinone (NMP)/PVdF as solvent/binder combination. However, the SLMP is thermodynamically and kinetically unstable when in contact with NMP solvent. The exothermal reaction prevents the incorporation of SLMP into the electrode by conventional slurry process. In this project, we are trying to explore SLMP compatible solvents and polymer binders to enable the preferred slurry coating process adopted widely in the battery industry and successfully fabricate the high quality electrode incorporated with SLMP. The first stage of the research is to identify the coating layer on the SLMP surface and other physical and chemical properties in order to provide insight for ultimate activation of SLMP.

**SLMP morphology and chemical composition characterization:** As indicates by the SEM measurement in Figure V - 224, the SLMP from FMC has a wide range of the particle size distribution with median size of 50 $\mu$ m in diameter. The surface coating layer is not homogeneous and showed island-like consistency with part of the surface scratched and exposed (Figure V - 224.)

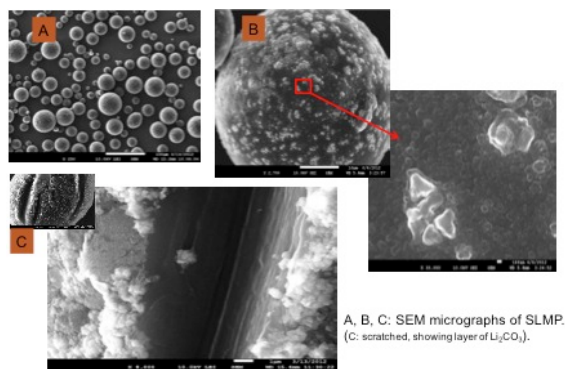


Figure V - 224: SLMP particle characterization by SEM technique.

To identify the surface coating of the SLMP sample from FMC, <sup>7</sup>Li-NMR measurement was conducted by suspending the SLMP powder in the anhydrous p-xylene and compared with the <sup>7</sup>Li NMR spectrum of standard Li<sub>2</sub>CO<sub>3</sub> suspension in the same solvent. NMR spectra confirmed that SLMP contains majority of lithium metal and a small amount of lithium compounds, i.e., Li<sub>2</sub>CO<sub>3</sub>, as shown in Figure V - 225.

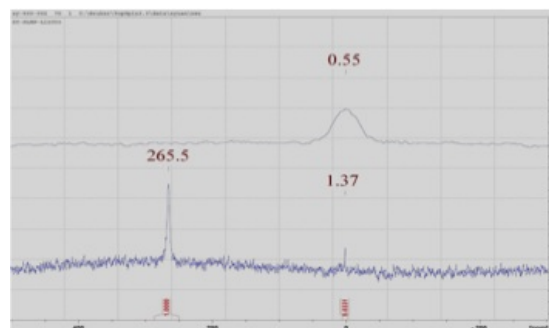
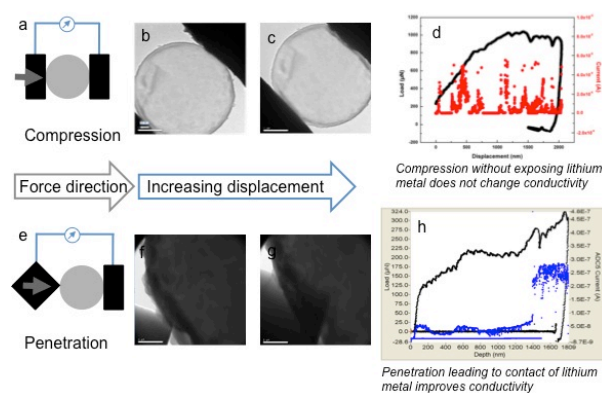


Figure V - 225: <sup>7</sup>Li-NMR spectra of surface-coated SLMP (lower spectrum, the major peak is from the bulk Li at 265.5ppm; the small peak at 1.37ppm indicates Li<sub>2</sub>CO<sub>3</sub> species; samples were measured in p-xylene solvent).

**SLMP material's mechanical properties and conductivity.** These were characterized with *in situ* TEM (in collaboration with Prof. Andrew Minor in National Center for Electron Microscopy at Berkeley Lab). Detailed electromechanical study of SLMP was conducted via an *in situ* probing technique with TEM (Figure V - 226) This technique allows concurrently monitoring the mechanical and electrical responses of single SLMP particles in real time. In the SLMP/graphite electrode, after applying a certain pressure on the electrodes to crush the Li<sub>2</sub>CO<sub>3</sub> shells, the fresh lithium metal is exposed and in contact with the graphite anode material. When electrolyte is added to wet the electrode, an electrochemical reaction takes place spontaneously between the exposed lithium and graphite particles to produce partially lithiated graphite anode. This lithiation happens prior to the cell charging process, therefore minimizing the irreversible capacity loss due to the lithium consumption events during formation, and lead to spontaneous SEI formation. Nanoscale Electrical Contact Resistance (nanoECR) system was used for performing coupled electromechanical tests of individual SLMP particles *in situ* in a transmission electron microscope (TEM). The nanoECR provides an electrical path from the conductive boron-doped diamond tip, through the sample and to the signal acquisition and measurement hardware. The nanoECR nanocompression technique therefore enables to directly observe the particle fracture events and quantify both the mechanical force and the electrical resistivity during compression in the TEM. The initial yield pressure at point d where the shell begins to fracture is ~15 MPa and the electrical conductivity of the Li<sub>2</sub>CO<sub>3</sub> shell to be a value of ~10<sup>-6</sup> S/cm as measured by this technique.



**Figure V - 226:** *In situ* TEM demonstrate the compression force required to break the SLMP particles and the electric conductivity of the carbonate coating layer. a. Schematic of compression in TEM chamber; b,c. SLMP particle before and after compression; d. load and conduction change during compression; e. Schematic of penetration; f,g. SLMP particle before and after penetration. h. load and conduction change during penetration.

#### Solvent compatibility with SLMP was investigated.

A large quantity of the solvent/polymer combinations and their reactivity with SLMP were investigated. Several compositions were optimized and used for electrode fabrication process. SLMP was found incompatible with N-methylpyrrolidinone (NMP), dimethylformamide (DMF), or dimethyl acetamide (DMA). New compatible solvents have been explored. Some of the recent results are summarized in Figure V - 227. Based on the compatibility test, toluene, anisole and dichlorobenzene are the more stable solvents for SLMP.

| Solvent  | None | THNA  | Ani-sole | DCL   | CL   | DMSO  | NMP  |
|--|------|-------|----------|-------|------|-------|------|
| Molecule Structure   |      |       |          |       |      |       |      |
| Mass of SLMP (mg)  | 18.3 | 21.2  | 20.6     | 21.0  | 19.5 | 21.0  | 21.6 |
| Test condition (glovebox)  | N/A  | 72 hr | 72 hr    | 72 hr | 4 d  | 48 hr | 24hr |
| Vol. of H <sub>2</sub> generated (mL) upon adding H <sub>2</sub> O | 27.2 | 32.2  | 31.7     | 32.5  | 28.4 | 28.6  | 1.2  |
| Vol. of H <sub>2</sub> (assuming 97% Li, mL)                       | 28.4 | 32.9  | 31.9     | 32.6  | 30.2 | 32.6  | 33.5 |
| Actual Li wt% based on test  | 92.9 | 94.9  | 96.2     | 96.7  | 91.0 | 85.1  | 7.8  |

**Figure V - 227:** Solvent-SLMP reactivity and compatibility test summary.

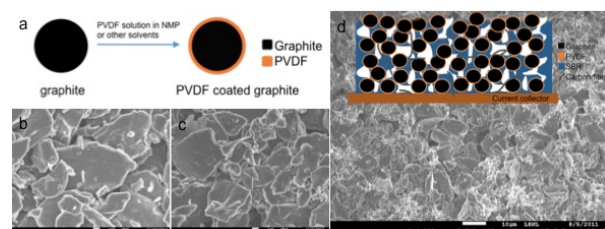


**Figure V - 228:** PVDF coated graphite enables SBR/toluene as binder solvent system for graphite and SLMP anode. a. Schematic of PVDF coated graphite particle; b. SEM of graphite; c. 2% PVDF coated graphite; d. electrode made with PVDF coated graphite and SBR/toluene binder system, inset is the schematic of the electrode.

**Development of new binder and solvent combinations that are stable towards SLMP in the slurry making process.** Toluene, a common industrial scale organic solvent, is very stable toward SLMP material. The combination of Styrene-Butadiene Rubber (SBR) with toluene was investigated as a suitable solvent/binder system for SLMP and graphite mixture. SBR has been widely used as a binder in lithium-ion anode via an aqueous based slurry process. SBR/toluene mixed with SLMP and graphite can form uniform slurry, and coat into uniform electrode laminate. However, the swelling of SBR in the electrolyte is very limited. Therefore, the lithium-ion transport through SBR is poor. SBR covered graphite particles tend to have degraded rate performance compared to the PVDF based graphite electrode. To solve the lithium-ion transport issue at the binder particle interface, a thin layer of PVDF or cross-linked PEO (1-2% by weigh) is coated on the surface of graphite to improve the electrolyte transport (Figure V - 228). This has led to significantly enhanced both rate and cycling performance of the SBR/toluene processed SBR/graphite electrode (Figure V - 229).

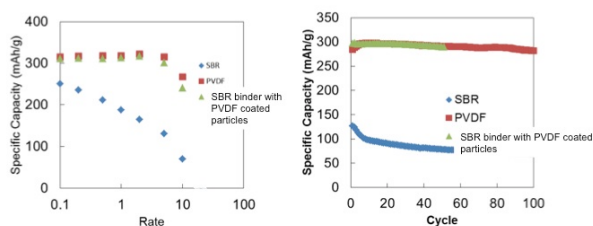


**Figure V - 229:** Both rate and cycling performance are not compromised at initial testing using SBR/toluene process when the graphite is coated with 2% of PVDF. a. rate performance; b. cycling performance.

A new type of binder suitable with SLMP compatible solvent was also developed (Binder A, the structure is not disclosed). A graphite anode was fabricated using the solvent of dichlorobenzene as an example with binder A. A mixture of MCMB (84 wt%), carbon black (4 wt%), Binder A (5-10 wt%) in dichlorobenzene SLMP (2 wt%) were added to a container inside a argon-filled glovebox, appropriate amount of dichlorobenzene was added for to adjust the viscosity of the resulted homogeneous slurry. The slurry was coated onto a copper foil using a Dr. Blade coater, and dried in the oven at 75°C for 0.5 hour to 3 hours, then further dried in vacuum oven under dynamic vacuum for overnight.

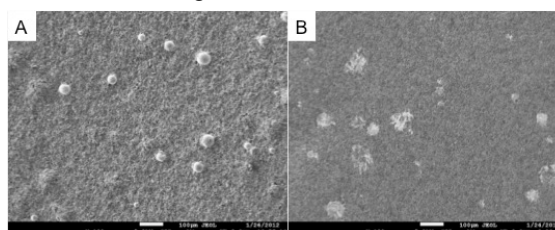


**Figure V - 230:** SEM image of the surface of graphite electrode doped with 2% by weight of SLMP in the laminate. a. As made electrode after

drying before compression; b. After compression/calendaring activation, inset is the anode potential after compression.

**Demonstration of the activation of SLMP in the electrode laminate.** With the stable binder and solvent compositions, the anode electrode of graphite and controlled amount of SLMP can be fabricated by mixing graphite particles and SLMP powder with binder and solvent to make a slurry, and use industrial state-of-the-art lithium-ion electrode coating process to coat electrode laminate. The laminate contains both graphite and SLMP. In this case, 2% SLMP by weight was incorporated into the electrode. When the electrode went through a compression/calendaring process, the SLMP particles were broken to expose lithium metal, which makes intimate contact with the graphite particles (Figure V - 230). When the electrolyte was added, the prelithiation happened without electrically charging the electrode. The potential of the graphite electrode measured after the electrolyte addition is around 0.4 V, below the SEI formation potential (0.8 V) required for graphite. A new activation method by using heating was developed: the aforementioned laminates were cut into certain size suitable as anode. The anode electrodes were then placed in an appropriate heating source to heat at 100-200°C for 5-10 minutes to activate the lithium inside the SLMP. The comparison of both activation methods is illustrated in Figure V - 231.

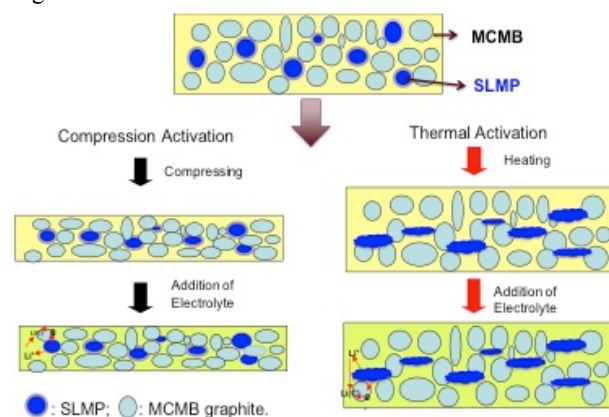


Figure V - 231: Schematic activation mechanism of SLMP.

#### Investigate formation effect with SLMP electrode.

Once SLMP is activated, it will deliver lithium ion to the graphite anode material. When the potential of the graphite comes down below 0.8 V, SEI forms spontaneously on the surface. It is important to understand the long-term stability of this SEI layer. Initial work has demonstrated that 2% SLMP addition in the electrode can significantly lower the anode potential down to 0.4 V (Figure V - 232). The electrodes were stored for different period of time ranging from no storage to 8 days of storage after cell assembly. It is shown that the storage time has improved both the cycling capacity and the initial cycling stability. Although lithium ion insertion from SLMP to the graphite happen immediately and spontaneously after the

electrolyte addition which bring the graphite to 0.4 V, the storage time allows the SEI protective layer to form and stabilize. The performance improvement is systematic along the storage time from no storage, one, two and four days. The cells at 4 days and 8 days of storage gave similar, and highest capacity and cycling stability. This shows the SLMP addition may open a door to a low manufacturing cost SEI formation process compared to the conventional electrical charge based process.

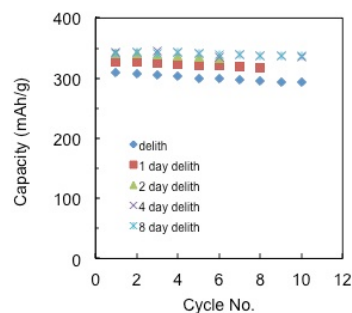
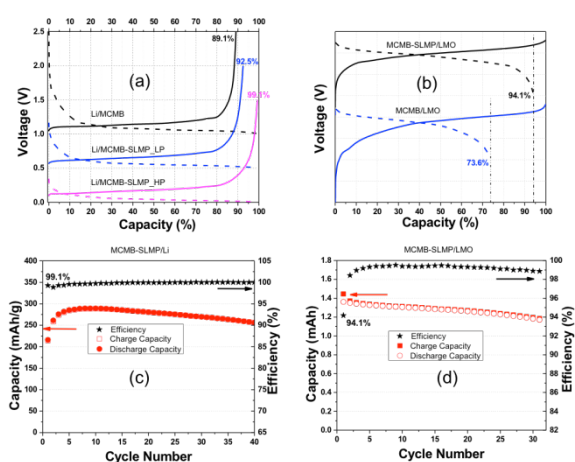


Figure V - 232: Cycling stability of the 2% SLMP doped graphite electrode after different duration of storage times. The blue diamond was no storage time.

**Initial Cycling performance of the SLMP-containing electrode.** After SLMP was activated through the above methods, the anode electrodes were used to assemble the half cell and the full cell. Upon addition of Gen 2 electrolyte (1.2 M LiPF<sub>6</sub> in EC/EMC (3/7)), the graphite anodes will be lithiated *in situ* by the activated SLMP. An illustration on the mechanism of lithiation process is shown in Figure V - 233a. The charge discharge profiles of these half cells indicated that the first cycle capacity loss of graphite electrode could be reduced to various levels depending on compression pressure. A MCMB-SLMP electrode was compressed and assembled into a coin cell type battery with LMO cathode and Gen 2 electrolyte. The charge discharge profiles of these batteries indicated that first cycle capacity loss could be greatly reduced as shown in Figure V - 233b. The cycle performance of MCMB-SLMP/LMO cell is shown in Figure V - 233d.



**Figure V - 233:** a First cycle voltage profiles and efficiency of MCMB anode with SLMP; b. first cycle voltage profiles and efficiency of MCMB-SLMP/LNMO full cell; c. Initial cycling data of MCMB-SLMP anode; d. Initial cycling data of MCMB-SLMP/LNMO full cell.

## Conclusions and Future Directions

This project has been focused on solving the main issues that impede the widespread acceptance of SLMP for battery manufacturers, and developed corresponding approaches to address these issues. The first issue is the chemical incompatibility between the SLMP and common battery manufacturing solvents. New binder and solvent compositions that are stable towards SLMP have been jointly developed. The second issue is related to the activation of SLMP. The  $\text{Li}_2\text{CO}_3$  coating chemistry and the effect of compression to the SLMP particles have been investigated. New activation processes has been developed and tested to be effective. Third, SLMP can be used as an additive in the negative electrode to accelerate the formation of SEI on negative material surface. The stability of the direct SEI formation by SLMP has been investigated, and extended storage after SLMP lithiation leads to improve stability. Initial lithium ion battery testing results indicated that the SLMP can be successfully introduced into the electrodes acting as an effective additive for to improve energy density.

Future work will be on combining and optimizing all the aspects of new binder, new activation process and formation process in testing lithium-ion chemistry at the guidance of industrial partners. Use modeling aid to understand the really cost reduction and energy gain in the cell level, and scale up this effort in pouch cells and large format cells with industrial partners.

## FY 2012 Publications/Patents/Presentations

### National Labs and Industries Joint Meetings and On-site Workshops

- Gao Liu, Vince Battaglia, Venkat Srinivasan, Zhengcheng Zhang, Khalil Amine, Marina Yakovleva, and Bridget Deveney, 2012 DOE Annual Peer Review

Meeting (AMR) Presentation, Washington DC. May 2012.

- Gao Liu, Vince Battaglia, Zhengcheng Zhang, Argonne-Lawrence Berkeley Joint workshop, Argonne, IL, Oct. 2012.
- Gao Liu, Zhengcheng Zhang, Marina Yakovleva, Argonne-Lawrence Berkeley-FMC Joint video-discussion, Berkeley, CA and Argonne, IL, Oct. 2012.
- Gao Liu, Vince Battaglia, Marina Yakovleva, and Bridget Deveney, LBNL-FMC-SAFT Joint Meeting, Cockeysville, MD, July 2012,
- Gao Liu, Vince Battaglia, Venkat Srinivasan, Zhengcheng Zhang, Marina Yakovleva, and Bridget Deveney, ANL-LBNL-FMC-SAFT Joint Meeting, Berkeley, CA Nov. 2011.

## Patent Disclosers and Application

- Polyvinylidene difluoride, polyethylene oxide, and derivative surface modified active material particles for styrene-butadiene rubber as binder for lithium-ion electrode applications, Gao Liu, Lei Wang and Sang-Jae Park, IB-3052 PCT filed in 2012.
- Lithium metal doped electrodes for lithium-ion rechargeable chemistry, Gao Liu, Vince Battaglia and Lei Wang, U.S. patent application serial no. 61/700,790 filed in Sept 2012.

## Publications

- Zheng, H.; Yang, R.; Liu, G.; Song, X.; Battaglia, V. S., "Cooperation between Active Material, Polymeric Binder and Conductive Carbon Additive in Lithium Ion Battery Cathode," *Journal of Physical Chemistry C* 2012, **116** (7), 4875-4882.
- Zheng, H.; Tan, L.; Liu, G.; Song, X.; Battaglia, V. S., "Calendering effects on the physical and electrochemical properties of Li Ni<sub>1/3</sub>Mn<sub>1/3</sub>Co<sub>1/3</sub>O<sub>2</sub> cathode," *J. Power Sources* 2012, **208**, 52-57.
- Zheng, H.; Sun, Q.; Liu, G.; Song, X.; Battaglia, V. S., "Correlation between dissolution behavior and electrochemical cycling performance for LiNi<sub>1/3</sub>Co<sub>1/3</sub>Mn<sub>1/3</sub>O<sub>2</sub>-based cells," *J. Power Sources* 2012, **207**, 134-140.
- Zheng, H.; Qu, Q.; Zhang, L.; Liu, G.; Battaglia, V. S., "Hard carbon: a promising lithium-ion battery anode for high temperature applications with ionic electrolyte," *Rsc Advances* 2012, **2** (11), 4904-4912.
- Zheng, H.; Li, J.; Song, X.; Liu, G.; Battaglia, V. S., "A comprehensive understanding of electrode thickness effects on the electrochemical performances of Li-ion battery cathodes," *Electrochim. Acta* 2012, **71**, 258-265.
- Xun, S.; Chong, J.; Song, X.; Liu, G.; Battaglia, V. S., "Li<sub>4</sub>P<sub>2</sub>O<sub>7</sub> modified high performance Li<sub>3</sub>V<sub>2</sub>(PO<sub>4</sub>)<sub>3</sub> cathode material," *Journal of Materials Chemistry* 2012, **22** (31), 15775-15781.

7. Wu, S.-L.; Zhang, W.; Song, X.; Shukla, A. K.; Liu, G.; Battaglia, V.; Srinivasan, V., "High Rate Capability of Li(Ni<sub>1/3</sub>Mn<sub>1/3</sub>Co<sub>1/3</sub>)O<sub>2</sub> Electrode for Li-Ion Batteries," *J. Electrochem. Soc.* 2012, **159** (4), A438-A444.
8. Liu, X.; Liu, J.; Qiao, R.; Yu, Y.; Li, H.; Suo, L.; Hu, Y.-s.; Chuang, Y.-D.; Shu, G.; Chou, F.; Weng, T.-C.; Nordlund, D.; Sokaras, D.; Wang, Y. J.; Lin, H.; Barbiellini, B.; Bansil, A.; Song, X.; Liu, Z.; Yan, S.; Liu, G.; Qiao, S.; Richardson, T. J.; Prendergast, D.; Hussain, Z.; de Groot, F. M. F.; Yang, W., "Phase Transformation and Lithiation Effect on Electronic Structure of Li<sub>x</sub>FePO<sub>4</sub>: An In-Depth Study by Soft X-ray and Simulations," *J. AM. CHEM. SOC.* 2012, **134** (33), 13708-13715.
9. Liu, G.; Zheng, H.; Song, X.; Battaglia, V. S., "Particles and Polymer Binder Interaction: A Controlling Factor in Lithium-Ion Electrode Performance," *J. Electrochem. Soc.* 2012, **159** (3), A214-A221.
10. Chong, J.; Xun, S.; Song, X.; Ridgway, P.; Liu, G.; Battaglia, V. S., "Towards the understanding of coatings on rate performance of LiFePO<sub>4</sub>," *J. Power Sources* 2012, **200**, 67-76.
11. Xun, S.; Song, X.; Wang, L.; Grass, M. E.; Liu, Z.; Battaglia, V. S.; Liu, G., "The Effects of Native Oxide Surface Layer on the Electrochemical Performance of Si Nanoparticle-Based Electrodes," *J. Electrochem. Soc.* 2011, **158** (12), A1260-A1266.
12. Xun, S.; Song, X.; Grass, M. E.; Roseguo, D. K.; Liu, Z.; Battaglia, V. S.; Liu, G., "Improved Initial Performance of Si Nanoparticles by Surface Oxide Reduction for Lithium-Ion Battery Application," *Electrochem. Solid State Lett.* 2011, **14** (5), A61-A63.
13. Liu, G.; Xun, S.; Vukmirovic, N.; Song, X.; Olalde-Velasco, P.; Zheng, H.; Battaglia, V. S.; Wang, L.; Yang, W., "Polymers with Tailored Electronic Structure for High Capacity Lithium Battery Electrodes," *Advanced Materials* 2011, **23** (40), 4679.
14. Kim, S.; Park, M. J.; Balsara, N. P.; Liu, G.; Minor, A. M., "Minimization of focused ion beam damage in nanostructured polymer thin films," *Ultramicroscopy* 2011, **111**, 191-199.
15. Chong, J.; Xun, S.; Zheng, H.; Song, X.; Liu, G.; Ridgway, P.; Wang, J. Q.; Battaglia, V. S., "A comparative study of polyacrylic acid and poly(vinylidene difluoride) binders for spherical natural graphite/LiFePO<sub>4</sub> electrodes and cells." *J. Power Sources* 2011, **196** (18), 7707-7714.

### Invited Talks

1. "Conductive polymer binder for lithium ion battery application - a scalable approach to assemble Si nanoparticles into electrode," DOE User Facility: The Molecular Foundry Annual Workshop, Berkeley, CA, October **2012**.
2. "New Binder Approaches for Advanced Anode Electrode," *5<sup>th</sup> International Conference on Advanced Lithium Batteries for Automobile Applications*, Istanbul, Turkey, September **2012**.
3. "An ALS XAS characterization and DFT calculation guided materials discovery of conductive polymer binders for high capacity Si anode electrode," US-China Electric Vehicle and Battery Technology Workshop, Boston, MA, August **2012**.
4. "An ALS XAS characterization and DFT calculation guided materials discovery of conductive polymer binders for high capacity Si anode electrode," ALS Seminar Series, Berkeley, CA, June **2012**.
5. "Conductive Polymer Binders with Tailored Electronic Structure for Si Alloy Anode," *MRS Spring Meeting*, San Francisco, CA, **2012**.
6. "Conductive Polymer Binder and Silicon Composite Anode for High Energy Lithium Ion Battery," *The Young Engineers and Scientists Symposium*, Berkeley, CA, March **2012**.
7. "A Solvent Processable Conductive Polymer Binder for Si Anode Electrode," *10X Advanced Battery R&D*, Santa Clara, CA, Jan. **2012**.
8. "Combined Adhesion with Electric Conduction in the Electrode Conductive Polymer Binders for Si Alloy Anode," *International Battery Association and Pacific Power Sources Symposium*, Waikoloa Village, Hawaii, Jan. **2012**.
9. "Particles and Polymer Binder Interaction - A Controlling Factor in Lithium-ion Electrode Performance," *General Motors Global R&D Symposium-Automotive Lightweight Materials and Battery Technology* in Shanghai China, Nov. **2011**.
10. "New Materials and Electrode Designs for Lithium-ion Rechargeable General Motors," Warren Michigan, Nov. **2011**.
11. "Probe Material and Interface Changes of an OLED Device," U.S. DOE EERE-BES SSL Roundtable meeting in Bethesda Maryland, Oct. **2011**
12. "Developing and understanding battery materials with combined techniques Part I. Introduction and materials," DOE User Facility: Advanced Light Sources user meeting at Lawrence Berkeley National Laboratory in Berkeley CA, Oct. 2011.

## V.G.3 Composite Electrolyte to Stabilize Metallic Lithium Anodes (ORNL)

Nancy Dudney, PI (Oak Ridge National Laboratory)  
Wyatt Tenhaeff, co-PI

Nancy Dudney  
Oak Ridge National Laboratory  
Material Science and Technology Division  
PO Box 2008, MS 6124  
Oak Ridge, TN 37831-6124  
Phone: (865) 576-4874  
E-mail: [dudneynj@ornl.gov](mailto:dudneynj@ornl.gov)

Start Date: October 2011

Projected End Date: September 2016

### Objectives

- Understand  $\text{Li}^+$  transport at the interface between two dissimilar solid electrolytes, e.g., ceramic/polymer.
- Develop composites of electrolyte materials with the requisite electrochemical and mechanical properties as guided by simulation.
- Fabricate thin membranes and demonstrate stability upon cycling of a thin metallic lithium anode with good power performance and long cycle life.

### Technical Barriers

Advanced lithium batteries, including Li-air and Li-S, require robust protection of the metallic lithium anode to maintain a mechanically and chemically stable lithium anode. Any reaction or roughening of the lithium will result in loss of capacity, degradation of performance and may also compromise safety. A robust solid electrolyte to protect the lithium while ensuring rapid cycling is the clear solution, yet identifying and fabricating a solid electrolyte with the required ionic transport, electrochemical stability, and mechanical strength is a technical challenge. In addition, the electrolyte must be very thin and light, and cost effective for large-scale manufacturing. To provide a lithium anode with significantly higher energy density than current Li-ion anodes, all components of the anode including the packaging, current collector, protective electrolyte, and indeed the lithium itself, must be minimized.

### Technical Targets

- Develop a solid electrolyte membrane that stabilizes the long-term, safe, and efficient cycling of lithium metal anodes to enable high energy density batteries.
- Provide an electrolyte protected anode to promote the equivalent electric range of 40 miles (PHEV) and 200-300 miles (EV).

- Enable battery anodes for very high energy Li-S Battery (500 Wh/kg) by 2020 and Li-Air Battery (700 Wh/kg) by 2030.

### Accomplishments

- Demonstration that small interfacial impedance across planar interfaces of dry PEO-based electrolytes with either Ohara (ceramic) or garnet-type lithium lanthanum zirconate ceramics can be achieved.
- Development of a method to achieve 60 vol.% loading of dispersed ceramic particles in a dry polyethylene oxide (PEO) matrix, ensuring networks for transport paths and mechanical stability.
- Demonstration that crystalline PEO has a relatively high elastic modulus (around 1 GPa), which is several orders of magnitude higher than conventional amorphous polymer electrolytes.



### Introduction

This program is based on the observation that no single solid electrolyte, either polymer, ceramic, or glass, can currently meet all of the requirements for a stable interface with the active lithium anode. Many inorganic materials are not stable in contact with lithium metal and also suffer from being too brittle when thinned to a light weight membrane. Polymer electrolytes, even those with rigid block co-polymer structures, gradually roughen with lithium cycling and are too resistive for room temperature operation. Formation of a composite polymer-ceramic structure offers a pragmatic approach to optimizing the electrolyte properties. Using the wealth of known solid electrolyte materials, this program is addressing the fabrication and testing of such composites, both experimentally and through simulation. A critical aspect of such a composite is the properties of the interface formed between two different electrolytes, which must offer mechanical integrity while not impeding the transport of lithium ions. Characterizing and modifying these interfaces is the primary focus of this program.

### Approach

**Preparation and electrochemical characterization of bi-layer electrolyte laminates.** Using well-studied electrolyte materials from a variety of sources, bi-layer structures create a simple planar interface to characterize the lithium transport from one material to another. Various synthesis approaches are investigated to either laminate or cast a polymer electrolyte over a ceramic plate. Only dry processing is used to eliminate all solvent effects. In

addition, investigations probe how the materials forming the interface can be functionalized or activated to promote good adhesion and high conductivity. By electrochemical impedance spectroscopy (EIS) with blocking electrodes, the measured impedance of the bilayer is compared to the series summation of the individual components. An interfacial impedance that is significant in magnitude relative to the bulk resistance can be readily resolved. Results from these investigations provide parameters for the interface phase used in simulations of the composite properties.

**Simulation of ion transport through composite structures.** Codes were developed in our earlier work to predict both ion transport and also elastic modulus of various composite electrolytes. The composite is considered as two bulk materials plus an interfacial phase; this adds complexity beyond existing models, such as effective medium studies. The composites evaluated are generally either layered composites or composites with dispersed hard ceramic particles. Additional sophistication is being added by using Comsol tools with a finer and flexible meshing routine. These simulations will help evaluate how variation in the interfacial resistivity alters the overall ionic conduction path and the uniformity of current through the composite electrolyte.

**Fabricating electrolyte components for improved ion transport and mechanical properties.** Based on results of bilayer and simulation studies, selected materials and selected mixtures are prepared as dispersed composites. Using EIS, ion transport measurements are compared against the simulations to evaluate the influence of the interfaces to block or direct the ionic current. Promising composite electrolytes are also prepared with metallic lithium contacts to evaluate the dc transport, transference number and electrochemical stability with Li. As work progresses, alternative fabrication methods and materials will be investigated to improve performance. This may require highly aligned structures and/or high volume fractions of the dispersed phase. Feasibility of preparing the membrane with platelet or flake morphology will be explored.

## Results

**Studies of bi-layer electrolyte laminates.** Following our earlier published studies of Lipon-glass/polymer interfaces, measurements of the interface resistance between dry PEO polymer electrolytes and two different ceramic electrolytes were obtained by EIS. Dense ceramic plates were either a  $\text{Li}_7\text{La}_3\text{ZrO}_{12}$ -based garnet (LLZO) from Prof. Jeff Sakamoto (Michigan State University) or a Nasion-type phosphate electrolyte purchased from Ohara Corp. (Ohara). These ceramics were coated using several melt lamination processes with PEO-polymer electrolytes having either LiTFSI or  $\text{LiCF}_3\text{SO}_3$  salts. Examples of the results are given in Figure V - 234 and Figure V - 235.

Figure V - 234 shows that the fabrication technique clearly influences the interfacial resistance. The low frequency semicircle that dominates the overall response shown in the upper figure is assigned to interfacial resistance between the Li garnet ceramic and the PEO electrolyte. This would certainly lead to a highly resistive composite electrolyte. However, the resistive interface is nearly eliminated for the same materials via an alternate fabrication as shown in the lower plot. This demonstrates that the fabrication technique is a key consideration, and issues such as wetting and adhesion must be carefully considered.

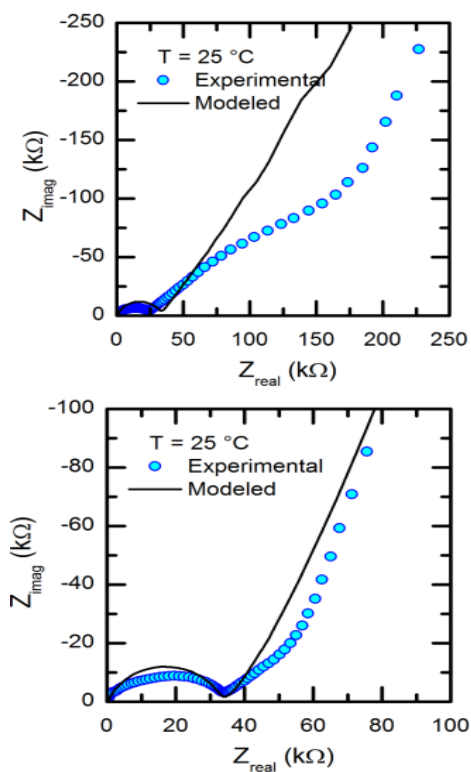


**Figure V - 234:** Impedance spectroscopy of laminated LLZO-PEO<sub>10</sub>:LiTFSI bilayers prepared by two different routes. The modeled response assumes a negligible interfacial resistance.

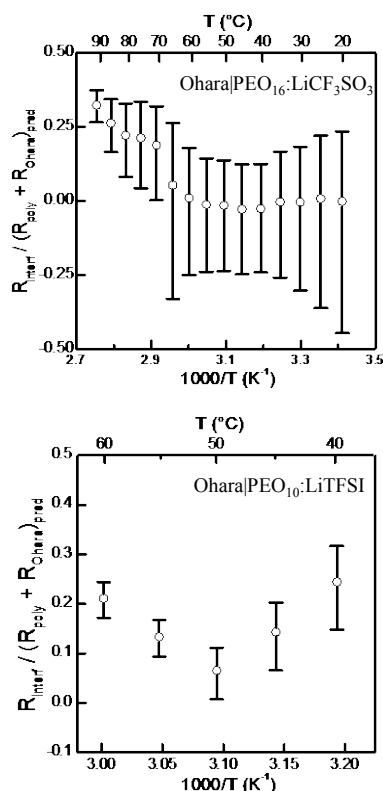


**Figure V - 235:** Interfacial resistances between a ceramic plate and two polymer electrolytes: PEO16:LiCF<sub>3</sub>SO<sub>3</sub> (top) and PEO10:LiTFSI (bottom). Values are normalized to the bulk resistance of the two layers. Melting temperatures are 60°C and 35°C, respectively.

In Figure V - 235, the relative interfacial resistance extracted from a similar EIS analysis is shown for a bilayer of Ohara ceramic and two different polymer electrolytes. Below the melting temperature, the interface resistance is near zero relative to the sum of the bulk resistances; being too low for accurate extraction, the error bars are quite large. Above the melting temperatures, the interfacial resistance increases. Possible sources of the interface resistance were examined by electron microscopy and x-ray spectroscopy. While the lithium salt is not homogeneously dispersed in the polymer, there is no indication of segregation along the interface which is well adhered and free of pores. Interestingly, for collected polymer/ceramic bilayers composed of different materials, the interfacial resistances followed an Arrhenius dependence with activation energies of  $100 \pm 6$  kJ/mol.

**Comparison to simulation.** The third figure illustrates a simulation for dispersed particles of the highly conductive garnet in a more resistive polymer electrolyte matrix. This shows that as the interface becomes more resistive, the ions flow around rather than through the conductive ceramic giving the suppression of the normalized conductivity to the left of the gold circle. Such simulations are currently being analyzed with respect to the bilayer results.

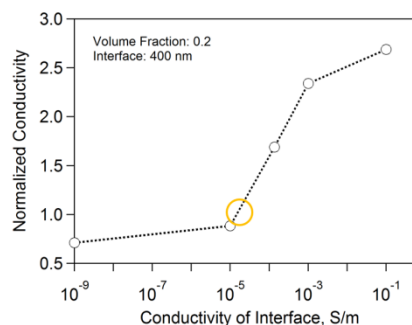


**Figure V - 236:** Simulated conductivity of a composite with 20 vol.% conductive ceramic particles assuming a range of interface conductivities.

**Dispersed particle composites.** Figure V - 237 shows a fracture edge of a dispersed composite containing 60 vol% Ohara ceramic particles. This is quite a high particle loading and should constitute a structurally stable composite and a percolating network of ceramic particles for the Li ion transport. Impedance studies are underway.

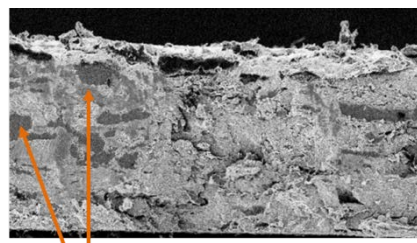


**Figure V - 237:** Fracture edge of composite with 60 vol.% ceramic particles. Arrows indicate polymer rich regions.

## Conclusions and Future Directions

Results from bilayer studies indicate that in some cases the interfacial resistance between a polymer and ceramic lithium electrolytes can be very large; this may be minimized by appropriate fabrication techniques, choice of materials and preparation of the surfaces. Simulations of dispersed composites are being developed to predict the relative conductivity and mechanical stability for a highly conductive ceramic, such as the garnet electrolytes, in a polymer electrolyte matrix. Fabrication of the experimental composites loaded heavily with the conductive ceramic phase will continue with attention to the formation of grain boundaries from larger particle contacts. These composites will then be evaluated for their mechanical properties and stability with lithium metal electrodes.

## FY 2012 Publications/Presentations

- 2012 DOE Annual Peer Review Meeting Poster Presentation.
- Nancy J. Dudney, Wyatt E. Tenhaeff, Erik G. Herbert, Sergiy Kalnaus, Kelly Perry, Kunlun Hong, Adrian S. Sabau. "Transport and mechanical properties of pure and composite solid lithium electrolytes." Invited

- presentation at the 5th meeting for Beyond Li-ion Batteries, June 2012. Berkeley, CA.
3. Nancy J. Dudney, Wyatt E. Tenhaeff Erik G. Herbert, Sergiy Kalnaus Kelly Perry, Kunlun Hong Adrian S. Sabau, "Solid Electrolytes for Li Battery Applications – Are lithium metal containing batteries a good idea?" Invited presentation at Electronic Materials and Applications, American Ceramic Society, Jan. 2012, Orlando FL.
  4. W. E. Tenhaeff, K. A. Perry, S. Kalnaus, N. J. Dudney. "Tough Solid Composite Electrolytes to Enable Lithium Metal Anodes." Prime Pacific Rim Meeting on Electrochemical and Solid-State Science. Honolulu, HI, Oct. 2012.
  5. W.E. Tenhaeff, K.A. Perry, N.J. Dudney. "Impedance characterization of Li ion transport at the interface between laminated ceramic and polymeric electrolytes." *J. Electrochem. Soc.*, accepted.